



UNIVERSITY OF  
LIVERPOOL

# Investigation into [4+6] porous organic cages and their use in porous liquids

**Rachel Joy Kearsey**

**Department of Chemistry**

**Supervisors: Professor Andrew Cooper,  
Dr Rebecca Greenaway**

## Table of contents

Acknowledgements.....	4
Abstract.....	5
Abbreviations.....	5
Chemical abbreviations.....	6
<b>Chapter 1: Introduction.....</b>	<b>8</b>
1.1 Porous materials.....	9
1.2 Definition of a porous liquid.....	10
1.3 Classes of solids used to make porous liquids.....	11
1.4 Strategies for designing porous liquids.....	24
1.5 Aims of the project.....	41
<b>Chapter 2: Using high-throughput automation in the discovery of highly soluble scrambled cages.....</b>	<b>42</b>
2.1 Introduction.....	43
2.2 Development of a high-throughput discovery workflow for discovering highly soluble cage/solvent combinations.....	46
2.3 Generating a scrambled cage library.....	54
2.4 Screening for suitable porous liquid solvents.....	62
2.5 High-throughput solubility screen.....	68
2.6 Scale up of highly soluble scrambled cage/solvent combinations.....	72
2.7 Conclusions.....	78
<b>Chapter 3: Study into the formation mechanism and properties of an isopropyl-decorated porous organic cage.....</b>	<b>80</b>
3.1 Introduction.....	81
3.2 Synthesis and characterisation of <b>CC21</b> .....	87
3.3 Study into the formation mechanism of <b>CC21</b> .....	90
3.4 Properties of <b>CC21</b> .....	100
3.5 Conclusions.....	105
<b>Chapter 4: Investigation into the properties of Type II scrambled porous liquids.....</b>	<b>106</b>
4.1 Introduction.....	107
4.2 Porosity screening of potential porous liquids.....	110
4.3 Naming Type II porous liquids.....	111
4.4 Effect of changing porous liquid solvent.....	112
4.5 Effect of changing scrambled cage component.....	119
4.6 Effect of changing the scrambled cage concentration.....	124
4.7 Investigation into guest release mechanisms.....	130
4.8 Gelation and sol-gel behaviour of porous liquids.....	133

4.9 Retention of guest in $3^3:13^3_{\text{HAP}}$ .....	135
4.10 Stability studies of $3^3:13^3_{\text{HAP}}$ .....	136
4.11 Recovery of scrambled cage from $3^3:13^3_{\text{HAP}}$ .....	137
4.12 Conclusions .....	138
<b>Chapter 5: Synthesis of organic cage salts to target porous ionic liquids .....</b>	<b>139</b>
5.1 Introduction .....	140
5.2 Designing a high-throughput methodology.....	145
5.3 Scale-up and characterisation of hits found in the high-throughput screen.....	152
5.4 ‘Scale out’ of liquids.....	154
5.5 Synthesis and characterisation of organic cage salts.....	157
5.6 Targeting Type II porous liquids .....	162
5.7 Conclusions .....	166
<b>Chapter 6: Conclusions and future work .....</b>	<b>168</b>
6.1 Conclusions .....	169
6.2 Future work .....	171
<b>Chapter 7: Experimental data and references .....</b>	<b>172</b>
7.1 General synthetic and analytical methods .....	173
7.2 Chapter 2 experimental data .....	177
7.3 Chapter 3 experimental data .....	192
7.4 Chapter 4 experimental data .....	198
7.5 Chapter 5 experimental data .....	203
7.6 References .....	213
<b>Appendices .....</b>	<b>227</b>
Chapter 2.....	228
Chapter 3.....	241
Chapter 4.....	243
Chapter 5.....	256
NMRs of new materials .....	261

## **Acknowledgements**

Firstly, I would like to thank Prof Andy Cooper and Dr Becky Greenaway for their academic support. Particularly for challenging me to be a better scientist, which has resulted in work I am proud to put my name to. Science is ultimately a collaboration so thank you to the others who assisted in the completion of my PhD, particularly to Dr Ben Alston for help with the high-throughput work, Dr Marc Little for x-ray diffraction, Aiting Kai for helping run the gas sorption, Mike Brand for collecting the HRMS data, and Jess Smith for the DSC data. Also, a special thanks to Rob Clowes, who provided essential help for using the Cooper Group equipment, without him the group would fall apart!

This PhD has been quite the journey and its challenges have been made easier by the friends I've made along the way. Thank you to Cath, Duncan and Andy, our (virtual) coffee trips and the daily Richard Madeley quotes provided essential motivation to get my thesis written. Thank you to Jess, not only for your academic support but for keeping me going when things were difficult. And to Fran, who quickly transitioned from being a colleague to my friend.

Thank you to my Dad, Michael, who painstakingly checks everything I write without complaint, this achievement is as much yours as it is mine. Also to my mum, Lynn, my sister, Ruth, and my grandparents – thank you for your love, support and inspiration to keep going. To Alison, Simon, Kieran, Bampi and Charlie, thank you for being an extension of my family, you all joined me during this journey and its only made it brighter. To Rach, who has been my friend all my adult life, thank you for telling me 'you've got this.'

I am looking forward to sharing this achievement with you all soon!

And lastly, thank you to my wonderful boyfriend, Dan, for the motivation and perspective when it seemed unachievable. This year has been especially tough on us all without having a thesis to write but the process was made so much easier with your unwavering confidence in me.

## **Abstract**

The field of porous liquids is relatively new compared to other porous materials but is rapidly developing and gaining interest. There is a diverse range of strategies in the literature to achieve porosity in the liquid state, including using porous organic cages as either soluble pores or neat liquid hosts. However, there are not enough examples to draw a comparison, so little is known about the design and limitations associated with these systems. In this thesis, we show how high-throughput automation can be applied to streamline discovery and expand the area of porous liquids with two different approaches. Firstly, the focus was on improving current systems and finding highly soluble porous organic cages in cavity-excluded solvents. This resulted in a library of porous liquids with increased cavity concentrations that allowed the exploration into how changing the solvent and cage components effects overall properties, such as gas uptake and viscosity. One problem associated with these soluble cages was the use of solvents with associated vapour pressure, which limits their study using gas sorption methods. Therefore, a second strategy was devised to explore low melting cage salts with large cavity-excluded anions. A high-throughput screen was developed that generated a small cage salt library with varying cages and counterions. The thermal behaviour of these systems was studied to determine the effect of changing these components on melting. Overall, the work carried out in this thesis developed high-throughput workflows that can be applied to larger screens and presented a series of design considerations for future systems.

## Abbreviations

BET	Brunauer-Emmett-Teller
DOSY	Diffusion ordered spectroscopy
DSC	Differential scanning calorimetry
ES-MS	Electrospray mass spectrometry
FT-IR	Fourier-Transform infrared spectroscopy
HPLC	High performance liquid chromatography
HRMS	High resolution mass spectrometry
HT	High-throughput
ICP	Inductively coupled plasma
NMR	Nuclear magnetic resonance
PXRD	Powder x-ray diffraction
QTOF	Quadrupole time-of-flight
Rt	Room temperature
SA	Surface area
SBU	Secondary building unit
SCXRD	Single crystal x-ray diffraction
SPE	Solid phase extraction
TGA	Thermogravimetric analysis

## Chemical abbreviations

ACC	Anionic covalent cage
BARF	Tetrakis[3,5-bis(trifluoromethyl)phenyl]borate
BDC	1,4-Benzenedicarboxylate
BMIM	1-Butyl-3-methylimidazolium
BPy	1-Butylpyridinium
CC	Covalent cage
CFC	Chlorofluorocarbon
CHDA	(±)- <i>trans</i> -1,2-Cyclohexanediamine
CMP	Conjugated microporous polymers
COF	Covalent organic framework
CTF	Covalent triazine frameworks
DBU	1,8-Diazabicyclo[5.4.0]undec-7-ene
DCBC	2,4-Dichlorobenzylchloride
DCM	Dichloromethane
DCT	2-Chloro-4-toluene
DMAC	Dimethylacetamide
DMF	Dimethylformamide
DMHDA	(3 <i>R</i> ,4 <i>R</i> )-2,5-Dimethylhexane-3,4-diamine dihydrochloride
DMSO	Dimethyl sulfoxide
EMIM	1-Ethyl-3-methylimidazolium
EtOAc	Ethyl acetate
EtOH	Ethanol
HAP	2-Hydroxyacetophenone
HCS	Hollow carbon sphere
HPEN	1,2-Bis(2-hydroxyphenyl) ethylenediamine
IL	Ionic liquid
IPA	Isophalate

KPEGS	Poly(ethylene glycol) sulfonate-based potassium salt
MMM	Mixed matrix membranes
MOC	Metal-organic cage
MOF	Metal organic framework
MOP	Metal organic polyhedra
MPDA	1,2-Diamino-2-methyl-propane
MS	Methyl salicylate
NEt <sub>3</sub>	Triethylamine
NMP	N-Methyl-2-pyrrolidone
NOHM	Nanoparticle organic hybrid materials
NSA	2-Naphthalenesulfonate
OS	Organosilane
P5mim.bFAP	1-propyl-3-methylimidazolium tris(heptafluoropropyl)trifluorophosphate
PAF	Porous aromatic framework
PCP	Perchloropropene
PEG	Polyethylene glycol
PEGS	Poly(ethylene glycol) sulfonate salt
PIL	Polymerised ionic liquid
PIM	Polymer of intrinsic microporosity
PL	Porous liquid
POC	Porous organic cage
polyMOC	Polymer-linked metal-organic cage
POP	Porous organic polymer
PS	Polymer surfactant
Py	Pyridinium
SBU	Secondary building units
SiNR	Silica shell nanorods
TBA	4-(Trifluoromethoxy)benzyl alcohol
TFA	Trifluoro acetic acid
TFB	1,3,5-Triformylbenzene
TFSA	Bis(trifluoromethanesulfonyl)amide
THF	Tetrahydrofuran
TMS	Tetramethylsilane
TSA	p-Toluenesulfonate
XSA	m-Xylene-4-sulfonic acid
ZIF	Zeolitic imidazolate framework
ZSM-5	Zeolite Socony Mobil-5

# **Chapter 1: Introduction**



## 1.1 Porous materials

The field of porous materials describes a diverse range of both solids and liquids, all containing cavities within their structures. The pore diameter is used in classification; those with pore sizes less than 2 nm are *microporous*, those between 2 and 50 nm are *mesoporous*, and those greater than 50 nm are *macroporous*.<sup>1-3</sup> Within the field, there are three main compositions: inorganic, organic, or a hybrid material containing both. They all have different arrangements in the solid state, resulting in either amorphous or crystalline materials that can be single molecular species or extended networks (**Figure 1.1**).<sup>4,5</sup> The high surface area and pore volume associated with these materials makes them useful in many applications, including catalysis,<sup>6</sup> molecular separations<sup>3</sup> and gas storage.<sup>7</sup> In order to be useful in industrial applications, materials must be produced on large scales and have long-term stability by not changing in arrangement, but for specific functions, the requirements can vary.<sup>5</sup>

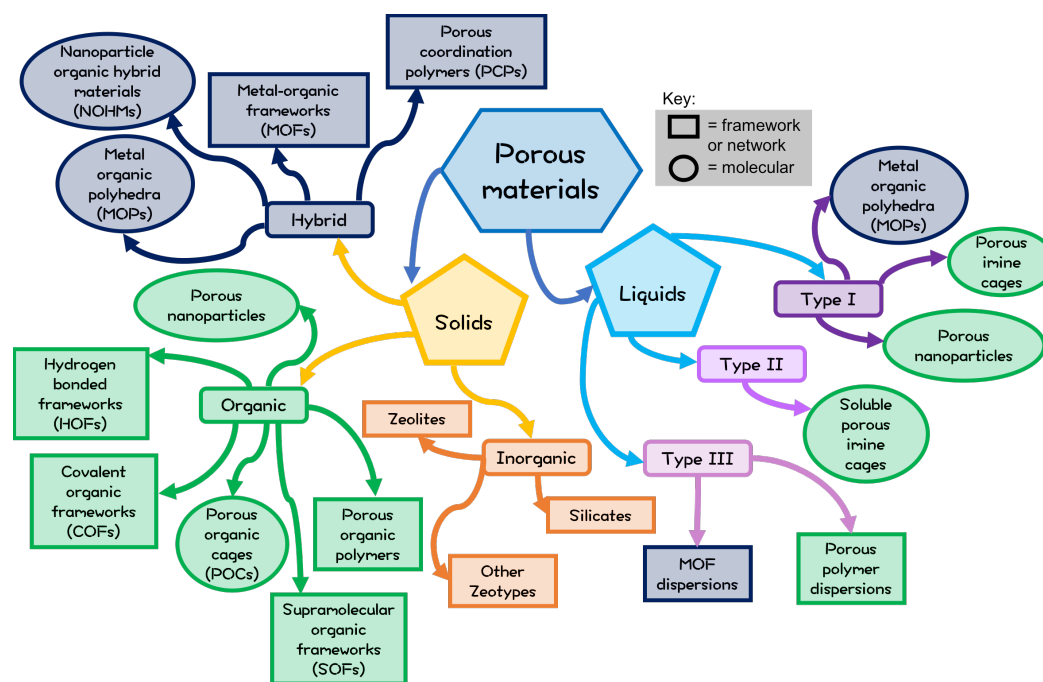


**Figure 1.1:** Summary of families of porous materials and their subcategories within the literature.

Until recently, there has been a focus on solids with high surface areas and uniformity in their pore structure, on the premise that this is required for ‘superior application properties’.<sup>3</sup> However, the literature has seen the emergence of systems with disorder that utilise defects,<sup>8-10</sup> or the liquid state,<sup>11</sup> to target specific applications. In this thesis, the interest lies in exploring the potential of using microporous materials in the liquid state, which can be formed with either extended frameworks and networks, or be composed of discrete molecules.

## 1.2 Definition of a porous liquid

While porous solids are common in many applications, such as molecular separations, translation into the liquid state could potentially enable easier implementation into current industrial plants and flow processes.<sup>12,13</sup> In 2007, James and co-workers proposed the concept of a new class of materials known as ‘porous liquids’.<sup>14</sup> These systems contain permanent ‘intrinsic’ porosity within the molecules that constitute the liquid, rather than the transient ‘extrinsic’ cavities found between those in a conventional liquid. Three different types of porous liquids were initially proposed: Type I was described as a neat liquid where the molecules themselves contain rigid intrinsic cavities, whereas Type II and III were described as a porous material either dissolved or dispersed in a cavity-excluded solvent, respectively (Figure 1.2).

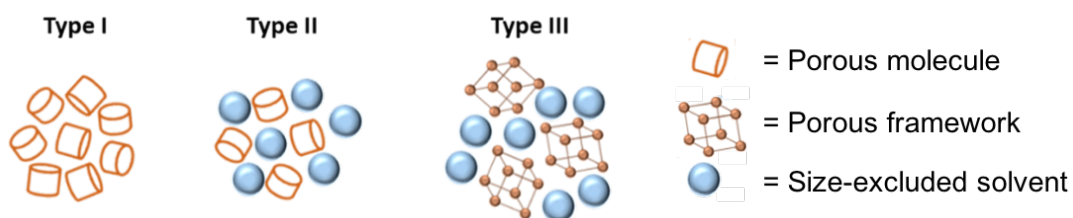


**Figure 1.2:** Schematic representing the structure of the three types of porous liquids proposed by James and co-workers.<sup>14</sup>

The definitions of the porous liquid types give a large scope for interpretation, as there are many examples of porous solids that could be adapted to form liquids with permanent porosity. To date, porous liquids have been formed with numerous molecular and extended framework materials, leading to a rapid diversification of the field. There may even be systems present in the literature prior to 2007 that meet the definitions and could be classified as porous liquids. On the other hand, many of the materials published since the initial concept article are porous in the liquid state but do not meet the original definitions of specific types of porous liquids.<sup>15,16</sup> As the field has developed, the employment of diverse strategies has generated a range of porous liquids, and this introduction will discuss several classes of porous materials and how they have been utilised to engineer porosity into the liquid state.

### 1.3 Classes of solids used to make porous liquids

With the fundamental definitions of a porous liquid in mind, there are several porous molecules or assemblies that are potential components for a porous liquid. A porous solid contains void spaces within the molecule or framework. These pores can be filled with solvent or other guest molecules that are not part of the porous material.<sup>17</sup> There are a variety of porous solids with different chemical compositions that give rise to diverse structures and properties.

One important consideration when designing a porous liquid from a solid is to understand the arrangement and behaviour in the solid state. Changing a system from the solid to the liquid phase will depend on the arrangement and interaction of the crystal lattice. Structures with different unit cells but with the same elemental composition are described as having *polymorphism*.<sup>18</sup>

The variation in the packing arrangement leads to changes in the free energy ( $\Delta G$ ) within the system, therefore, polymorphs can possess different lattice energies and physical properties, including solubility and melting point. The arrangement with the lowest energy will be the most stable form and others will eventually rearrange to this despite appearing stable. This means a stronger, more uniform lattice will require more energy to change phase and will result in a higher melting point and lower dissolution rate.<sup>18,19</sup> Materials that do not pack in a long-ranged, ordered arrangement in the solid state are called *amorphous* and have very different properties to the crystal form. ‘Disordered’ structures or those with defects in their arrangements have less regular solid state packing, which lowers the lattice energy associated with the material. Therefore, the energy barrier for dissolution of the material is lower and the material is more soluble.<sup>19</sup> For example, they do not exhibit a melting point but a *glass transition temperature*, where a major change in mobility is seen but a clear ‘melt’ is not, where ‘glassy’ is used to describe these types of systems in this work.

Throughout this thesis, the physical appearance of materials is a key observation when finding suitable materials for a porous liquid. Some systems are seen to form a *gel*, which is a ‘non-fluid colloidal or polymer network that is expanded throughout its whole volume by a fluid’ and *gelation* describes the process of passing through the point of forming a chemical or physical network.<sup>20</sup> There are a large number of categories associated with these systems, depending on their formation, structure and behaviours in this state. Although there is a large amount of research into different gels and their assembly, the general observation seems to be that they are between the solid and liquid behaviours.<sup>21</sup> When the term is used during the subsequent results and discussion chapters, it refers to the liquid state not becoming a free flowing solid, but an extended structure.

### 1.3.1 Inorganic

One subclass of porous solids are inorganic microporous frameworks such as zeolites. These are 3-dimensional materials, with the general formula  $M_{x/n}[(AlO_2)_x(SiO_2)_y] \cdot mH_2O$ , consisting of corner sharing  $[SiO_4]^{4-}$  and  $[AlO_4]^{5-}$  tetrahedra building blocks.<sup>22-25</sup> These clusters form 2, 3 or 4 vertices to create oxygen bridges that construct the larger secondary building units (SBUs). Within the structure, the Si/Al ratio can vary, therefore, a purely  $[SiO_4]$  framework is known as a silicate.<sup>22</sup> However, substituting the Si with Al changes the valance and gives an anionic material, which is balanced with cations held electrostatically within the zeolite. Changing the Si/Al directly affects the cation content, as well as the structure of the extended framework. The chemical composition determines the cavity and channel size, which directly impacts the porosity of the system.<sup>23</sup> The resulting chemical and thermal stability of zeolites makes them useful in several applications, including catalysis.<sup>25,26</sup>

### 1.3.2 Hybrid nanoparticles

Hybrid materials, defined above as having both inorganic and organic components, are increasingly common as they often possess unique properties and are beginning to evolve into use in porous liquids. One such example includes nanoparticle organic hybrid materials (NOHMs). These consist of a nano-core, ranging from silica, oxide, or metallic nanoparticles, to carbon nanotubes, with a corona linker (usually a silane or thiol) that covalently or ionically bonds to polymer chains. These functionalities typically result in a range of states, from a liquid to a gel or solid-like behaviour, with zero vapour pressure.<sup>27</sup>

Within the literature, there is a diverse range of nanoparticle hybrid materials and many use silica as the nano-core. This includes work by Wang *et al.*, who reported a NOHM consisting of a silica core with a polyetheramine canopy covalently linked to a 3-glycidyloxypropyltrimethoxysilane corona (**Figure 1.3**).<sup>28</sup> The authors observed that the NOHM had liquid-like behaviour, confirmed by differential scanning calorimetry (DSC), and a melting temperature of  $-9$  °C. These were used to form mixed matrix membranes (MMM) by dispersing in Pebax®, which improved the CO<sub>2</sub>/N<sub>2</sub> separation capability of the system. Overall, many of the silica nano-core based systems possess liquid-like character., for example, Lin *et al.* also demonstrated that the use of either ionic or covalent bonding to tether the corona-canopy does not affect the physical state, but can be used to change the gas sorption properties.<sup>29</sup>

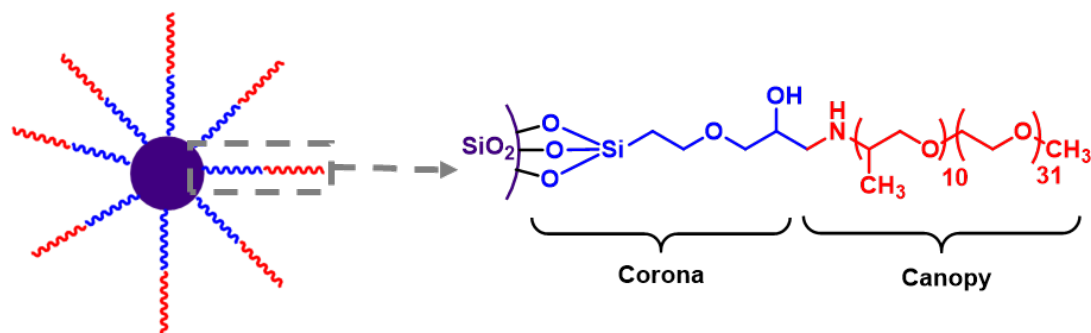


**Figure 1.4:** Silica nanoparticle functionalised with a 3-glycidyloxypropyltrimethoxysilane corona and a polyetheramine canopy presented by Wang *et al.*<sup>28</sup>

The use of carbon nanotubes as the nano-core can also result in a liquid-like NOHM. Li *et al.* presented a series of nanofluids with varying polyetheramine canopies and their resulting properties (**Figure 1.4**).<sup>30</sup> It was found that changing the structure of the polyetheramine chain has a direct impact on the melting temperature of the NOHM. The DSC traces showed T5000 had the lowest melting point ( $-64\text{ }^{\circ}\text{C}$ ) compared to the other systems, which is likely due to the branching present in the chains. The addition of the oxygenated and amine functionality to the carbon nanotubes significantly improved the  $\text{CO}_2$  capture capacity compared to the uptake in the single carbon nanotubes and the polyetheramines. The viscosity of the nanofluids reduced with increasing temperature, which also resulted in a higher  $\text{CO}_2$  uptake. The authors rationalised that this was due to weaker intermolecular forces at higher temperatures, allowing an increased  $\text{CO}_2$  capacity.

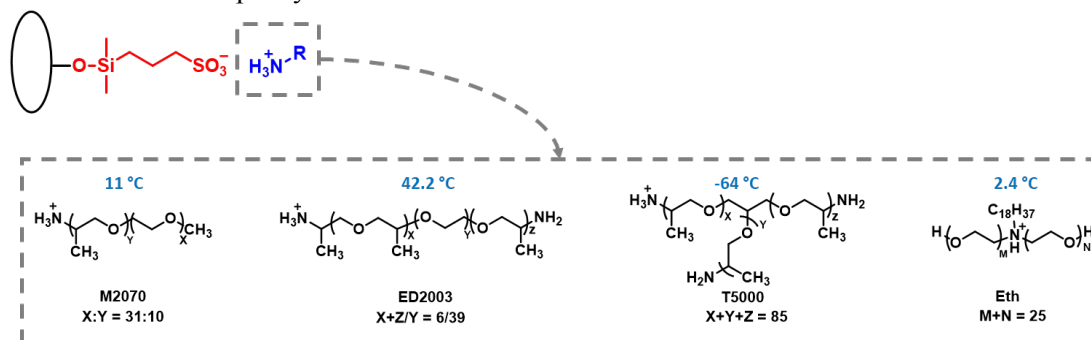


**Figure 1.3:** A series of nanofluids presented by Li *et al.* using carbon nanotubes as the core with the structures of a range of polyetheramine canopies.<sup>30</sup>

The ability to tune the properties of NOHMs could provide an effective strategy when forming a porous liquid. The examples presented here do not appear to use a hollow porous nano-core and, in the case of Wang *et al.*, molecular modelling showed that the  $\text{CO}_2$  molecules bind to the outer surface of the  $\text{SiO}_2$  core. The use of hollow spheres could result in porous liquids, as the flexible organic chains induce liquid-like behaviour and improve the stability of dispersions.<sup>29</sup>

### 1.3.3 Metal-organic frameworks (MOFs)

The use of coordination chemistry to form extended porous materials has seen a rapid expansion in recent years, the area of metal-organic frameworks (MOFs). These structures consist of metal ion clusters (secondary building units, SBUs) linked together through organic ligands to form hybrid one-, two-, or three-dimensional frameworks (**Figure 1.5**).<sup>31</sup> Changing the metal in the SBUs, or the length and functionality of the organic linkers directly affects the overall chemical and physical properties of a MOF, which allows for targeted design towards a particular function.<sup>32,33</sup>

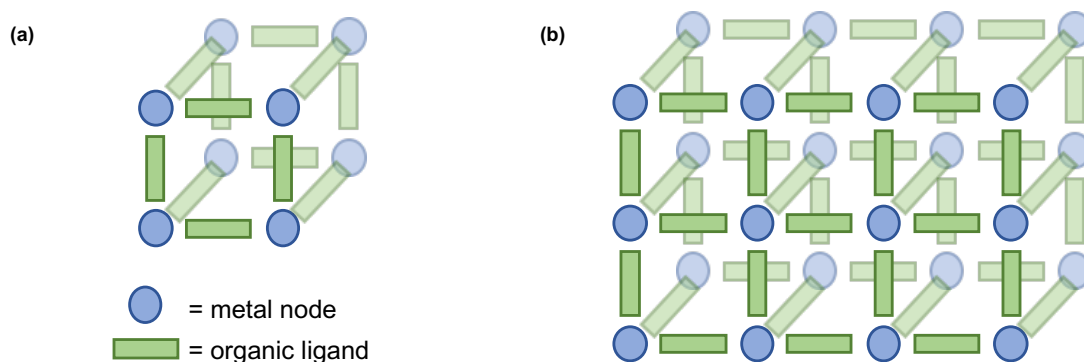


**Figure 1.5:** Graphical representation of a metal-organic framework structure with (a) a single unit, and (b) the extended network.

Li *et al.* presented one of the first MOFs with permanent micro-porosity in 1999.<sup>34</sup> Known as MOF-5, its structure consisted of tetranuclear clusters,  $Zn_4(O)(CO_2)_6$ , connected together by 1,4-benzenedicarboxylate (BDC), to form a cubic lattice with a Langmuir surface area of  $310 \text{ m}^2\text{g}^{-1}$ .<sup>31,34</sup> Since then, there have been a significant number of MOFs with varying SBUs, organic linkers, and topologies, which has resulted in a diverse range of applications including molecular separations<sup>35</sup>, drug delivery<sup>36</sup>, catalysis,<sup>37,38</sup> and gas storage.<sup>39</sup>

Traditionally, MOFs are synthesised as ordered crystalline materials but this diverse area is now expanding into frameworks with engineered defects and disorder.<sup>40</sup> As these are large structures, defects are introduced in the formation mechanism, which could result in ‘mismatched growth and gelation’.<sup>41,42</sup> Defects in the framework are increasingly being exploited and have been shown to enhance the properties of certain MOFs,<sup>42</sup> which is further diversifying an assorted area of research. For example, Wu *et al.* demonstrated that varying the missing linker concentration in MOF UiO-66 enhances the pore volume by up to ~150%, and increases the absorption of  $CO_2$  by ~50%.<sup>43</sup>

The introduction of defects into the structure can also change the MOFs overall chemical and physical properties.<sup>42</sup> Partial substitution of the imidazolate linker in ZIF-4 during synthesis to create ZIF-62 lowers the melting temperature from 550 °C to 410 °C respectively.<sup>44</sup> Bennett *et al.* report that reducing a MOF's melting point changes the structure from a crystalline state to a thermo-mechanically stable glass. MOF glasses, formed by heating above the melting point and cooling again, maintain the framework connectivity observed in the crystalline state.<sup>42,44,45</sup> Several MOF glasses have now been reported and their melting mechanisms explored in more detail. For example, ZIF-76 possesses a melting transition at 451 °C, allowing the casting of a glass at 310 °C. The amorphous glass still maintained the connectivity seen in the crystalline material, alongside maintaining some of the porosity.<sup>46</sup> These hybrid MOF materials may not possess the high surface areas and porosity seen in their crystalline counterparts, but the ability to process structures with inherent mechanical stability provides the possibility for use in many applications, including chemical separations, catalysis, and ion conductivity.<sup>42,45,46</sup>

The self-assembly of MOFs usually results in a highly ordered structure, but increasing the rate of crystallisation can cause aggregation and defective coordination, resulting in gel formation.<sup>42</sup> Li *et al.* presented an aluminium metal-organic aerogel formed through the gelation of MOF nanoparticles.<sup>41</sup> Crystalline MOF, and its gel counterpart, had comparable bonding and connectivity but different overall structural 'regularity'. Interrupting the coordination by competing interactions leads to mismatched growth and gelation. The aerogel also retained porosity and the authors were able to demonstrate H<sub>2</sub> and CO<sub>2</sub> separation.

The recent advances in hybrid MOF materials demonstrates that introducing disorder or defects into a structure can change the chemical, physical and mechanical properties. Traditionally crystalline materials, MOFs have some degree of dynamic behaviour due to the entropy of the system (**Figure 1.6**), which can be exploited to form other functional materials; such as gels and glasses.<sup>40,42</sup> Crystalline solids can be difficult to incorporate into commercial settings so processing into different forms allows for alternative applications to be targeted.

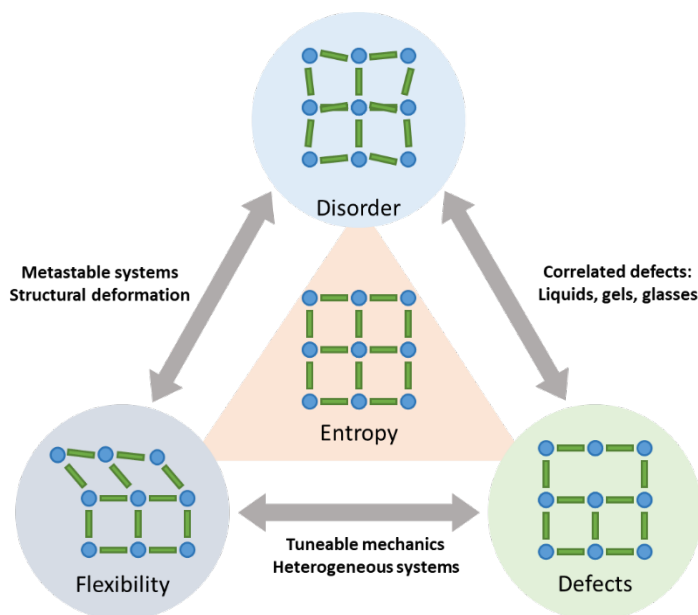


**Figure 1.6:** Graphical representation of the links between the structural variations seen in metal-organic framework structures due to entropy proposed by Bennett *et al.*<sup>42</sup>

### 1.3.3 Porous organic polymers (POPs)

Not all extended porous structures are crystalline, many are amorphous and contain covalent bonding. One such classification includes porous organic polymers (POPs), which are highly cross-linked, microporous materials.<sup>47–49</sup> This constitutes a broad area, from covalent triazine frameworks (CTFs),<sup>49–51</sup> to conjugated microporous polymers (CMPs).<sup>49,52–55</sup> One example of a porous organic polymer was synthesised by Ben *et al.*, who used theoretical simulations to design the structure of a porous aromatic framework, PAF-1 (**Figure 1.7**).<sup>56</sup> This extended network consisted of a diamond-like structure with the covalent C-C single bonds replaced with phenyl rings. As a result, an insoluble amorphous framework was produced with robust internal cavities that was thermally stable up to 520 °C. The exceptionally high Brunauer-Emmett-Teller surface area ( $S_{\text{BET}} = 5600 \text{ m}^2 \text{ g}^{-1}$ ) also translated to a high uptake capacity for a number of gases, including  $\text{H}_2$  (10.7 wt% at 48 bar, 77K), and  $\text{CO}_2$  (1300  $\text{mg g}^{-1}$  at 298 K, 40 bar). Additionally, the organic nature of PAF-1 meant the framework could adsorb organic vapours, such as benzene (16.74  $\text{mmol g}^{-1}$ ) and toluene (14.73  $\text{mmol g}^{-1}$ ), which is of particular interest to environmental applications. Since the first report of PAF-1 in 2009, there have been numerous studies into its properties, as well as modification of the structure to form analogous frameworks.<sup>57–61</sup> The pore size of the PAF can be altered by changing the size and length of the aromatic precursor, which allows structures to be tailored towards a specific guest or separation.<sup>57</sup>



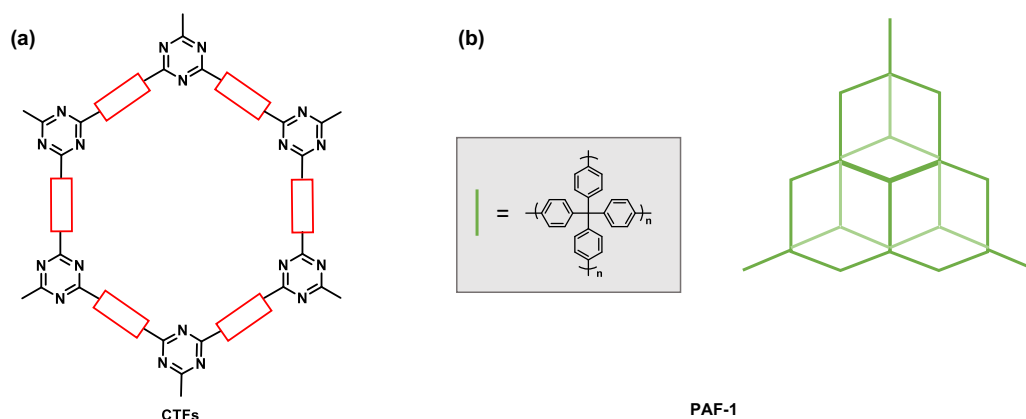


**Figure 1.7:** Structure of common porous organic polymers: **(a)** the general structure for covalent triazine frameworks (CTFs), which can be connected by a variety of linkers<sup>37</sup> and **(b)** the extended structure for the porous aromatic framework, PAF-1, with the structure of the linker.<sup>56</sup>

### 1.3.4 Metal organic polyhedra (MOPs)

Framework materials, as discussed above, are often insoluble and unsuitable for certain applications, such as biochemical or biomedical treatments. Alternative classes of porous materials contain discrete, cage-like molecules with defined structures and cavities accessible through open windows.<sup>62,63</sup> These are often formed through the self-assembly of pre-organised components into well-defined structures,<sup>64</sup> allowing for the properties of the resulting cage to be tailored by changing the precursors used. To be porous, cage molecules need to be robust enough so that they do not undergo self-filling and are shape-persistent when desolvated. An advantage is their ability to form co-crystals through molecular recognition,<sup>65–67</sup> which allows for the bulk structure to be changed for particular applications. As a result, there are a range of cages in the literature with different size cavities, functionalities on the periphery, and chemical environments.

One particular type of porous molecular materials are metal organic polyhedra or cages (MOPs or MOCs), which like MOFs, comprise of metal centres linked together by organic ligands.<sup>63</sup> Unlike MOFs, MOPs are soluble in common laboratory solvents.<sup>63,68</sup> Due to the number of different coordination geometries associated with metal ions, MOPs can be formed in a large variety of topologies, from simple tetrahedrons to more elaborate cuboctahedrons,<sup>69</sup> which allow for many applications to be targeted.

By carefully selecting the metal salt and organic ligands, a MOP's structure is tailorable to meet a specific function. In particular, the solubility and metal sites allows for the design of synthetic biochemical environments, such as artificial ion channels, drug delivery systems, enzymes, and biological sensors, and are considerably more suitable than insoluble frameworks.<sup>63,70,71</sup> Other functions for MOPs in materials chemistry are based on the ability

to exploit the host-guest behaviour of a system. Their symmetry and structure can sometimes lead to chirality in the cage, which enables enantioselective separations.<sup>68,72,73</sup> Additionally, like other porous materials, MOPs are also used for guest capture and separations as their cavity size can be tailored for a specific molecule.<sup>74,75</sup> Early examples appeared to have limited porosity in the solid state as they seemed to lack structural integrity once solvent was removed,<sup>76</sup> but there have been recent improvements in the gas adsorption of MOPs. Lorzing *et al.* reported a coordination cage,  $\text{Mo}_{24}(\text{}^t\text{Bu-bdc})_{24}$  ( $\text{bdc}^{2-} = 1,3\text{-benzenedicarboxylate}$ ), with one of the highest surface areas to date ( $\text{SA}_{\text{BET}} = 1321 \text{ m}^2/\text{g}$ ).<sup>76,77</sup> While there is significant increase in reported surface areas, they still remain considerably lower than MOFs.

One challenge in MOP synthesis is generating multi-component cages due to the source of error associated with self-assembly, because often self-recognition and isolating the desired product can be difficult. Li *et al.* demonstrated an alternative strategy for preparing multi-component MOPs by partially or completely substituting the bridging ligands after synthesis.<sup>78</sup> This allows for structures that might not be realised, or are difficult to form, as there is already a preformed cage to act as a template. The methodology relies on the solubility of MOPs and their precursors, along with their stability in the reaction solvent. The authors presented a series of  $\text{Cu}_2(\text{O}_2\text{CR})_4$  cages with carboxylate bridging ligands (**Figure 1.8**), with varying cavity sizes and geometries. They also demonstrated that the solvent often coordinated to the metal centre and had an influence on the resulting MOP structure. Changing the functionality on the cage periphery influences the cavity size, and therefore, the gas sorption properties. For example, a MOP with *t*-butyl groups in the windows selectively absorbed  $\text{H}_2$  and  $\text{O}_2$  over  $\text{N}_2$ , as well as  $\text{CO}_2$  over  $\text{CH}_4$ , which was attributed to the bulky groups blocking the windows of neighbouring cages in the solid state.

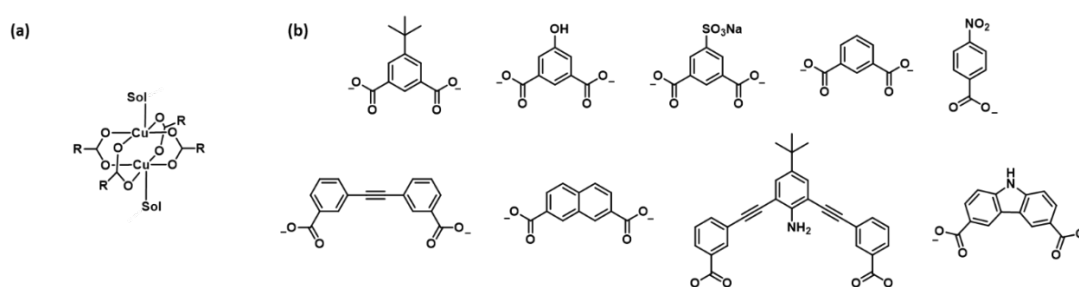


**Figure 1.8:** Chemical structures of metal-organic cage components synthesised by Li *et al.*: **(a)** Copper paddlewheel unit, where R = bridging ligand and Sol = solvent molecules, and **(b)** carboxylate bridging ligands.<sup>78</sup>

The work by Li *et al.* is not the only example of utilising the solubility of MOPs for a specific function. Bolliger *et al.* demonstrated the usefulness of a water-soluble  $\text{Fe}^{2+}$  cage in the encapsulation of large molecular guests (**Figure 1.9**).<sup>79</sup> The  $[\text{Fe}_4\text{L}_6]$  (where L = ligand) was formed from diaminoterphenylene, which self-assembled into a tetrahedral cage with a 16.1 Å radius. The glyceryl substituents, located on the periphery, were responsible for making the cage water-soluble, and computational modelling inferred they pointed outwards. The hydrophobic nature of the pore was exploited to bind several hydrophobic guests, confirmed by diffusion-ordered NMR spectroscopy (DOSY), which could be useful for the removal of organic contaminants from water. The cage was highly soluble in water, but a crystal structure was not reported, so it is unclear whether the water is excluded from the cage cavities because of this hydrophobic environment.

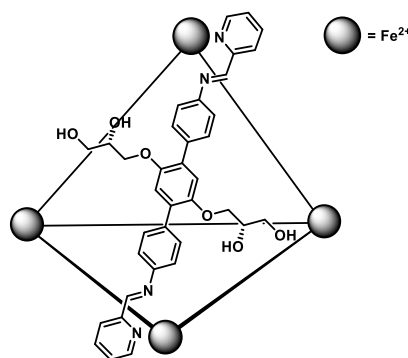


**Figure 1.9:** The structure of the water-soluble  $[\text{Fe}_4\text{L}_6]$  cage presented by Bolliger *et al.* (L = diaminoterphenylene).<sup>79</sup>

The solubility and functionalisation of MOPs has allowed hybrid materials to be developed. Due to their ability to act as secondary building blocks, these metal cages can also be used to form frameworks through their vacant metal coordination sites.<sup>80,81</sup> Other, more unusual examples include using the metal sites in a MOP to form highly branched gels. Zhukhovitskiy *et al.* reported two MOCs, linked together by polymers, to form gels (polyMOCs).<sup>82</sup> The authors synthesised two poly(ethylene glycol) (PEG) terminated organic ligands, with bis-*para*-pyridine and bis-*meta*-pyridine, that had free metal coordination sites (**Figure 1.10**). These were used to form two MOPs but as the terminal groups were connected by PEG chains, this resulted in the formation of supramolecular gels. These polyMOCs had increased branching and loop defects, which are polymer chains where both ends are attached to the same metal atom or metal-ligand cluster. The simple isomeric change between the two gels gave a different overall structure, with gel-1 having covalent tendencies, and gel-2 behaving like traditional supramolecular gels with less loop defects. This work, in particular, shows the versatility of using discrete porous molecules. Traditionally, a MOP is an ordered, rigid

material, however, their discrete molecular structure allows for the design of materials with unique, disordered characteristics.

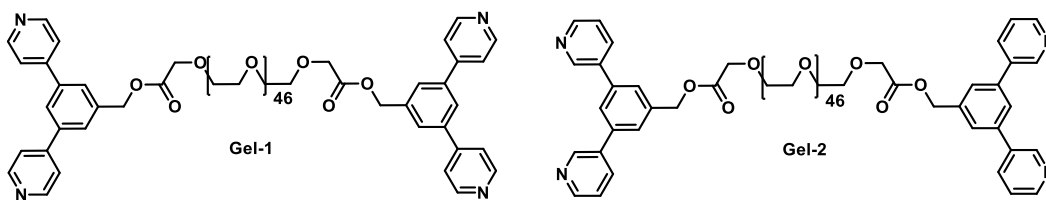


**Figure 1.10:** The structure of the organic PEG ligands used by Zhukhovitskiy *et al.* to form highly branched metallogels.<sup>82</sup>

### 1.3.4 Porous organic cages (POCs)

Other discrete molecular assemblies may be solely comprised of organic components, for example, porous organic cages (POCs) are another class of microporous materials. These are discrete organic molecules that contain intrinsic, shape persistent cavities accessible through windows, which make them ideal candidates for many applications.<sup>83</sup> POCs can form extended pore networks based on solid state packing, held together by non-covalent interactions. As a result, many examples are ‘solution processable’, meaning they can be dissolved in common organic solvents with the individual cage molecules remaining intact.<sup>84</sup> There are a range of bond forming chemistries that can be used to form organic cages, with dynamic covalent reactions being the most common. These allow self-correction to form discrete cage species.

Dynamic covalent chemistry is a useful strategy to form 3-dimensional, molecular structures by allowing equilibration to the thermodynamic product. A substantial number of POC syntheses have exploited imine condensations. For example, Cooper and co-workers have reported several imine cages formed from 1,3,5-triformylbenzene with vicinal diamine precursors (**Figure 1.11**). Each cage molecule is formed from four equivalents of an aldehyde and six equivalents of diamine to give a [4+6] stoichiometry.<sup>84</sup> Varying the functionality on the cage periphery allows the tailoring of a POC’s overall properties for a specific function, and the choice of precursors is important as small changes can have a large effect on both the size and geometry of the resulting cage.<sup>83,85</sup> There is also a possibility of forming amorphous polymer networks or the collapse of intrinsic cavities upon desolvation.<sup>83</sup>

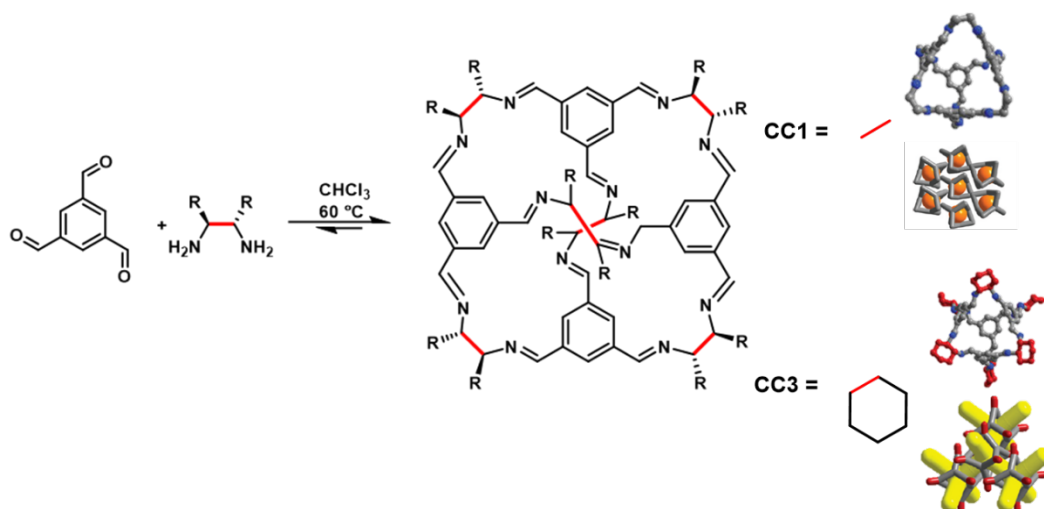


**Figure 1.11:** General reaction scheme for the synthesis of POCs reported by Cooper and co-workers.<sup>84</sup>

Lauer *et al.* also presented examples of porous imine cages formed from 1,3,5-triaminobenzene and 1,3,5-triformylbenzene derivatives (**Figure 1.12**). The authors observed that the presence of ethyl groups on the triamine were required for cage formation, which was due to the added alkyl functionality pre-configuring the conformation of the methylamine groups into the correct orientation to form a cage. The resulting product was a [4+4] truncated tetrahedral cage with a shape-persistent structure. Addition of ethyl groups on the trialdehyde precursor also formed a cage, albeit with a lower surface area and porosity due to the chains blocking the windows. However, the di-ethyl substituted cage formed in a higher yield than the analogous species containing hydrogen atoms.<sup>86</sup> This work demonstrates that the conformation of the precursors dictates the rate of formation and geometry of the resulting cage, and highlights that pre-organisation can be important when designing a POC.

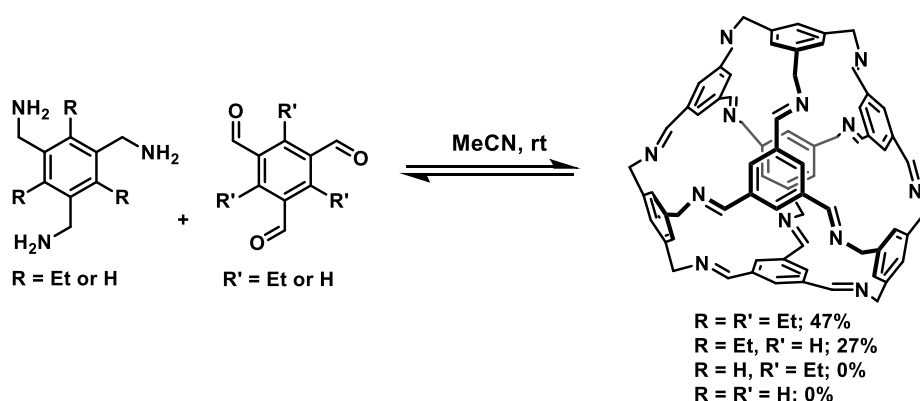


**Figure 1.12:** The synthesis of two porous imine cages reported by Lauer *et al.* from 1,3,5-triaminobenzene and 1,3,5-triformylbenzene derivatives.<sup>86</sup>

Other work has utilised orthogonal dynamic covalent chemistries to form mixed structures. For example, Pattillo *et al.* recently reported a tetrahedral organic cage formed using both imine condensation and alkyne metathesis (**Figure 1.13**).<sup>87</sup> The authors used a two-step synthesis to prepare the mixed cage structure, starting with an imine condensation between a trialdehyde and an amine to form a pre-configured cage precursor with six alkyne metathesis sites, which subsequently underwent intramolecular cyclisation to form a POC. The alkyne/imine cage possessed a tetrahedral structure, confirmed by NMR spectroscopy. While attempts to obtain a crystal structure were unsuccessful, and no gas sorption data was available, high resolution mass spectroscopy (HRMS) confirmed the presence of the cage species and 2D NMR spectroscopy confidently determined the tetrahedral stoichiometry. Further studies showed the imine vertex could be removed to form a macrocycle by adding  $\text{Sc}(\text{OTf})_3$  through transimination, which could be reversed to reform the cage by  $\text{Sc}(\text{III})$  catalysis. Whilst the cage was unable to be isolated, this work demonstrated the possibility of creating complex cage structures with mixed functionality.

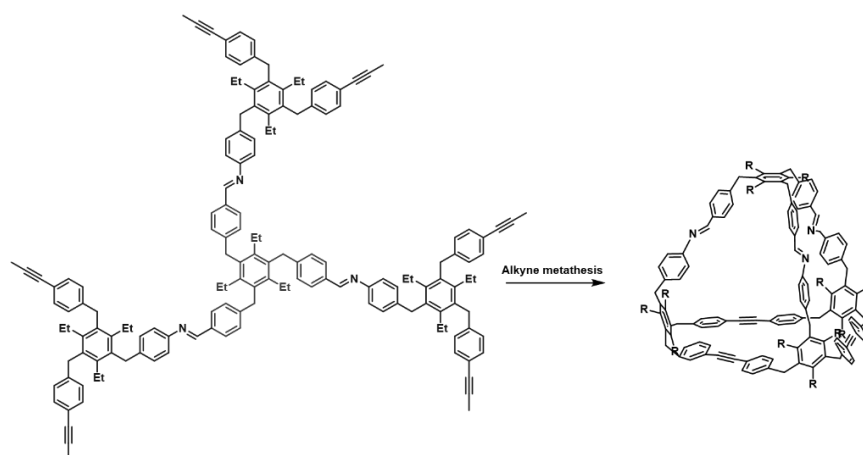


**Figure 1.13:** Formation of a tetrahedral POC using both imine condensation and alkyne metathesis by Pattillo *et al.*, where the imine vertex can be reversibly removed using  $\text{Sc}(\text{III})$  catalysis.<sup>87</sup>

One disadvantage with POCs is their limited solubility in common organic solvents, which can restrict their usefulness in some applications. Cooper and co-workers demonstrated that ‘dynamic covalent scrambling’ could be used to increase the solubility of cage mixtures.<sup>88</sup> Unlike other examples, which show self-sorting, synthesising organic cages with a mixture of functionality on the periphery leads to the production of porous soluble materials. The co-reaction of two different vicinal diamines gave a ‘scrambled’ distribution of POCs, made up of varying ratios of functionality, that disrupts the ability of the individual structures to pack efficiently. As a result, there was an increase in solubility and porosity compared to their crystalline counterparts (**Figure 1.14**). It was found that the product distribution could be

altered by changing the diamine ratio, which allows tuning of the gas selectivity of the scrambled cage for a range of gases.

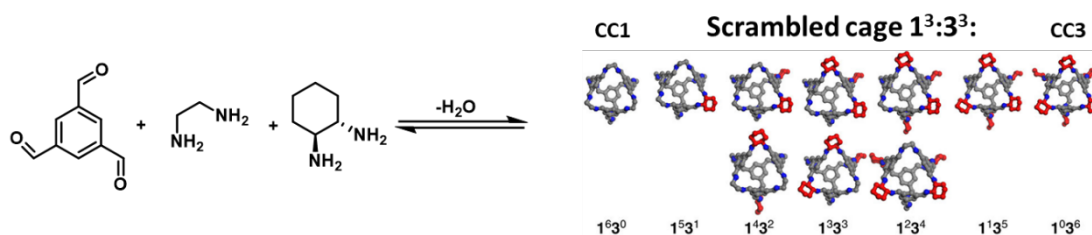


**Figure 1.14:** The 'scrambled' POC mixtures synthesised by Cooper and co-workers.<sup>88</sup> The naming is depicted as follows,  $1^n 3^{6-n}$  (1 and 3 represent the diamines used to form CC1 and CC3 respectively,  $n$  = number of diamines on the vertices of the different cages).

There are very few examples of scrambled POCs in the literature, with self-sorting seeming more prevalent. Lee *et al.* studied the equilibration of an alkyne metathesis cage (**Figure 1.15**), which were the kinetic product and, due to their high stability, the dominant species.<sup>89</sup> Dynamic scrambling was used to demonstrate the 'kinetic trapping' observed in the reaction pathway. Under alkyne metathesis conditions, the pre-formed parent cages (**Figure 1.15, aaaa** and **bbbb**) with higher catalyst loadings, showed no evidence of further equilibration or a scrambled distribution, and the parent cages remained intact. The alkyne metathesis precursors, with different alkyl functionality, were also reacted in equimolar quantities to see the effects on product distribution. There were five cage species with mixed functionality observed in the HRMS data, corresponding to the various scrambled systems, rather than the self-sorted parent cages, **aaaa** and **bbbb**. While POCs can have limited solubility, they provide an appealing strategy to target porous liquids as their dynamic covalent chemistry allows the tailoring of their properties for specific functions.

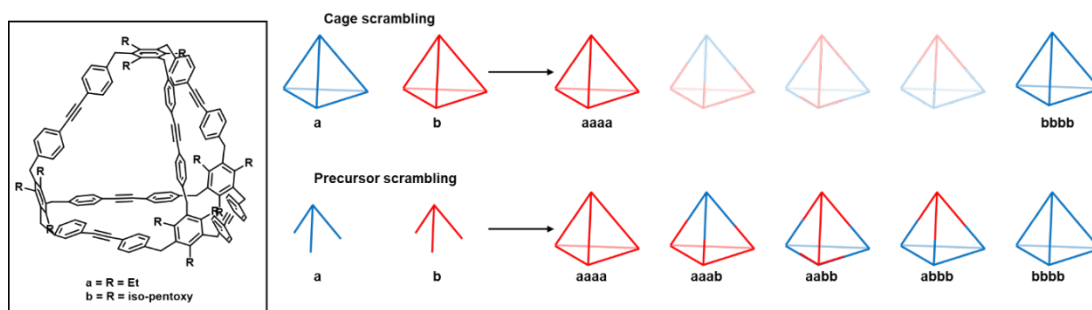


**Figure 1.15:** The alkyne POCs reported by Lee *et al.* and the mixtures synthesised when scrambled reactions, using either the pre-formed cages or precursors, were attempted.<sup>89</sup>

## 1.4 Strategies for designing porous liquids

With such a diverse range of porous materials presented in the literature, this provides a large scope for different strategies to target porous liquids. In the case of designing a porous liquid, the formation is the most important consideration. Whether the components are crystalline or amorphous in the solid state does not really have an impact, as the intrinsic porosity is important in a porous liquid, not the extrinsic. With this in mind, the development of porous liquids has presented challenges not necessarily observed in their solid counterparts. Arguably, finding a single, low melting species to generate a Type I porous liquid is highly challenging and remains the most difficult to achieve. Type II and III porous liquids, however, rely on another component to fluidise a porous material and are easier to target, if a cavity-excluded solvent can be found.

### 1.4.1 Examples of porous liquids within the literature

Although the definition of a porous liquid is relatively new, there are arguably several examples in the literature that met the requirement to be classed as a porous liquid prior to the concept article and the first reported examples. In a recent review, Bavykina *et al.* discussed a number of organic cages that dissolve in cavity-excluded solvents, and are therefore, technically Type II porous liquids.<sup>11</sup> One of the first examples was in 1994 by Cram and co-workers, who described a hemicarcerand capsule with cavities too small to encapsulate diphenyl ether (**Figure 1.15a**).<sup>90</sup> NMR studies confirmed the cavities remained empty when the hemicarcerand was evacuated of *N,N*-dimethylacetamide in the diphenyl ether solvent. However, the crystal structures provided were all of complexes with much smaller guests, so there was no other confirmation that diphenyl ether was cavity-excluded.

Another example, provided by Bavykina *et al.*, described the host-guest chemistry of cryptophanes. Chaffee *et al.* presented the work in 2009 before the first named porous liquid was reported (**Figure 1.15b**).<sup>91</sup> Cryptophane-111 had a small cavity (~8.1 Å) and NMR experiments showed no evidence of chloroform, dichloromethane, or propane in the pores. The authors rationalised that chloroform, although similar in molecular volume to xenon (a guest with a high affinity for the cryptophane), had a different geometry and electronic properties, so binding was unfavourable. In the case of dichloromethane and propane, these guests were larger and unlikely to fit in the cage cavity, now considered as size-excluded.<sup>71</sup> Solely organic molecules are not the only example of potential Type II porous liquids presented within the literature. Hsu *et al.* reported a ‘molecular box’ formed from Co<sub>4</sub>Ru<sub>4</sub> linked together with CN ligands (**Figure 1.15c**).<sup>93</sup> The crystal structure of the molecular box



indicated that the cavity remained empty when acetonitrile was present, allowing the host-guest chemistry to be studied without competition from the solvent.<sup>11</sup>

The work presented here illustrates the potential other systems that meet the requirements to be classified as a porous liquid, but were not described as such. The term ‘porous liquid’ remains relatively unknown and is not yet a common description for fluid systems that have permanent porosity. This is likely to change and revisiting previous examples might lead to their exploration as porous liquids in detail. However, the concentration of the porous species within the solution needs consideration when determining if it is relevant for a system to be described as a Type II porous liquid. For example, the hemicarcerand capsule, presented by Cram and co-workers, was dissolved at ~28 mg per 1 mL of diphenyl ether,<sup>90</sup> and Chaffee *et al.* performed their host-guest studies at ~1.0-1.4 mg per 1 mL.<sup>91</sup> It could be argued that in these examples, the concentration of the solution would be too low in order to add significant pore volume to be appreciable, a consideration not taken into account by the original definitions.

#### 1.4.2 Porous liquids formed from porous nano-particles

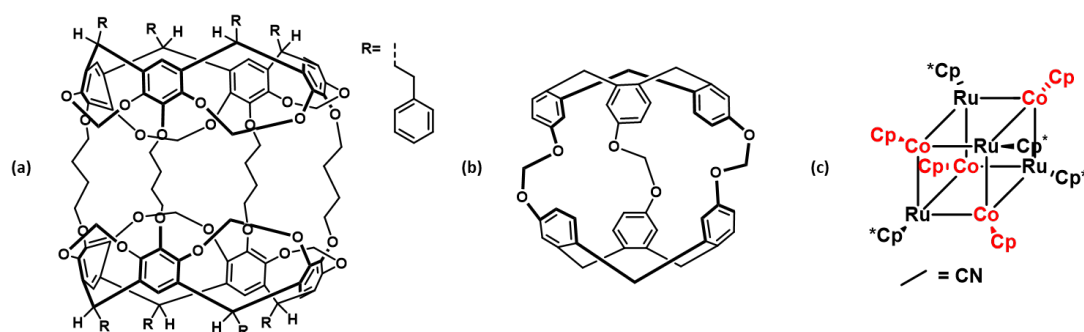


**Figure 1.16:** The structures of porous systems reported by Bavykina *et al.* and identified as potential Type II porous liquids. **(a)** Hemicarcerand capsule by Cram and co-workers<sup>72</sup> **(b)** Cryptophane-111 by Chaffee *et al.*,<sup>91</sup> and **(c)** Molecular box by Hsu *et al.*<sup>93</sup>

There have been a few examples of neat Type I porous liquids reported in the literature, including a hollow silica porous liquid presented by Zhang *et al.* (**Figure 1.17**).<sup>94</sup> The authors functionalised hollow silica nanoparticles to make a system that was liquid at room temperature. First, an organosilane moiety was reacted with hydroxyl groups on the silica core, and then PEG chains were added to the outer surface salt-exchange to induce liquid-like behaviour. Nitrogen sorption indicated that the silica core with the corona attached possessed empty cavities that remained unchanged with the attached PEG. The long chains on the silica core do not occupy the cavities and are size-excluded. The system also demonstrated high

thermal stability and negligible vapour pressure, useful characteristics for gas separations. The selectivity of CO<sub>2</sub> over N<sub>2</sub> was also demonstrated, probably due to the enhanced solubility of CO<sub>2</sub> in the liquid. The authors acknowledged the low gas permeability of the system compared to conventional microporous solids. However, there is scope for improving the properties of the porous liquid. For example, varying the functionality tethered on the nanoparticle could improve gas selectivity and uptake. The size-excluded chain and robust nature of the system lends itself well to having a variety of groups without the worry of occupation of the cavities.

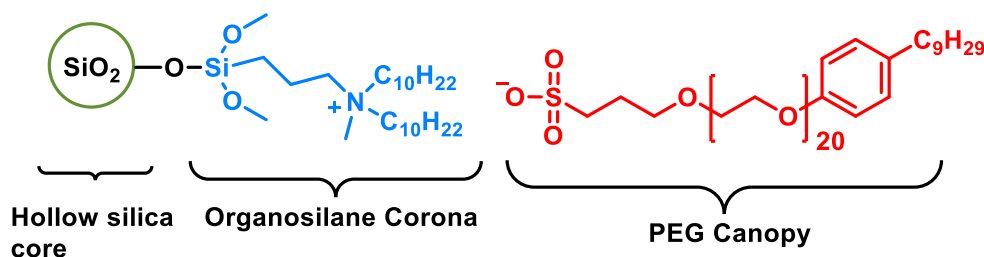


**Figure 1.17:** Schematic representing the structure of hollow silica nanoparticles with organosilane and PEG functionality by Zhang *et al.*<sup>94</sup>

Hemming *et al.* used a similar methodology to target a porous liquid based on an organosilica nanosphere (**Figure 1.18**).<sup>16</sup> The approach was based on the synthesis presented by Zhang *et al.* and involved functionalising the exterior of a hollow SiO<sub>2</sub> sphere with an organosilane group and a poly(ethylene glycol) sulfonate (PEGS) anion. The authors also prepared silica spheres with additional thiol groups in order to encapsulate metal nanoparticles, which included Au, Pt, and Pd functionalised with the same corona-canopy. The metal-nanoparticle size significantly increased on addition of the corona-canopy and subsequent modification into a porous liquid. These steps contribute to aggregation due to limited binding with the thiol groups. The metal concentration was found to also decrease by introducing the extra functionality, likely due to substantial removal of unbound metal nanoparticles when the porous liquid was synthesised.

In a following study, Hemming *et al.* also explored the use of the metal nanoparticle encapsulated porous liquid as a catalyst for the hydrogenation of alkenes and nitroarenes, which is the first reported example of a porous liquid being employed in catalysis.<sup>95</sup> Specifically, the authors studied the Pt doped porous liquid, along with the solid intermediates, in ethanol and a poly(ethylene glycol) sulfonate-based potassium salt (KPEGS), which was thought to be cavity-excluded, to give a comparison of each system's properties. The catalytic activity increased on dispersing the porous liquid in ethanol, compared to the solid

intermediates. However, using KPEGS as the solvent decreased the catalytic activity, likely due to the higher viscosity of the system. While the catalytic rate was lower for the porous liquid in KPEGS, the process could be repeated three times with no loss in activity. While the system showed catalytic activity as a dispersion, based on the original definitions, it would technically no longer be a porous liquid.

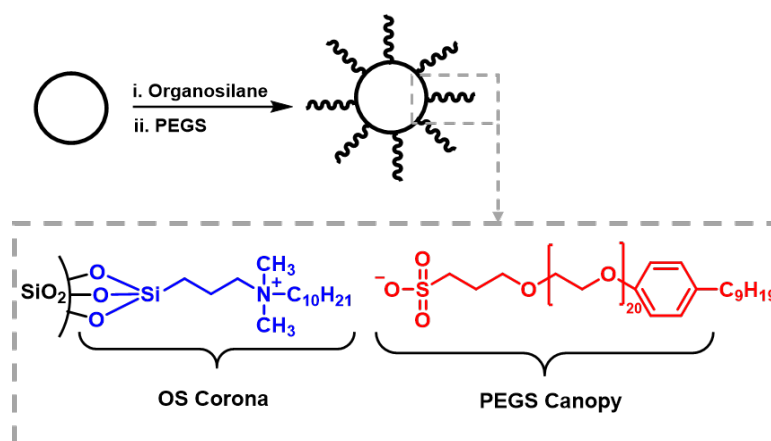


**Figure 1.18:** The functionalised organosilica nanospheres used as a porous liquid presented by Hemming *et al.*<sup>16,95</sup>

However, the work presents a limited investigation into the permanent porosity of the system, compared to work of a similar nature. The N<sub>2</sub> isotherm shows that functionalising the silica nanospheres reduced the surface area for the solid intermediates, but there is limited evidence for the gas uptake in the corresponding porous liquids. Argon displaced from the liquid using chloroform was the only evidence of a gas in the system, but there was no stated overall volume to indicate a quantifiable uptake. There is no subsequent data to suggest the porosity remains intact and how the loss of metal nanoparticles from the silica spheres effects the gas uptake of the system. Overall, the authors expanded the work on organosilica nanosphere porous liquids by exploring the encapsulation of metal nanoparticles and their use in catalysis. As the first reported example for using porous liquids in this type of application, there is a large scope for future research.

Kumar *et al.*, who described a similar methodology as discussed previously (**Figure 1.19**), presented another example of an organosilane porous liquid.<sup>96</sup> The covalent coupling of hollow silica shell nanorods (SiNR) to an organosilane canopy (OS) and then electrostatically grafting to a polymer surfactant (PS) support, gave a liquid with a melting point of 15 to 20 °C by DSC. The gas sorption properties of the liquid were explored by comparing the N<sub>2</sub> isotherms to the solid intermediate. The liquid appeared to be non-porous to nitrogen at -197 °C, which was thought to be linked to the polymer surfactant forming a glass around the silica nanorods as the T<sub>g</sub> was -60 to -70 °C. However, when the gas sorption of CO<sub>2</sub> was attempted at 0 °C, an uptake of 17 to 25 cm<sup>3</sup> g<sup>-1</sup> was observed at 0.03 P/P<sub>0</sub>, which equated to 3.3 to 4.8% w/w (depending on the aspect ratio) and was comparable to solid mesoporous silica.

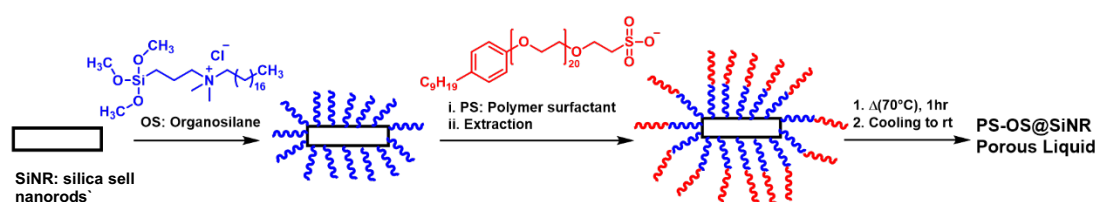


**Figure 1.19:** A functionalised silica nanorod based porous liquid presented by Kumar *et al.*<sup>96</sup>

An alternative approach, presented by Li *et al.*, utilised hollow carbon spheres (HCS) as the porous backbone instead of silica (**Figure 1.20**). Unlike hollow silica, the carbon's surface is chemically inert, therefore, covalent functionalisation with a corona – canopy was not possible. Instead, the imidazolium cation on a polymeric ionic liquid (PIL) and the HCS creates a strong electrostatic force of attraction that binds the cation to the carbon surface. The liquid character was then achieved by replacing the bromide counter-ion with a poly(ethylene glycol) sulfonate salt (PEGS), which stabilised the hollow PILs@HCS with strong ionic interactions, to give a porous liquid at room temperature. Despite not possessing covalent bonds, the authors demonstrated the electrostatic forces were strong enough to give a stable porous liquid that remained unchanged for over 6 months under reduced pressure. They also observed no mass loss before decomposition by thermogravimetric analysis (TGA), indicating a zero vapour pressure, which allowed the study of gas sorption properties. It was found that while the addition of the porous ionic liquid to the HCS reduced the specific surface area slightly (465 to 314 cm<sup>3</sup> g<sup>-1</sup>), it did not remove the porosity completely. The subsequent porous liquid was also shown to have a higher CO<sub>2</sub> uptake at both 1 bar (0.445 wt%) and 10 bar (2.54 wt%) compared to the control species, including neat PEGS and a PIL-PEGS composite. However, the porous liquid appeared to be non-porous to N<sub>2</sub>, demonstrating the potential for application in CO<sub>2</sub>/N<sub>2</sub> separation.<sup>97</sup>

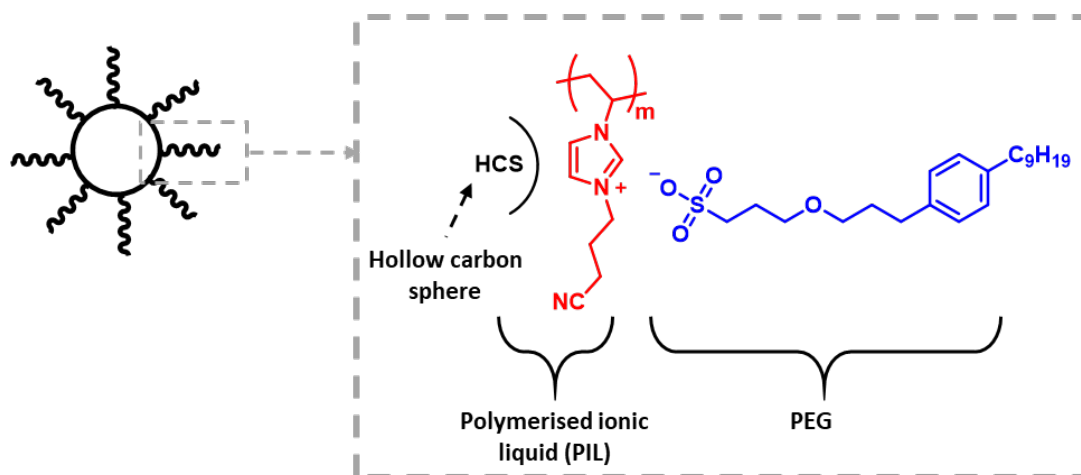


**Figure 1.20:** Hollow carbon spheres functionalised with a polymerised ionic liquid and a poly(ethylene glycol) sulfonate salt to give a porous liquid by Li *et al.*<sup>97</sup>

Overall, these systems were described as Type I porous liquids. However, the original terminology stated empty ‘molecular’ hosts constitute a Type I porous liquid, rather than empty colloidal spheres with pore sizes on the nanometer scale. This is likely because the proposed definitions did not anticipate the range of strategies that would be employed to generate porous liquids, illustrated by several examples presented in the literature.

As the area of porous liquids continues to develop, it is difficult to directly compare the reported gas uptakes, in particular when comparing the organosilica nanoparticles. Zhang *et al.* used the permeability of their system to demonstrate permanent porosity (quoted in Barrer)<sup>94</sup>, whereas Kumar *et al.* gave their gas uptake measurements in  $\text{cm}^3 \text{g}^{-1}$  and % w/w. The differences in reported values make it challenging to directly compare the systems, despite the similarities in their structures, and determine which has a higher porosity. There is also a limited investigation into the liquid properties of organosilica and carbon nanoparticle porous liquids, specifically the viscosity. Highly viscous systems might pose a challenge for implementation in future applications. However, there is scope to study the porosity in these systems in more detail because, due to their low vapour pressures, traditional sorption techniques are applicable – as demonstrated by Kumar *et al.* and Li *et al.* Therefore, there is the possibility for investigating the porosity, recyclability, and reproducibility in more depth.

### 1.4.3 Dispersions of extended frameworks

One of the most recent and common strategies for generating porous liquids is the dispersion of extended frameworks in cavity-excluded solvents, often an ionic liquid (IL) or oil. This is a simple but effective method of fluidising a porous material because it does not rely on solubility, or on the porous material being a liquid at room temperature. However, the dispersed particles do need to form a stable dispersion in the solvent, and not separate over a short period in order to be useful. The use of MOFs, particularly ZIFs, has become an increasingly popular way to improve the gas uptake in Type III porous liquids compared to the neat liquid component.<sup>98–106</sup>

Since 2014, there has been a steady increase in reports of Type III porous liquid systems based on stable MOF dispersions in size-excluded solvents (**Figure 1.21**, **Table 1.1**), with ZIF-8 being predominate because of its thermal and chemical stability.<sup>102</sup> However, a significant challenge that has arisen is comparing the gas uptakes of these porous liquids, as there is currently not a standard unit or method. Many of the examples, including work by Lui,<sup>101,105</sup> Wang,<sup>100</sup> and Cahir<sup>103</sup> *et al.* (**Table 1.1**, entries 1, 4, 7 and 8), perform gas uptake measurements on custom equipment and this often leads to a range of conditions.

**Table 1.1:** Summary of the Type III porous liquids presented in the literature based on MOFs

Entry	Author	MOF	Solvent	Highest MOF concentration	Gas uptake / units	Sorption method	Sorption conditions	Year	Ref
1	Liu <i>et al.</i>	ZIF-8	Liquid glycols (glycol-2-methylimidazole solution)	15 wt%	1.25 mol L <sup>-1</sup> at 1 bar, CO <sub>2</sub>	Custom experimental set-up	Up to 20 bar	2014	105
2	Shan <i>et al.</i>	ZIF-8	[DBU-PEG] [NTf <sub>2</sub> ] IL	30 wt%	1.54 mmol g <sup>-1</sup> , CO <sub>2</sub>	Intelligent Gravimetric Analyser	rt, up to 10 bar	2018	102
3	Gomes <i>et al.</i>	ZIF-8	[P <sub>6,6,6,14</sub> ] [NTf <sub>2</sub> ] IL	5 % w/w	0.4672 10 <sup>-3</sup> mol g <sup>-1</sup> , CO <sub>2</sub>	Intelligent Gravimetric Analyser	303 K and 5 bar	2018	107
4	Liu <i>et al.</i>	ZIF-8	[Bpy] [NTf <sub>2</sub> ] IL	1.4 wt%	2.5 wt% CO <sub>2</sub>	Custom experimental set-up	10 bar at 298 K	2018	101
5	Zhao <i>et al.</i>	UiO-66 with polyether amine	[M2070] [IPA] IL	50 wt%	7.32 wt%, CO <sub>2</sub>	Intelligent Gravimetric Analyser	10 bar	2019	104
6	Li <i>et al.</i>	H-ZSM-5	[P <sub>6,6,6,14</sub> ] [Br] IL	Unclear	2.95 wt%, CO <sub>2</sub>	Intelligent Gravimetric Analyser	Up to 10 bar	2019	108
7	Wang <i>et al.</i>	ZIF-8	[C <sub>4</sub> Py] [NTf <sub>2</sub> ] and [C <sub>4</sub> Py] [N(CN) <sub>2</sub> ] IL	16.96 and 11.55 wt%	0.47 mole fraction for CO <sub>2</sub> solubility in ZIF-8 [C <sub>4</sub> Py] [NTf <sub>2</sub> ]	Custom experimental set-up	303.15 to 333.15 K	2019	100
8	Cahir <i>et al.</i>	Several	Bio-oils and glycols	12.5 to 25 wt%	0.82 mmol g <sup>-1</sup>	Custom experimental set up	298, 323, 348K, up to 5 bar	2020	105

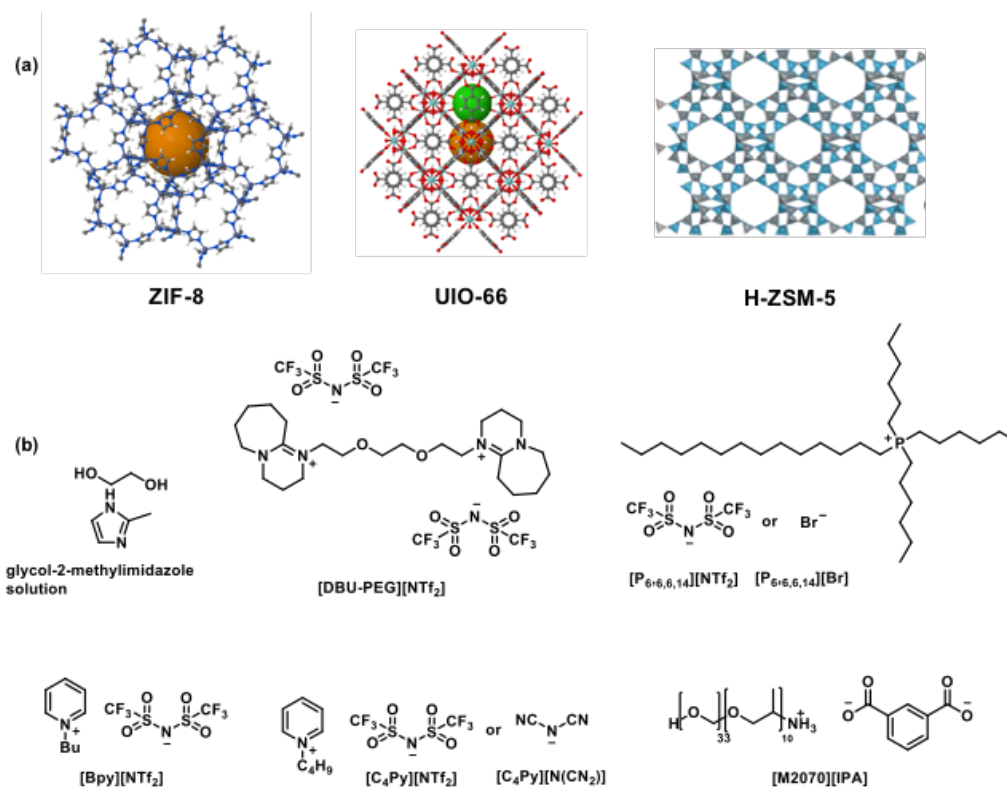


**Figure 1.21:** Structures of the components in reported Type III porous liquids: (a) MOFs (images from chemtube3d.com); (b) Size-excluded solvents.

One of the first examples of a Type III system was originally described as a porous slurry, but possessed the characteristics to be classified as a porous liquid. Liu *et al.* studied CO<sub>2</sub> uptakes and a range of separations for dispersions of ZIF-8 in glycol and glycol-2-methylimidazole solutions.<sup>105</sup> ZIF-8 in glycol-2-methylimidazole, in particular, possessed a high CO<sub>2</sub> capacity (1.25 mol L<sup>-1</sup> at 1 bar). This value is higher than several ionic liquids used for CO<sub>2</sub> capture, including [p5mim] [bFAP] (0.048 mol L<sup>-1</sup>), and the neat glycol-2-methylimidazole solution. A series of separations showed the slurry was selective for CO<sub>2</sub> from several gases, including H<sub>2</sub>, N<sub>2</sub>, and CH<sub>4</sub>. The values were considerably higher than other reported MOFs, and achievable at a range of pressures, which makes the slurry suitable for numerous feed gases.

Zhao *et al.* presented a Type III porous liquid based on the dispersion of UiO-66, another Zn based MOF, functionalised with polyether amine (D2000, **Figure 1.22**), and dispersed in a polymeric ionic liquid ([M2070] [IPA]), to give a stable liquid at ambient temperatures (**Figure 1.21**).<sup>104</sup> The addition of the polyether amine chains to the MOF nanoparticles aimed to stabilise the framework in the ionic liquid, which was found to be stable after storage in a vacuum oven at 45 °C for 6 months. The UiO-66 liquid possessed enhanced CO<sub>2</sub> uptake compared to the neat [M2070] [IPA] (7.32 vs. 2.86 wt% at 10 bar, respectively), showing that the introduction of the MOF nanoparticles improved the system's uptake capacity. The porous

liquid still has lower CO<sub>2</sub> uptake than solid UiO-66 (16.30 wt%) but this a common occurrence in these types of materials, and could be due to added hinderance from the solvent reducing the diffusion of guest into the MOF. To date, this remains one of the highest concentration MOF-doped porous ionic liquids, with a loading of 50 wt% UiO-66, that still maintains a stable dispersion.

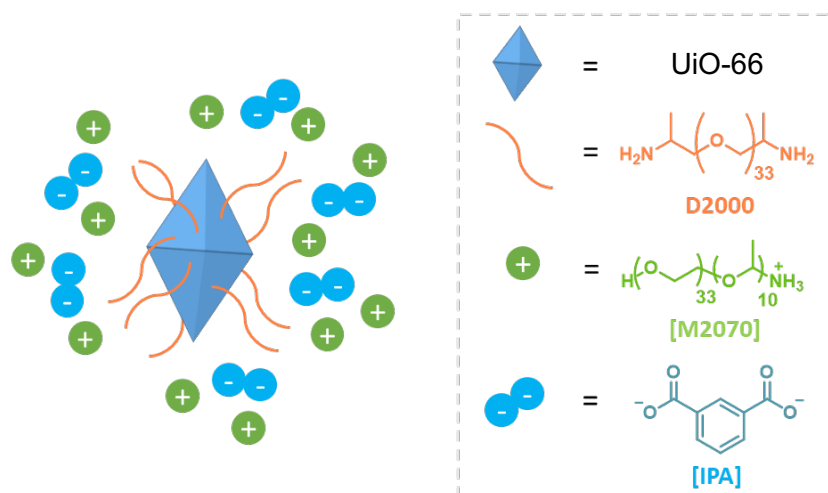


**Figure 1.22:** Graphical representation of the Type III porous liquid presented by Zhao *et al.* with polyether amine (D2000) functionalised UiO-66 dispersed in [M2070] [IPA], a polymeric ionic liquid.<sup>104</sup>

Many reports in the literature included only one or two systems, however, Cahir *et al.* presented an extensive study into different porous solids (including MOFs, zeolites, and porous organic polymers) dispersed in a range of oils.<sup>103</sup> Many of the dispersions possessed enhanced gas uptake compared to the parent solvent, notably, PAF-1 in Genesorb® 1753 had a significantly higher CO<sub>2</sub> uptake compared to the neat solvent (0.72 vs. 0.23 mmol g<sup>-1</sup>). The stability of the systems, and the ability to tailor them towards specific applications, including gas separations, was reported. Compared to some of the ionic liquids used in other studies, the solvents are cheaper and more sustainable.

As briefly mentioned, a major challenge in comparing different porous liquids is the diversity in conditions and units used to study the gas uptake. However, Zhao *et al.* presented a comprehensive assessment of a number of porous liquids in the literature and reported the CO<sub>2</sub> uptake in wt%, which makes comparison easier (**Table 1.2**). This included the uptakes for a range of Type III MOF dispersions and the Type I nanoparticle corona-canopy based systems. The UiO-66 liquid appeared to have the highest MOF loading (50 wt%) and the highest CO<sub>2</sub> uptake (7.32 wt% at 10 bar and 298 K) compared to the rest of the porous liquids (**Table 1.2**, Entry 1). Although the low melting nanoparticle porous liquids are ‘neat’ systems, they have considerably lower uptakes compared to the MOF dispersions (**Table 1.2**, Entries 2 and 3).



This could be due to their viscosities being higher, which could have an effect on the diffusion of the guests, or their affinity for CO<sub>2</sub>.

**Table 1.2:** Summary of the CO<sub>2</sub> uptakes in a range of reported porous liquids, adapted from work presented by Zhao *et al.*<sup>104</sup>

Entry	Porous material	Solvent	MOF concentration	Adsorption		Ref
				Capacity	Conditions	
1	UiO-66 with polyether amine	[M2070] [IPA]	50 wt%	7.32 wt%	10 bar, 298 K	104
				4.99 wt%	5 bar, 298 K	
				1.95 wt%	1 bar, 298 K	
2	Hollow carbon sphere	n/a	n/a	1.9 wt%	10 bar, 298 K	97
				0.445 wt%	1 bar, 298 K	
3	Hollow silica nanorods	n/a	n/a	3.3 to 4.8% w/w	0 °C	96
4	ZIF-8	[DBU-PEG] [NTf <sub>2</sub> ]	30 wt%	6.86 wt%	10 bar, 298 K	102
5	ZIF-8	[Bpy] [NTf <sub>2</sub> ]	1.4 wt%	2.5 wt%	10 bar, 298 K	101
6	ZIF-8	[P6,6,6,14] [Br]	Unclear	2.21 wt %	5 bar, 298 K	107
7	ZIF-8	glycol	15 wt%	5.5 g L <sup>-1</sup>	1 bar, 303 K	105

#### 1.4.4 Porous liquids based on MOPs/MOCs

As discussed previously, the extended metal-organic frameworks are inherently insoluble, and although dispersions are an easy method to introduce fluidity, they still pose stability issues over time. Designing a neat molecular porous system that is a liquid at ambient temperature is arguably the most challenging strategy to achieve a porous liquid. However, Ma *et al.* presented a metal coordination cage (MOC), with a low melting temperature, that retained permanent porosity in the liquid state (**Figure 1.23**).<sup>109</sup> A MOC was functionalised on the periphery with PEG – imidazolium chains, which were shown to be imperative in lowering the melting point of the corresponding cage. When coordination cages with shorter PEG chains were synthesised as a comparison, these were found to be solid at room temperature.



data at 70 °C sharpened the peaks in the spectra.<sup>109</sup> Practically, having to use a higher temperature might limit the applications of the material, as more volatile guests, such as those studied for CFC capture, would be difficult to work with. Ma *et al.* also did not provide gas uptakes, which could be determined from the integration of the guest peaks compared to the cage, discussed later in this chapter. However, the work presented by Ma *et al.* provides an in-depth study into the first stable low melting coordination cage for use as a porous ionic liquid, and is the first example that has been applied in liquid guest separations, and for the capture of larger gaseous guests.

### 1.4.5 Porous liquids based on POCs

Since the original concept paper in 2007, there are now a handful of examples of porous liquids presented in the literature, with a considerable number based on porous organic cages (POCs). First, James and co-workers targeted Type I porous liquids and reported several porous alkylated imine cages with low melting points. The addition of alkyl chains to the cage's periphery resulted in a reduction in melting temperature from  $\geq 300$  °C for un-functionalised POCs synthesised by Cooper *et al.*,<sup>84</sup> to as low as 50 °C for the cages containing octyl chains (Figure 1.24).<sup>110</sup> These molecular species melted at low temperatures because of the disruption of crystal packing by the alkyl chains on the periphery.<sup>110,111</sup> For the analogues where single crystals could be grown, irregular packing and disorder was observed, with partial interlocking of the alkyl chains. While the solids appeared to melt readily, they did not appear to absorb significant quantities of nitrogen. The authors predicted that in the liquid state, the cages were unlikely to possess microporosity due to the alkyl chains occupying neighbouring cavities.<sup>110</sup>

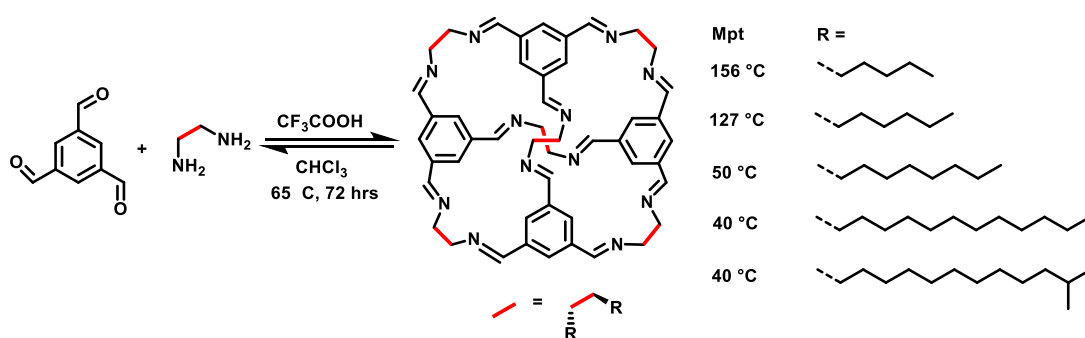


Figure 1.24: Synthesis of alkylated POCs by Giri *et al.* and their corresponding melting points<sup>110</sup>

Melaugh *et al.* reported subsequent computational simulations to rationalise the reduction in porosity for the alkylated POCs in their neat liquid state.<sup>111</sup> All systems showed a transition between a disordered solid to a fluid phase, attributed to the addition of the alkyl chains. The authors also demonstrated how the terminal groups on the peripheral chains occupied the

cavities of neighbouring cages, as predicted by Giri *et al.*, and reduced the overall porosity of the system. However, in the case of the pentyl-substituted cage, predictions suggested 30% of the cavities remained unoccupied. Therefore, theoretically, this POC could be defined as permanently porous in its liquid state.

Overall, the work presented by Giri *et al.* and Melaugh *et al.* does seem to suggest that the alkylated POCs are potentially porous liquids. The long alkyl chains reduce the melting point of the cages, with the longer chains having the lowest melting point of those synthesised. However, computational modelling demonstrated a loss of porosity in the melted cages.<sup>111</sup> The pentyl-substituted cage had a high melting point of 158 °C, but it is predicted that it retains some microporosity in the liquid state. Currently, it would be difficult to prove these theoretical predictions with experimental data. This work demonstrates the potential in reducing the melting point of alkyl-substituted cages to access a liquid phase at room temperature, but also could also be expanded to finding a bulky solvent that would result in a Type II porous liquid.

In 2015, Giri *et al.* reported two alternative strategies for synthesising a Type II porous liquid.<sup>13</sup> The first system looked at solving the occupancy of the cage cavities by flexible alkyl chains by adding ‘tethered groups’ instead (**Figure 1.25**). The POC, functionalised with six crown-ether moieties, was found to dissolve in 15-crown-5 at high concentration and it was too large to enter the pores. The gas solubility of methane increased from 6.7  $\mu\text{mol g}^{-1}$  in the pure 15-crown-5 solvent, to 52  $\mu\text{mol g}^{-1}$  in the crown-ether Type II porous liquid at 293 K. Molecular modelling suggested this was due to the methane molecules being in the intrinsic cage pores rather than in transient cavities.<sup>13</sup> However, the crown-ether cage has a difficult six-step synthesis, several of which involve dangerous intermediates with large exotherms as indicated by DSC. The problems faced in the synthesis meant the crown-ether porous liquid was unsuitable for scale-up, and additionally its high viscosity made it impractical for use in industrial systems.

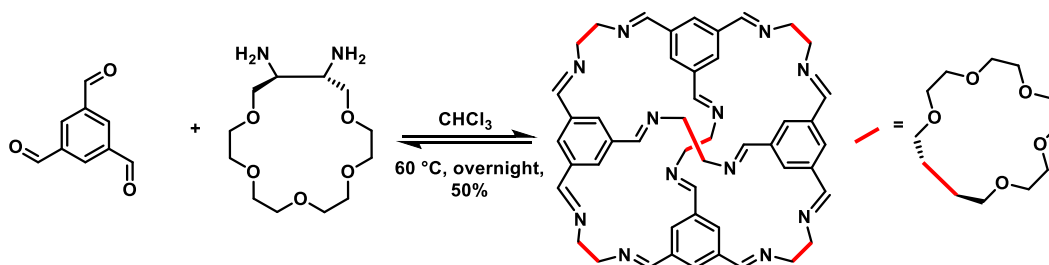


**Figure 1.25:** General reaction scheme for the synthesis of the tethered POC used to form a Type II porous liquid by Giri *et al.*<sup>13</sup>

The second system used an alternative strategy adapted from the dynamic covalent scrambling methodology first pioneered by Jiang *et al.*<sup>88</sup> Giri *et al.* presented a Type II porous liquid formed from the scrambled cage mixture between CC3 and CC13, with the same [4+6] POC core used in the ‘tethered’ cage, dissolved in the size-excluded perchloropropene (PCP).<sup>13</sup> The design strategy was described in more detail in a subsequent study by Greenaway *et al.*, who screened the solubility of 25 different scrambled cages with 6 bulky solvents, chosen based on the likelihood of being size-excluded. Out of the 150 combinations, a 3:3 ratio of cyclohexyl and dimethyl functionality on the cage periphery ( $3^3:13^3$ ) in PCP was found to have the highest solubility ( $200 \text{ mg mL}^{-1}$ ), with most being less than  $30 \text{ mg mL}^{-1}$ .  $3^3:13^3$  was shown to have improved solubility, compared to the parent cages, in both chloroform and PCP (Figure 1.26), showing this is an effective method for improving solubility of POCs because of the poor packing in the solid state.<sup>112</sup> The resulting Type II porous liquid gave substantially higher gas uptakes than neat PCP for a range of gases, including methane ( $51 \text{ } \mu\text{mol g}^{-1}$  vs  $6.7 \text{ } \mu\text{mol g}^{-1}$  at 293 K, respectively).<sup>13,112</sup>

The scrambled porous liquid was more scalable than the crown-ether derivative, as  $3^3:13^3$  was synthesised on a multi-gram scale. However, PCP, although size-excluded, has an acute toxicity, has limited commercial availability, and is expensive. Both porous liquids presented by Giri *et al.* are effective at proving the concept of a Type II porous liquid, but they have associated problems that make them impractical for use on a large scale.

Using scrambled cages in Type II porous liquids is effective because of their scalability and high solubility. However, the method of discovery by Greenaway *et al.* has scope for improvement, as a screen of 150 solvents and scrambled cage combinations only led to the discovery of a single porous liquid. If the screening process could be streamlined to make it more efficient, this might improve the probability of finding more than one Type II porous liquid.

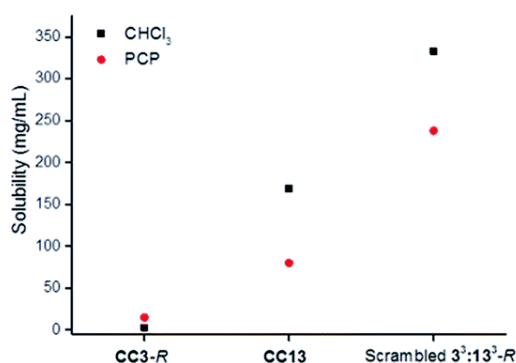
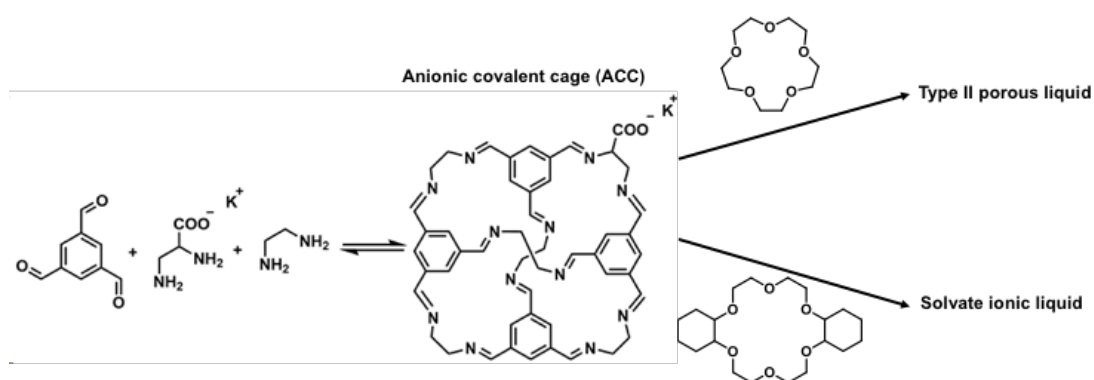


Figure 1.26: Solubility of CC3-R, CC13 and the scrambled  $3^3:13^3$  cage, in chloroform and PCP.

Jie *et al.* presented an alternative approach by targeting porous ionic liquids from POCs by functionalising CC1 with a potassium carboxylate group to form an anionic covalent cage (ACC).<sup>113</sup> The authors aimed to use ‘supramolecular complexation’ of the potassium ion in a crown ether, thereby acting as the cation in a resulting porous liquid rather than ion exchange for a larger cation because the POC decomposed in water (**Figure 1.27**). When attempting this strategy, mixing the anionic cage with 15-crown-5 in a 1:2 ratio only resulted in solids being formed, but increasing to a 1:7 ratio gave a viscous liquid at room temperature. In contrast, using dicyclohexano-18-crown-6 in a 3:1 ratio with the cage formed a liquid. Comparison of the gas sorption properties for each liquid, the neat crown ethers, and the solid cage, confirmed they were permanently porous. While the solid cage had a higher CO<sub>2</sub> adsorption (1.062 mmol g<sup>-1</sup>), both the porous liquids demonstrated a significant increase (0.375 and 0.429 mmol g<sup>-1</sup>) compared to dicyclohexano-18-crown-6, which was too low for detection (15-crown-5 was excluded from measurements due to its high volatility).



**Figure 1.27:** The [4+6] POC presented by Jie *et al.* and supramolecular complexation into porous liquids.<sup>113</sup>

The melting characteristics of both porous liquids using DSC was also studied. This indicated that the 15-crown-5 based porous liquid was a Type II system, based on it possessing two melting transitions, but the dicyclohexano-18-crown-6 derived liquid was a Type I system because it had a single transition, confirming the formation of a complex. However, whilst described as a neat Type I porous ionic liquid, this complexation strategy can be thought of as more of a solvation method for POCs. It seems closer to a solvate ionic liquid – a relatively new class of ionic liquids consisting of a coordinating solvent and a salt to form a complex with very similar properties to ionic liquids.<sup>114–117</sup> This would also account for the single observed transition by DSC, but would suggest that the system is closer to a Type II porous liquid with no vapour pressure. This further highlights that the original definitions are quite broad, and as the field has advanced, there are examples that do not fit the initial descriptions

for each porous liquid type. The composition and behaviour of the examples indicate the complexity of the emerging field.

The examples of POC-derived porous liquids discussed so far had varying functionality on the diamine precursor to either induce melting or increase solubility. However, more recently, Egleston *et al.* investigated the effect of varying the window size on gas uptakes in structurally analogous POCs (**Figure 1.28**).<sup>118</sup> The properties of **3<sup>3</sup>:13<sup>3</sup>**, described earlier, and **CC15-R**, which was synthesised using 1,3,5-triacetylbenzene instead of 1,3,5-triformylbenzene were compared.<sup>119</sup> The additional methyl groups on **CC15-R** resulted in a much smaller window (1.7 vs 4.0 Å, respectively) and cavity (4.61 and 5.85 Å) size than **3<sup>3</sup>:13<sup>3</sup>**, the same as **CC3**, which gave the potential to tune gas selectivity in a subsequent porous liquid. Both cages were soluble in PCP, but **CC15 $\alpha$**  had a much lower solubility of 50 mg mL<sup>-1</sup> (5% w/v). **CC15 $\alpha$**  packs window-to-arene, whereas **3<sup>3</sup>:13<sup>3</sup>** is thought to have a frustrated packing similar to **1<sup>3</sup>:3<sup>3</sup>**<sup>120</sup> and this improves the solubility compared to the single cage species. Therefore, to allow direct comparison, the porous liquids were prepared at the same equimolar concentrations (39  $\mu\text{mol}_{\text{cage}}$  in 1 mL<sub>PCP</sub>).

The authors studied the gas uptake in these two Type II porous liquids using gas displacement and <sup>1</sup>H NMR spectroscopy for a range of guests. The porous liquids had a higher gas uptake, for most gases, over the neat PCP solvent, due to the addition of the cage cavities. The gas evolved from each porous liquid, carried out using a similar methodology described by Greenaway *et al.*, demonstrated the effect of changing the cage window size. For example, xenon usually has a high affinity for [4+6] imine cages due to its high binding preference, as observed for **3<sup>3</sup>:13<sup>3</sup>** but not for **CC15-R**. The xenon uptake for the **CC15-R** porous liquid was considerably lower, and rationalised by the presence of the methyl groups in the cage windows that reducing the accessibility. Interestingly, this is not the case in the solid state, as the xenon uptakes are considerably higher than the porous liquids. This can be rationalised by the loss of the interconnected pore network in the liquid state, as Type II porous liquids exclusively possess intrinsic cavities. To explain this observation, the authors demonstrated the differences between the porous liquids using NMR spectroscopy. When in a cage cavity, the guest experiences an upfield shift, and gives an indication into the gas uptake in a porous liquid. For **3<sup>3</sup>:13<sup>3</sup>** in PCP, xenon experienced a large upfield shift compared to neat PCP ( $\Delta\delta = -38.6$  ppm), however, **CC15-R** exhibited a much smaller change ( $\Delta\delta = -4.7$  ppm) and cannot as easily occupy the cage cavities.<sup>118</sup>

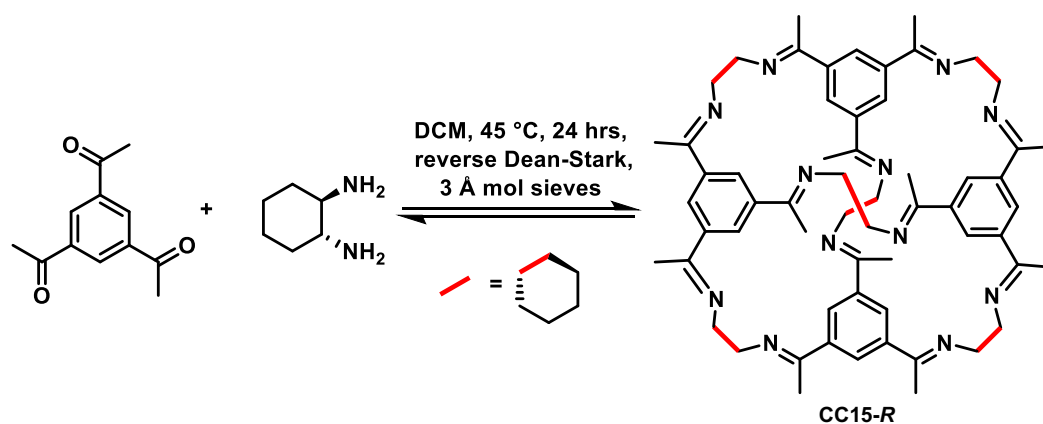


**Figure 1.28:** Structure of CC15-R used by Egleston *et al.* to generate a Type II porous liquid in PCP.<sup>118</sup>

The work presented by Egleston *et al.* gave a useful insight into the behaviour of two analogous porous liquids when the cage window size was changed. Designer porous liquids could be selective to separate one gas from another. NMR spectroscopy is a useful technique in studying porous liquids, particularly those susceptible to vacuum. Unlike gas evolution measurements, NMR spectroscopy gives an indication as to the location of a guest within a porous liquid by the extent of the upfield shift. Using a calibrated capillary, this allows the calculation of a guest's concentration, as demonstrated by several examples. However, there are limitations with this method, as the guests being studied need to be NMR active.

Recent research has shown the potential for using POCs as components in porous liquids. The discrete molecular nature of POCs can lead to both Type I and Type II porous liquids with their formation through self-assembly enabling access to a diverse range of structures, targeting low melting and highly soluble species. However, there are still a number of limitations with the resulting systems, and therefore, there is scope to expand the area by further investigating the use of POCs. For example, there is currently a threshold cavity concentration of 200 mg mL<sup>-1</sup> within the Type II porous liquid systems, particularly with the scrambled porous liquids, but changing the functionality on the periphery could lead to species that are more soluble. There is also a problem with using volatile solvents, such as PCP, as these limit the studies and applications.



## 1.5 Aims of the project

Whilst the field of porous liquids is still in its infancy, there are now a number of fundamental examples reported. However, there are still a range of potential strategies for synthesising and improving the current systems. In particular, porous organic cages provide scope for developing porous liquids of all three types, particularly Type I and II. Despite the limited solubility of early [4+6] imine cages, there are methods to tailor the properties available, including varying the melting point and solubility by changing the functionality on the cage periphery. Prior to this work, one of the highest concentration Type II porous liquids was **3<sup>3</sup>:13<sup>3</sup>** scrambled cage in perchloropropene. While the cage is highly scalable, the solvent has inherent problems with toxicity and cost, and therefore, while this system outlined a successful approach to generating a Type II porous liquid with enhanced gas uptake compared to the neat solvent, it has potential to be improved.

The aim of this thesis was to expand on the work carried out by Giri and Greenaway *et al.* to generate a library of Type II scrambled porous liquids, with a range of scrambled cages and cavity-excluded solvents. Having a range of interchangeable species would allow us to study how changing these components affects other properties, and enable design rules to be generated. Not only is there a limited fundamental understanding in the design of Type II scrambled porous liquids, there is a limited cavity concentration - the highest concentration to date was 200 mg per 1 mL of solvent,<sup>13,112</sup> and a more concentrated porous liquid was yet to be realised. It was hypothesised that increasing the pore volume would enable higher gas uptakes to be achieved, and it was desirable to determine if there was a maximum viable concentration before gas uptake plateaus.

Additionally, the current Type II scrambled porous liquids suffer from an inherent volatility associated with the solvent components. As reduced pressure would affect these systems, as the solvent would evaporate under vacuum, this limits their study and applications. Therefore, finding a low melting ionic system or a cage that dissolves to a reasonable concentration in an ionic liquid would negate these issues.

**Chapter 2:**  
Using high-throughput automation  
in the discovery of highly soluble  
scrambled cages

## 2.1 Introduction

### 2.1.1 Using porous organic cages to form porous liquids

When designing a Type II porous liquid – a molecular porous species dissolved in a cavity-excluded solvent – a key consideration is the solubility of the porous material in the chosen solvent. Generally, it could be expected that by increasing the number of cavities per volume, the overall porosity could be increased. Therefore, in the case of POCs, the more soluble a cage is in a size-excluded solvent, the more likely the corresponding porous liquid will have higher gas uptake due to the increased number of cavities. However, despite dissolution in a number of organic solvents being possible, imine cages tend to have low solubility, for example, **CC3-Ra** has a solubility of just 9 mg mL<sup>-1</sup> in chloroform.<sup>121,122</sup> To overcome this limitation, several strategies have therefore been employed to improve the solubility of these molecules in common organic solvents.<sup>13,112,113,123</sup> One particularly successful method utilises dynamic covalent ‘scrambling’, which was first pioneered by Jiang *et al.*, to create disordered cage mixtures (**Figure 2.1**).<sup>88</sup> The process involves the co-reaction of two or more vicinal diamines to give a statistical distribution of cages where the functionality on the periphery differs. An observed increase in porosity and solubility in organic solvents, compared to their crystalline counterparts, was thought to be due to the disruption of the ability of the cages to pack efficiently.<sup>120,124</sup> Further, the distribution of cage products can be varied, with the ratio being dictated by the diamine feed ratio (**Figure 2.1**). For example, the use of 5 equivalents of ethylenediamine (used to form **CC1**) and 1 equivalent of cyclohexyldiamine (used to form **CC3**) leads to a mixture favouring the **1<sup>5</sup>3<sup>1</sup>** cage species, whereas the use of 3 equivalents of each forms a more Gaussian distribution of cages, with the **1<sup>3</sup>3<sup>3</sup>** species now favoured. The

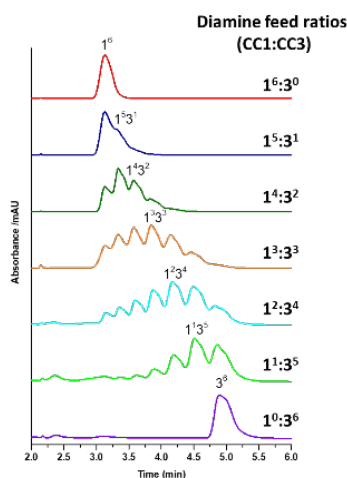


**Figure 2.1:** The HPLC traces showing how changing the diamine feed ratio effects the final statistical distribution ethylenediamine (used to form **CC1**) and cyclohexyldiamine (used to form **CC3**). The individual cage names are depicted as follows: **1<sup>n</sup>3<sup>6-n</sup>** (1/3 = diamines used based on parent cage names, and n = number of diamines on the cage vertices).

modular nature of this approach could enable guest selectivity for a range of gases to be tuned.<sup>88,124</sup>

Giri *et al.* used this same scrambling approach for the synthesis of a Type II porous liquid, which was based on a 3:3 feed ratio of the diamines used to form **CC3** and **CC13**, forming a scrambled cage mixture denoted as **3<sup>3</sup>:13<sup>3</sup>** (**Figure 2.2**) which was dissolved in a size-excluded solvent, perchloropropene (PCP).<sup>13</sup> The system had a reasonable solubility (200 mg of scrambled cage in 1 mL of solvent) and showed improved gas uptake over the neat parent solvent, which included an eight fold increase in CH<sub>4</sub> uptake.<sup>112</sup> This successfully

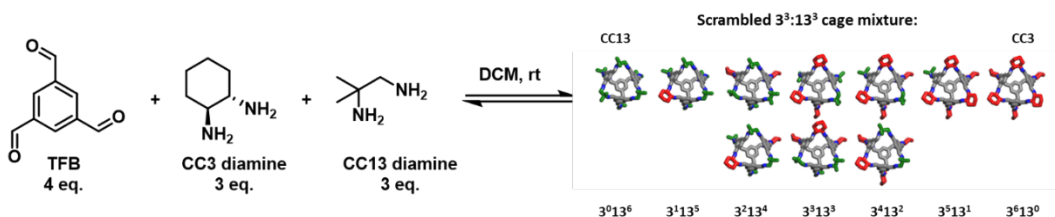


**Figure 2.2:** Reaction scheme illustrating the synthesis of the scrambled cage mixture used to form a Type II porous liquid. The individual cage names are depicted as follows: **3<sup>n</sup>13<sup>6-n</sup>** (3/13 = diamines used based on parent cage names, and n = number of those diamines on the cage vertices).

demonstrated that the combination of scrambled cages and a bulky organic solvent was an effective method for forming a Type II porous liquid.<sup>13,112</sup>

With only a single example of a scrambled porous liquid in the literature, there remained a large scope for further investigation into their design and properties. Scrambled cage mixtures containing different functionalities could potentially vary the properties of the corresponding porous liquids, including improving the solubility to increase cavity concentration, and therefore the porosity or tailor towards specific guests. However, there is an infinite number of scrambled cage/solvent combinations that could be theoretically investigated, and using a manual trial and error approach to do this would be extremely time consuming. Therefore, the development of an efficient workflow where large numbers of cage/solvent pairings could be synthesised and screened could be beneficial in discovering new Type II porous liquids with improved properties.

### 2.1.2 Targeting the ideal Type II porous liquid

Type II porous liquids are fundamentally comprised of two components: a soluble porous species, typically molecular in nature, and a cavity-excluded solvent. These components should have complementary properties in order to be fit for purpose. In the case of scrambled porous liquids, the scrambled organic cage mixtures need to be highly soluble and stable to the solvent, whereas the latter should ideally have low viscosity, cost, vapour pressure, and

toxicology. The most important pre-requisite, however, is finding a solvent that does not occupy the cage cavities, either by size-exclusion or having unfavourable binding interactions, in order to ensure permanent porosity is introduced and retained in the liquid state.

There are potential benefits to a two component porous liquid system, and continuing the work on scrambled porous liquids gives scope to target many applications. The overall properties, such as viscosity and gas uptake capacity, of a Type II porous liquid could be tuned by changing components, including the pore concentration. If a library of porous liquids could be designed, with interchangeable scrambled cage mixtures and complementary solvents, the porous liquids could be tailor-made to perform specific tasks. For example, specific gas separations could be targeted by changing the scrambled cage or solvent to switch the guest preference. Further, gaining a more in-depth understanding of these systems would also reduce any limitations that might be detrimental to their usefulness in commercial settings. For example, a maximum porosity threshold might be reached before other properties, such as viscosity, start to impede their practicality in gas diffusion or flow applications.

### **2.1.3 High-throughput methodology in chemical synthesis**

High-throughput synthesis and physiochemical testing are becoming more common in areas such as drug discovery<sup>125–127</sup> and materials chemistry.<sup>128–133</sup> For example, recently we reported an effective high-throughput workflow that enabled a large organic cage library to be synthesised and characterised from binary mixtures of precursors.<sup>134</sup> Although scrambled cages are typically formed using three precursors,<sup>88</sup> they require similar reaction conditions to those used by Greenaway *et al.*, and therefore should be translatable onto an automated synthesis platform. Additionally, solubility testing has been demonstrated using automated methodology,<sup>126</sup> but such approaches have yet to be applied in the discovery of new porous liquids. There is a large scope for combining such methods to design a high-throughput workflow incorporating the synthesis, purification, characterisation, and solubility testing of scrambled cages, with the ultimate aim being the discovery of new Type II porous liquids.

Furthermore, along with accelerating the discovery process and exploring a larger chemical space, this approach has the potential to allow the elucidation of relationships between the components that constitute the porous liquid and its resulting properties. Currently, little is known about the ideal characteristics needed to create new Type II porous liquids, and one of the main challenges for improving on the first generation is introducing sufficient cavity concentration per volume in order to increase the overall porosity. Generally, investigations into the design of new scrambled porous liquids, and their resulting properties, could help establish important design considerations for future work.

This work aimed to demonstrate the benefits of utilising automation to accelerate the discovery of next generation Type II porous liquids, which could be studied further to understand their properties.

## **2.2 Development of a high-throughput discovery workflow for discovering highly soluble cage/solvent combinations**

### **2.2.1 Choosing suitable precursors**

Typically, porous imine cages are synthesised in a one-pot poly-condensation reaction, and isolated using simple purification procedures.<sup>13,88,112</sup> The nature of this synthesis has been previously translated into a high-throughput workflow for organic cages derived from two precursors,<sup>134</sup> and therefore, should allow the development of an analogous methodology for three component scrambled cage mixtures.

First, the choice of cage precursors needs to be carefully considered. While the reversibility associated with imine chemistry allows for statistical distributions of cages to be formed, when using three precursors (one trialdehyde and two vicinal diamines), other reactions could potentially occur. This can include social self-sorting into a single new cage species, or narcissistic self-sorting into separate binary ‘parent’ cages (**Figure 2.3**).<sup>135</sup> POCs have also been shown to self-assemble through chiral recognition: this was observed when using different chiral forms of the diamine precursor, resulting in the formation of homochiral cages.<sup>135–139</sup> Chiral recognition in cage racemates has also been found to greatly decrease solubility,<sup>136,137,140</sup> which is undesirable in the design of a scrambled porous liquid. Overall, having two diamines with unknown selectivity and reactivity increases the risk of other side reactions occurring, as it is difficult to predict the composition of the final products. Additionally, whilst all manner of different diamines could be investigated in a high-throughput screen, not all would be guaranteed to form cages, with the formation of oligomers or polymers also possible. Therefore, while it was important to select a variety of diamines containing a range of functionalities, using a completely untested precursor family would be counter-intuitive since the synthesis of scrambled cages has not previously been automated. With this in mind, several diamines were selected that are known to make both parent and scrambled cages. These would act as controls to check the validity of the high-throughput workflow, confirming whether scrambled cage synthesis can be translated onto automated platforms. Once the methodology and workflow has been developed and optimised, then new combinations could easily be incorporated and screened in the future.

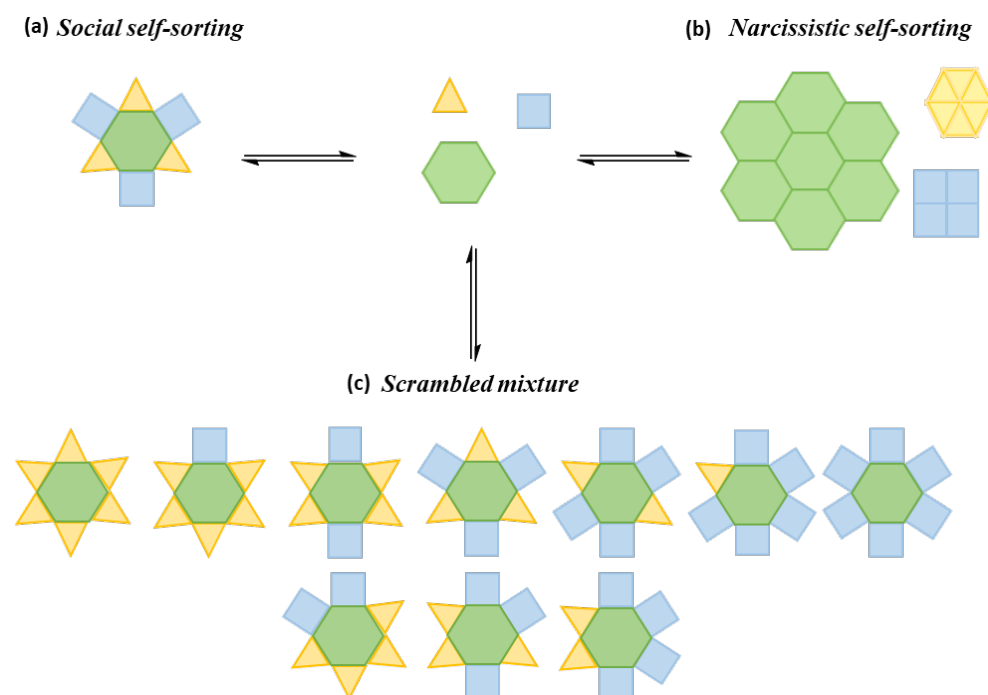


**Figure 2.3:** Graphical representation of how a mixture of 3 precursors can self-sort into a range of different products.

To simplify the search space, the achiral 1,2-diamino-2-methyl-propane (Amine A, **Figure 2.4**) was selected as one of the scrambling partners because it reliably forms **CC13 $\beta$** , our most soluble parent cage to date, and has previously been shown to scramble with other vicinal diamines.<sup>13,122</sup> The other scrambling partners were chosen based on their structural diversity and availability. The scrambling diamines were required to feed the high-throughput screen with sufficient material, so needed to either be commercially sourced, or synthesisable on a gram scale. For example, Amines **B** to **F**, and Amine **K**, (**Figure 2.4**) were selected because they were structurally diverse, some are known to readily form scrambled cages (Amines **B-E**, and **K**)<sup>112</sup>, and they were readily available from chemical suppliers.

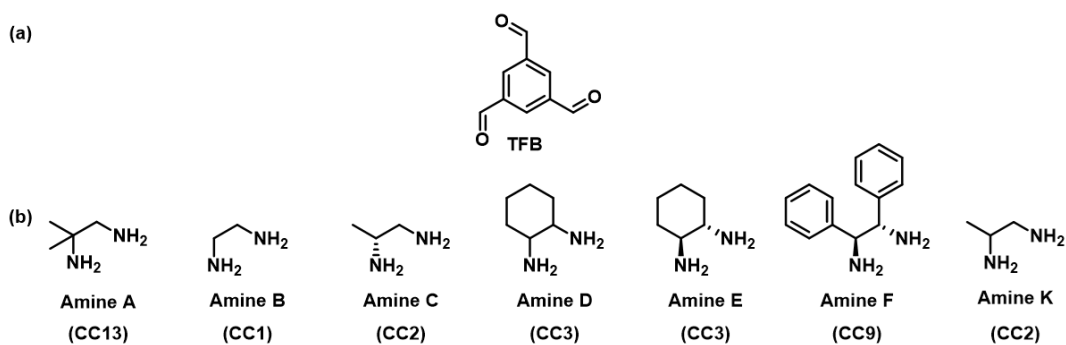


**Figure 2.4:** Structure of the commercial precursors selected for use in the high-throughput screen: (a) 1,3,5-triformylbenzene (TFB), paired with (b) a range of diamines.

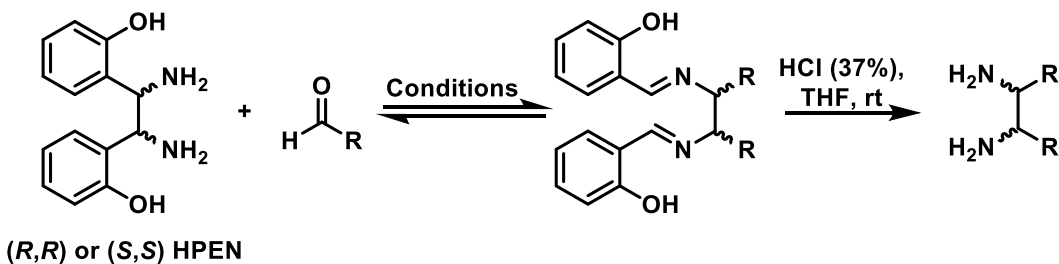
Given the modular nature of cage synthesis, different functionalities can be introduced onto the periphery of a cage,<sup>141</sup> and therefore, introducing custom diamines into the precursor library for a high-throughput screen would potentially diversify the range of accessible scrambled cage mixtures. However, high yielding precursors are required in order to provide an adequate feedstock for the entire workflow. Insufficient quantities of the starting diamines would lead to not enough scrambled cage being formed for use in subsequent large scale solubility screening, which is an important consideration when choosing suitable starting materials. Therefore, to expand on the selection of commercially available precursors and the range of included functionality, the first step was producing a library of structurally diverse vicinal diamines that could be used to synthesise the scrambled cages needed for subsequent solubility testing. These diamines are common precursors in the formation of imine POCs,<sup>85</sup> and are easily synthesised using the Diaza-Cope rearrangement. This reaction forgoes the need for a metal catalyst that are typically required in other common types of chiral diamine synthesis.<sup>142–144</sup> In addition, the ease of synthesis and generally high yields in the literature offers an effective method for incorporating custom diamines as precursors in the high-throughput screen.<sup>145–149</sup>

Diaza-Cope rearrangements allow for a variety of substituents to be introduced onto the diamine backbone, and after acid hydrolysis, result in an enantiomerically pure diamine with either symmetrical or asymmetrical moieties.<sup>147,150</sup> Stereospecificity is beneficial in organic cage synthesis because, as discussed earlier, a racemic mixture of diamines typically results in chiral self-sorting of the cage products.<sup>138</sup> Specifically, the racemic mixture is considerably less soluble than a single homochiral cage species,<sup>137</sup> which would be an issue when forming a Type II porous liquid as a high solubility is required to introduce reasonable porosity into the liquid state.

With this in mind, a precursor library was synthesised based on methodology previously optimised for a variety of alkyl and aryl substituted chiral diamines.<sup>110,145,151</sup> These species were prepared from a single ‘mother’ diamine ((*R,R* or *S,S*) 1,2-bis(2-hydroxyphenyl) ethylenediamine, HPEN) and a range of commercially available aldehydes (**Table 2.1**).



**Table 2.1:** Summary of the reaction scheme and the diamines synthesised using a Diaza-Cope rearrangement followed by an acid hydrolysis.



	R=	Conditions	Yield (%)	Outcome
1		Toluene, Dean-Stark apparatus, 120 °C	23	Unable to form diimine
2		Toluene, Dean-Stark apparatus, 120 °C	79	Isolated as HCl salt
3		Toluene, Dean-Stark apparatus, 120 °C	79	Isolated as free diamine
4		Toluene, Dean-Stark apparatus, 120 °C	89	Isolated as free diamine
5		Toluene, Dean-Stark apparatus, 120 °C	93	Isolated as HCl salt
6		Ethanol, rt	93	Isolated as HCl salt
7		Toluene, Dean-Stark apparatus, 120 °C	23	Hydrolysis reaction unsuccessful
8		Toluene, Dean-Stark apparatus, 120 °C	29	Hydrolysis reaction unsuccessful

Previously, vicinal diamines containing long alkyl functionality were used to form POCs,<sup>110</sup> and while their synthesis required harsher conditions, alkylated diamines formed via the Diaza-Cope rearrangement can be isolated in high yields and purity. First, incorporation of a *tert*-butyl substituent was of particular interest because branched functionality on the cage periphery could prevent occupation of neighbouring cage cavities, as observed with alkylated cages,<sup>111,123</sup> and reduce the melting point by disrupting the solid state packing. However,

HPEN and 2,2-dimethylpropanal failed to form the desired diimine (**Table 2.1**, Entry 1). Instead, a stable five-membered ring intermediate was observed, with an increased number of aromatic peaks corresponding to an asymmetrical fused ring system apparent in the  $^1\text{H}$  NMR spectrum (**Figure 2.5**), which has previously been reported in the literature.<sup>152</sup> Attempts to promote the rearrangement under harsher conditions, such as refluxing the reaction in DMSO, still yielded the same result. Therefore, as an alternative, an isopropyl group was instead incorporated as this forms in a high yield and purity,<sup>149</sup> so enough material could be synthesised for a high-throughput screen (**Table 2.1**, Entry 2).

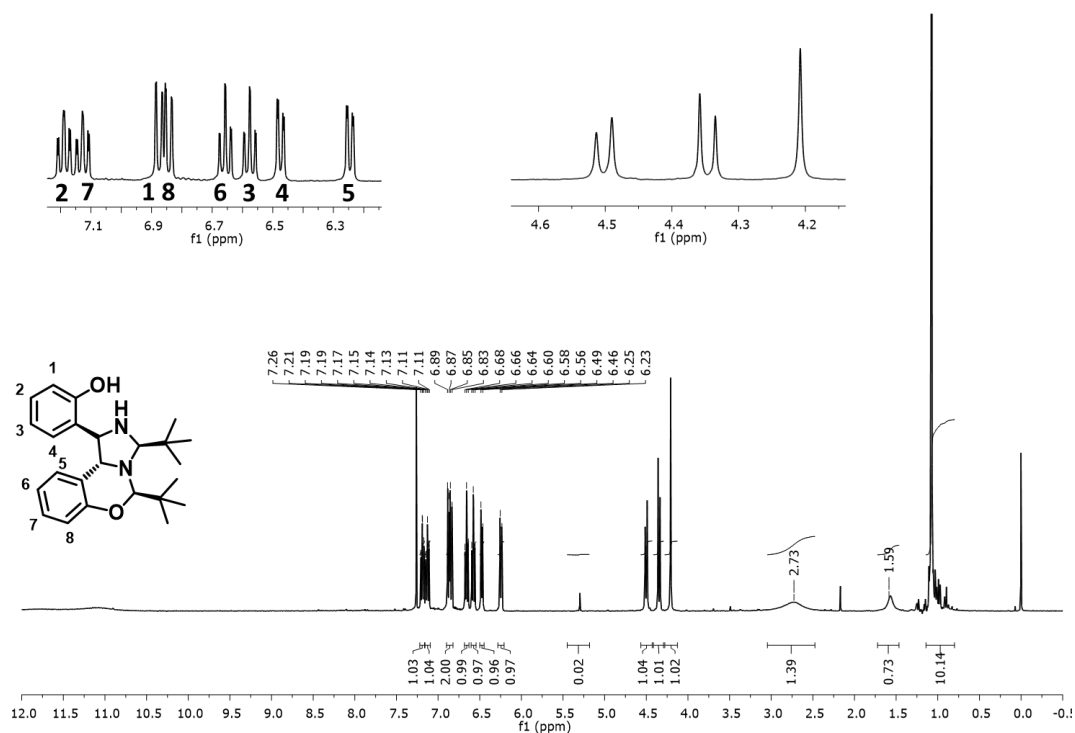


**Figure 2.5:**  $^1\text{H}$  NMR spectrum ( $\text{CDCl}_3$ ) and expansions for the cyclic product formed between HPEN and 2,2-dimethylpropanal.

Next, given that diamines with alkyl handles readily form both parent and scrambled cages, several custom diamines were included to enable incorporation of solubilising groups, which included various chain lengths and cyclic species, to study their effects on the scrambled cage properties (**Table 2.1**, Entries 3-5). Although these required harsher conditions to form, due to the nature of the formation mechanism,<sup>149,152,153</sup> these diamines were isolated in high yield and purity.

Aromatic aldehydes were found to easily undergo the Diaza-Cope reaction, forming compounds such as the dipyridyl-substituted diamine (**Table 2.1**, Entry 6), but previous studies have shown they are difficult to incorporate into a POC.<sup>154,155</sup> For example, aryl

substituted diamines were used to access functionalised [4+6] imine cages in previous work, but these required much harsher conditions, were isolated in low yield, and scrambled mixtures have yet to be realised.<sup>154,155</sup> With this in mind, the custom aryl diamine (**Table 2.1**, Entry 6) was deemed unsuitable to be used in high-throughput screening and only Amine **F** (**Figure 2.4**), which is commercially available, was included to determine if aryl functionality could be integrated into scrambled cages.

Finally, the diimine intermediate containing a fluorinated substituent was low yielding compared to the other analogues in the library (**Table 2.1**, Entry 7), which could be due to the electron withdrawing nature of this group. Within the literature, there does not appear to be any extensive studies of the effect of electron donating or electron withdrawing alkyl substituents on the outcome of the Diaza-Cope rearrangement. However, electron donating substituents on aryl groups have been shown to reduce the rate of the [3,3]-sigmatropic rearrangement, because the intermediate is stabilised through conjugation with the aryl ring.<sup>153</sup> As a result, more side products seem to form and further purification was needed to isolate the diimine. A similar effect was observed when HPEN was combined with an aldehyde containing a silanol substituent (**Table 2.1**, Entry 8). However, the boiling point of this aldehyde was similar to that of toluene, the reaction solvent, so was likely refluxed and potentially removed by the Dean-Stark apparatus used to remove the water produced as a side-product. The synthesis was repeated at a lower temperature with other solvents, such as DMSO and chloroform, to try and negate this issue, but these conditions gave a lower product yield.

Unfortunately, the subsequent acid hydrolysis of both the fluorinated and silanol substituted diimines was unsuccessful (**Table 2.1**, Entries 8-9). The Diaza-Cope rearrangement is reversible, and competes with the hydrolysis – the introduction of functional groups with varying electronics or steric bulk could promote this rearrangement over the desired acid hydrolysis. The reaction conditions were varied to try and improve the conversion to the desired diamine, including the reaction time and temperature, but hydrolysis still proved ineffective. Therefore, these precursors could not be used in the subsequent high-throughput screen.

The successful custom diamines from the Diaza-Cope study (**Figure 2.6**), along with the selected commercial precursors (**Figure 2.4**), provided a large feedstock for use in the high-throughput screen. As a result, the precursor library contained 11 diamines, which would give a diverse selection of scrambled cages for solubility testing.

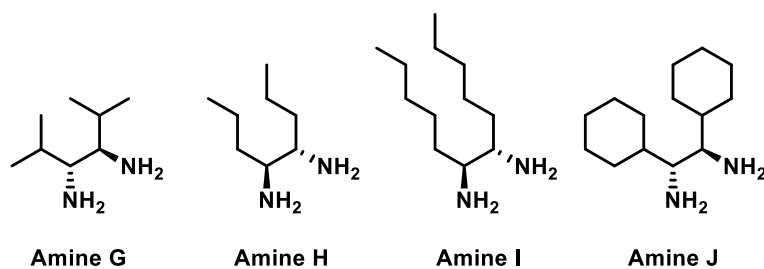


**Figure 2.6:** Structure of the custom diamines synthesised via Diaza-Cope rearrangements, which were chosen for use in in high-throughput scrambled cage synthetic screen.

### 2.2.2 Choosing suitable conditions for translation onto automated platforms

POCs are usually synthesised using high dilution to avoid the formation of kinetic products and impurities such as polymers or oligomers.<sup>83,84</sup> However, there is a limit to the maximum volume of solvent that can be accommodated by the reaction vessels on the robotic platform (60 mL). In order to capitalise on the material generated, preliminary investigations were carried out to determine the highest viable reaction concentration that still avoids polymeric by-product formation, because this can cause handling problems on the platform. Therefore, prior to the high-throughput synthetic screen, the synthesis of the scrambled cage **3<sup>3</sup>:13<sup>3</sup>** was attempted at a three-fold increase in concentration compared to the original conditions used by Giri *et al.* (**Figure 2.2**). This would allow the maximum concentration that would be suitable to use in a scrambled cage synthesis to be determined. The same scale which would be used in the high-throughput screen was used in the trial reactions, but unfortunately, reducing the scale appeared to have a dramatic impact on the yield when the reaction was carried out at the original concentration (**Table 2.2**, Reaction 1).

However, overall, the <sup>1</sup>H NMR spectra showed the cage had formed in reasonable purity (**Figure 2.7**) and the yield was not greatly affected by polymer formation at the higher concentration of 0.13 M (**Table 2.2**, **Reaction 2**). The high performance liquid chromatography (HPLC) also gave the expected statistical distribution corresponding to the expected ratio of cages (**Figure 2.7**).

Based on these findings, it was decided that the high-throughput scrambled cage screen could be carried out at a higher concentration, where there was sufficient starting material, to maximise the resulting product yield and quantity of material produced for subsequent solubility testing.

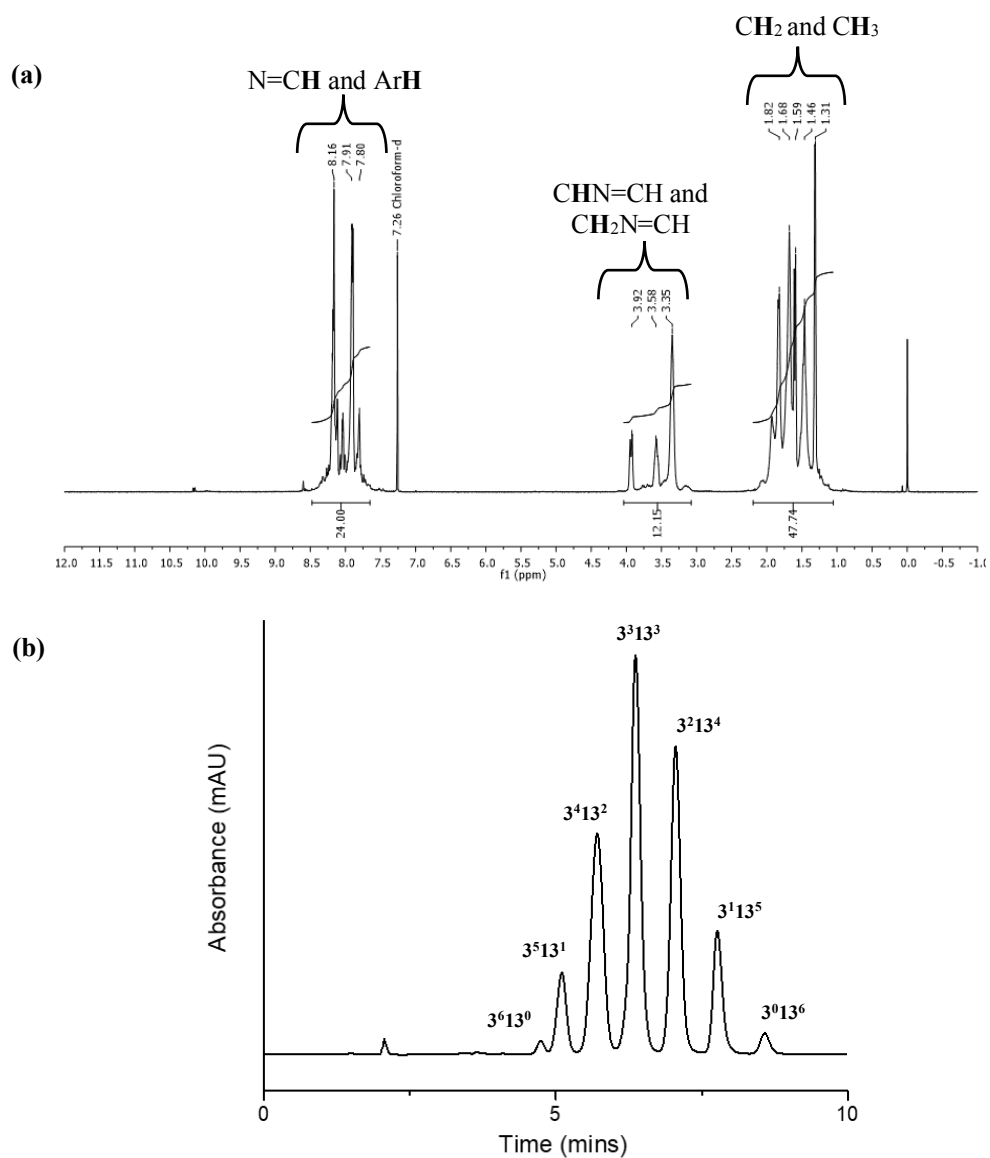


**Figure 2.7:** The analytical data for the scrambled  $3^3:13^3$  cage produced at 0.13 M. (a)  $^1\text{H}$  NMR spectrum ( $\text{CDCl}_3$ ); (b) HPLC trace.

**Table 2.2:** Conditions for the trial 3<sup>3</sup>:13<sup>3</sup> scrambled cage synthesis \*

	TFB		Amine A		Amine E		DCM (mL)	Mass recovery (g)	Molarity (Σmmol/V <sub>sol</sub> )	Yield (%)
	mg	mmol	mg	mmol	mg	mmol				
<b>Reported procedure</b> <sup>13</sup>	7500	46.25	3058	34.69	3961	34.69	2700	14.71	0.043	61
<b>Reaction 1</b>	166.0	1.024	88.0	0.77	67.7	0.77	60	0.25	0.043	24
<b>Reaction 2</b>	498.0	3.071	263.0	2.30	203.0	2.30	60	0.57	0.13	54

## 2.3 Generating a scrambled cage library

### 2.3.1 High-throughput synthesis

Having generated a suitable precursor library and selected the initial cage-forming conditions, a high-throughput synthetic screen was designed using an automated platform (Chemspeed Accelerator SLT-100, **Figure 2.8**). This included 1,3,5-triformylbenzene (TFB) and Amine **A** being combined with the different partner diamines (Amines **B-K**) in varying stoichiometric ratios by dispensing as stock solutions on the platform (**Figure 2.9**). To ensure each reaction was at the correct concentration, an additional calculated volume of chloroform was dispensed to make the total volume up to 60 mL. The vessels were then vortexed at ambient temperature for 3 days to give the reactions enough time to equilibrate, before being transferred into vials (3 x 20 mL for each vessel). Carrying out a total of four runs could result in 61 possible scrambled cage distributions.

Overall, the automated synthesis of a scrambled cage library significantly reduced the time required to complete the syntheses compared to manual methods. For example, although the precursor stock solutions needed preparing manually, they were dispensed by the platform with minimal error and the overall preparation time was reduced. Several known scrambled cages were also incorporated to act as controls, to check the reactions on the platform were successful, ensuring each run was valid.

\* Using 1,2-diamino-2-methylpropane (Amine **A**) and (1*S*,2*S*)-(+)-1,2-diaminocyclohexane (Amine **E**) with 1,3,5-triformylbenzene (TFB) in DCM (60mL). Briefly, a solution of Amine **A** (3.0 eq.) in DCM (15 mL), and a solution of Amine **E** (3.0 eq.) in DCM (15 mL), were added to TFB (4 eq.) in DCM (30mL), and the resulting solution was stirred at room temperature for 72 hours. The solvent was then removed under reduced pressure, and the crude product re-dissolved in DCM and filtered to remove any insoluble precipitate. The solvent was removed *in vacuo*, before the solid was subsequently washed with ethyl acetate and the purified product collected by filtration.

**Chapter 2:** Using high-throughput automation in the discovery of highly soluble scrambled cages

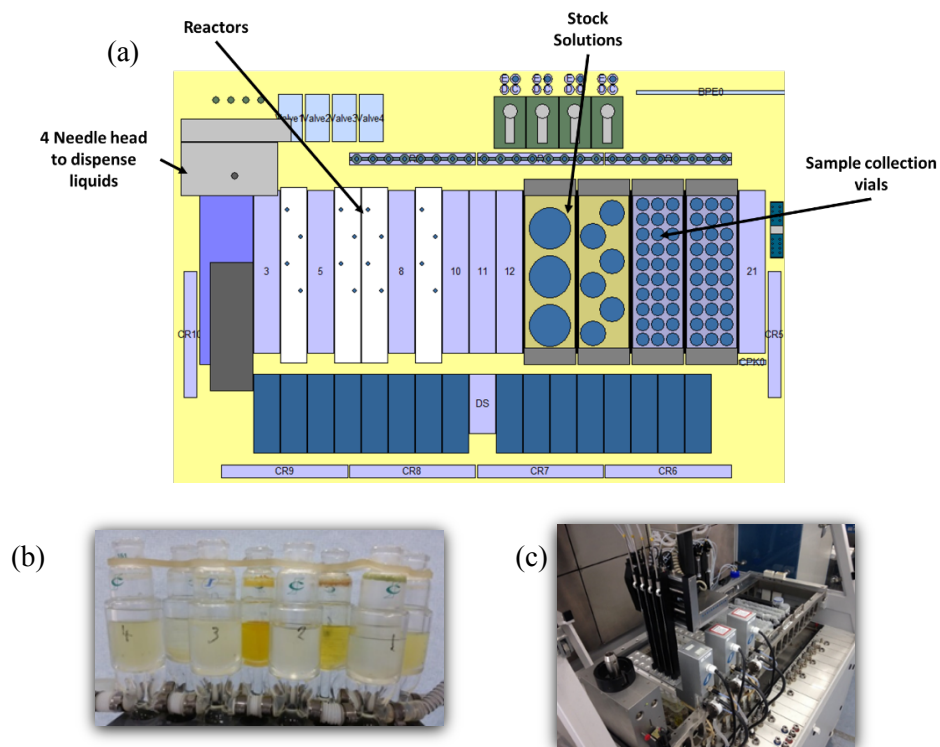


**Figure 2.8:** (a) Graphical representation of the deck layout used in the synthesis of the scrambled cage library; (b) Photo of the individual reactors; (c) Photo of the Chemspeed Accelerator SLT-100.

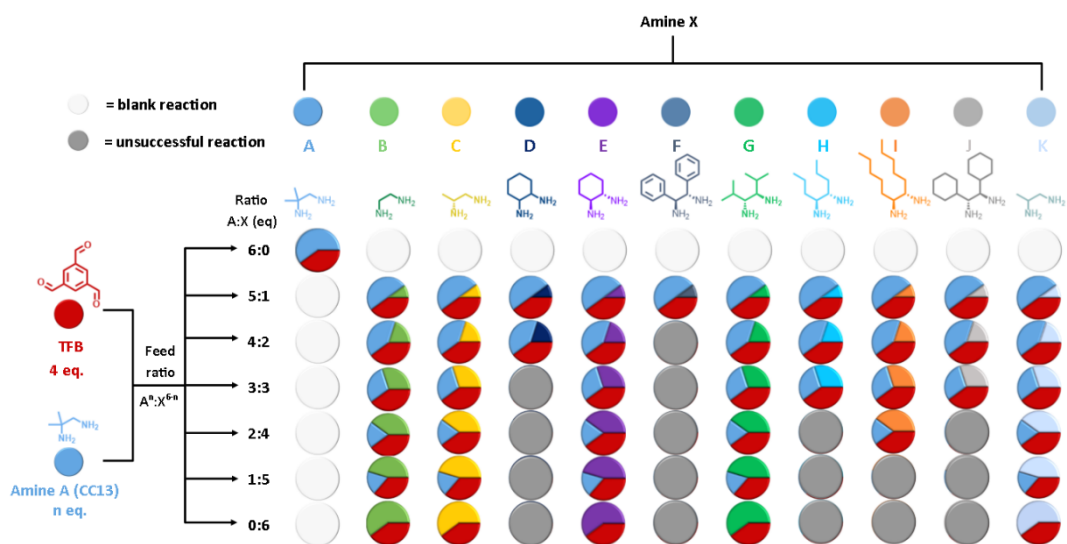


**Figure 2.9:** Graphical representation of the scrambled cage mixtures targeted in the high-throughput synthetic screen: the feed ratio of precursors added to each reaction vessel is defined by the diamine combination  $A^n:X^{6-n}$  (where A is 1,2-diamino-2-methylpropane, X represents the partner diamine (B-K), and n is the number of equivalents). Unsuccessful or low yielding reactions are marked with a grey circle.

**Chapter 2:** Using high-throughput automation in the discovery of highly soluble scrambled cages

Usually the purification and isolation of products is a bottleneck in a high-throughput workflow. However, in this work, several parallel isolation and purification techniques were employed. First, the solvent was removed from the scrambled cage reactions using a Combidancer high-throughput evaporator (**Figure 2.10a**). After isolation, DCM (10 mL) was added to each vial, and the mixtures were filtered in parallel using a Supelco SPE vacuum manifold (**Figure 2.10b**) to remove any insoluble polymer. This does mean some low yielding reactions could be a result of poorly soluble cages, therefore, the filtrate should be analysed to check no cage was missed. The filtrates were then concentrated using the Combidancer, and the procedure repeated using THF for those reactions starting with a diamine chloride salt, as the side-product triethylamine hydrochloride salts were insoluble in this solvent. Finally, all cages were dried in a vacuum oven overnight at 90 °C to remove any residual solvent.

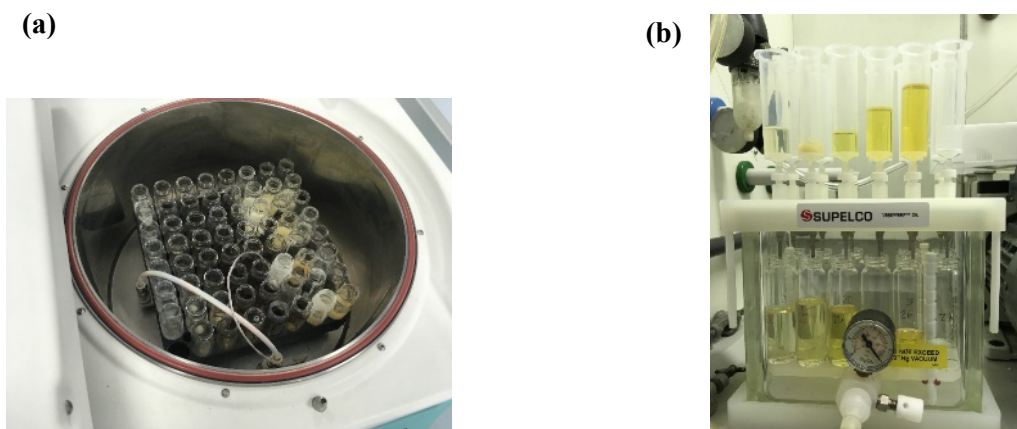


**Figure 2.10:** Parallel isolation and purification techniques: (a) Combidancer high-throughput evaporator; (b) Filtration using a Supelco SPE vacuum manifold.

Although all of the reactions from the screen could be partially purified using the parallel methods as described above, not all of the impurities were removed, as determined by  $^1\text{H}$  NMR spectroscopy. Common soluble impurities in POC syntheses include aldehyde and amine-based oligomers. Therefore, implementing suitable parallel purification methods into future workflows would be beneficial. As one step of the current process is filtration through solid phase extraction (SPE) cartridges, adding an SPE scavenger resin to remove impurities containing specific functionality would potentially improve the workflow for future work. As a result, an investigation into the effectiveness of SPE resins at purifying scrambled cages during the filtration was performed. SPE resins based on silica or polymer supports, and incorporating functional groups designed to remove specific impurities were chosen, primarily targeting aldehyde and amine oligomers (**Figure 2.11**).



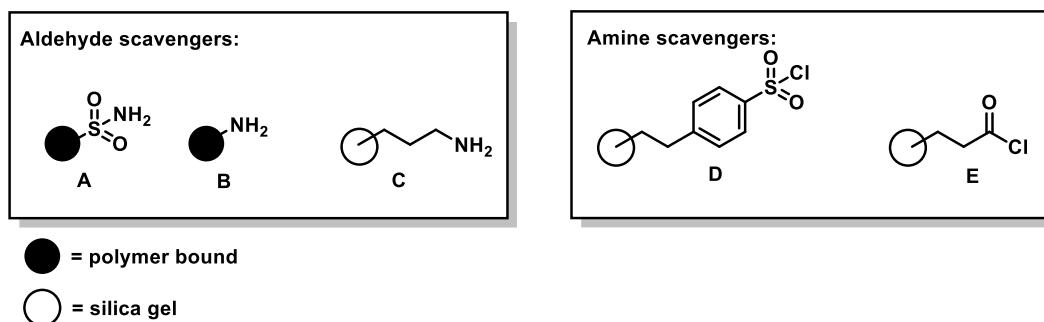


**Figure 2.11:** The structure of the solid phase extraction (SPE) resins (A-E) used in a series of cage purification tests, functionalised to act as aldehyde and amine scavengers.

First, determining if the SPE resins suffered from degradation in the solvents used in cage synthesis would be important in implementing this methodology into the high-throughput workflow. Chloroform and DCM are common solvents used for cage synthesis and did not appear to degrade or dissolve any of the resins. However, methanol and THF both appeared to dissolve several or all of the columns, which indicates these solvents would not be suitable for use in SPE purifications.

Ideally, purification using an SPE column would remove both aldehyde and amine functionalities (including residual starting material), but would leave the cage product unchanged. Therefore, each resin was tested with separate solutions of TFB and (*1S,2S*)-cyclohexane-1,2-diamine (the diamine used to form **CC3**) respectively. All of the screened SPE resins appeared to remove the majority of both TFB and **CC3** diamine.

The next objective was to purify a known cage from the high-throughput screen, so the parent cage **CC13** (formed using TFB with Amine **A**) was selected to carry out preliminary studies. This reaction has previously been reported to form cleanly on the slow addition of TFB to a diamine solution.<sup>122</sup> However, during the high-throughput screen a number of impurities were observed, which could be due to the faster rate of addition, the higher concentration, or the temperature used (room temperature compared to the cooled solution reported). Several resins were effective at removing the aldehyde impurities from the crude cage reaction, which was shown in the <sup>1</sup>H NMR spectrum (**Figure 2.12**, Resins A-C). However, the removal of amine-based oligomers and purification was less successful for a novel cage, **CC21**, which is discussed in **Chapter 3**, with no change or even degradation being observed.

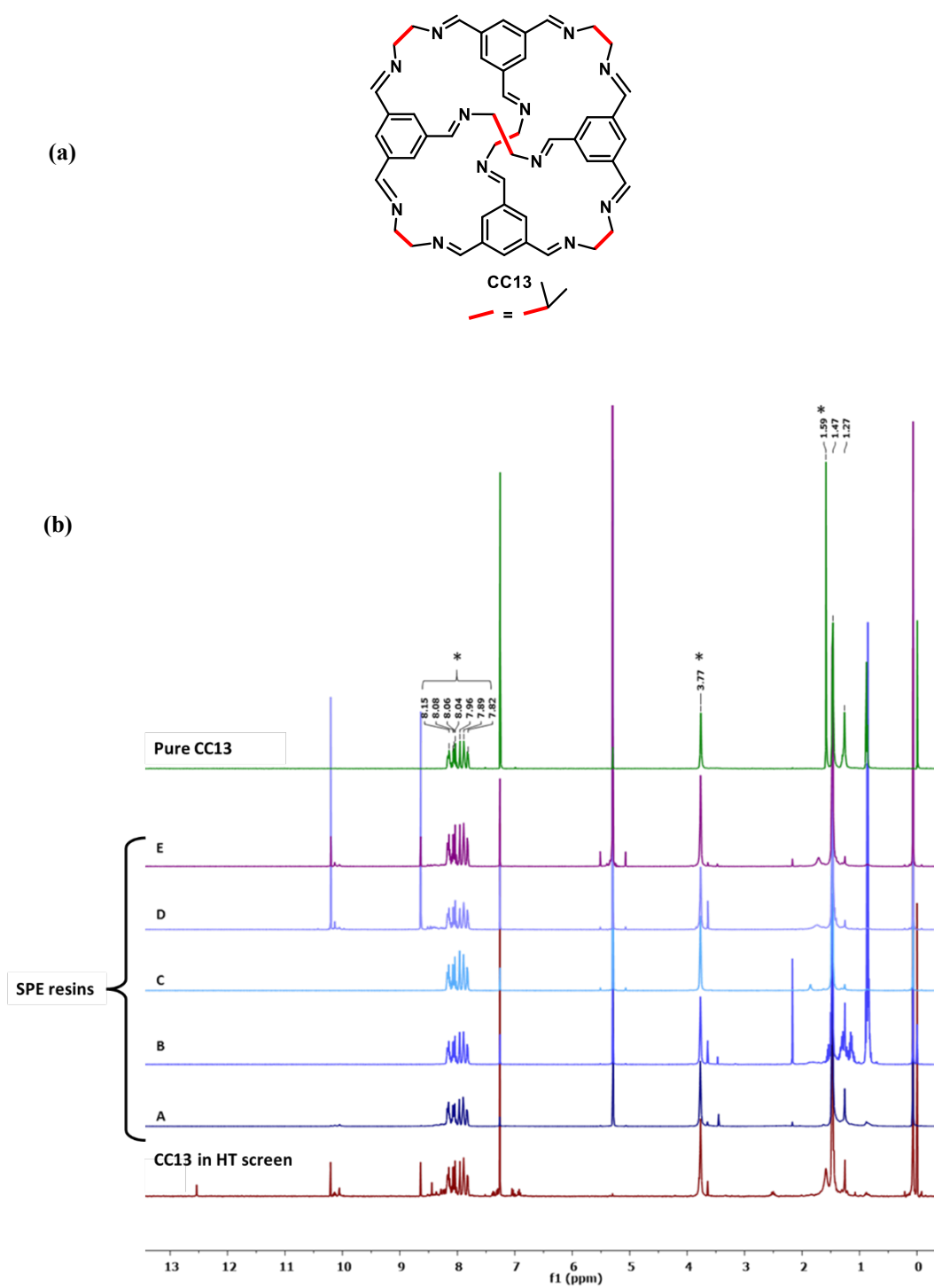


**Figure 2.11:** (a) The structure of **CC13**; (b)  $^1\text{H}$  NMR spectra ( $\text{CDCl}_3$ ) of **CC13** solution passed through SPE resins A-E, compared to **CC13** taken directly from the high-throughput (HT) screen, and pure **CC13** formed using conventional batch synthesis. \* shows peaks corresponding to **CC13**.

Overall, this study shows the potential for implementing scavenger resins through SPE purifications in future high-throughput workflows. Whilst there were some issues with maintaining a consistent flow rate, **CC13** was purified successfully using an SPE resin (**Figure 2.12**, Resins A-C), which shows the potential for using this method to purify organic cages. However, given the purification was found to not translate well to another novel cage, **CC21**, this approach needs further investigation before implementing into future workflows. This might be overcome by screening a larger number of resins with different functionalities, as only a small selection were tested in this study.

After isolating each scrambled cage from the high-throughput screen, each product was analysed using a variety of methods using high-throughput modes to increase the efficiency of data collection. A combination of  $^1\text{H}$  NMR spectroscopy, HPLC, and high-resolution mass spectroscopy (HRMS), were all used to identify successful reactions. Additionally, powder x-ray diffraction (PXRD), provided information on the crystallinity of the samples, with the majority of scrambled cages being poorly crystalline; an example can be seen in **Figure 2.13**.<sup>88</sup> For the **A:B** series, the parent cages (0:6 and 6:0) are semi-crystalline and do not seem to look like the reported PXRD spectra, which could be due to how the solvent was removed during purification.<sup>84,156</sup> One characteristic indicative of a scrambled cage mixture is that the cage distributions are governed by the diamine feed ratio. As a result, a distribution of products can be seen in the HPLC chromatograms, and can be confirmed by the identification of the corresponding masses in the mass spectra. The combined data for each scrambled cage family (**A<sup>n</sup>:X<sup>6-n</sup>** where **A** and **X** are the diamine number, and **n** is the number of amine equivalents used) were analysed together to compare the variation in changing ratio.

Generally, a reaction was deemed successful if it gave sufficient material for subsequent solubility testing ( $\geq 0.2$  g) of reasonable purity ( $\geq 80\%$ ; based on  $^1\text{H}$  NMR data) (**Table 2.3**). For example, the cage family with Amine **D**, *rac*-CHDA, appeared to have a scrambled cage present in good purity, but could not be used in the high-throughput solubility screen due to insufficient quantities being formed through precursor addition error or product being lost during purification – likely to the poor solubility of this cage. While these reactions could arguably be repeated, the reaction yield was low, and therefore the material would not be scalable for use in a porous liquid. Overall, using the selection criteria, 42 reactions gave adequate conversion to either the parent or scrambled cage mixtures to be used in the high-throughput solubility screen, a 72% success rate.

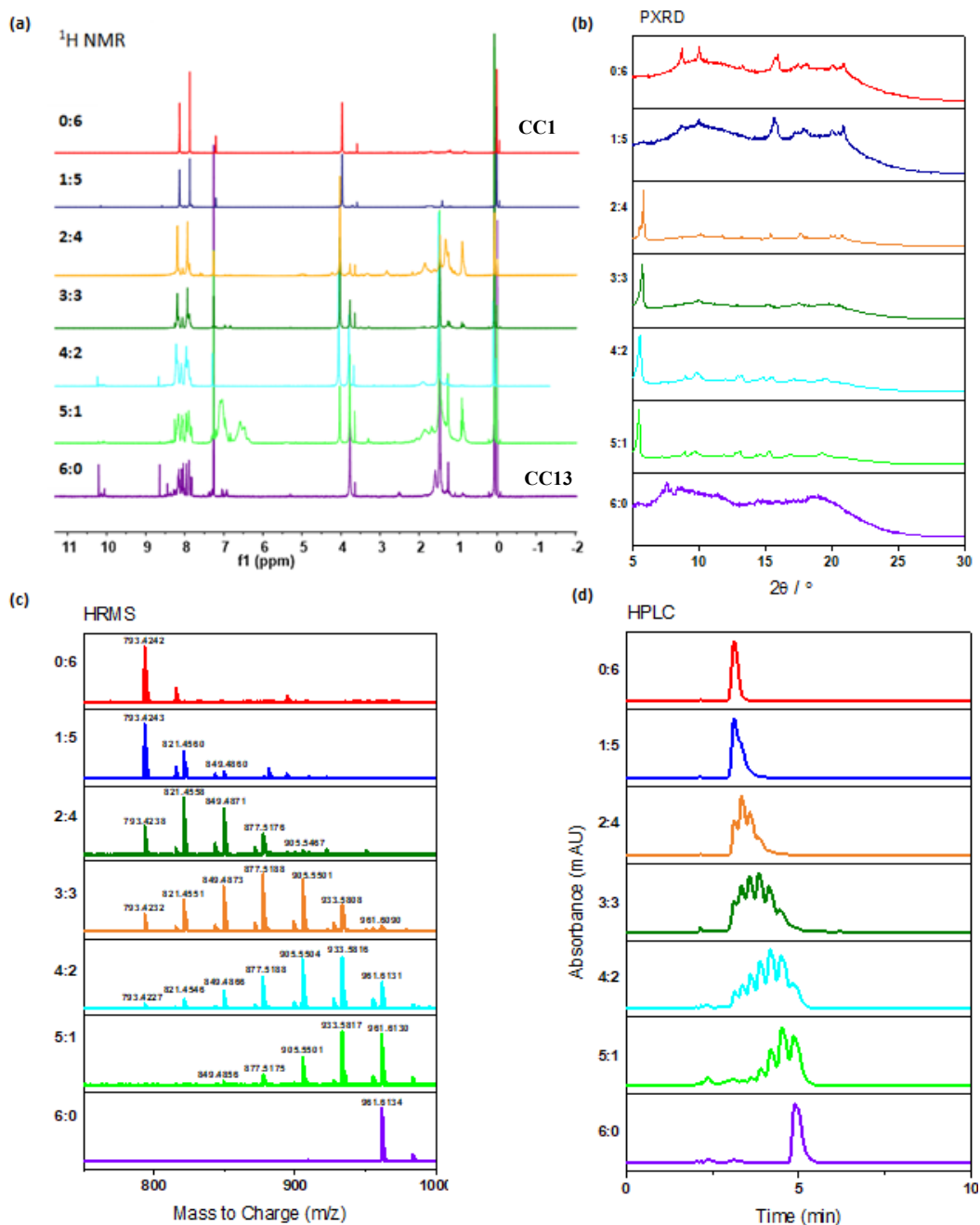
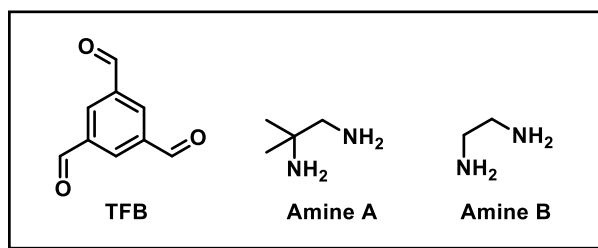
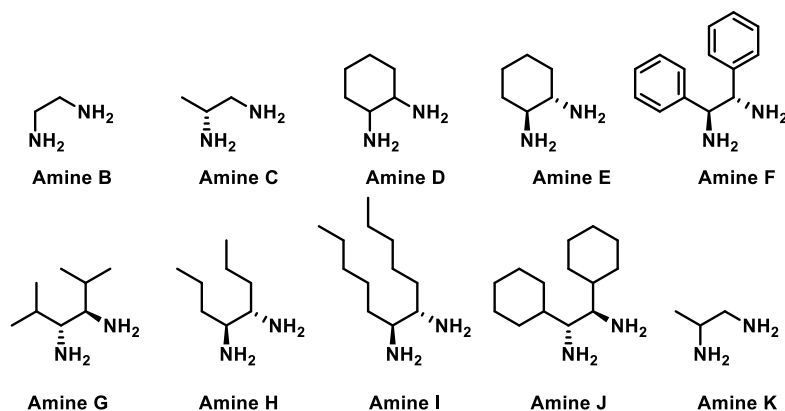


**Figure 2.13:** The structure of the precursors used in the **AB** scrambled cage series, and an example dataset for  $\text{A}^n\text{B}^{6-n}$ : (a)  $^1\text{H NMR}$  spectra in  $\text{CDCl}_3$ ; (b) PXRD patterns showing the formation of semi-crystalline/ amorphous material; (c) HRMS spectra with expected masses observed for  $\text{A}^6\text{B}^0$ ,  $\text{A}^5\text{B}^1$ ,  $\text{A}^4\text{B}^2$ ,  $\text{A}^3\text{B}^3$ ,  $\text{A}^2\text{B}^4$ ,  $\text{A}^1\text{B}^5$ , and  $\text{A}^0\text{B}^6$  at 960.6003, 932.5690, 904.5377, 876.5064, 848.4751, 820.4438 and 792.4125; (d) HPLC chromatograms showing the formation of scrambled cages. The parent cages  $\text{A}^0\text{B}^6$  (**CC1**) and  $\text{A}^6\text{B}^0$  (**CC13**) are shown at the top (red) and bottom (purple) of each set of stacked data respectively.

**Table 2.3:** Summary of scrambled cage reaction outcome (feed ratios of Amine A:Amine X) with structures of the diamine precursors.



Amine	5:1	4:2	3:3	2:4	1:5	0:6
A	-	-	-	-	-	✓
B	✓	✓	✓	✓	✓	✓
C	✓	✓	✓	✓	✓	✓
D	✗	✗	✗	✗	✗	✗
E	✓	✓	✓	✓	✓	✓
F	✓	✗	✗	✗	✗	✗
G	✓	✓	✓	✓	✓	✓
H	✓	✓	✓	✓	✗	✗
I	✓	✓	✓	✗	✗	✗
J	✓	✓	✓	✗	✗	✗
K	✓	✓	✓	✓	✓	✓

Although data collection was efficient, the main challenge was the manual data processing required to determine whether a cage had formed. In order to limit this ‘bottleneck’, full characterisation of the reaction mixtures was not performed – if there was evidence of a cage then the product was investigated further. It is worth noting that high-throughput screening can lead to false negatives, for example, some reactions might not have resulted in cage formation because the selected conditions were not optimal for that product to form. After subsequent solubility testing, any porous liquids that were identified would need scaling up, at which point the synthesis of the scrambled cage component could be explored to increase yield and purity. Overall, a successful high-throughput synthetic workflow was designed for the formation of new scrambled cages, with incorporation of automation and parallel techniques where appropriate (**Figure 2.14**). In the future, this workflow could be streamlined further by implementing a computational screening methodology that could process the large volumes of data quickly, identifying successful reactions from key peaks or characteristics.

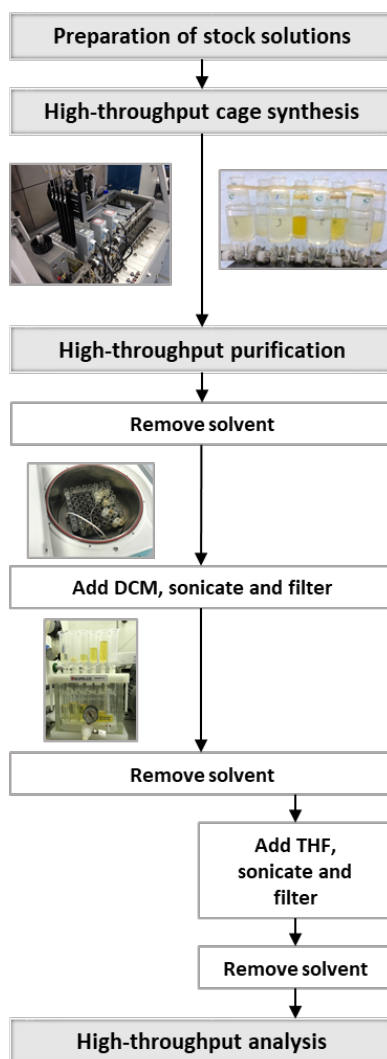


**Figure 2.14:** General scheme showing the overall high-throughput workflow used to synthesise and purify a series of scrambled cages.

## 2.4 Screening for suitable porous liquid solvents

One of the main difficulties in designing a Type II porous liquid is choosing a solvent that is both size-excluded from the cage cavities and is able to dissolve the porous molecule at a high concentration. Additionally, previous work in the group has not focused on studying the solubility trends of POCs. Therefore, identifying suitable solvent-scrambled cage pairings that form Type II porous liquids remains challenging. With such a large scope of possible combinations, a systematic approach was needed to increase the likelihood of discovering hits. In an attempt to address this, a series of preliminary tests were designed to rationalise the choice of size-excluded solvents for use in subsequent high-throughput solubility testing.

### 2.4.1 Solubility screen of scrambled 3<sup>3</sup>:13<sup>3</sup> cage in common laboratory solvents

First, the general solubility trends of a known scrambled cage, 3<sup>3</sup>:13<sup>3</sup> (A<sup>3</sup>:E<sup>3</sup> from the scrambled cage library), were determined in a range of common laboratory solvents, which would then inform the choice of bulkier analogues. These solvents were added in 0.1 mL increments to 30 mg samples of scrambled cage until visual inspection showed the solid had dissolved, or a lower solubility limit of 50 mg mL<sup>-1</sup> had been reached (Figure 2.15). This initial study suggested that certain halogenated and aromatic solvents might be suitable to form porous liquids, with 3<sup>3</sup>:13<sup>3</sup> having high solubility in solvents such as chloroform, trifluoroethanol, and anisole (2-methoxybenzene). Solvents with a low or zero vapour pressure would be preferable for use in a porous liquid, but many of these fell below the hit threshold, including two ionic liquids that were investigated.

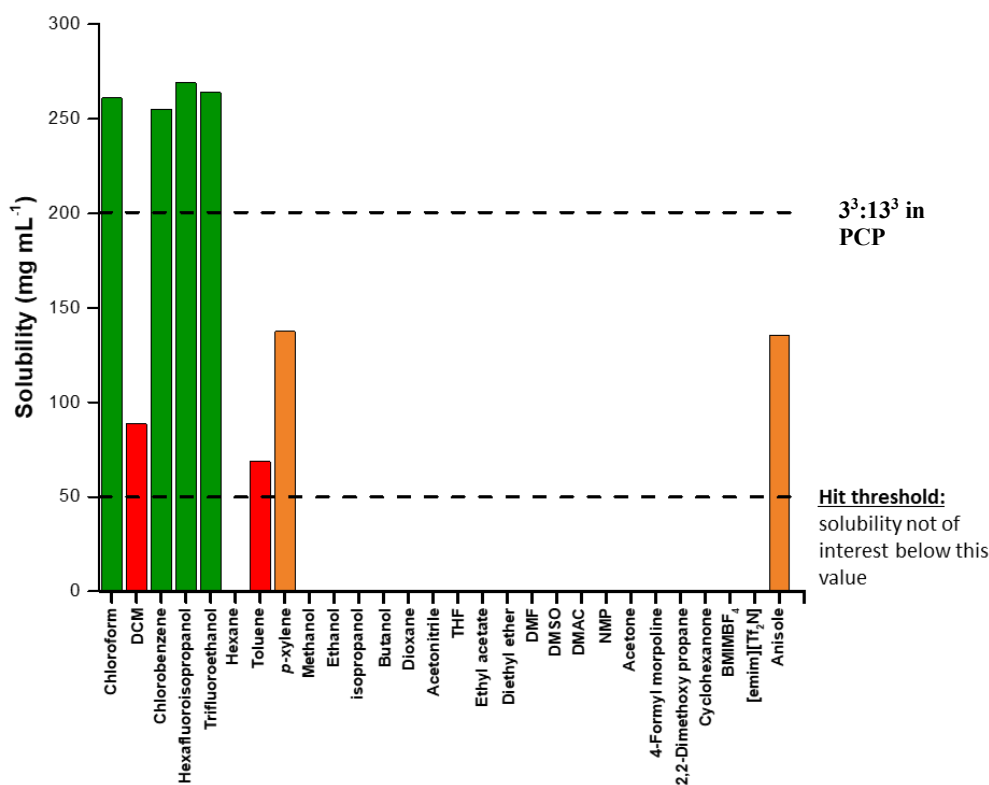


**Figure 2.15:** Comparison of the solubility of scrambled 3<sup>3</sup>:13<sup>3</sup> cage in a range of common laboratory solvents. A lower threshold limit of 50 mg mL<sup>-1</sup> was used (shown as a dashed line), and only a solubility above this threshold was classified as a hit – any that fell below this limit are not shown on the graph as an accurate solubility was not recorded. Green = a high solubility, orange = a reasonable solubility and red = a low solubility.

### 2.4.2 Solubility screen of scrambled 3<sup>3</sup>:13<sup>3</sup> cage in bulky solvents

The results from the common laboratory solubility screen in Section 2.4.1 gave some indication to solvent types in which the scrambled cage (3<sup>3</sup>:13<sup>3</sup>) was highly soluble. These findings were translated into selecting bulkier, less-common analogues to use in forming Type II porous liquids. The scope of the search was narrowed further by only including room temperature liquids with relatively high molecular weights (>100 g mol<sup>-1</sup>), to favour cavity exclusion, and elevated boiling points (>150 °C).

The scrambled cage 3<sup>3</sup>:13<sup>3</sup> was highly soluble in chlorinated (chloroform, chlorobenzene), fluorinated (hexafluoropropanol, trifluoroethanol), methoxy-substituted (anisole), and certain aromatic (chlorobenzene, *p*-xylene) solvents, which informed the choice of several bulkier analogues (Figure 2.16). These were chosen based on having similar functionality but with higher molecular weights. Further, additional solvents with mixed functionality, and bulky equivalents of solvents in which the scrambled cage was poorly soluble, were included for comparison. Using this selection of bulkier solvents, a second solubility screen was conducted using the same procedure and scrambled cage to determine if there was a correlation between the solubility of 3<sup>3</sup>:13<sup>3</sup> in the common smaller laboratory solvents, and the potential size-excluded solvents. The solubility of 3<sup>3</sup>:13<sup>3</sup> was investigated to the same lower solubility threshold value of >50 mg mL<sup>-1</sup> by adding each solvent in 0.1 mL increments - any that fell below this value were not investigated further.

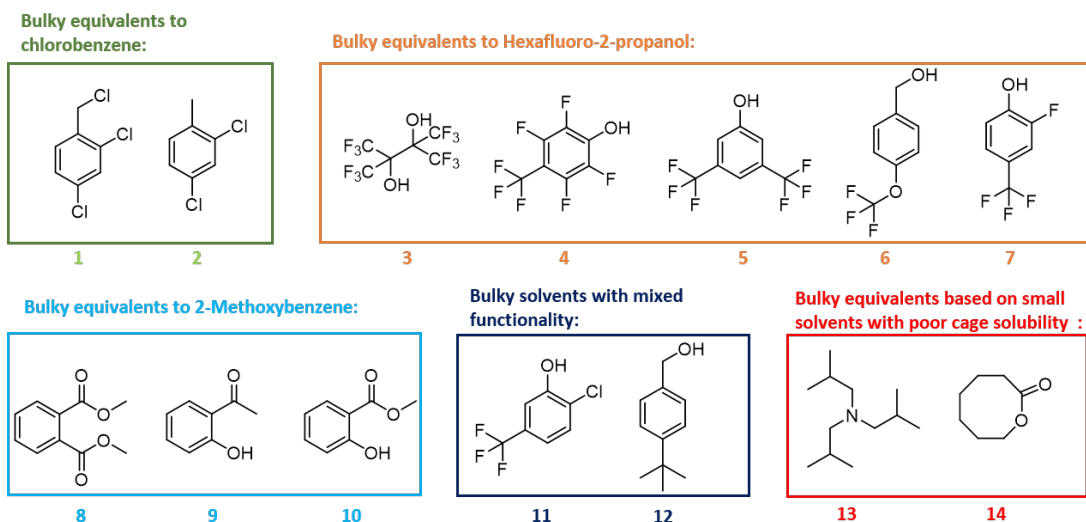
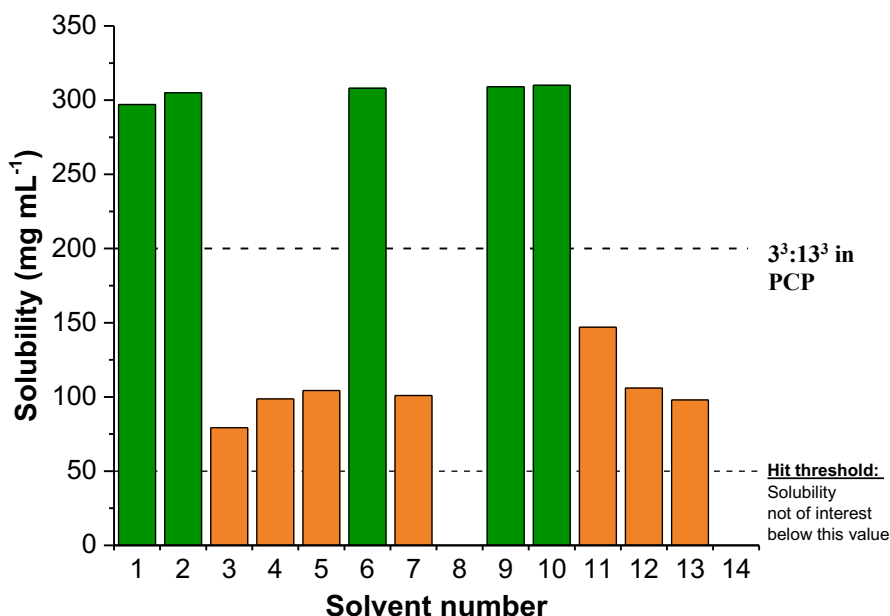


Figure 2.16: Structures of the bulkier solvent analogues used in the solubility screen – solvents are grouped into different families and labelled 1-14.



In this subsequent screen, five bulky solvents in particular were found to dissolve the scrambled cage,  $3^3:13^3$ , at potentially  $\geq 300 \text{ mg mL}^{-1}$  (**Figure 2.17**), which is substantially higher than the concentration of the first Type II porous liquid formed using this scrambled cage ( $200 \text{ mg mL}^{-1}$ ).  $3^3:13^3$  was also reasonably soluble in seven other solvents, all of which were analogues of small laboratory solvents. Therefore, there is potentially a correlation between the solubility in the smaller solvents and their bulkier analogues. The  $3^3:13^3$  cage mixture was also part of the scrambled cage library ( $A^3:E^3$ ), so these new porous liquids would act as control systems and be ‘rediscovered’ during the subsequent high-throughput solubility testing with the top 5 bulky solvents from this screen.



**Figure 2.17:** Solubility screen of the scrambled  $3^3:13^3$  cage in 14 bulky solvents: the highly soluble combinations ( $\sim 300 \text{ mg mL}^{-1}$ ) are highlighted in green; any combinations which fell below a  $50 \text{ mg mL}^{-1}$  solubility threshold (i.e., solvents 8 & 14) were not investigated further.

### 2.4.3 Using xenon displacement to determine size exclusivity

The key requirement of a porous liquid is that the pores remain permanently vacant, and in the case of a scrambled Type II porous liquid, the solvent molecules must not occupy the cavities of the cage. Previous work within the group has demonstrated that gas evolution measurements can give an indication of the gas uptake and selectivity in porous liquids.<sup>112</sup> The addition of a small non-excluded liquid guest, such as chloroform, to a gas-loaded porous liquid, can displace the gas from the cage pores, whereas bulkier size-excluded solvents do not.<sup>13,112</sup> This concept of guest selectivity was adapted here to create a simple test to screen the potential porous liquid solvents, discovered in the bulky analogue solubility screen (**Section 2.4.2**), for cavity exclusion by attempting to displace gas from a known porous liquid.

The xenon gas displaced from the original  $3^3:13^3$  scrambled porous liquid, formed using PCP, was measured for these studies and also compared to neat PCP. A single molecule of xenon can fit inside each cage cavity,<sup>157</sup> which allows the maximum total expected volume of gas to be calculated using the ideal gas equation (**Figure 2.18a**; 4.6 cm<sup>3</sup> for 200 mg  $3^3:13^3$  in 1 mL PCP). For the scrambled  $3^3:13^3$  cage, the cavity and windows are assumed to be the same size as all the scrambled cages in the library, and therefore, if a solvent was found to be size-excluded from  $3^3:13^3$ , it should also be size-excluded for all cages used in the high-throughput screen. Generally, if a significant volume of xenon is released upon addition of a candidate solvent, the solvent in question has entered the cage cavities and is therefore not size-excluded. In contrast, the absence of gas evolution indicates the potential solvent is size-excluded and suitable for use in the high-throughput solubility screen for discovering new Type II porous liquids (**Figure 2.18b**). In this study, a single gas evolution measurement for each potential bulky solvent was used for rapid screening.

**(a) Calculation for expected volume of xenon occupying the  $3^3:13^3$  scrambled cage using the ideal gas equation:**

$$V_{Xe} = \frac{nRT}{P} = \frac{(0.192 \times 10^{-3}) \times 8.31 \times 298}{101325} = 4.6 \text{ cm}^3$$

Mass of cage used	200 mg
Moles of cage	0.192 mmol
MW	1039.34

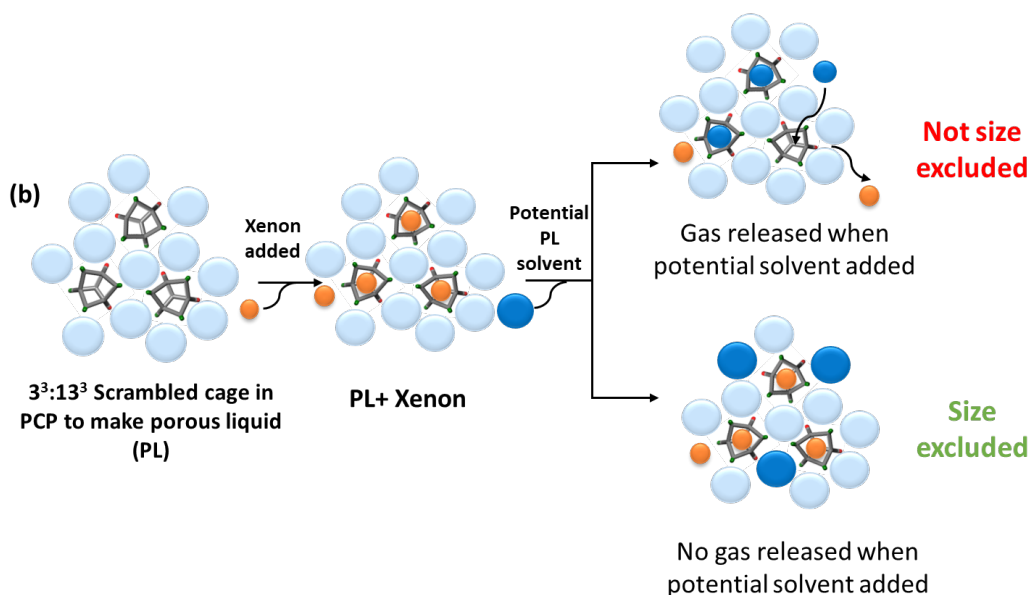


**Figure 2.18:** (a) Calculation showing the expected total volume of xenon to be evolved from a sample of scrambled porous liquid using 200 mg of cage and the ideal gas equation; (b) Scheme illustrating the size-exclusion screen for potential porous liquid solvents – each candidate solvent was added to a known xenon-loaded porous liquid (20% w/v  $3^3:13^3$  in PCP). If little or no gas was evolved upon solvent addition, the solvent was deemed to be size-excluded.

Therefore, each potential porous liquid solvent that had reasonable to high solubility in **Section 2.4.2** was added to a sample of xenon-saturated porous liquid (20% w/v  $3^3:13^3$  in PCP), and the volume of xenon evolved was recorded. All of the potential candidate solvents appeared to displace very little xenon from the porous liquid, indicating they are size-excluded from, or have unfavourable binding with, the cage cavities (**Figure 2.19**). The small volume that was displaced on addition is comparable to that evolved from the neat parent solvent, PCP, which suggests the xenon evolved is not due to displacement from the cage cavities. One possible explanation for the small volume displaced from PCP is a decrease in gas solubility in the neat solvent to differing extents on addition of the potential size-excluded solvents, resulting in different quantities being released. This will be due to the different base solubility of xenon in the new potential solvents, which is studied in **Chapter 4** alongside the corresponding porous liquids. After the bulkier solvent had been added, an additional equivalent of chloroform was added to displace any remaining xenon from the porous liquid to demonstrate the total gas uptake of the system.

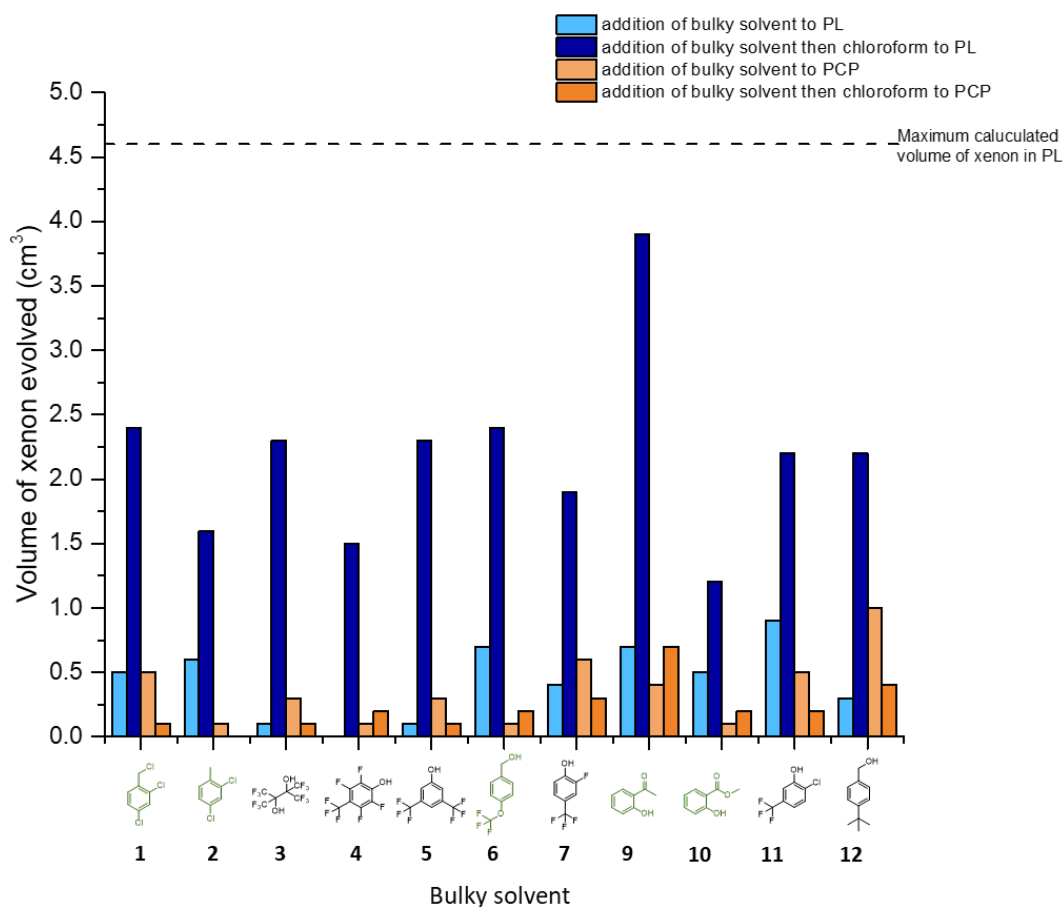


**Figure 2.19:** Comparison of the amount of xenon evolved when a series of potential porous liquid solvents (shown along the bottom axes) were added to the original scrambled  $3^3:13^3$  porous liquid (200 mg in 1 mL PCP, 20% w/v) and the neat solvent, PCP. Green = solvents that were both highly solubilising and size excluded.

Of all the potential solvents tested, five were selected for use in subsequent high-throughput solubility screening, with the eventual aim being the discovery of new Type II porous liquids. Not only did they dissolve the scrambled  $3^3:13^3$  cage at a higher concentration than the previously reported scrambled porous liquid ( $300 \text{ mg mL}^{-1}$  vs  $200 \text{ mg mL}^{-1}$ ), they were deemed cavity-excluded in the xenon displacement study (**Figure 2.20**).

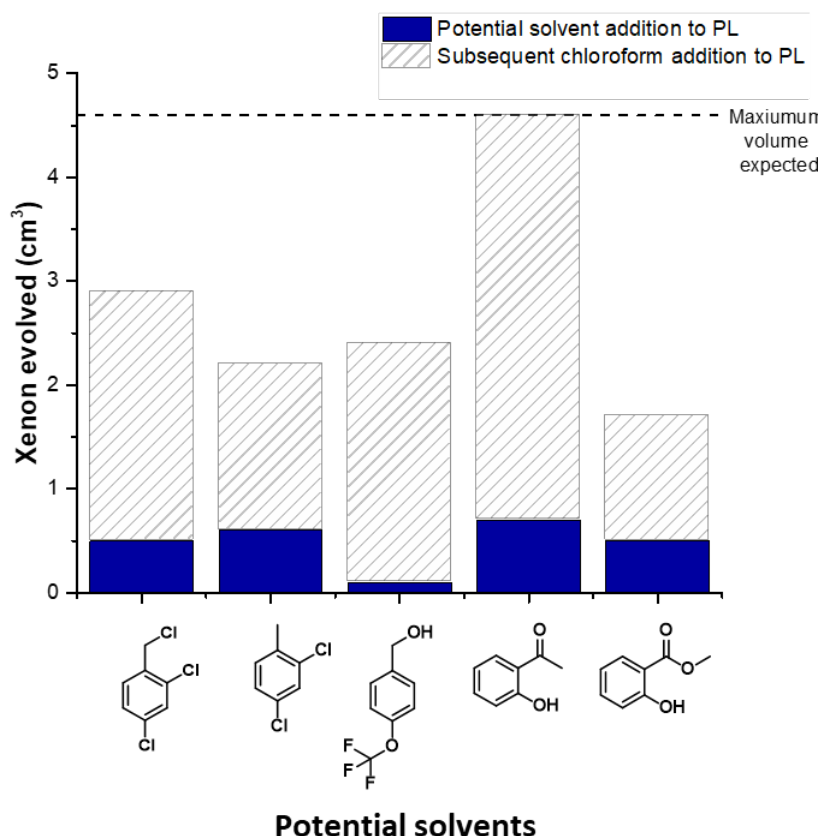


**Figure 2.20:** The five highly solubilising candidate solvents all displaced small volumes of xenon from the known porous liquid (blue bars), but not equating to the total volume in the system, as demonstrated by a subsequent addition of chloroform (grey bars). It could be concluded that the candidate solvents were size-excluded from the cage cavities.

## 2.5 High-throughput solubility screen

The five best solvents that were both size-excluded and dissolved the most scrambled  $3^3:13^3$  cage ( $A^3:E^3$ ,  $\geq 300 \text{ mg mL}^{-1}$ ), along with PCP, were selected for use in the high-throughput solubility screen to target Type II porous liquids (**Figure 2.21a**). First, using a Chemspeed Swing automated platform (**Figure 2.21b**), the scrambled cages were dispensed into vials as stock solutions ( $0.1 \text{ mL}$  portion of a  $300 \text{ mg mL}^{-1}$  concentration in chloroform) to remove the need for manual and repetitive weighing of small masses. Liquid dispensing of stock solutions was used, rather than dispensing solids directly on the platform, due to the physical nature of the scrambled cages. These ranged from fine powders to waxy or glassy solids, which made

them challenging to handle using a solid dispenser. After the addition of appropriate stock solutions, the solvent was then removed under reduced pressure and the vials subsequently dried in a vacuum oven at 90 °C to ensure all samples were fully desolvated prior to solubility testing.

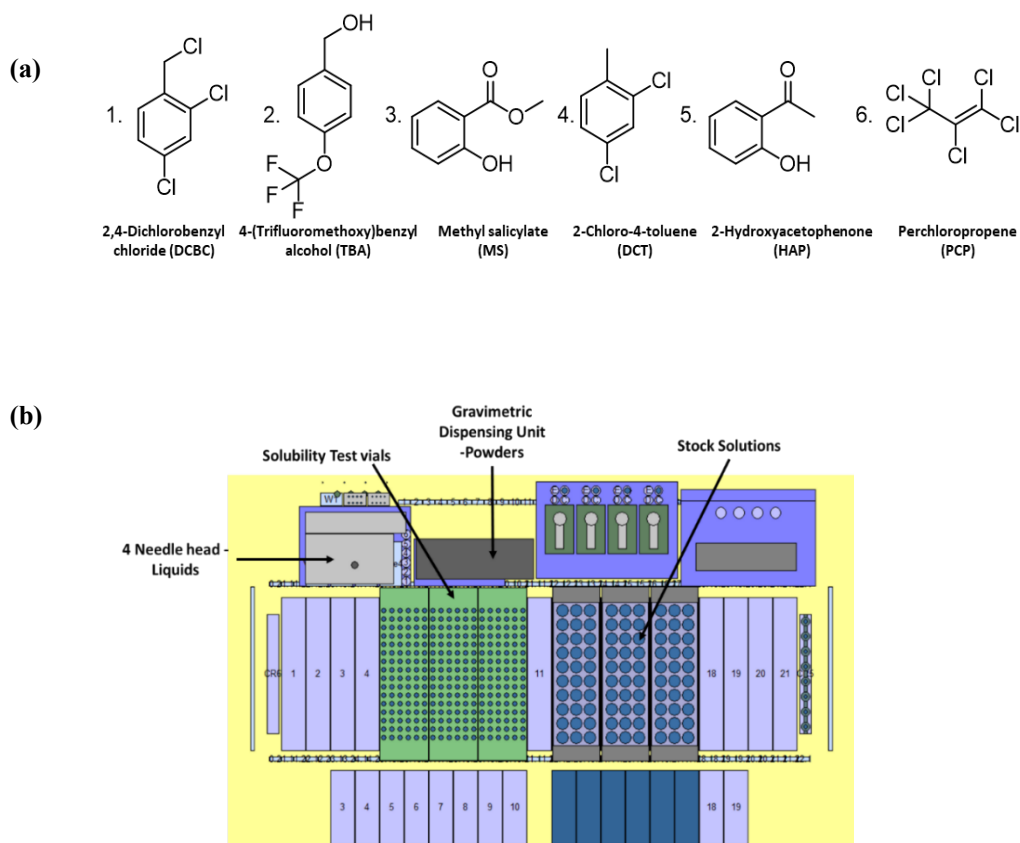


**Figure 2.21:** (a) The six size-excluded solvents used in the high-throughput solubility screen. (b) Graphical layout and photograph of the Chemspeed Swing platform used during the high-throughput solubility testing.

The high-throughput solubility screen utilised the same automated liquid dispensing to add the selected size-excluded solvents in 0.1 mL increments to each scrambled cage in the library. A 300 mg mL<sup>-1</sup> upper limit was set in order to conserve material, because reaching this value would give ‘hits’ with a concentration already ~50% greater than the previously reported scrambled cage porous liquid (**3<sup>3</sup>:13<sup>3</sup>** in PCP, 200 mg mL<sup>-1</sup>). Any combinations that achieved the upper limit would be scaled up to determine a maximum concentration, and their porosity subsequently investigated. Since there are known combinations that form solutions at high concentrations, the lower boundary was capped at 100 mg mL<sup>-1</sup> (3 × 0.1 mL additions) and any that fell below this value were not investigated further. The sample was manually inspected after each addition to determine if the solid had fully dissolved.

Overall, a streamlined methodology for rapid, high-throughput solubility testing was devised and implemented in screening the solubility of a scrambled cage library in six pre-determined size-excluded solvents (**Figure 2.22**) – a total of 357 potential porous liquid combinations. In doing so, the time efficiency of the process was improved compared to manual solubility testing, with a large number of additions being performed at a faster rate. To ensure the small volume dispensed by the platform was reliable and would not introduce a large potential for error, several empty vials were distributed in each run to act as controls to check the platform was dispensing the correct volume of solvent. Overall, the automated liquid dispensing was more accurate, and had a lower margin for error than repetitive, manual solvent additions.

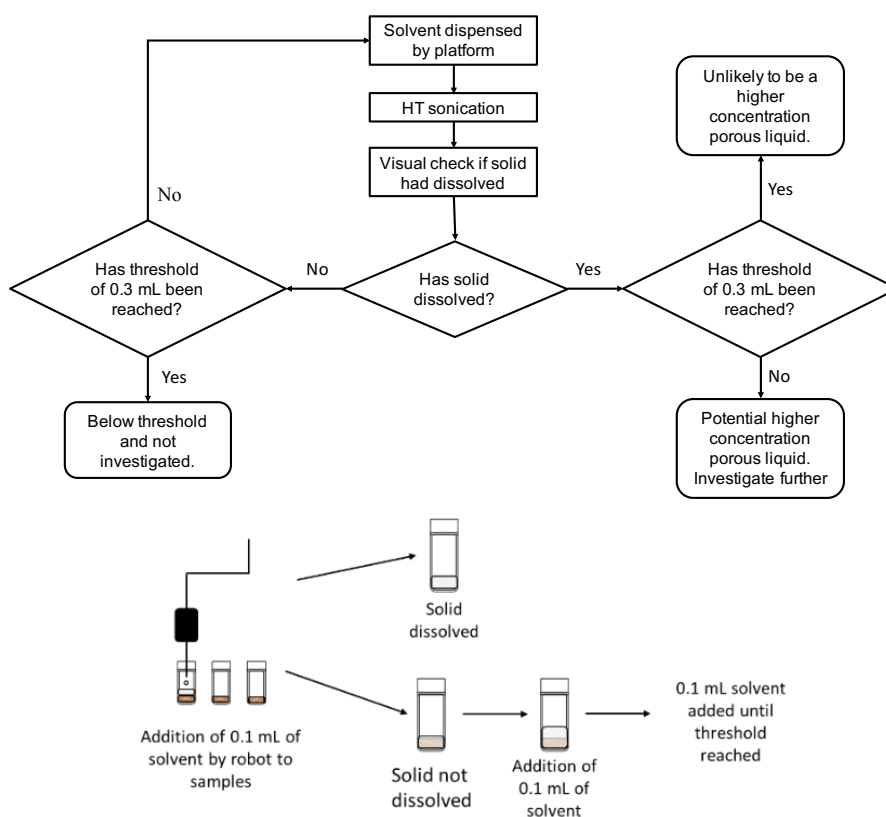


**Figure 2.22:** Graphical representation of the methodology used during the high-throughput solubility screen with size-excluded solvents

A key factor to take into account when calculating concentration and solubility is that the scrambled cages used are isolated as mixtures. As it is non-trivial to calculate an average molecular weight for scrambled mixtures of cages, the molecular weight of the pre-dominant cage species formed based on the diamine feed ratio was calculated (see **Table 2.4** for an example of  $A^3:E^3$ ).

Table 2.4: Calculating the average molecular weight for scrambled cage  $A^3:E^3 - 1039.43$

Precursor	Chemical formula	Equivalents	MW in cage
TFB	$C_9H_6O_3$	4	264.46
Amine A	$C_4H_{12}N_2$	3	342.58
Amine E	$C_6H_{14}N_2$	3	648.58
Sum =			1255.61
Minus $12H_2O$			1039.43

The high-throughput solubility screen found 40 new scrambled cage/bulky solvent pairings with a solubility  $\geq 300$  mg mL<sup>-1</sup>, and a further 27 with a similar concentration to the original scrambled porous liquid ( $3^3:13^3$  in PCP). Overall, 250 combinations were within the threshold limits ( $\geq 300$ -100 mg mL<sup>-1</sup>), a 70% success rate (Figure 2.23). Generally, it appeared that the most soluble scrambled cages were those formed with a 3:3 feed ratio of diamines (Figure 2.24a). This particular distribution of scrambled cage species could potentially give the most soluble mixtures because the 3:3 distributions are ‘maximally scrambled’, and therefore most effectively lower the lattice energy required to solubilise these materials. Additionally, the scrambled combinations using amines A:G gave the most hits above the solubility threshold (Figure 2.24b), suggesting that the addition of isopropyl substituents aids in solubilising the scrambled cage, perhaps due to the periphery disrupting solid state packing causing inefficient arrangement of molecules and lowering the lattice energy.

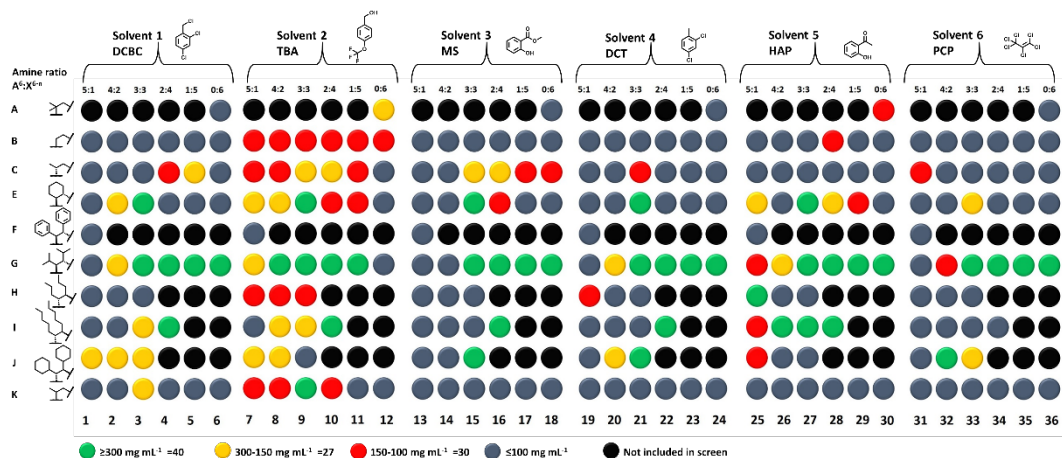
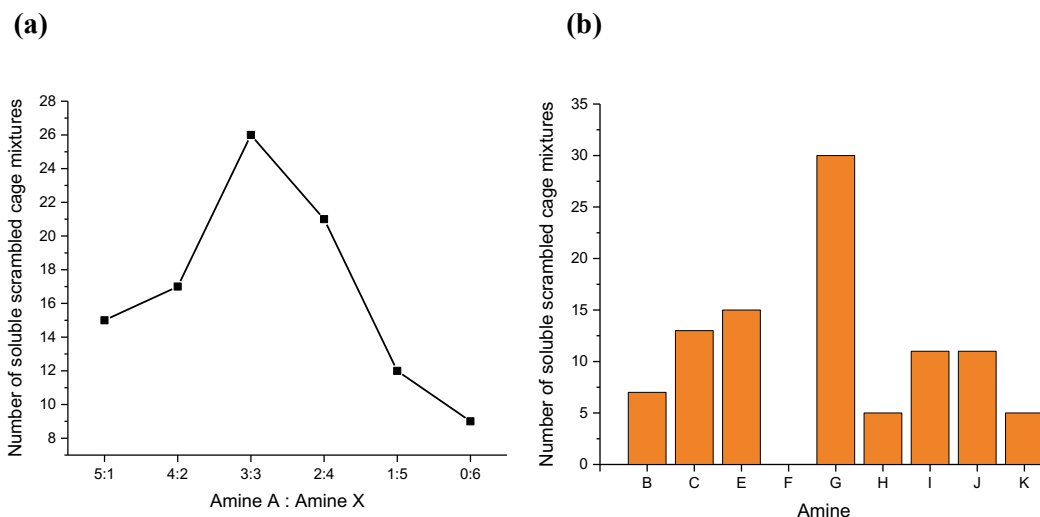


Figure 2.23: Graphical summary of the results from the high-throughput solubility screen – the solubility of the scrambled cage library was tested in six different bulky solvents (5 new solvents, plus PCP). A ‘hit’ was determined to be a cage/solvent combination with a concentration  $\geq 300$  mg mL<sup>-1</sup> (green); cage-solvent combinations with a concentration between 150 and 300 mg mL<sup>-1</sup> shown in yellow; 150 to 100 mg mL<sup>-1</sup> in red; combinations below the 100 mg mL<sup>-1</sup> threshold are shown in grey. All combinations involved diamine A. Each potential porous liquid was assigned a name based on the partner scrambling amine used in the high-throughput synthetic screen (A-K, left), plus a number assigned to each solvent/scrambling ratio combination (1-36, bottom); for example, the 3:3 scrambling ratio of diamine A with diamine B in solvent 2 is B9; the 2:4 scrambling ratio of diamine A with diamine I in solvent 3 is I16, etc.



**Figure 2.24:** Graphical representation of the number of soluble scrambled cage mixtures for (a) each diamine ratio between  $\geq 300$  and  $100 \text{ mg mL}^{-1}$ , and (b) each scrambling diamine.

Overall, the incorporation of high-throughput screening, alongside determining solubility trends and pre-screening for size-exclusivity, has streamlined the discovery of potential Type II porous liquids.

## 2.6 Scale up of highly soluble scrambled cage/solvent combinations

With 40 highly soluble scrambled cage/solvent combinations, and therefore 40 new potential Type II porous liquids with a higher concentration than the originally reported system, the next step was to scale up and study their gas uptake in more detail. However, given PCP (solvent 6) was used in the first porous liquid system and has inherent problems with toxicity, availability, and purification, these combinations were removed from further study. For the remaining combinations, both the solvent needed purifying, and the scrambled cages scaled up and purified, prior to studying their capability for gas uptake, which is discussed in **Chapter 4**.

### 2.6.1 Purification of solvents

Impurities in the solvent used to form Type II porous liquids can lead to a reduction in overall gas uptake, which has been observed in previous work.<sup>112</sup> Trace impurities, if they are small enough, can occupy the cage cavities and compete with other guests. With any new size-excluded solvent, it was therefore important to ensure they were pure enough that the gas uptake of the resulting porous liquids was not affected.

Therefore, the size-excluded solvents used in the high-throughput screen were purified using a variety of methods. To determine if the use of purified solvents in the porous liquids



improved uptake, they were combined with the scrambled cage  $3^3:13^3$  ( $A^3:E^3$ ), and the xenon displacement experiments repeated. As the xenon uptake had already been investigated when choosing the new size-excluded solvents, an expected evolved volume was already known, and so a direct comparison could be made. Additionally, if there was not a clear reduction in impurity peaks in the solvent's  $^1H$  NMR spectra after purification, gas evolution would confirm if there was any improvement in solvent purity.

For most systems, an increased amount of xenon was evolved from the porous liquid after distillation of the solvent, with 2,4-dichlorobenzyl chloride (solvent 1, DCBC), methyl salicylate (solvent 3, MS), and 2-hydroxyacetophenone (solvent 5, HAP), showing improvement with a significant order of magnitude (**Figure 2.25**). Subsequent measurements for porous liquids using these solvents were therefore carried out with distilled solvents, dried over molecular sieves and stored under an inert atmosphere, in order to prevent uptake of moisture.

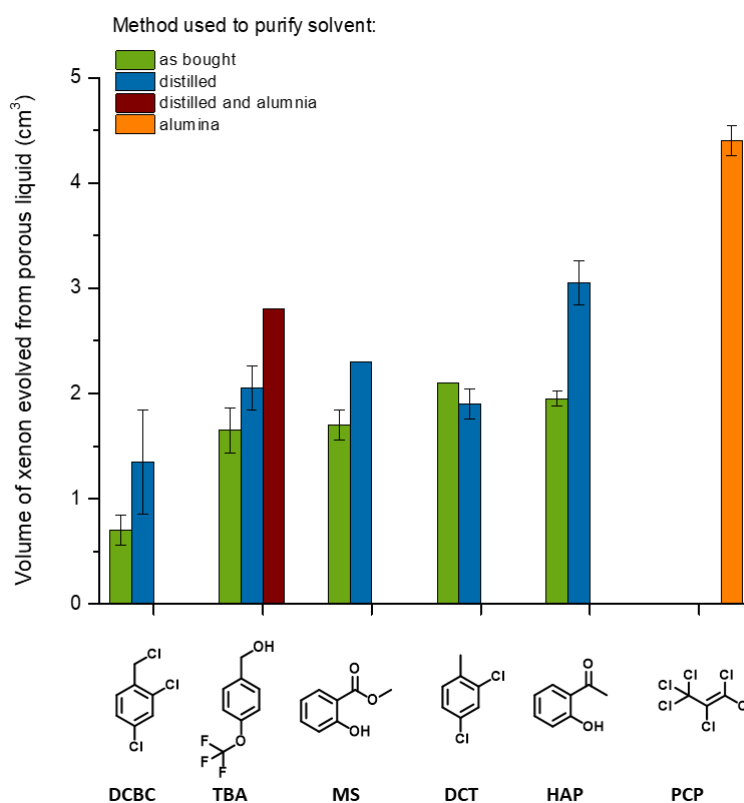


**Figure 2.25:** Comparison of the volume of xenon released from porous liquids using scrambled  $A^3:E^3$  cage in the solvents purified using a number of different methods. Purifying the solvent before use is important as this can increase the gas uptake in the resulting porous liquid.

4-(Trifluoromethoxy)benzyl alcohol (solvent 2, TBA) and 2,4-dichlorotoluene (solvent 4, DCT) were purified by distillation, but minimal improvement in gas evolution was observed. A small scale purification screen was therefore attempted with different resins (silica, alumina, and Celite<sup>®</sup>) as, in previous work, perchloropropene (solvent 6, PCP) has been purified using basic alumina to give improved gas uptake.<sup>112</sup>

For TBA (solvent 2), a marginal improvement in xenon uptake was observed after distillation, although not to the same extent as the other solvents. The neat solvent was then passed over an alumina plug to determine if this would remove more of the impurities. The resulting <sup>1</sup>H NMR spectra showed a higher reduction in impurities, and the corresponding porous liquid also showed an improvement in xenon uptake (**Figure 2.26**). Therefore, TBA was purified by distillation and by passing through basic alumina before using in a porous liquid in subsequent studies.

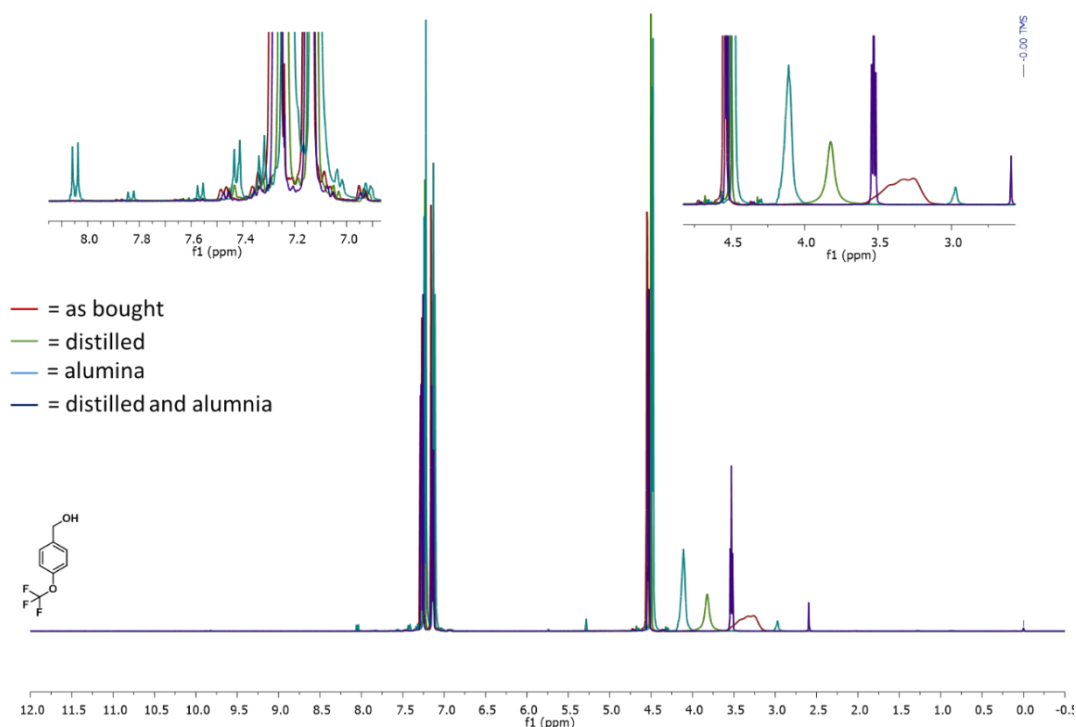


**Figure 2.26:** Overlaid <sup>1</sup>H NMR spectra (CDCl<sub>3</sub>) for 4-(trifluoromethoxy)benzyl alcohol (solvent 2, TBA) as bought and after purification using different methods.

Distillation of DCT (solvent 4) before use did not appear to show any improvement in the gas uptake of the corresponding porous liquid (**Figure 2.27**). Therefore, other methods of purification were again attempted by passing through different resins. However, little improvement in purity was observed and several showed degradation, with the appearance of additional peaks (**Figure 2.27**). Therefore, DCT was only purified by distillation for subsequent investigations.

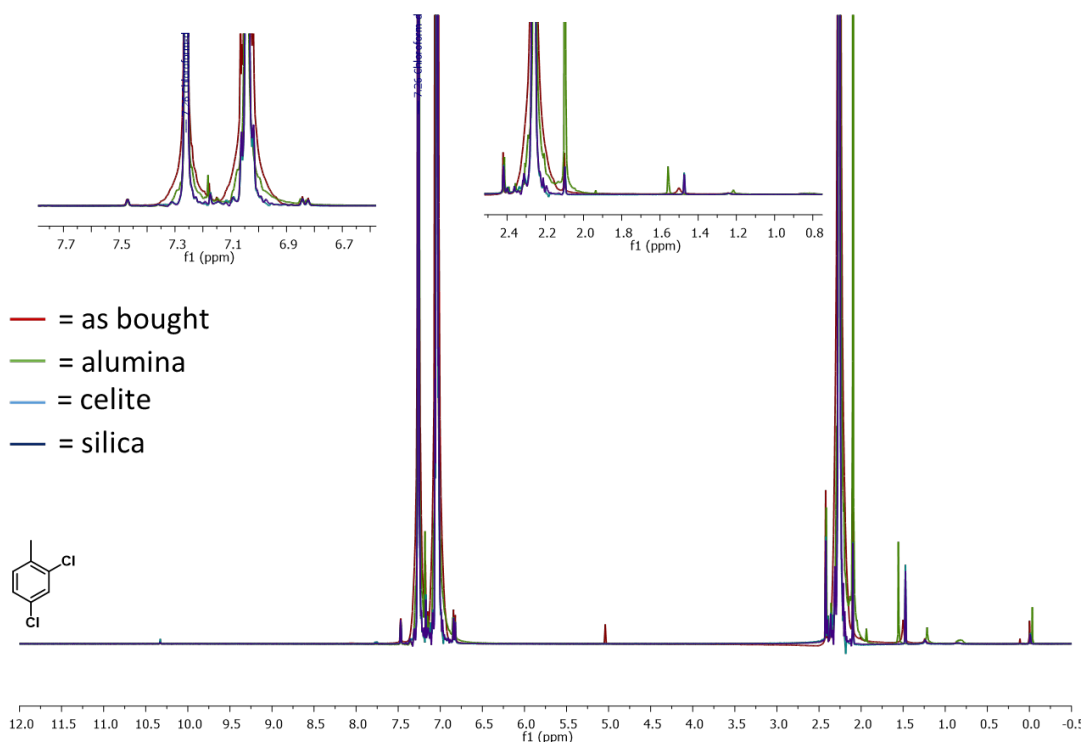


**Figure 2.27:** Overlaid  $^1\text{H}$  NMR spectra ( $\text{CDCl}_3$ ) for 2,4-dichlorotoluene (solvent 4, DCT) as bought and after passing over alumina, Celite<sup>®</sup>, and silica resins.

## 2.6.2 Scale up of scrambled cages

Next, the scrambled cages from the remaining 36 hits were scaled up using conventional batch synthesis, and the reaction conditions optimised. This is because the generalised conditions used for the robotic screen did not necessarily result in the optimal conversion for each specific cage. Depending on the precursors, POCs typically require different reaction conditions to form, which can include elevated temperatures and different reaction solvents. A minimum purity of 95% was targeted to ensure small oligomers did not affect the gas uptake of the subsequent porous liquids. Overall, the synthesis of  $\text{A}^3:\text{E}^3$ ,  $\text{A}^4:\text{G}^2$ ,  $\text{A}^3:\text{G}^3$ ,  $\text{A}^2:\text{G}^4$ ,  $\text{A}^1:\text{G}^5$ ,  $\text{A}^5:\text{H}^1$ ,  $\text{A}^4:\text{I}^2$ ,  $\text{A}^3:\text{I}^3$ ,  $\text{A}^2:\text{I}^4$ , and  $\text{A}^3:\text{K}^3$  were scaled up and optimised (**Figure 2.28**).

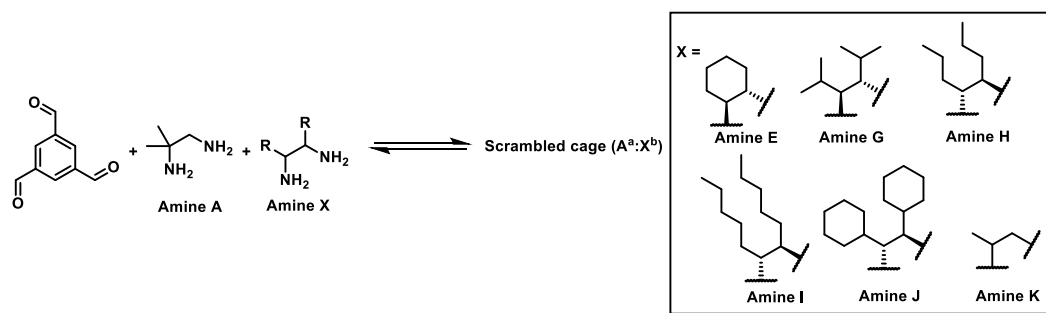


**Figure 2.28:** General scheme for the formation of scrambled cages from 1,3,5-triformylbenzene (TFB, 4.0 equiv.) and two vicinal diamines in varying ratios (total = 6.0 equiv.). The result is a statistical distribution of [4+6] cages.

Several of the scrambled cages were found to scale well, with the synthesis  $A^3:E^3$  ( $3^3:13^3$ ) being carried out on a 30 g batch in a 74% yield. The synthesis of this scrambled cage mixture was originally modified by Giri *et al.*, and therefore, reaction conditions that gave a high yield and purity were already known.<sup>13</sup> However, several of the other scrambled cages from the high-throughput screen had not been previously reported, including the  $A:G$  series.

The synthesis of  $A^4:G^2$ ,  $A^3:G^3$ , and  $A^2:G^4$ , were attempted using several different reaction conditions, including solvents, temperature and using the free diamine. However, those used for the high-throughput screen (chloroform at ambient temperature) were found to give the best conversion to the desired scrambled cages. During the scale-up of  $A^1:G^5$ , several conditions were also trialled, which included changing the reaction solvent. Unusually, the parent cage ( $A^0G^6$ ) was isolated when chloroform was used as the reaction medium in the presence of an equivalent of the diamine used to form **CC13** (Amine **A**), whereas the scrambled cage mixture was isolated when DCM was used instead. This gives an interesting insight into the formation of imine cages. Therefore, the formation mechanism and properties of this cage were studied in more detail, which is outlined in **Chapter 3**.

The synthesis of  $A^5:H^1$ ,  $A^4:I^2$ ,  $A^3:I^3$ , and  $A^2:I^4$ , were all carried out in chloroform at ambient temperature during the high-throughput screen. However, previous work has shown that these alkylated cages typically require harsher conditions to form preferentially.<sup>110</sup> Therefore, when the scrambled cages, using amines **H** and **I**, were scaled up, the synthesis was carried out at reflux and the resulting cages were formed in higher purity, as seen by the reduction in side-products in the  $^1H$  NMR spectrum for  $A^2:I^4$  (**Figure 2.29**).

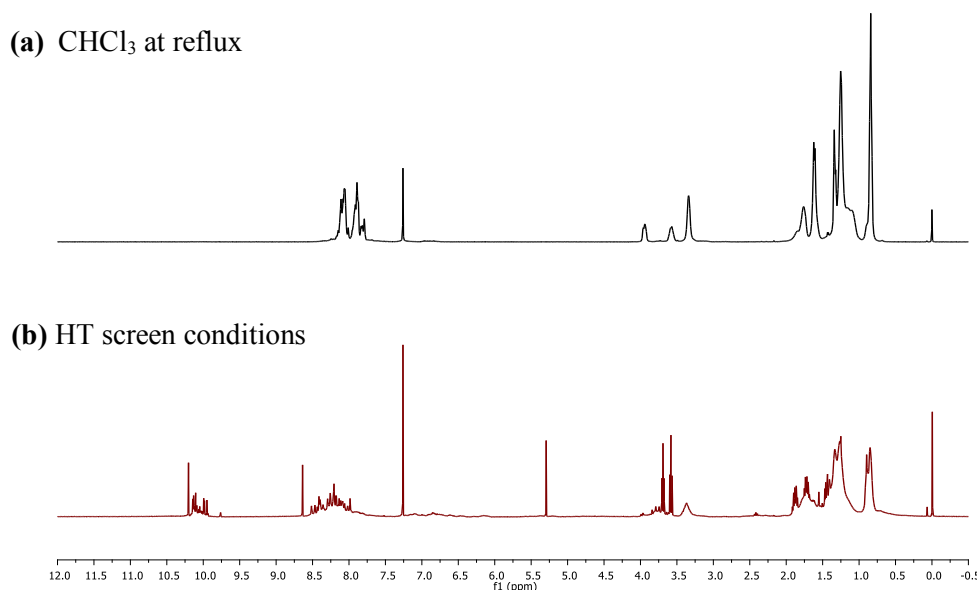


**Figure 2.29:**  $^1H$  NMR ( $CDCl_3$ ) spectra for the synthesis of  $A^2:I^4$  using different conditions: (a)  $CHCl_3$  at reflux, and (b) high-throughput synthesis -  $CHCl_3$  at room temperature.

On scale-up, some combinations from the high-throughput screen that used other custom diamines, such as  $A^3:J^3$ , were lower yielding and contained impurities in spite of multiple purification attempts and screening of different reaction conditions (**Figure 2.30**). These particular scrambled cages would not be suitable to be used in a porous liquid, due to the impurities being able to compete with other guests for occupation of the cage cavities, and were therefore not carried forward.

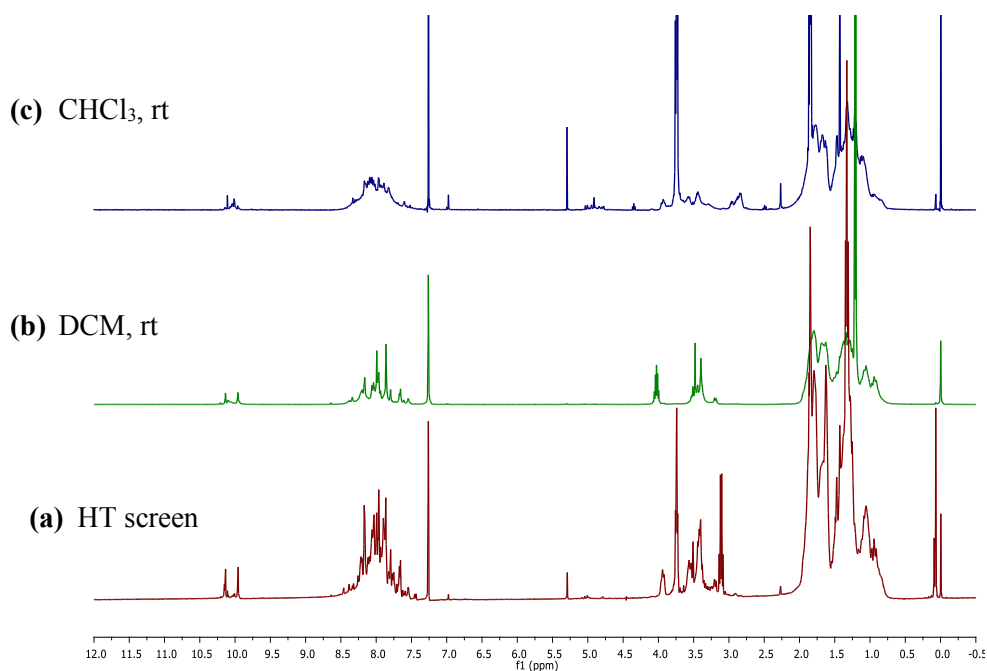


**Figure 2.30:**  $^1\text{H}$  NMR spectra ( $\text{CDCl}_3$ ) for the attempted synthesis of  $A^3:J^3$  in (a) the high-throughput screen, (b) dichloromethane, and (c) chloroform, showing the consistent formation of a large number of impurities.

Finally, other scrambled cages were easily optimised by simply adjusting the reaction solvent.  $A^3:K^3$ , in particular, showed better conversion to the scrambled cage on an 18 g scale in dichloromethane, rather than chloroform, and was isolated in an 89% yield (**Figure 2.31**), which indicates that solvent choice is an important factor in POC synthesis.

Given the importance of ensuring no competing guests can occupy the cavity in a porous liquid, the scrambled cages that possessed poor purity were not studied further, leaving 30 potential systems to investigate as Type II porous liquids in more detail, which is presented in **Chapter 4**.

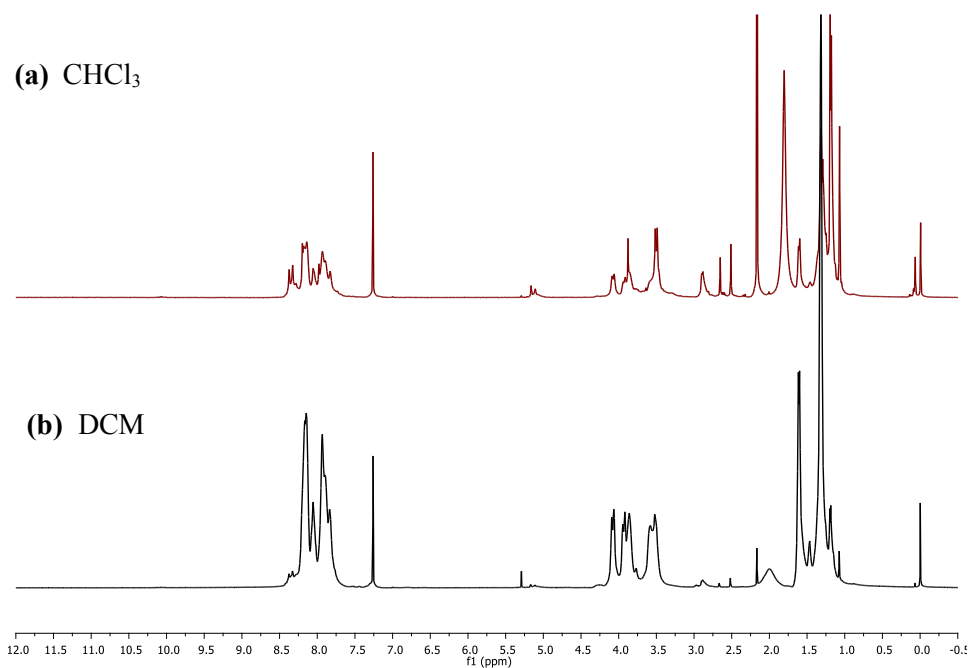


**Figure 2.31:**  $^1\text{H}$  NMR spectra ( $\text{CDCl}_3$ ) for the synthesis of  $\text{A}^3\text{K}^3$  in (a) chloroform, and (b) dichloromethane.

## 2.7 Conclusions

Until now, there have been limited examples of scrambled Type II porous liquids in the literature. This chapter explored how designing a high-throughput workflow could improve the rate of discovering scrambled porous liquids. A methodology was developed that implemented automated platforms and other high-throughput or parallel equipment to streamline the synthesis of scrambled cages, which resulted in a library of 42 systems. Alongside this, a parallel workflow was designed to select pre-determined size-excluded solvents to use in the subsequent solubility testing. Suitable solvent candidates were chosen based on a series of laboratory experiments, which screened for high solubility and size-exclusivity. As a result, 6 solvents were chosen for use in the high-throughput solubility screen. An automation platform was used to dispense a set volume of the size-excluded solvents to test the solubility of the scrambled cages. From this screen, 40 combinations were found to have a concentration at  $\geq 300 \text{ mg mL}^{-1}$ , which was higher than the first scrambled porous liquid ( $200 \text{ mg mL}^{-1}$ ) reported. The solvents from the high-throughput screen were also purified to remove any impurities that would affect the gas uptake of a system, and the scrambled cages were scaled up to give sufficient material to study in further detail. During this process, the formation of a parent cage was observed over a scrambled cage, which is a rare occurrence with these POCs. This gives an interesting insight into the formation mechanism of [4+6] cages and will be investigated in a subsequent chapter. Overall, 30 potential Type II porous liquids were discovered across a range of solvents and scrambled

**Chapter 2:** Using high-throughput automation in the discovery of highly soluble scrambled cages

cage families. This gives the potential to study the effect of changing the components in a scrambled porous liquid on its properties and gas uptake, which is discussed in **Chapter 4**.

**Chapter 3:**  
Study into the formation mechanism  
and properties of an isopropyl-  
decorated porous organic cage



### 3.1 Introduction

#### 3.1.1 Dynamic covalent chemistry of porous organic cages

As porous organic cages are primarily formed through dynamic covalent chemistries such as imine condensations, and rely on the self-assembly of multiple components during their formation, there is often a number of different possible reaction outcomes. For example, as discussed in **Chapter 2**, having several starting diamines in the same reaction mixture can result in a ‘scrambled’ mixture (or statistical distribution) of functionality in the final products.<sup>120</sup> However, this is not the only possible outcome for a multi-component reaction. POCs can undergo self-sorting, which is described as self-recognition between molecules within complex mixtures.<sup>158</sup> This definition can be divided into systems that show an affinity for themselves (*narcissistic self-sorting*) and those that form mixed structures (*social self-sorting*), as illustrated in **Figure 3.1**.<sup>158–160</sup>

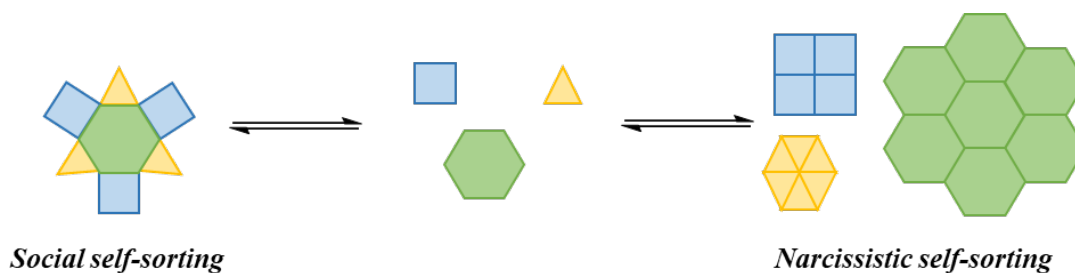


**Figure 3.1:** Graphical representation of the different types of self-sorting; those that show an affinity for themselves (*narcissistic self-sorting*) and those that form mixed structures (*social self-sorting*)<sup>158–160</sup>

The composition of a system is also affected by whether the reaction has reached thermodynamic equilibrium, or a species is trapped under kinetic control.<sup>158</sup> For example, the product can be trapped due to large kinetic barriers, highly stable intermediates, or precipitation.<sup>86,89,160,161</sup> Additionally, the targeted product, such as an organic cage, may not be the most thermodynamically favourable product, and if left to equilibrate further, will form other species including interlocked systems.<sup>134,139,160,162–164</sup>

There are several studies in the literature that explore the dynamic equilibrium of imine-derived POCs. Cooper *et al.* and Lee *et al.* both described the effect of cage scrambling when multiple diamine precursors were used in a one-pot reaction (see **Chapter 2** for details).<sup>10,120</sup> Additionally, the imine cage reported by Lauer *et al.* was also observed as a scrambled distribution when a mixture of trialdehydes (1,3,5-triformylbenzene and 2,4,6-triethylbenzene-1,3,5-tricarbaldehyde) were reacted with a triamine (2,4,6-triethylbenzene-1,3,5-trimethanamine), with the mixed functionality observed by mass spectrometry (**Figure 3.2**).<sup>86</sup>

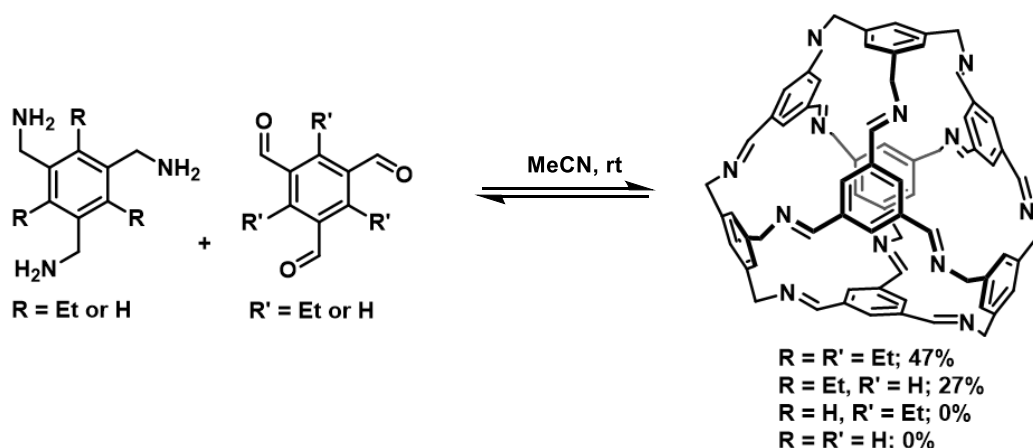


**Figure 3.2:** Porous organic cage presented by Lauer *et al.* which undergoes dynamic covalent scrambling when two different trialdehydes are used.<sup>86</sup>

Other organic cages have been shown to undergo narcissistic self-sorting, which were selective for specific components. Acharyya *et al.* presented a study into the dynamic equilibrium of organic cages formed through the imine condensation between two equivalents of a triamine and three equivalents of a dialdehyde (**Figure 3.3a**).<sup>165</sup> The reaction was found to be specific for a combination of partners (**A<sub>3</sub>D<sub>2</sub>** and **B<sub>3</sub>D<sub>2</sub>**; **Figure 3.3b**), and even when using two triamines and one dialdehyde in a single reaction, this did not result in a cage with mixed functionality. When four precursors were present in one-pot, the same two cages were also observed in the final product composition. The self-sorting could be caused by the poor solubility of the four cages in the reaction solvent ( $\text{CHCl}_3:\text{EtOH}$ , 1:10), with the precipitation of the two fastest forming cages preventing the reaction from progressing further.<sup>160,165</sup> A series of  $^1\text{H}$  NMR experiments (in  $\text{CDCl}_3$ ) of each individual cage formation showed that **A<sub>3</sub>D<sub>2</sub>** and **B<sub>3</sub>D<sub>2</sub>** had the fastest reaction kinetics, and had the highest percentage conversion after 5 hours.<sup>165</sup>

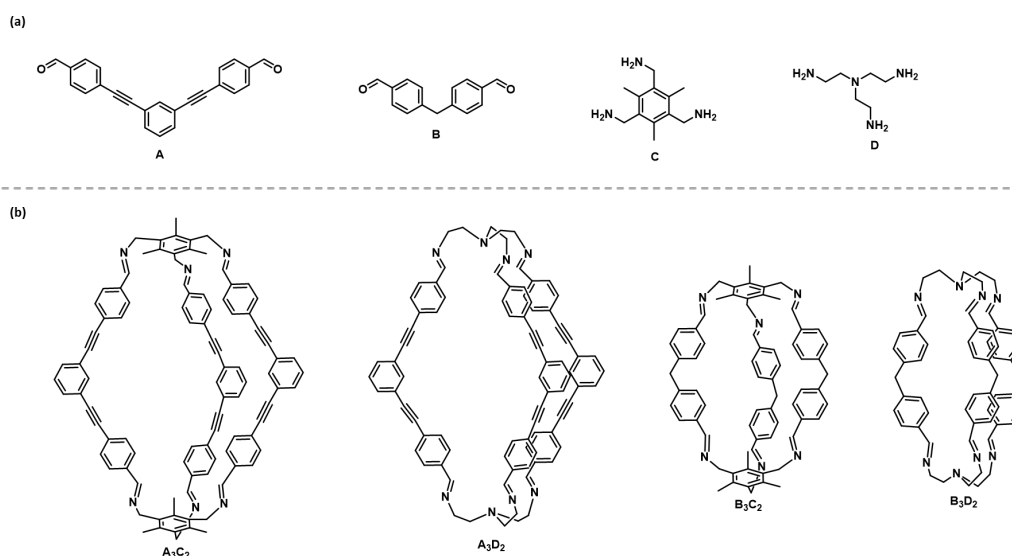


**Figure 3.3:** (a) The four precursors used, and (b) the structures of the organic cages presented by Acharyya *et al.*<sup>165</sup>

Overall, this study demonstrated that the isolated product can be dictated by both entropy and the reaction solvent when several precursors are used during the formation of porous imine cages. This could lead to interesting and unexpected product distributions.

There are also other examples of narcissistic self-sorting during the formation of organic cages using imine condensations. Jiao *et al.* reported a series of tetrahedral and triangular prism cages formed using extended trialdehydes and triamines.<sup>166</sup> The authors showed the conformation of the starting aldehyde precursors influenced the resulting cage structures. In particular, self-sorting could be induced by using two different trialdehyde precursors with tris(2-aminoethyl)amine (**Figure 3.4**). The precursor, 1,3,5-triethyl-2,4,6-tris(4-formylphenyl)benzene, has a twisted conformation due to the steric bulk on the central benzene ring from the alternating ethyl and aryl substituents. This promoted favourable CH- $\pi$  interactions that led to the tetrahedral [4+4] cage being formed. Whereas, when the central benzene ring was replaced with a triazine core to form, 1,3,5-tris(4-formylphenyl)triazine, a [2+3] triangular prismatic structure was formed instead. The more planar precursor meant it was more energetically demanding for this precursor to adopt the required conformation to form the tetrahedral structure. Additionally, using a less substituted variant of the initial precursor, 1,3,5-tris(4-formylphenyl)benzene, resulted in less self-sorting being observed, with the reaction being tuneable towards a particular cage topology depending on the ratio of precursors employed. Changing the ethyl substituent to a hydrogen on this trialdehyde resulted in less steric strain, which meant the precursor could adopt both the twisted and planar conformations, and therefore could form both the tetrahedral and prismatic cages. These studies by Jiao *et al.* illustrate how small changes to the precursors can affect the conformation. The interaction of the precursors can have a drastic effect on what cage structure is formed, and can drive the preference for formation of a particular cage depending on the energy requirements.

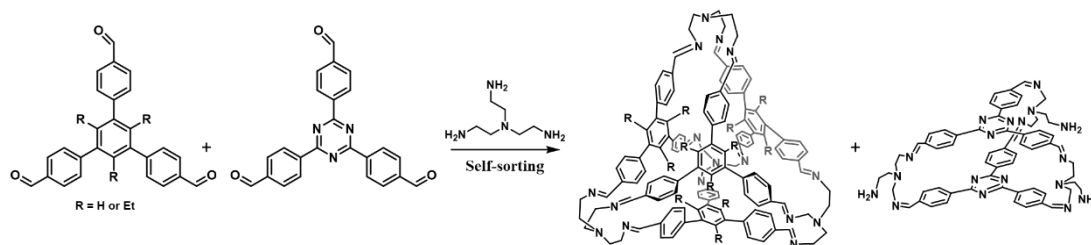


**Figure 3.4:** Reaction scheme showing narcissistic self-sorting of the organic cages formed from extended trialdehydes and tris(2-aminoethyl)amine by Jiao *et al.*<sup>166</sup>

The bond arrangement in precursors was also demonstrated to affect the final cage composition by Beaudoin *et al.*, who reported the chiral self-sorting of [2+3] salicylimine cages (**Figure 3.5**).<sup>167</sup> The reaction between the two isomers of triaminotribenzotriquinacene and bis(salicylaldehyde) resulted in narcissistic self-sorting, which was confirmed in the cage crystal structures. The authors studied the reaction in a range of solvents to observe the effects on the self-sorting process. In most cases, narcissistic self-sorting was observed, except when precipitation occurred during the reaction, at which point a cage containing both isomers was isolated. The mixed cage was isolated due to its lower solubility in ethyl acetate than the other species, therefore, is enthalpically trapped, whereas narcissistic self-sorting is entropically favoured.

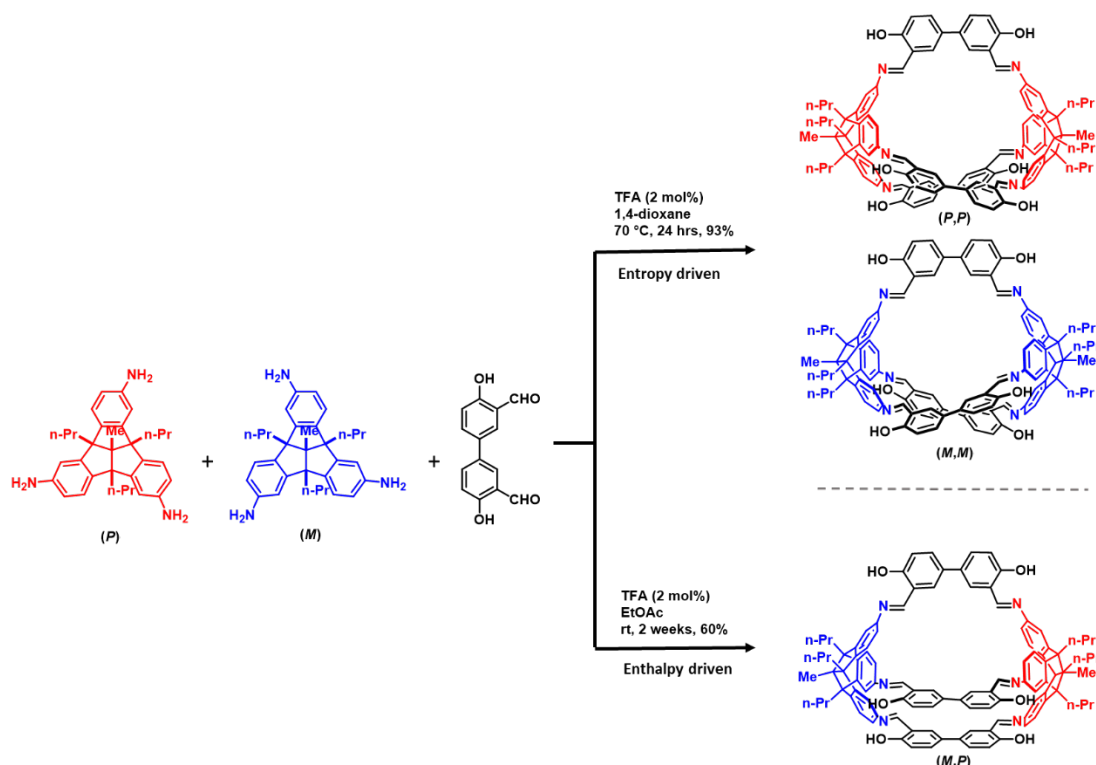


**Figure 3.5:** Structures of the self-sorted [2+3] salicylimine cages reported by Beaudoin *et al.*<sup>167</sup>

For [4+6] imine cages, as discussed in **Chapter 2**, there are very few reports of self-sorting, with scrambling to form statistical distributions typically occurring.<sup>120</sup> An example of chiral self-sorting in these species has been reported, for example, if ( $\pm$ )-*trans*-1,2-cyclohexanediamine (CHDA) is used in the synthesis of **CC3**, a racemic co-crystal is formed from the homochiral derivatives, **CC3-R** (formed from *R,R*-CHDA) and **CC3-S** (formed from *S,S*-CHDA).<sup>168</sup> However, Slater *et al.* discovered the presence of two additional isomers of **CC3**, which contained both *R,R*-CHDA and *S,S*-CHDA in the same cage species in solution, named **CC3-RS** and **CC3-SR**, while the homochiral cages (**CC3-R** and **CC3-S**) precipitated as the racemic co-crystal.<sup>169</sup> Each dissymmetric cage possessed three (*R,R*)-CHDA and three

(*S,S*)-CHDA vertices, with the cyclohexyl groups positioned in different directions. The authors rationalised that the racemic dissymmetric cages are kinetically trapped due to the precipitation of the homochiral enantiomers from solution. Interestingly, these were the only products observed, other than the homochiral cage species, unlike the distribution of  $\geq 12$  mixed cage species observed on scrambling a mixture of two vicinal diamines. Despite varying the ratio of *R,R*-CHDA and *S,S*-CHDA, only the homochiral and 3:3 mixed cages were observed, which suggests these are the most stable enantiomers.

Another example of self-sorting in a [4+6] cage was reported by Slater *et al.*, who synthesised a methylated CC3 derivative (**Figure 3.6**).<sup>170</sup> The authors attempted to synthesise a [4+6] imine cage with an analogue of TFB containing three methyl groups on the aromatic ring ( $\text{Me}_3\text{TFB}$ ). However, despite optimising the conditions, only 1 equivalent of the aldehyde was incorporated into the cage structure, with the other 3 equivalents being TFB. The added steric hindrance from the methyl groups prevented the formation of the expected [4+6] cage. Self-sorting experiments showed a mixture of TFB and  $\text{Me}_3\text{TFB}$  only resulted in **CC14-R**, independent of the aldehyde ratio. Overall, this study demonstrated the sterics of the starting aldehydes can direct the final cage products.

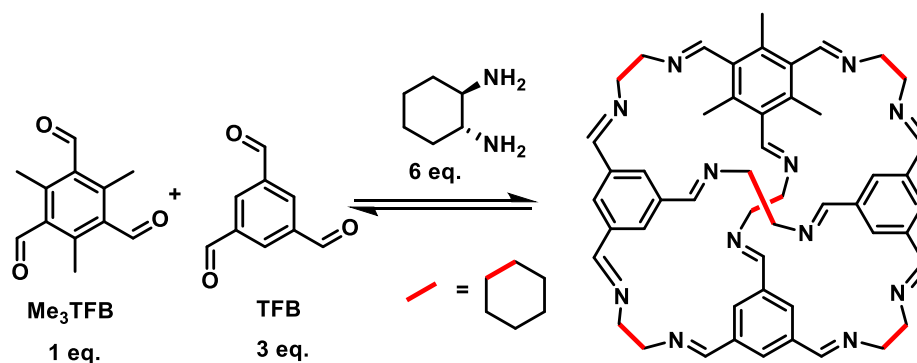


**Figure 3.6:** Reaction scheme for the synthesis of **CC14-R** by Slater *et al.*<sup>170</sup>

Finally, an example of social self-sorting was presented by Greenaway *et al.*, who used a combination of computational prediction and high-throughput screening to discover a three component organic cage pot (**Figure 3.7**).<sup>171</sup> These species were formed from a tri-topic amine, di-topic amine, and a tri-topic aldehyde, that self-assembled into a capsule with an open window. While DFT calculations suggested that the energetic driving force favours narcissistic self-sorting, the socially self-sorted cage pots were the major product in the reaction. There are other factors, such as entropic differences, kinetic trapping, and solvent choice, that can influence the product formed. In this particular example, the entropic contributions were calculated and the advantages were found to outweigh the difference in

energy formation, supporting the argument that the formation of the cage pots was favoured thermodynamically.

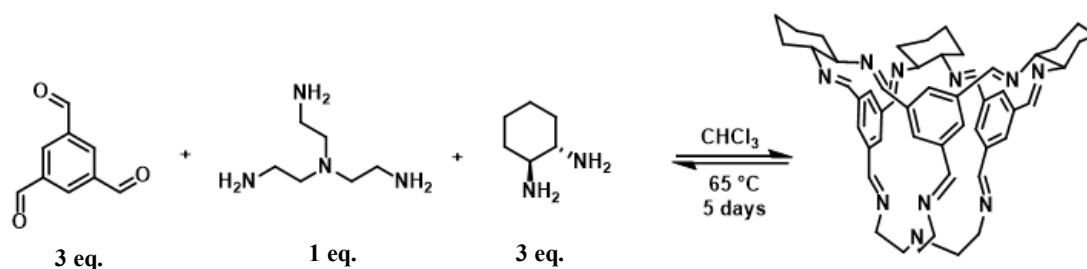
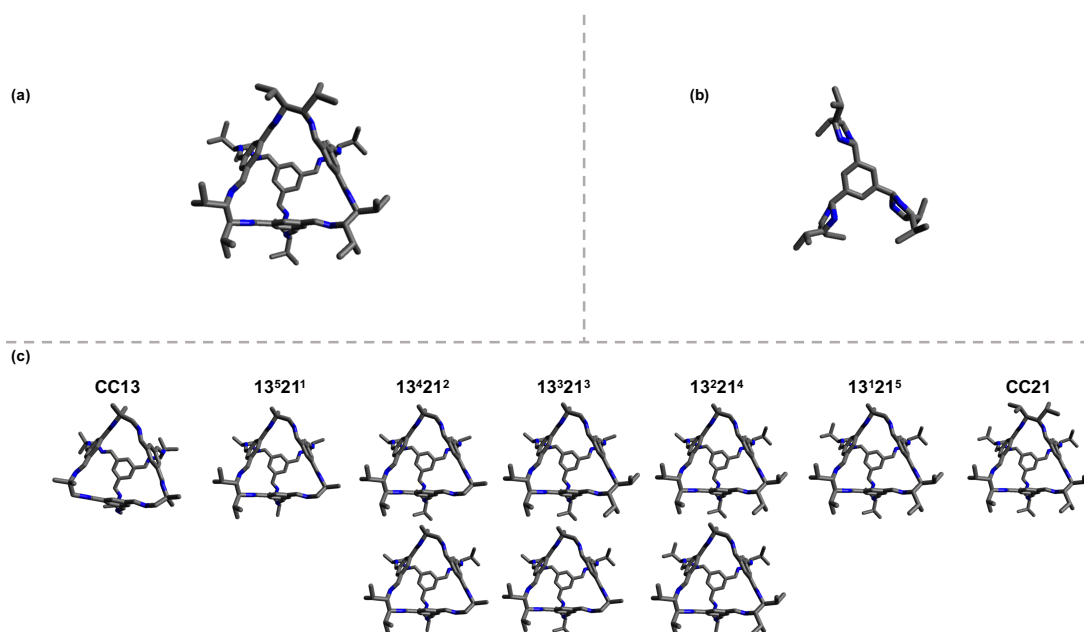


**Figure 3.7:** Synthesis of organic cage pots presented by Greenaway *et al.*<sup>171</sup>

### 3.1.2 Discovery of an isopropyl-decorated porous organic cage using high-throughput screening

Following the high-throughput screen discussed in **Chapter 2**, the highly soluble scrambled cage hits were scaled up and their synthesis optimised. During this process, several reaction conditions were adjusted in order to improve the isolated yield and overall purity of the product. The synthesis of one scrambled cage in particular, **A<sup>1</sup>:G<sup>5</sup>** from the high-throughput screen, illustrated some unusual behaviour when it was scaled up. This scrambled cage comprised of 1 equivalent of 1,2-diamino-2-methylpropane (MPDA, diamine used to form **CC13**) and 5 equivalents of (3*R*,4*R*)-2,5-dimethylhexane-3,4-diamine dihydrochloride (DMHDA, diamine used to form **CC21**), and will be referred to as **13<sup>1</sup>:21<sup>5</sup>** throughout this chapter.

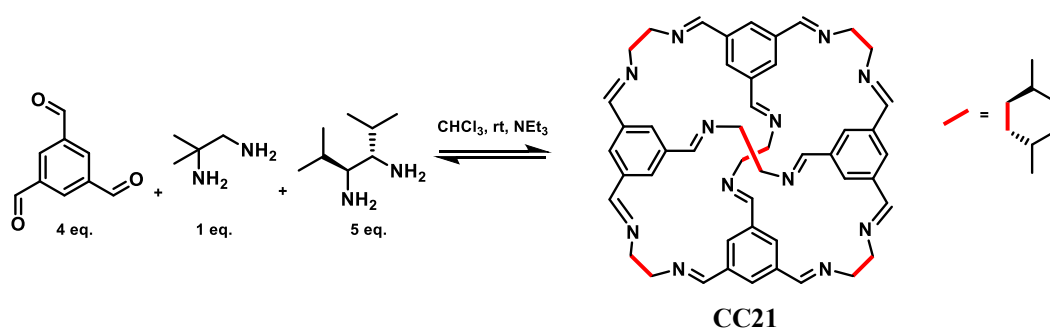
During the scale-up studies of **13<sup>1</sup>:21<sup>5</sup>**, different reaction solvents were trialled as this can affect cage formation, in an attempt to improve the yield of the reaction. When DCM was used as the reaction solvent, the expected scrambled **13<sup>1</sup>:21<sup>5</sup>** cage was observed and isolated by precipitation using methanol. However, when the synthesis of **13<sup>1</sup>:21<sup>5</sup>** was attempted in chloroform on a larger scale, and methanol was added to isolate the product, only the parent cage, **CC21**, (**Figure 3.8a**) was isolated as a single product. Finally, when the same reaction was carried out in the absence of MPDA to target solely **CC21**, the isolated product from the reaction was neither the scrambled cage (**13<sup>1</sup>:21<sup>5</sup>**, **Figure 3.8b**) nor the parent cage (**CC21**), but an alternative amination trimer product with a [1+3] stoichiometry (**Figure 3.8c**). These results prompted us to study the formation and properties of **CC21** in more detail, especially since this cage had not previously been reported.



**Figure 3.8:** Structures of the products isolated during synthetic optimisation for the reaction between TFB, MPDA, and DMHDA: (a) CC21; (b) [1+3]-3H<sub>2</sub>O and (c) scrambled 13<sup>1</sup>:21<sup>5</sup> cage distribution.

### 3.2 Synthesis and characterisation of CC21

As briefly summarised above, when the conditions in the reaction between TFB, DMHDA, and MPDA, were changed, different products were isolated. During the optimisation of 13<sup>1</sup>:21<sup>5</sup>, several factors were changed in an attempt to improve the yield and purity of the final scrambled mixture, which included the reaction solvent (**Table 3.1**). In particular, when chloroform was used, the parent cage (**CC21**) was isolated instead of the expected scrambled cage, albeit in low yield (**Figure 3.9**).

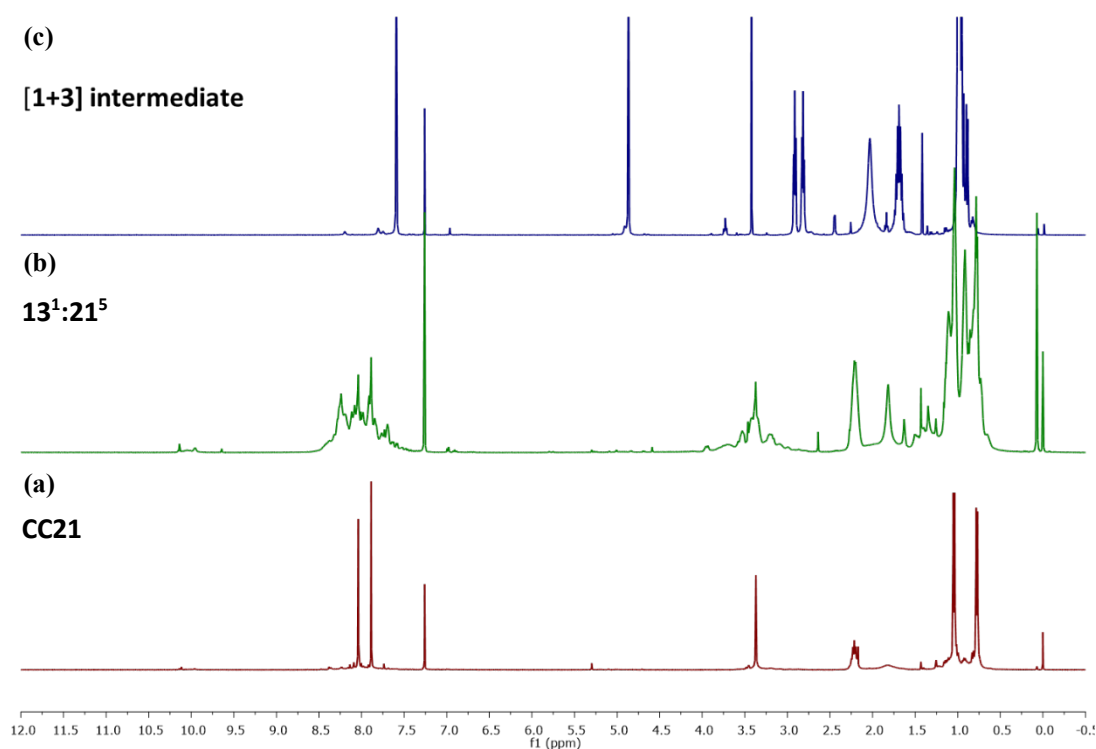


**Figure 3.9:** Reaction scheme for the synthesis of CC21.

**Table 3.3:** Summary of the reaction conditions used during cage synthesis, and the resulting isolated product.

Reaction	Solvent	TFB		DMHDA		MPDA		Product	Yield (%)
		Mmol	Eq.	Mmol	Eq.	Mmol	Eq.		
1	Chloroform	2.055	4	2.570	5	0.514	1	CC21	5
2	DCM	3.100	4	3.900	5	0.800	1	13 <sup>1</sup> :21 <sup>5</sup>	11
3	Chloroform	6.170	4	9.260	6	0.000	0	[1+3]	33

Even in the presence of MPDA (the diamine used to form **CC13**), carrying out the reaction in chloroform resulted in a single cage species, **CC21**, being isolated (**Table 3.1**, Reaction 1), with two distinct singlets at ~7.75-8.25 ppm corresponding to the aromatic and imine protons (**Figure 3.10a**).


**Figure 3.10:** Stacked <sup>1</sup>H NMR (CDCl<sub>3</sub>) spectra for (a) **CC21**, (b) **13<sup>1</sup>:21<sup>5</sup>**, and (c) the [1+3] intermediate isolated when the reaction conditions were changed.

When the same reaction was carried out in DCM (**Table 3.1**, Reaction 2), however, the scrambled **13<sup>1</sup>:21<sup>5</sup>** cage was apparent in the <sup>1</sup>H NMR spectrum with the broad peaks between 7.5 and 8.5 ppm being indicative of a mixture of products (**Figure 3.10b**). Interestingly, on removing the MPDA from the reaction in chloroform to target **CC21** (**Table 3.1**, Reaction 3), only a single peak was apparent in the aromatic region of the <sup>1</sup>H NMR spectrum, with no indication of an imine shift (**Figure 3.10c**), corresponding to an unexpected, symmetrical



product. High-resolution mass spectrometry suggested the main molecular mass ion was 541.4958, which corresponded to a [1+3]-3H<sub>2</sub>O species. In combination with the <sup>1</sup>H NMR data, this confirmed the formation of a symmetrical tri-aminal species, with a single peak for the proton on the aminal (H<sup>b</sup>) present, and one for the proton on the iPr group (H<sup>c</sup>), in contrast to the two observed in the isopropyl-decorated parent cage, **CC21** (Figure 3.11).

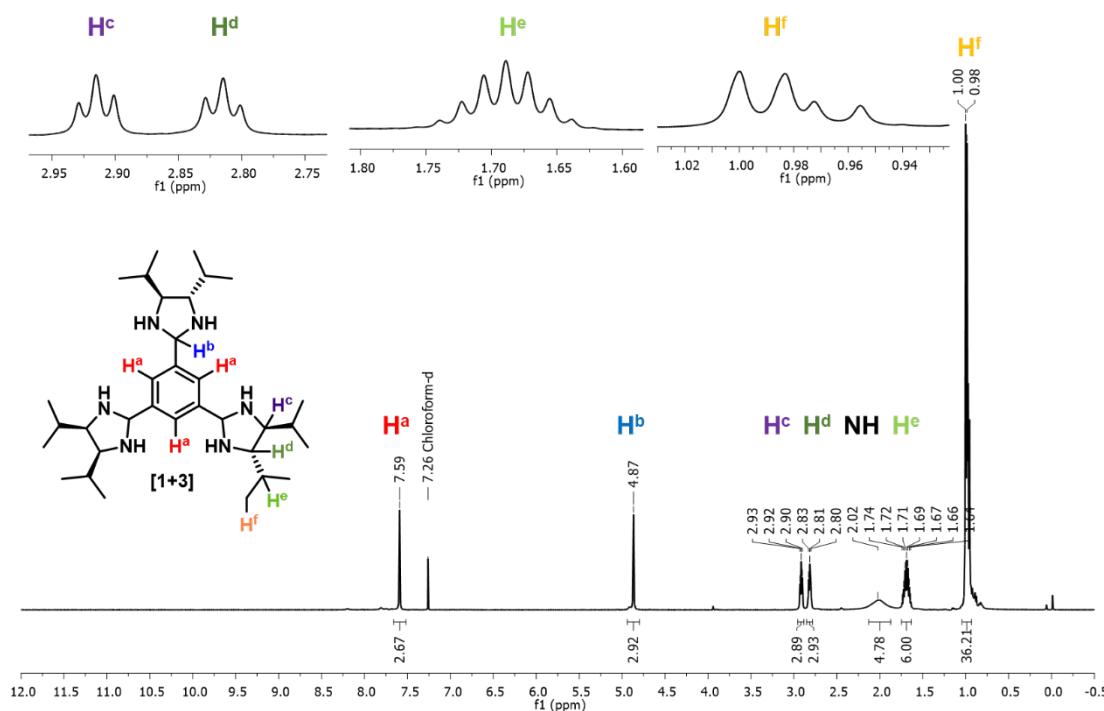


**Figure 3.11:** <sup>1</sup>H NMR spectrum (CDCl<sub>3</sub>) for the [1+3] tri-aminal species isolated from the reaction between TFB and (3*R*,4*R*)-2,5-dimethylhexane-3,4-diamine dihydrochloride in chloroform.

To date, there are limited reports on the formation mechanism of these types of porous imine cages. However, Zhu *et al.* presented a combined experimental and computational study into the intermediates formed during the synthesis of **CC3** and their relative energies.<sup>172</sup> They monitored the formation of **CC3-R** using electrospray mass spectrometry (ES-MS) over a two hour period and identified the intermediates present. From this, seven key species were deduced, beginning with the smaller oligomers that later re-arranged into larger intermediates. Interestingly, a [2+3] species was a re-occurring intermediate throughout the reaction pathway. Previously, it was considered that the [4+6] cage (**CC3-R**) was the thermodynamically stable product, but in this study, computational modelling suggested that the [2+3] species has a slightly lower formation energy than the [4+6] species. This work provides an interesting insight into the formation mechanism of porous imine cages, and illustrates how dynamic covalent chemistry allows for multiple species to be formed with

similar energies, which could help to explain the presence of the [1+3] species observed when attempting the formation of **CC21**.

Despite attempts to optimise the synthesis of **CC21**, the product recovery was still very low, suggesting that the cage is not the major product that is formed. There could be several reasons for the low cage yield, and the different species being isolated, including complex energetics in the mechanism and kinetic traps. Therefore, inspired by the study by Zhu *et al.*, the formation mechanism of **CC21** was investigated.

### 3.3 Study into the formation mechanism of **CC21**

First, the formation mechanism of **CC21** (TFB + DMHDA) was studied in further detail by monitoring the reaction progress in CDCl<sub>3</sub> using <sup>1</sup>H NMR spectroscopy and HRMS (run by Michael Brand). The <sup>1</sup>H NMR spectra showed the complexity of the formation mechanism, with **CC21** not formed as the major product even after 42 days (**Figure 3.12**). Periodically, HRMS data was collected to help identify the intermediates present in the reaction mixture – based on the observed mass ions, structures of the different oligomeric species were proposed (**Figure 3.13** and **3.14**). In particular, the following species were identified: [1+2]-2H<sub>2</sub>O, [1+3]-3 H<sub>2</sub>O, [2+3]-5 H<sub>2</sub>O, [2+4]-6 H<sub>2</sub>O, [3+4]-8 H<sub>2</sub>O, [3+5]-9 H<sub>2</sub>O and [4+6]-12 H<sub>2</sub>O (where [X+Y], X = equivalents of trialdehyde incorporated, Y = equivalents of diamine incorporated). However, for the species identified where a free amine could be present based on the stoichiometry of trialdehyde:diamine, it is unclear if the species are in the cyclised aminal or open amine form, as they both possess the same mass.

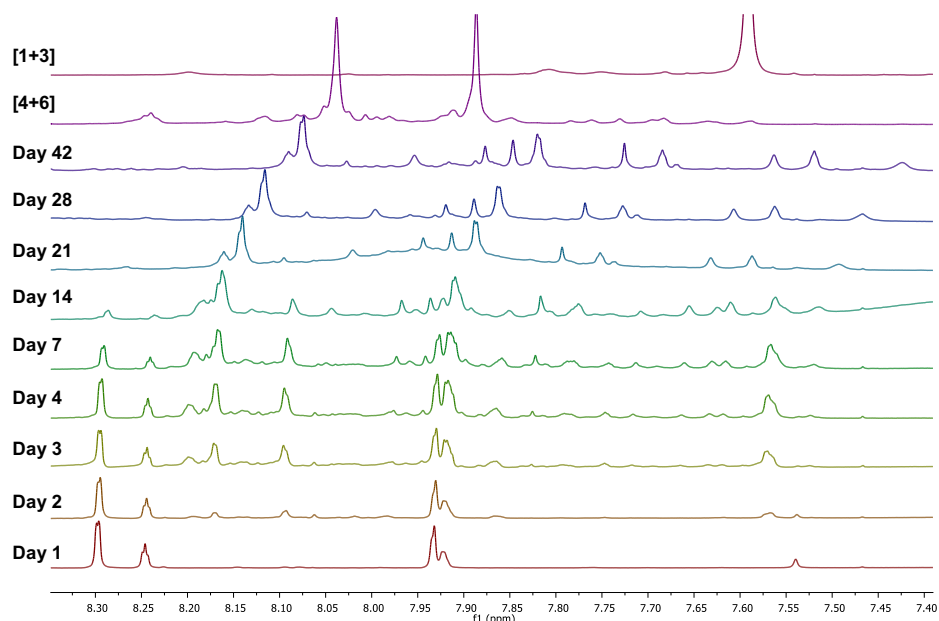


**Figure 3.12:** Stacked <sup>1</sup>H NMR (CDCl<sub>3</sub>) data for the reaction between TFB and DMHDA in CDCl<sub>3</sub> monitored over 42 days.

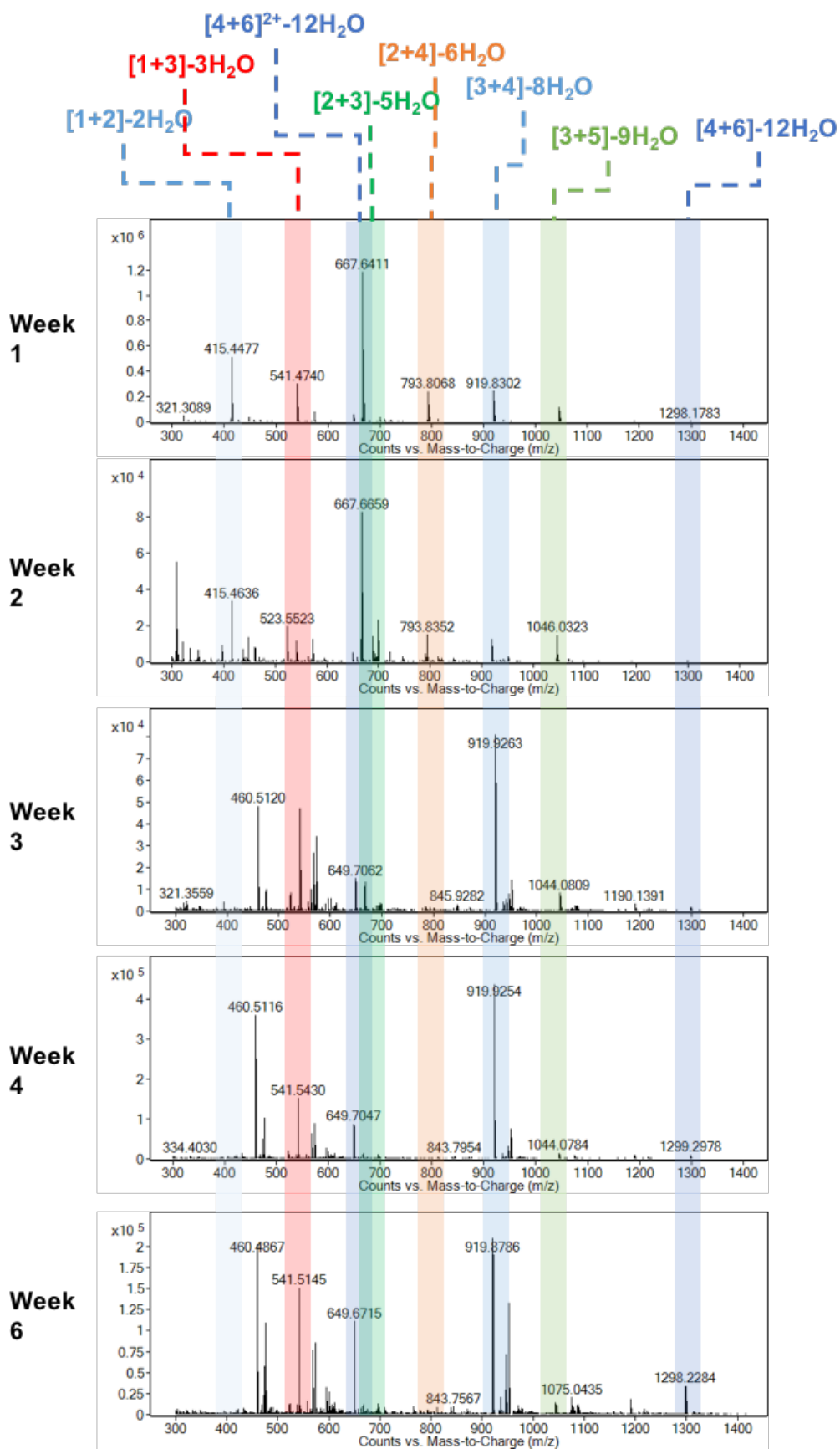
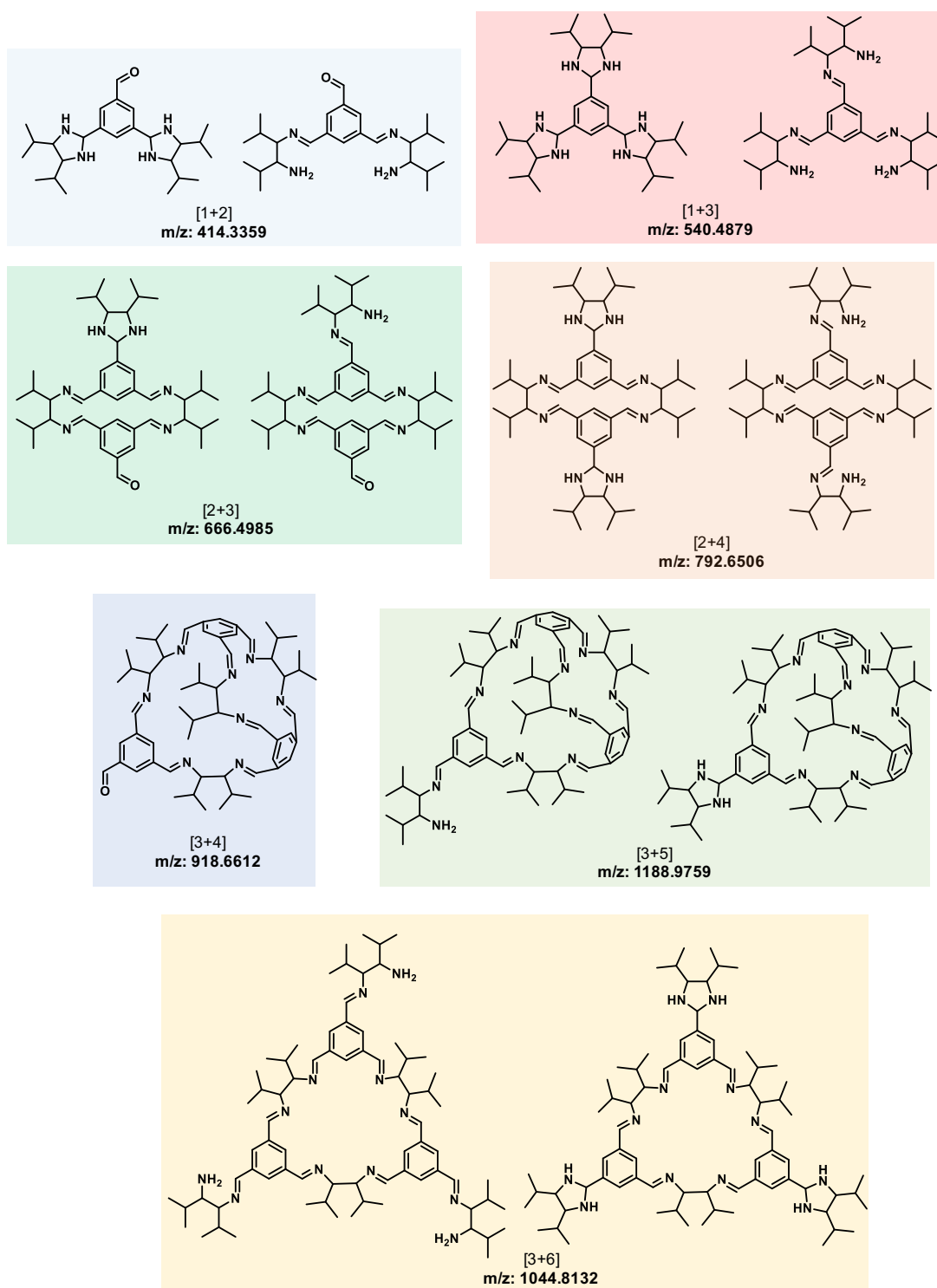


Figure 3.13: Stacked HRMS data for the reaction between TFB and DMHDA in CDCl<sub>3</sub> monitored over 42 days, with the identified intermediates highlighted.

**Chapter 3: Study into the formation mechanism and properties of an isopropyl-decorated POC**



**Figure 3.14:** Potential structures of the intermediates identified during CC21 formation and their expected mass values. In cases where a free amine is present, the species can also form the cyclised aminal, which has the same molecular weight.

Additionally, a range of reactions with varying conditions were monitored to observe the effect of changing the solvent and the addition of an equivalent of MPDA on **CC21** formation (**Table 3.2**). For each combination, HRMS was used to determine the intermediates present at each stage of the reaction. There were several key species that were re-occurring in each reaction, for example, the [1+3]-3H<sub>2</sub>O species (with an expected m/z of 540.4879) was common, indicating that this was a key intermediate with potentially good stability. **CC21** started to become apparent as the reactions progressed, but remained a small percentage of the overall composition as confirmed by the <sup>1</sup>H NMR spectra, which suggested there are either more stable intermediates or the species have similar energies. For the reactions that included MPDA, the mass ion for **CC13** was not observed, and therefore, the diamines do not appear to self-sort into both binary parent cages, and instead MPDA may facilitate the formation of **CC21**. This was confirmed by using isobutylamine instead (**Table 3.2**, Entry 5), which also showed the formation of several of the previously identified key intermediates alongside **CC21**.

**Table 3.4:** The mass ions identified during the reactions used to study the formation of **CC21**.

Entry	Conditions (at room temp)	Identified intermediates in HRMS					
		Week 1	Week 2	Week 3	Week 4	Week 6	
1	TFB, DMHDA, MPDA, NEt <sub>3</sub> , CDCl <sub>3</sub>	[M+H] <sup>+</sup>	415.4441	415.4441	541.5444	541.5434	541.5113
			541.4703	541.4964	811.7678	811.7665	811.7215
			667.6369	667.6661	919.9274	919.9258	919.3727
			793.8001	919.8640	1186.1554	1186.1535	1186.0855
919.8237					1298.2181		
		[M+H] <sup>2+</sup>	649.6228	-	649.7049	649.7043	649.6679
		[M+2H] <sup>2+</sup>	-	460.9693	460.5127	460.5117	460.4834
2	TFB, DMHDA, MPDA, NEt <sub>3</sub> , CD <sub>2</sub> Cl <sub>2</sub>	[M+H] <sup>+</sup>	415.4489	415.4643	415.5055	415.5055	541.5134
			541.4758	541.4928	541.5422	541.5433	919.8765
			667.644	667.6632	667.7213	919.9244	1046.0371
			919.8327		919.9283	1046.0952	1186.0912
1045.9959			1046.1006	1186.1534	scrambled		
		[M+2H] <sup>2+</sup>	-	523.5509	460.5124	460.5124	460.4858
				523.5994	523.5990	523.5717	
3	TFB, DMHDA, NEt <sub>3</sub> , CDCl <sub>3</sub>	[M+H] <sup>+</sup>	415.4477	415.4636	415.5079	541.5430	541.5145
			541.4740	541.4946	541.5455	919.9254	919.8786
			667.6411	667.6659	793.8961	1044.0784	1044.0235
			793.8068	793.8352	919.9263	1299.978	1298.2284
919.8302	919.8626		1044.0809				
	1045.9943	1046.0323	1190.1391				
	1298.1783						
		[M+H] <sup>2+</sup>	-	649.6528	649.7062	649.7047	649.6715
		[M+2H] <sup>2+</sup>	-	460.4674	460.5141	460.5116	460.4867
				523.5527	523.6032	523.5955	
4	TFB, DMHDA, NEt <sub>3</sub> , CD <sub>2</sub> Cl <sub>2</sub>	[M+H] <sup>+</sup>	415.4489	415.4637	415.5079	415.5054	541.5151
			541.4751	541.4940	541.5455	541.5438	919.8960
			667.6426	667.6654	667.7222	919.9245	1046.0425
			793.8092	793.8350	919.9216	1046.0960	1298.2305
919.8321	919.8639		1046.1030	1299.2981			
	1045.9967	1046.0317					
	1299.1843						
		[M+H] <sup>+</sup>	-	-	649.7092	649.7052	649.6727
		[M+2H] <sup>2+</sup>	-	460.9661	460.5105	460.5115	460.4873
				523.5524	523.5996	523.5995	523.5722

5	TFB, DMHDA, isobutylamine, NEt <sub>3</sub> , CDCl <sub>3</sub>	[M+H] <sup>+</sup>	415.4488	415.4641	541.5410	541.5431	541.5431
			541.4767	541.4960	811.7724	919.3797	919.9253
			667.6440	667.6666	919.9222	1298.2308	
			811.6799	919.8650	1046.0877		
			919.8336	1046.0328			
			1045.9968				
		[M+H] <sup>2+</sup>	-	-	-	649.6727	649.7047
		[M+2H] <sup>2+</sup>	-	460.4661	460.5098	460.4857	460.5116
				523.5503			

Two reactions were also carried out using the isolated [1+3] tri-aminal species to give further insight into the formation of **CC21**. When TFB was reacted with the [1+3] species, a number of the other intermediates were observed, along with **CC21**, after 2 months (**Table 3.3**, Entry 6). This suggests that the [1+3] species can rearrange and equilibrate into other species, but that this process is slow as **CC21** is not the major product. Finally, as previously observed, changing the solvent from CDCl<sub>3</sub> to CD<sub>2</sub>Cl<sub>2</sub> (**Table 3.2**, Entry 2) had an impact on the reaction composition, with the scrambled cage mixture being formed instead of the parent cage, **CC21**. However, when **CC13** and the [1+3] species were reacted together in CDCl<sub>3</sub>, the scrambled cage was observed, indicating that **CC13** is not involved in the reaction mechanism of **CC21** directly.

**Table 3.5:** Reactions of the pre-formed [1+3] species and the mass ions identified in the HRMS after 2 months.

Entry	Conditions	Main cage intermediates in HRMS after 2 months
6	TFB, [1+3] intermediate, CDCl <sub>3</sub> at room temperature	[M+H] <sup>+</sup> 541.4990, 793.6630, 1045.8255, 1189.9837, 1297.9814
7	<b>CC13</b> , [1+3] intermediate, CDCl <sub>3</sub> at room temperature	[M+H] <sup>+</sup> scrambled

Overall, comparison of the final compositions in the mass spectra for each reaction revealed the most common intermediate was the [1+3]-3H<sub>2</sub>O species, which could be why this was an isolatable product (**Table 3.4**). It also appeared to be consistently present throughout the reactions (**Table 3.2**), suggesting it is stable and not all of it rearranges into other components. Solvent has also been shown to affect the formation of [4+6] imine cage species, in particular, the solubility of the intermediate and final cage species can result in a low yielding reaction.<sup>173</sup> However, in this case, no precipitate was observed, despite a lower solubility of the reactants in DCM. Whilst DCM facilitated the formation of the scrambled cage mixture over **CC21** from the starting reagents, the scrambled cage seemed to form best directly from **CC13**, as this gave clean <sup>1</sup>H NMR and HRMS spectra, with no other intermediates apparent (**Table 3.4**,

Entry 7). In general, these mechanistic studies aided in the identification of a number of stable intermediates present throughout the reaction, and the complexity of the  $^1\text{H}$  NMR spectra, even after 42 days, suggested there was not a major overall product. This helps account for the low isolated yield of **CC21**, and the fact that the [1+3] species was also isolated in a reasonable yield.

**Table 3.6:** Summary of the cage intermediates present in the HRMS after <sup>(a)</sup> 6 weeks and <sup>(b)</sup> 2 months

Identified intermediate [TFB+DMHDA]	Calc. m/z	Present in reaction mixture						
		Entry 1 <sup>a</sup>	Entry 2 <sup>a</sup>	Entry 3 <sup>a</sup>	Entry 4 <sup>a</sup>	Entry 5 <sup>a</sup>	Entry 6 <sup>b</sup>	Entry 7 <sup>b</sup>
[1+2]-2H <sub>2</sub> O	414.3357							
[1+3]-3H <sub>2</sub> O	540.4877							
[2+3]-5H <sub>2</sub> O	666.4982							
[2+4]-6H <sub>2</sub> O	792.6502							
[2+4]-5H <sub>2</sub> O	810.6608							
[3+4]-8H <sub>2</sub> O	918.6607							
[3+5]-9H <sub>2</sub> O	1044.8127							
[3+6]-9H <sub>2</sub> O	1188.9753							
[4+6]-12H <sub>2</sub> O	1296.9752							

Whilst the HRMS data gave useful information about the intermediates present in a reaction mixture, it does not give a quantifiable ratio of species. The complexity of the  $^1\text{H}$  NMR spectra also prevents the ratio of the species from being determined, and therefore it is difficult to rationalise the reaction on these techniques alone. Therefore, computational modelling was carried out (by Dr Andrew Tarzia, Jelfs Group, Imperial College London) to determine the formation energies of each identified intermediate, which were normalised per imine bond to allow direct comparison of different stoichiometric species. Additionally, both the open amine and the cyclised aminal forms of the intermediates were modelled, based on the knowledge that these species can form experimentally, as seen with the isolated [1+3]-3H<sub>2</sub>O species.

Overall, the simulations showed that the aminal forms of the intermediates had lower energies than the free amine counterparts (**Figure 3.15**). Some of the more persistent species in the mechanism seem to be the aminal intermediates, including the [1+3]-3H<sub>2</sub>O species which was isolated in reasonable yield, and has the second lowest energy. This helps to explain why the reaction kinetics to **CC21** are slow compared to other analogous cage formations (e.g. **CC1** forms in 1 day, **CC3** forms in 5 days, and **CC13** forms in 3 days – all are carried out in DCM and at room temperature).<sup>67,84,156</sup> This may explain why the reaction does not reach full conversion to **CC21** – whilst the imine intermediates have very similar energies so are likely able to equilibrate, if an aminal forms, these are substantially more stable and are likely acting as traps during the reaction.

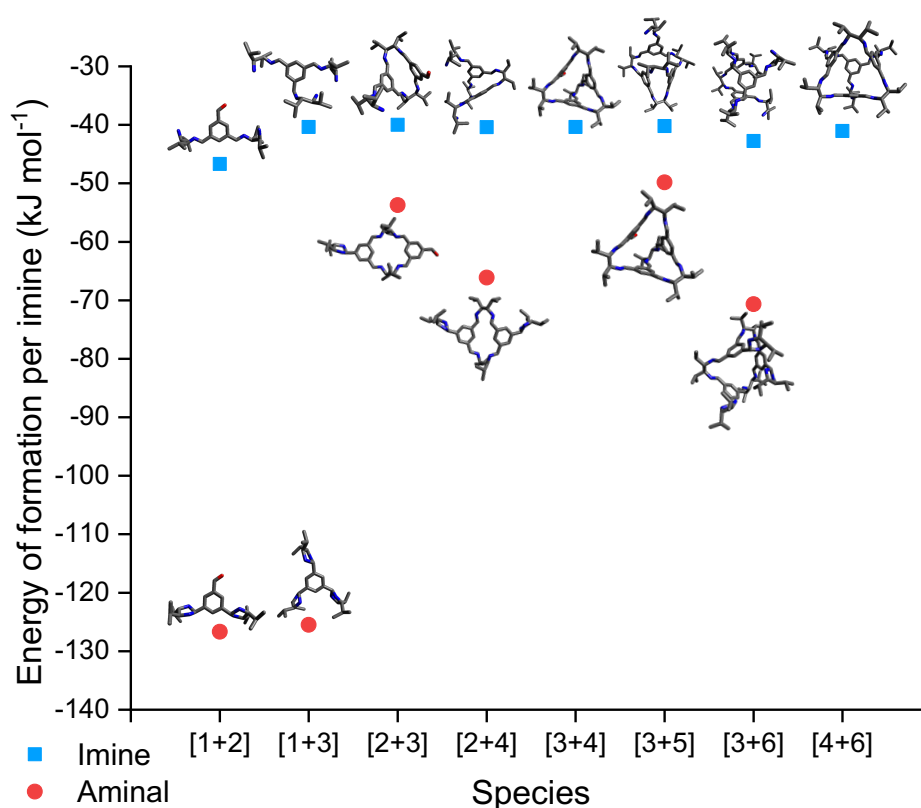


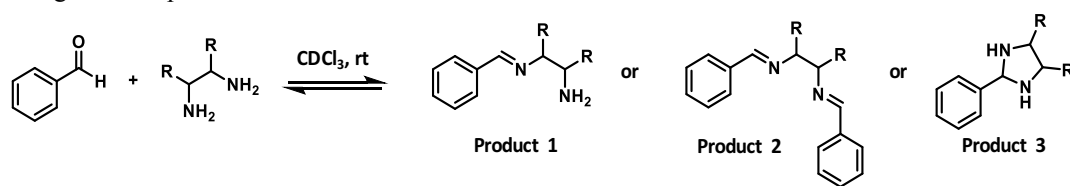
**Figure 3.15:** Formation energies per imine bond for the identified intermediate species during the formation of **CC21**.

The computational calculations suggested that the aminal forms of the intermediates were the most favourable and lowest in energy during **CC21** formation. Therefore, a series of control reactions were carried out to investigate the preferred products formed when a series of diamines, used for the synthesis of **CC21** and in the synthesis of common [4+6] imine cages (**CC1**, **CC3**, and **CC13**), were reacted with benzaldehyde in CDCl<sub>3</sub> at ambient temperature (**Table 3.5**). A <sup>1</sup>H NMR spectrum was collected after 72 hours to determine the composition of the reaction mixture.



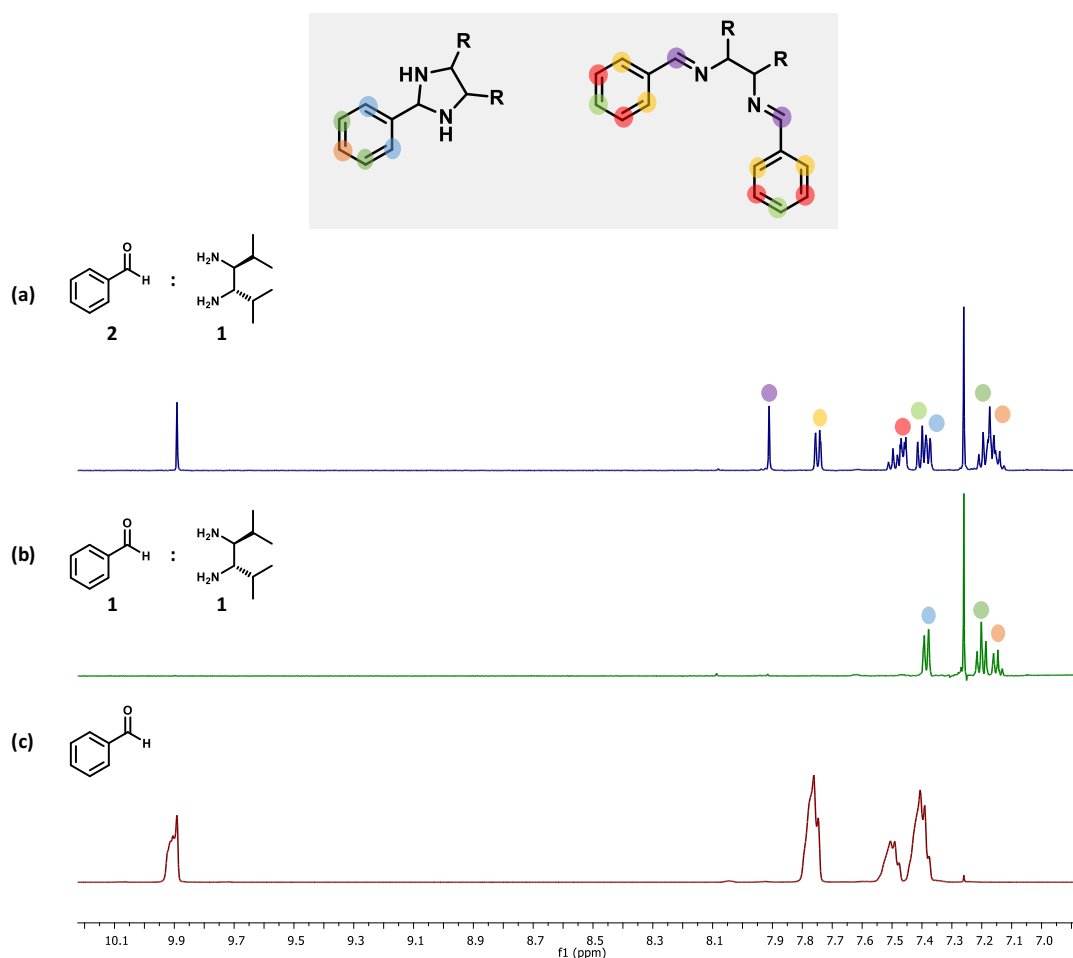
**Chapter 3:** Study into the formation mechanism and properties of an isopropyl-decorated POC

**Table 3.7:** General reaction scheme for the control reactions between benzaldehyde (1.0 or 2.0 equivalents) and either the **CC21** diamine or an alternative common cage diamine (1.0 equivalent), along with the products formed in each reaction.



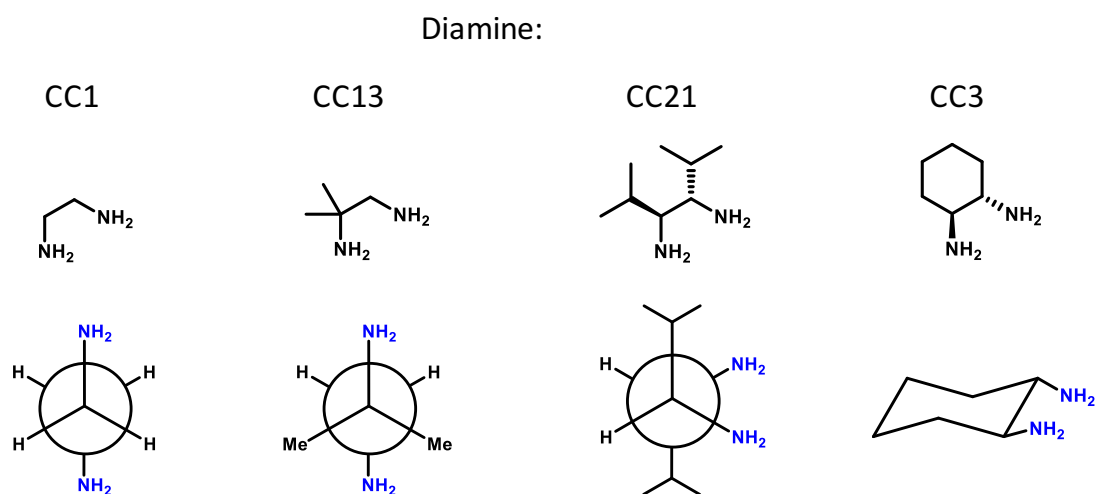
Entry	Diamine	Equivalent of benzaldehyde	Product
1		1	Product 1 and 2
2		2	Product 2
3		1	Product 1 and 2
4		2	Product 2
5		1	Product 1
6		2	Product 1 and 2
7		1	Product 3
8		2	Product 2 and 3

All of the reactions showed either the mono- or di-imine formed preferentially, depending on the equivalents of benzaldehyde present, except for the diamine used to form **CC21** ((3*R*,4*R*)-2,5-dimethylhexane-3,4-diamine dihydrochloride, DMHDA). When a single equivalent of benzaldehyde was used, full conversion to the aminal product was observed, rather than the imine, whereas when two equivalents of benzaldehyde were used, a mixture of imine and aminal species was apparent (**Figure 3.16**). In the case of **CC21**, an excess of TFB could promote imine formation over the aminal to increase the cage yield but further investigation is needed.



**Figure 3.29:** Expansion of the aromatic region in the  $^1\text{H}$  NMR spectra ( $\text{CDCl}_3$ ) for the reactions between benzaldehyde and (3*R*,4*R*)-2,5-dimethylhexane-3,4-diamine dihydrochloride (DMHDA), used to form **CC21**, with benzaldehyde as reference.

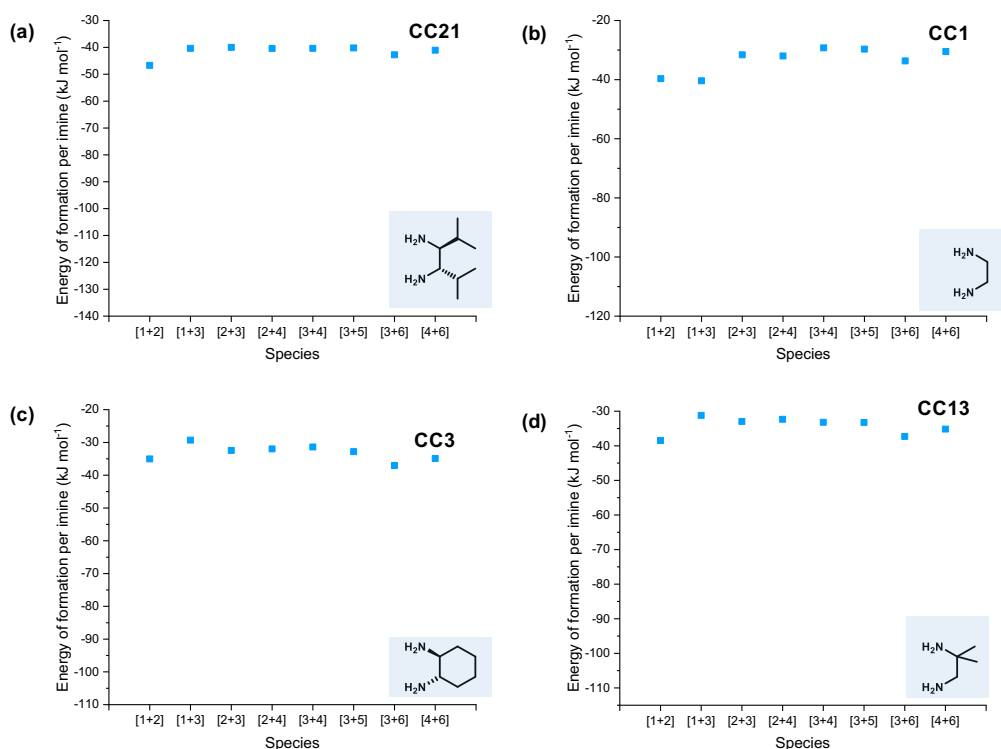
To try and rationalise the findings that most of the diamines do not form a cyclic aminal product, but DMHDA used to form **CC21** diamine does, the Newman projections for each of the diamines were compared (**Figure 3.17**). The isopropyl substituents provide a large amount of steric clash so they orientate themselves as far away from each other as possible. This positions the amines in close proximity to each other, and are therefore more likely to internally cyclise to form an aminal. For the diamines used to form **CC1** and **CC13**, the amine groups are able to position themselves away from each other, and although the geminal-dimethyl groups in the **CC13** diamine create steric hindrance, the amines can still position themselves away from each other.



**Figure 3.17:** Structures of the diamines used to form **CC1**, **CC13**, **CC21**, and **CC3**, along with their Newman projections or chair structure.

Overall, the study into the formation mechanism of **CC21** gave an interesting insight into how the addition of sterically bulky groups can affect cage formation. While the rate of formation is slow compared to other cage reactions, comparison of the **CC21** imine intermediates to the same intermediates for **CC1**, **CC3** and **CC13** indicated that they are in fact of similar in formation energies and reaction pathways (**Figure 3.18**), and therefore, it is the formation of more stable aminals that are likely acting as traps during the reaction.

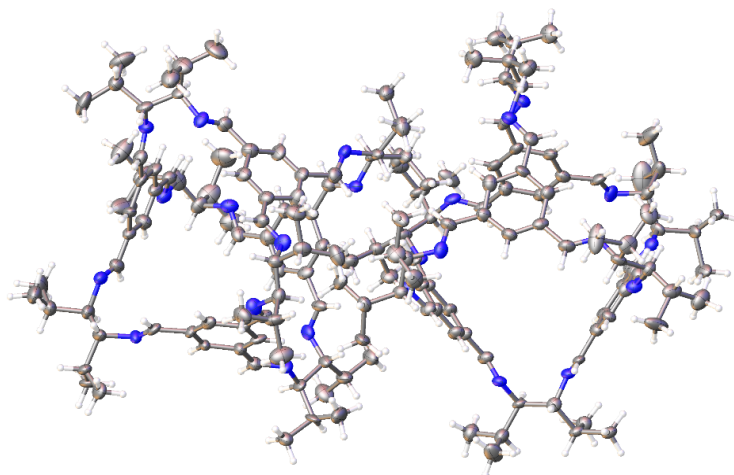
Whilst the use of DCM promoted scrambling, the presence of another amine species in chloroform aids the reaction progression towards **CC21** rather than forming a scrambled mixture. This could be an alternative method to accessing [4+6] imine cages that previously seemed unable to form.



**Figure 3.18:** Formation energies for the intermediates formed during [4+6] imine cage reaction: (a) CC21; (b) CC1; (c) CC3 and (d) CC13.

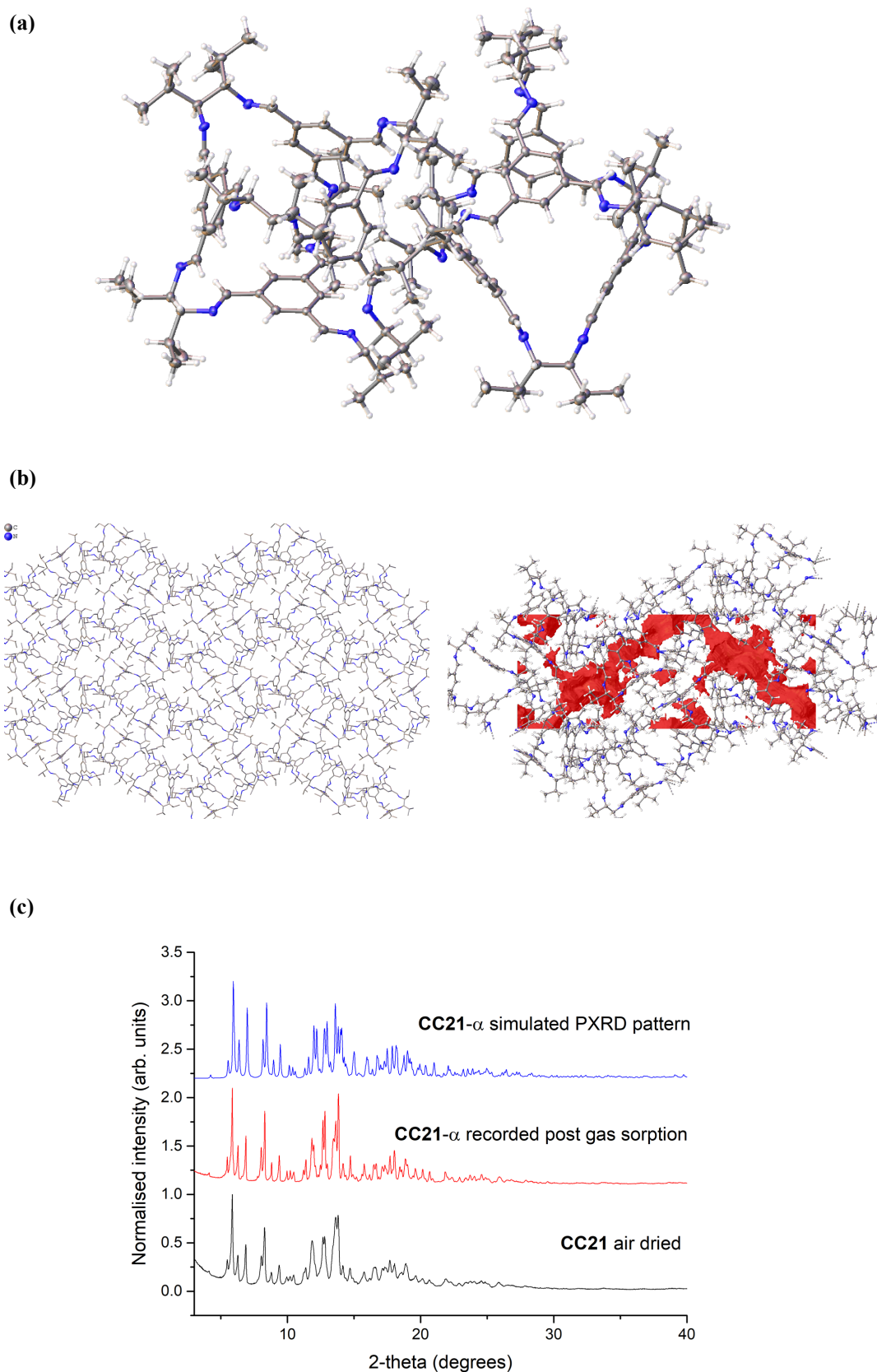
### 3.4 Properties of CC21

Although CC21 was isolated in low yield, the addition of isopropyl groups onto the cage periphery may have an effect on the overall properties. Therefore, the reaction was repeated until sufficient material was generated for subsequent studies. The solid-state packing of the CC21 molecules was of particular interest, so solvated crystals suitable for single crystal X-ray diffraction (run by Dr Marc Little), were grown from the slow diffusion of methanol into a solution of CC21 in chloroform. The solvated crystal structure showed the CC21·CHCl<sub>3</sub>·MeOH possessed a frustrated packing arrangement, with the isopropyl groups on the cage vertices disrupting the usual window-to-window or window-to-arene arrangement often observed with these [4+6] POCs (Figure 3.19), creating extrinsic voids on the cage vertices.<sup>121,122</sup>



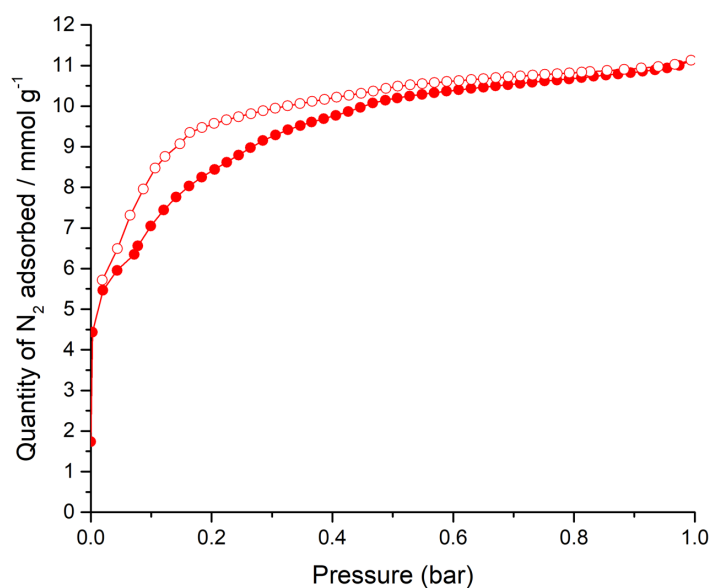
**Figure 3.19:** Displacement ellipsoid plot of the asymmetric unit from the single crystal structure,  $2(\text{CC21}) \cdot 9(\text{CHCl}_3) \cdot 10.5(\text{CH}_4\text{O}) \cdot (\text{H}_2\text{O})$ . Ellipsoids displayed at 30% probability level; disordered solvent omitted for clarity. C = grey, H = white, N = blue.

The crystal structure and packing of the bulk material of **CC21** was also studied after recrystallisation from slowly evaporating DCM from a saturated solution at ambient temperature. The isolated material was dried under vacuum at 363 K, and analysed by single crystal and powder X-ray diffraction (performed by Dr Marc Little). This gave a new phase, **CC21 $\alpha$** , which had a similar bulk structure to **CC21**·CHCl<sub>3</sub>·MeOH, but with a 15% smaller unit cell volume (**Figure 3.20a**) due to denser packing of the **CC21** molecules. The extended structure showed the molecules in the unit cell pack with a staggered arrangement in the solid state (**Figure 3.20b**), which is unlike other analogues in the series as they seem to pack either window to window or window to arene. The added steric bulk on the periphery by the isopropyl groups seems to disrupt and prevent the usual arrangement demonstrated by cages with the same core shape. However, this does seem similar to **CC13 $\alpha$** , which also has a staggered arrangement and no direct window-to-window connections, suggesting these cages could be isostructural. The PXRD pattern of the bulk **CC21 $\alpha$** , from CD<sub>2</sub>Cl<sub>2</sub>, matched the simulated pattern (**Figure 3.20c**).



**Figure 3.20:** (a) Displacement ellipsoid plot of the asymmetric unit from the single crystal structure, **CC21 $\alpha$** . Ellipsoids displayed at 30% probability level. C = grey, H = white, N = blue, (b) The extended structure of **CC21 $\alpha$**  unit cell with the voids highlighted in red, and (c) PXRD patterns for **CC21**: crystallised from  $\text{CH}_2\text{Cl}_2$  and air dried (bottom, black); recorded after activation at 363 K under dynamic vacuum and subjected to gas sorption analysis (middle, red); simulated pattern for **CC21 $\alpha$**  from the single crystal structure recorded at 100 K.

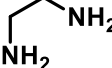
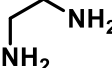
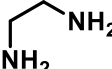
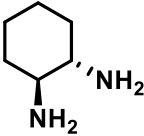
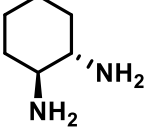
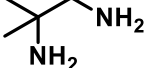
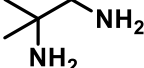
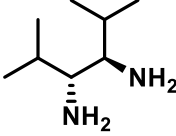
The desolvated **CC21 $\alpha$**  phase was found to absorb 11.1 mmol g<sup>-1</sup> of N<sub>2</sub> at 1 bar and 77.3 K (gas sorption run by Dr Marc Little and Rob Clowes), and also has a S<sub>A</sub>BET of 699 m<sup>2</sup>g<sup>-1</sup> (**Figure 3.21**). The PXRD data post-sorption showed the structure did not change phase, and therefore, the bulky isopropyl groups do not affect its stability and **CC21** is shape-persistent in the solid state (**Figure 3.20b**). Compared to other cages in the series, **CC21** has a reasonably high surface area and gas uptake (**Table 3.6**). The addition of the isopropyl groups on the periphery caused inefficient crystal packing. **CC13**, a cage with two geminal methyl groups, also packed in a staggered manner with no window-to-window connectivity.<sup>122</sup> In the  $\alpha$  phase, **CC13** has higher gas uptake than **CC1** and **CC3** (other cages in the series), but **CC21 $\alpha$**  has the highest. The additional steric bulk, compared to **CC1** that has only hydrogens on the periphery, forces the cages further apart in the solid-state. However, the cyclohexyl groups in **CC3** fill the extrinsic pore volume, whereas, in **CC13 $\alpha$**  the methyl groups create additional pore volume.<sup>122</sup> A similar effect could be seen in the crystal structure of **CC21 $\alpha$** , where solvent molecules were occupying these extrinsic voids, and could explain the increase in N<sub>2</sub> uptake. However, **CC13 $\beta$**  has a higher gas sorption value due to directed packing of the molecules by re-crystallising with dioxane, which causes the cages to pack window-to-window. The dioxane stabilises this phase and helps create an intrinsic pore network.<sup>122</sup> The same could be attempted for **CC21** to access other phases and increase the gas uptake further. It would be interesting to observe how the bulkier isopropyl groups interact and if window-to-window packing can occur.



**Figure 3.21:** N<sub>2</sub> sorption isotherm for **CC21 $\alpha$**  recorded at 77.3 K. Adsorption points are shown as closed symbols; desorption points are shown as open points.

As the isopropyl groups disrupt the bulk packing of **CC21**, this could improve the cage's solubility. Although imine cages are discrete molecules and can dissolve in a range of common solvents, they usually have poor solubility due to ordered packing in the solid state. The solubility of **CC21** in chloroform was tested and compared to other [4+6] cages in the series. While **CC21** had a slightly lower solubility than **CC13 $\beta$**  (165 vs. 200 mg mL<sup>-1</sup>, respectively), it far exceeded the solubility of other cages such as **CC3** (9 mg mL<sup>-1</sup>).<sup>122</sup> This demonstrates that the addition of disordered, bulky groups on the periphery could be responsible for improving solubility.

**Table 3.8:** Summary of the properties for common [4+6] imine cages found in the literature compared to **CC21- $\alpha$**

Entry	Cage	Starting diamine	Crystal packing	N <sub>2</sub> sorption at 1 bar and 77.3 K (mmol g <sup>-1</sup> )	S <sub>ABET</sub> (m <sup>2</sup> g <sup>-1</sup> )	Ref
1	CC1 $\alpha$		Window-to-arene	Non porous	23	[84]
2	CC1 $\beta$		Window-to-arene	Non porous	30	[174]
3	CC1•1,4 dioxane		Window-to-window	3.9	333	[122]
4	CC3 $\alpha$		Window-to-window	8.17	624	[84]
5	CC3 $\beta$		Window-to-face	6.1	555	[175]
6	CC13 $\alpha$		Window-to-arene	9.2	517	[122]
7	CC13 $\beta$		Window-to-window	13.5	946	[122]
8	CC21 $\alpha$		Frustrated	11.1	699	This work



### **3.5 Conclusions**

In this chapter, the synthesis and properties of a new [4+6] imine cage, **CC21**, were investigated. The addition of bulky isopropyl groups onto the cage periphery were seen to have an effect on the reaction mechanism, with  $^1\text{H}$  NMR spectra and HRMS data showing several stable intermediates. Computational modelling showed the energies of the imine intermediates were very similar, but the aminated species were more stable. Further experimental studies indicated that for the isopropyl diamine, the aminated species is preferred and supported the findings from the calculations. These observations gave an insight into imine cage formation that had not been explored before. The properties of **CC21** were also investigated and an unusual frustrated bulk packing was observed in the crystal structure, where the isopropyl groups created extra extrinsic voids. This disordered packing contributed to a higher solubility in chloroform than most other cages in the same series, and a high  $\text{N}_2$  uptake.

**Chapter 4:**  
Investigation into the properties of  
Type II scrambled porous liquids

## 4.1 Introduction

### 4.1.1 Study of previous scrambled porous liquids

In the current literature, there are only a few porous liquids formed using organic molecular cages, and up until this study, only one that utilised a scrambled cage mixture. Scrambled porous liquids have different properties compared to conventional porous solids. This poses new challenges for measuring gas uptake. The first example of this type, a scrambled cage ( $3^3:13^3$ ) dissolved in PCP at  $200 \text{ mg mL}^{-1}$  (**Figure 4.1**), could not be studied using traditional gas sorption measurements due to the vapour pressure associated with PCP.<sup>13</sup> As a result of these restrictions, alternative methods were needed to determine if this scrambled cage solution was permanently porous and a Type II porous liquid. Therefore, gas uptake measurements were performed using gas displacement and NMR spectroscopy; this demonstrated that the system had increased porosity compared to neat PCP.<sup>13</sup>

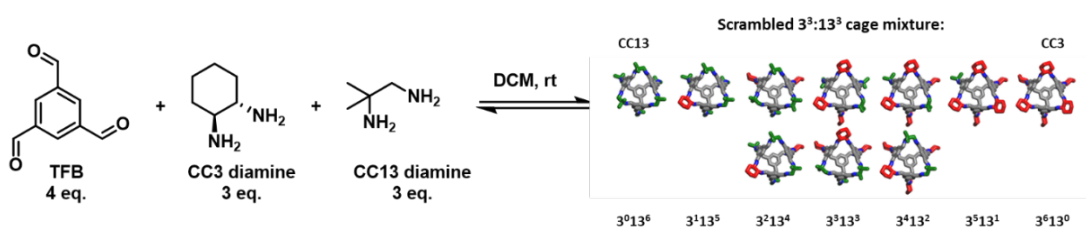


**Figure 4.1:** General reaction scheme for the synthesis of  $3^3:13^3$  scrambled cage mixture, formed from 1,3,5-triformylbenzene (TFB, 4.0 equiv.), (1S,2S)-(+)-1,2-diaminocyclohexane (diamine used to form CC3, 3.0 equiv.), and 1,2-diamino-2-methyl-propane (diamine used to form CC13, 3.0 equiv.) in DCM at room temperature.

Building on the initial report, Greenaway *et al.* carried out an in-depth study on the gas uptake properties of  $3^3:13^3$  in PCP at  $200 \text{ mg mL}^{-1}$ , using several techniques to demonstrate the uptake of different gases in the porous liquid. Initially FTIR was used to detect the distinctive stretch given by  $\text{CO}_2$ , which allowed quantitative analysis using neat samples in a liquid cell. The porous liquid showed an overall three-fold increase in uptake compared to neat PCP (**Figure 4.2a**).<sup>112</sup>

Understandably, FTIR was only suitable for certain gases, so other techniques were needed to measure the uptakes of alternative guests. In both reports studying  $3^3:13^3$  in PCP, chemical displacement was a quick and effective method for estimating the gas uptake in the porous liquid (**Figure 4.2b**). This involved saturating a porous liquid with a gas using optimised conditions ( $50\text{--}60 \text{ mL min}^{-1}$  for 5 min per 1 mL of PCP used), before displacement of the gas from the cage cavities using a small liquid guest, such as chloroform. The gas was collected

in an inverted burette prefilled with water, and the volume evolved related to the uptake in the overall system.<sup>13,112</sup>

This technique was particularly useful because uptakes for a number of gases, including those that are IR inactive, could be tested and compared, including N<sub>2</sub>, CH<sub>4</sub>, CO<sub>2</sub>, Xe, and SF<sub>6</sub>. High volumes of both Xe and SF<sub>6</sub> were displaced from the scrambled porous liquid (72.8 and 74.3 μmol g<sub>PL</sub><sup>-1</sup>, equating to 72% and 74% cage occupancies, respectively). Additionally, the displaced volume of CH<sub>4</sub> was in close agreement with the value calculated using <sup>1</sup>H NMR spectroscopy (45.8 vs 51.0 μmol g<sub>PL</sub><sup>-1</sup>).<sup>112</sup> This demonstrates that gas displacement studies can give a reliable indication of porosity. However, there are some limitations with using this method to determine gas uptake in a porous liquid – the volume recorded does not give any information on the guest’s location within the system, nor does this value account for the inherent solubility of the gas in the solvent. As a result, gas displacement alone cannot provide a complete picture of the gas uptake behaviour in a porous liquid.

Another very useful technique for measuring and studying the gas uptake in a scrambled porous liquid is NMR spectroscopy. The uptake of CH<sub>4</sub> was monitored using the distinct chemical shift which appeared at <0 ppm in the scrambled porous liquid.<sup>13</sup> A dramatic shift was observed for the CH<sub>4</sub> signal compared to the neat solvent ( $\Delta\delta = -2.56$  ppm), which indicated that the CH<sub>4</sub> was occupying the cage cavities in the porous liquid on the NMR timescale.<sup>13,112</sup> This shielding effect was also observed during the uptake of other gases, including Xe (<sup>129</sup>Xe NMR) and SF<sub>6</sub> (<sup>19</sup>F NMR), both of which showed a peak shift, alongside peak broadening (**Figure 4.2c**).<sup>112</sup> The authors used a sealed calibrated capillary (*d*<sub>2</sub>-DCM/TMS) to reference the spectrum – not only did this prevent the deuterated solvent from acting as a competing guest, it also enabled the CH<sub>4</sub> uptake over a range of concentrations to be measured and calculated.

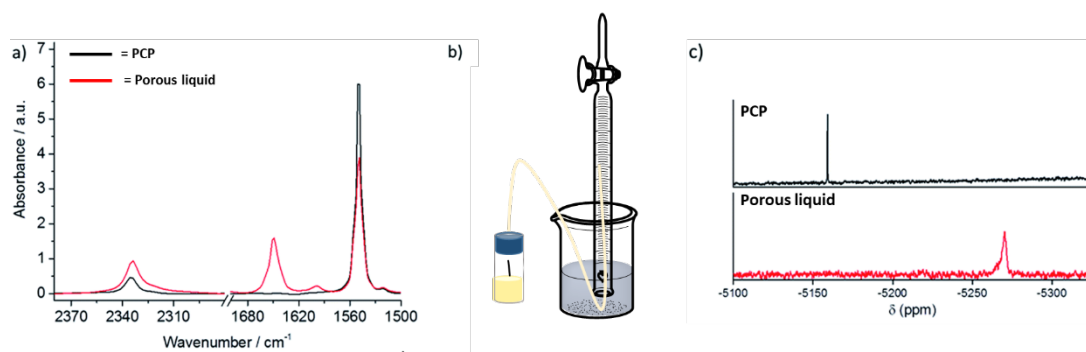


**Figure 4.2:** (a) Liquid cell-FTIR spectra for the scrambled porous liquid (3<sup>3</sup>:13<sup>3</sup> in PCP) and neat PCP after saturation with CO<sub>2</sub>; (b) General set up for gas displacement measurements using an inverted burette; (c) <sup>129</sup>Xe NMR spectra showing the Xe uptake in PCP and the corresponding porous liquid (3<sup>3</sup>:13<sup>3</sup> in PCP). Figure adapted from work presented by Greenaway *et al.*<sup>112</sup>

These in-depth studies into the gas uptake properties of  $3^3:13^3$  in PCP provide a range of techniques for reliable measurement of the gas uptake in a scrambled porous liquid. Overall, Greenaway *et al.* developed methodology to prove that the porous liquid had substantially increased gas uptake over neat PCP. Additionally, by using a non-porous control molecule, the authors were able to demonstrate that the presence of cavities in the scrambled porous liquid were responsible for this observed increase. Further, by carrying out saturation studies and varying other conditions, such as gas flow rate in the gas uptake experiments, optimised conditions were reported. As a result, a reliable methodology was presented that could be used to study the scrambled cage/bulky solvent combinations discovered in **Chapter 2**, to facilitate the determination of porosity in the liquids.

#### **4.1.2 Design considerations for Type II porous liquids**

Type II porous liquids are comprised of two components, a pores molecule and a size-excluded solvent, as such, an understanding of how these interact and influence the overall properties would be an important advance in the field. In the case of scrambled porous liquids, for example, the scrambled cage would ideally have high solubility and be stable to the chosen size-excluded solvent. The solvent also needs complementary properties in order for the system to have practical applications, which includes low viscosity, toxicity, and cost. Additionally, a vapour pressure of zero (or near zero) would be preferable because this would allow the use of modified gas sorption techniques to study a system, alongside the use of temperature or pressure swings for the reversible uptake of different guests.

Having a library of scrambled porous liquids enables an investigation into how changing the components in a Type II porous liquid has an effect on its overall properties. For example, determining whether the same cage in different solvents affects the selectivity for guests, or how changing the cage functionality changes the diffusion of gases, could allow for tailored porous liquids towards a specific application. Additionally, with very few examples in the current literature, the limitations of Type II porous liquids are relatively unknown. Investigations into how increasing the pore concentration has an effect on the overall properties could determine if there is an optimum cage concentration before the viscosity becomes too high to be practical in flow applications. Therefore, understanding the potential limitations associated with porous liquids would be beneficial when studying new applications, and potentially implementing them into a commercial setting.

## 4.2 Porosity screening of potential porous liquids

In **Chapter 2**, a library of highly soluble scrambled cage/bulky solvent combinations was discovered using a high-throughput workflow. These were scaled-up in order to study them further and to determine whether any were porous liquids. Initially this involved comparing the gas uptakes in the system and the neat solvents. However, as discussed above, traditional gas sorption techniques are not usually suitable for scrambled porous liquids.<sup>13,112</sup> To confirm that the liquids in this study could not be subjected to reduced pressure, the parent solvents were exposed to vacuum for 24 hours and the mass loss recorded. All of the solvents tested saw a decrease in mass, indicating they have an associated volatility. Therefore, an alternative method was employed, which measured the displacement of xenon to determine the gas uptake of the scrambled cage/solvent combinations from the high-throughput screen (**Figure 4.3**).

Each of the potential porous liquid combinations was prepared using 200 mg of the corresponding scrambled cage in 1 mL of the size-excluded solvent (20% w/v). At this concentration, however, some combinations (**A<sup>3</sup>:K<sup>3</sup>** in solvent 2) formed a gel rather than a free-flowing solution, which is unsuitable for use as a porous liquid. POCs have been shown to self-assemble in the solid state to form interconnected pore networks.<sup>83,122,157,161,176</sup> At these higher solution concentrations, the scrambled cages may start forming ordered structures, which could explain the observed gel formation. While this occurrence was interesting, it was not useful in targeting porous liquids, so this system was removed from further study, leaving 29 potential combinations. The initial scrambled porous liquid (**A<sup>3</sup>:E<sup>3</sup>** (200 mg) in PCP (1 mL), **E33**, **Figure 4.1**) provided a benchmark uptake of xenon ( $4.4 \pm 0.2 \text{ cm}^3 \text{ Xe evolved}$ , equating to  $95.6 \mu\text{mol g}_{\text{PL}}^{-1}$ ) enabling direct comparison with new systems containing the same mass of cage (200 mg). The potential porous liquids were therefore loaded with xenon gas, which was subsequently displaced with chloroform, and the volume evolved was measured by collection in an inverted burette.

Using this simple screen, it was easy to determine the porosity of the new systems by comparing the xenon uptakes to that in the initial scrambled porous liquid, **A<sup>3</sup>:E<sup>3</sup>** in PCP (**3<sup>3</sup>:13<sup>3</sup><sub>PCP</sub>**). Of the combinations tested, three had similar xenon uptakes to **3<sup>3</sup>:13<sup>3</sup><sub>PCP</sub>** (**Figure 4.3**). One of these hits (**A<sup>2</sup>:G<sup>4</sup>** in solvent 3), however, again suffered from gelation when prepared on a larger scale and was not investigated further. The two final porous liquids contained the same scrambled cage (**A<sup>3</sup>:E<sup>3</sup>**) as **3<sup>3</sup>:13<sup>3</sup><sub>PCP</sub>**, but in different solvents; 2-hydroxyacetophenone (HAP) and 4-(trifluoromethoxy)benzyl alcohol (TBA).

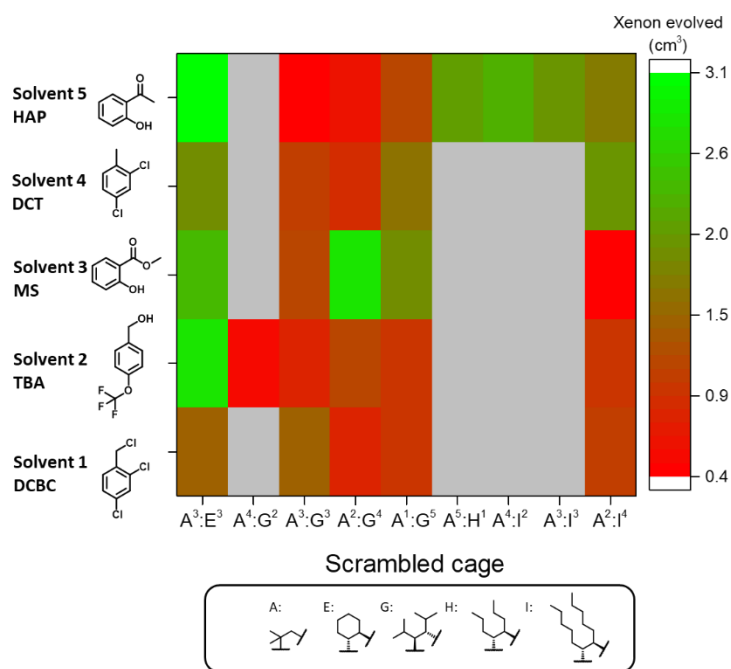


**Figure 4.3:** Graphical representation summarising the results from the screen for porosity in new scrambled cage/bulky solvent combinations in the search for new porous liquids. Green indicates a higher xenon evolution on displacement with chloroform. Grey indicates combinations not tested.

However, in addition to the two highly porous combinations, the porosity screen indicated potential trends within porous liquid families with reasonable xenon uptake across several solvents ( $A^3:E^3$  in solvents 1 to 5) and scrambled cages ( $A^3:E^3$ ,  $A^5:H^1$ ,  $A^4:I^2$ , and  $A^3:I^3$ , all in solvent 5). With the effect of changing the different components of a Type II porous liquid poorly understood, further studies could provide insight into designing future systems. In addition,  $3^3:13^3_{HAP}$  and  $3^3:13^3_{TBA}$  also potentially had a higher pore concentration, and therefore might demonstrate higher gas uptake than  $3^3:13^3_{PCP}$ , which would allow the effects of changing the cage concentration to be investigated.

### 4.3 Naming Type II porous liquids

Prior to discussing the porous liquids studied in this chapter, a new naming system is presented (**Figure 4.4**). Previously, each combination was assigned a unique identifying code during the high-throughput solubility screen; for clarity the names were changed to describe both the scrambled cage component and the solvent used in the composition of the porous liquid.  $A^3:E^3$  is a known scrambled cage, and has been called  $3^3:13^3$  previously, but the other cages did not have a similar name, and therefore, retained the code relating to the incorporated amines used earlier in the study.

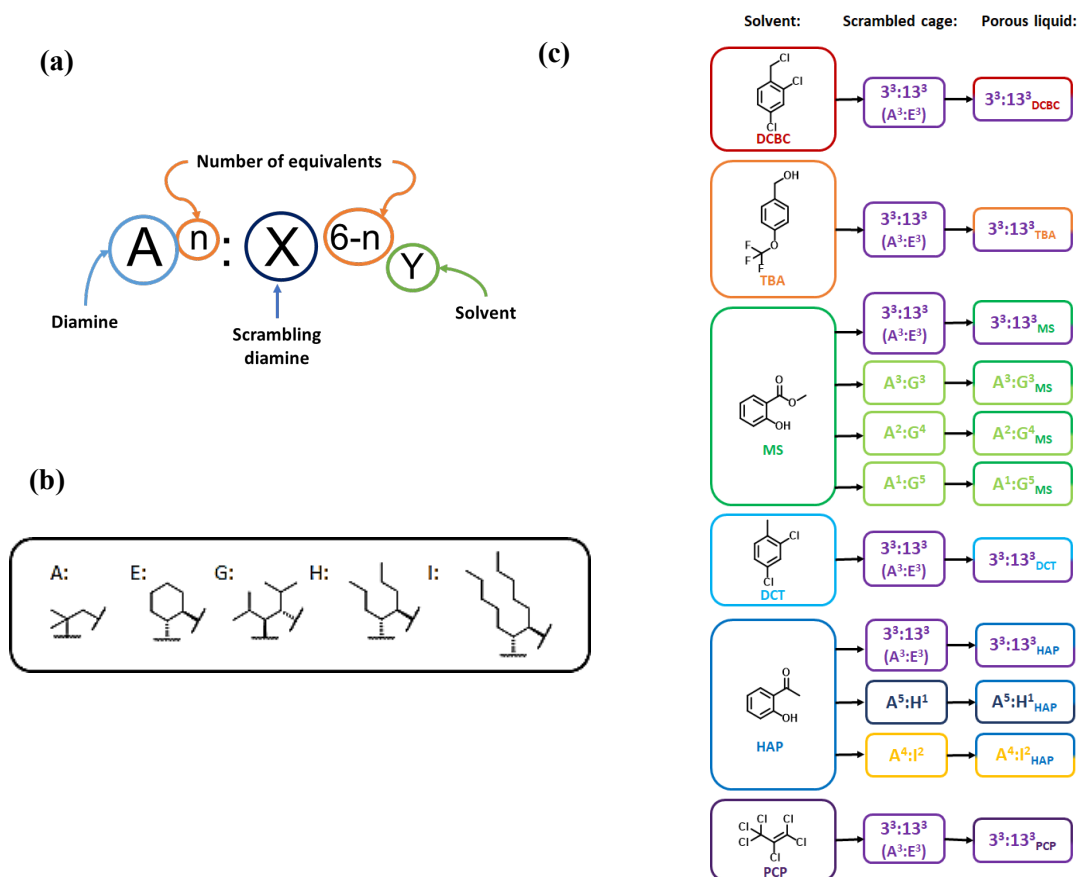


**Figure 4.4:** Naming system for new Type II scrambled porous liquids: (a) general scheme for the naming system,  $A^n:X^{6-n}$  ( $A/X$  = diamine, and  $n$  = number of diamines on cage vertices); (b) functionality on the porous organic cage periphery; (c) the names of the porous liquids studied further. For example,  $3^3:13^3$  ( $A^3:E^3$ ) in 2,4-dichlorobenzyl chloride (DCBC) is referred to as  $3^3:13^3_{DCBC}$ .

#### 4.4 Effect of changing porous liquid solvent

The size-excluded solvent is an important component of a Type II porous liquid, and has the potential to change the overall properties, as well as the diffusion of a guest into the cage pores. Previously, there have been no studies carried out to determine how changing the solvent affects the gas uptake of the system when the cage component remains the same. A family of Type II porous liquids was discovered during the high-throughput screen which contained the same scrambled cage,  $3^3:13^3$  ( $A^3:E^3$  in the high-throughput screen), in six different size-excluded solvents (Figure 4.5). Therefore, we were able to determine what effect varying the solvent had on the overall gas uptake and properties for the first time.



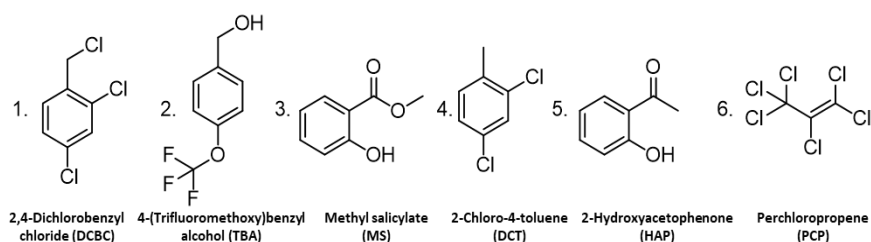


Figure 4.5: Structures of the size-excluded porous liquid solvents

#### 4.4.1 Studying xenon uptake using gas displacement

As discussed previously, the xenon uptake of a scrambled porous liquid can be measured by gas displacement using a small guest, such as chloroform (Figure 4.6). The original scrambled porous liquid, 20% w/v  $3^3:13^3$  in PCP, had a calculated uptake of 183.0  $\mu\text{mol}$  xenon, and using this methodology, could be compared to the other porous liquids in the family.<sup>13,112</sup>

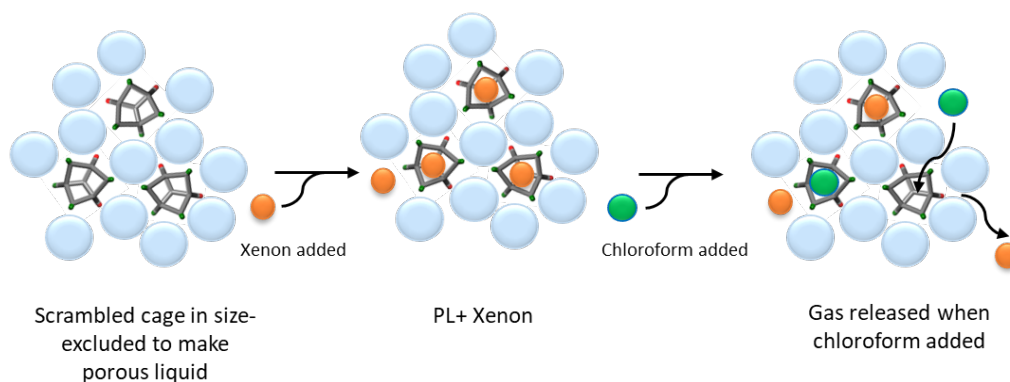
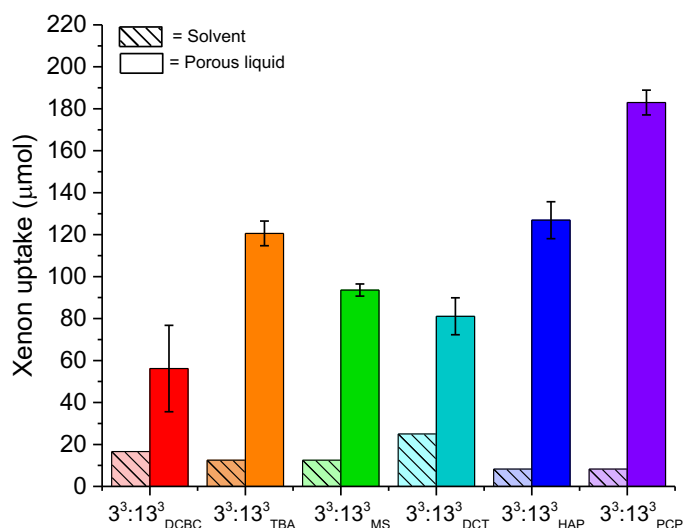


Figure 4.6: General scheme showing the measurement of xenon uptake using gas displacement from a porous liquid using a small guest (PL = porous liquid).

The xenon uptake was compared for the family of porous liquids formed using  $3^3:13^3$  in the six bulky solvents, with all of the samples formed using 200 mg of scrambled cage in 1 mL of each solvent (20% w/v). The volume of xenon collected was converted from mL to  $\mu\text{mol}$  using the ideal gas equation

Overall, all of the porous liquids in the family demonstrated a dramatic increase in xenon uptake compared to their neat parent solvents (Figure 4.7). However, the quantities of xenon displaced varied considerably in the new porous liquids, ranging from 56.2  $\mu\text{mol}$  to 126.9  $\mu\text{mol}$ , with  $3^3:13^3_{\text{PCP}}$  exhibiting a much higher uptake of 183.0  $\mu\text{mol}$ . The same quantity of  $3^3:13^3$  scrambled cage was present in each porous liquid sample, and is equivalent to the same concentration of cavities based on their calculated pore volume (ranging from 0.63-0.66%), which shows the solvent component directly impacts the overall gas uptake.



**Figure 4.7:** Effect of changing the size-excluded solvent on xenon uptake in a family of porous liquids. Average xenon uptake measured by displacement from the neat solvents (1 mL, dashed lines) and from each porous liquid (200 mg  $3^3:13^3$  with 1 mL solvent, 20% w/v) using chloroform (1.0 molar equivalents relative to cage) – average of 3 measurements, with the standard deviation shown as error bars.

† Given the cage is the same in all of the porous liquids and only the solvent is changing, the volume of xenon displaced from each porous liquid gives an indication into the affinity of the guest for the cage cavities within the porous liquid. In previous work, the percentage occupancy was calculated for a range of gases, with  $3^3:13^3_{PCP}$  showing a high affinity for xenon.<sup>112</sup> The same principle was applied to the porous liquids in this study for comparison – the percentage occupancy for each porous liquid was calculated from the volume of xenon displaced (**Figure 4.8**). This calculation assumes that 100% of the xenon had been evolved, all of the guest molecules reside in the cage cavities, and is compared to the maximum expected value based on 1:1 Xe:cage binding (4.6 cm<sup>3</sup> from 200 mg cage in 1 mL of solvent). Interestingly,  $3^3:13^3_{PCP}$  (95.7% occupancy) gave a much higher value compared to the study carried out previously (72.8%),<sup>13</sup> which could be due to the smaller volume of porous liquid used in this study. There are some limitations with using the calculated percentage occupancy as an indication for affinity of a guest molecule with the cage cavity in a porous liquid. For example, the value does not account for any guest dissolved in the solvent, and it assumes all the gas has been displaced from the cage cavities.

† There is a large experimental error due to the nature of the gas displacement experiments. The small volume of 1 mL leads to more variation in result as not all gas is removed from the porous liquid as some remains in the solvent

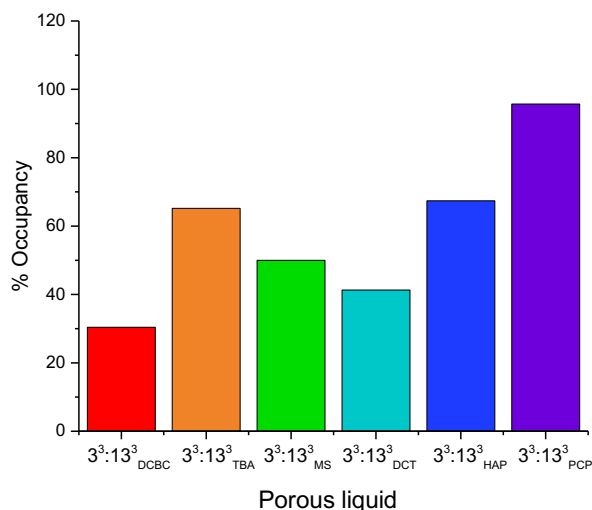


**Figure 4.8:** The percentage occupancy of xenon in the cage cavities for the  $3^3:13^3$  porous liquid series in different bulky solvents at 20% w/v.

#### 4.4.2 Studying methane uptake using $^1\text{H}$ NMR spectroscopy

Although gas displacement measurements can give an indication of the overall porosity of a system, they cannot confirm if a liquid is permanently porous, or that the gas is located within the cage cavities. However,  $^1\text{H}$  NMR spectroscopy can be used to investigate the host-guest behaviour, and give more of an indication of whether the liquids in question have permanent porosity. In addition, the methane uptake can be measured quantitatively using a calibrated capillary; it has previously been reported that the methane is shielded by the cage when it is located in the cavity.<sup>112</sup> These methods were used to study this family of porous liquids. A varying shift in the methane peak was observed in all cases, confirming that there is a solvent effect as the cage species remained the same. Although the new porous liquids exhibited substantially lower methane uptakes compared to  $3^3:13^3_{PCP}$  at the same concentration, they still all showed an enhancement over their respective neat parent solvents (**Figure 4.9**).

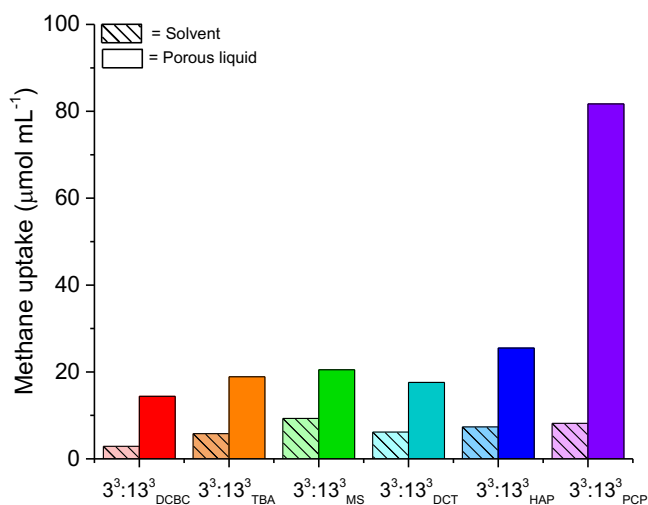


**Figure 4.9:** Methane uptake in neat solvents and porous liquids (20% w/v) measured using  $^1\text{H}$  NMR spectroscopy with a calibrated TMS/  $\text{CD}_2\text{Cl}_2$  capillary.

Previous studies have shown that the methane signal experiences an upfield shift in the  $^1\text{H}$  NMR spectra when compared to the neat parent solvent.<sup>13,112</sup> The new porous liquids also demonstrated a similar effect to varying degrees (**Figure 4.10**), indicating the gas molecules enter the cage cavities on the NMR timescale and experience a shielding effect. The most pronounced shifts seem to correlate with the liquids that exhibited the highest overall methane uptakes. Although  $\text{CH}_4$  is in dynamic equilibrium between the cage cavities and occupying the solvent, two separate chemical shifts for the bound and unbound guest was not observed. Work carried out by Komulainen demonstrated that xenon has a bound and unbound peak in the Xe NMR spectra of **CC3** and equilibrium is established between the two shifts. As a result, an average of the two peaks is present when is loaded with xenon.<sup>177</sup> However, there is no value for the completely bound methane so it is assumed the same happens in this case. The increase in the upfield shift seen when there was a higher uptake in a porous liquid was likely due to the higher concentration of  $\text{CH}_4$  present, meaning it moves closer towards the fully bound peak and further from the unbound seen in the neat solvent.

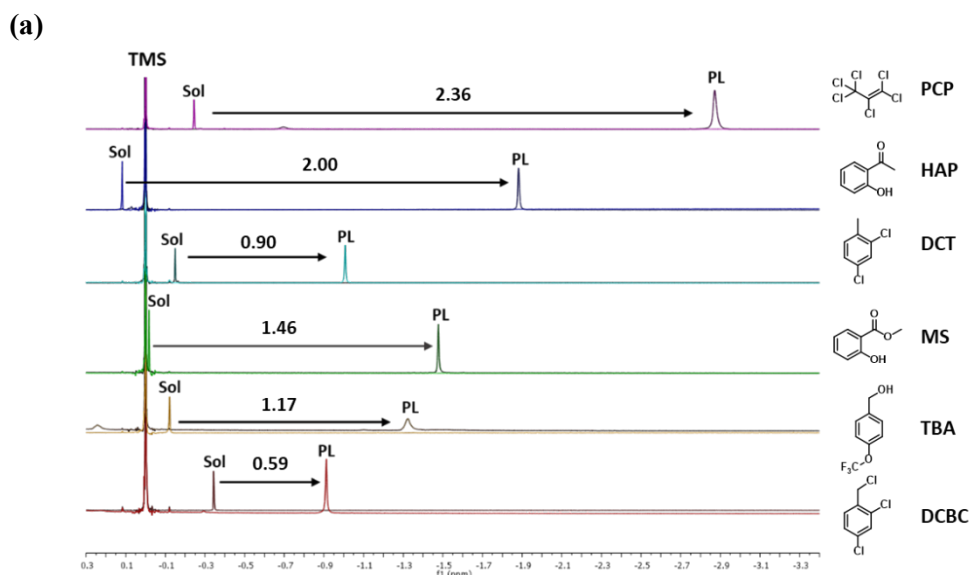


**Figure 4.10:** Comparison of the methane upfield shifts in the neat solvents and the porous liquids (Sol - indicates  $\text{CH}_4$  in neat solvent, PL - indicates  $\text{CH}_4$  in porous liquid).

Overall, the general trends that started to emerge within the scrambled  $3^3:13^3$  porous liquid family gave an insight into the effect changing the size-excluded solvent has on the methane uptake. As the same cage ( $3^3:13^3$ ) was used in each porous liquid, it suggests that the interaction and solubility of a guest in the solvent directly influences the overall gas uptake in the system. A higher methane uptake in the parent solvent resulted in a higher uptake and greater change in chemical shift in the corresponding porous liquids (**Figure 4.11**). This suggests that a high solubility in the neat solvent is more likely to result in the methane molecules entering and occupying the cage cavities in the porous liquid. For example, neat PCP dissolves the highest concentration of methane compared to the other solvents in the

study ( $7.1 \mu\text{mol mL}^{-1}$ ) and the porous liquid,  $3^3:13^3_{\text{PCP}}$ , gives the highest overall methane uptake ( $81.7 \mu\text{mol mL}^{-1}$ ), whereas  $3^3:13^3_{\text{DCBC}}$ , and its solvent (2,4-dichlorobenzyl chloride) gave the lowest values ( $14.2$  and  $2.8 \mu\text{mol mL}^{-1}$ , respectively).  $3^3:13^3_{\text{DCT}}$  and  $3^3:13^3_{\text{MS}}$  did not appear to follow this trend to the same degree as the other porous liquids, which could be due to other factors influencing the equilibrium kinetics between the methane inside and outside the cavities.

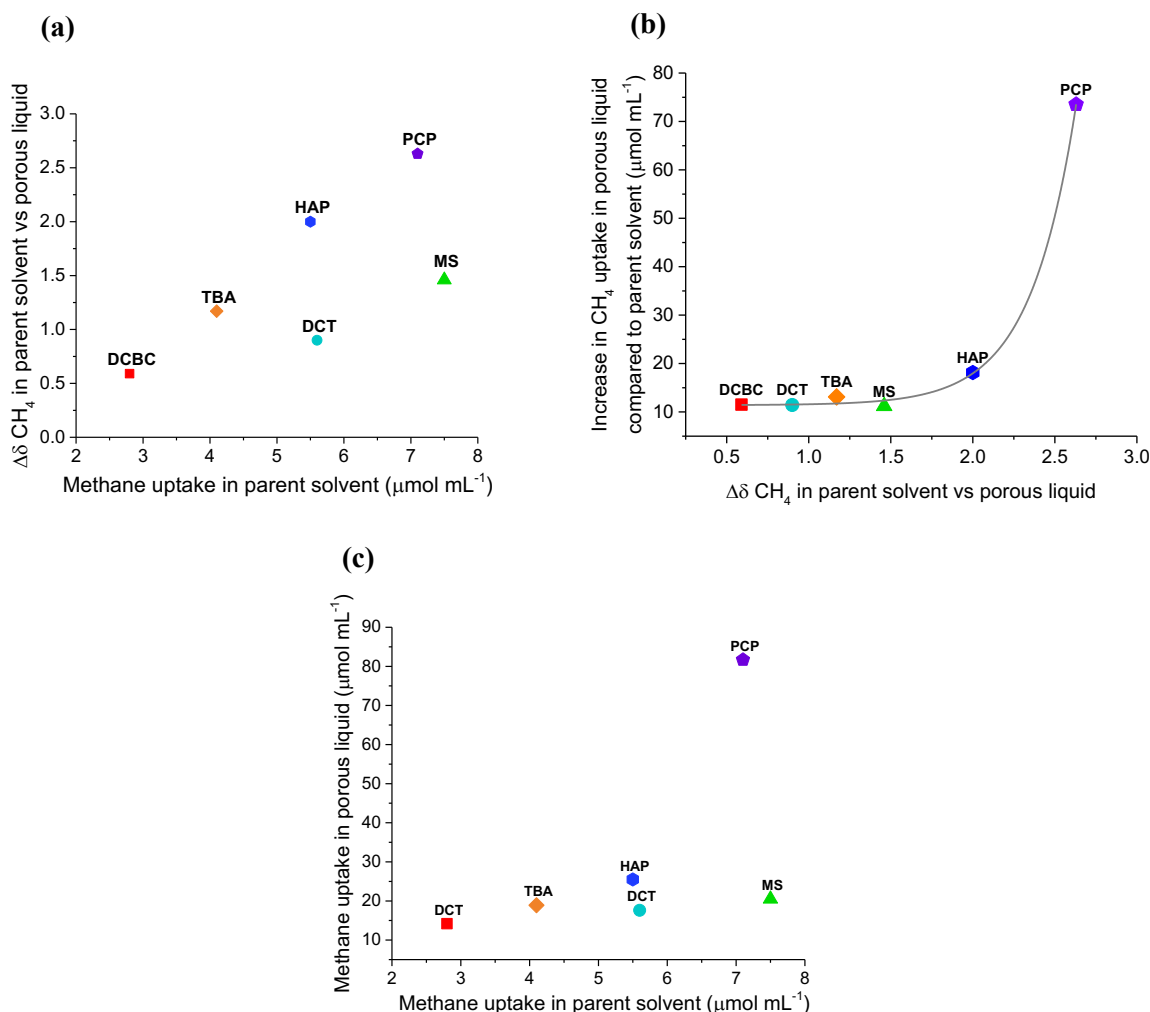


**Figure 4.11:** The relationship between (a) methane uptake in the parent solvent of a porous liquid and the change in methane chemical shift between the parent solvent and porous liquid; (b) changes in methane chemical shift compared to the increase in methane uptake between the parent solvent and the corresponding porous liquid; (c) the methane uptake ( $\mu\text{mol mL}^{-1}$ ) in the neat solvent and the corresponding porous liquid at 20% w/v.

In previous work, diffusion NMR spectroscopy has been used to calculate the length of time that methane resides in the cage cavities in  $3^3:13^3_{\text{PCP}}$ , by comparing the diffusion coefficients of  $\text{CH}_4$  in neat PCP and the porous liquid.<sup>112</sup> However, when this was attempted for the other porous liquids in the  $3^3:13^3$  series, reliable diffusion coefficients could not be measured. PCP

has no protons, meaning it is  $^1\text{H}$  NMR inactive, whilst the other solvents in the study are – this made it challenging to run diffusion NMR.

#### 4.4.3 General trends in changing solvent on gas uptake

One key consideration when reporting gas uptake in a Type II porous liquid is the units of measure used. Changing the porous liquid solvent has an impact: 1 mL of sample for each porous liquid does not have the same overall mass. However, the porous liquids in this part of the study do all possess the same quantity of cage, and as a result, the same number of cage cavities. This allowed a direct comparison of the porous liquids.

In order to compare the uptakes of different gases in the same porous liquids, the xenon uptakes were converted from  $\mu\text{mol}$  (Figure 4.7) to  $\mu\text{mol mL}^{-1}$ , to allow a direct comparison to the measured  $\text{CH}_4$  uptakes (Figure 4.12). All of the porous liquids have a higher xenon uptake than  $\text{CH}_4$ , likely due to the preferred binding of xenon in the cage cavity, as discussed earlier. Overall,  $3^3:13^3_{\text{PCP}}$  had the highest uptake for both gases ( $81.7 \mu\text{mol mL}^{-1} \text{CH}_4$ , and  $155.0 \mu\text{mol mL}^{-1} \text{Xe}$ ). Interestingly,  $3^3:13^3_{\text{TBA}}$  has the biggest difference between the two gas uptakes ( $86.6 \mu\text{mol mL}^{-1}$ ), which could mean this system is suitable for use in gas separations. The investigation into the xenon and  $\text{CH}_4$  uptake showed that varying the solvent component of a porous liquid has a direct impact on the gas uptake of a system.

In previous work, a correlation between the heats of absorption of the gases in the solid state, and the uptake in the porous liquid, was observed,<sup>112</sup> but these additional findings also show that the solvent influence is just as important.

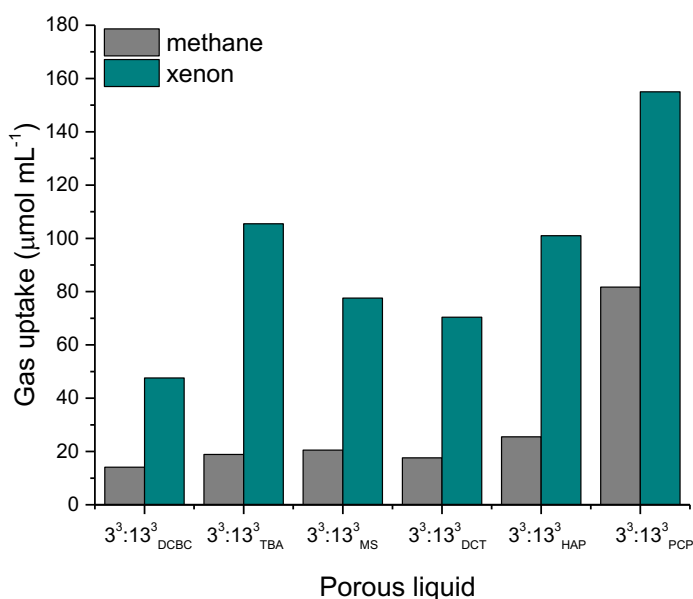


**Figure 4.12:** Comparison of the methane and xenon uptakes in the scrambled  $3^3:13^3$  porous liquids at 20% w/v using the different solvents from the high-throughput screen.

## 4.5 Effect of changing scrambled cage component

As well as families of porous liquids containing the same cage with different solvents, there were several where the scrambled cage varied in the same solvent (**Figure 4.13**). Therefore, the effect of changing the cage component on gas uptake was also investigated, particularly in respect to the effect on the selectivity and the overall uptake.<sup>‡</sup>

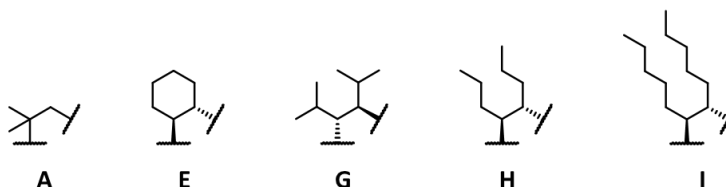


**Figure 4.13:** Structures of the functionality on the scrambled cages used in the study.

### 4.5.1 Effect of changing the diamine feed ratio on gas uptake

The gas uptake in porous liquids that were formed using scrambled cages from the same diamines, but with different feed ratios ( $A^3:G^3$ ,  $A^2:G^4$ ,  $A^1:G^5$ ), in a single solvent (methyl salicylate, MS) at 20% w/v (200 mg in 1 mL, equating to ~15 wt%) were compared. The xenon uptake seemed to vary considerably with changing diamine ratio (50.0–116.5  $\mu\text{mol mL}^{-1}$ ; **Figure 4.14**). Overall,  $A^2:G^4$  gave the highest xenon uptake (116.5  $\mu\text{mol mL}^{-1}$ ), even compared to the  $3^3:13^3_{\text{MS}}$  porous liquid (95.6  $\mu\text{mol mL}^{-1}$ ), as  $3^3:13^3$  has been the best performing scrambled cage to date, albeit not in MS (**Figure 4.3**).

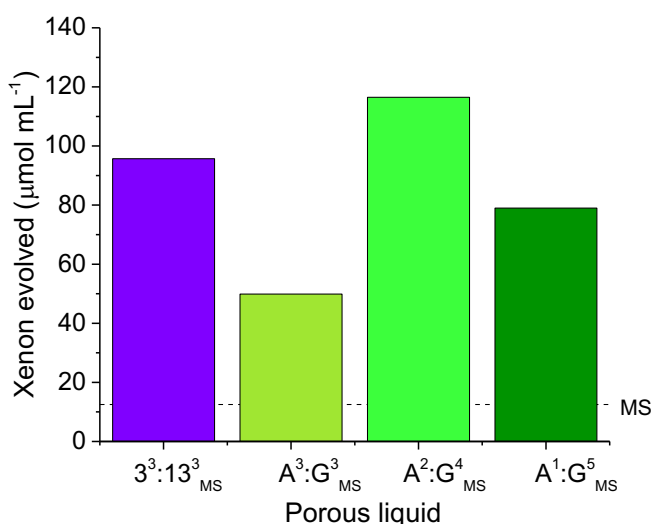


**Figure 4.14:** The effect of changing the diamine feed ratio on the xenon uptake in the  $A:G_{\text{MS}}$  porous liquid family at 20% w/v.

<sup>‡</sup> These experiments were not repeated due to the limited amount of scrambled cage available.

The CH<sub>4</sub> uptake in the A:G scrambled cage family was also studied using <sup>1</sup>H NMR spectroscopy, as previously discussed. Interestingly, the diamine feed ratio did not affect the methane uptake, with very similar solubility measured for all the porous liquids tested (18.9–20.6 μmol mL<sup>-1</sup>, **Figure 4.15a**). However, the <sup>1</sup>H NMR spectra gave an insight into the equilibrium kinetics: a higher ratio of isopropyl functionality (A<sup>1</sup>:G<sup>5</sup>) led to a larger methane peak shift than observed for the other porous liquids in the family, which suggests the average chemical shift is closer to the fully bound shift (**Figure 4.15b**). The guest could potentially be spending more time in the pores on an NMR timescale because of the steric bulk provided by the extra isopropyl groups, slowing down the rate of diffusion.

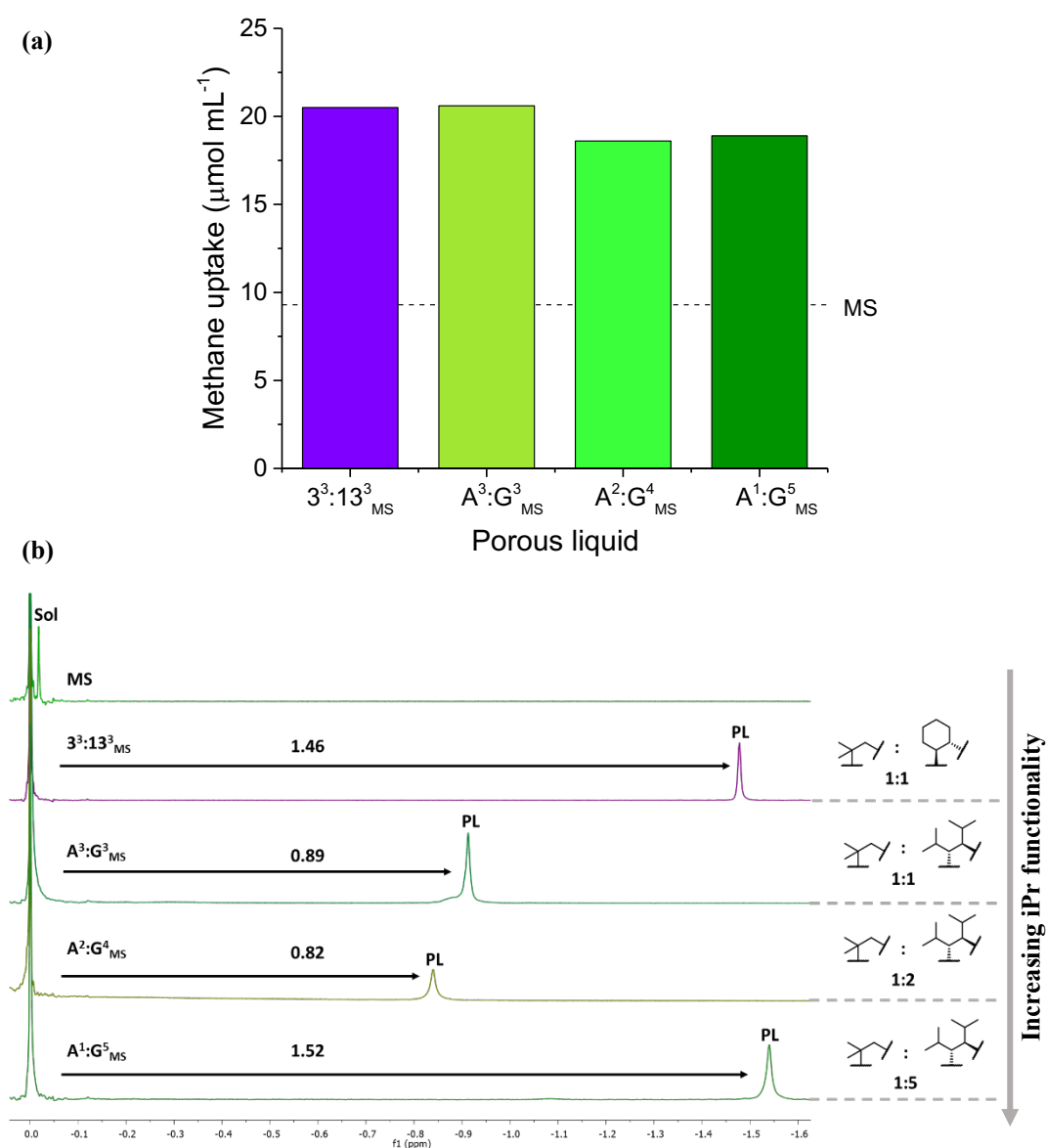


**Figure 4.15:** (a) Effect of changing the diamine feed ratio on methane uptake; (b) Comparison of the methane upfield shifts in the <sup>1</sup>H NMR spectra for the neat solvent (MS) and the porous liquids (Sol – indicates CH<sub>4</sub> in neat solvent, PL - indicates CH<sub>4</sub> in porous liquid).



Whilst there appeared to be a correlation between the overall CH<sub>4</sub> uptake and the chemical shift when the porous liquid solvent was changed, there is not a clear trend when the diamine feed ratio is changed (**Figure 4.16a**). In this case, the change in chemical shift gives more of an indication of the kinetic behaviour of the guest, and the preference it has for occupying the cage cavity. The number of isopropyl groups on the periphery of the cage appears to change the preference of some guests over others. For example, two systems (**A<sup>2</sup>:G<sup>4</sup>** and **A<sup>3</sup>:G<sup>3</sup>**) seemed each to have a preference for xenon or methane, respectively (**Figure 4.16b**) – **A<sup>2</sup>:G<sup>4</sup>** appeared to have a high xenon uptake (116.5 μmol mL<sup>-1</sup>), whereas in **A<sup>3</sup>:G<sup>3</sup>** (which contained less isopropyl functionality) it appeared that the xenon uptake was reduced (50.0 μmol mL<sup>-1</sup>). This effect demonstrates the possibility of tuning the selectivity in porous liquids by varying the functionality on the periphery.

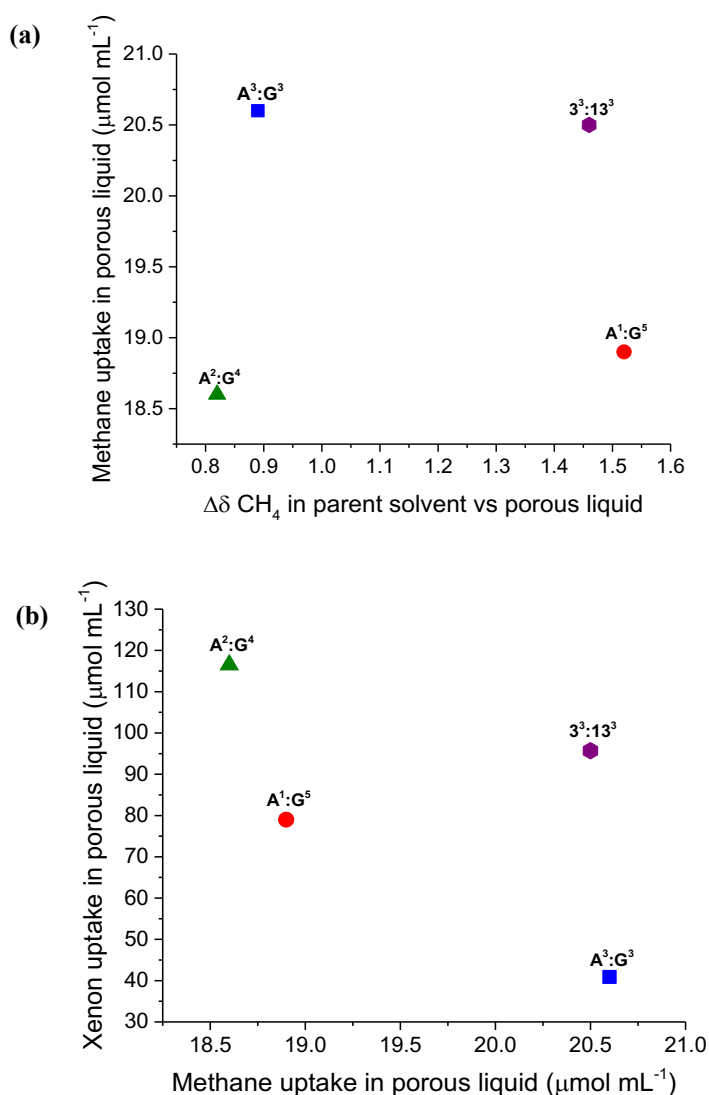


**Figure 4.16:** Graphical representation of the relationship between (a) the change in methane chemical shift and methane uptake, and (b) the methane and xenon uptakes in porous liquids formed using cages containing different diamine feed ratios.

#### 4.5.2 Effect of changing the diamine chain length on gas uptake

Another family of porous liquids discovered in the high-throughput screen contained different length alkyl chains on the cage periphery (*n*-propyl in  $A^5:H^1$ , *n*-pentyl in  $A^4:I^2$ , compared to the cyclohexyl groups in  $A^3:E^3$ ) in the same solvent (2-hydroxyacetophenone, HAP). The gas uptake in each of these porous liquids at 20% w/v was compared to determine if chain length can also alter the uptake and selectivity of a system.

Overall, the addition of a linear chain on the cage periphery reduced the xenon uptake in the porous liquids compared to those that contained cyclohexyl functionality (**Figure 4.17**). The linear alkyl chains could reduce the porosity of the system by preventing the diffusion of guests into the cage cavity, or by occupying the cavities of neighbouring cages. The addition of alkylated functionality of increasing chain length has been shown to reduce the porosity of neat Type I porous liquids based on organic cages, and therefore it is likely that this is also occurring in the Type II systems.<sup>110</sup>

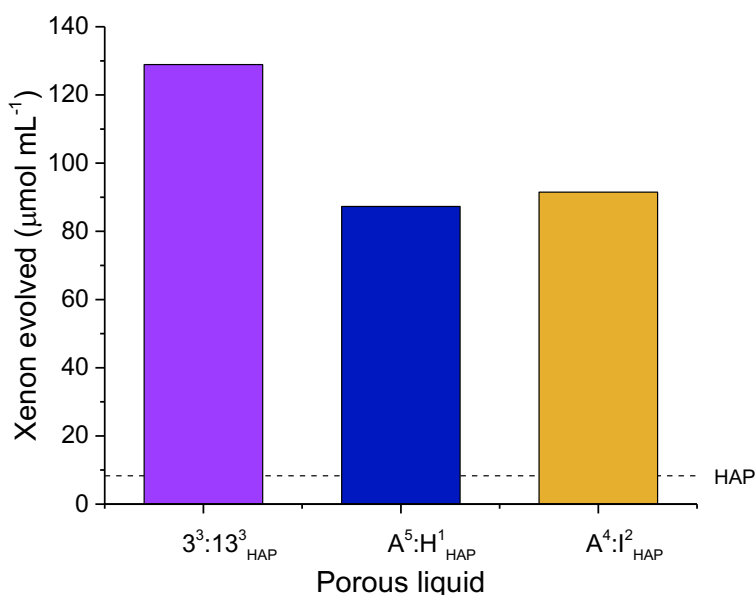


**Figure 4.17:** Effect of changing the diamine alkyl chain length on xenon uptake

Whilst the xenon uptake reduced as the length of the alkyl substituent increased, a similar methane uptake was observed –  $25.5 \mu\text{mol mL}^{-1}$  in  $A^3:E^3_{\text{HAP}}$ ,  $23.3 \mu\text{mol mL}^{-1}$  in  $A^5:H^1_{\text{HAP}}$ , and  $19.0 \mu\text{mol mL}^{-1}$  in  $A^4:I^2_{\text{HAP}}$  (**Figure 4.18a**). This suggests that the exterior functionality of the cage species can have a direct effect on the overall gas uptake, but that this effect may not be the same for all gases, perhaps offering an opportunity to tune gas selectivity. The  $^1\text{H}$  NMR spectrum also gives an insight into the kinetics and host-guest behaviour of the methane when the alkyl chains on the cage periphery are changed. Not only is the methane uptake similar in the porous liquids, but so is the change in methane chemical shift (**Figure 4.18b**).

Although  $A^4:I^2_{HAP}$  had low  $CH_4$  uptake, this porous liquid had a larger chemical shift compared to  $A^5:H^1_{HAP}$ , which is likely due to the equilibrium being towards the  $CH_4$  molecules spending more time in the cage cavities. There does appear to be some broadening of the peak in  $A^2:I^4_{HAP}$ , which suggests a slower equilibrium between the guests being in and out of the cage cavities on an NMR timescale, and could be due to the longer alkyl chains slowing down the rate of diffusion.

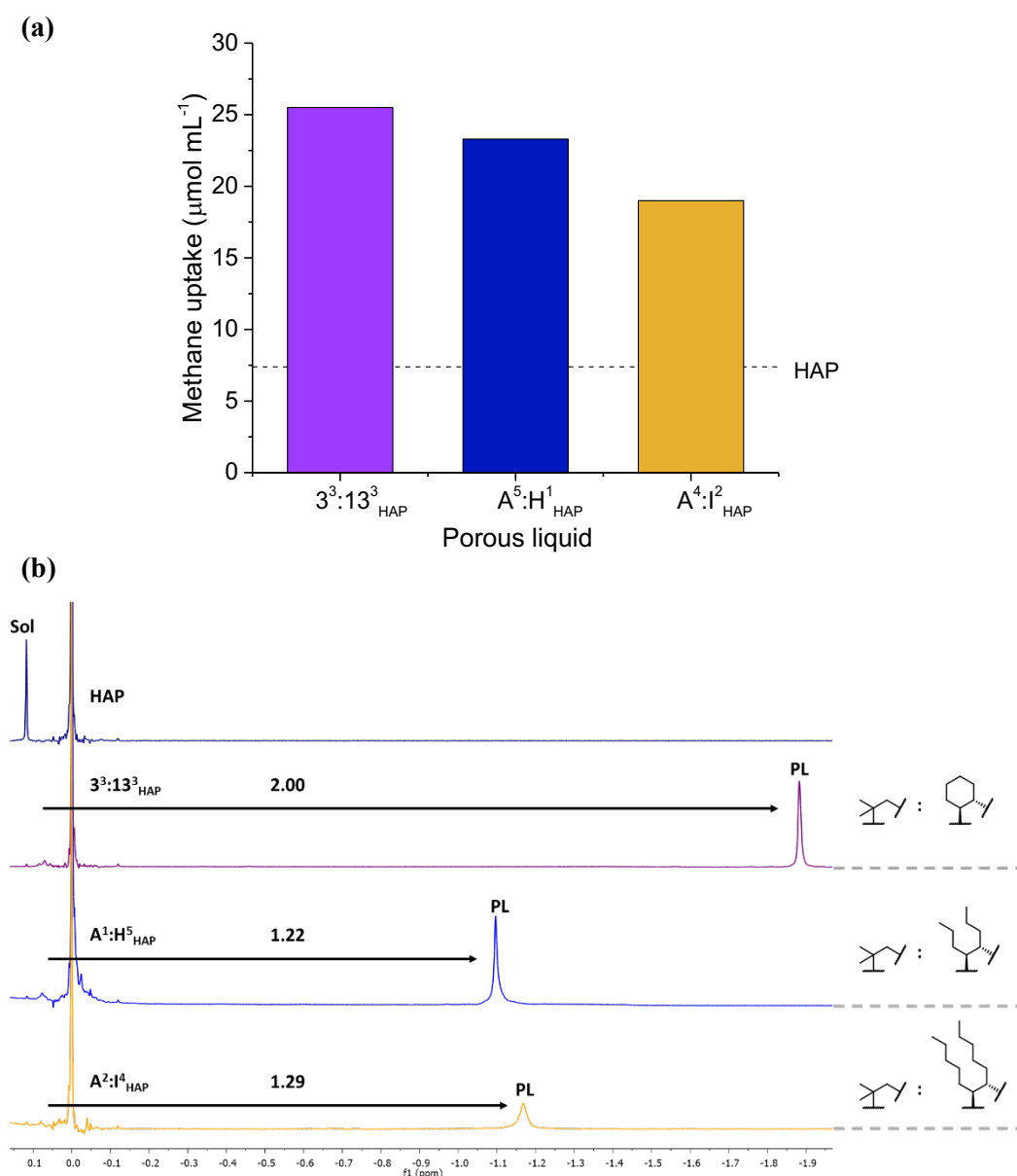


Figure 4.18: Effect of changing the diamine functionality on (a) methane uptake, and (b) the methane chemical shift in different porous liquids compared to the parent solvent

## 4.6 Effect of changing the scrambled cage concentration

While the effect of changing both the solvent and scrambled cage components was investigated and gave an indication of the effect on gas uptakes in Type II porous liquids, the studies were carried out at the same concentration of cage (200 mg in 1 mL of solvent). A key aim of this study was to find Type II scrambled porous liquids with a higher cavity concentration, and therefore increased gas uptake, compared to the first reported example ( $3^3:13^3_{\text{PCP}}$ ,  $95.6 \mu\text{mol g}^{-1}$  Xe uptake at 20% w/v).

### 4.6.1 The effect of changing the cage concentration on xenon uptake and viscosity

The high-throughput solubility screen, carried out in **Chapter 2**, had an upper limit of 30% w/v. Therefore, all of the discovered porous liquids that met this criterion had a higher cavity concentration compared to  $3^3:13^3_{\text{PCP}}$ . When these were scaled up and screened for porosity, three systems were found with comparable xenon uptake at 20% w/v, indicating that they might be good candidates for higher concentration porous liquids. One of these hits ( $A^2:G^4$  in methyl salicylate) however, showed some gelation and was not investigated further, leaving two porous liquids for further study. These systems both contained the same  $3^3:13^3$  scrambled cage ( $A^3:E^3$ ), but in different solvents: 2-hydroxyacetophenone (HAP) and 4-(trifluoromethoxy)benzyl alcohol (TBA).

The xenon uptake in  $3^3:13^3_{\text{HAP}}$  and  $3^3:13^3_{\text{TBA}}$  ( $98.7$  and  $83.4 \mu\text{mol g}^{-1}$ , respectively) was comparable to  $3^3:13^3_{\text{PCP}}$  ( $95.6 \mu\text{mol g}^{-1}$ ) at 20% w/v. However, after determining and taking the density into account, the volumetric xenon uptake of  $3^3:13^3_{\text{HAP}}$  ( $\rho = 1.0240 \text{ g mL}^{-1}$ ,  $101 \mu\text{mol mL}^{-1}$ ) and  $3^3:13^3_{\text{TBA}}$  ( $\rho = 1.2648 \text{ g mL}^{-1}$ ,  $105.5 \mu\text{mol mL}^{-1}$ ) were both found to be lower than  $3^3:13^3_{\text{PCP}}$  ( $\rho = 1.6193 \text{ g mL}^{-1}$ ,  $155 \mu\text{mol mL}^{-1}$ ) at 20% w/v. By increasing the cage concentration in these systems, the aim was to find porous liquids with higher porosity because the solubility of  $3^3:13^3$  was substantially higher in both HAP and TBA than PCP. As a result, Type II scrambled porous liquids with ~25-35 wt% cage concentrations were formed and studied, which was higher than the previously reported  $3^3:13^3_{\text{PCP}}$  (10 wt%). Xenon displacement experiments were performed on these higher concentration systems to study if the porosity changed.

When the concentration of  $3^3:13^3_{\text{HAP}}$  was increased from 16 to 27 wt%, the volume of xenon evolved showed a proportional increase from  $101$  to  $194.7 \mu\text{mol mL}^{-1}$ , which equates to a 93% increase in gas solubility when going from 200 mg to 400 mg of scrambled cage in 1 mL of solvent (**Figure 4.19a**). The gravimetric xenon solubility of  $3^3:13^3_{\text{HAP}}$  also significantly exceeds the first scrambled porous liquid,  $3^3:13^3_{\text{PCP}}$  ( $155 \mu\text{mol mL}^{-1}$ ),<sup>112</sup> with the 27 wt%

$3^3:13^3_{\text{HAP}}$  sample demonstrating a 26% increase in xenon uptake compared to the 10 wt%  $3^3:13^3_{\text{PCP}}$  system ( $194.7 \mu\text{mol mL}^{-1}$  vs.  $155 \mu\text{mol mL}^{-1}$ ).

However, increasing the cage concentration in  $3^3:13^3_{\text{TBA}}$  from 14 to 24 wt%, did not have the same effect on the xenon uptake – the gas evolution seemed to plateau or even to decrease (Figure 4.19b). A similar occurrence was observed for  $3^3:13^3_{\text{HAP}}$  at 35 wt% (equating to 600 mg scrambled cage in 1 mL solvent) – the volume of xenon displaced using chloroform was substantially lower than expected for the increase in cage concentration (Figure 4.19a). Both  $3^3:13^3_{\text{TBA}}$  (24 wt%) and  $3^3:13^3_{\text{HAP}}$  (35 wt%) were noticeably more viscous at these concentrations, which was thought to be influencing the diffusion of guests into the cage cavities.

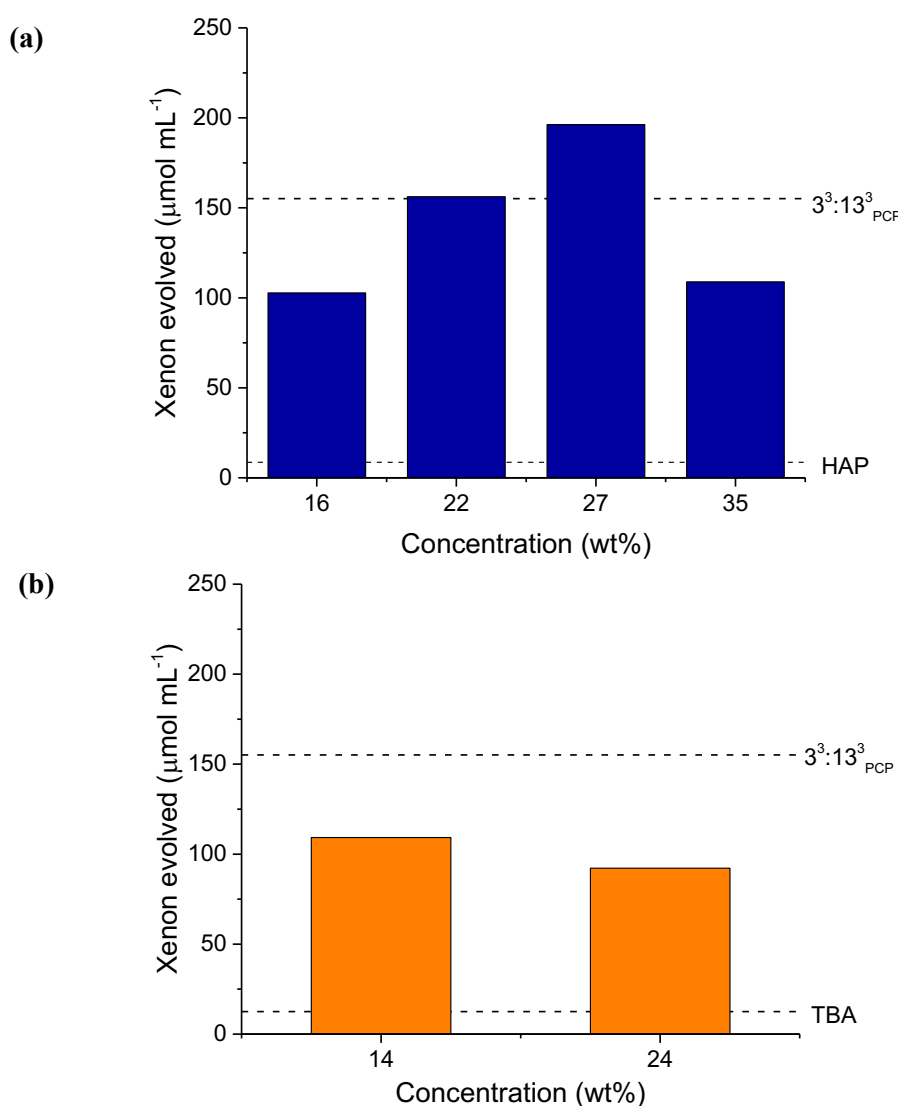


**Figure 4.19:** Xenon uptake in (a)  $3^3:13^3_{\text{HAP}}$  at different concentrations (200, 300, 400 and 600 mg in 1 mL solvent, equating to 16, 22, 27 and 35 wt% solutions), and (b)  $3^3:13^3_{\text{TBA}}$  at different concentrations (200 and 400 mg in 1 mL solvent, equating to 14 and 24 wt% solutions), measured by displacement with chloroform (1.0 molar equiv. per cage). Compared to the uptake in the neat solvents (HAP and TBA) and the maximum xenon uptake in  $3^3:13^3_{\text{PCP}}$  at 10 wt%.

In an attempt to rationalise the plateau in xenon uptake, the viscosity was measured for  $3^3:13^3_{\text{HAP}}$  and  $3^3:13^3_{\text{TBA}}$  at various concentrations (Figure 4.20). In both porous liquids, the viscosity increased with increasing cage concentration, but  $3^3:13^3_{\text{TBA}}$  had a significantly higher viscosity at 24 wt% ( $298.07 \pm 1.8$  cP) than the 14 wt% solution ( $32.46 \pm 0.53$  cP), and  $3^3:13^3_{\text{HAP}}$  at 27 wt% ( $62.64 \pm 0.095$  cP). Therefore, it is possible that the significant increase in viscosity for  $3^3:13^3_{\text{TBA}}$  at 24 wt% is responsible for the reduction in xenon uptake.

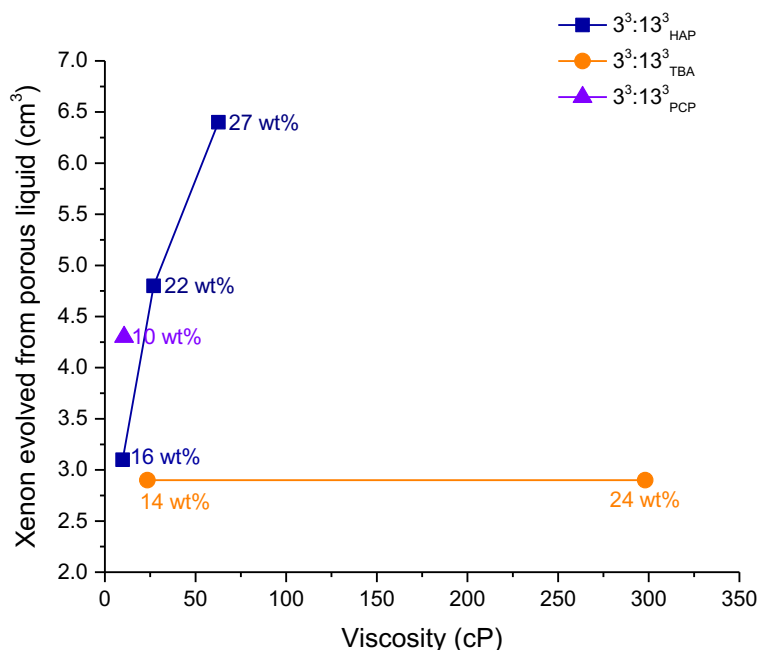
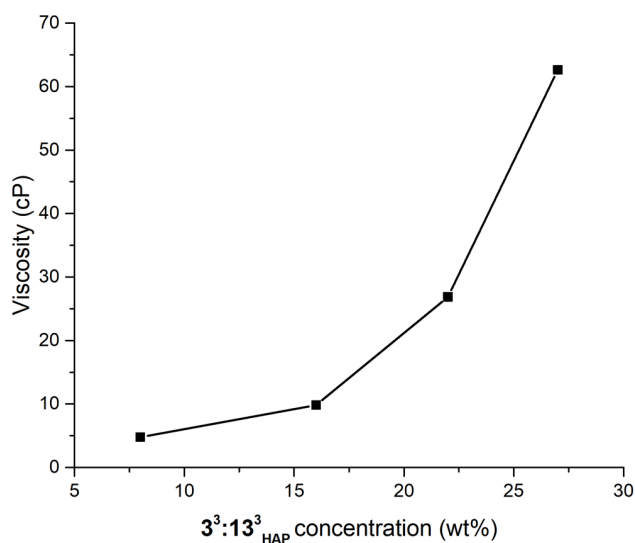


Figure 4.20: The volume of xenon evolved from  $3^3:13^3_{\text{HAP}}$  and  $3^3:13^3_{\text{TBA}}$  at different concentrations compared to their viscosities, with  $3^3:13^3_{\text{PCP}}$  at 10 wt% plotted for comparison.

However, the observed reduction in gas uptake for 35 wt%  $3^3:13^3_{\text{HAP}}$  could also be due to the addition of chloroform to displace the gas, which partially precipitated the cage from solution, and suggests the sample is at saturation. Since  $3^3:13^3_{\text{HAP}}$  could form porous liquids at varying concentrations, the maximum concentration was capped at 27 wt% for subsequent gas uptake studies.

In summary, changing the cage concentration of a Type II porous liquid appears to affect the overall properties, including the viscosity, which can affect the gas uptake. For example, increasing the amount of cage in  $3^3:13^3_{\text{HAP}}$  also increases the viscosity of the system (Figure 4.21). While this does not seem to affect the gas uptake up to 27 wt% (Figure 4.20), other systems, such as  $3^3:13^3_{\text{TBA}}$ , were shown to have reduced gas uptake at increasing concentration and higher viscosities. These findings suggest that viscosity is an important parameter when designing new porous liquids and there could be an optimum pore concentration for maximum gas uptake in each system.



**Figure 4.21:** The relationship between the concentration of scrambled cage in  $3^3:13^3_{\text{HAP}}$  and the viscosity of the porous liquid.

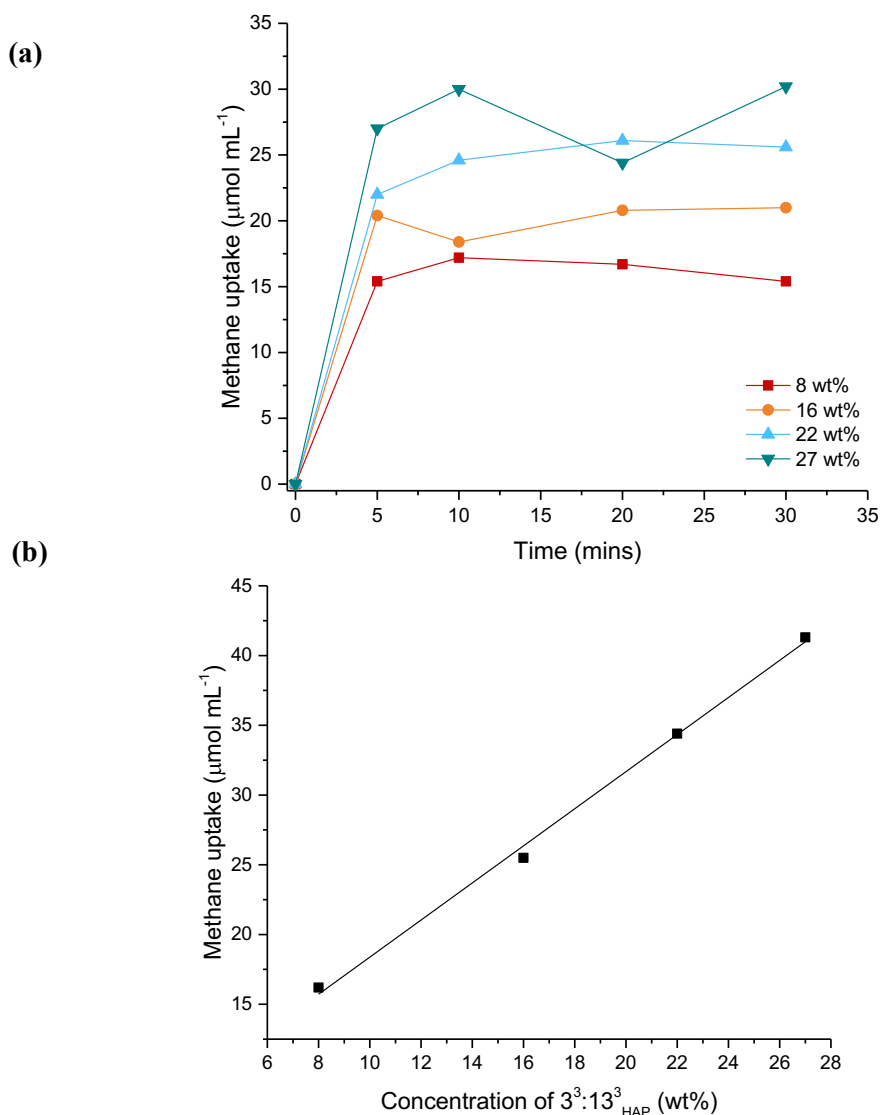
#### 4.6.2 Changing the cage concentration and its effect on methane uptake

The porous liquid  $3^3:13^3_{\text{HAP}}$  showed proportional xenon uptake with cavity concentration and, therefore, this porous liquid was chosen to study in further detail. Since  $3^3:13^3_{\text{HAP}}$  could form porous liquids at varying concentrations, the  $\text{CH}_4$  uptake was studied in this system using  $^1\text{H}$  NMR spectroscopy.

First, saturation studies were carried out (using  $^1\text{H}$  NMR spectroscopy) to determine the time required for the porous liquid to reach its maximum occupancy. Methane was added at 50 to 60  $\text{mL min}^{-1}$  flow rate to different  $3^3:13^3_{\text{HAP}}$  samples at various concentrations (8, 15, 21, and 26 wt%) over five-minute intervals, and a  $^1\text{H}$  NMR spectrum was recorded. Each porous liquid reached full saturation within five minutes, with only small fluctuations apparent after this time (**Figure 4.22a**). Based on this, for all subsequent experiments, the  $3^3:13^3_{\text{HAP}}$  porous liquid samples were purged with a gas for 10 minutes per 1 mL of solvent used to ensure saturation.

With the time needed to saturate  $3^3:13^3_{\text{HAP}}$  at various concentrations now known, the porous liquid could be investigated further. Overall, there was a linear correlation between the  $\text{CH}_4$  uptake and the cage concentration in  $3^3:13^3_{\text{HAP}}$  (**Figure 4.22b**), suggesting that the uptake in this system corresponds directly to the increased number of accessible cavities. Although the xenon uptake in 27 wt%  $3^3:13^3_{\text{HAP}}$  was the highest of the systems studied, the porous liquid had a lower  $\text{CH}_4$  uptake compared to  $3^3:13^3_{\text{PCP}}$  ( $41.3 \mu\text{mol mL}^{-1}$  for  $3^3:13^3_{\text{HAP}}$  at 27 wt%, compared to  $81.7 \mu\text{mol mL}^{-1}$  for  $3^3:13^3_{\text{PCP}}$  at 10 wt%). This could be due to the increased viscosity (62.64 vs. 4.30 cP), or that neat HAP dissolves less methane than neat PCP ( $5.5$  vs.  $7.1 \mu\text{mol mL}^{-1}$ , respectively).

Although the methane uptake for  $3^3:13^3_{\text{HAP}}$  at 27 wt% did not exceed that of  $3^3:13^3_{\text{PCP}}$ , the  $^1\text{H}$  NMR data also gives information on the behaviour of the guests when the cage concentration is increased. As expected, the ratio of cage to solvent molecules decreases with increasing cage concentration (Table 4.1), which has an interesting effect on the  $\text{CH}_4$  molecules in the porous liquid. The methane's chemical shift gives an indication for the preference of the guest to reside in the cage cavities. Increasing the concentration of  $3^3:13^3_{\text{HAP}}$  also shifts the  $\text{CH}_4$  peak more upfield (Figure 4.23), which suggests an increased preference of the guest for the cage pores, or the  $\text{CH}_4$  is spending more time on average in the cage cavities on the NMR timescale.

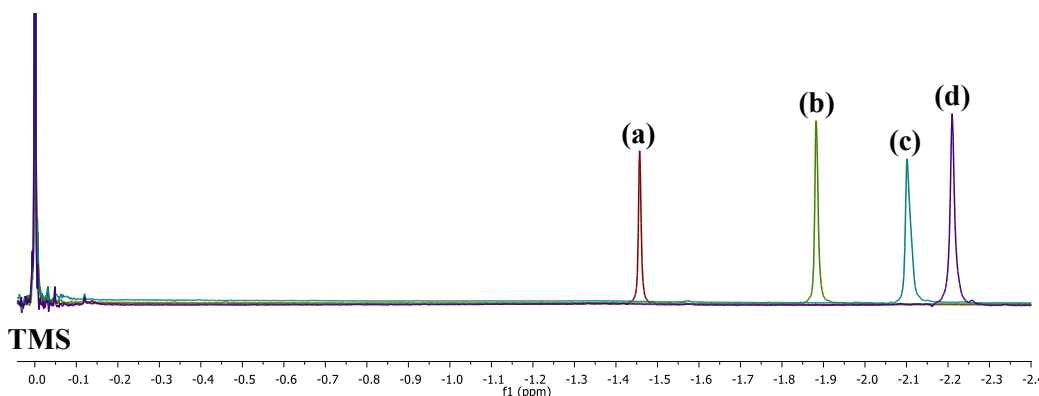


**Figure 4.22:** (a) The methane concentration in  $3^3:13^3_{\text{HAP}}$  at 8, 16, 22 and 27 wt% calculated from the  $^1\text{H}$  NMR spectra after being purged for five minute intervals (all of the samples were saturated after 5 minutes), and (b) methane uptake in  $3^3:13^3_{\text{HAP}}$  at different concentrations measured by  $^1\text{H}$  NMR spectroscopy.

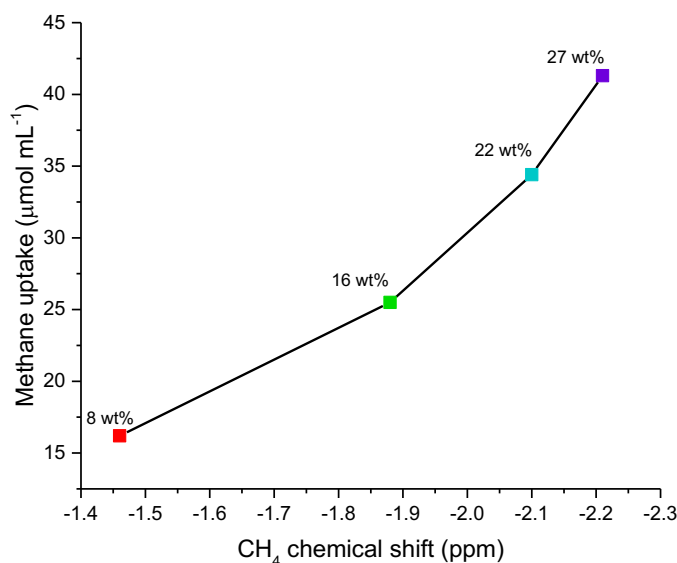


**Table 4.9:** Summary of component amounts in  $3^3:13^3_{\text{HAP}}$  at various concentrations and the calculated cage to solvent ratios.

Concentration (wt %)	Mmol cage	Mmol solvent	Cage: Solvent
8	0.0962	8.307	1:86
16	0.192	8.307	1:43
22	0.289	8.307	1:29
27	0.385	8.307	1:22


**Figure 4.23:** Overlaid  $^1\text{H}$  NMR spectra ( $\text{CD}_2\text{Cl}_2/\text{TMS}$  capillary) for different concentrations of  $3^3:13^3_{\text{HAP}}$  loaded with methane at (a) 8, (b) 16, (c) 22 and (d) 27 wt%, showing the shift corresponding to methane relative to TMS.

There is also a correlation between the methane chemical shift and the overall uptake in  $3^3:13^3_{\text{HAP}}$  with increasing cage concentration (**Figure 4.24**). The  $\text{CH}_4$  molecules could be spending longer in the cage cavities compared to the solvent, because there are more cages per volume of porous liquid at higher concentrations. Additionally, the increased viscosity of the system could slow down the rate of diffusion.


**Figure 4.24:** Graphical representation of the relationship between the methane chemical shift in  $3^3:13^3_{\text{HAP}}$  at various concentrations and the calculated methane uptake in the porous liquids.

## 4.7 Investigation into guest release mechanisms

In this chapter so far, small liquid additives were used to displace the gas within the cavities of the porous liquid. In previous work, sonication was demonstrated as an additional and effective gas release mechanism for repeated cycles.<sup>112</sup> Although sonication is a more effective method of displacement than the use of a chemical additive, both procedures are not practical mechanisms for large scale gas capture and release. Temperature and pressure swings are conventional techniques used to remove gas from liquids, but lowering the pressure of a Type II porous liquid is challenging due to the solvent's associated vapour pressure. Temperature release, however, could be a viable way to liberate xenon from a pre-loaded porous liquid, and the effect of heating  $3^3:13^3_{\text{HAP}}$  was investigated.

Initially, on increasing the temperature of a  $3^3:13^3_{\text{HAP}}$  sample, there appeared to be an increase in the rate xenon was released from the porous liquid. However, above 80 °C, the liquid also increased in viscosity and appeared to foam. As a result, an unexpected increase in gas was observed after a certain point, which could be due to some decomposition of the porous liquid, with either the cage or solvent being affected. As identification of the gas is difficult with gas displacement experiments, the temperature was capped at 80 °C to prevent any decomposition from occurring.

A sample of  $3^3:13^3_{\text{HAP}}$  at 16 wt% (200 mg in 1mL) appeared to evolve xenon when it was heated to 40-65 °C (**Figure 4.25a**). During the first cycle,  $97.8 \pm 2.3 \mu\text{mol mL}^{-1}$  of gas was released from the porous liquid, which was comparable to the volume collected using chemical displacement ( $101 \mu\text{mol mL}^{-1}$ ). The process could be repeated on the same sample to give a similar, although slightly reduced evolved volume of xenon ( $78.1 \pm 11.4 \mu\text{mol mL}^{-1}$ ). With the reversibility associated with imine cages, decomposition of a porous liquid might be expected on heating. Unfortunately, the 16 wt%  $3^3:13^3_{\text{HAP}}$  sample appeared to decompose after the second temperature release cycle, which could account for the decrease in collected xenon. There was a change in physical appearance of the sample, with an increase in viscosity and gelation being observed, and therefore, a third cycle could not be performed (**Figure 4.25b**).

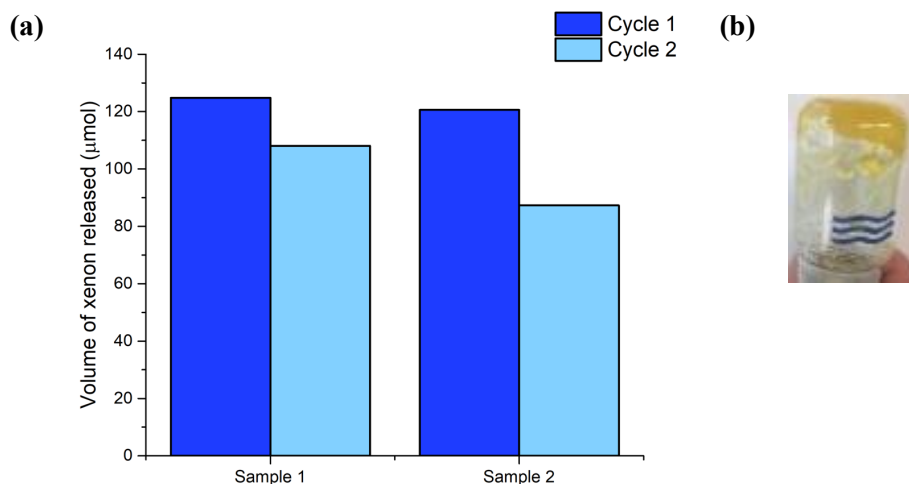


**Figure 4.25:** (a) Results of the temperature release experiments when heating xenon-loaded 16 wt%  $3^3:13^3_{\text{HAP}}$  porous liquid samples at 60-70 °C, and (b) the physical appearance of  $3^3:13^3_{\text{HAP}}$  after 2 cycles.

The temperature displacement of  $3^3:13^3_{\text{HAP}}$  at higher concentrations (22 and 27 wt%) was also comparable to the volume collected by chemical displacement. However, the 35 wt% porous liquid showed a significantly higher xenon evolution ( $213.3 \pm 9.6 \mu\text{mol mL}^{-1}$ ) than when using chloroform ( $108.9 \mu\text{mol mL}^{-1}$ ). As seen previously, the porous liquid appears to be at saturation with a cage concentration at 35 wt%, and addition of chloroform causes the cage to precipitate from solution. Heating the porous liquid seems to avoid this problem and a proportional volume of xenon is released from the cavities (**Figure 4.26**).

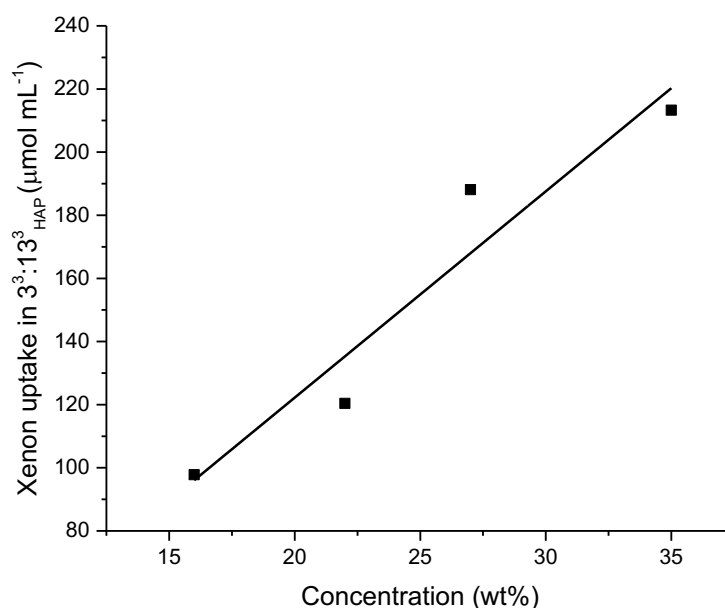


**Figure 4.26:** The volume of xenon evolved from  $3^3:13^3_{\text{HAP}}$  porous liquids at various concentrations using temperature release

Overall, a temperature swing is a preferable method for releasing gaseous guests from a porous liquid because it is more suitable for commercial settings, and in particular, flow applications. However, the higher concentration porous liquids, in this case, are not reusable and can only be heated once. The cage appears to undergo decomposition, and the  $^1\text{H}$  NMR spectrum shows the presence of new peaks at  $\sim 2$  and 13 ppm, which do not correspond to the starting cage or solvent (**Figure 4.27**).

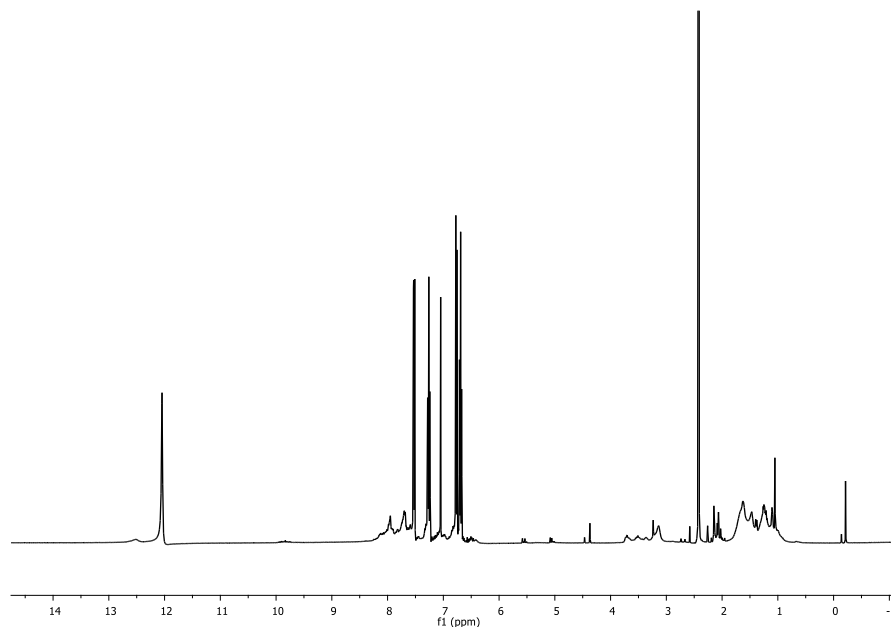


**Figure 4.27:**  $^1\text{H}$  NMR ( $\text{CDCl}_3$ ) spectra of  $3^3:13^3_{\text{HAP}}$  at 35 wt% after temperature release of xenon.

The physical appearance of both the 27 and 35 wt% samples changed through heating, and the viscosity increased with foaming occurring, while xenon was released from the porous liquid (**Figure 4.28**). The physical change means using high concentration  $3^3:13^3_{\text{HAP}}$  in flow applications would not be possible, and the increased viscosity also makes it difficult to reuse the porous liquid in a second cycle. However, there is still scope to use  $3^3:13^3_{\text{HAP}}$  in other gas capture and release applications.

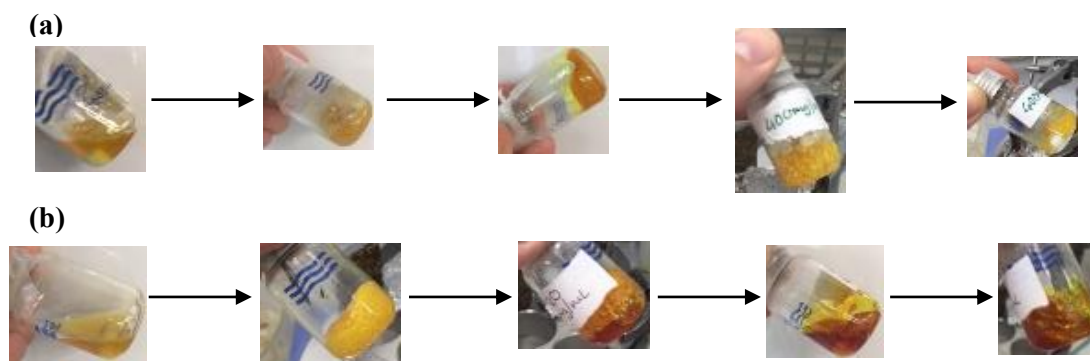


**Figure 4.28:** The physical state of  $3^3:13^3_{\text{HAP}}$  at (a) 27 wt%, and (b) 35 wt%, when heated at 60-80  $^{\circ}\text{C}$  during guest release.

#### 4.8 Gelation and sol-gel behaviour of porous liquids

During the study of  $3^3:13^3_{\text{HAP}}$  at higher concentrations, an interesting observation was made – increasing the cage concentration impacts the viscosity of the system, as shown previously, and appears to cause gelation of the samples if left undisturbed for prolonged time periods. Other reports have shown that supramolecular assemblies can possess thermo-responsive sol-gel behaviour, with cooling promoting gel formation, and heating reforming the solution.<sup>178</sup> Therefore, the ability of  $3^3:13^3_{\text{HAP}}$  at 27 and 35 wt% to act as a sol-gel was investigated as a capture-release mechanism for gases. The porous liquids at these concentrations were saturated with xenon and cooled between 0-6 °C until gelation occurred. The temperature was not lowered further due to the risk of the cage precipitating from solution, rather than promoting gel formation. The gel was then heated to between 60-80 °C to reform the liquid and release the trapped gas. For both concentrations, the xenon evolution was comparable ( $181 \mu\text{mol mL}^{-1}$  for 27 wt%, and  $240 \mu\text{mol mL}^{-1}$  for 35 wt%) to those obtained for chemical displacement or heating the liquid sample (Figure 4.29).

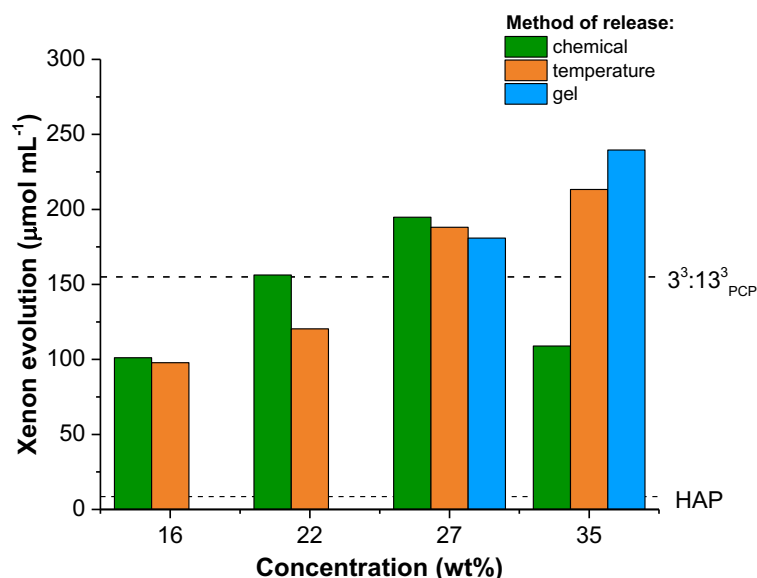


**Figure 4.29:** Comparison of the xenon evolved from  $3^3:13^3_{\text{HAP}}$  at different concentrations and using different release mechanisms (chemical displacement with chloroform - green; increased temperature – orange; formation of gel and release on heating – blue).

The physical properties, such as the colour and viscosity, of  $3^3:13^3_{\text{HAP}}$  at higher concentrations appear to change after a sol-gel cycle (Figure 4.30a). Foaming also occurs as the xenon gas is released from the system. The process of heating scrambled porous liquids has already been shown to alter the physical appearance of the system. As imine bonds are labile, it is unsurprising the porous liquids in this study might experience decomposition –  $3^3:13^3_{\text{HAP}}$  at 35 wt% does not retain its liquid state after releasing the guest from the cavities, and the <sup>1</sup>H

NMR spectrum shows slight decomposition between 1-4 ppm (**Figure 4.30b**). In order to evacuate the sample of xenon completely,  $3^3:13^3_{\text{HAP}}$  was heated to  $\leq 80^\circ\text{C}$  and this could cause the decomposition of the scrambled cage. As a result, the sol-gel process could not be repeated for the 35 wt% sample. The 27 wt% porous liquid, however, does not appear to decompose after a single temperature release experiment from the gel, with the  $^1\text{H}$  NMR spectrum matching both the parent solvent and scrambled cage (**Figure 4.30b**).

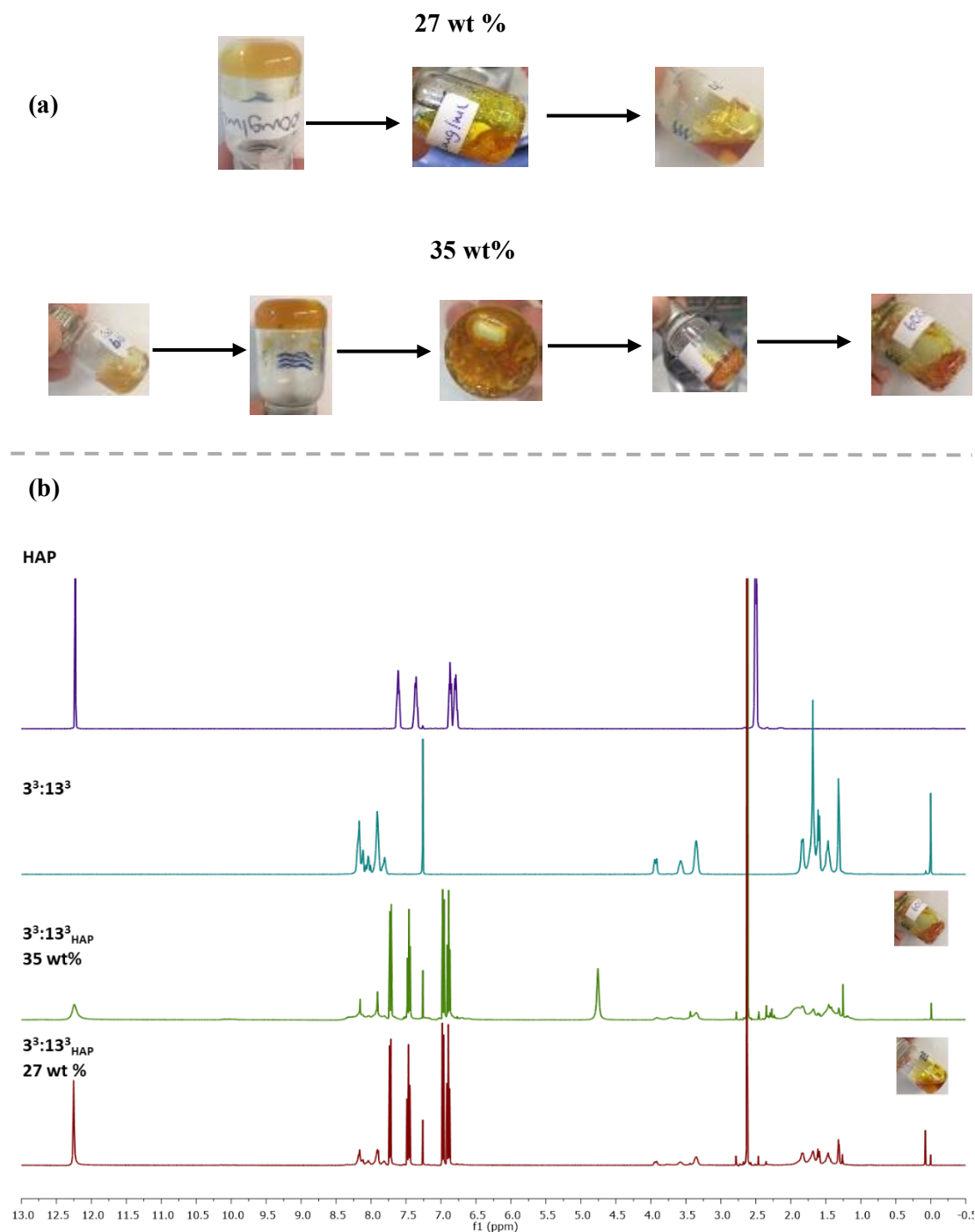


**Figure 4.30:** (a) The physical states of  $3^3:13^3_{\text{HAP}}$  at 27 and 35 wt % when the gel was heated to release the trapped guest, and (b)  $^1\text{H}$  NMR ( $\text{CDCl}_3$ ) spectra of  $3^3:13^3_{\text{HAP}}$  at 27 and 35 wt % after a temperature release cycle compared to  $3^3:13^3$  and HAP.

To determine if  $3^3:13^3_{\text{HAP}}$  at 27 wt% had retained any porosity after the sol-gel process, the same sample was re-saturated with xenon and a second gas displacement was attempted with a small chemical additive. The volume released was comparable to the neat solvent, which suggested the porous liquid no longer possessed any porosity (Table 4.2).

**Table 4.10:** The volume of xenon evolved from  $3^3:13^3_{\text{HAP}}$  at 27 wt% when heated at 60-85 °C (Cycle 1), followed by chemical displacement carried out on the same sample re-saturated with xenon (Cycle 2).

Porous liquid	Cycle 1	Cycle 2
	Temperature release	Chemical release
$3^3:13^3_{\text{HAP}}$ at 27 wt%	6.2 mL	0.2 mL

#### 4.9 Retention of guest in $3^3:13^3_{\text{HAP}}$

The increased viscosity of  $3^3:13^3_{\text{HAP}}$  at higher concentrations gives rise to the ability of the porous liquid to act as a sol-gel. Even though the sol-gel capture–release process was not cyclable, it could be an effective method for gas storage. Therefore, the retention of xenon gas in the porous liquid was studied in a 35 wt% gelled sample. The first experiment demonstrated a large proportion of the gas was retained in the porous liquid after 48 hours, with 64% of the original volume of xenon evolved by temperature release (Table 4.3).

**Table 4.11:** Volume of xenon released and percentage retained by  $3^3:13^3_{\text{HAP}}$  liquid after immediate release, and after 48 hours.

Time (hrs)	Volume of xenon released (mL)	Volume of xenon released ( $\mu\text{mol mL}^{-1}$ )	% Xe retained over time (%)
0	6.4	196.3	-
48	4.4	126.2	64

As there appeared to be a high percentage of xenon retained in the gel after 48 hours, loaded  $3^3:13^3_{\text{HAP}}$  samples were left undisturbed for extended periods of time. It was found that xenon could be retained within the gel at 35 wt% for over 28 days, with 68% of gas remaining after 7 days, and 50% after 28 days, based on temperature release (Table 4.4 and Figure 4.31). The sol-gel behaviour of  $3^3:13^3_{\text{HAP}}$  could lead to interesting capture–release applications where the gaseous guest could be loaded into the system in the liquid state, stored as a gel, and then released after heating to reform the liquid.

**Table 4.12:** Volume of xenon released from  $3^3:13^3_{\text{HAP}}$  gel after being left to stand for set amounts of time.

Time after preparation (days)	Volume of xenon released (mL)	Volume of xenon released ( $\mu\text{mol mL}^{-1}$ )	% Xe retained over time (%)
1	8.8	222.4	-
7	6.0	151.6	68
28	4.4	111.2	50

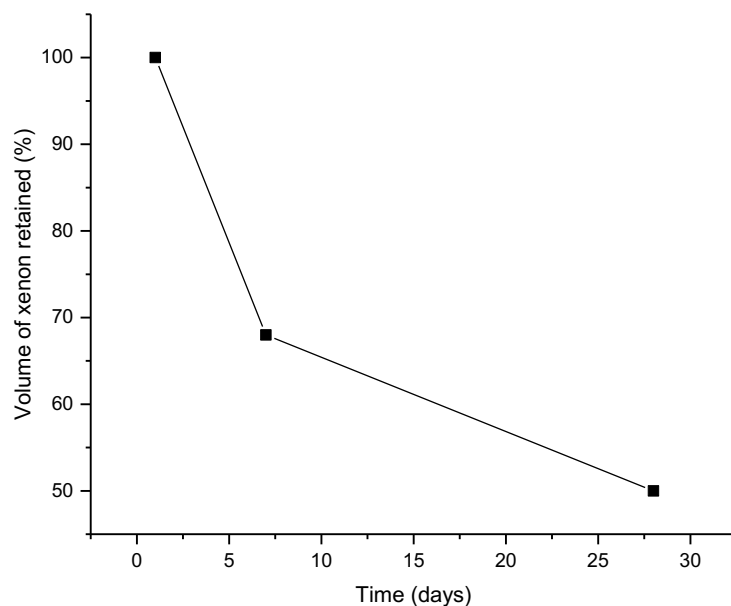


**Figure 4.31:** Retention of xenon in  $3^3:13^3_{\text{HAP}}$  gel over 28 days.

#### 4.10 Stability studies of $3^3:13^3_{\text{HAP}}$

It is important to ensure the porous liquid is stable during use as imine chemistry is reversible in solution. If  $3^3:13^3_{\text{HAP}}$  is left standing, it appears to set as a gel, but this is reversible if heated at 80 °C to reform the liquid (Figure 4.32). The gelation can be avoided if the porous liquid is stirred continuously.

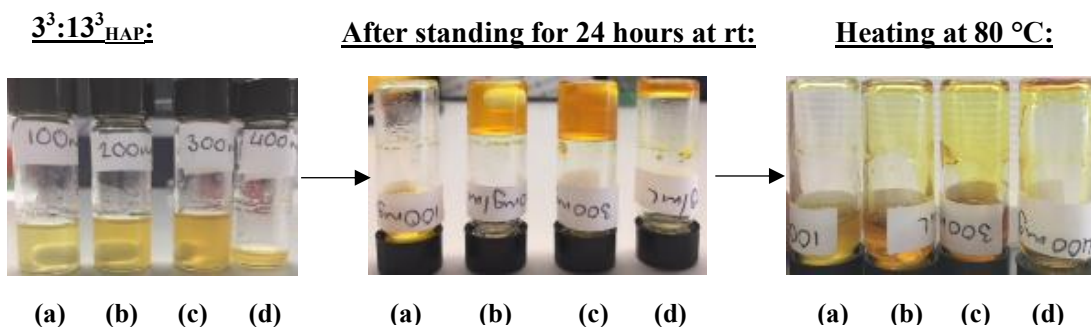


**Figure 4.32:** Stability of  $3^3:13^3_{\text{HAP}}$  at several concentrations: (a) 8, (b) 16, (c) 22, and (d) 27 wt%. Gelation occurs after 24 h but this can be reversed by heating to 80 °C.



### 4.11 Recovery of scrambled cage from $3^3:13^3_{\text{HAP}}$

Although in some cases the porous liquid cannot be reused due to changes in physical appearance, the solvents used in this study, aside from PCP, are readily available and inexpensive. Therefore, recovery and reuse of the scrambled cage would be beneficial as this would help to make the porous liquids more cost effective. Addition of acetone to a porous liquid caused the precipitation of the  $3^3:13^3$  scrambled cage from solution. The  $^1\text{H}$  NMR spectrum of the recovered cage is comparable to the initial starting cage mixture with no signs of decomposition (**Figure 4.33**).

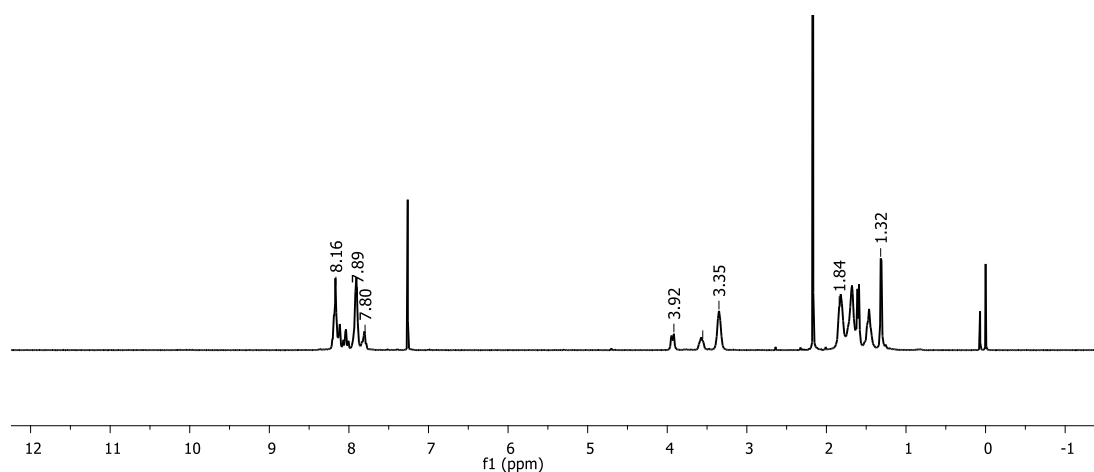


**Figure 4.33:**  $^1\text{H}$  NMR ( $\text{CDCl}_3$ ) spectrum of  $3^3:13^3$  after recovery from a porous liquid by precipitation with acetone.

After collection by filtration and drying under vacuum, the cage was reused in freshly made porous liquids (200 mg in 1 mL, 20% w/v). The gas displacement measurements from two subsequent porous liquids were similar to the values reported previously (**Table 4.5**).

**Table 4.13:** Volume of xenon released from 20% w/v porous liquids formed using recycled scrambled cage.

Porous liquid	Mass of cage (mg)	Volume of xenon evolved (mL)	Volume of xenon evolved from recycled PL ( $\mu\text{mol mL}_{\text{PL}}^{-1}$ )	Volume of xenon evolved from original PL ( $\mu\text{mol mL}_{\text{PL}}^{-1}$ )
$3^3:13^3_{\text{TBA}}$	200	2.3	83.3	$105.5 \pm 5.1$
$3^3:13^3_{\text{HAP}}$	200	2.8	92.8	$101.0 \pm 7.0$

## 4.12 Conclusions

The development of a high-throughput workflow led to a library of highly soluble scrambled cage/bulky solvent combinations. These were scaled up and screened for porosity by displacing xenon from a 20% w/v sample (200 mg of scrambled cage in 1 mL of solvent) using chloroform. This screen led to the discovery of Type II porous liquid families, and enabled studies into how changing the different components changed the overall properties. We investigated a series with the same scrambled cage ( $3^3:13^3$ ) in a range of different solvents, and demonstrated that gas uptake in the parent solvent has an impact on the gas uptake of the porous liquid. Changing the scrambled cage, including the diamine feed ratio and the alkyl chain length on the cage periphery, was also shown to change the methane and xenon uptake in a porous liquid.

Porous liquids with higher cage concentrations were also discovered, with up to 55% more xenon uptake than the first reported system,  $3^3:13^3_{PCP}$ . However, increased cage solubility does not always translate into improved porosity, as other properties, such as viscosity, can limit gas uptake or cause gelation. The gelation at the higher concentrations gave a new method for capturing and storing xenon, with temperature used to release a trapped guest from a gelled porous liquid. Overall, there are several factors that need to be considered when designing Type II porous liquids, which have been explored for the first time.

**Chapter 5:**  
Synthesis of organic cage salts to  
target porous ionic liquids

## 5.1 Introduction

### 5.1.1 Challenges associated with Type II scrambled porous liquids

Porous liquids have scope to be used in a variety of applications, but there are considerations that need to be taken into account when targeting a specific purpose, as discussed in previous chapters. Using porous imine cages in Type II porous liquids has some associated limitations, particularly in relation to stability and re-usability. Additionally, the solvents used in the Type II systems in this thesis also have certain restrictions, with the associated vapour pressures reducing the suitability for certain purposes. Targeting a neat Type I porous liquid, based on non-reversible porous organic cages, would overcome previous limitations by improving the system's prolonged stability. The associated vapour pressure would also be removed and enable the porous liquid to be exposed to reduced pressure.

### 5.1.2 Modification of porous organic cages

Whilst the reversibility of imine formation allows equilibration of precursors and oligomers into multi-component cage species, it can also cause chemical instability in the resulting product. POCs containing imine bonds are often prone to water/acid hydrolysis, and decomposition in the presence of moisture. Post-synthetic modification can be used as a strategy to overcome such issues. For example, reduction of the imines to the corresponding amines improves the stability and can be readily functionalised.<sup>179</sup>

Previously, Cooper *et al.* have reported several methods for functional group modification of imine-derived POCs (**Figure 5.1**). This includes the reduction of **CC1** (compound **a** in **Figure 5.1**) to an amine derivative using sodium borohydride (compound **b**). Unfortunately, the resulting reduced cage was found to collapse, probably due to the increased flexibility of the structure, resulting in a lack of shape-persistent pores.<sup>180</sup> In subsequent research, the amine cage (compound **b**) was then reduced further to an amide cage containing a range of functionality (compound **c**). The authors demonstrated substitution on the 12 amines with sterically bulky groups, rather than changing the cage core. The amide bond helped to reduce the free rotation inherent in the flexible amine cage, but not all of the analogues were porous.<sup>180</sup> However, the potential for incorporating different functionality after synthesising a cage could be a valid method for tailoring the solubility or melting point for a potential porous liquid.

Alternatively, an additional method to limit the flexibility of the reduced amine cage was to 'tie' the vertices by adding bridging groups onto the diamines to form rigid aminal rings (compound **d** in **Figure 5.1**). This produces shape-persistent and porous amine cages with enhanced chemical stability over their imine counterparts. Reduced **CC3** (**RCC3**) was tied using both acetone and formaldehyde to see the effects of varying the substitution on the

aminal. The acetone tied cage was more rigid compared to **RCC3** but did not remain permanently porous, collapsing over several days due to it containing a single aminal. As an alternative, the use of formaldehyde proved more successful, as the resulting shape-persistent cage was porous and chemically stable, even when subjected to boiling at pH 12.<sup>181</sup> The reduction and ‘tying’ method has the potential to increase the stability of cages for their use in porous liquids. This would allow the system to undergo multiple temperature swings, or the addition/removal of other species without decomposition.

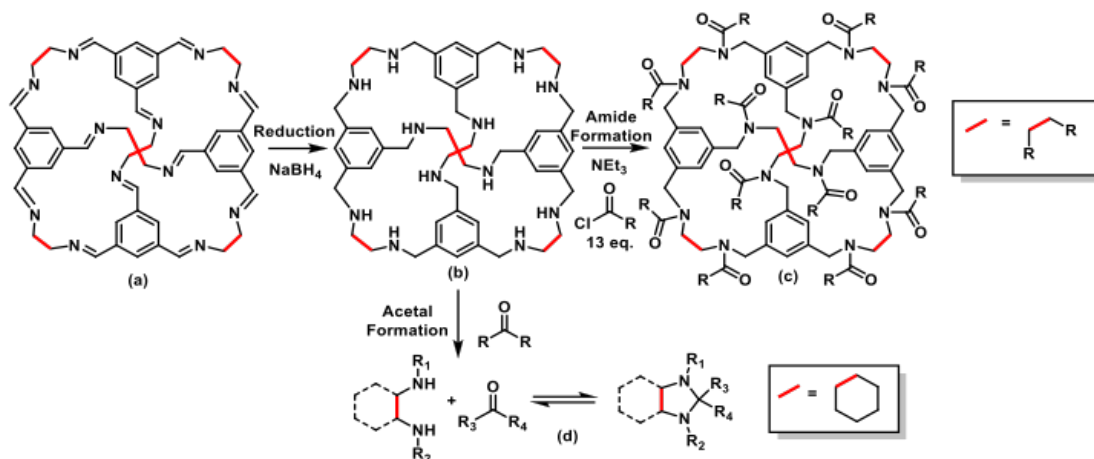


**Figure 5.30:** Post-synthetic modification of imine cages (a) to its amide (c) and acetal (d) analogues by Cooper *et al.*<sup>179–181</sup>

Cooper *et al.* also reported several cage salts based on ionised derivatives of organic cages with varying anions, for example, **CC1** was reduced and protonated to make the corresponding salt (**Figure 5.2**). The crystal structures of the protonated cages demonstrated the anions were important in maintaining packing as both  $\text{Cl}^-$  and  $\text{SO}_4^{2-}$  are strong hydrogen bond acceptors. Computational modelling showed that the chloride anions in  $[\text{H}_{12}\text{RCC1}]^{12+} \cdot 12\text{Cl}^-$  remain outside the cage windows, as these are crucial in the proton conductivity mechanism, but water molecules occupy the cavities. The larger sulphate ions in the  $[\text{H}_{12}\text{RCC1}]^{12+} \cdot 6\text{SO}_4^{2-}$  species were found to occupy the cage windows and some of the cage cavities. Therefore, 3D hydrogen bond networks were formed between the anions and the water molecules, which contributed to altering the cage conformation in the crystal structure.<sup>182</sup> The finding that the anions in the organic cage salts are likely to be located outside the cage cavities could potentially be useful in the field of porous liquids. Finding a low melting cage salt, with a bulky anion, would remove the vapour pressure associated with using a bulky organic solvent and could potentially form a room temperature ionic liquid.

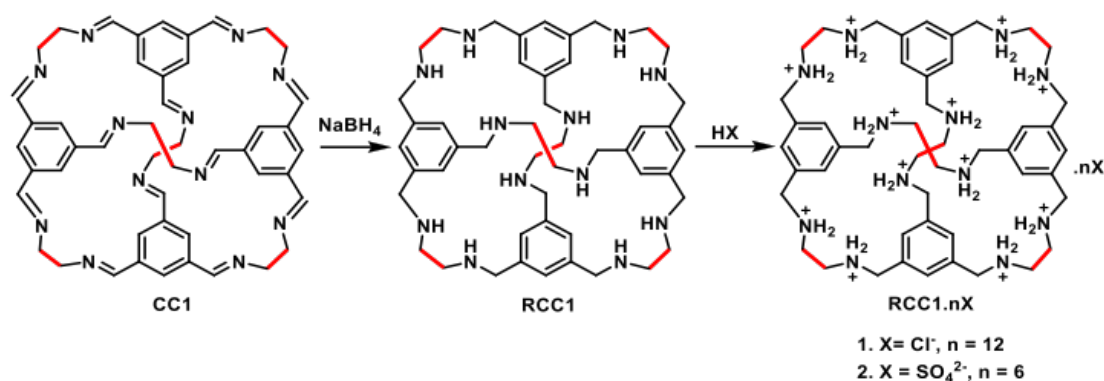


Figure 5.2: Synthesis of organic cage salts by Cooper *et al.*<sup>182</sup>

### 5.1.3 Ionic liquids

The volatility and vapour pressure associated with the solvents currently used in the Type II scrambled porous liquids, discussed both in this thesis and the literature,<sup>13,112</sup> can be problematic when studying the gas uptake in these systems. Generating porous liquids using non-volatile components, such as ionic liquids, could overcome these issues. For example, an ionic liquid based on a stable organic cage could form a neat, non-volatile porous liquid, that could be subjected to vacuum, and therefore used in several new applications.

Ionic liquids are defined as a subset of molten salts with melting points below 373 K ( $T_m$ ),<sup>183,184,185</sup> and the chemical structure of the cation or anion can be varied to influence the melting point directly.<sup>183</sup> The tuneable properties,<sup>185</sup> along with them having zero or near zero volatility and good thermal stability,<sup>183</sup> make them an ideal candidate for use in the field of porous liquids. There are several different subclasses of ionic liquids that can be categorised based on their molecular structure (**Figure 5.3**), giving numerous functionalities that could be incorporated into the structure of organic cages.

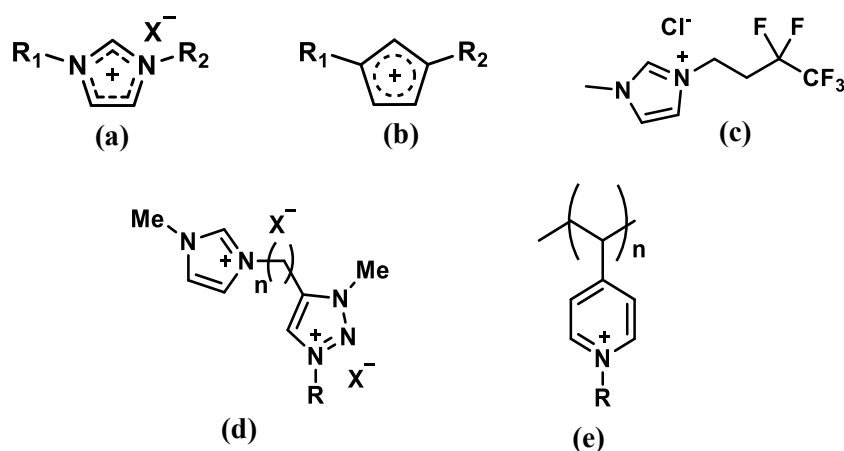


Figure 5.3: Examples of ionic liquids: (a) protic<sup>184,188,202</sup>; (b) aprotic<sup>184</sup>; (c) fluoro<sup>184,203</sup>; (d) dicationic<sup>184,204</sup>; (e) polymeric.<sup>184,205</sup>



a low melting ionic cage species. Additionally, James *et al.* reported the effect of increasing the alkyl chain length on the cage periphery, which decreased the melting point, reiterating the observations made by Kaliner *et al.*<sup>187</sup> However, there are pitfalls associated with cages possessing long alkyl chains; these are likely to lead to a reduction in porosity by interpenetration of neighbouring cage cavities. A large counter-ion would also be needed in order to be size-excluded from the cage cavity and contribute to a lower melting point.

#### 5.1.4 Strategies for synthesising an ionic cage liquid

The formation of organic cage salts provides a strategy to target a low melting ionic liquid that remains permanently porous. Previous work in the Cooper Group, as mentioned above in **Figure 5.2**, has shown that **CC1** can be reduced to an amine cage (**RCC1**) and protonated to form a salt (**RCC1.nX**). Replacement of the chloride counter-ion with a bulkier, cavity-excluded analogue, would potentially leave the cage cavities unoccupied. Additionally, these ionic cage salts could be exposed to traditional gas sorption techniques without the liquid being affected.

Previous work in the group has built on the findings by Liu *et al.*<sup>182</sup> to exchange the chloride ions for a bulkier anion. This unpublished work found **RCC1.12BARF** was a potentially low melting ionic cage salt, but the porosity was not investigated in greater detail (**Figure 5.5**). Building on these preliminary results and adapting the findings from work carried out earlier, there is scope to design a high-throughput methodology to screen combinations of different organic cages and bulky anions targeting a low melting cage salt whose porosity could be investigated.

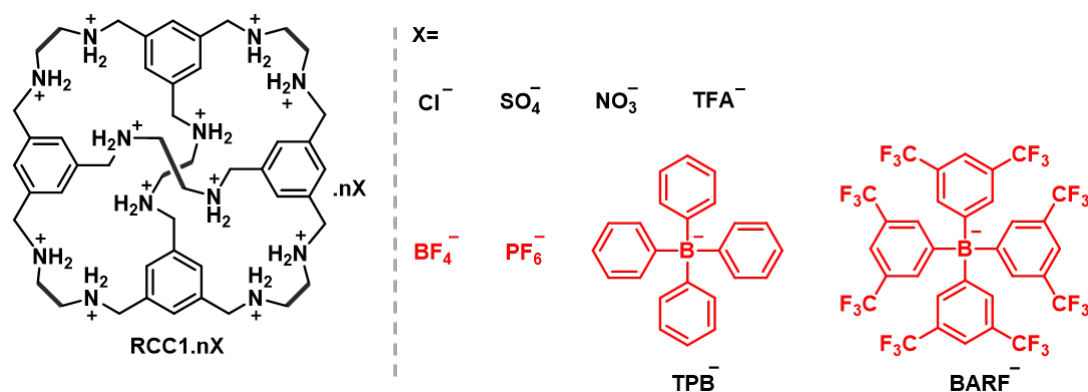


**Figure 5.5:** **RCC1** and a selection of anions trialled by Liu *et al.* with the aim of synthesising a low melting ionic cage salt. The bulky anions are highlighted in red.



## 5.2 Designing a high-throughput methodology

The aim of this work was to develop a high-throughput workflow to screen and synthesise new organic cage salts, which incorporated potential size-excluded anions.

### 5.2.1 Small scale trial reactions

When designing a high-throughput workflow, it is important to ensure the reliability of the data generated. First, since salt exchange of organic cage hydrochloride salts is not well established, a purification method would need to be determined, especially because changing the anion could change the solubility of the resulting cage salt in common solvents. Additionally, as discussed in the scrambled porous liquid workflow, having several control reactions that are known to work is important to include in a high-throughput screen. Therefore, predetermining if the selected anions undergo salt exchange ‘offline’ would be beneficial in designing a reliable workflow that could be then used in subsequent, larger screens.

For the preliminary studies, **RCC1.12HCl** was chosen as the starting cage salt because Liu *et al.* had already shown this can undergo salt exchange with bulkier anions, including [BARF]. The known success of salt exchange with the [BARF] anion makes a sensible control reaction, although it does have a substantially high molecular weight, and with 12 counter-ions, the ionic cage salt has a high cage:anion mass ratio (829.2774:10358.6424). Therefore, only a small volume of porosity would be introduced in a cage-[BARF] salt, so lower molecular weight anions were also considered. The literature provided a selection of anions commonly found in ionic liquids,<sup>183,184,188</sup> which led to a range of commercially available ionic salts being selected for the preliminary studies.

The work carried out on scrambled porous liquids in previous chapters provided an insight into the type of molecule that would be size-excluded from a [4+6] cage cavity – the same size used in this study. Several of the size-excluded solvents were functionalised aromatic rings, and therefore this criterion was applied when choosing counter-ions to narrow the search space. Sulfates are also a predominant functionality found in ionic liquids as the anions, and there are many commercially available sodium aryl sulfate salts. Therefore, a series of aryl sulfates (**Figure 5.6**: TSA, XSA, and NSA) were selected as counter-ions that were likely to be size-excluded. Bis(trifluoromethanesulfonyl)amide (TFSA) is also used regularly as an anion in ionic liquids, and has been proven in unpublished work in the group to be size-excluded from **CC3**, which has the same cavity size as **CC1** (**Figure 5.6**). All of the anions were purchased as sodium salts, apart from TFSA, which was obtained as the lithium salt

because it was cheaper than the sodium analogue, an important consideration when designing high-throughput workflows.

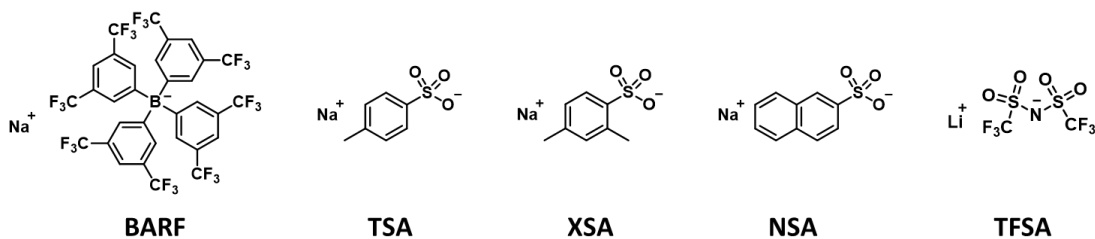


**Figure 5.6:** The ionic salts used in the trial reactions for salt exchange with **RCC1.12HCl**

Overall, this gave five counterions to use in preliminary salt exchange reactions with **RCC1.12HCl**, and potentially in subsequent high-throughput screens. Small scale reactions were therefore performed to determine the conditions required for translation onto the automated platform, with concentration being an important factor to consider, as discussed previously. The salt exchange reactions with **RCC1.12HCl** were carried out in methanol with 12 equivalents of each bulky salt (**Figure 5.7**).

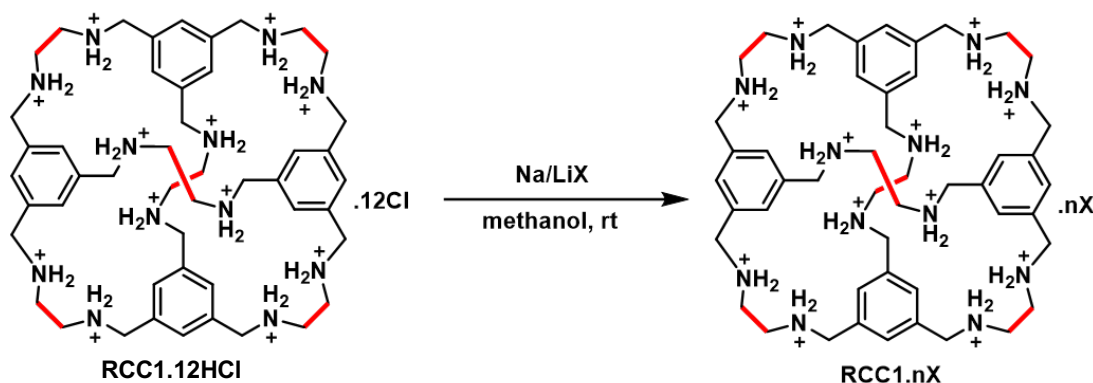


**Figure 5.7:** General reaction scheme for salt exchange between **RCC1.12HCl** and different sodium or lithium-based salts.

The next challenge was to develop methods to purify each reaction. Given the simplicity of the salt exchange, there should theoretically have been very few impurities and only a metal chloride salt to remove. However, despite **RCC1.12HCl** being water soluble, the salt-exchanged ionic salts had different solubility profiles and were more difficult to isolate. Therefore, different anti-solvents were trialled, based on literature findings. Liu *et al.* found the cage BARF salt precipitated on addition of water to methanol, but the remaining sulfate salts were water soluble, so this method was unsuitable. The TSA, XSA and NSA cage salts of **RCC1** were found to be soluble in DCM, and the NaCl was precipitated by addition of

diethyl ether. Finally, the TFSA cage salt was separated by addition of THF to precipitate the LiCl (Table 5.1).

**Table 5.14:** Summary of the purification methods used to remove NaCl or LiCl from salt exchange reactions with **RCC1.12HCl**.

Salt	Solvent	Method of purification
<b>NaBARF</b>	Methanol/water	Cage salt solution added dropwise to water ( $10 \times V_{\text{MeOH}}$ ). Cage salt filtered
<b>NaTSA</b>	DCM/diethyl ether	Cage salt dissolved in minimum volume of DCM. Diethyl ether added to precipitate NaCl, filtered and solvent removed
<b>NaXSA</b>	DCM/diethyl ether	Cage salt dissolved in minimum volume of DCM. Diethyl ether added to precipitate NaCl, filtered and solvent removed
<b>NaNSA</b>	DCM/diethyl ether	Cage salt dissolved in minimum volume of DCM. Diethyl ether added to precipitate NaCl, filtered and solvent removed
<b>LiTFSA</b>	THF	THF added to the concentrated reaction mixture and LiCl precipitate filtered

As illustrated in previous chapters, an important part of a high-throughput workflow is the analytical techniques used to determine if a reaction is deemed successful. The targeted materials in this project are ionic salts, and therefore required techniques for determining if both the cage and counterion were present.

Typically, NMR analysis is particularly effective in identifying if a cage species has formed. However, as the counterions constitute a high proportion of the overall mass due to their large molecular weight, these dominate the spectra and the cage signals are difficult to identify. For example, the aromatic signal of **RCC1** is hard to observe in the aromatic region due to the BARF signals, as observed for **RCC1.12BARF** (Figure 5.8a). However, used in conjunction with NMR data, HRMS confirms the presence of the cage species in the salt. For **RCC1.12BARF**, both **RCC1** and **RCC1+12H** were identified at 817.6156 and 829.6154 ( $[\text{M}+\text{H}]^+$ ), but the  $\text{BARF}^-$  counter-ion was not apparent, which has been observed previously in these ionic cage salts.<sup>189</sup> Additionally, FTIR confirms the presence of both the counter-ion, and in most cases, the reduced cage. For example, the BARF anion has a distinctive stretch at  $\sim 1100 \text{ cm}^{-1}$ , which was evident in the FTIR spectrum of **RCC1.12BARF**, and several NH stretches (at  $3500\text{-}3300 \text{ cm}^{-1}$  and  $1650\text{-}1550 \text{ cm}^{-1}$ ) were present corresponding to the reduced cage (Figure 5.8c).

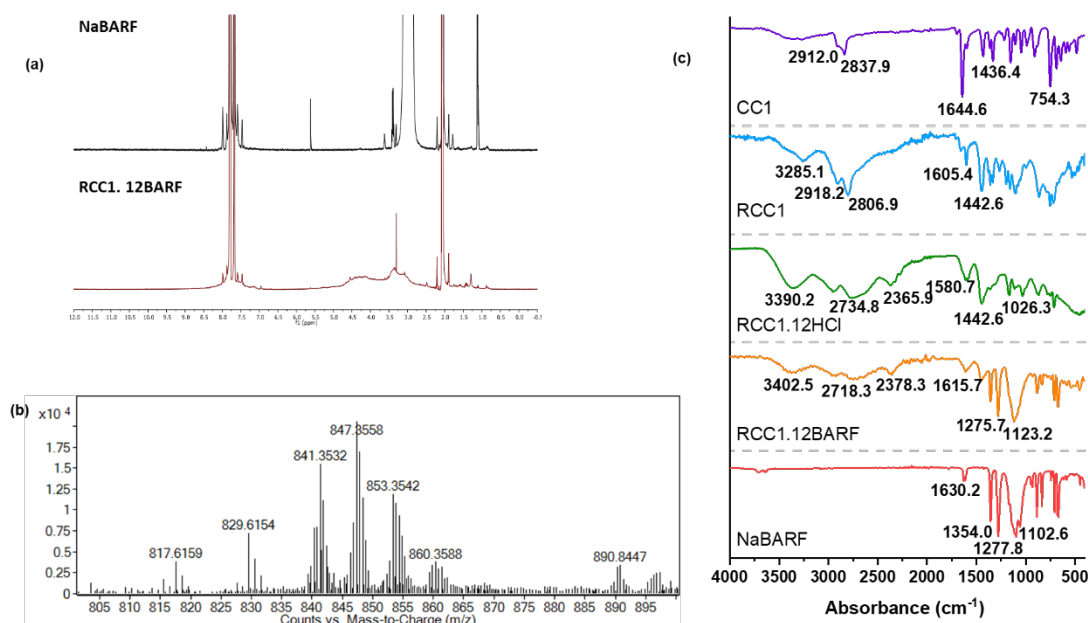


**Figure 5.8:** Analytical data for **RCC1.12BARF**: (a) stacked <sup>1</sup>H NMR spectra of **RCC1.12BARF** and NaBARF in acetone-d<sub>6</sub>; (b) HRMS data; (c) stacked FTIR spectra for **CC1**, **RCC1**, **RCC1** cage salts and NaBARF.

These methods were used to confirm the formation of the **RCC1.12X** salt series, and interestingly, **RCC1.12TFSA** appeared to be a liquid at ambient temperature. Therefore, it was decided that, alongside HRMS and FTIR data, visual inspection of the physical state of the isolated salts would be used to determine if any ionic cage liquids were formed in the high-throughput screen. Any hits would be subsequently scaled up and characterised fully, including determination of the overall purity, and/or investigation of the liquid and melting behaviour.

### 5.2.2 Choosing suitable precursors for the high-throughput screen

A small cage precursor library was selected that contained some organic cage salts that were simple to synthesise and well known in the literature (**Figure 5.9**). **RCC1.12HCl** was successfully used in the trial salt exchange reactions and would, therefore, provide a series of control reactions. **RCC3.12HCl** and **RCC13.12HCl** were selected on the basis that they might form cage salts with more rigid cavities due to the functionalisation on the periphery. The two scrambled cages (**R3<sup>3</sup>:R13<sup>3</sup>.12HCl** and **R1<sup>3</sup>:R3<sup>3</sup>.12HCl**) in the screen were chosen based on our previous findings that mixed functionality disrupts the packing, and might increase the likelihood of discovering a low melting cage salt.

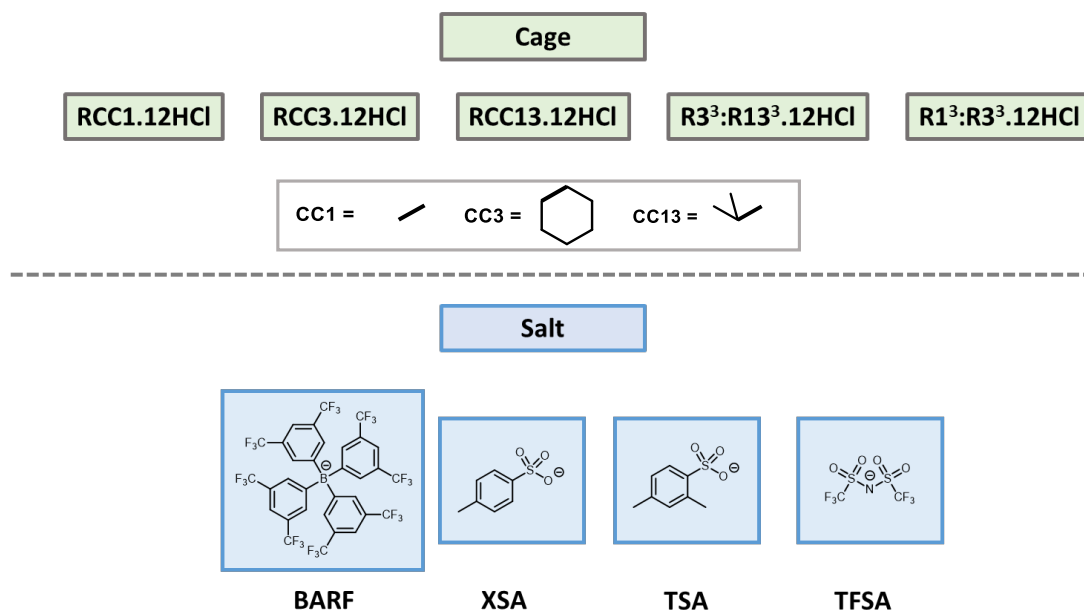


**Figure 5.9:** The precursors selected for the high-throughput screen of ionic organic cage salts.

As discussed previously, the solubility of precursors is an important consideration when implementing a workflow on an automated platform. If a compound is poorly soluble, this can limit the maximum mass of product formed in a single reaction, or if precipitation occurs, can cause blockages. Taking this into consideration, NaNSA was deemed unsuitable for use in the high-throughput screen as it was poorly soluble in methanol, the reaction solvent. This left four ionic salts to screen with the chosen reduced cage hydrochloride salts (**Figure 5.9**), giving 20 possible new cage salts that could be investigated further.

### 5.2.3 High-throughput synthesis of organic cage salts

With a small precursor library selected to develop a high-throughput workflow for the discovery of organic cage salts, their synthesis via salt exchange was performed using an I-Synth Chemspeed automated platform (**Figure 5.10a**). Stock solutions of reduced cage hydrochlorides and ionic salts in methanol were dispensed into reactors and, to ensure all the reactions were at the correct concentration, an additional pre-programmed volume of methanol was added to make the total volume up to 10 mL. The vessels were then vortexed for 72 hours at ambient temperature, before the solvent was removed using a Combidancer parallel evaporator (**Figure 5.10b**). After isolation, the crude samples were each purified using the procedures determined prior to the high-throughput screen (**Table 5.1**) and analysed using HRMS and FTIR spectroscopy.

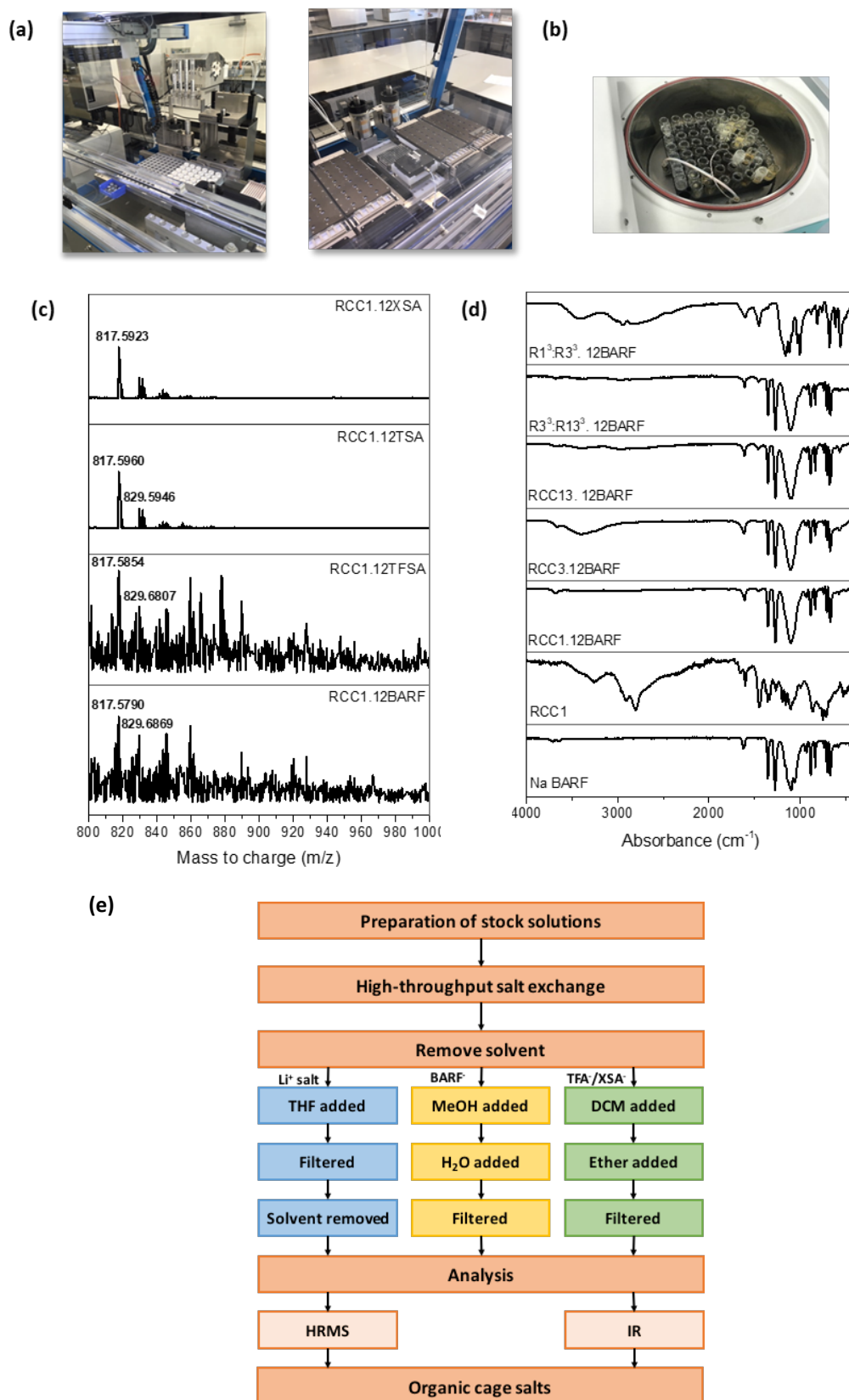


**Figure 5.10:** (a) Photographs of the Chemspeed ISynth platform used for high-throughput synthesis; (b) Combindancer parallel evaporator; (c) Example HRMS dataset of the **RCC1.12X** family of salts; (d) Example IR spectra dataset for the **BARF<sup>-</sup>** family of salts; (e) Overall schematic showing the high-throughput workflow for the synthesis of organic cage salts.

While all 20 reactions from the high-throughput screen appeared to have some evidence of successful salt exchange, very few met the full set of criteria, with only four of the cage salts being classified as ‘hits’. These had evidence of both the reduced cage and the expected anion, and appeared to be liquid at ambient temperature (Figure 5.11). The liquid hits all contained the same TFSA counterion, although the **RCC13.12TFSA** did not show significant evidence in the FTIR spectrum for the presence of the reduced cage so was not pursued further.

Overall, the TFSA derived cage salts were potential candidates for being porous organic cage ionic liquids. However, the high-throughput screen did not give any indication of the overall purity or porosity of the systems. Therefore, hits were scaled up, fully characterised, and screened for porosity.

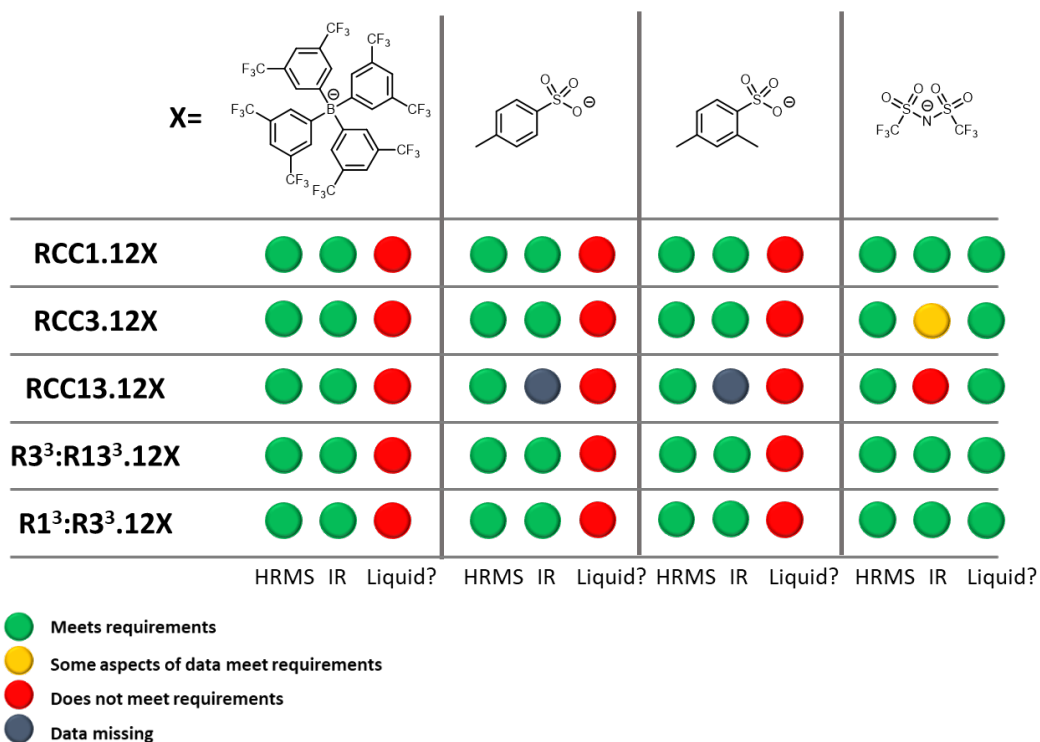


**Figure 5.11:** Graphical summary of the high-throughput salt exchange screen, with the results from the HRMS and FTIR spectra, and visual inspection of the physical state. Samples that met the requirements are highlighted in green, i.e. reduced cage in HRMS, counterion in FTIR, and visually a liquid.

### 5.3 Scale-up and characterisation of hits found in the high-throughput screen

First, the reaction of **RCC1.12HCl** and LiTFSA was repeated on a 10 mL scale, at 10 mg mL<sup>-1</sup> concentration, to optimise the conditions and confirm the results from the high-throughput screen were reproducible (**Figure 5.12a**). Alongside this, as TFSA<sup>-</sup> contains no protons, this allowed <sup>1</sup>H NMR spectroscopy to be used to confirm the presence of the reduced cage, particularly in the aromatic region, with peak broadening occurring as a result of protonation of the NH groups (**Figure 5.12b**). However, a large amount of residual solvent and several impurities were apparent; these needed to be removed prior to studying the properties. While the <sup>1</sup>H NMR data provided information on the purity of the cage salt, FTIR spectroscopy confirmed the presence of both the reduced cage and TFSA anion in the sample (**Figure 5.12b**). Therefore, NMR spectroscopy was also used to study the organic cage salt series during scale-up.

To determine if **RCC3.12TFSA** should be scaled up and investigated further, the reaction of **RCC3.12HCl** with LiTFSA was also repeated, as the FTIR data from the high-throughput screen did not give a clear indication of whether the reaction had been successful. The <sup>1</sup>H NMR spectrum showed the presence of the reduced cage, and the FTIR spectra also indicated that both the reduced cage and counter anion were present (**Figure 5.12c**). Therefore, **RCC3.12TFSA** was also classed as a hit, and therefore would be studied in more detail.

As the organic cage salts found in the high-throughput screen were reproducible, the reactions were therefore attempted on a larger scale – the batch reactions of the TFSA cage salt series were all attempted at the same concentration as used in the high-throughput screen, but at a higher volume (50-200 mL). However, none of the cage salts appeared to be scalable, with **RCC1.12TFSA** and **RCC3.12TFSA** containing solid particulates after isolation and purification, and the scrambled cages not forming the desired product at all. This indicated that uniform salt exchange had not occurred and scale-up in batch might not be suitable for this reaction.



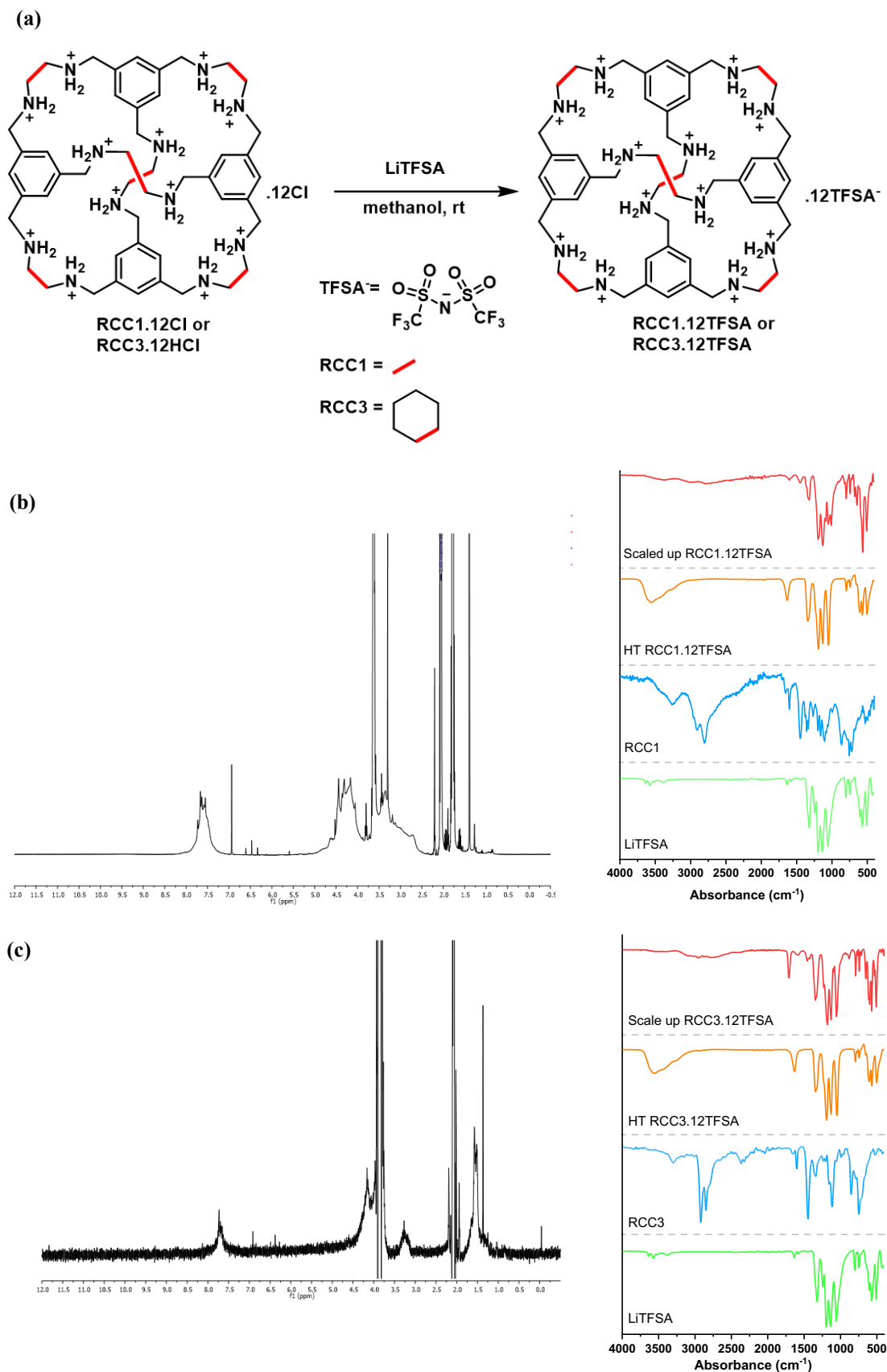


**Figure 5.12:** (a) Reaction scheme for the synthesis of **RCC1.12TFSA** and **RCC3.12TFSA** from the cage hydrochloride salt and LiTFSA, with the corresponding  $^1\text{H}$  NMR and FTIR spectra for (b) **RCC1.12TFSA**, and (c) **RCC3.12TFSA**

## 5.4 ‘Scale out’ of liquids

As the larger scale batch reactions of the TFSA cage salt series were unsuccessful, an alternative strategy was devised. Given the reaction conditions on a 10 mL scale had proven to be reproducible, a ‘scaling out’ approach was investigated, instead of ‘scaling up’. This meant performing a large number of smaller scale reactions in parallel to generate enough material to study the gas sorption properties. However, this method is often time consuming when carried out manually. Therefore, using the same approach from the high-throughput screen, a ‘scale out’ method was designed utilising the liquid dispensing of the automated Chemspeed ISynth platform.

First, the scale-out synthesis of **RCC3.12TFSA**, from **RCC3.12HCl** and LiTFSA (**Figure 5.13a**), was investigated because it was easier to handle practically, due to being more soluble than **RCC1.12HCl**. Overall, 48 identical parallel reactions were prepared using liquid dispensing of the prepared stock solutions and methanol added (total volume in each reactor = 10 mL). The vessels were then vortexed for 72 hours, before all the reactions were combined, the solvent removed, and the crude material purified using THF (**Figure 5.13b**).

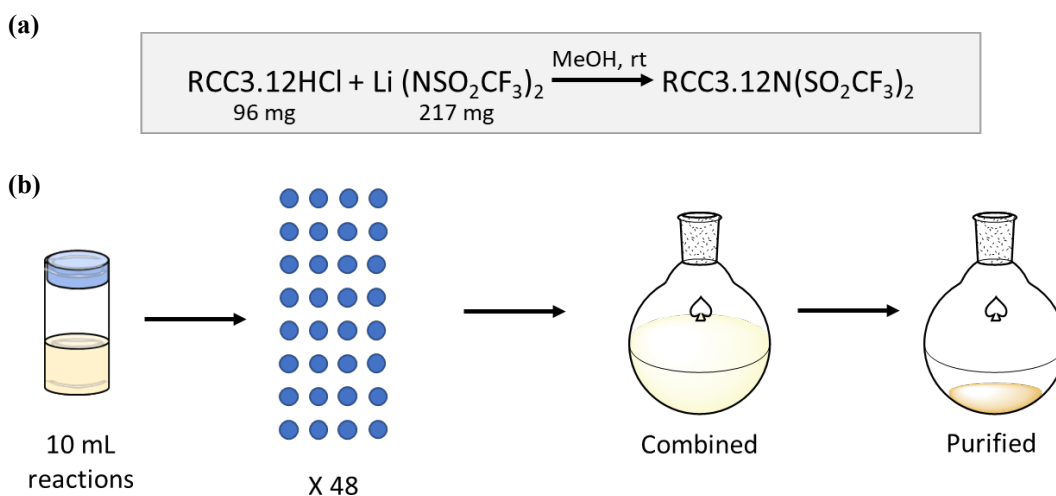


**Figure 5.13:** (a) Reaction scheme, and (b) graphical representation, for the scale out process used for the synthesis of **RCC3.12TFSA**.

Next, the resulting liquid was analysed – the initial data confirmed that the **RCC3**<sup>12+</sup> cage and the TFSA anion were both present in the sample, but there was also a large amount of THF apparent in the <sup>1</sup>H NMR spectra (**Figure 5.14a-c**). This proved difficult to remove from the sample, even on drying the liquid overnight in a vacuum oven at 90 °C – this could potentially be due to coordination between the solvent and the cage salt, or favourable encapsulation of the THF in the cage cavity. For example, THF is known to be an aprotic organic donor and often used as a Lewis acid,<sup>190</sup> so there could be strong hydrogen bonding between the NH<sub>2</sub><sup>+</sup> of

the cage and the oxygen atom in the THF. However, this was not the only observation during purification, with the appearance of a crystalline solid occurring after subjecting the liquid to vacuum (**Figure 5.14d**). Investigation into this solid contaminant showed a large concentration of LiCl still remained in the liquid, which was confirmed by ICP analysis (run by Steven Moss, University of Liverpool analytical services). Both halide and alkali metal salt by-products have been known to remain dissolved in ionic liquids after synthesis,<sup>188,191</sup> a likely occurrence in this case. Overall, the mass recovery exceeded the expected yield, which is explained by the residual THF and LiCl.

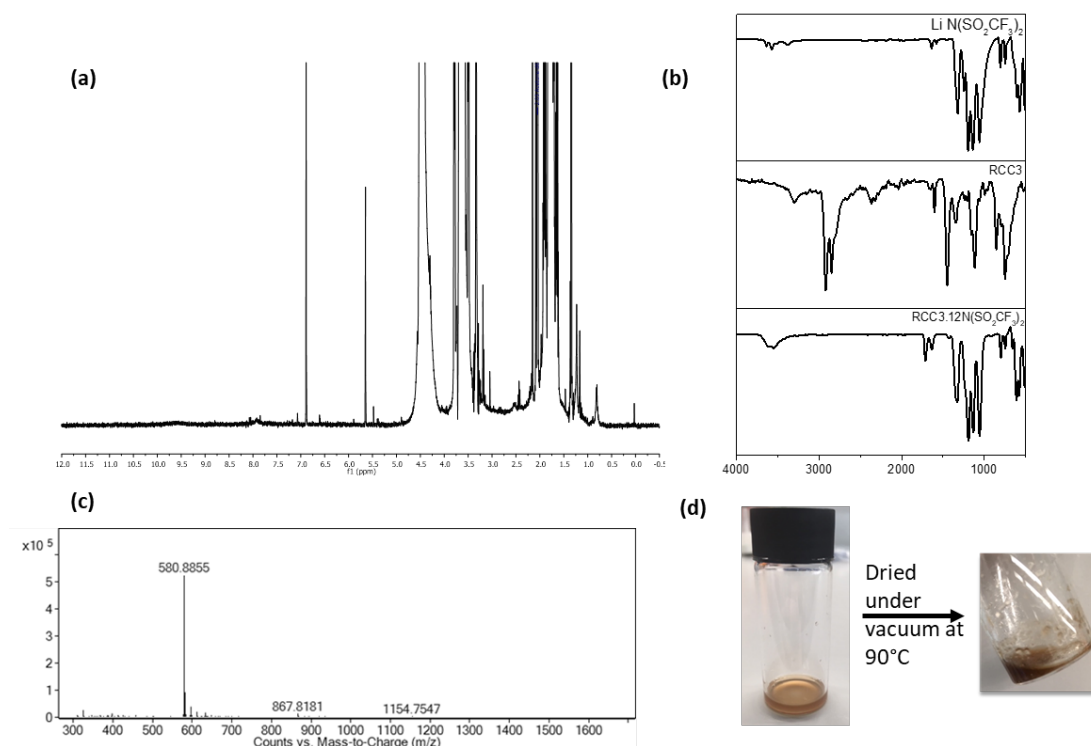


**Figure 5.14:** Analytical data for **RCC3.12TFSA** scaled out using an automated platform: **(a)** <sup>1</sup>H NMR spectrum in acetone-d<sub>6</sub>; **(b)** FTIR spectrum compared to LiTFSA and **RCC3**; **(c)** HRMS data; **(d)** physical appearance of the liquid before and after being dried under vacuum.

Given the use of LiTFSA as the starting ionic salt was problematic, an alternative was needed, particularly to mitigate the need for using THF in the purification stage. Lithium salts have a good solubility in ionic liquids due to their partial covalent bonding character. However, sodium salts maintain a large degree of ionic behaviour and are less likely to be solvated by ionic liquids.<sup>192</sup> Therefore, the reaction was repeated using NaTFSA for salt exchange because the by-product, NaCl, should be easier to remove from the reaction during purification. Additionally, **RCC3.12TFSA** was soluble in acetone, in which NaCl has poor solubility, providing an ideal alternative solvent for simple purification of the cage salt, removing the need to use THF. The product from a test reaction on a 10 mL scale using NaTFSA, and

purified using acetone, was successful. The  $^1\text{H}$  NMR spectrum showed the characteristic broad peaks corresponding to the reduced cage (**Figure 5.15a**), and the IR spectrum indicated that both the cage and the anion were present (**Figure 5.15b**). Elemental analysis was also performed – the results were comparable to the calculated composition (**Figure 5.15c**), suggesting the cage salt had been isolated.

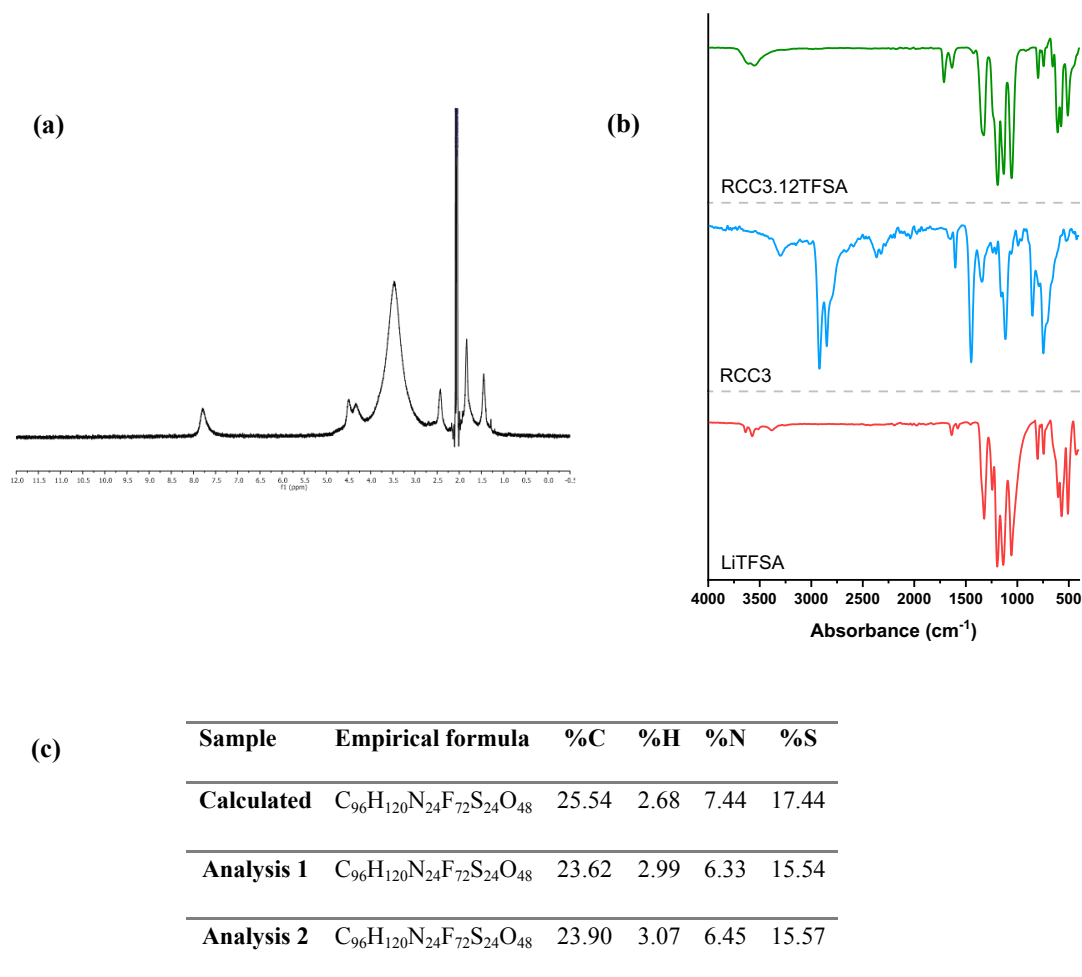


**Figure 5.15:** Analytical data for **RCC3.12TFSA** formed using **RCC3.12HCl** and NaTFSA: (a)  $^1\text{H}$  NMR spectrum in acetone- $d_6$ ; (b) FTIR data compared to **RCC3** and **LiTFSA**; (c) elemental analysis.

Given the successful replacement of LiTFSA with NaTFSA, the scale out was repeated for both the synthesis of **RCC3.TFSA** and **RCC1.TFSA** using the Chemspeed ISynth. **RCC1.12HCl** had limited solubility in methanol, which meant the stock solution was dispensed as a dispersion. Once the stock solutions had been dispensed, the vessels were vortexed at ambient temperature for 72 hours. As before, the reactions were then combined and the solvent removed under reduced pressure, before acetone was added to precipitate the sodium chloride by-product. The solid was removed by filtration and the solvent removed

from the filtrate. The purification was repeated until no more solid precipitated from solution, at which point the cage salt was dissolved in ethanol, filtered through a syringe filter, and the solvent removed under reduced pressure.

After purification, the isolated cage salts were dried further under vacuum, and unlike previous observations, then appeared to be solid. This is likely due to the higher purity of the isolated cage salt, formed using the optimised synthesis, as the purity of ionic salts has been demonstrated to vary between batches. It is often difficult to quantify the residual by-products in ionic liquids, such as halide salts, due to them being NMR silent, and this can result in changes to overall properties, which includes variation in the observed melting points.<sup>193</sup> Additionally, the solvent used during the purification can also be difficult to remove if it interacts with the formed ionic salt, which was observed with THF in the formation of ionic cage salts here. Whilst none of the formed cage salts were liquid once pure, this highlights the importance of determining the purity of synthesised ionic liquids and how it can affect the final properties of the material. However, organic cage salts with large anions have yet to be studied in greater detail, and determining their behaviour in the solid state could still inform the design of future cage salts, such as evaluating if the anions are size-excluded from the cage cavities. Therefore, these scaled-out organic cage salts were studied in further detail.

### 5.5 Synthesis and characterisation of organic cage salts

A range of the cage salts synthesised in the high-throughput screen, including the scaled up **RCC3.TFSA** and **RCC1.TFSA**, were studied further to explore how changing both the cage and the anion effects the properties of the ionic cage salts (**Figure 5.16**).

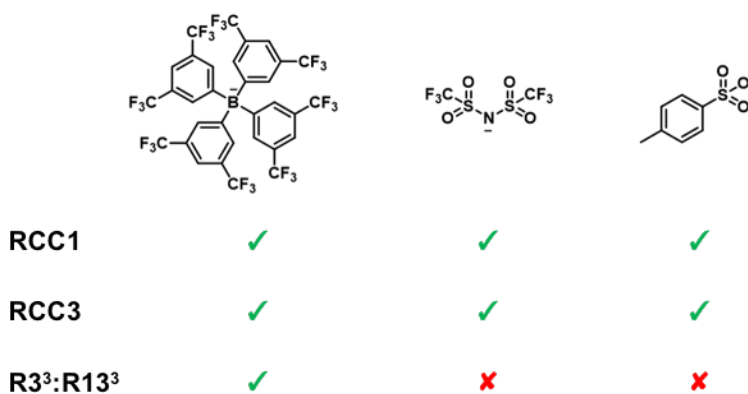


**Figure 5.16:** The structure of the cage salts selected to investigate the effect of changing the cage and anion on the properties and gas uptake. (✓ = cage salts synthesised and studied, ✗ = synthesis not successful).

The scale out of **RCC3.12TFSA** resulted in a high isolated yield (3.725 g, 55%), which meant there was plenty of material to study this organic cage salt in depth. However, the synthesis of the other cage salts needed repeating in order to generate sufficient quantities for characterisation. The synthesis of **RCC1.12TFSA** was also repeated because of the low yield from the scale out (<0.2 g). For several of the other cage salts there was insufficient material produced for subsequent characterisation, therefore they were not studied in further detail. This gave seven salts, which were isolated in high purity and fully characterised using the analytical techniques discussed earlier, before investigating their properties.

### 5.5.1 Investigation into melting characteristics of cage salts

As discussed previously, a glass transition occurs when a liquid is rapidly cooled and crystallization is avoided. The molecules in the liquid are frozen in their movement, therefore, rather than having enough time to form an ordered crystalline structure, an amorphous glass is formed. The cooling rate is an important factor in the glass formation because changing how fast a sample is cooled will change the glass transition temperature ( $T_g$ ). Increasing the cooling rate, also increases the  $T_g$  and will affect the resulting material's properties (**Figure 5.17**).<sup>194</sup> It is important to report the cooling rate when discussing the thermal behaviour of materials as this will vary the onset of  $T_g$ . In most cases, the standard practice is to use  $10 \text{ K min}^{-1}$  when determining the glass transition using differential scanning calorimetry (DSC) for calibration and to account for thermal lag.<sup>195</sup> In this work,  $5 \text{ K min}^{-1}$  was used as the cooling rate and will be referred to as the fictive temperature ( $T_f$ ) as the glass transition ( $T_g$ ) as the cooling rate of  $10 \text{ K min}^{-1}$ . Changing the rate of cooling also affects the temperature at which the atoms/molecules slow down and a glass is formed over a different temperature region. To compare materials, the glass transition is defined at  $10 \text{ K min}^{-1}$  and at other rates, the notation, *fictive temperature* is used.

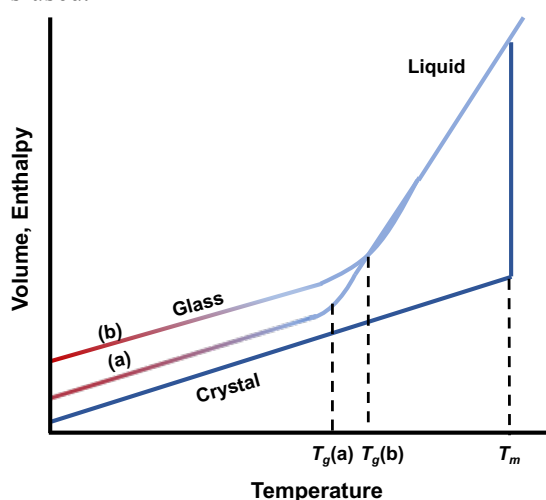


**Figure 5.17:** A graphical representation of the how a liquid's volume or enthalpy depends on the temperature. Cooling a sample at a slower rate gives  $T_g(a)$ , whereas at a faster rate gives  $T_g(b)$ .  $T_m$  is the melting temperature observed in a crystalline sample.<sup>194</sup>

One property of interest when targeting a liquid or meltable organic cage salt is its behaviour on heating. Thermogravimetric analysis (TGA) was carried out on the organic cage salts in the library to determine their decomposition temperature ( $T_d$ ), which ranged from 200 to 300 °C (Table 5.2). With the  $T_d$  known, the thermal characteristics of the cage salts were investigated in greater detail using differential scanning calorimetry (DSC, carried out by Jess Smith). Each sample was heated at 5 °C/min to just below their  $T_d$  cooled, and then reheated, to study their phase behaviour (Table 5.2 and Figure 5.18) – several of the organic cage salts potentially exhibited melting behaviour ( $T_m$ ), fictive temperature ( $T_f$  (5 K min<sup>-1</sup>)), and re-solidification on cooling ( $T_s$ ), and it was apparent that changing both the cage species and the anion seemed to have an effect on the  $T_f$ (5 K min<sup>-1</sup>) and  $T_m$ .

Across the BARF anion series (**RCC1.12BARF**, **RCC3.12BARF**, and **R3<sup>3</sup>:R13<sup>3</sup>.12BARF**), no distinct melting transitions were apparent, but a glass transition was observed for each cage salt. This value varied depending on the reduced cage, for example, the salt containing **RCC1** had a lower phase transition than that containing **R3<sup>3</sup>:R13<sup>3</sup>**, which was lower than that formed with **RCC3** ( $T_f$ (5 K min<sup>-1</sup>) ~60 °C, ~70 °C, and ~80 °C, respectively) – this can be rationalised due to the increasing steric bulk on the outer periphery when going from **RCC1** to **R3<sup>3</sup>:R13<sup>3</sup>** to **RCC3**, contributing to the observed increases in fictive temperature.

Changing the anion to TFSA gave a much more complex DSC trace. Unlike the BARF series, the TFSA cage salts exhibited both a broad endothermic melt and a corresponding exothermic transition in the downcycle, which is attributed to the liquid cage salt re-solidifying (**RCC1.12TFSA**:  $T_m$  170-220 °C,  $T_s$  160-190 °C; **RCC3.12TFSA**:  $T_m$  190-250 °C,  $T_s$  180-210 °C). Additionally, for both **RCC1.12TFSA** and **RCC3.12TFSA**, whilst the  $T_f$ (5 K min<sup>-1</sup>) followed the same trend in relation to the cages (**RCC3**>**RCC1**), they were significantly lower than the BARF analogues (**RCC1.12TFSA**:  $T_f$ (5 K min<sup>-1</sup>) -50 °C; **RCC3.12TFSA**:  $T_f$ (5 K min<sup>-1</sup>) -20 °C) – this is likely due to the smaller and less bulky TFSA anion compared to BARF. Contrasting with the previously reported alkylated cages, the  $T_m$  was also still observed on the second upcycle, even after a phase transition had occurred.<sup>110</sup> The additional endotherm at ~150 °C observed for **RCC1.12TFSA** is potentially an irreversible phase change that would need further investigation using other characterization techniques, such as PXRD, to confirm without doubt.

The salts containing the TSA anion did not appear to follow the same trend as the other cage salts, with the  $T_f$ (5 K min<sup>-1</sup>) for **RCC1.12TSA** and **RCC3.12TSA** being higher than both the corresponding BARF and TFSA salts (**RCC1.12TSA**:  $T_f$ (5 K min<sup>-1</sup>) 75 °C; **RCC3.12TSA**:  $T_f$ (5 K min<sup>-1</sup>) 140 °C). However, in unpublished work carried out in the

group, the DSC trace of **RCC3** possessed a similar transition at 138 °C to **RCC3.12TSA**. Therefore, this counter-ion may not affect the thermal properties in the same way as BARF or TFSA, possibly because it is not cavity excluded. This would need further investigations in order to elucidate any structure-property relationships.

In several of the DSC traces there were other transitions that require further investigation in future work. To confirm if the  $T_f$  values were glass transitions, the DSC would need repeating at a ramp rate of 10 K per min. This also includes an unexpected exothermic transition for **RCC3.12TFSA** at ~250 °C, which was towards the end of the first upcycle (**Figure 5.18**). Overall, this preliminary investigation into the thermal properties of the organic cage salts illustrates how changing both the cage and anion can change the melting and phase behaviour.

**Table 5.15:** Summary of the thermal behaviour of organic cage salts based on analysis by TGA and DSC

Entry	Organic cage salt	$T_d$ (°C)	$T_m$ (°C)	$T_f$ (5 K $\text{min}^{-1}$ ) (°C)	$T_s$ (°C)	Notes
1	<b>RCC1.12BARF</b>	200	n/a	60	n/a	
2	<b>RCC1.12TFSA</b>	310	170 to 220	-50	160 to 190	Endotherm at 147 °C
3	<b>RCC1.12TSA</b>	300	n/a	75	n/a	
4	<b>RCC3.12BARF</b>	200	n/a	80	n/a	
5	<b>RCC3.12TFSA</b>	250	190 to 250	-20	180 to 210	Exotherm at 244 °C
6	<b>RCC3.12TSA</b>	280	n/a	140	n/a	Endotherm at 199 °C
7	<b>R3<sup>3</sup>:R13<sup>3</sup>.12BARF</b>	200	n/a	70	n/a	



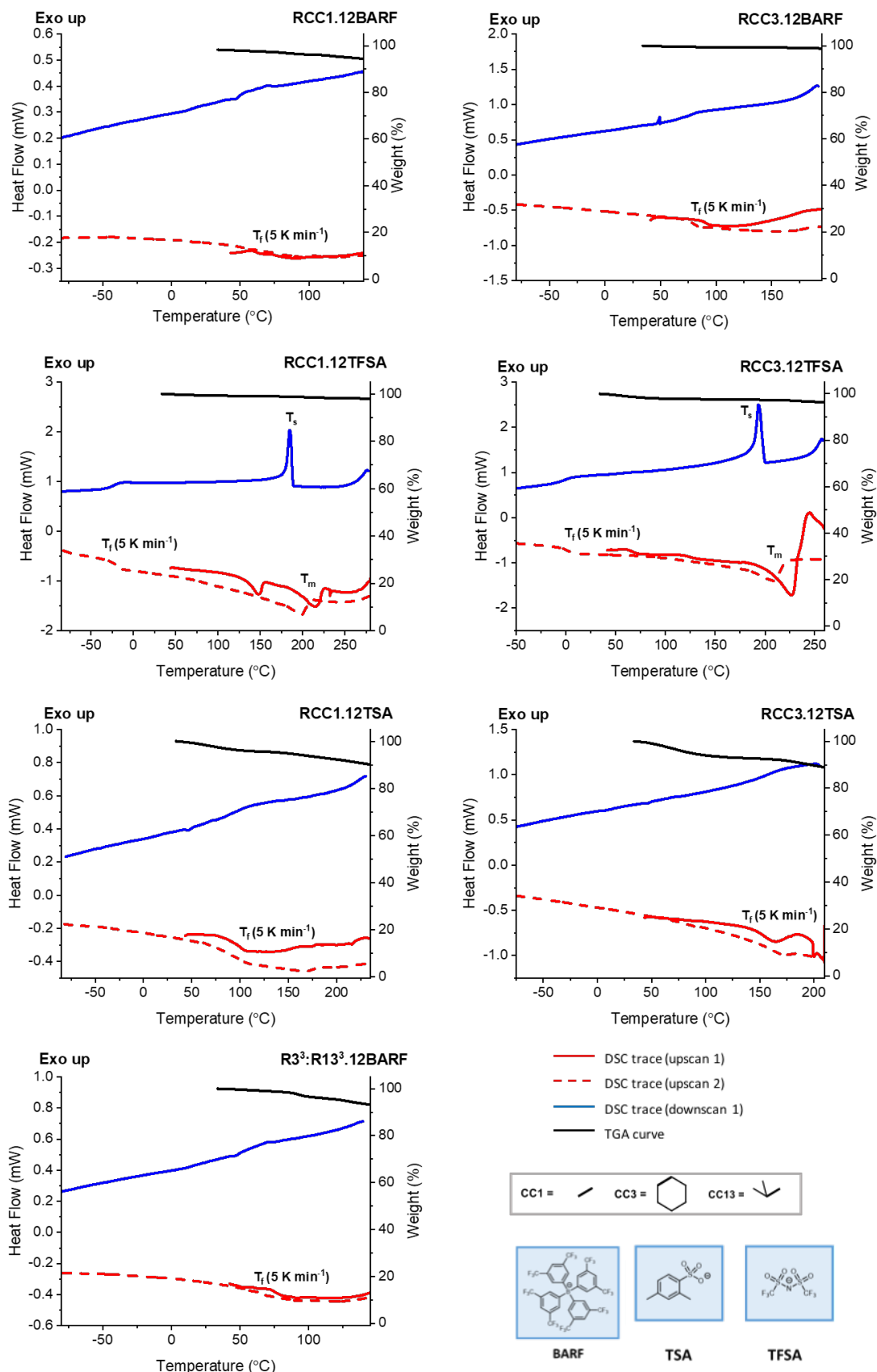


**Figure 5.18:** DSC traces and corresponding TGA curves (black) for a series of organic cage salts subjected to a heat-cool-heat cycle to below their decomposition temperatures. DSC traces: initial upscan shown as solid red line, downscan as a solid blue line, and second upscan as a dashed red line. Exotherm pointing up.

Gas sorption was also attempted on solid **RCC3.12TFSA** but it exhibited a negligible surface area, indicating the solid is non-porous compared to other imine cages. This could mean that the TFSA anions are not completely cavity-excluded from the cage, or that reduction of the imine bonds has led to collapse of the cage cavity, which is more likely based on previous reports.<sup>196</sup> However, there could be enough accessible porosity maintained in the liquid state to increase the porosity of an ionic liquid as a Type II system. As the cage salts in this study are solid at ambient temperature, investigations could be carried out into their bulk packing in the solid state. Attempts to grow single crystals for X-ray diffraction were attempted, but **RCC3.12TFSA** and **RCC3.12BARF**, in particular, are highly soluble so suitable crystals have yet to be obtained. However, obtaining crystal structures of the cage salts would give an insight into the interactions of anions with the cages and determine which are size-excluded. Future work would explore the gas sorption of the other cage salts and how changing the anion changes this property.

## 5.6 Targeting Type II porous liquids

Although the high-throughput screen did not result in a low melting cage salt, it did provide several potential precursors for Type II porous liquids. Unlike the scrambled cages in **Chapter 2**, the cage salts could potentially be more soluble in ionic liquids, and therefore could allow Type II porous liquids with zero vapour pressure to be targeted. **RCC1.12TFSA** and **RCC3.12TFSA** were chosen as the cage salt to be used as a potential Type II porous liquid because they were synthesised on a reasonable scale, and would demonstrate the effect of having two contrasting groups on the cage periphery on gas uptake.

### 5.6.1 Solubility testing of cage salts in ionic liquids

The requirement for a Type II porous liquid, as seen previously, is a porous molecule dissolved in a cavity-excluded solvent. Therefore, a small scale screen was designed to test the solubility of **RCC1.12TFSA** and **RCC3.12TFSA** in several ionic liquids with the same counterion (TFSA). Although a high-throughput workflow was developed in **Chapter 2**, this method was not suitable to test the cage salts in ionic liquids because they are inherently more expensive and more viscous than the solvents used in the scrambled porous liquids. Therefore, a small scale solubility screen was devised based on choosing ionic liquids with similar functionality to the cage salts.

A range of ionic liquids were chosen that were either commercially available or had been synthesised in the group (**Figure 5.19**). Trifluoromethanesulfonamide (TFSA) salts are more common than the other anions used in this study, so a varied range could be chosen from. As

there is limited prior solubility data for cage salts in ionic liquids, a simple methodology was devised to start elucidating general trends. Ionic liquids were chosen with similar functionality to the amine cages, and large cations to increase the likelihood of being cavity-excluded. Through the purification procedures, the cage salts appeared to have a reasonable solubility in methanol, ethanol and, acetone so, where possible, this was taken into consideration when choosing ionic liquids. As seen in **Chapter 2**, there was an apparent correlation between the solubility of the scrambled cage in the small solvent and in the bulky analogues, therefore, a similar approach was taken here. Several ionic liquids with alcohol functionality was selected to test with **RCC3.12TFSA**.

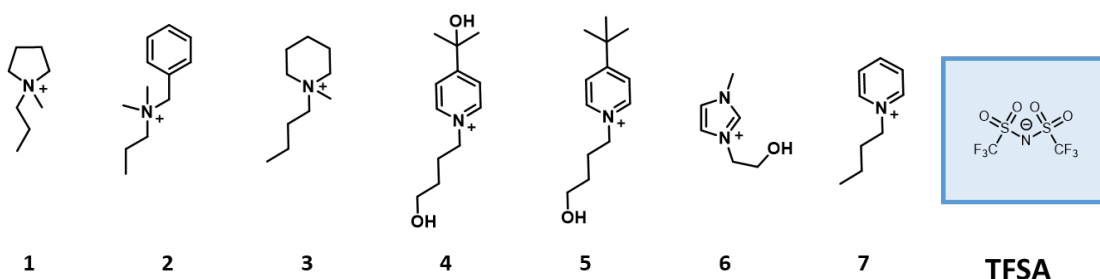


**Figure 5.19:** Structures of the TFSA ionic liquids used in the solubility screen for Type II porous liquids and the TFSA anion .

A procedure was designed to test the solubility of both **RCC1.12TFSA** and **RCC3.12TFSA** in the chosen ionic liquids, which was based on the one developed in **Chapter 2**. In order to conserve material, 30 mg of cage salt was used and 0.1 mL increments of each ionic liquid were added until the solid dissolved. When a positive outcome was reached, this value was set as a lower bound in order to conserve material. As a result, three potential Type II porous liquids were found with a concentration of 100 mg mL<sup>-1</sup> (**Figure 5.20**).

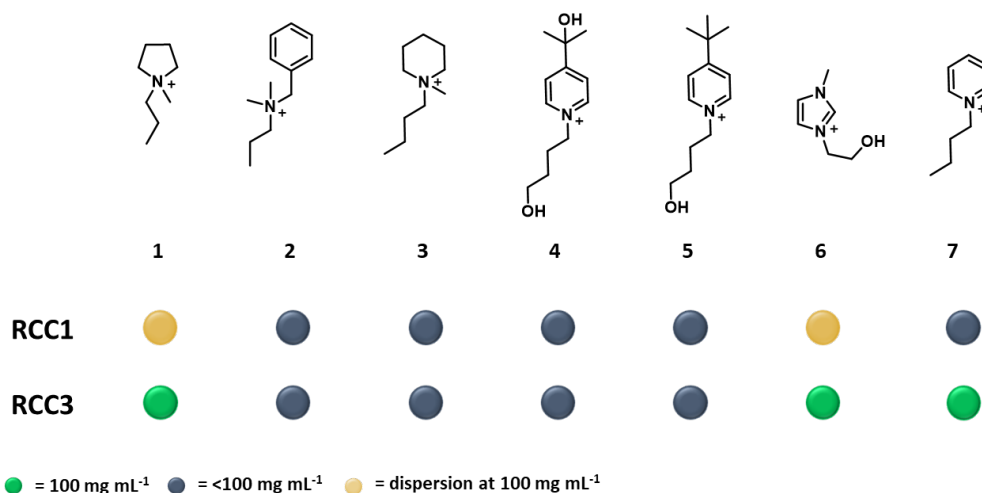


**Figure 5.20:** Results from the solubility screen of **RCC1.12TFSA** and **RCC3.12TFSA** in a range of ionic liquids. Green = a positive 'hit' at 100 mg mL<sup>-1</sup>, yellow = a dispersion at 100 mg mL<sup>-1</sup> and grey = solubility <100 mg mL<sup>-1</sup>.

In addition, as a comparison, to demonstrate how changing the anion affects solubility, both **RCC3** and **RCC3.12HCl** were tested in ionic liquid **1** using the same methodology. Both cage species were insoluble in the ionic liquid at  $<100 \text{ mg mL}^{-1}$ , whereas **RCC3.12TFSA** showed higher solubility at  $100 \text{ mg mL}^{-1}$ . Using TFSA as the cage salt anion appears to improve the solubility in some ionic liquids that contain the same anion and, generally, **RCC3.12TFSA** was more soluble than **RCC1.12TFSA**.

### 5.6.2 Gas sorption of cage ionic liquids

With a selection of potential Type II porous ionic liquids in hand, the next step was to investigate the gas uptake of these systems. Unlike the scrambled porous liquids in previous chapters, the cage ionic liquids did not contain volatile solvents so could be studied using more traditional gas sorption techniques. Traditional gas sorption equipment is enclosed and not easily modified, which makes it difficult to test liquid samples that require stirring to ensure equilibration during gas addition, or heating to their melting temperature. Therefore, a modified liquid gas sorption program was setup on a Quantachrome Nova (by Dr Becky Greenaway) and calibrated using several commercially available liquids with reported literature values. This provides a reliable method for testing gas sorption of porous liquid samples with negligible vapour pressure up to 1 bar. The Quantachrome Nova is a piece of commercial equipment, which is stripped back to allow stirrer plates and heating mantles to be fitted for a range of different porous liquid types to be tested.

In this study, the  $\text{CO}_2$  and  $\text{CH}_4$  uptakes were therefore investigated in the potential Type II porous ionic liquids (carried out by Aiting Kai). The liquids were prepared using **RCC3.12TFSA** (100 mg) and ionic liquids (1 mL), which were dried under vacuum at  $90 \text{ }^\circ\text{C}$  to remove any atmospheric water. A 0.5 to 1.0 mL sample was then degassed at 298 K, with stirring, for 18 hours. The gas absorption was run at 0.05 to 1.00 bar with stirring to give an isotherm. The data were given as P (mmHg) and V ( $\text{cc g}^{-1}$ ), so the units were converted to  $\mu\text{mol g}^{-1}$  using the ideal gas law, and the pressure was converted to bar. Finally, the procedure was repeated on the same sample in order to determine if the gas uptake was repeatable.

The gas sorption values differed between each porous liquid (**Figure 5.21**). There was a slight increase in  $\text{CO}_2$  uptake in both PIL-1 and PIL-2 over the neat ionic liquids, with PIL-1 having the highest value compared to neat IL-1 (88.6 vs  $72.4 \mu\text{mol g}^{-1}$ , respectively). This demonstrates the potential proof-of-concept for increasing the gas uptake in ionic liquids by incorporating organic cage salts into ionic liquids to improve gas solubility. The methane uptake in the porous liquids experienced only a marginal increase compared to the neat liquids,

suggesting that if the gas capacity can be increased, these systems may have potential in CO<sub>2</sub>/CH<sub>4</sub> separations in future work.

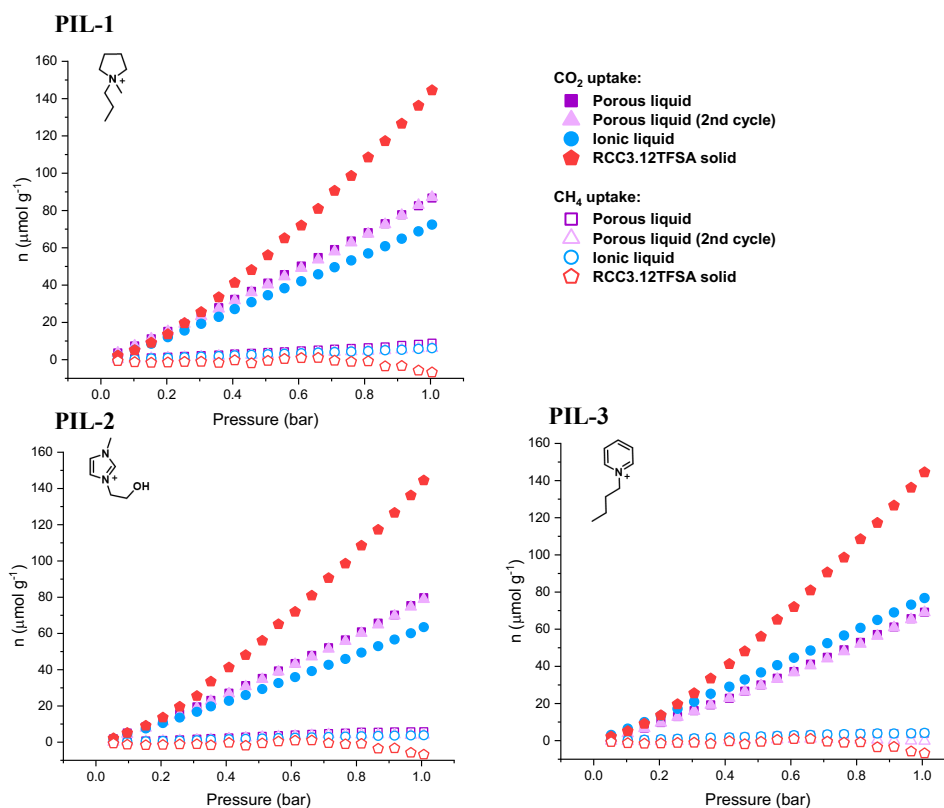


**Figure 5.21:** Gas uptake for Type II porous ionic liquids formed from RCC1.12TFSA (100 mg) in a range of TFSA ionic liquids.

Repeating the gas sorption on each porous liquid showed the uptakes were reproducible on the same sample. Further investigation would be needed to demonstrate how many cycles could be carried out on the same sample, but there is potential for multiple cycles to be performed without the cage decomposing. The gas uptakes would also need repeating between batches to see if concordant results could be obtained and to get an average uptake measurement. This was briefly attempted and similar uptakes were observed for PIL-3 but PIL-1 and PIL-2 gave lower values. The gas sorption needs to be repeated to confirm the reproducibility and give an average uptake. In this case, the samples may have been inadequately dried under vacuum as ionic liquids have a high affinity for water, which could affect the overall gas uptake.<sup>197,198</sup>

## 5.7 Conclusions

Throughout this chapter, an alternative strategy towards non-volatile porous liquids has been explored. Post-synthetic modification of imine organic cages allowed for the development of a high-throughput workflow to screen for organic cage salts with bulky counter-anions. The simplicity of the salt-exchange methodology meant it translated well onto the high-throughput platform, and provides scope for larger scale screens in future work. Overall, dispensing the precursors as stock solutions using an automated system improves the accuracy and time efficiency of a workflow. Although only 20 combinations were tested in this project, this would be particularly useful with larger precursor libraries.

During the purification step of the workflow, the procedures were carried out in parallel but using manual additions of the solvents. While this was not an issue for the 20 cages in this screen, it could be a limiting step with a larger number of reactions to purify. However, dispensing solvents using liquid addition using the high-throughput platform would make the purification more time efficient, along with using the Supelco SPE vacuum filtration manifold in the filtration step (seen in **Chapter 2**). This work also explored the analytical techniques suitable for identifying the formation of a cage salt.  $^1\text{H}$  NMR spectroscopy is not always useful if the anion is NMR active – this is because the large mass ratio compared to the cage makes the relevant peaks associated with the cage species difficult to identify. However, the cage component is often visible by mass spectrometry, but without the anion. For a high-throughput screen, a mixture of methods should be used to determine the presence of both constituents in the cage salt. However, the purity of the resulting cage salt was difficult to determine, as illustrated throughout this project. Detecting residual halide salts can be problematic because they cannot be seen in traditional analytical techniques, such as  $^1\text{H}$  NMR spectroscopy. These can affect the physical state of an ionic salt, as observed in **RCC3.12TFSA**, which was isolated as a high melting solid when the halide salt was removed.

Although the high-throughput screen did not result in a cage salt that was liquid at ambient temperature, a methodology was designed that could be applied to a much larger dataset. Some of the fundamental considerations have been considered when designing a screen for liquid cage salts. Further, a series of the synthesised solid organic cage salts were also studied using DSC and TGA. These showed interesting characteristics, and while none were low melting, they did exhibit fictive temperatures. Future work will involve collecting NMR and PXRD data to check if these are glass transitions, are stable and still molecular in nature, as well as studying the porosity. A porous ionic cage glass would allow casting in the liquid state and the formation of new functional materials.

Finally, the library of synthesised cage salts was screened for solubility in ionic liquids, to form non-volatile Type II porous liquids. **RCC3.12TFSA** was found to be highly soluble in three ionic liquids and possessed some improved gas uptake over the neat ionic liquid. This provides scope for testing other TFSA cage salts in ionic liquids with functionality to improve solubility, such as bulky groups on the periphery, or scrambled cages. There is also the potential to study the materials as dispersions to form Type III porous liquids. Overall, this study has provided further understanding into the behaviour of organic cage salts, and fundamental strategies towards the targeted design of non-volatile porous liquids.

# **Chapter 6:**

## Conclusions and future work



## 6.1 Conclusions

The work presented in this thesis has attempted to develop the understanding into the design of scrambled porous liquids. In order to streamline the discovery of new Type II systems, a high-throughput methodology was developed for the synthesis, characterization, analysis and solubility testing of scrambled cages. Using automation, where appropriate, allowed a large library of diamines to be screened in a more time efficient manner. A parallel workflow also predetermined if the solvents were cavity-excluded before the high-throughput solubility testing, which increased the probability of finding a highly soluble scrambled cage. From the combined workflow, 40 scrambled cages were identified with higher solubility in 6 cavity-excluded solvents than the previously reported example. From the selection potential porous liquids, the scrambled cages were scaled up and the solvents purified in order to test the porosity of the identified combinations. These were screened for porosity using a gas displacement method, where xenon was loaded into the porous liquid and the volume collected after displacement with a small guest equated to the gas uptake. The porosity screen gave a library of Type II porous liquids with varying scrambled cages and bulky solvents. Therefore, the effect of changing these components on the overall properties was investigated. A series of scrambled porous liquids with the same cage but different solvents had varying gas uptake using gas displacement measurements and  $^1\text{H}$  NMR spectroscopy. The same was also observed when the scrambled cage was changed, with the diamine feed ratio and functionality both having an effect.

An aim of the high-throughput screen was to find a porous liquid with a higher pore concentration. One particular system, comprised of  $3^3:13^3$  and 2-hydroxyacetophenone, possessed a higher solubility of 27 wt% compared to the first reported system ( $3^3:13^3_{\text{PCP}} = 10$  wt%). This porous liquid also had a 26 % increase xenon uptake ( $194.7 \mu\text{mol mL}^{-1}$  vs.  $155 \mu\text{mol mL}^{-1}$ ), however, the methane remained lower, which further demonstrated the effect of the solvent. Another property affected by the concentration of scrambled cage in the porous liquid was the viscosity. Increasing the cage concentration did not always increase the gas uptake in a system and can actually be detrimental, and also lead to gelation. This allowed for an alternative xenon capture method, where the gas could be trapped in the porous liquid and released by heating. Prior gas displacement measurements were performed using chemical release by a small liquid guest, such as chloroform, however, this is not practical and did not allow for recycling of the porous liquid. Therefore, temperature release was demonstrated as an alternative for displacing the xenon trapped in the porous liquid. Overall, a library of Type II scrambled liquids was discovered and, for the first time, factors for designing a new system were considered. Both the size-excluded solvent and scrambled cage were shown to be

important considerations when designing a Type II porous liquid. In particular, a combination was discovered with a higher pore concentration with a less expensive, less toxic solvent compared to the first reported system.

From the high-throughput synthesis screen, a new porous organic cage (**CC21**) was discovered with isopropyl groups on the periphery. When the synthesis of **13<sup>1</sup>:21<sup>5</sup>** was optimised, the binary **CC21** parent cage was the isolated product instead. However, without the added equivalent of 1,2-diamino-2-methyl-propane (used to form **CC13**), a [1+3] amination species was observed - intermediates that had not previously been isolated. <sup>1</sup>H NMR and HRMS studies showed a complex formation mechanism with a number of reoccurring intermediates. Since **CC21** was not the major product, unlike other cages in the series, further investigation was needed to rationalise the formation mechanism. Computational calculations for the formation energies of the imine bonds in each intermediate revealed the amination species were more stable than the imine analogues. Experimental control reactions showed the amination was preferential with the **CC21** diamine but other diamines, such as **CC1**, **CC3** and **CC13**, exclusively formed the imine. This helped explain the slow mechanism as the amination intermediates were more stable, acting as traps in the reaction. **CC21** also possessed a reasonably high surface area ( $S_{\text{BET}} = 669 \text{ m}^2 \text{ g}^{-1}$ ) and  $\text{N}_2$  uptake ( $11.1 \text{ mmol g}^{-1}$ ) compared to similar [4+6] analogues. The above average solubility was due to the frustrated packing in the solid state due to the disorder provided by the isopropyl groups. This could lead to interesting gas separation applications in future work. The low yield made it unsuitable for use in a porous liquid during the high-throughput screen but the cage could be investigated in a Type II PL in future work.

For some applications, the scrambled porous liquids are unsuitable because of the vapour pressure associated with the size-excluded solvents. Therefore, another strategy was explored using post-synthetic modification of the imine cages into amine cage salts. Another high-throughput workflow was designed to screen for low melting organic cage salts. A series of scalable [4+6] cage hydrochloride salts were salt exchanged with several bulky halide salts, with the aim of being excluded from the cage cavities. Although a low melting organic cage salt was not discovered, the importance of the purification for this ionic system was demonstrated. The metal halide salt by-product was difficult to detect and remove from the desired product, which can affect the melting point of the organic cage salt. However, the high-throughput screen did generate a library of organic cage salts with varying cages and anions. This allowed the study into the thermal behaviour of cage salts using TGA and DSC and showed how changing the components affects the glass transitions and melting points of the ionic cage salts. Changing the anion from a  $\text{Cl}^-$  to a  $\text{N}(\text{SO}_2\text{CF}_3)_2^-$  also improved the

solubility of **RCC3.12N(SO<sub>2</sub>CF<sub>3</sub>)<sub>2</sub>** in a number of ionic liquids. The gas sorption of this system demonstrated an improved uptake over the neat ionic liquid.

## 6.2 Future work

Overall, this thesis has demonstrated the usefulness of high-throughput screening in streamlining materials discovery, in particular for advancing a new field. However, the area of porous liquids remains underdeveloped. In the case of the Type II scrambled porous liquids, there is now scope to further diversify the scrambled cage library. In order to develop the methodology, many of the diamines selected were known to produce scrambled cages, however, now there is a reliable workflow, more complex custom diamines could be screened. This could allow for low melting organic cages to be targeted, particularly if longer, branched alkylated chains were used. Other combinations of scrambled cages could be used, instead of limiting to **CC13**, which could give more highly soluble combinations. A more extensive library of Type II porous liquids would allow the investigation into specific applications by tuning the scrambled cage / solvent combinations for separating gas mixtures.

Finding a low melting organic cage salt remains a challenge and further investigation is needed to find an anion that significantly reduces the melting point. Another approach would be to alter the functionality on the cage periphery in order to disrupt the solid state packing. The alkylated cages presented by James *et al.* had lower melting points than other imine cages,<sup>111,123</sup> which could translate when modified to the amine cage salt. Determining if the anions are excluded from the cage cavities would also be useful prior to future screens. As the organic cage salts in this study are solid, single crystal x-ray diffraction would give a useful insight into the solid state behaviour, which could also inform about the liquid phase. Continuing the study into the thermal behaviour of organic cage salts would allow for interesting hybrid materials to be developed.

## **Chapter 7: Experimental data and references**

## 7.1 General synthetic and analytical methods

**Materials:** 1,3,5-Triformylbenzene was purchased from Manchester Organics (UK). Other chemicals were purchased from Fluorochem UK, TCI UK or Sigma-Aldrich. Solvents were reagent or HPLC grade purchased from Fischer Scientific. All materials were used as received unless stated otherwise.

**Synthesis:** All reactions were stirred magnetically using Teflon-coated stirrer bars. Where heating was required, the reactions were warmed using a stirrer hotplate with heating blocks, with the stated temperature being measured externally to the reaction flask with an attached probe. Removal of solvents was done using a rotary evaporator.

**High-throughput synthesis and solubility screening:** High-throughput automated synthesis was carried out using a Chemspeed Accelerator SLT-100 or an I-SYNTH Chemspeed automated synthesis platform, and the high-throughput solubility testing was performed on a ChemSpeed Swing platform. Organic solvents were removed using a Combidancer evaporator.

**IR Spectra:** Infra-red (IR) spectra were recorded on a Bruker Tensor 27 FT-IR using ATR measurements for oils and solids as neat samples, or using transmission mode on a 96-well silica wafer deposited as a thin film as part of the high-throughput analysis.

**NMR Spectra:**  $^1\text{H}$  Nuclear magnetic resonance (NMR) were recorded using an internal deuterium lock for the residual protons in  $\text{CDCl}_3$  ( $\delta = 7.26$  ppm),  $\text{D}_2\text{O}$  ( $\delta = 4.79$  ppm), or  $\text{CD}_2\text{Cl}_2$  ( $\delta = 5.32$  ppm) at ambient probe temperature on either a Bruker Avance 400 (400 MHz) or Bruker DRX500 (500 MHz) spectrometer. NMR studies of porous liquids were conducted using an in-house calibrated capillary of TMS in  $\text{d}_2$ -DCM (made using 100  $\mu\text{L}$  sample from 10  $\mu\text{L}$  TMS in 0.5 mL  $\text{d}_2$ -DCM).

Data are presented as follows: chemical shift, integration, peak multiplicity (s = singlet, d = doublet, t = triplet, q = quartet, quint = quintet, m = multiplet, br = broad), coupling constants ( $J$ / Hz), and assignment. Chemical shifts are expressed in ppm on a  $\delta$  scale relative to  $\delta_{\text{TMS}}$  (0 ppm),  $\delta_{\text{D}_2\text{O}}$  (4.79 ppm),  $\delta_{\text{CD}_2\text{Cl}_2}$  (5.32 ppm), or  $\delta_{\text{CDCl}_3}$  (7.26 ppm). Assignments were determined either on the basis of unambiguous chemical shift or coupling patterns, or by analogy to fully interpreted spectra for structurally related compounds.

$^{13}\text{C}$  NMR Spectra were recorded using an internal deuterium lock using  $\text{CDCl}_3$  ( $\delta = 77.16$  ppm) at ambient probe temperatures on the following instruments: Bruker Avance 400 (101 MHz) or Bruker DRX500 (126 MHz).

**Calibration of d<sub>2</sub>-DCM/TMS sealed capillaries:**

The same calibrated capillary (2) was used in this work as used previously by Greenaway *et al.* which was calibrated using **3<sup>3</sup>:13<sup>3</sup>** in perchloropropene (**Figure 7.1**)<sup>112</sup>

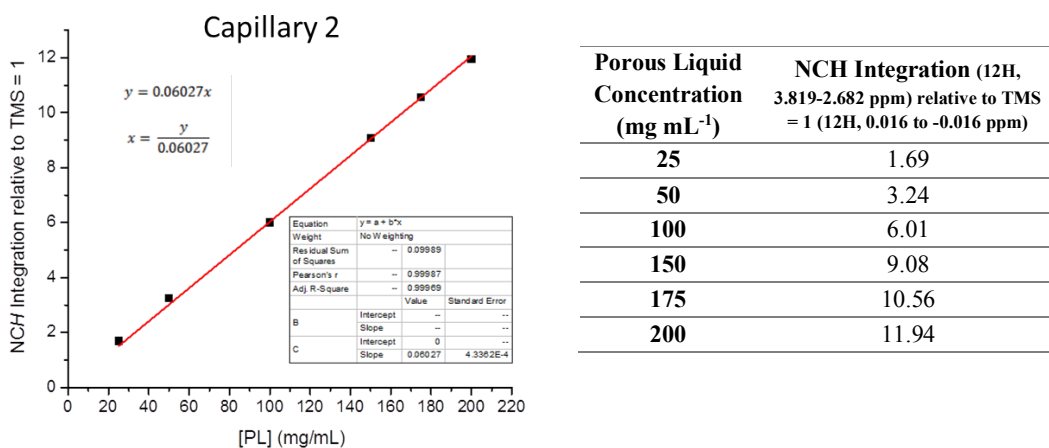


**Figure 7.1:** Calibration curve generated by Greenaway *et al.* for the sealed TMS/CD<sub>2</sub>Cl<sub>2</sub> capillary by plotting the NCH integration, relative to TMS = 1, against the porous liquid concentration<sup>112</sup>

**HPLC Spectra:** HPLC analysis was carried out using a Dionex UltiMate 3000 with a diode array UV detector using a Thermo-Scientific Synchronis C8 column, 150 x 4.6 mm, 3 μm (SN 10136940, Lot 12459). The mobile phase was isocratic MeOH at a flow rate of 1 mL/min for a 10-30 min run time, and the column temperature was set to 30 °C. The injection volume was 10 μL and the sample concentration was approximately 1 mg/mL. Detection for UV analysis was conducted at 254 nm.

**HRMS spectra:** High resolution mass spectrometry (HRMS) was carried out using an Agilent Technologies 6530B accurate-mass QTOF Dual ESI mass spectrometer (capillary voltage 4000 V, fragmentor 225 V) in positive-ion detection mode. The mobile phase was MeOH + 0.1% formic acid at a flow rate of 0.25 mL/min.

**PXRD:** Laboratory powder X-ray diffraction data were collected in transmission mode on samples held on a black opaque 96-shallow well microplate (ProxiPlate-96 Black) on a Panalytical X'Pert PRO MPD equipped with a high-throughput screening (HTS) XYZ stage, X-ray focusing mirror and PIXcel detector, using Ni-filtered Cu K $\alpha$  radiation. Data were measured over the range 5–30° in ~0.013° steps over 15 minutes.

**Gas uptake and evolution studies:** All uptakes in the porous liquid samples were measured using gases purchased from BOC of the following grades: methane (N4.5) and xenon (N5.0), in 10 mL GC headspace vials (22 mm x 45 mm screw top, ThermoScientific). All samples

had gas addition and measurements conducted between 23-25 °C in a temperature-controlled laboratory.

The gas flow rate was measured and controlled using a Gilmont calibrated flowmeter (tube size 0, Gilmont EW-03201-22) with a stainless steel (SS) float and 0-100 scale. The flow rate for each gas was calculated using the correlated flow table for air from the supplier, and the general correction equations. These equations approximate the gas flow compared to air by using each gas density (g/mL) at standard conditions (taken from the NIST Chemistry WebBook<sup>199</sup> and Gilmont calibrated at 1 atm, 294 K), with corrections for temperature and pressure. Each gas was maintained at a ~50-60 mL/min flow rate by setting the regulator output pressure to 0.5 bar and fine-controlling the flow with a needle valve to the calculated scale readings (see table below).

The gas evolved from the porous liquids was collected and measured by water displacement in an inverted Rotaflo stopcock 25 mL burette (0.1 mL graduations) in a crystallisation dish of water. The GC vial containing the sample was connected to the burette using a needle/tubing cannula.

#### General correction equations:

Gas flow from air flow:

$$q_G^o = q_A^o \sqrt{\frac{\rho_{Air}^o}{\rho_G^o}}$$

Correction for temperature and pressure:

$$q_G' = q_G^o \sqrt{\frac{p}{p^o} \cdot \frac{T^o}{T}}$$

Standard conditions:  $p^o = 1 \text{ atm}$   $T^o = 21 \text{ °C}/294 \text{ K}$

$q_A^o$  = standard air flow reading from meter (mL/min)

$q_G^o$  = standard gas flow (mL/min)

$\rho_{Air}^o$  = density of air at standard conditions (g/mL)

$\rho_G^o$  = density of gas at standard conditions

$q_G'$  = gas flow at p and T with volume corrected to measurement at standard conditions (mL/min)

p = absolute pressure of gas inlet (atm)

T = absolute temperature

#### Calculated gas flow from air flow and Gilmont flowmeter reading:

Gas	Density of gas (g/mL) at standard conditions (1 atm, 21 °C/294 K) from NIST WebBook <sup>199</sup>	Gilmont Scale Reading (SS Float)	Calibrated Air Flow $q_A^o$ at standard conditions (mL/min)	Corrected Gas Flow $q_G^o$ from Air Flow $q_A^o$ at standard conditions (mL/min)
Air	$\rho_{Air}^o = 0.00120$	39-43	49.69–58.40	N/A
Xe	$\rho_G^o = 0.00546$	60–66	105.2–124.7	49.31–58.46
CH <sub>4</sub>	$\rho_G^o = 0.00066$	32–36	36.50–43.76	49.21–59.00

**Viscosity measurements:** Viscosity measurements were carried out using a calibrated RheoSense  $\mu$ VISC viscometer (0.01–100 or 10–2000 cP) with a temperature controller (18–50 °C). Measurements were repeated a minimum of three times with the average viscosity reported along with a standard deviation.

**Differential Scanning Calorimetry (DSC):** Performed on a TA Instruments Q200 DSC, under nitrogen flow, and with heating and cooling rates of 5 °C/min.

**Single crystal X-ray Crystallography:** SC-XRD data sets were measured on a Rigaku MicroMax-007 HF rotating anode diffractometer (Mo-K $\alpha$  radiation,  $\lambda = 0.71073$  Å, Kappa 4-circle goniometer, Rigaku Saturn724+ detector). Structures were solved with SHELXT<sup>200</sup> and refined by full-matrix least squares on  $|F|^2$  by SHELXL,<sup>200</sup> interfaced through the programme OLEX2.<sup>201</sup> Absolute configuration was based on experimental synthetic procedures. Due to solvent disorder in the crystal structure, 2(CC21)·9(CHCl<sub>3</sub>)·10.5(CH<sub>4</sub>O)·(H<sub>2</sub>O), the CHCl<sub>3</sub> and MeOH solvent molecules were refined with bond distance restraints (DFIX and DANG in SHELX) and rigid bond restraints (RIGU in SHELX).

**Gas sorption analysis for solids:** Surface areas were measured by nitrogen sorption at 77.3 K. Powder samples were degassed on the analysis port under vacuum. Isotherm measurements were performed using a Micromeritics 3flex surface characterization analyzer, equipped with a Cold-Edge technologies liquid helium cryostat chiller unit for temperature control.

**Gas sorption analysis for liquids:** Samples contained in a 9 mm sample cell with a large bulb (P/N: 74064), fitted with a filler glass rod (P/N: 74105-L) and a glass coated stirrer bar. Liquids were degassed at 298 K for 18 hours with stirring and no filler rod, including a He backfill. CO<sub>2</sub> and CH<sub>4</sub> sorption measurements were performed using a modified Quantachrome Nova, fitted with a magnetic stirring hotplate. Benchmarked using commercially available liquids, including BMIM.NTf<sub>2</sub>, Genesorb 1753 and 15-crown-5.

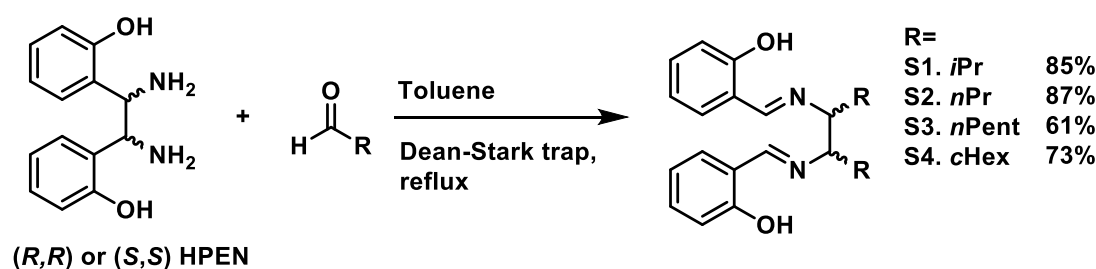


## 7.2 Chapter 2 experimental data

### 7.2.1 Synthesis and characterisation of diamine precursors

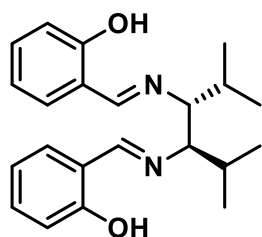
1,2-Diamino-2-methylpropane (Amine **A**), ethylenediamine (Amine **B**), (*R*)-propane-1,2-diamine (Amine **C**), 1,2-diaminocyclohexane (Amine **D**), (1*S*,2*S*)-(+)-1,2-diaminocyclohexane (Amine **E**), (1*S*,2*S*)-(-)-1,2-diphenylethylenediamine (Amine **F**), and 1,2-diaminopropane (Amine **K**), were purchased from TCI UK, Sigma Aldrich, or Fluorochem UK. Amines **G-J** were synthesised according to the steps below.

#### Step 1:



**General procedure:** A modification of the procedure by Kim *et al.* was used for these reactions.<sup>149</sup> Aldehyde (2.5 eq.) was added to a solution of either (*R,R*) or (*S,S*)-1,2-bis-(2-hydroxyphenyl)-1,2-diaminoethane (HPEN) (1.0 eq) in toluene, and the resulting solution refluxed at 120 °C for 72 hours fitted with a pre-filled Dean-Stark trap. The resulting mixture was cooled to room temperature and the solvent was removed under reduced pressure. The reaction product was then purified by either: **(1)** the addition of methanol and the resulting precipitate collected by filtration; **(2)** the crude product was dissolved in the minimum amount of DCM possible, followed by the addition of hexane to precipitate the product which was collected by filtration.

#### 2,2'-((1*E*,1'*E*)-((3*R*,4*R*)-2,5-Dimethylhexane-3,4-diyl)bis(azaneylylidene))bis(methaneylylidene))-diphenol (**P1**)

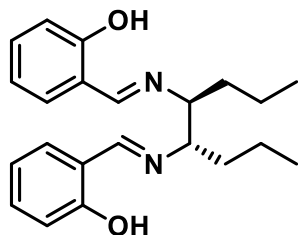


Prepared according to the general procedure using (*S,S*)-HPEN (10.00 g, 40.9 mmol) and isobutyraldehyde (7.38 g, 102.3 mmol) in toluene (135 mL). Purified using method **(1)** to give **S1** (12.20 g, 34.6 mmol, 85%) as a yellow powder.

<sup>1</sup>H NMR (400 MHz, CDCl<sub>3</sub>): δ 13.54 (2H, br s, OH), 8.16 (2H, s, imine CH), 7.27–7.21 (2H, m, ArH), 7.13 (2H, dd, *J* = 7.7, 1.6 Hz, ArH), 6.93 (2H, d, *J* = 8.0 Hz, ArH), 6.78 (2H, t, *J* = 8.0 Hz, ArH), 3.22 (2H, s, NCH), 2.17–2.03 (2H, m, CH), 0.97

(6H, d,  $J = 6.8$  Hz, CH<sub>3</sub>), 0.89 (6H, d,  $J = 6.8$  Hz, CH<sub>3</sub>); <sup>13</sup>C NMR (101 MHz, CDCl<sub>3</sub>): δ 165.43 (Imine CH), 161.13 (ArCH), 132.02 (ArCH), 131.23 (ArCH), 118.25 (ArCH), 118.22 (ArCH), 116.78 (ArCH), 75.98 (NCH), 28.23 (CH), 20.32 (CH<sub>3</sub>), 17.16 (CH<sub>3</sub>); HRMS (CI+) calculated for C<sub>22</sub>H<sub>28</sub>N<sub>2</sub>O<sub>2</sub> 352.2151; found [M+H]<sup>+</sup> 353.2235. Data in accordance with literature values.<sup>149,152</sup>

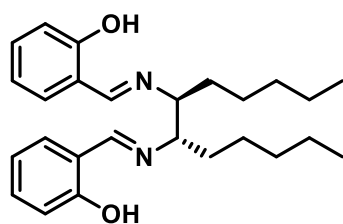
**2,2'-((1*E*,1'*E*)-((4*S*,5*S*)-Octane-4,5-diyl)bis(azaneylylidene))bis(methaneylylidene)diphenol (P2)**



Prepared according to the general procedure using (*R,R*)-HPEN (4.00 g, 16.4 mmol) and butyraldehyde (2.94 g, 40.9 mmol) in toluene (100 mL). Purified using method (2) to give **S2** (5.03 g, 14.3 mmol, 87%) as a yellow powder.

<sup>1</sup>H NMR (400 MHz, CDCl<sub>3</sub>): δ 13.39 (2H, br s, OH), 8.25 (2H, s, Imine H), 7.27 (2H, t,  $J = 8.0$  Hz, ArH), 7.20 (2H, dd,  $J = 7.5, 1.6$  Hz, ArH), 6.96 (2H, d,  $J = 8.0$  Hz, ArH), 6.83 (2H, t,  $J = 7.5$  Hz, ArH), 3.32–3.27 (2H, m, NCH), 1.67–1.63 (4H, m, CH<sub>2</sub>), 1.31–1.24 (4H, m, CH<sub>2</sub>), 0.95 (9H, t,  $J = 7.3$  Hz, CH<sub>3</sub>); <sup>13</sup>C NMR (101 MHz, CDCl<sub>3</sub>): δ 165.00 (Imine CH), 161.42 (ArCH), 132.35 (ArCH), 131.48 (ArCH), 118.60 (ArCH), 118.60 (ArCH), 117.20 (ArCH), 73.63 (NCH), 34.81 (CH<sub>2</sub>), 19.54 (CH<sub>2</sub>), 13.99 (CH<sub>3</sub>); HRMS (CI+) calculated for C<sub>22</sub>H<sub>28</sub>N<sub>2</sub>O<sub>2</sub> 352.2151; found [M+H]<sup>+</sup> 353.2242.

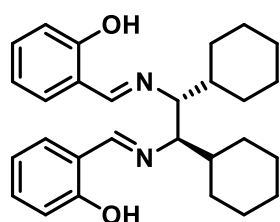
**2,2'-((1*E*,1'*E*)-((6*S*,7*S*)-Dodecane-6,7-diyl)bis(azaneylylidene))bis(methaneylylidene)diphenol (P3)**



Prepared according to the general procedure using (*R,R*)-HPEN (4.28 g, 17.5 mmol) and hexanal (4.38 g, 43.8 mmol) in toluene (100 mL). Purified using method (2) to give **S3** (4.40 g, 10.8 mmol, 61%) as a yellow powder.

<sup>1</sup>H NMR (400 MHz, CDCl<sub>3</sub>): δ 13.45 (2H, s, OH), 8.25 (2H, s, Imine H), 7.31–7.25 (2H, m, ArH), 7.21 (2H, dd,  $J = 7.7, 1.6$  Hz, ArH), 6.97 (2H, d,  $J = 7.9$  Hz, ArH), 6.84 (2H, td,  $J = 7.5, 1.6$  Hz, ArH), 3.29–3.26 (2H, m, NCH), 1.69–1.59 (4H, m, CH<sub>2</sub>), 1.27 (12H, br s, CH<sub>2</sub>), 0.85 (6H, t,  $J = 6.5$  Hz, CH<sub>3</sub>); <sup>13</sup>C NMR (101 MHz, CDCl<sub>3</sub>): δ 165.31 (Imine CH), 161.75 ArCH, 132.66 (ArCH), 131.81 (ArCH), 119.00 (ArCH), 118.91 (ArCH), 117.53 (ArCH), 74.17 (NCH), 32.89 (CH<sub>2</sub>), 32.09 (CH<sub>2</sub>), 26.38 (CH<sub>2</sub>), 22.99 (CH<sub>2</sub>), 14.48 (CH<sub>3</sub>); HRMS (CI+) calculated for C<sub>26</sub>H<sub>36</sub>N<sub>2</sub>O<sub>2</sub> 408.2777; found [M+H]<sup>+</sup> 409.2897. Data in accordance with literature values.<sup>123</sup>

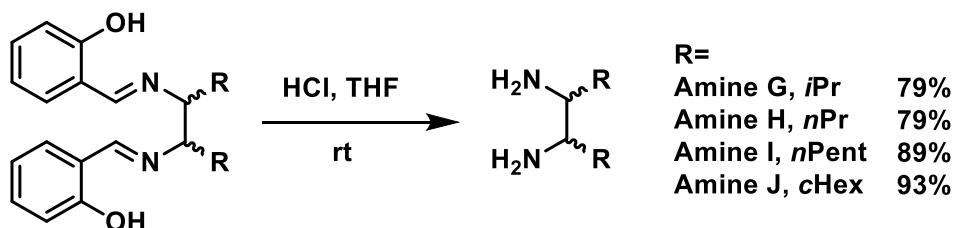
**2,2'-((1*E*,1'*E*)-(((1*R*,2*R*)-1,2-dicyclohexylethane-1,2-diyl)bis(azaneylylidene))bis(methaneylylidene)) diphenol (P4)**



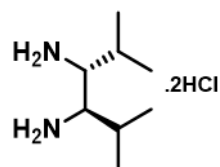
Prepared according to the general procedure using (*S,S*)-HPEN (4.35 g, 17.8 mmol) and cyclohexanecarboxaldehyde (4.98 g, 44.5 mmol) in toluene (100 mL). Purified using method (1) to give **S4** (5.61 g, 13.0 mmol, 73%) as a yellow powder.

<sup>1</sup>H NMR (400 MHz, CDCl<sub>3</sub>): δ 13.62 (2H, s, OH), 8.11 (2H, s, Imine H), 7.27–7.22 (2H, m, ArH), 7.12 (2H, dd, *J* = 7.7, 1.6 Hz, ArH), 6.93 (2H, d, *J* = 8.0 Hz, ArH), 6.84 (2H, td, *J* = 7.5, 1.6 Hz, ArH), 3.26 (2H, s, NCH), 1.76 - 1.55 (12H, m, CH and CH<sub>2</sub>), 1.21–0.96 (10H, m, CH<sub>2</sub>); <sup>13</sup>C NMR (101 MHz, CDCl<sub>3</sub>): δ 165.11 (Imine CH), 161.20 (ArCH), 131.96 (ArCH), 131.18 (ArCH), 118.19 (ArCH), 118.21 (ArCH), 116.80 (ArCH), 74.85 (NCH), 38.01 (CH), 30.70 (CH<sub>2</sub>) 27.84 (CH<sub>2</sub>), 26.12 (CH<sub>2</sub>), 26.06 (CH<sub>2</sub>), 25.97 (CH<sub>2</sub>); HRMS (CI<sup>+</sup>) calculated for C<sub>28</sub>H<sub>36</sub>N<sub>2</sub>O<sub>2</sub> 432.2777; found [M+H]<sup>+</sup> 433.2861. Data in accordance with literature values.<sup>149,152</sup>

**Step 2:**

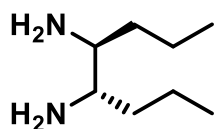


**General Procedure:** A modification of the procedure by James *et al.* and Kim *et al.* was used in these reactions.<sup>123,149</sup> A solution of hydrochloric acid (37%, aqueous) in THF was added to a solution of the diimine (formed in Section 2.1.) in THF, and the reaction mixture stirred at room temperature for 48 hours. The diamine was then isolated by either: (1) the resulting precipitated hydrochloride salt in the crude reaction mixture was collected by filtration; (2) diethyl ether (100 mL) was added to the reaction mixture and the organic layer extracted with H<sub>2</sub>O (3 x 50 mL), then the aqueous phase was basified with aqueous NaOH (1M), extracted with chloroform (3 x 50 mL), dried (Na<sub>2</sub>SO<sub>4</sub>), and the solvent removed under reduced pressure to afford the diamine.

**(3*R*,4*R*)-2,5-Dimethylhexane-3,4-diamine dihydrochloride (Amine G)**

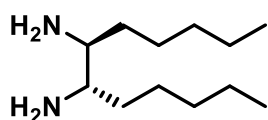
Prepared according to the general procedure using **S1** (3.93 g, 10.3 mmol) in THF (50 mL), and a solution of HCl (3 mL, 37%) in THF (50 mL). **Amine G** was purified using method (1) and collected as a colourless powder (1.77 g, 8.2 mmol, 79%).

$^1\text{H NMR}$  (400 MHz,  $\text{D}_2\text{O}$ ):  $\delta$  3.48 (2H, d,  $J = 8.0$  Hz, CH), 2.19 (2H, m, CH), 1.10 (12H, t,  $J = 6.6$  Hz,  $\text{CH}_3$ );  $^{13}\text{C NMR}$  (101 MHz,  $\text{D}_2\text{O}$ ):  $\delta$  56.67 (NCH) 27.26 (CH) 18.55 ( $\text{CH}_3$ ) 17.13 ( $\text{CH}_3$ ); **HRMS** (CI+) calculated for  $\text{C}_8\text{H}_{20}\text{N}_2$  144.1626; found  $[\text{M}+\text{H}]^+$  145.1660. Data in accordance with literature values.<sup>149,152</sup>

**(4*S*,5*S*)-Octane-4,5-diamine (Amine H)**

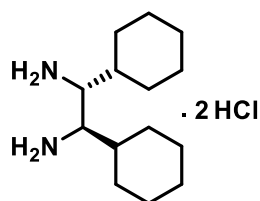
Prepared according to the general procedure using **S2** (5.03 g, 14.3 mmol) in THF (50 mL), and a solution of HCl (4 mL, 37%) in THF (50 mL). **Amine H** was purified using method (2) and collected as an orange oil (1.62 g, 11.2 mmol, 78%).

**IR** ( $\nu_{\text{max}}/\text{cm}^{-1}$ ): 2943, 2892, 2692, 1569, 1538, 1476, 1435, 1235, 1170, 1123, 1085, 1001;  $^1\text{H NMR}$  (400 MHz,  $\text{CDCl}_3$ ):  $\delta$  2.62 (2H, s, CH), 1.23 (8H, s,  $\text{CH}_2$ ), 0.84 (6H, s,  $\text{CH}_3$ );  $^{13}\text{C NMR}$  (101 MHz,  $\text{CDCl}_3$ ):  $\delta$  55.04 (CH), 37.24 ( $\text{CH}_2$ ), 20.89 ( $\text{CH}_2$ ), 14.32 ( $\text{CH}_3$ ); **HRMS** (ES+) calculated for  $\text{C}_8\text{H}_{20}\text{N}_2$  144.1626; found  $[\text{M}+\text{H}]^+$  145.1699.

**(6*S*,7*S*)-Dodecane-6,7-diamine (Amine I)**

Prepared according to the general procedure using **S3** (4.23 g, 10.0 mmol) in THF (50 mL), and a solution of HCl (3.1 mL, 37%) in THF (50 mL). **Amine I** was purified using method (2) and collected as an orange oil (1.79 g, 8.9 mmol, 89%).

$^1\text{H NMR}$  (400 MHz,  $\text{CDCl}_3$ ):  $\delta$  2.54 (2H, br s, CH), 1.29 (16H, m,  $\text{CH}_2$ ), 0.88 (6H, m,  $\text{CH}_3$ );  $^{13}\text{C NMR}$  (101 MHz,  $\text{CDCl}_3$ ):  $\delta$  55.04 (CH), 34.72 ( $\text{CH}_2$ ), 31.85 ( $\text{CH}_2$ ), 26.07 ( $\text{CH}_2$ ), 22.89 ( $\text{CH}_2$ ), 13.87 ( $\text{CH}_3$ ); **HRMS** (ES+) calculated for  $\text{C}_{12}\text{H}_{28}\text{N}_2$  200.2252; found  $[\text{M}+\text{H}]^+$  201.2327. Data in accordance with literature values.<sup>123</sup>

**(1*R*,2*R*)-1,2-Dicyclohexylethane-1,2-diamine dihydrochloride (Amine J)**

Prepared according to the general procedure using **S4** (5.60 g, 12.9 mmol) in THF (60 mL), and a solution of HCl (3.0 mL, 37%) in THF (60 mL). **Amine J** was purified using method (1) and collected as a colourless powder (3.57 g, 12.0 mmol, 93%).

$^1\text{H NMR}$  (400 MHz,  $\text{D}_2\text{O}$ ):  $\delta$  3.46 (2H, d,  $J = 8.0$  Hz, NCH), 1.78–1.61 (12H, m, cyclohexane H), 1.23–1.06 (10H, m, cyclohexane H);  $^{13}\text{C NMR}$  (101 MHz,  $\text{D}_2\text{O}$ ):  $\delta$  57.59 (NCH), 38.59 (CH), 31.59 ( $\text{CH}_2$ ), 30.49 ( $\text{CH}_2$ ), 27.58 ( $\text{CH}_2$ ), 27.40 ( $\text{CH}_2$ ), 27.37 ( $\text{CH}_2$ ); **HRMS** (ES+) calculated for  $\text{C}_{14}\text{H}_{28}\text{N}_2$  224.2252; found  $[\text{M}+\text{H}]^+$  225.2330. Data in accordance with literature values.<sup>149,152</sup>

**7.2.2 High-throughput synthesis screen**

Usually, high dilution is used during the synthesis of organic cages formed by imine condensations because there is a risk of polymer or oligomer formation. However, there is a limit to the maximum volume of solvent that can be used in a single reactor on the synthesis platform, and with a large amount of material required for the solubility screen, it was desirable to obtain the highest quantity of scrambled cage possible in each. Therefore, we first investigated if the previously reported reaction concentration used for scrambled cage synthesis could be increased.<sup>13</sup>

In order to determine the maximum concentration that could be used, a trial scrambled  $3^3:13^3$  cage synthesis was carried out to determine the yield at up to three times the original concentration (**Figure 7.2**).

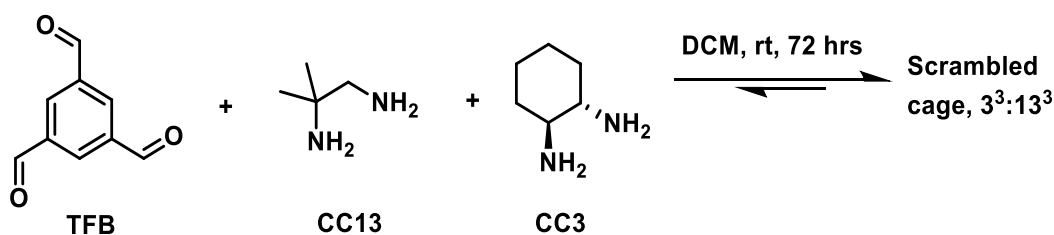


**Figure 7.2:** General reaction scheme for the synthesis of scrambled cage  $3^3:13^3$

Overall, the yield was not greatly affected by polymer formation at the higher concentration (**Appendix Table 1**), and the  $^1\text{H NMR}$  spectra confirmed the formation of cage in reasonable purity. Therefore, the high-throughput screen was carried out at three times the original concentration where there was enough available starting material.

**General high-throughput synthetic screening procedure:** All precursors (TFB and Amines A-K, Figure 7.3) were dissolved in chloroform to make stock solutions (20-30 mg/mL) for use in the high-throughput screen (Appendix Table 2). Where the diamine was used as a hydrochloride salt, triethylamine (3.3 eq.) was added to the stock solution. Over 4 runs on a Chemspeed Accelerator SLT-100 platform, the required volume of the TFB stock solution, followed by the required volume of each amine stock solution, was added to jacketed reactors (16 reactors with 75 mL total volume per run, 60 combinations and 2 control reactions) *via* liquid dispensing, followed by additional chloroform to make each total volume up to 60 mL (Appendix Table 3). The resulting solutions were vortexed at 800 rpm at room temperature for 72 hours, before the reaction mixtures were removed from the reactors and dispensed into vials (3 x 20 ml for each reactor) for subsequent isolation and purification.

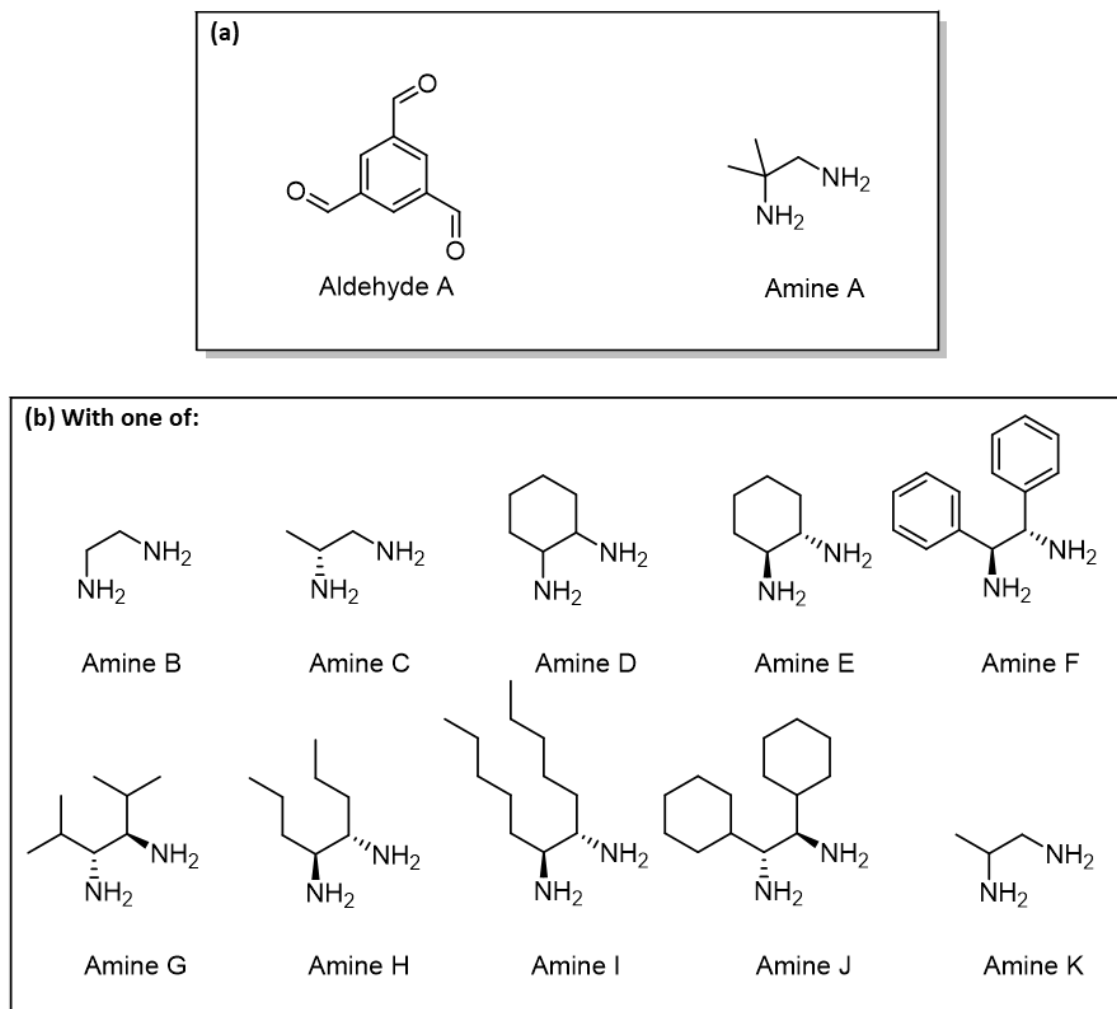


**Figure 7.2:** The range of precursors used in the high-throughput synthetic screen targeting scrambled cage combinations: (a) Structures of the precursors used to form CC13 which was scrambled with different diamine partners; (b) Structures of the scrambling diamine partners used in this study.

**General isolation and purification procedure:** The solvent from each reaction was removed under reduced pressure using a Combidancer high-throughput evaporator. To each of the isolated solids was added DCM (10 mL), and the mixtures filtered in parallel through empty, fritted SPE cartridges to remove any insoluble precipitate. The solvent was again removed using the Combidancer and the procedure repeated with THF for those reactions containing triethylamine to remove the formed triethylamine hydrochloride salt. The purified cages were then dried overnight in a vacuum oven at 90 °C prior to characterisation (see **Appendix Table 4**)

### 7.2.3 Selection of suitable solvents

The initial investigations for selecting potential porous liquid solvents were carried out manually, and once selected, the methodology was translated onto an automation platform for the high-throughput solubility screen.

**General procedure:** Scrambled  $3^3:13^3$  ( $A^3:E^3$ ) cage (30 mg) was manually weighed into a 2 mL vial and solvent was added in 0.1 mL increments using a disposable syringe. Between each addition, the sample was sonicated for 30 minutes and visually inspected to see if the solid had dissolved. If not, the procedure was repeated until dissolved or the lower threshold limit of 50 mg/mL had been reached. For a summary of the results see **Appendix Table 5-6**.

### 7.2.4 Xenon uptake measurements using chemical displacement

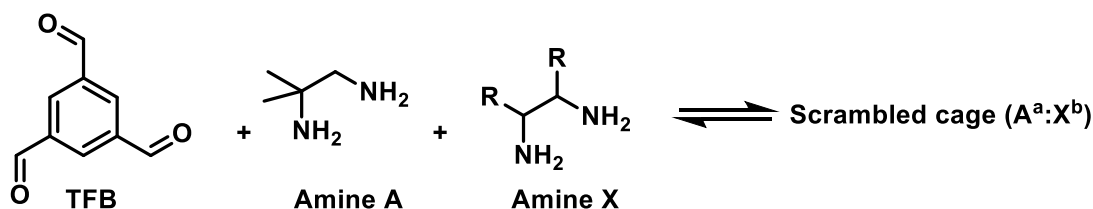
**General procedure:** Samples of porous liquid were prepared by dissolving scrambled  $3^3:13^3$  cage (200 mg), desolvated in a vacuum oven at 90 °C overnight, in purified perchloropropene (1 mL) by vortexing – see *Chem. Sci.*, **2017**, *8*, 2640 for further details. Xenon was then added to the porous liquid by bubbling the gas through the sample at ~50-60 mL/min (60-66 on Gilmont flowmeter scale with a stainless-steel float) for 10 min. The potential size-excluded solvent (1.0 eq. relative to cage) was then added and the displacement of water measured in an inverted burette over 10 minutes. Chloroform (16  $\mu$ L, 1.0 eq. relative to cage) was then added to evolve the remaining xenon and the displacement of water was again measured over 10 minutes (see **Appendix Table 7**).

### 7.2.5 High-throughput solubility testing

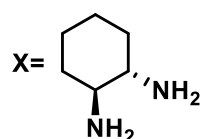
**General procedure:** Stock solutions of the scrambled cage hits (300 mg) in chloroform (10 mL) were prepared and 1 mL of each stock solution was liquid dispensed into 250 pre-weighed vials using a Chemspeed Swing platform. The solvent was then removed under reduced pressure and the scrambled cage samples dried overnight in a vacuum oven at 90 °C, before

the dispensed mass of cage was recorded – these were re-adjusted if needed to ensure ~30 mg of sample was in each vial. Using the Chemspeed Swing platform, the six size-excluded solvents (0.1 mL) were then added to the samples in the vials using liquid dispensing, before the resulting mixture was sonicated for 30 minutes (if samples heated up during sonication, they were left to cool to room temperature). The mixture was visually inspected to determine if the solid had dissolved and the outcome recorded. If the solid had not fully dissolved, further increments of solvent (0.1 mL) were added *via* liquid dispensing, followed by sonication for 30 minutes, until the solid dissolved or the lower threshold of 100 mg/mL was reached. *NB.* The 3<sup>3</sup>:13<sup>3</sup> (A<sup>3</sup>:E<sup>3</sup>) cage used in the reported original scrambled porous liquid<sup>13</sup> was included as a control to ensure the solubility screen was successful, as it is known to be soluble at 200 mg/mL in perchloropropene (PCP). See **Appendix Table 8** for complete results.

### 7.2.6 Synthesis of scrambled cages



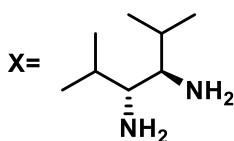
#### A<sup>3</sup>:E<sup>3</sup> (3<sup>3</sup>:13<sup>3</sup>)



In a 5 L jacketed vessel equipped with an overhead stirrer, TFB (30.0 g, 185 mmol, 4.0 eq.) was dissolved in DCM (2.5 L). A solution of 1,2-diamino-2-methyl-propane (Amine A, 12.23 g, 138.7 mmol, 3.0 eq.) and (*R,R*)-1,2-diaminocyclohexane (Amine E, 15.87 g, 138.7 mmol, 3.0 eq.) in DCM (1.5 L) was then added. The reaction mixture was stirred for 72 h at room temperature. The resulting solution was dried (MgSO<sub>4</sub>) and the solvent removed under reduced pressure. The crude product was re-dissolved in DCM (500 mL) and the solution filtered to remove any insoluble precipitate. The solvent was removed under reduced pressure and the resulting solid washed with ethyl acetate (500 mL) to afford A<sup>3</sup>:E<sup>3</sup> (35.61 g, 34.3 mmol, 74%) as an off-white powder.

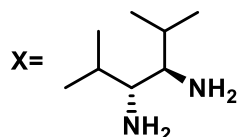
<sup>1</sup>H NMR (400 MHz, CDCl<sub>3</sub>): δ 8.18–7.80 (24H, m, N=CH and ArH), 3.92–3.35 (12H, m, CHN=CH and CH<sub>2</sub>N=CH), 1.82–1.31 (42H, m, CH<sub>2</sub> and CH<sub>3</sub>). Data in agreement with literature values.<sup>13</sup>



**A<sup>4</sup>:G<sup>2</sup>**

To a solution of TFB (0.33 g, 2.04 mmol, 4.0 eq.) dissolved in chloroform (30 mL), was added solutions of 1,2-diamino-2-methyl-propane (Amine **A**, 0.18 g, 2.04 mmol, 4.0 eq.) in chloroform (15 mL), and (3*R*,4*R*)-2,5-dimethylhexane-3,4-diamine dihydrochloride (Amine **G**, 0.22 g, 1.03 mmol, 2.0 eq.) in chloroform (15 mL), followed by triethylamine (0.2 mL, 1.7 mmol, 3.3 eq.). The reaction mixture was stirred for 72 h at room temperature before the solvent was removed under reduced pressure. The crude product was dissolved in THF (50 mL), filtered to remove triethylamine hydrochloride salts, and the solvent removed under reduced pressure. The crude product was redissolved in DCM (50 mL) and filtered to remove any insoluble polymer. The solvent was removed under reduced pressure to afford the product (0.11 g, 0.1 mmol, 20%) as a cream solid.

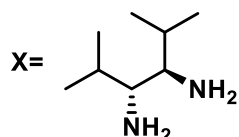
**IR** ( $\nu_{\max}$  /cm<sup>-1</sup>): 2974, 2860, 1709, 1657 (imine N=C), 1599, 1448, 1367, 1261; **<sup>1</sup>H NMR** (400 MHz, CDCl<sub>3</sub>):  $\delta$  8.17–7.83 (24H, m, ArH and N=CH), 3.94–3.42 (12H, m, CHN=CH and CH<sub>2</sub>N=CH), 2.22–2.20 (4H, m, CH), (15H, m, CH), 1.62–0.72 (48H, m, CH<sub>3</sub>); **<sup>13</sup>C NMR** (101 MHz, CDCl<sub>3</sub>): (due to scrambling, all singlets appear as broad multiplets)  $\delta$  161.71, 160.21, 155.93, 137.08, 129.87, 125.98, 72.88, 61.69, 46.25, 30.78, 28.93, 21.84, 16.20; **HRMS** (ES<sup>+</sup>) calc. for scrambled cages **A<sup>6</sup>G<sup>0</sup>**, **A<sup>5</sup>G<sup>1</sup>**, **A<sup>4</sup>G<sup>2</sup>**, **A<sup>3</sup>G<sup>3</sup>**, **A<sup>2</sup>G<sup>4</sup>**, **A<sup>1</sup>G<sup>5</sup>**, **A<sup>0</sup>G<sup>6</sup>** = 960.6003, 1016.6629, 1072.7255, 1128.7881, 1184.8507, 1240.9133, 1296.9759; found [M+H]<sup>+</sup> at: 961.5915, 1017.6505, 1073.7108, 1129.7697, 1185.8276, 1241.8854, 1298.9463.

**A<sup>3</sup>:G<sup>3</sup>**

To a solution of TFB (0.60 g, 3.7 mmol, 4.0 eq.) dissolved in chloroform (60 mL), was added solutions of 1,2-diamino-2-methyl-propane (Amine, **A**, 0.24 g, 2.8 mmol, 3.0 eq.) in chloroform (30 mL), and (3*R*,4*R*)-2,5-dimethylhexane-3,4-diamine dihydrochloride (Amine **G**, 0.60 g, 2.8 mmol, 3.0 eq.) in chloroform (30 mL), followed by triethylamine (0.39 mL, 2.8 mmol, 3.3 eq.). The reaction mixture was stirred for 72 h at room temperature before the solvent was removed under reduced pressure. The crude product was dissolved in THF (60 mL), filtered to remove triethylamine hydrochloride salts, and the solvent removed under reduced pressure. The resulting oil was triturated in methanol (50 mL) and the purified scrambled cage collected as a colourless solid by filtration (0.76 g, 6.8 mmol, 73%).

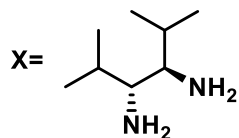
**IR** ( $\nu_{\max}$  /cm<sup>-1</sup>): 2949, 2841, 1709, 1655 (imine N=C), 1599, 1456, 1259; **<sup>1</sup>H NMR** (400 MHz, CDCl<sub>3</sub>):  $\delta$  8.32–7.72, (24H, m, N=CH and ArH), 3.95–3.24 (12H, m, CHN=CH and

$\text{CH}_2\text{N}=\text{CH}$ ), 2.20-1.62 (6H, m, CH), 1.09-0.77 (54H, m,  $\text{CH}_3$ );  $^{13}\text{C}$  NMR (101 MHz,  $\text{CDCl}_3$ ): (due to scrambling, all singlets appear as broad multiplets)  $\delta$  160.19, 159.70, 137.55, 136.60, 129.62, 50.87, 28.49, 28.27, 21.61, 21.44, 15.87; HRMS (ES+) calc. for scrambled cages  $\text{A}^6\text{G}^0$ ,  $\text{A}^5\text{G}^1$ ,  $\text{A}^4\text{G}^2$ ,  $\text{A}^3\text{G}^3$ ,  $\text{A}^2\text{G}^4$ ,  $\text{A}^1\text{G}^5$ ,  $\text{A}^0\text{G}^6$  = 960.6003, 1016.6629, 1072.7255, 1128.7881, 1184.8507, 1240.9133, 1296.9759; found  $[\text{M}+\text{H}]^+$  at: 1073.7226, 1129.7846, 1185.8456, 1241.9053, 1297.9669.

**A<sup>2</sup>:G<sup>4</sup>**

To a solution of TFB (0.50 g, 3.1 mmol, 4.0 eq.) dissolved in chloroform (30 mL), was added solutions of 1,2-diamino-2-methyl-propane (Amine A, 0.14 g, 1.55 mmol, 2.0 eq.) in chloroform (15 mL), and (3*R*,4*R*)-2,5-dimethylhexane-3,4-diamine dihydrochloride (Amine G, 0.75 g, 3.1 mmol, 4.0 eq.) in chloroform (15 mL), followed by triethylamine (0.30 mL, 2.6 mmol, 3.3 eq.). The reaction mixture was stirred for 72 h at room temperature before the solvent was removed under reduced pressure. The crude product was dissolved in THF (50 mL), filtered to remove triethylamine hydrochloride salts, and the solvent removed under reduced pressure. The resulting oil was triturated in methanol (50 mL) and the purified scrambled cage was collected as a colourless solid (0.44 g, 3.7 mmol, 48%).

IR ( $\nu_{\text{max}}$  / $\text{cm}^{-1}$ ): 2970, 2860, 1709, 1641 (imine  $\text{N}=\text{C}$ ), 1595, 1452, 1381, 1267;  $^1\text{H}$  NMR (400 MHz,  $\text{CDCl}_3$ ):  $\delta$  8.20–7.63 (24H, m,  $\text{N}=\text{CH}$  and ArH), 3.75–2.87 (12H, m,  $\text{CHN}=\text{CH}$  and  $\text{CH}_2\text{N}=\text{CH}$ ), 2.20 (8H, br s, CH), 1.10-0.79 (60H, m,  $\text{CH}_3$ );  $^{13}\text{C}$  NMR (101 MHz,  $\text{CDCl}_3$ ): (due to scrambling, all singlets appear as broad multiplets) 161.61, 159.84, 136.73, 129.76, 76.42, 67.59, 61.29, 32.20, 28.62, 28.41, 28.15, 21.96, 21.76, 21.57, 20.92, 18.82, 16.23, 15.99; HRMS (ES+) calc. for scrambled cages  $\text{A}^6\text{G}^0$ ,  $\text{A}^5\text{G}^1$ ,  $\text{A}^4\text{G}^2$ ,  $\text{A}^3\text{G}^3$ ,  $\text{A}^2\text{G}^4$ ,  $\text{A}^1\text{G}^5$ ,  $\text{A}^0\text{G}^6$  = 960.6003, 1016.6629, 1072.7255, 1128.7881, 1184.8507, 1240.9133, 1296.9759; found  $[\text{M}+\text{H}]^+$  at: 1073.7506, 1129.8139, 1185.8771, 1241.9393, 1298.0007.

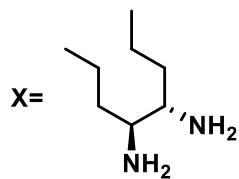
**A<sup>1</sup>:G<sup>5</sup>**

To a solution of TFB (0.50 g, 3.1 mmol, 4.0 eq.) dissolved in DCM (50 mL), was added solutions of 1,2-diamino-2-methyl-propane (Amine A, 0.07 g, 0.8 mmol, 1.0 eq.) in DCM (25 mL), and (3*R*,4*R*)-2,5-dimethylhexane-3,4-diamine dihydrochloride (Amine G, 0.84 g, 3.9 mmol, 5.0 eq.) in DCM (25 mL), followed by triethylamine (0.4 mL, 5.1 mmol, 3.3 eq.). The reaction mixture was stirred for 72 h at room temperature before the solvent was removed under reduced pressure.

The crude product was dissolved in THF (50 mL), filtered to remove the triethylamine hydrochloride salts, and the solvent removed under reduced pressure. The crude material was then re-dissolved in DCM, filtered to remove any polymer, and the solvent removed under reduced pressure. Methanol (50 mL) was added to precipitate the scrambled cage which was collected by filtration as a colourless powder (0.40 g, 0.3 mmol, 42%).

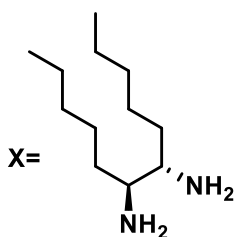
**IR** ( $\nu_{\max}/\text{cm}^{-1}$ ): 2968, 2860, 1701, 1659 (imine N=C), 1595, 1466, 1364, 1259;  **$^1\text{H NMR}$**  (400 MHz,  $\text{CDCl}_3$ ):  $\delta$  8.24–7.68 (24H, m, N=CH and ArH), 3.96–3.18 (12H, m, CHN=CH and  $\text{CH}_2\text{N}=\text{CH}$ ), 2.21 and 1.35 (10H, m, CH), 1.11–0.77 (60H, m,  $\text{CH}_3$ );  **$^{13}\text{C NMR}$**  (101 MHz,  $\text{CDCl}_3$ ): (due to scrambling chemical shifts appear as multiplets) 159.70, 136.59, 129.87, 61.16, 28.49, 28.28, 21.61, 21.43, 16.12, 15.85; **HRMS** (ES+) calc. for scrambled cages  $\text{A}^6\text{G}^0$ ,  $\text{A}^5\text{G}^1$ ,  $\text{A}^4\text{G}^2$ ,  $\text{A}^3\text{G}^3$ ,  $\text{A}^2\text{G}^4$ ,  $\text{A}^1\text{G}^5$ ,  $\text{A}^0\text{G}^6$  = 960.6003, 1016.6629, 1072.7255, 1128.7881, 1184.8507, 1240.9133, 1296.9759; found  $[\text{M}+\text{H}]^+$  at: 1129.8253, 1185.8900, 1241.9539, 1298.0147.

### $\text{A}^5\text{H}^1$



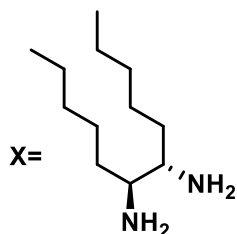
To a solution of TFB (0.64 g, 4.0 mmol, 4.0 eq.) dissolved in chloroform (30 mL), was added solutions of 1,2-diamino-2-methyl-propane (Amine **A**, 0.44 g, 5.0 mmol, 5.0 eq.) in chloroform (15 mL), and (4*S*,5*S*)-octane-4,5-diamine (Amine **H**, 0.19 g, 1.3 mmol, 1.0 eq.) in chloroform (15 mL). The reaction mixture was stirred at 60 °C for 72 h before being allowed to cool to room temperature, and the solvent was removed under reduced pressure. The crude product was re-dissolved in DCM (40 mL), filtered to remove insoluble polymer, and the solvent removed under reduced pressure. Acetone (50 mL) was added to precipitate the scrambled cage product which was collected by filtration as a colourless powder (0.16 g, 0.2 mmol, 16%).

**IR** ( $\nu_{\max}/\text{cm}^{-1}$ ): 2960, 2856, 1705, 1651 (imine N=C), 1456, 1250;  **$^1\text{H NMR}$**  (400 MHz,  $\text{CDCl}_3$ ):  $\delta$  8.15–7.83 (24H, m, N=CH and ArH), 3.95–3.35 (12H, m, CHN=CH and  $\text{CH}_2\text{N}=\text{CH}$ ), 1.74–1.25 (44H, m,  $\text{CH}_2$  and  $\text{CH}_3$ );  **$^{13}\text{C NMR}$**  (101 MHz,  $\text{CDCl}_3$ ): (due to scrambling, all singlets appear as broad multiplets)  $\delta$  161.38, 155.67, 137.04, 129.68, 75.91, 72.82, 61.64, 53.83, 32.33, 26.29, 23.02, 14.52; **HRMS** (ES+): calc. for scrambled cages  $\text{A}^6\text{H}^0$ ,  $\text{A}^5\text{H}^1$ ,  $\text{A}^4\text{H}^2$ ,  $\text{A}^3\text{H}^3$ ,  $\text{A}^2\text{H}^4$ ,  $\text{A}^1\text{H}^5$ ,  $\text{A}^0\text{H}^6$  = 960.6003, 1016.6629, 1072.7255, 1128.7881, 1184.8507, 1240.9133, 1296.9759; found  $[\text{M}+\text{H}]^+$  at: 961.6157, 1015.6232, 1073.7418, 1127.7487, 1185.8712, 1297.9926.

**A<sup>4</sup>:I<sup>2</sup>**

To a solution of TFB (0.46 g, 2.9 mmol, 4.0 eq.) dissolved in chloroform (30 mL), was added solutions of 1,2-diamino-2-methyl-propane (Amine **A**, 0.25 g, 2.9 mmol, 4.0 eq.) in chloroform (15 mL), and (6*S*,7*S*)-dodecane-6,7-diamine (Amine **I**, 0.27 g, 1.4 mmol, 2.0 eq.) in chloroform (15mL). The reaction mixture was stirred at 60 °C for 72 h before being allowed to cool to room temperature, and the solvent was removed under reduced pressure. The crude product was re-dissolved in DCM (40 mL), filtered to remove insoluble polymer, and the solvent removed under reduced pressure. Acetone (50 mL) was added to precipitate the scrambled cage product which was collected by filtration as a colourless powder (0.11 g, 0.093 mmol, 18%).

**IR** ( $\nu_{\max}/\text{cm}^{-1}$ ): 2968, 2849, 1705, 1643 (imine N=C), 1448, 1379, 1263; **<sup>1</sup>H NMR** (400 MHz, CDCl<sub>3</sub>):  $\delta$  8.15–7.83 (24H, m, N=CH and ArH), 3.93–3.34 (12H, m, CHN=CH and CH<sub>2</sub>N=CH), 1.75–0.84 (68H, m, CH<sub>2</sub> and CH<sub>3</sub>); **<sup>13</sup>C NMR** (101 MHz, CDCl<sub>3</sub>): (due to scrambling, all singlets appear as broad multiplets)  $\delta$  161.70, 137.55, 129.86, 61.70, 31.39, 29.84, 23.04, 14.55; **HRMS** (ES<sup>+</sup>): calc. for scrambled cages **A<sup>6</sup>I<sup>0</sup>**, **A<sup>5</sup>I<sup>1</sup>**, **A<sup>4</sup>I<sup>2</sup>**, **A<sup>3</sup>I<sup>3</sup>**, **A<sup>2</sup>I<sup>4</sup>**, **A<sup>1</sup>I<sup>5</sup>**, **A<sup>0</sup>I<sup>6</sup>** = 960.6003, 1072.7255, 1184.8507, 1296.9759, 1409.1011, 1521.2263 and 1633.3515; found [M+H]<sup>+</sup> at: 961.6129, 1073.7396, 1185.8681, 1297.9899.

**A<sup>3</sup>:I<sup>3</sup>**

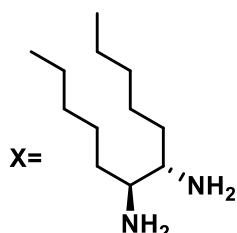
To a solution of TFB (0.46 g, 2.9 mmol, 4.0 eq.) dissolved in chloroform (30 mL), was added solutions of 1,2-diamino-2-methyl-propane (Amine **A**, 0.19 g, 2.2 mmol, 3.0 eq.) in chloroform (15 mL), and (6*S*,7*S*)-dodecane-6,7-diamine (Amine **I**, 0.43 g, 2.2 mmol, 3.0 eq.) in chloroform (15mL). The reaction mixture was stirred at 60 °C for 72 h before being allowed to cool to room temperature, and the solvent was removed under reduced pressure. The crude product was re-dissolved in DCM (40 mL), filtered to remove insoluble polymer, and the solvent removed under reduced pressure. Acetone (50 mL) was added to precipitate the scrambled cage product which was collected by filtration as a colourless powder (0.27 g, 0.2 mmol, 29%).

**IR** ( $\nu_{\max}/\text{cm}^{-1}$ ): 2968, 2854, 1647 (imine N=C), 1445, 1364, 1261; **<sup>1</sup>H NMR** (400 MHz, CDCl<sub>3</sub>):  $\delta$  8.17–7.83 (24H, m, N=CH and ArH), 3.94–3.34 (12H, m, CHN=CH and CH<sub>2</sub>N=CH), 1.76–0.84\* (77H, m, CH<sub>2</sub> and CH<sub>3</sub>); **<sup>13</sup>C NMR** (101 MHz, CDCl<sub>3</sub>): (due to scrambling, all singlets appear as broad multiplets)  $\delta$  161.14, 155.52, 137.20, 129.59, 61.38, 31.98, 22.31, 14.26; **HRMS** (ES<sup>+</sup>): calc. for scrambled cages **A<sup>6</sup>I<sup>0</sup>**, **A<sup>5</sup>I<sup>1</sup>**, **A<sup>4</sup>I<sup>2</sup>**, **A<sup>3</sup>I<sup>3</sup>**, **A<sup>2</sup>I<sup>4</sup>**, **A<sup>1</sup>I<sup>5</sup>**,

$A^0I^6 = 960.6003, 1072.7255, 1184.8507, 1296.9759, 1409.1011, 1521.2263$  and  $1633.3515$ ; found  $[M+H]^+$  at:  $1073.7399, 1073.7399, 1185.8644, 1297.9908, 1411.1186$ .

\*85H expected but 77H observed, possibly due to a slightly different scrambling distribution forming over the targeted

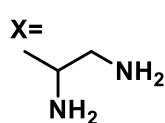
### $A^2:I^4$



To a solution of TFB (0.46 g, 2.9 mmol, 4.0 eq.) dissolved in chloroform (30 mL), was added solutions of 1,2-diamino-2-methyl-propane (Amine A, 0.13 g, 1.4 mmol, 2.0 eq.) in chloroform (15 mL), and (6*S*,7*S*)-dodecane-6,7-diamine (Amine I, 0.60 g, 2.9 mmol, 4.0 eq.) in chloroform (15 mL). The reaction mixture was stirred at 60 °C for 72 h before being allowed to cool to room temperature, and the solvent was removed under reduced pressure. The crude product was re-dissolved in DCM (40 mL), filtered to remove insoluble polymer, and the solvent removed under reduced pressure. Acetone (50 mL) was added to precipitate the scrambled cage which was collected by filtration as a colourless powder (0.16 g, 0.1 mmol, 45%).

**IR** ( $\nu_{\max}/\text{cm}^{-1}$ ): 2964, 2851, 1647 (imine N=C), 1456, 1263;  **$^1\text{H NMR}$**  (400 MHz,  $\text{CDCl}_3$ ):  $\delta$  8.07–7.79 (24H, m, N=CH and ArH), 3.94–3.34 (12H, m, CHN=CH and  $\text{CH}_2\text{N=CH}$ ), 1.76–0.84 (95H, m,  $\text{CH}_2$  and  $\text{CH}_3$ );  **$^{13}\text{C NMR}$**  (101 MHz,  $\text{CDCl}_3$ ): (due to scrambling, all singlets appear as broad multiplets)  $\delta$  161.14, 159.46, 137.19, 136.75, 129.65, 129.40, 75.59, 61.41, 31.96, 29.65, 26.17, 22.75, 22.72, 22.27, 14.25; **HRMS** (ES+) calc. for scrambled cages  $A^6I^0, A^5I^1, A^4I^2, A^3I^3, A^2I^4, A^1I^5, A^0I^6 = 960.6003, 1072.7255, 1184.8507, 1296.9759, 1409.1011, 1521.2263$  and  $1633.3515$ ; found  $[M+H]^+$  at: 1185.8460, 1297.9703, 1411.0961, 1523.2191.

### $A^3:K^3$



To a solution of TFB (15.00 g, 0.093 mol, 4.0 eq) dissolved in DCM (1.5 L), was added solutions of 1,2-diamino-2-methyl-propane (Amine A, 6.11 g, 0.069 mol, 3.0 eq) in DCM (250 mL), and racemic propane-1,2-diamine (Amine K, 5.11g, 0.069 mol, 3.0 eq) in DCM (250 mL). The reaction mixture was stirred at room temperature for 72 h before the solvent was removed under reduced pressure. The crude product was re-dissolved in DCM (250 mL), filtered to remove insoluble polymer, and the solvent removed under reduced pressure. The resulting solid was washed with ethyl acetate (250 mL) and collected to give the scrambled cage as a colourless solid (19.0 g, 20.7 mmol, 89%).

**IR** ( $\nu_{\max}/\text{cm}^{-1}$ ): 2970, 2851, 1707, 1649 (imine N=C), 1601, 1447, 1383, 1265, 1149;  **$^1\text{H NMR}$**  (400 MHz,  $\text{CDCl}_3$ ):  $\delta$  8.17–7.83 (24H, m, N=CH and ArH) 3.92–3.52 (15H, m, CHN=CH

and  $\text{CH}_2\text{N}=\text{CH}$ ) 1.60–1.19(27H, m,  $\text{CH}_3$ );  $^{13}\text{C}$  NMR (101 MHz,  $\text{CDCl}_3$ ): (due to scrambling, all singlets appear as broad multiplets)  $\delta$  162.79, 159.26, 154.97, 136.98, 136.28, 129.35, 72.13, 68.22, 66.64, 61.03, 60.19, 50.42, 29.22, 28.58, 21.86, 20.75, 14.00; HRMS (ES+) calc. for scrambled cages  $\text{A}^6\text{K}^0$ ,  $\text{A}^5\text{K}^1$ ,  $\text{A}^4\text{K}^2$ ,  $\text{A}^3\text{K}^3$ ,  $\text{A}^2\text{K}^4$ ,  $\text{A}^1\text{K}^5$ ,  $\text{A}^0\text{K}^6$  = 960.6003, 946.5846, 932.569, 918.5533, 904.5377, 890.522 and 876.5064; found  $[\text{M}+\text{H}]^+$  at: 947.5812, 933.5684, 919.5531, 905.5372, 891.5213, 877.5066.

### 7.2.7 Purification of solvents

**General procedure for xenon evolution measurements:** Samples of the porous liquid were prepared by dissolving scrambled  $3^3:13^3$  cage (200 mg), desolvated in a vacuum oven at 90 °C overnight, in either the ‘as bought’ or purified solvent (1.0 mL) by sonication and stirring. Xenon was then added to the porous liquid by bubbling the gas through the sample at ~50-60 mL/min (60-66 on Gilmont flowmeter scale with a stainless steel float) for 10 mins per 1 mL of solvent used. Chloroform (16  $\mu\text{L}$ , 1.0 eq. relative to cage) was then added to evolve the xenon and the displacement of water was measured in an inverted burette over 30 minutes (see **Appendix Table 9**) – a maximum of 4.6 mL of evolved xenon is expected based on 1:1 occupancy of the cages for a 200 mg sample.

**General procedure for solvent purification by distillation:** Each solvent was heated slowly in 10 °C increments in distillation apparatus under vacuum. Fractions were collected as they condensed with the first and last 10% discarded. The purified solvent was stored under  $\text{N}_2$  in an oven-dried Schlenk tube over activated 4 Å sieves. If further purification was needed, the solvent was filtered 5 times through 5 separate activated basic alumina plugs (5 × 150 g aluminium oxide, activated, basic, Brockmann I, CAS 1344-28-1, Sigma-Aldrich).

**2,4-Dichlorobenzyl chloride (DCBC, solvent 1)** was collected after distillation as a colourless liquid.  $^1\text{H}$  NMR (400 MHz,  $\text{CDCl}_3$ ):  $\delta$  7.32-7.29 (2H, m, , ArH), 7.16 (1H, d,  $J$  = 8.0 Hz, ArH), 4.58 (2H, s,  $\text{CH}_2$ );  $^{13}\text{C}$  NMR (101 MHz,  $\text{CDCl}_3$ ):  $\delta$  135.02 (ArC), 134.67 (ArC), 133.62 (ArC), 131.52 (ArC), 129.55 (ArC), 127.49 (ArC), 42.46 ( $\text{CH}_2$ ).

**4-(Trifluoromethoxy)benzyl alcohol (TBA, solvent 2)** was collected as a colourless liquid after distillation and passing over alumina.  $^1\text{H}$  NMR (400 MHz,  $\text{CDCl}_3$ ):  $\delta$  7.29 (2H, d,  $J$  = 8.0 Hz, ArH), 7.16 (2H, d,  $J$  = 8.0 Hz, ArH), 4.56 (2H, d,  $J$  = 3.0 Hz,  $\text{CH}_2$ ), 3.10 (1H, br s, OH);  $^{13}\text{C}$  NMR (101 MHz,  $\text{CDCl}_3$ ):  $\delta$  148.74, (ArC), 139.59 (ArC), 128.36 (ArC/ $\text{CF}_3$ ), 121.14 (ArC), 64.36 ( $\text{CH}_2$ ) -  $\text{CF}_3$  not observed- possibly due to overlap with ArC.

**Methyl salicylate (MS, solvent 3)** was collected after distillation as a colourless liquid.  $^1\text{H}$  NMR (400 MHz,  $\text{CDCl}_3$ ):  $\delta$  10.76 (1H, s, OH), 7.82 (1H, d,  $J$  = 8.0 Hz, ArH), 7.44 (1H, t,  $J$  = 16.0 Hz, ArH), 6.97 (1H, d,  $J$  = 8.0 Hz, ArH), 6.86 (1H, t,  $J$  = 16.0 Hz, ArH), 3.92 (3H, s,

$\text{CH}_3$ );  $^{13}\text{C}$  NMR (101 MHz,  $\text{CDCl}_3$ ):  $\delta$  170.43 (CO), 161.48 (ArCOH), 135.53 (ArC), 129.76 (ArC), 119.00 (ArC), 117.41 (ArC), 112.24 (ArC), 52.09 ( $\text{CH}_3$ ).

**2,4-Dichlorotoluene (DCT, solvent 4)** was collected after distillation as a colourless liquid.  $^1\text{H}$  NMR (400 MHz,  $\text{CDCl}_3$ ):  $\delta$  7.27 (1H, s, ArH), 7.05 (2H, s, ArH), 2.27 (3H, s,  $\text{CH}_3$ );  $^{13}\text{C}$  NMR (101 MHz,  $\text{CDCl}_3$ ):  $\delta$  135.00 (ArC), 134.54 (ArC), 132.01 (ArC), 131.60 (ArC), 128.83 (ArC), 126.80 (ArC), 19.48 ( $\text{CH}_3$ ).

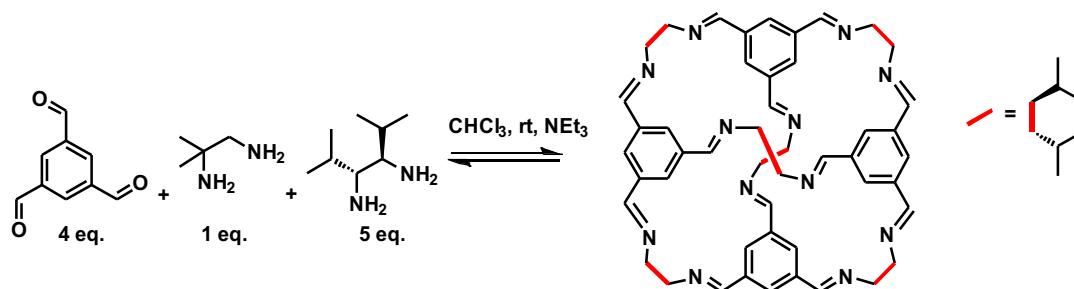
**2-Hydroxyacetophenone (HAP, solvent 5)** was collected after distillation as a colourless liquid.  $^1\text{H}$  NMR (400 MHz,  $\text{CDCl}_3$ ):  $\delta$  12.24 (1H, s, OH), 7.63–7.60 (1H, m, ArH), 7.40–7.36 (1H, m, ArH), 6.89–6.86 (1H, m, ArH), 6.77–6.67 (1H, m, ArH), 2.52–2.50 (3H, m,  $\text{CH}_3$ );  $^{13}\text{C}$  NMR (101 MHz,  $\text{CDCl}_3$ ):  $\delta$  204.75 (CO), 162.48 (ArC), 136.56 (ArC), 130.95 (ArC), 119.82 (ArC), 119.08 (ArC), 118.41 (ArC), 26.65 ( $\text{CH}_3$ ).

## 7.3 Chapter 3 experimental data

### 7.3.1 Synthesis of porous organic species

The (3*R*,4*R*)-2,5-Dimethylhexane-3,4-diamine dihydrochloride was synthesised using the same procedure as used previously (See Section 7.2.1).

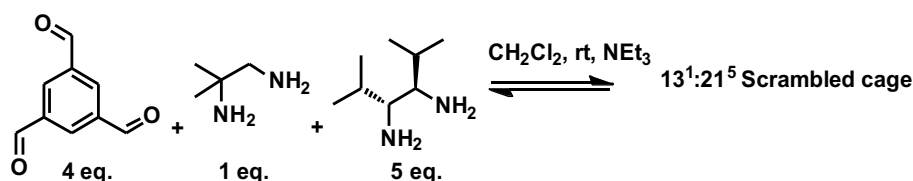
#### Synthesis of CC21 with catalytic 1,2-diamino-2-methyl-propane



TFB (0.33 g, 2.055 mmol, 4 eq.) was dissolved in chloroform (30 mL). 1,2-diamino-2-methylpropane (0.045 g, 0.514 mmol, 1 eq.) in chloroform (15 mL) and (3*R*,4*R*)-2,5-dimethylhexane-3,4-diamine (0.59 g, 2.570 mmol, 5 eq.) in chloroform (15 mL) with triethylamine (0.2 mL, 1.7 mmol, 3.3 eq.) were added. The reaction mixture was stirred for 72 hrs at rt. The solvent was removed under reduced pressure. The crude product was dissolved in THF, filtered and the solvent removed under reduced pressure. The resulting oil was triturated in methanol and the purified parent cage was collected as a white solid (52.4 mg, 0.04 mmol, 5%).

**IR** ( $\nu_{\text{max}}$  / $\text{cm}^{-1}$ ): 2959, 2865, 1647, 1595, 1457, 1377, 1243, 1148, 1057, 979, 878, 688; **<sup>1</sup>H NMR** (400 MHz,  $\text{CDCl}_3$ ):  $\delta$ 8.04 (s, 12H, ArH), 7.88 (s, 12H, ArH), 3.37 (s, 12H, CHN), 2.23-2.19 (m, 12H, CH), 1.05 (d, 36H, 6.7Hz,  $\text{CH}_3$ ) 0.78, (d, 36H, 6.7Hz,  $\text{CH}_3$ ); **<sup>13</sup>C NMR**: 159.85 (ArC), 136.76 (ArC), 129.77 (ArC), 28.65 (CH), 21.59 ( $\text{CH}_3$ ), 16.02 ( $\text{CH}_3$ ); **HRMS** (QTOF) calc at 1296.9790. Found at:  $[\text{M}+2\text{H}]^+$  1298.0221,  $[\text{M}+\text{H}]^{2+}$  649.5070 ; **Elemental Analysis**: C, 75.76; H 9.03; N 12.65 (C, 77.73; H 9.32; N 12.95 calculated for  $\text{C}_{84}\text{H}_{120}\text{N}_{12}$ ) (See Appendix Figure 1 and 2 for NMR spectra).

#### Synthesis of 13<sup>1</sup>:21<sup>5</sup> scrambled cage



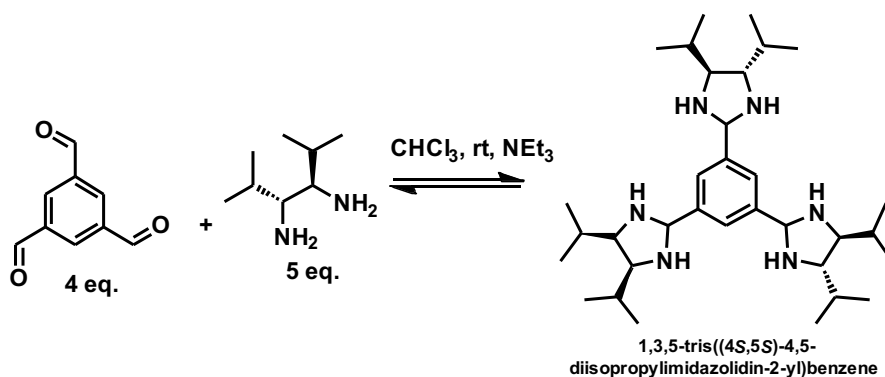
TFB (0.50 g, 3.10 mmol, 4 eq.) was dissolved in dichloromethane (50 mL). 1,2-diamino-2-methylpropane (0.07 g, 0.80 mmol, 1 eq.) in dichloromethane (25 mL) and (3*R*,4*R*)-2,5-



dimethylhexane-3,4-diamine (0.84 g, 3.90 mmol, 5 eq.) in dichloromethane (25 mL) and triethylamine (0.4 mL, 5.1 mmol, 3.3 eq.) were added. The reaction mixture was set to stir at rt for 72 hrs. The solvent was removed under reduced pressure. THF (50 mL) was added, filtered to remove the triethylamine salts and solvent removed. The crude material was then re-dissolved in dichloromethane, filtered to remove any polymer and the solvent was removed under reduced pressure. Methanol was added to precipitate and give the scrambled cage (0.40 g, 0.3 mmol, 11%) as a white powder.

**IR** ( $\nu_{\text{max}}$  / $\text{cm}^{-1}$ ): 2968, 2860, 1701, 1659 (imine N=C), 1595, 1466, 1364, 1259;  **$^1\text{H}$  NMR** (400 MHz,  $\text{CDCl}_3$ ):  $\delta$  8.24-7.70 (m, 24H, N=CH and ArH), 3.51-3.21 (m, 12H, CHN=CH), 2.20-1.82 (m, 15H, CH), 1.11-0.77 (m, 60H,  $\text{CH}_2$  and  $\text{CH}_3$ );  **$^{13}\text{C}$  NMR** (101 MHz,  $\text{CDCl}_3$ ): (due to scrambling chemical shifts appear as multiplets) 160.00, 136.74, 130.02, 61.34, 28.64, 28.43, 28.16, 21.98, 21.61, 21.57, 16.26, 16.00, 1.16; **HRMS** (QTOF) calc. for scrambled cages  $13^6:21^0$ ,  $13^5:21^1$ ,  $13^4:21^2$ ,  $13^3:21^3$ ,  $13^2:21^4$ ,  $13^1:21^5$ ,  $13^0:21^6$  = 961.3200, 1017.4280, 1073.5360, 1129.6440, 1185.7520, 1241.8600, 1297.9680 Found  $[\text{M}]^+$  or  $[\text{M}+\text{H}]^+$  at: 1129.8253, 1185.8900, 1241.9539, 1298.0147

#### Synthesis of 1,3,5-tris(4,5-diisopropylimidazolidin-2-yl)benzene



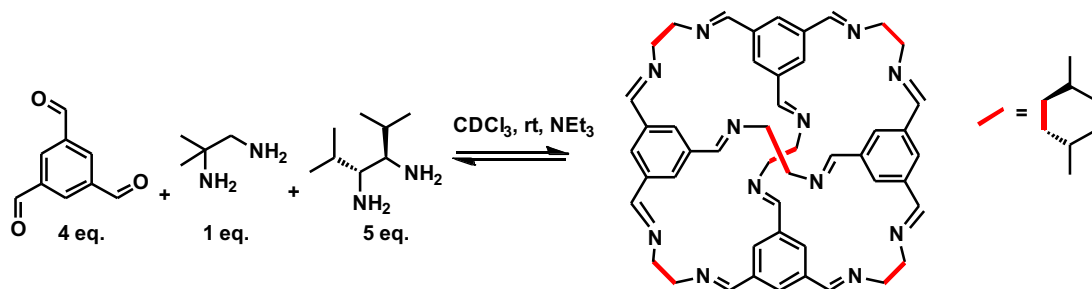
TFB (0.5 g, 6.17 mmol, 4 eq.) was dissolved in chloroform (60 mL). (3R,4R)-2,5-dimethylhexane-3,4-diamine (2.01 g, 9.26 mmol, 6 eq.) and triethylamine (0.37 mL, 3.3 eq.) in chloroform (60 mL) was added. The reaction was stirred at rt for 72 hrs when the solvent was removed *in vacuo*. The purified product was precipitated with methanol. 1,3,5-tris(4,5-diisopropylimidazolidin-2-yl)benzene (1.11g, 2.05 mmol, 33%) was collected as a pink power.

**$^1\text{H}$  NMR** ( $\text{CDCl}_3$ ):  $\delta$  7.59 (3H, s, ArH), 4.87 3H, (s, ArNCH), 2.87 (6H, dt,  $J=40.0, 5.7$  Hz, NCHiPr) 2.02 (6H, br s, NH), 1.72-1.66 (6H, m, CHiPr), 1.00-0.96 (36H, m,  $\text{CH}_3$ );  **$^{13}\text{C}$  NMR** ( $\text{CDCl}_3$ ):  $\delta$  142.28 (ArC), 124.88 (ArC), 67.96 (ArCN), 67.57 (ArCN), 32.75 (CHN), 32.29 (CHN), 20.98 (CHiPr), 20.86 (CHiPr), 18.78 ( $\text{CH}_3$ ), 18.64 ( $\text{CH}_3$ ); **HRMS**:  $[\text{C}_{33}\text{H}_{60}\text{N}_6]$  calc

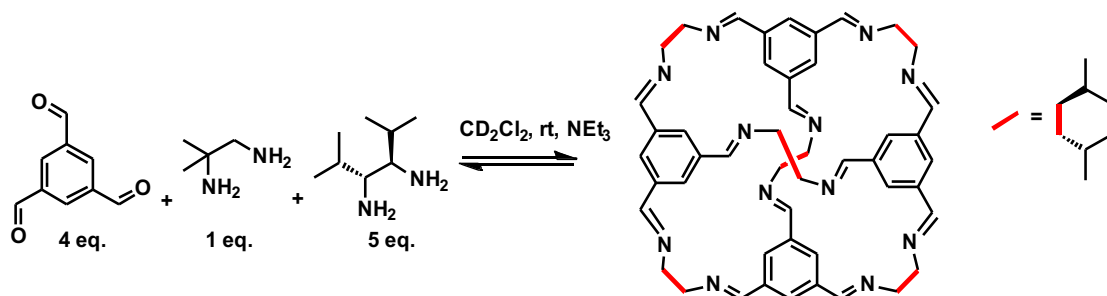
at: 540.4879. Found  $[M+H]^+$  at: 541.4958; Elemental analysis: C, 72.09 H, 11.20 N, 15.37 (calculated for  $C_{33}H_{60}N_6$  at C, 73.28 H, 11.18 N, 15.54). (See Appendix Figure 3 and 4 for NMR spectra).

### 7.3.2 Formation mechanism studies

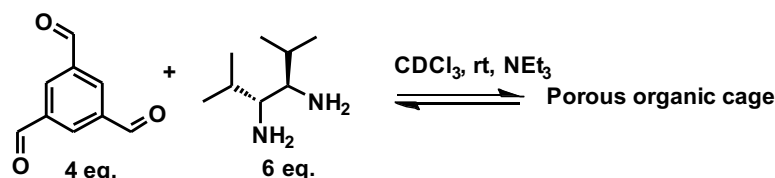
See **Appendix Table 10** for full list of possible intermediates during the formation of CC21.



TFB (33 mg, 0.2055 mmol, 4 eq.) was dissolved in  $CDCl_3$  (3 mL) and 1,2-diamino-2-methylpropane (4.5 mg, 0.0514 mmol, 1 eq.) in  $CDCl_3$  (1.5 mL) and (3*R*,4*R*)-2,5-dimethylhexane-3,4-diamine (5.9 mg, 0.257 mmol, 5 eq.) in  $CDCl_3$  (1.5 mL) with triethylamine (0.12 mL, 0.848 mmol, 3.3 eq.) were added. The reaction was set to stir at rt. The progress monitored by running  $^1H$  NMR analysis on crude samples.

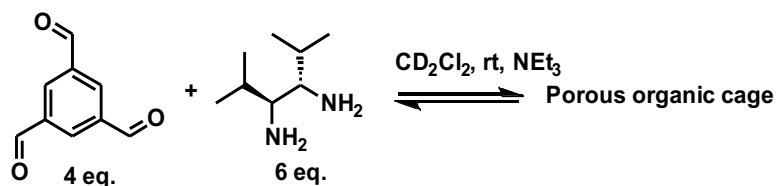


TFB (50 mg, 0.617 mmol, 4 eq.) was dissolved in  $CD_2Cl_2$  (5 mL) and 1,2-diamino-2-methylpropane (7.0 mg, 0.154 mmol, 1 eq.) in  $CD_2Cl_2$  (2.5 mL) and (3*R*,4*R*)-2,5-dimethylhexane-3,4-diamine (80.4 mg, 0.771 mmol, 5 eq.) in  $CD_2Cl_2$  (2.5 mL) with triethylamine (0.36 mL, 2.54 mmol, 3.3 eq.) were added. The reaction was set to stir at rt for 7 days. The progress monitored by running  $^1H$  NMR analysis on crude samples.

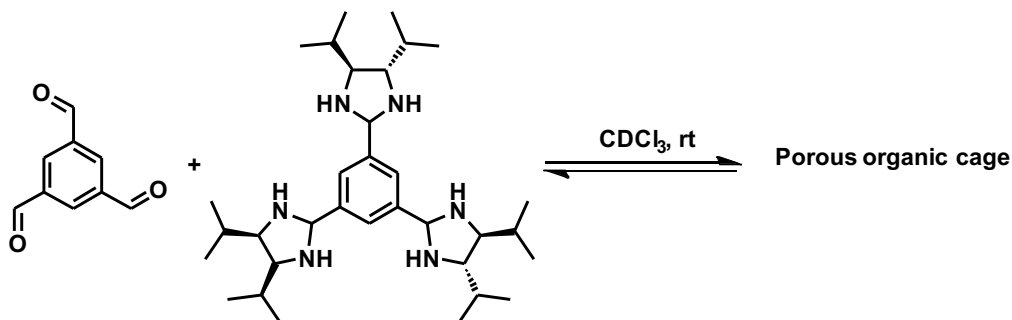


TFB (0.033 g, 0.206 mmol, 4 eq) was dissolved in  $CDCl_3$  (3 mL) and (3*R*,4*R*)-2,5-dimethylhexane-3,4-diamine (0.067 g, 0.308 mmol, 6 eq.) and triethyl amine (0.14 mL, 1.02

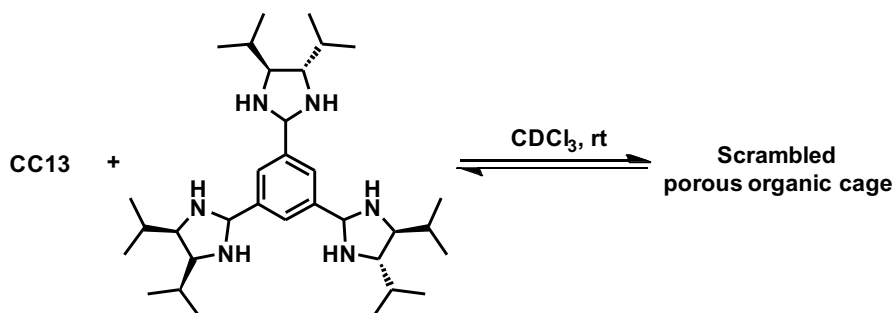
mmol, 3.3 eq.) in  $\text{CDCl}_3$  (3 mL) was added. The reaction was set to stir at rt and monitored using  $^1\text{H}$  NMR spectroscopy.



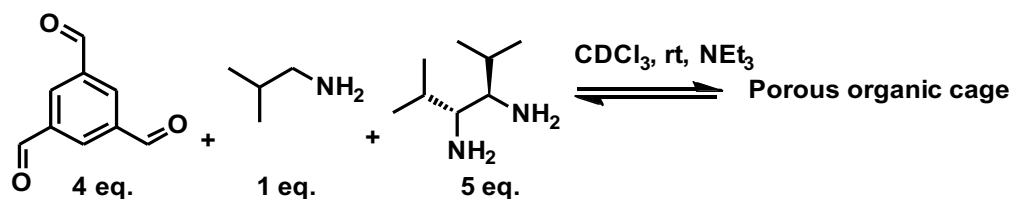
TFB (0.05 g, 0.617 mmol, 4 eq.) was dissolved in  $\text{CD}_2\text{Cl}_2$  (5 mL) and (3*R*,4*R*)-2,5-dimethylhexane-3,4-diamine (0.10 g, 0.926 mmol, 6 eq.) and triethyl amine (0.43 mL, 3.05 mmol, 3.3 eq.) in  $\text{CD}_2\text{Cl}_3$  (5 mL) was added. The reaction was set to stir at rt and monitored using  $^1\text{H}$  NMR spectroscopy.



TFB (30 mg, 0.250 mmol, 4 eq.) was dissolved in  $\text{CDCl}_3$  (3 mL) and 1,3,5-tris(4,5-diisopropylimidazolidin-2-yl)benzene (20 mg, 0.370 mmol, 6 eq.) in  $\text{CDCl}_3$  (3 mL) added. The reaction was set to stir at rt for 7 days and monitored by  $^1\text{H}$  NMR spectroscopy by running spectra of the crude reaction mixture.

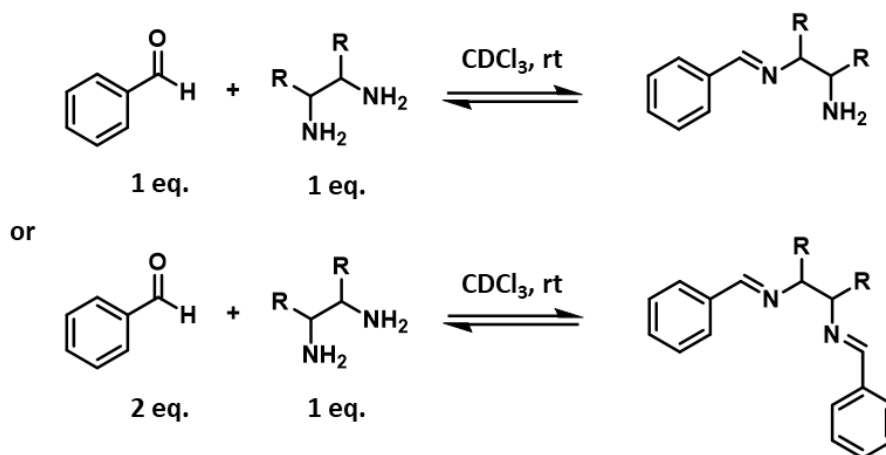


CC13 (240 mg, 0.250 mmol, 4 eq.) was dissolved in  $\text{CDCl}_3$  (3mL) and 1,3,5-tris(4,5-diisopropylimidazolidin-2-yl)benzene (200 mg, 0.370 mmol, 6 eq.) in  $\text{CDCl}_3$  (3 mL) added. The reaction was set to stir at rt for 7 days and monitored by  $^1\text{H}$  NMR spectroscopy by running spectra of the crude reaction mixture.



TFB (37 mg, 0.226, 4 eq.) was dissolved in  $\text{CDCl}_3$  (3 mL) and isobutylamine (4.1 mg, 0.0566 mmol, 1 eq.) in  $\text{CDCl}_3$  (1.5 mL) and (3*R*,4*R*)-2,5-dimethylhexane-3,4-diamine (61.5 mg, 0.283 mmol, 5 eq.) in  $\text{CDCl}_3$  (0.13 mL, 0.934 mmol, 3.3 eq.) with triethylamine (0.02 mL, 0.17 mmol, 3.3 eq.) were added. The reaction was set to stir at rt for 7 days. The progress monitored by running  $^1\text{H}$  NMR analysis on crude samples.

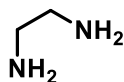
### 7.3.3 Control reactions



#### General procedure:

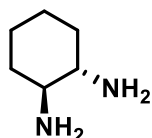
Benzaldehyde (1 or 2 eq.) was dissolved in  $\text{CDCl}_3$  (3 mL) and diamine (1 eq.) in  $\text{CDCl}_3$  (3 mL) was added. The reaction mixture was set to stir at rt for 72 hours, when a  $^1\text{H}$  NMR spectrum was run to determine the composition.

R=



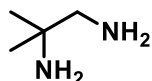
**Reaction 1:** benzaldehyde (43.6 mg, 0.4110 mmol, 2 eq.) and ethylene diamine (12.4 mg, 0.2055 mmol, 1 eq.).

**Reaction 2:** benzaldehyde (21.8 mg, 0.2055 mmol, 1 eq.) and ethylene diamine (12.4 mg, 0.2055 mmol, 1 eq.).



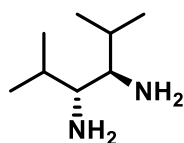
**Reaction 1:** benzaldehyde (43.6 mg, 0.4110 mmol, 2 eq.) and (1S,2S)-1,2-cyclohexanediamine (23.5 mg, 0.2055 mmol, 1 eq.).

**Reaction 2:** benzaldehyde (21.8 mg, 0.2055 mmol, 1 eq.) and (1S,2S)-1,2-cyclohexanediamine (23.5 mg, 0.2055 mmol, 1 eq.).



**Reaction 1:** benzaldehyde (43.6 mg, 0.4110 mmol, 2 eq.) and 1,2-Diamino-2-methylpropane (18.1 mg, 0.2055 mmol, 1 eq.).

**Reaction 2:** benzaldehyde (21.8 mg, 0.2055 mmol, 1 eq.) and 1,2-Diamino-2-methylpropane (18.1 mg, 0.2055 mmol, 1 eq.).



**Reaction 1:** benzaldehyde (43.6 mg, 0.4110 mmol, 2 eq.), (3R,4R)-2,5-dimethylhexane-3,4-diamine (44.6 mg, 0.2055 mmol, 1 eq.) and triethylamine (0.95 mL, 0.678 mmol, 3.3 eq.).

**Reaction 2:** benzaldehyde (21.8 mg, 0.2055 mmol, 1 eq.), (3R,4R)-2,5-dimethylhexane-3,4-diamine (44.6 mg, 0.2055 mmol, 1 eq.) and triethylamine (0.95 mL, 0.678, 3.3 eq.).

### 7.3.4 Single crystal X-ray diffraction

Single crystals were grown of **CC21** by dissolving **CC21** in chloroform and methanol added by slow vapour diffusion. For the full refinement details, see **Appendix Table 11**.

## 7.4 Chapter 4 experimental data

### 7.4.1 Solubility and porosity screen

**Solvent volatility:** A small volume of solvent (5 mL) was added to a round-bottom flask and the mass recorded. The solvent was subjected to house vacuum for 24 hrs and the mass recorded (**Appendix Table 12**)

**General procedure for porosity screen:** The selected solvent (1 mL) was added to a scrambled cage (200 mg) and stirred until dissolved. Any cages which did not dissolve or formed a gel at this concentration at the higher volume, were discounted. Xenon was added to the porous liquid at  $\sim 50\text{-}60\text{ mL min}^{-1}$  for 10 mins per 1 mL of solvent. Chloroform (1.0 eq. relative to cage) was then added to evolve the xenon and the displacement of water was measured in an inverted burette over 30 minutes. This screen of the potential new porous liquids was carried out to narrow down the hits further, and the systems with the highest volume evolved were investigated further at higher concentrations (**Appendix Table 13**).

### 7.4.2 Effect of changing porous liquid components

**Viscosity measurements:** Scrambled  $3^3:13^3$  cage (200 mg) was dissolved in one of the bulky solvents (1 mL), and the viscosity of the sample measured using a RheoSense  $\mu$ VISC viscometer (using either a 0.01–100 or 10–2000 cP microfluidic chip) with the temperature set at 25 °C (See **Appendix Table 14**). The procedure was repeated three times to calculate the average viscosity and standard deviation, as well as for the neat solvents (**Appendix Table 15**).

**Density measurements:** Scrambled cage (200 mg) was dissolved in one of the bulky solvents (1 mL), before a sample of each porous liquid was added to a pre-weighed 1 mL volumetric flask. The volumetric flask was then re-weighed and the density of the porous liquid (20% w/v) calculated (**Appendix Table 16**). The procedure was repeated three times to calculate the average density and standard deviation, as well as for the neat solvents (**Appendix Table 17**).

**Calculating total pore volume:** using the previously reported method, the total pore volume for the scrambled  $3^3:13^3$  porous liquid family can be calculated and compared for 200 mg of scrambled  $3^3:13^3$  cage dissolved in 1 mL of each solvent (**Appendix Tables 19 and 20**).<sup>112</sup>

**General Procedure for xenon uptake using gas displacement:** Samples of each porous liquid were prepared by dissolving scrambled cage (200 mg, 0.192 mmol), desolvated in a vacuum oven at 90 °C overnight, in each of the purified solvents (1.0 mL) by sonication and stirring. Xenon was then added to each porous liquid by bubbling the gas through the sample

at ~50-60 mL min<sup>-1</sup> (60-66 on Gilmont flowmeter scale with a stainless-steel float) for 10 mins per 1 mL of solvent used. Chloroform (16 µL, 0.192 mmol, 1.0 eq. relative to cage) was then added to evolve the xenon and the displacement of water was measured in an inverted burette over 30 minutes. The theoretical maximum volume of xenon that can be evolved based on a 1:1 cage:Xe ratio is 4.6 cm<sup>3</sup> (**Appendix Table 21**). There is a large uncertainty associated with the xenon displacement experiments, likely due to the small volume of porous liquid used (in order to conserve material), as well as the inability to determine if all the gas had been displaced from the liquid and the cage pores.

**Calculation of xenon uptake in µmol:** To compare the xenon uptakes in the different scrambled porous liquids at 20% w/v, the measurements were converted to moles using the ideal gas equation (**Appendix Table 22 and 23**).

$$n \text{ (mol)} = \frac{pV}{RT}$$

$$P \text{ (Pa)} = 101325$$

$$T \text{ (K)} = 293$$

$$R \text{ (J K}^{-1} \text{ mol}^{-1}\text{)} = 8.314$$

$$V \text{ (m}^3\text{)}$$

$$\text{Example for 20\% w/v } 3^3:13^3_{\text{HAP}}: n = \frac{101325 \times 0.0000029}{8.314 \times 293} = 0.126 \text{ mmol}$$

**Calculation of xenon uptake in µmol g<sub>PL</sub><sup>-1</sup>:** To further compare the gas uptake in each scrambled 3<sup>3</sup>:13<sup>3</sup> porous liquid at 20% w/v, the xenon uptake was also converted to µmol g<sub>PL</sub><sup>-1</sup> (**Appendix Table 24**)

**Step 1:**

$$\text{Overall mass of porous liquid} = M_{\text{cage}} + M_{\text{solvent}}$$

**Step 2:**

$$n \text{ (mol)} = \frac{pV}{RT}$$

$$P \text{ (Pa)} = 101325$$

$$T \text{ (K)} = 293$$

$$R \text{ (J K}^{-1} \text{ mol}^{-1}\text{)} = 8.314$$

$$V \text{ (m}^3\text{)}$$

**Step 3:**

$$\mu\text{mol/g}_{\text{PL}} = \frac{\text{mmol uptake for whole sample}}{\text{mass of whole sample}}$$

**Example for 20% w/v 3<sup>3</sup>:13<sup>3</sup><sub>DCBC</sub>:**

$$0.2 \text{ g} + 1.3468 \text{ g} = 1.5438 \text{ g}$$

$$n = \frac{101325 \times 0.0000017}{8.314 \times 293} = 70.7 \mu\text{mol}$$

$$\frac{70.7 \mu\text{mol}}{1.5438 \text{ g}} = 45.8 \mu\text{mol}/g_{PL}$$

**Calculation of xenon uptake in  $\mu\text{mol mL}_{PL}^{-1}$ :** In order to compare xenon and subsequent methane uptakes, the gas uptake was converted to  $\mu\text{mol mL}_{PL}^{-1}$  (**Appendix Table 25**):

$$\mu\text{mol mL}^{-1} = \mu\text{mol g}^{-1} \times \rho (\text{g mL}^{-1})$$

**General Procedure for xenon uptake in neat solvents using gas displacement:** Xenon gas was added to each purified parent solvent (1 mL) by bubbling the gas through the sample at  $\sim 50\text{-}60 \text{ mL min}^{-1}$  (60-66 on Gilmont flowmeter scale with a stainless-steel float) for 10 mins per 1 mL of solvent used. Chloroform (16  $\mu\text{L}$ , 0.192 mmol, 1.0 eq.) was then added to evolve the xenon and the displacement of water was measured in an inverted burette over 30 minutes (**Appendix Table 26**).

**General procedure for measuring methane uptake in porous liquids:** Scrambled cage (200 mg), desolvated in vacuum oven at  $90 \text{ }^\circ\text{C}$  before use in a porous liquid, was dissolved in each solvent (1 mL) by vortexing. Methane was added to the new porous liquids at  $\sim 50\text{-}60 \text{ mL min}^{-1}$  for 10 mins per 1 mL of solvent used.  $^1\text{H}$  NMR spectra were recorded of the porous liquids using a calibrated TMS/ $\text{CD}_2\text{Cl}_2$  capillary. The integration of the methane peak was compared to that of the NCH stretch for the scrambled cage, and the overall cage concentration was determined by comparing the integration to the TMS peak at 0.00 ppm (**Appendix Table 27 and 28**).

**General procedure for measuring methane uptake in neat solvents:** Methane was added to each neat solvent (1 mL) at  $\sim 50\text{-}60 \text{ mL min}^{-1}$  for 10 mins per 1 mL of solvent used.  $^1\text{H}$  NMR spectra were recorded of the porous liquids using a calibrated TMS/ $\text{CD}_2\text{Cl}_2$  capillary. The integration of the methane peak was compared to the integration to the TMS peak at 0.00 ppm (**Appendix Table 29**).

**Conversion to  $\mu\text{mol g}_{PL}^{-1}$ :** The methane uptakes calculated from the NMR studies can also be converted from  $\mu\text{mol mL}^{-1}$  to  $\mu\text{mol g}^{-1}$  (**Appendix Table 32 and 33**).

$$\frac{\mu\text{mol}}{g_{PL}} = \frac{\mu\text{mol/ml}}{\rho (\text{g/ml})}$$

**Example for 20% w/v  $3^3\text{:}13^3_{\text{DCBC}}$ :**

$$\frac{14.2 \mu\text{mol/mol}}{1.3099 \text{ g/mL}} = 10.9 \mu\text{mol}/g_{PL}$$



### 7.4.3 Effect of changing porous liquid concentration on $3^3:13^3_{\text{HAP}}$ and $3^3:13^3_{\text{TBA}}$

The  $3^3:13^3_{\text{HAP}}$  and  $3^3:13^3_{\text{TBA}}$  porous liquid families were studied at different concentrations to determine the effect on gas uptake and other scrambled porous liquid properties.

**Porous liquid sample preparation:** Scrambled  $3^3:13^3$  cage (200 to 600 mg) was dried in a vacuum oven overnight at 90 °C before being dissolved in purified 2-hydroxyacetophenone or 4-(trifluoromethoxy)benzyl alcohol (1 mL) using prolonged stirring and sonication.

**Density measurements of  $3^3:13^3_{\text{HAP}}$  and  $3^3:13^3_{\text{TBA}}$  at varying concentrations:** Scrambled  $3^3:13^3$  cage (200 to 600 mg) was dissolved in each solvent (1 mL), before a sample of each porous liquid was added to a pre-weighed 1 mL volumetric flask. The volumetric flask was then re-weighed and the density of the porous liquid calculated. The procedure was repeated three times to calculate the average density and standard deviation (**Appendix Table 34 and 35**).

**Viscosity measurements of  $3^3:13^3_{\text{HAP}}$  and  $3^3:13^3_{\text{TBA}}$  at varying concentrations:** Scrambled cage (200 to 600 mg) was dissolved in bulky solvent (1 mL) and the viscosity of the sample measured using RheoSense  $\mu$ VISC viscometer (using either 0.01–100 or 10–2000 cP chip) with the temperature set at 25 °C. The procedure was repeated three times to calculate the average viscosity and standard deviation (**Appendix Table 39**).

### 7.4.4 Studies of $3^3:13^3_{\text{HAP}}$ at different concentrations

**General procedure for xenon uptake using gas displacement for various concentrations:** Samples of  $3^3:13^3_{\text{HAP}}$  at 16, 22, 27 and 35 wt%, and  $3^3:13^3_{\text{TBA}}$  at 14 and 24 wt%, were prepared and xenon gas was then added to each porous liquid by bubbling the gas through the sample at  $\sim 50\text{--}60 \text{ mL min}^{-1}$  (60–66 on Gilmont flowmeter scale with a stainless steel float) for 10 mins per 1 mL of solvent used. Chloroform (1.0 eq. relative to cage) was then added to evolve the xenon and the displacement of water was measured in an inverted burette over 30 minutes (**Appendix Table 40–43**).

**Methane saturation studies:**  $3^3:13^3_{\text{HAP}}$  was then investigated further as the xenon uptake varied with concentration. Saturation studies were carried out with methane and investigated using  $^1\text{H}$  NMR spectroscopy. Methane was added to different  $3^3:13^3_{\text{HAP}}$  samples at different concentrations (8, 15, 21 and 26 wt%) over five-minute intervals. Each porous liquid seemed to reach full saturation within five minutes, with only small fluctuations after this time (**Appendix Table 44–47**). For all subsequent experiments, porous liquid samples were purged with a gas for 10 min per 1 mL of solvent used to ensure saturation.

**Methane uptake measurements for  $3^3:13^3_{\text{HAP}}$  at different concentrations:** Using the findings from the saturation study, a sample of  $3^3:13^3_{\text{HAP}}$  at 8, 16, 22, and 27 wt% was loaded with methane gas for 10 min per 1 mL of solvent used, and the uptake calculated using  $^1\text{H}$  NMR analysis. Overall, the methane uptake increases with increasing concentration, as well as the methane peak shifting more downfield, indicating a preference for the cage cavity (**Appendix Table 48 and 49**).

#### 7.4.5 Temperature release experiments

**General procedure:** Scrambled  $3^3:13^3$  cage (200 to 600 mg) was dissolved in 2-hydroxyacetophenone (1 mL) and purged with xenon at  $\sim 50\text{-}60$  mL/min for 10 min per mL of solvent. The porous liquid was then heated slowly to the required temperature and the water displacement measured by collecting the gas released in an inverted burette (**Appendix Table 50-55**).

#### 7.4.6 Sol-gel behaviour of $3^3:13^3_{\text{HAP}}$

**General procedure:** Scrambled  $3^3:13^3$  cage (400 or 600 mg) was dissolved in 2-hydroxyacetophenone (1 mL) and saturated with xenon at  $\sim 50\text{-}60$  mL  $\text{min}^{-1}$  for 10 min per mL of solvent. The xenon-loaded porous liquid was then cooled to between 0 and 6 °C until the solution underwent gelation. The gel was then heated at 60-85 °C for the 27 wt% sample, and 80-120 °C for the 35 wt% sample, to release the guest which was measured by water displacement in an inverted burette (**Appendix Table 56-57**).

#### 7.4.7 Retention of guest in $3^3:13^3_{\text{HAP}}$

**General procedure for 27 wt% sample:** The scrambled  $3^3:13^3$  cage (400 mg) was dissolved in 2-hydroxyacetophenone (1 mL) and purged with xenon at  $\sim 50\text{-}60$  mL  $\text{min}^{-1}$  for 10 min per mL of solvent. The sample was sealed and left undisturbed. After 48 h, the sample was heated to release the trapped guest, which was collected in an inverted burette in water. The volume of water displaced equated to the volume of xenon in the porous liquid (**Appendix Table 58**).

**General procedure for 35 wt% sample:** The scrambled  $3^3:13^3$  cage (600 mg) was dissolved in 2-hydroxyacetophenone (1 mL) and purged with xenon at  $\sim 50\text{-}60$  mL/min for 10 min per mL of solvent. Several samples were prepared in this manner and left standing at ambient temperature. Periodically, a sample was heated to release the trapped guest, which was collected in an inverted burette in water. The volume of water displaced equated to the volume of xenon retained in the porous liquid (**Appendix Table 59**).

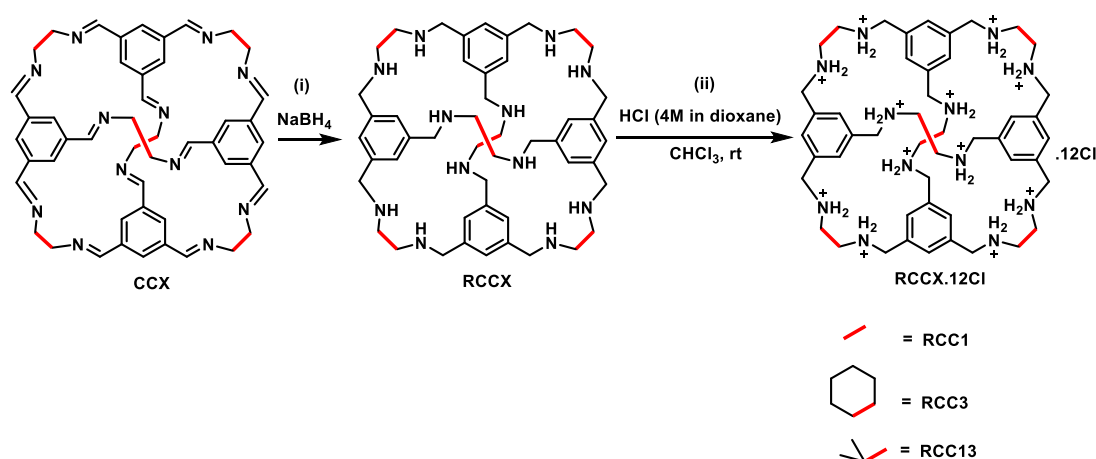
### 7.4.8 Recovery of 3<sup>3</sup>:13<sup>3</sup> scrambled cage

**General procedure:** Acetone was added to 3<sup>3</sup>:13<sup>3</sup><sub>HAP</sub> until precipitation of the scrambled cage occurred. The solid was collected by filtration and dried at 70 °C in a vacuum oven. The scrambled cage was recovered as a white solid, and the <sup>1</sup>H NMR spectrum confirmed pure material had been recovered (Appendix Table 60).

## 7.5 Chapter 5 experimental data

### 7.5.1 Synthesis of RCCX.12HCl

All cage precursors were prepared using literature procedures.<sup>13,84,88,156,179,181</sup>



- (i) **General procedure for cage reduction:** Porous imine cage (1 eq.) dissolved in chloroform: methanol (1:1) and sodium borohydride (32 eq.) added batch-wise. The reaction was set to stir at rt for 24 hrs. Water was added and stirred for a further 12 hrs before the solvent removed under reduced pressure. Another portion of water (100 mL) was added and extracted with chloroform (2 x 100 mL). The organics combined, dried ( $\text{MgSO}_4$ ), filtered and the solvent removed under reduced.
- (ii) **General procedure for formation of hydrochloride salt:** Reduced porous organic cage (1 eq.) dissolved in chloroform and HCl (4M, dioxane, 15 eq.) was added dropwise. The reaction mixture was stirred at rt for 2 hrs and the solid filtered through a nylon membrane. To prevent polymerisation, the solid was dissolved in methanol before drying on the filter paper and solvent removed *in vacuo*. Procedure adapted from methodology used by Liu *et al.*<sup>189</sup>

**RCC1.12HCl**

**RCC1** (0.8 g, 0.98 mmol, 1 eq.) dissolved in chloroform (20 mL) and HCl (2.5 mL, 14.7 mmol, 15 eq.) added. **RCC1.12HCl** (0.729 g, 0.59 mmol, 60 %) was collected as a white powder and dried under vacuum.

<sup>1</sup>H NMR (400 MHz, D<sub>2</sub>O): δ 7.47 (s, 12H, ArH), 4.14 (s, 24H, Ar-CH<sub>2</sub>), 3.13 (s, 24H, NH<sub>2</sub>); <sup>13</sup>C NMR (400 MHz, D<sub>2</sub>O): δ 134.54, 130.86, 50.94, 43.98; IR (V<sub>max</sub>/ cm<sup>-1</sup>): 3361.3, 2955.3, 2749.2, 2376.2, 1605.4, 1450.9, 1172.6, 1036.6, 869.7, 713.1; HRMS (QTOF): Calculated for C<sub>48</sub>H<sub>72</sub>N<sub>12</sub> 816.6003, found [M+H]<sup>+</sup> 817.5898; **Elemental analysis calculated for (H<sub>12</sub>RCC1)<sup>12+</sup>.12HCl (%)**: C 46.17, H 6.30, N 13.46; found at: C 41.50, H 7.27, N, 11.87; in concordance with literature values <sup>189</sup>

**RCC3.12HCl**

**RCC3** (0.21 g, 0.18 mmol, 1 eq.) dissolved in chloroform (10 mL) and HCl (1.0 mL, 2.68 mmol, 15 eq.) added. **RCC3.12HCl** (0.20 g, 1.00 mmol, 72%) was collected as a white powder and dried under vacuum.

<sup>1</sup>H NMR (400 MHz, D<sub>2</sub>O): δ 7.66 (s, 12H, ArH), 4.53 (d, 12H, J<sub>Z</sub>= 13.5 Hz, ArCH<sub>2</sub>), 4.30 (d, 12H, J<sub>Z</sub> = 13.5 Hz, ArCH<sub>2</sub>), 3.78-3.75 (m, 16H, NCH<sub>2</sub>), 2.42-2.39 (m, 12H, CH<sub>2</sub>), 1.85 (br s, 24H, CH<sub>3</sub>), 1.54 (s, 12H, CH<sub>2</sub>); <sup>13</sup>C NMR (400 MHz, D<sub>2</sub>O): 132.36, 131.68, 66.53, 57.19, 48.34, 25.46, 21.29; IR (V<sub>max</sub>/ cm<sup>-1</sup>): 3353.1, 2930.6, 2689.5, 1593.1, 1450.9, 1384.9, 1123.2, 1018.1, 873.8; HRMS (QTOF): calculated for C<sub>72</sub>H<sub>120</sub>N<sub>12</sub> 1140.8820, found [M+H]<sup>+</sup> 1141.8725; **Elemental analysis calculated for (H<sub>12</sub>RCC3)<sup>12+</sup>.12HCl (%)**: C 54.94 H 7.36 N 10.68; found at: C 46.39 H 7.69 N 8.80.

**RCC13.12HCl**

The synthesis of **R1<sup>3</sup>:R3<sup>3</sup>.12HCl** was started from imine cage and the reduced cage not isolated.

**CC13** (0.6 g, 0.624 mmol, 1 eq.) dissolved in chloroform: methanol (1:1, 100 mL) cooled on ice and sodium borohydride (0.80 g, 20.2 mmol, 32 eq.) added batch-wise. The reaction mixture was set to stir at rt for 24 hrs and then water (1 mL) added. The reaction was left to stir for a further 12 hrs before the solvent was removed under reduced pressure. A further portion of water (100 mL) was added and extracted with chloroform (2 x 100 mL). The organics were collected, dried (MgSO<sub>4</sub>), filtered and solvent removed under reduced pressure. The resulting **RCC13** cage was dissolved in chloroform (50 mL) and HCl (1.0 mL, 3.12 mmol, 15 eq.) added dropwise. After stirring at rt for 4 hrs, the precipitate was filtered under reduced

pressure and washed with chloroform. The crude material was triturated with ether, filtered.  
**RCC13.12HCl** (0.24 g, 0.206 mmol, 33%)

<sup>1</sup>H NMR (400 MHz, D<sub>2</sub>O): δ7.66-7.62 (m, 12H, ArH), 4.19-4.08 (m, 24H, ArCH<sub>2</sub>), 3.36-3.18 (m, 12H, NCH<sub>2</sub>), 2.28 (br s, CH<sub>3</sub>), 1.81-1.37 (m, 42H, CH<sub>3</sub>); <sup>13</sup>C NMR (400 MHz, D<sub>2</sub>O): 132.66, 130.87-130.35 (m), 58.56, 51.62, 48.11, 27.35, 22.97, 22.97, 21.61 (peaks appeared as broad multiplets); IR (V<sub>max</sub>/ cm<sup>-1</sup>): 3353.1, 2959.4, 2741.0, 2598.8, 2405.1, 1584.8, 1413.8, 1170.6, 1024.3, 882.1, 702.8; HRMS (QTOF): calculated for C<sub>60</sub>H<sub>84</sub>N<sub>12</sub> 984.7881, found [M+H]<sup>+</sup> 985.7808; **Elemental analysis calculated for (H<sub>12</sub>RCC13)<sup>12+</sup>.12HCl (%)**: C 50.82 H 7.32 N 11.85; found at: C 42.87 H 7.67 N 9.97

### **R3<sup>3</sup>:R13<sup>3</sup>.12HCl**

**R3<sup>3</sup>:R13<sup>3</sup>** (0.8 g, 0.77 mmol, 1 eq.) dissolved in chloroform (20 mL) and HCl (2.0 mL, 11.5 mmol, 15 eq.) added. **R3<sup>3</sup>:R13<sup>3</sup>.12HCl** (0.886 g, 0.59 mmol, 77%) was collected as a white powder.

<sup>1</sup>H NMR (400 MHz, D<sub>2</sub>O): δ7.63-7.47 (m, 12H, ArH), 4.22-4.01 (m, 24H, Ar-CH<sub>2</sub>), 3.35-3.15 (m, 12H, NCH<sub>2</sub>), 2.28 (br s, 6H, CH), 1.82-1.37 (m, 41H, CH<sub>2</sub>+ CH<sub>3</sub>); <sup>13</sup>C NMR (400 MHz, D<sub>2</sub>O): δ132.55-132.22 (m), 58.64-57.59 (m), 51-26-50.82 (m), 48.50-48.14 (m), 45.06-44.76 (m), 26.04-25.35 (m), 21.77-21.38 (m); IR (V<sub>max</sub>/ cm<sup>-1</sup>): 3351.0, 2936.8, 2732.7, 2409.2, 1582.8, 1446.7, 1382.9, 1166.5, 1119.1, 1022.2, 869.7; HRMS (QTOF): calculated for scrambled cages 3<sup>0</sup>13<sup>6</sup>, 3<sup>1</sup>13<sup>5</sup>, 3<sup>2</sup>13<sup>4</sup>, 3<sup>3</sup>13<sup>3</sup>, 3<sup>4</sup>13<sup>2</sup>, 3<sup>5</sup>13<sup>1</sup>, 3<sup>6</sup>13<sup>0</sup> = 984.7881, 1010.8037, 1036.8194, 1062.8350, 1088.8507, 1114.8663, 1140.8820, found [M+H]<sup>+</sup> 985.7751, 1011.7930, 1037.8099, 1063.8257, 1089.8405, 1115.8538, 1141.8661; **Elemental analysis calculated for (H<sub>12</sub>R3<sup>3</sup>:R13<sup>3</sup>)<sup>12+</sup>.12HCl (%)**: C 53.06 H 7.22 N 11.25; found at: C 47.88 H 7.44 N 10.08

### **R1<sup>3</sup>:R3<sup>3</sup>.12HCl**

The synthesis of **R1<sup>3</sup>:R3<sup>3</sup>.12HCl** was started from imine cage and the reduced cage not isolated.

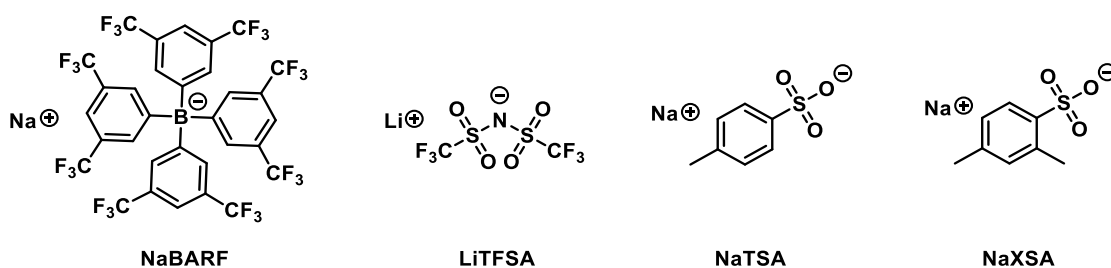
**1<sup>3</sup>:3<sup>3</sup>** (0.6 g, 0.69 mmol, 1 eq.) dissolved in CHCl<sub>3</sub>: MeOH (1:1, 50 mL), cooled on ice and sodium borohydride (0.80 g, 20.2 mmol, 32 eq.) added batch-wise. The reaction mixture was set to stir at rt for 24 hrs and then water (1 mL) added. The reaction was left to stir for a further 12 hrs before the solvent was removed under reduced pressure. A further portion of water (100 mL) was added and extracted with chloroform (2 x 100 mL). The organics were collected, dried (MgSO<sub>4</sub>), filtered and solvent removed under reduced pressure. The resulting **R1<sup>3</sup>:R3<sup>3</sup>** cage was dissolved in chloroform (50 mL) and HCl (0.36 mL, 4M in dioxane) added dropwise. After stirring at rt for 4 hrs, the precipitate was filtered under reduced pressure and washed

with chloroform. The crude material was triturated with ether, filtered and **R1<sup>3</sup>:R3<sup>3</sup>.12HCl** (0.40 g, 0.176 mmol, 41%) was collected as a white powder.

<sup>1</sup>H NMR (400 MHz, D<sub>2</sub>O): δ 7.80-7.57 (m, 12H ArH), 4.64-4.61 (m, 12H, ArCH<sub>2</sub>), 4.35-4.28 (m, 12H, ArCH<sub>2</sub>), 3.84-3.42 (m, 16H, NCH<sub>2</sub>), 2.46-2.39 (m, 12H, CH<sub>2</sub>), 1.85-1.41 (m, 46H, CH<sub>2</sub>+CH<sub>3</sub>); <sup>13</sup>C NMR (400 MHz, D<sub>2</sub>O): δ 132.41, 131.66, 57.24, 52.14, 51.26, 48.36, 29.20, 25.51, 22.69, 21.35; IR (V<sub>max</sub>/cm<sup>-1</sup>): 3373.7, 2930.6, 2736.9, 1580.7, 1452.9, 1185.0, 1026.3, 877.9; HRMS (QTOF): calculated for scrambled cages 1<sup>6</sup>3<sup>0</sup>, 1<sup>5</sup>3<sup>1</sup>, 1<sup>4</sup>3<sup>2</sup>, 1<sup>3</sup>3<sup>3</sup>, 1<sup>2</sup>3<sup>4</sup>, 1<sup>1</sup>3<sup>5</sup>, 1<sup>0</sup>3<sup>6</sup> = 816.6003, 870.6472, 924.6942, 978.7411, 1032.7880, 1086.8350, 1140.8820, found [M+H]<sup>+</sup> 817.6136, 1087.8200, 1141.8685; **Elemental analysis calculated for (H<sub>12</sub>R1<sup>3</sup>:R3<sup>3</sup>)<sup>12+</sup>.12HCl (%)**: C 51.11 H 6.79 N 11.92; found at: C 45.26 H 7.60 N 9.47

### 7.5.2 High-throughput salt exchange

**General high-throughput synthetic procedure:** All precursors (cage hydrochloride salts and sodium/lithium salts) were dissolved in methanol, (2.4-150 mg) depending on solubility studies (**Appendix Table 61**), for use in the high-throughput screen. The run was carried out on a Chemspeed ISYNTH platform by liquid dispensing of the required cage hydrochloride salt stock solution into capped 20 mL vials. The sodium/ lithium salt stock solution was then added, also by liquid dispensing, followed by the addition of methanol to make the total volume up to 15 mL. The resulting solutions were vortexed at 200 rpm at room temperature for 72 hrs. The reaction conditions were carried out twice to give 40 reactions in total (see **Appendix Table 62 and 63**).



### 7.5.3 Characterisation of cage salts

The cage salts from the high-throughput screen were analysed using IR spectroscopy and HRMS, which is summarised in **Appendix Table 64-65**.

### 7.5.4 Scale out of cage salts

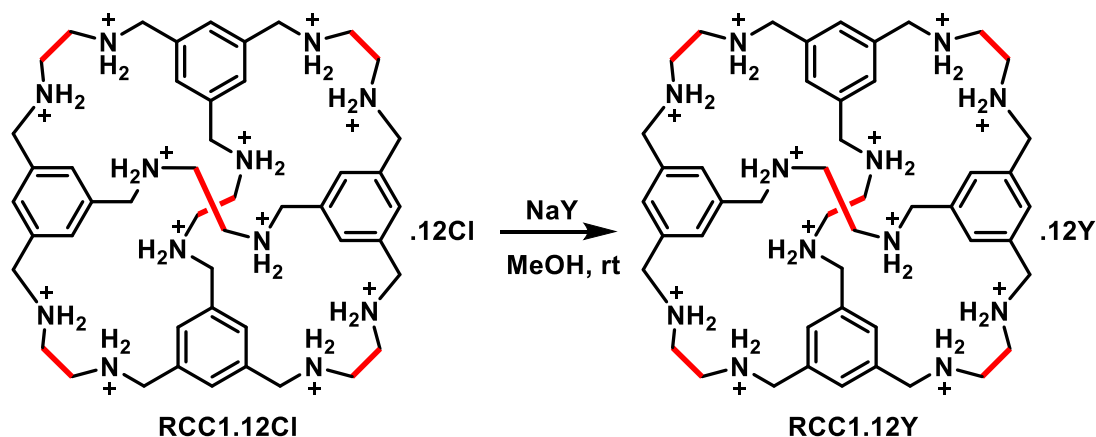
**General procedure:** All precursors (**RCC1.12HCl**, **RCC3.12HCl** and Sodium trifluoromethanesulfonimide) were dissolved in methanol as stock solutions (**Appendix Table 66**). These were dispensed using a Chemspeed ISYNTH platform, using liquid addition, into

capped 20 mL vials (**Appendix Table 67**). The reaction vessels were vortexed at ambient temperature for 72 hrs. The reactions containing the same cage were combined and the solvent removed under reduced pressure. Acetone was added, the precipitate filtered and the solvent removed under reduced pressure. The purification procedure was repeated until no more precipitation occurred.  $^{13}\text{C}$  NMR spectroscopy was attempted but was difficult to get quality spectra so was not reported here. The cage salts were characterised using other standard techniques.

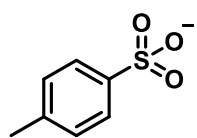
The procedure for **RCC1.12TFSA** was repeated in the laboratory, see **Section 6.5.5** for full characterisation.

**RCC3.12TFSA** (3.725 g, 0.825 mmol, 55%) was collected as a yellow powder.  $^1\text{H}$  NMR (400 MHz, MeOD):  $\delta$ 7.79 (s, 12H, ArH), 4.30 (s, 24H, ArCH<sub>2</sub>), 3.70 (s, 12H, Cyclohexane-CH), 2.35 (s, 12H, Cyclohexane-CH<sub>2</sub>) 1.82 (s, 24H, Cyclohexane-CH<sub>2</sub>), 1.57 (s, 12H, Cyclohexane-CH<sub>2</sub>);  $^{19}\text{F}$  NMR (376 MHz, MeOD):  $\delta$ -79.92; IR ( $V_{\text{max}}/\text{cm}^{-1}$ ): 3087.2, 2947.1, 2726.6, 1607.5, 1461.2, 1323.1, 1197.4, 1051.1, 795.5, 744.0; HRMS (ES<sup>+</sup>): calculated for C<sub>72</sub>H<sub>108</sub>N<sub>12</sub> 1140.8820, found at  $[\text{M}+\text{H}]^{2+}$  571.5935; **Elemental analysis calculated for (H<sub>12</sub>RCC3)<sup>12+</sup>.12TFSA (%)**: C 25.54 H 2.68 N 7.44 S 17.44; found at C 20.39 H 2.60 N 6.18 S 17.00. (See **Appendix Figure 5** and **6** for NMR data).

### 7.5.5 Scale up of RCC1 cage salts

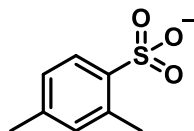


A modified procedure from the scale out was used to synthesis the cage salts manually. Each reaction was carried out four times and combined before purification. Therefore, the yield is based on the 4 x the starting cage.



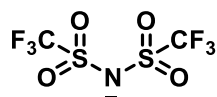
**RCC1.12HCl** (30.0 mg, 0.0241 mmol, 1 eq.) was dissolved in methanol (5 mL) and Sodium *p*-toluenesulfonate (56.2 mg, 2.896 mmol, 12 eq.) in methanol (5 mL) was added. The mixture was stirred at rt for 72 hrs and the reactions combined. The solvent was removed under reduced pressure, DCM added (10 mL) added and filtered to remove the residual sodium chloride. The solvent was removed under reduced pressure and the procedure repeated with ethanol. **RCC1.12 *p*-toluenesulfonate** (0.0597 g, 0.0207 mmol, 21%) was collected as a brown powder.

**IR** ( $V_{\max}/\text{cm}^{-1}$ ): 3406.7, 3015.1, 2786.3, 2433.9, 1605.4, 1455.0, 1172.2 1055.7, 816.1, 682.2, 560.6;  **$^1\text{H NMR}$**  (400 MHz, MeOD):  $\delta$ 7.81-7.21 (m, 4H, ArH), 3.33-3.32 (m, 3H, CH<sub>3</sub>); **HRMS** (ES<sup>+</sup>): calculated for calculated for C<sub>48</sub>H<sub>72</sub>N<sub>12</sub> 816.6003, found at 817.7617; **Elemental analysis calculated for (H<sub>12</sub>RCC1)<sup>12+</sup>.12 *p*-toluenesulfonate (%)**: C 54.98 H 5.87 N 5.83 S 13.34, found at C 48.50 H 6.03 N 6.00 S 10.50. (See **Appendix Figure 7** for NMR data).



**RCC1.12HCl** (30.0 mg, 0.0241 mmol, 1 eq.) was dissolved in methanol (5 mL) and Sodium 2,4-dimethylbenzenesulfonate (65.6 mg, 2.898 mmol, 12 eq.) in methanol (5 mL) added. The reaction mixture was stirred at rt for 72 hrs. . The solvent was removed under reduced pressure, DCM added (10 mL) added and filtered to remove the residual sodium chloride. The solvent was removed under reduced pressure and the procedure repeated with ethanol. **RCC1.12 (2,4-dimethyl)-benzenesulfonate** (0.269 g, 0.088 mmol, 91%) was collected as a yellow powder.

**IR** ( $V_{\max}/\text{cm}^{-1}$ ):291.5, 2687.4, 1603.4, 1450.9, 1147.9, 1005.7, 822.3, 678.0, 562.6; (400 MHz, MeOD):  $\delta$ 7.85-7.83 (m, 2H, ArH), 7.07 (s, 1H, ArH), 7.00 (d, 1H,  $J = 8$  Hz, ArH), 2.63 (s, 3H, CH<sub>3</sub>), 2.30 (s, CH<sub>3</sub>, CH<sub>3</sub>); **HRMS** (ES<sup>+</sup>): calculated for calculated for C<sub>48</sub>H<sub>72</sub>N<sub>12</sub> 816.6003, found at 817.7616; **Elemental analysis calculated for (H<sub>12</sub>RCC1)<sup>12+</sup>.12 (2,4-dimethyl)benzenesulfonate (%)**: C 56.67 H 6.34 N 5.51 S 12.61, found at C 50.78 H 6.42 N 6.12 S 10.00. (See **Appendix Figure 8** for NMR data).

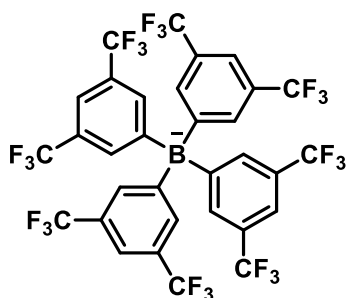


**RCC1.12HCl** (100 mg, 0.080 mmol, 1 eq.) was dissolved in methanol (10 mL) and Sodium trifluoromethanesulfonimide (291.0 mg, 0.960 mmol, 12 eq.) in methanol (10 mL) was added. The reaction mixture was stirred at rt for 72 hrs and each reaction combined. The solvent was removed under reduced pressure and acetone (10 mL) added. The precipitate filtered and the solvent removed under reduced pressure. The



procedure repeated until no precipitation occurred and the resulting solid was dried under vacuum at 90 °C. **RCC1.12 trifluoromethanesulfonimide** (0.4668 g, 0.111 mmol, 35%) was collected as a yellow powder.

**IR** ( $V_{\max}/\text{cm}^{-1}$ ): 3377.8, 2986.2, 2763.7, 1609.6, 1457.1, 1319.0, 1197.4, 1133.5, 1055.2, 799.6, 645.1, 564.7, 511.1;  **$^1\text{H}$  NMR** (400 MHz, MeOD):  $\delta$ 7.82 (s, 12H, ArH), 4.39 (s, 24H, ArCH<sub>2</sub>), 3.51 (s, 24H, NCH<sub>2</sub>);  **$^{19}\text{F}$  NMR** (376 MHz, MeOD):  $\delta$ -79.92; **HRMS** (ES+): calculated for C<sub>48</sub>H<sub>72</sub>N<sub>12</sub> 816.6003, Found at: 817.7868; **Elemental analysis calculated for (H<sub>12</sub>RCC1)<sup>12+</sup>.12 trifluoromethanesulfonimide (%)**: C 20.63 H 2.02 N 8.02 S 18.36, found at C 15.62 H 1.16 N 6.44. (See **Appendix Figure 9** and **10** for NMR data).

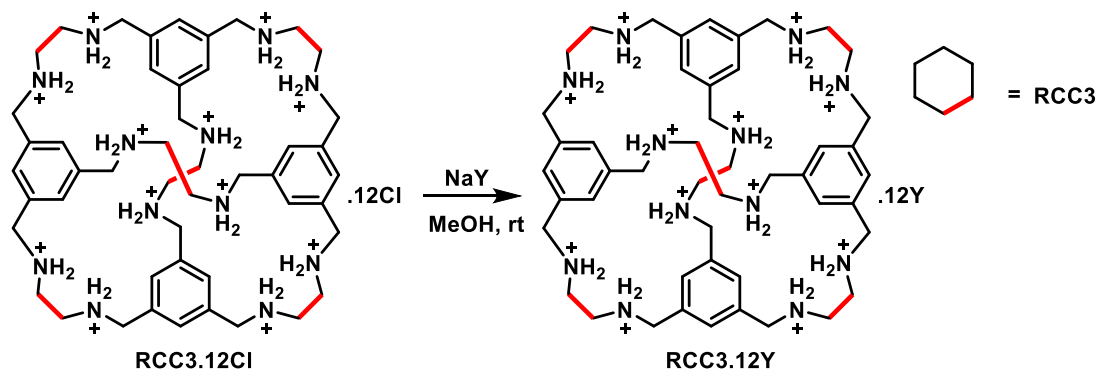


**RCC1.12HCl** (78.3 mg, 0.063 mmol, 1 eq.) was dissolved in methanol (10 mL) and sodium tetrakis[3,5-bis(trifluoromethyl)phenyl]borate (673.5 mg, 0.76 mmol, 12 eq.) was added batch-wise. The reaction was set to stir at rt for 4 hrs and then added to water (100 mL) dropwise. The resulting precipitate was filtered through a nylon filter and

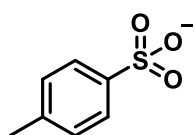
**RCC1.12BARF** (0.125 g, 0.0111 mmol, 18%) was collected as a white powder.

**IR** ( $V_{\max}/\text{cm}^{-1}$ ): 3367.5, 2961.5, 2757.5, 2361.8, 1611.6, 1452.9, 1354.0, 1279.8, 1114.9, 882.1, 834.7, 711.0, 671.9;  **$^1\text{H}$  NMR** (400 MHz, acetone-d<sub>6</sub>):  $\delta$ 7.79-7.78 (m, 2H, ArH), 7.67 (s, 1H, ArH);  **$^{19}\text{F}$  NMR** (376 MHz, acetone-d<sub>6</sub>):  $\delta$  -64.28; **HRMS** (ES+): C<sub>48</sub>H<sub>72</sub>N<sub>12</sub> 816.6003, found at 817.6159; **Elemental analysis calculated for (H<sub>12</sub>RCC1)<sup>12+</sup>.12 BARF (%)**: C 46.38 H 2.05 N 1.50, found at C 44.30 H 2.08 N 1.42. (See **Appendix Figure 11** and **12** for NMR data).

## 7.5.6 Scale up of RCC3 cage salts

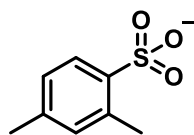


A modified procedure from the scale out was used to synthesis the cage salts manually. Each reaction was carried out four times and combined before purification. Therefore, the yield is based on the 4 x the starting cage.



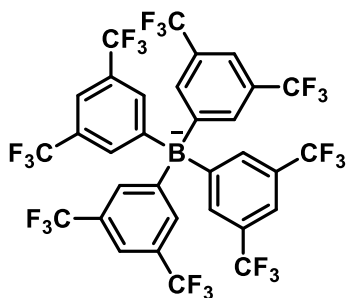
**RCC3.12HCl** (49.9 mg, 0.0315 mmol, 1 eq.) was dissolved in methanol (5 mL) and Sodium *p*-toluenesulfonate (73.4 mg, 0.378 mmol, 12 eq.) in methanol (5 mL) was added. The reaction mixture was stirred at rt for 72 hrs. The solvent was removed under reduced pressure, DCM added (10 mL) added and filtered to remove the residual sodium chloride. The solvent was removed under reduced pressure and the procedure repeated with ethanol. **RCC3.12 *p*-toluenesulfonate** (0.360 g, 0.112 mmol, 89%).

**IR** ( $V_{\text{max}}/\text{cm}^{-1}$ ): 3412.8, 2940.9, 2670.9, 2411.2, 1601.3, 1448.8, 1160.2, 1117.0, 1005.7, 816.1, 680.1, 562.6; ; **<sup>1</sup>H NMR** (400 MHz, MeOD):  $\delta$ 7.78 (d, 2H,  $J = 8$  Hz, ArH), 7.29 (d, 2H,  $J = 8$  Hz, ArH), 2.39 (s, 3H, CH<sub>3</sub>); **HRMS** (ES<sup>+</sup>): calculated for calculated for C<sub>72</sub>H<sub>108</sub>N<sub>12</sub> 1140.8820, found at [M+H]<sup>2+</sup>571.5941; **Elemental analysis calculated for (H<sub>12</sub>RCC3)<sup>12+</sup>.12 *p*-toluenesulfonate (%)**: C 58.41 H 6.41 N 5.24 S 11.99, found at C 54.01 H 7.16 N 7.44 S 6.50. (See **Appendix Figure 13** for NMR data).



**RCC3.12HCl** (49.9 mg, 0.0315 mmol, 1 eq.) was dissolved in methanol (5 mL) and Sodium 2,4-dimethylbenzenesulfonate (83.7 mg, 0.378 mmol, 12 eq.) in methanol (5 mL) added. The reaction mixture was stirred at rt for 72 hrs. The solvent was removed under reduced pressure, DCM added (10 mL) added and filtered to remove the residual sodium chloride. The solvent was removed under reduced pressure and the procedure repeated with ethanol. **RCC3.12 (2,4-dimethyl)-benzenesulfonate** (0.141 g, 0.042 mmol, 33%) was collected a yellow powder.

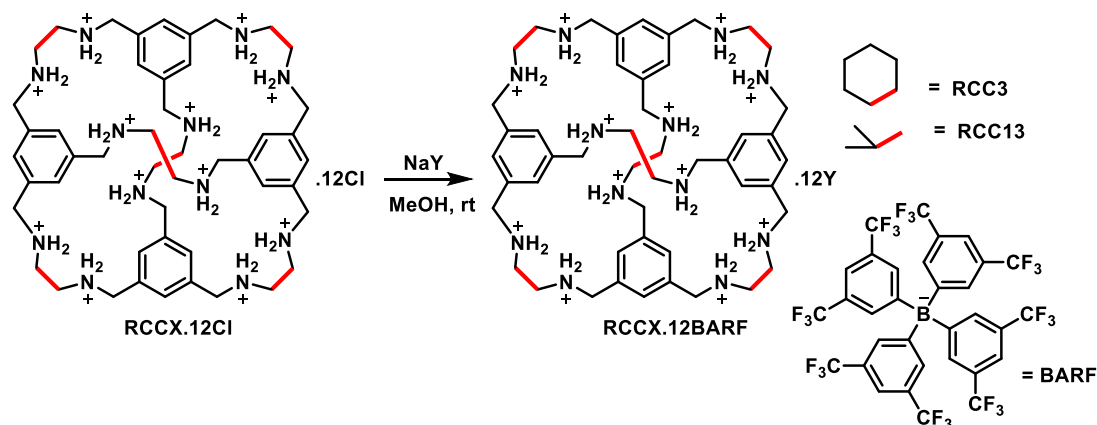
IR ( $V_{\max}/\text{cm}^{-1}$ ): 3414.9, 2955.3, 2815.2, 1603.4, 1446.7, 1160.3, 1084.0, 1011.9, 810.2, 678.0, 568.8;  $^1\text{H NMR}$  (400 Mz, MeOD):  $\delta$ 7.75 (d, 1H,  $J = 8$  Hz, ArH), 7.08 (s, 1H, ArH), 7.00 (d, 1H,  $J = 8$  Hz, ArH), 2.61 (s, 3H, ArCH<sub>3</sub>), 2.31 (s, 3H, ArCH<sub>3</sub>); **HRMS** (ES<sup>+</sup>): calculated for calculated for C<sub>72</sub>H<sub>108</sub>N<sub>12</sub> 1140.8820, found at  $[\text{M}^{12+}+\text{H}]^{2+}$  577.7996; **Elemental analysis calculated for (H<sub>12</sub>RCC3)<sup>12+</sup>.12 (2,4-dimethyl)-benzenesulfonate (%)**: C 56.76 H 6.81 N 4.98 S 11.39, found at C 59.71 H 7.84 N 7.04 S 850. (See **Appendix Figure 14** for NMR data).



**RCC3.12BARF** (100 mg, 0.063 mmol, 1 eq.) was dissolved in methanol (10 mL) and sodium tetrakis[3,5-bis(trifluoromethyl)phenyl]borate (673.5 mg, 0.76 mmol, 12 eq.) was added batch-wise. The reaction was set to stir at rt for 4 hrs and then added to water (100 mL) dropwise. The resulting precipitate was filtered through a nylon filter and **RCC3.12BARF** (0.211 g, 0.0183 mmol, 29%) was collected as a white powder.

IR ( $V_{\max}/\text{cm}^{-1}$ ): 3668.4, 2947.1, 1607.5, 1455.0, 1356.1, 1110.8, 888.2, 834.7, 708.9, 671.9;  $^1\text{H NMR}$  (400 MHz, acetone-d<sub>6</sub>):  $\delta$ 7.79 (br s, 2H, ArH), 7.67 (br s, 1H, ArH);  $^{19}\text{F NMR}$  (376 MHz, acetone-d<sub>6</sub>):  $\delta$ -64.28; **HRMS** (ES<sup>+</sup>): calculated for C<sub>72</sub>H<sub>108</sub>N<sub>12</sub> 1140.8820, found at  $\{\text{M}+\text{H}\}^{2+}$  571.4491; **Elemental analysis calculated for (H<sub>12</sub>RCC3)<sup>12+</sup>.12 BARF (%)**: C 46.17 N 6.30 H 13.46, found at C 45.83, 7.05, 12.93. (See **Appendix Figure 15** and **16** for NMR data).

### 7.5.7 Scale up of other BARF salts



**General procedure:** Reduced cage hydrochloride salt (1 eq.) dissolved in methanol (10 mL) and sodium tetrakis[3,5-bis(trifluoromethyl)phenyl]borate (12 eq.) batch-wise. The reaction was set to stir at rt for 4 hrs and the resulting precipitate was filtered through a nylon filter.

**RCC13.12BARF**

**RCC13** (44.4 mg, 0.0315 mmol, 1 eq.) and sodium tetrakis[3,5-bis(trifluoromethyl)phenyl]borate (335.0 mg, 0.378 mmol, 12 eq.) added. **RCC13.12BARF** (80 mg, 0.00704 mmol, 22%) collected as a brown solid.

**IR** ( $V_{\max}/\text{cm}^{-1}$ ): 3682.8, 2963.6, 1607.5, 1354.0, 1275.7, 1108.8, 884.1, 838.8, 671.9; **<sup>1</sup>H NMR** (400 MHz, acetone- $d_6$ ):  $\delta$  7.78 (br s, 2H, ArH), 7.66 (br s, ArH); **HRMS** (ES+): calculated for  $\text{C}_{60}\text{H}_{104}\text{N}_{12}$  984.7881, found at:  $[\text{M}+\text{H}]^{2+}$  493.3953; **Elemental analysis calculated for  $(\text{H}_{12}\text{RCC13})^{12+}$ .12 BARF (%)**: C 46.92 H 2.20 N 1.48, found at C 42.58 H 1.99 N 0.99. (See **Appendix Figure 17** for NMR data).

**R3<sup>3</sup>:R13<sup>3</sup>.12BARF**

**R3<sup>3</sup>:R13<sup>3</sup>** (93.8 mg, 0.063 mmol, 1 eq.) and sodium tetrakis[3,5-bis(trifluoromethyl)phenyl]borate (673.5 mg, 0.76 mmol, 12 eq.) added. **R3<sup>3</sup>:R13<sup>3</sup>.12BARF** (0.0195 g, 0.00187 mmol, 3%) was collected as a brown solid.

**IR** ( $V_{\max}/\text{cm}^{-1}$ ): 3695.2, 2973.9, 1613.7, 1356.1, 1275.7, 1112.9, 884.1, 711.0, 673.9, 451.3; **<sup>1</sup>H NMR** (400 MHz, acetone- $d_6$ ):  $\delta$  7.79 (br s, 2H, ArH), 7.67 (s, 2H, ArH); **HRMS** (ES+): calculated for  $3^013^6$ ,  $3^113^5$ ,  $3^213^4$ ,  $3^313^3$ ,  $3^413^2$ ,  $3^513^1$ ,  $3^613^0$ : 984.7881, 1010.8037, 103.8194, 1062.8350, 1088.8507, 1114.8663, 1140.8200, found at: 506.5236, 518.4049, 531.4114, 544.4198, 557.4262; **Elemental analysis calculated for  $(\text{H}_{12}\text{R3}^3:\text{R13}^3)^{12+}$ .12 BARF (%)**: C 47.27 H 2.27 N 1.47, found at C 45.43 H 2.39 N 1.86. (See **Appendix Figure 18** for NMR data).

**7.5.8 Solubility testing**

**General procedure:** **RCCX.12 trifluoromethanesulfonimide** (30 mg) was manually weighed into a 2 mL vial and ionic liquid was added in 0.1 mL increments using a disposable syringe. Between each addition, the sample was sonicated for 30 minutes and visually inspected to see if the solid had dissolved. If not, the procedure was repeated until the solid had dissolved.

**7.5.9 Gas sorption of cage ionic liquids**

**General procedure:** All materials were dried in a vacuum oven at 90 °C prior to measurements to remove any residual solvent. **RCC3.12TFSA** (100 mg) was dissolved in the selected ionic liquid (1 mL) using stirring and sonication. The porous liquid was degassed on the Quantachrome Nova at 298 K for 18 hours. After which, the gas sorption was run at 298

K up to 1 bar. The raw data was converted from P (mmHg) to P (bar) and from V (cc/g) to ( $\mu\text{mol g}^{-1}$ ) using the ideal gas law ( $n = PV/RT$ ). For the full data set, see **Appendix Table 68**.

## 7.6 References

- 1 M. Sun, C. Chen, L. Chen and B. Su, *Front. Chem. Sci. Eng.*, 2016, **10**, 301–347.
- 2 *International union of pure and applied chemistry physical chemistry division commission on colloid and surface chemistry including catalysis reporting physisorption data for gas/solid systems with Special Reference to the Determination of Surface Area and Porosity Reporting physisorption data for gas/solid systems-with special reference to the determination of surface area and porosity*, 1985.
- 3 M. E. Davis, *Nature*, 2002, 417, 813–821.
- 4 C. J. Kepert, *Porous Materials*, John Wiley & Sons, Incorporated, 1st edn., 2010.
- 5 A. G. Slater and A. I. Cooper, *Science*, 2015, **348**, 8075–8075.
- 6 C. M. A. Parlett, K. Wilson and A. F. Lee, *Chem. Soc. Rev.*, 2013, 42, 3876–3893.
- 7 Porous Materials: Process technology and applications - Kozo Ishizaki, Sridhar Komarneni, Makoto Nanko - Google Books, (accessed 5 November 2019).
- 8 Z. Fang, B. Bueken, D. E. De Vos and R. A. Fischer, *Angew. Chemie Int. Ed.*, 2015, **54**, 7234–7254.
- 9 C. Tang, B. Wang, H.-F. Wang and Q. Zhang, *Adv. Mater.*, 2017, **29**, 1703185.
- 10 G. Zhu, Y. Liu, L. Flores, Z. R. Lee, C. W. Jones, D. A. Dixon, D. S. Sholl and R. P. Lively, *Chem. Mater.*, 2018, **30**, 262–272.
- 11 A. Bavykina, A. Cadiau and J. Gascon, *Coord. Chem. Rev.*, 2019, **386**, 85–95.
- 12 J.-H. Zhang, S.-M. Xie, B.-J. Wang, P.-G. He and L.-M. Yuan, *J. Chromatogr. A*, 2015, **1426**, 174–182.
- 13 N. Giri, M. G. Del Pópolo, G. Melaugh, R. L. Greenaway, K. Rätzke, T. Koschine, L. Pison, M. F. C. Gomes, A. I. Cooper and S. L. James, *Nature*, 2015, **527**, 216–220.

- 14 N. O'Reilly, N. Giri and S. L. James, *Chem. - A Eur. J.*, 2007, **13**, 3020–3025.
- 15 J. Zhang, S.-H. Chai, Z.-A. Qiao, S. M. Mahurin, J. Chen, Y. Fang, S. Wan, K. Nelson, P. Zhang and S. Dai, *Angew. Chemie Int. Ed.*, 2015, **54**, 932–936.
- 16 E. B. Hemming, A. F. Masters and T. Maschmeyer, *Chem. Commun.*, 2019, **55**, 11179–11182.
- 17 J. T. Culp, *Flexible Solid Sorbents for CO<sub>2</sub> Capture and Separation*, Elsevier B.V., 2015.
- 18 H. G. Brittain, *Polymorphism in pharmaceutical solids*, Informa Healthcare, London, Second., 2009.
- 19 M. E. Aulton, *Aulton's Pharmaceutics: The design and manufacture of medicines*, Elsevier, Fifth., 2018.
- 20 J. Alemán, A. V. Chadwick, J. He, M. Hess, K. Horie, R. G. Jones, P. Kratochvíl, I. Meisel, I. Mita, G. Moad, S. Penczek and R. F. T. Stepto, *Pure Appl. Chem.*, 2007, **79**, 1801–1829.
- 21 P. J. Lu, E. Zaccarelli, F. Ciulla, A. B. Schofield, F. Sciortino and D. A. Weitz, *Nature*, 2008, **453**, 499–503.
- 22 A. Smart, Lesley E.; Moore, E, *Solid State Chemistry A n i n t r o d u c t i o n*, CRC Press, Fourth., 2012.
- 23 L. B. McCusker and C. Baerlocher, in *Studies in Surface Science and Catalysis*, 2007, vol. 168, pp. 13–37.
- 24 T. Maesen, in *Studies in Surface Science and Catalysis*, 2007, vol. 168, pp. 1–12.
- 25 B. F. Sels and L. M. Kustov, *Zeolites and Zeolite-like Materials*, Elsevier, 2016.
- 26 E. A. Pidko and E. J. M. Hensen, in *Zeolites and Zeolite-like Materials*, 2016, pp. 111–135.
- 27 Y. Park, K. Y. A. Lin, A. H. A. Park and C. Petit, *Front. Energy Res.*, 2015, 3, 42.
- 28 D. Wang, S. Song, W. Zhang, Z. He, Y. Wang, Y. Zheng, D. Yao, Y. Pan, Z. Yang, Z. Meng and Y. Li, *Sep. Purif. Technol.*, 2020, **241**, 116708.
- 29 K.-Y. A. Lin, C. Petit and A.-H. A. Park, *Energy & Fuels*, 2013, **27**, 4167–4174.

- 30 P. Li, R. Yang, Y. Zheng, P. Qu and L. Chen, *Carbon N. Y.*, 2015, **95**, 408–418.
- 31 C. J. Kepert, in *Porous Materials*, 2010, pp. 1–67.
- 32 J. R. Long and O. M. Yaghi, *Chem. Soc. Rev.*, 2009, 38, 1213–1214.
- 33 J. L. C. Rowsell and O. M. Yaghi, *Microporous Mesoporous Mater.*, 2004, 73, 3–14.
- 34 H. Li, M. Eddaoudi, M. O’Keeffe and O. M. Yaghi, *Nature*, 1999, **402**, 276–279.
- 35 X. Cui, K. Chen, H. Xing, Q. Yang, R. Krishna, Z. Bao, H. Wu, W. Zhou, X. Dong, Y. Han, B. Li, Q. Ren, M. J. Zaworotko and B. Chen, *Science*, 2016, **353**, 141–144.
- 36 P. Horcajada, T. Chalati, C. Serre, B. Gillet, C. Sebrie, T. Baati, J. F. Eubank, D. Heurtaux, P. Clayette, C. Kreuz, J. S. Chang, Y. K. Hwang, V. Marsaud, P. N. Bories, L. Cynober, S. Gil, G. Férey, P. Couvreur and R. Gref, *Nat. Mater.*, 2010, **9**, 172–178.
- 37 H. Furukawa, K. E. Cordova, M. O’Keeffe and O. M. Yaghi, *Science*, 2013, 341.
- 38 L. Alaerts, E. Séguin, H. Poelman, F. Thibault-Starzyk, P. A. Jacobs and D. E. De Vos, *Chem. - A Eur. J.*, 2006, **12**, 7353–7363.
- 39 R. E. Morris and P. S. Wheatley, *Angew. Chemie Int. Ed.*, 2008, **47**, 4966–4981.
- 40 A. J. Tansell, C. L. Jones and T. L. Easun, *Chem. Cent. J.*, 2017, **11**, 100.
- 41 L. Li, S. Xiang, S. Cao, J. Zhang, G. Ouyang, L. Chen and C.-Y. Su, *Nat. Commun.*, 2013, **4**, 1774.
- 42 T. D. Bennett, A. K. Cheetham, A. H. Fuchs and F. X. Coudert, *Nat. Chem.*, 2016, 9, 11–16.
- 43 H. Wu, Y. S. Chua, V. Krungleviciute, M. Tyagi, P. Chen, T. Yildirim and W. Zhou, *J. Am. Chem. Soc.*, 2013, **135**, 10525–10532.
- 44 T. D. Bennett, Y. Yue, P. Li, A. Qiao, H. Tao, N. G. Greaves, T. Richards, G. I. Lampronti, S. A. T. Redfern, F. Blanc, O. K. Farha, J. T. Hupp, A. K. Cheetham and D. A. Keen, *J. Am. Chem. Soc.*, 2016, **138**, 3484–3492.
- 45 J. M. Tuffnell, C. W. Ashling, J. Hou, S. Li, L. Longley, M. L. Ríos Gómez and T. D. Bennett, *Chem. Commun.*, 2019, **55**, 8705–8715.

- 46 C. Zhou, L. Longley, A. Krajnc, G. J. Smales, A. Qiao, I. Erucar, C. M. Doherty, A. W. Thornton, A. J. Hill, C. W. Ashling, O. T. Qazvini, S. J. Lee, P. A. Chater, N. J. Terrill, A. J. Smith, Y. Yue, G. Mali, D. A. Keen, S. G. Telfer and T. D. Bennett, *Nat. Commun.*, 2018, **9**, 5042.
- 47 Y. Zhang and S. N. Riduan, *Chem. Soc. Rev.*, 2012, **41**, 2083–2094.
- 48 L. Zou, Y. Sun, S. Che, X. Yang, X. Wang, M. Bosch, Q. Wang, H. Li, M. Smith, S. Yuan, Z. Perry and H. C. Zhou, *Adv. Mater.*, 2017, **29**, 1–35.
- 49 P. Kaur, J. T. Hupp and S. T. Nguyen, *ACS Catal.*, 2011, **1**, 819–835.
- 50 M. Liu, L. Guo, S. Jin and B. Tan, *J. Mater. Chem. A*, 2019, **7**, 5153–5172.
- 51 M. J. Bojdys, J. Jeromenok, A. Thomas and M. Antonietti, *Adv. Mater.*, 2010, **22**, 2202–2205.
- 52 Y. Xu, S. Jin, H. Xu, A. Nagai and D. Jiang, *Chem. Soc. Rev.*, 2013, **42**, 8012–8031.
- 53 A. I. Cooper, *Adv. Mater.*, 2009, **21**, 1291–1295.
- 54 R. Dawson, A. Laybourn, R. Clowes, Y. Z. Khimiyak, D. J. Adams and A. I. Cooper, *Macromolecules*, 2009, **42**, 8809–8816.
- 55 Y. Xie, T. T. Wang, X. H. Liu, K. Zou and W. Q. Deng, *Nat. Commun.*, 2013, **4**, 1–7.
- 56 T. Ben, H. Ren, S. Ma, D. Cao, J. Lan, X. Jing, W. Wang, J. Xu, F. Deng, J. M. Simmons, S. Qiu and G. Zhu, *Angew. Chemie Int. Ed.*, 2009, **48**, 9457–9460.
- 57 C. Pei, T. Ben and S. Qiu, *Mater. Horizons*, 2015, **2**, 11–21.
- 58 J. R. Holst, E. Stöckel, D. J. Adams and A. I. Cooper, *Macromolecules*, 2010, **43**, 8531–8538.
- 59 G. Wu, X. Chen, Y. Li and Z. Jia, *Microporous Mesoporous Mater.*, 2019, **279**, 19–25.
- 60 U. Díaz and A. Corma, *Coord. Chem. Rev.*, 2016, **311**, 85–124.
- 61 T. Ben and S. Qiu, *CrystEngComm*, 2013, **15**, 17–26.
- 62 J. D. Evans, C. J. Sumby and C. J. Doonan, *Chem. Lett.*, 2015, **44**, 582–588.



- 63 N. Ahmad, H. A. Younus, A. H. Chughtai and F. Verpoort, *Chem. Soc. Rev.*, 2015, **44**, 9–25.
- 64 T. M. Phan and J. C. Huie, *Guided molecular self-assembly: a review of recent efforts Recent citations Catalystlike role of impurities in speeding layer-by-layer growth Guided molecular self-assembly: a review of recent efforts*, 2003.
- 65 S. Tothadi, M. A. Little, T. Hasell, M. E. Briggs, S. Y. Chong, M. Liu and A. I. Cooper, *CrystEngComm*, 2017, **19**, 4933–4941.
- 66 T. Frišćić, *Chem. Soc. Rev.*, 2012, **41**, 3493–3510.
- 67 T. Hasell, S. Y. Chong, K. E. Jelfs, D. J. Adams and A. I. Cooper, *J. Am. Chem. Soc.*, 2012, **134**, 588–598.
- 68 M. Pan, K. Wu, J. H. Zhang and C. Y. Su, *Coord. Chem. Rev.*, 2019, **378**, 333–349.
- 69 D. J. Tranchemontagne, Z. Ni, M. O’Keeffe and O. M. Yaghi, *Angew. Chemie Int. Ed.*, 2008, **47**, 5136–5147.
- 70 M. Jung, H. Kim, K. Baek and K. Kim, *Angew. Chemie Int. Ed.*, 2008, **47**, 5755–5757.
- 71 T. Kikuchi, S. Sato and M. Fujita, *J. Am. Chem. Soc.*, 2010, **132**, 15930–15932.
- 72 K. Wu, K. Li, Y.-J. Hou, M. Pan, L.-Y. Zhang, L. Chen and C.-Y. Su, *Nat. Commun.*, 2016, **7**, 10487.
- 73 T. Liu, Y. Liu, W. Xuan and Y. Cui, *Angew. Chemie Int. Ed.*, 2010, **49**, 4121–4124.
- 74 K. Li, L. Y. Zhang, C. Yan, S. C. Wei, M. Pan, L. Zhang and C. Y. Su, *J. Am. Chem. Soc.*, 2014, **136**, 4456–4459.
- 75 F. J. Rizzuto, L. K. S. von Krbek and J. R. Nitschke, *Nat. Rev. Chem.*, 2019, **3**, 204–222.
- 76 E. J. Gosselin, C. A. Rowland and E. D. Bloch, *Chem. Rev.*, 2020, **120**, 8987–9014.
- 77 G. R. Lorzing, E. J. Gosselin, B. A. Trump, A. H. P. York, A. Sturluson, C. A. Rowland, G. P. A. Yap, C. M. Brown, C. M. Simon and E. D. Bloch, *J. Am. Chem. Soc.*, 2019, **141**, 12128–12138.
- 78 J. R. Li and H. C. Zhou, *Nat. Chem.*, 2010, **2**, 893–898.

- 79 J. L. Bolliger, A. M. Belenguer and J. R. Nitschke, *Angew. Chemie Int. Ed.*, 2013, **52**, 7958–7962.
- 80 J. R. Li, D. J. Timmons and H. C. Zhou, *J. Am. Chem. Soc.*, 2009, **131**, 6368–6369.
- 81 M. H. Alkordi, J. A. Brant, L. Wojtas, V. C. Kravtsov, A. J. Cairns and M. Eddaoudi, *J. Am. Chem. Soc.*, 2009, **131**, 17753–17755.
- 82 A. V. Zhukhovitskiy, M. Zhong, E. G. Keeler, V. K. Michaelis, J. E. P. Sun, M. J. A. Hore, D. J. Pochan, R. G. Griffin, A. P. Willard and J. A. Johnson, *Nat. Chem.*, 2016, **8**, 33–41.
- 83 M. E. Briggs and A. I. Cooper, *Chem. Mater.*, 2017, **29**, 149–157.
- 84 T. Tozawa, J. T. A. Jones, S. I. Swamy, S. Jiang, D. J. Adams, S. Shakespeare, R. Clowes, D. Bradshaw, T. Hasell, S. Y. Chong, C. Tang, S. Thompson, J. Parker, A. Trewin, J. Bacsá, A. M. Z. Slawin, A. Steiner and A. I. Cooper, *Nat. Mater.*, 2009, **8**, 973–978.
- 85 T. Hasell and A. I. Cooper, *Nat. Rev. Mater.*, 2016, **1**, 16053.
- 86 J. C. Lauer, W. S. Zhang, F. Rominger, R. R. Schröder and M. Mastalerz, *Chem. - A Eur. J.*, 2018, **24**, 1816–1820.
- 87 C. C. Pattillo and J. S. Moore, *Chem. Sci.*, 2019, **10**, 7043–7048.
- 88 S. Jiang, J. T. A. Jones, T. Hasell, C. E. Blythe, D. J. Adams, A. Trewin and A. I. Cooper, *Nat. Commun.*, 2011, **2**, 207.
- 89 S. Lee, A. Yang, T. P. Money Penny and J. S. Moore, *J. Am. Chem. Soc.*, 2016, **138**, 2182–2185.
- 90 T. A. Robbins, C. B. Knobler, D. R. Bellew and D. J. Cram, *J. Am. Chem. Soc.*, 1994, **116**, 111–122.
- 91 K. E. Chaffee, H. A. Fogarty, T. Brotin, B. M. Goodson and J.-P. Dutasta, *J. Phys. Chem. A*, 2009, **113**, 13675–13684.
- 92 A. Bavykina, A. Cadiou and J. Gascon, *Coord. Chem. Rev.*, 2019, **386**, 85–95.
- 93 S. C. N. Hsu, M. Ramesh, J. H. Espenson and T. B. Rauchfus, *Angew. Chemie - Int. Ed.*, 2003, **42**, 2663–2666.

- 94 J. Zhang, S. H. Chai, Z. A. Qiao, S. M. Mahurin, J. Chen, Y. Fang, S. Wan, K. Nelson, P. Zhang and S. Dai, *Angew. Chemie - Int. Ed.*, 2015, **54**, 932–936.
- 95 E. B. Hemming, A. F. Masters and T. Maschmeyer, *Chem. – A Eur. J.*, 2020, **26**, 7059-7064.
- 96 R. Kumar, P. Dhasaiyan, P. M. Naveenkumar and K. P. Sharma, *Nanoscale Adv.*, 2019, **1**, 4067–4075.
- 97 P. Li, J. A. Schott, J. Zhang, S. M. Mahurin, Y. Sheng, Z.-A. Qiao, X. Hu, G. Cui, D. Yao, S. Brown, Y. Zheng and S. Dai, *Angew. Chemie*, 2017, **129**, 15154–15158.
- 98 M. Costa Gomes, L. Pison, C. Červinka and A. Padua, *Angew. Chemie Int. Ed.*, 2018, **57**, 11909–11912.
- 99 P. Li, H. Chen, J. A. Schott, B. Li, Y. Zheng, S. M. Mahurin, B. De-En Jiang, G. Cui, X. Hu, Y. Wang, L. Li and S. Dai, *Nanoscale*, 2019, **11**, 1515–1519.
- 100 X. Wang, D. Shang, S. Zeng, Y. Wang, X. Zhang, X. Zhang and J. Liu, *J. Chem. Thermodyn.*, 2019, **128**, 415–423.
- 101 S. Liu, J. Liu, X. Hou, T. Xu, J. Tong, J. Zhang, B. Ye and B. Liu, *Langmuir*, 2018, **34**, 3654–3660.
- 102 W. Shan, P. F. Fulvio, L. Kong, J. A. Schott, C.-L. Do-Thanh, T. Tian, X. Hu, S. M. Mahurin, H. Xing and S. Dai, *ACS Appl. Mater. Interfaces*, 2018, **10**, 32–36.
- 103 J. Cahir, M. Y. Tsang, B. Lai, D. Hughes, M. A. Alam, J. Jacquemin, D. Rooney and S. L. James, *Chem. Sci.*, 2020, **11**, 2077–2084.
- 104 X. Zhao, Y. Yuan, P. Li, Z. Song, C. Ma, D. Pan, S. Wu, T. Ding, Z. Guo and N. Wang, *Chem. Commun.*, 2019, **55**, 13179–13182.
- 105 H. Liu, B. Liu, L.-C. Lin, G. Chen, Y. Wu, J. Wang, X. Gao, Y. Lv, Y. Pan, X. Zhang, X. Zhang, L. Yang, C. Sun, B. Smit and W. Wang, *Nat. Commun.*, 2014, **5**, 5147.
- 106 S. He, L. Chen, J. Cui, B. Yuan, H. Wang, F. Wang, Y. Yu, Y. Lee and T. Li, *J. Am. Chem. Soc.*, 2019, **141**, 19708–19714.
- 107 M. Costa Gomes, L. Pison, C. Červinka and A. Padua, *Angew. Chemie*, 2018, **130**, 12085–12088.

- 108 P. Li, H. Chen, J. A. Schott, B. Li, Y. Zheng, S. M. Mahurin, D. Jiang, G. Cui, X. Hu, Y. Wang, L. Li and S. Dai, *Nanoscale*, 2019, **11**, 1515–1519.
- 109 L. Ma, C. J. E. Haynes, A. B. Grommet, A. Walczak, C. C. Parkins, C. M. Doherty, L. Longley, A. Tron, A. R. Stefankiewicz, T. D. Bennett and J. R. Nitschke, *Nat. Chem.*, 2020, **12**, 270–275.
- 110 N. Giri, C. E. Davidson, G. Melaugh, M. G. Del Pópolo, J. T. A. Jones, T. Hasell, A. I. Cooper, P. N. Horton, M. B. Hursthouse and S. L. James, *Chem. Sci.*, 2012, **3**, 2153.
- 111 G. Melaugh, N. Giri, C. E. Davidson, S. L. James and M. G. Del Pópolo, *Phys. Chem. Chem. Phys.*, 2014, **16**, 9422–9431.
- 112 R. L. Greenaway, D. Holden, E. G. B. Eden, A. Stephenson, C. W. Yong, M. J. Bennison, T. Hasell, M. E. Briggs, S. L. James and A. I. Cooper, *Chem. Sci.*, 2017, **8**, 2640–2651.
- 113 K. Jie, N. Onishi, J. A. Schott, I. Popovs, D. en Jiang, S. Mahurin and S. Dai, *Angew. Chemie - Int. Ed.*, 2020, **59**, 2268–2272.
- 114 D. Y. Oh, Y. J. Nam, K. H. Park, S. H. Jung, S.-J. Cho, Y. K. Kim, Y.-G. Lee, S.-Y. Lee and Y. S. Jung, *Adv. Energy Mater.*, 2015, **5**, 1500865.
- 115 K. Ueno, K. Yoshida, M. Tsuchiya, N. Tachikawa, K. Dokko and M. Watanabe, *J. Phys. Chem. B*, 2012, **116**, 11323–11331.
- 116 T. Mandai, K. Yoshida, K. Ueno, K. Dokko and M. Watanabe, *Phys. Chem. Chem. Phys.*, 2014, **16**, 8761.
- 117 D. J. Eyckens, M. E. Champion, B. L. Fox, P. Yoganantharajah, Y. Gibert, T. Welton and L. C. Henderson, *European J. Org. Chem.*, 2016, **2016**, 913–917.
- 118 B. D. Egleston, K. V. Luzyanin, M. C. Brand, R. Clowes, M. E. Briggs, R. L. Greenaway and A. I. Cooper, *Angew. Chemie*, 2020, **132**, 7432–7436.
- 119 A. G. Slater, P. S. Reiss, A. Pulido, M. A. Little, D. L. Holden, L. Chen, S. Y. Chong, B. M. Alston, R. Clowes, M. Haranczyk, M. E. Briggs, T. Hasell, G. M. Day and A. I. Cooper, *ACS Cent. Sci.*, 2017, **3**, 734–742.
- 120 S. Jiang, J. T. A. Jones, T. Hasell, C. E. Blythe, D. J. Adams, A. Trewin and A. I. Cooper, *Nat. Commun.*, 2011, **2**, 207.

- 121 T. Tozawa, J. T. A. Jones, S. I. Swamy, S. Jiang, D. J. Adams, S. Shakespeare, R. Clowes, D. Bradshaw, T. Hasell, S. Y. Chong, C. Tang, S. Thompson, J. Parker, A. Trewin, J. Bacsa, A. M. Z. Slawin, A. Steiner and A. I. Cooper, *Nat. Mater.*, 2009, **8**, 973–978.
- 122 T. Hasell, J. L. Culshaw, S. Y. Chong, M. Schmidtman, M. A. Little, K. E. Jelfs, E. O. Pyzer-Knapp, H. Shepherd, D. J. Adams, G. M. Day and A. I. Cooper, *J. Am. Chem. Soc.*, 2014, **136**, 1438–1448.
- 123 N. Giri, C. E. Davidson, G. Melaugh, M. G. Del Pópolo, J. T. A. Jones, T. Hasell, A. I. Cooper, P. N. Horton, M. B. Hursthouse and S. L. James, *Chem. Sci.*, 2012, **3**, 2153.
- 124 M. E. Briggs, A. G. Slater, N. Lunt, S. Jiang, M. A. Little, R. L. Greenaway, T. Hasell, C. Battilocchio, S. V. Ley and A. I. Cooper, *Chem. Commun.*, 2015, **51**, 17390–17393.
- 125 E. H. Kerns, *J. Pharm. Sci.*, 2001, **90**, 1838–1858.
- 126 J. Alsenz and M. Kansy, *Adv. Drug Deliv. Rev.*, 2007, **59**, 546–567.
- 127 K. Kwon and S. N. Peterson, *Methods Mol. Biol.*, 2014, **1140**, 75–88.
- 128 F. Blanc, S. Y. Chong, T. O. McDonald, D. J. Adams, S. Pawsey, M. A. Caporini and A. I. Cooper, *J. Am. Chem. Soc.*, 2013, **135**, 15290–15293.
- 129 T. Willhammar, J. Su, Y. Yun, X. Zou, M. Afeworki, S. C. Weston, H. B. Vroman, W. W. Loneragan and K. G. Strohmaier, *Inorg. Chem.*, 2017, **56**, 8856–8864.
- 130 R. Banerjee, A. Phan, B. Wang, C. Knobler, H. Furukawa, M. O’Keeffe and O. M. Yaghi, *Science*, 2008, **319**, 939–943.
- 131 R. Lai, B. S. Kang and G. R. Gavalas, *Angew. Chemie - Int. Ed.*, 2001, **40**, 408–411.
- 132 P. Wollmann, M. Leistner, U. Stoeck, R. Grünker, K. Gedrich, N. Klein, O. Throl, W. Grählert, I. Senkovska, F. Dreisbach and S. Kaskel, *Chem. Commun.*, 2011, **47**, 5151.
- 133 S. Han, Y. Huang, T. Watanabe, Y. Dai, K. S. Walton, S. Nair, D. S. Sholl and J. C. Meredith, *ACS Comb. Sci.*, 2012, **14**, 263–267.
- 134 R. L. Greenaway, V. Santolini, M. J. Bennison, B. M. Alston, C. J. Pugh, M. A. Little, M. Miklitz, E. G. B. Eden-Rump, R. Clowes, A. Shakil, H. J. Cuthbertson, H. Armstrong, M. E. Briggs, K. E. Jelfs and A. I. Cooper, *Nat. Commun.*, 2018, **9**, 2849.

- 135 D. Beaudoin, F. Rominger and M. Mastalerz, *Angew. Chemie Int. Ed.*, 2017, **56**, 1244–1248.
- 136 J. T. A. Jones, T. Hasell, X. Wu, J. Bacsa, K. E. Jelfs, M. Schmidtman, S. Y. Chong, D. J. Adams, A. Trewin, F. Schiffman, F. Cora, B. Slater, A. Steiner, G. M. Day and A. I. Cooper, *Nature*, 2011, **474**, 367–371.
- 137 T. Hasell, S. Y. Chong, K. E. Jelfs, D. J. Adams and A. I. Cooper, *J. Am. Chem. Soc.*, 2012, **134**, 588–598.
- 138 T. Hasell, M. A. Little, S. Y. Chong, M. Schmidtman, M. E. Briggs, V. Santolini, K. E. Jelfs and A. I. Cooper, *Nanoscale*, 2017, **9**, 6783–6790.
- 139 F. Beuerle and B. Gole, *Angew. Chemie Int. Ed.*, 2018, **57**, 4850–4878.
- 140 T. Hasell, S. Y. Chong, M. Schmidtman, D. J. Adams and A. I. Cooper, *Angew. Chemie Int. Ed.*, 2012, **51**, 7154–7157.
- 141 P. S. Reiss, M. A. Little, V. Santolini, S. Y. Chong, T. Hasell, K. E. Jelfs, M. E. Briggs and A. I. Cooper, *Chem. - A Eur. J.*, 2016, **22**, 16547–16553.
- 142 F. Huguenot, T. Brigaud, R. Cedex, L. Synthe and M. G. V, 2006, **71**, 7075–7078.
- 143 M. T. Reetz, R. Jaeger, R. Drewlies and M. Hübel, *Angew. Chemie Int. Ed. English*, 1991, **30**, 103–106.
- 144 Z. Zhang, S. Hu, J. Song, W. Li, G. Yang and B. Han, *ChemSusChem*, 2009, **2**, 234–238.
- 145 A. S. Kucherenko, A. A. Kostenko, V. V. Gerasimchuk and S. G. Zlotin, *Org. Biomol. Chem.*, 2017, **15**, 7028–7033.
- 146 A. S. Kucherenko, A. A. Kostenko, G. M. Zhdankina, O. Y. Kuznetsova and S. G. Zlotin, *Green Chem.*, 2018, **20**, 754–759.
- 147 J. Chin, S. H. Kwon, H. Kim, P. Chin, S. M. So and B. M. Kim, *European J. Org. Chem.*, 2014, **2014**, 725–730.
- 148 H. Kim, Y. Nguyen, A. J. Lough and J. Chin, *Angew. Chemie - Int. Ed.*, 2008, **47**, 8678–8681.
- 149 H. Kim, M. Staikova, A. J. Lough and J. Chin, *Org. Lett.*, 2009, **11**, 157–160.

- 150 M. Kim, H. Kim, H. Kim and J. Chin, *J. Org. Chem.*, 2017, **82**, 12050–12058.
- 151 H. Kim, Y. Nguyen, C. P. H. Yen, L. Chagal, A. J. Lough, B. M. Kim and J. Chin, *J. Am. Chem. Soc.*, 2008, **130**, 12184–12191.
- 152 H. Kim, *Phd Thesis*.
- 153 D. N. Lee, H. Kim, L. Mui, S. W. Myung, J. Chin and H. J. Kim, *J. Org. Chem.*, 2009, **74**, 3330–3334.
- 154 S. M. Xie, J. H. Zhang, N. Fu, B. J. Wang, L. Chen and L. M. Yuan, *Anal. Chim. Acta*, 2016, **903**, 156–163.
- 155 M. J. Bojdys, M. E. Briggs, J. T. A. Jones, D. J. Adams, S. Y. Chong, M. Schmidtman and A. I. Cooper, *J. Am. Chem. Soc.*, 2011, **133**, 16566–16571.
- 156 T. Hasell, J. L. Culshaw, S. Y. Chong, M. Schmidtman, M. A. Little, K. E. Jelfs, E. O. Pyzer-Knapp, H. Shepherd, D. J. Adams, G. M. Day and A. I. Cooper, *J. Am. Chem. Soc.*, 2014, **136**, 1438–1448.
- 157 L. Chen, P. S. Reiss, S. Y. Chong, D. Holden, K. E. Jelfs, T. Hasell, M. A. Little, A. Kewley, M. E. Briggs, A. Stephenson, K. M. Thomas, J. A. Armstrong, J. Bell, J. Busto, R. Noel, J. Liu, D. M. Strachan, P. K. Thallapally and A. I. Cooper, *Nat. Mater.*, 2014, **13**, 954–960.
- 158 M. M. Safont-Sempere, G. Fernández and F. Würthner, *Chem. Rev.*, 2011, **111**, 5784–5814.
- 159 A. Wu and L. Isaacs, *J. Am. Chem. Soc.*, 2003, **125**, 4831–4835.
- 160 K. Ono and N. Iwasawa, *Chem. – A Eur. J.*, 2018, **24**, 17856–17868.
- 161 A. Avellaneda, P. Valente, A. Burgun, J. D. Evans, A. W. Markwell-Heys, D. Rankine, D. J. Nielsen, M. R. Hill, C. J. Sumbly and C. J. Doonan, *Angew. Chemie Int. Ed.*, 2013, **52**, 3746–3749.
- 162 T. Hasell, X. Wu, J. T. A. Jones, J. Bacsa, A. Steiner, T. Mitra, A. Trewin, D. J. Adams and A. I. Cooper, *Nat. Chem.*, 2010, **2**, 750–755.
- 163 Q. Wang, C. Yu, H. Long, Y. Du, Y. Jin and W. Zhang, *Angew. Chemie Int. Ed.*, 2015, **54**, 7550–7554.

- 164 G. Zhang, O. Presly, F. White, I. M. Oppel and M. Mastalerz, *Angew. Chemie Int. Ed.*, 2014, **53**, 1516-1520.
- 165 K. Acharyya, S. Mukherjee and P. S. Mukherjee, *J. Am. Chem. Soc.*, 2013, **135**, 554–557.
- 166 T. Jiao, G. Wu, L. Chen, C.-Y. Wang and H. Li, *J. Org. Chem.*, 2018, **83**, 12404–12410.
- 167 D. Beaudoin, F. Rominger and M. Mastalerz, *Angew. Chemie Int. Ed.*, 2017, **56**, 1244–1248.
- 168 G. Zhu, C. D. Hoffman, Y. Liu, S. Bhattacharyya, U. Tumuluri, M. L. Jue, Z. Wu, D. S. Sholl, S. Nair, C. W. Jones and R. P. Lively, *Chem. - A Eur. J.*, 2016, **22**, 10743–10747.
- 169 A. G. Slater, M. A. Little, M. E. Briggs, K. E. Jelfs and A. I. Cooper, *Mol. Syst. Des. Eng.*, 2018, **3**, 223–227.
- 170 A. G. Slater, P. S. Reiss, A. Pulido, M. A. Little, D. L. Holden, L. Chen, S. Y. Chong, B. M. Alston, R. Clowes, M. Haranczyk, M. E. Briggs, T. Hasell, G. M. Day and A. I. Cooper, *ACS Cent. Sci.*, 2017, **3**, 734–742.
- 171 R. L. Greenaway, V. Santolini, A. Pulido, M. A. Little, B. M. Alston, M. E. Briggs, G. M. Day, A. I. Cooper and K. E. Jelfs, *Angew. Chemie*, 2019, **131**, 16421–16427.
- 172 G. Zhu, Y. Liu, L. Flores, Z. R. Lee, C. W. Jones, D. A. Dixon, D. S. Sholl and R. P. Lively, *Chem. Mater.*, 2018, **30**, 262–272.
- 173 V. Santolini, M. Miklitz, E. Berardo and K. E. Jelfs, *Nanoscale*, 2017, **9**, 5280–5298.
- 174 J. T. A. Jones, D. Holden, T. Mitra, T. Hasell, D. J. Adams, K. E. Jelfs, A. Trewin, D. J. Willock, G. M. Day, J. Bacsá, A. Steiner and A. I. Cooper, *Angew. Chemie - Int. Ed.*, 2011, **50**, 749–753.
- 175 M. A. Little, S. Y. Chong, M. Schmidtman, T. Hasell and A. I. Cooper, *Chem. Commun.*, 2014, **50**, 9465–9468.
- 176 J. Tian, P. K. Thallapally and B. P. McGrail, *CrystEngComm*, 2012, **14**, 1909.
- 177 S. Komulainen, J. Roukala, V. V. Zhivonitko, M. A. Javed, L. Chen, D. Holden, T. Hasell, A. Cooper, P. Lantto and V.-V. Telkki, *Chem. Sci.*, 2017, **8**, 5721–5727.
- 178 X. Zhou, P. fei Xie, J. Wang, B. bei Zhang, M. ming Liu, H. lan Liu and X. han Feng, *J.*



- Chromatogr. A*, 2011, **1218**, 3571–3580.
- 179 M. Liu, M. A. Little, K. E. Jelfs, J. T. A. Jones, M. Schmidtman, S. Y. Chong, T. Hasell and A. I. Cooper, *J. Am. Chem. Soc.*, 2014, **136**, 7583–7586.
- 180 S. I. Swamy, J. Bacsá, J. T. A. Jones, K. C. Stylianou, A. Steiner, L. K. Ritchie, T. Hasell, J. A. Gould, A. Laybourn, Y. Z. Khimyak, D. J. Adams, M. J. Rosseinsky and A. I. Cooper, *J. Am. Chem. Soc.*, 2010, **132**, 12773–12775.
- 181 J. L. Culshaw, G. Cheng, M. Schmidtman, T. Hasell, M. Liu, D. J. Adams and A. I. Cooper, *J. Am. Chem. Soc.*, 2013, **135**, 10007–10010.
- 182 M. Liu, L. Chen, S. Lewis, S. Y. Chong, M. A. Little, T. Hasell, I. M. Aldous, C. M. Brown, M. W. Smith, C. A. Morrison, L. J. Hardwick and A. I. Cooper, *Nat. Commun.*, 2016, **7**, 12750.
- 183 S. Mallakpour and M. Dinari, in *Green Solvents II: Properties and Applications of Ionic Liquids*, Springer Netherlands, Dordrecht, 2012, pp. 1–32.
- 184 R. Hayes, G. G. Warr and R. Atkin, *Chem. Rev.*, 2015, **115**, 6357–6426.
- 185 Y. Yoshimura, T. Takekiyo, Y. Imai and H. Abe, *Most*, 2011, 171–186.
- 186 P. A. Hunt, C. R. Ashworth and R. P. Matthews, *Chem. Soc. Rev.*, 2015, **44**, 1257–1288.
- 187 M. Kaliner and T. Strassner, *Tetrahedron Lett.*, 2016, **57**, 3453–3456.
- 188 B. Clare, A. Sirwardana and D. R. MacFarlane, in *Topics in Current Chemistry*, Springer, Berlin, Heidelberg, 2009, vol. 290, pp. 1–40.
- 189 M. Liu, L. Chen, S. Lewis, S. Y. Chong, M. A. Little, T. Hasell, I. M. Aldous, C. M. Brown, M. W. Smith, C. A. Morrison, L. J. Hardwick and A. I. Cooper, *Nat. Commun.*, 2016, **7**, 12750.
- 190 L. C. Brown, J. . Hogg and M. Swadzba-Kwasny, *Polymerized Ionic Liquids - Google Books*, 2018.
- 191 J. H. Davis Jr, C. M. Gordon, C. Hilgers and P. Wasserscheid, *Synthesis and purification of ionic liquids*, Elsevier B.V., 2002.

- 192 S. Chen, J. Ishii, S. Horiuchi, M. Yoshizawa-Fujita and E. I. Izgorodina, *Phys. Chem. Chem. Phys.*, 2017, **19**, 17366–17372.
- 193 A. Stark, P. Behrend, O. Braun, A. Müller, J. Ranke, B. Ondruschka and B. Jastorff, *Green Chem.*, 2008, **10**, 1152.
- 194 P. G. Debenedetti and F. H. Stillinger, *Nature*, 2001, **410**, 259.
- 195 J. M. Hutchinson, *J. Therm. Anal. Calorim.*, 2009, **98**, 579–589.
- 196 M. Liu, L. Chen, S. Lewis, S. Y. Chong, M. A. Little, T. Hasell, I. M. Aldous, C. M. Brown, M. W. Smith, C. A. Morrison, L. J. Hardwick and A. I. Cooper, *Nat. Commun.*, 2016, **7**, 12750.
- 197 B. F. Goodrich, J. C. de la Fuente, B. E. Gurkan, Z. K. Lopez, E. A. Price, Y. Huang and J. F. Brennecke, *J. Phys. Chem. B*, 2011, **115**, 9140–9150.
- 198 S. Stevanovic, A. Podgoršek, A. A. H. Pádua and M. F. Costa Gomes, *J. Phys. Chem. B*, 2012, **116**, 14416–14425.
- 199 NIST Chemistry WebBook, <https://webbook.nist.gov/chemistry/>, (accessed 1 August 2018).
- 200 G. M. Sheldrick, *Acta Crystallogr. Sect. A Found. Adv.*, 2015, **71**, 3–8.
- 201 O. V. Dolomanov, L. J. Bourhis, R. J. Gildea, J. A. K. Howard and H. Puschmann, *J. Appl. Crystallogr.*, 2009, **42**, 339–341.
- 202 O. Kuzmina and J. P. Hallett, *Application, Purification, and Recovery of Ionic Liquids*, 2016.
- 203 B. R. Caes, J. B. Binder, J. J. Blank and R. T. Raines, *Green Chem.*, 2011, **13**, 2719.
- 204 R. Fareghi-Alamdari and R. Hatefipour, *J. Mol. Liq.*, 2017, **225**, 793–799.
- 205 D. Mecerreyes, *Prog. Polym. Sci.*, 2011, **36**, 1629–1648.

# Appendices

## Chapter 2

**Appendix Table 1:** Conditions for the trial **3<sup>3</sup>:13<sup>3</sup>** scrambled cage synthesis using 1,2-diamino-2-methylpropane (Amine **A**) and (1*S*,2*S*)-(+)-1,2-diaminocyclohexane (Amine **E**) with 1,3,5-triformylbenzene (TFB) in DCM (60mL). Briefly, a solution of Amine **A** (3.0 eq.) in DCM (15 mL), and a solution of Amine **E** (3.0 eq.) in DCM (15 mL), were added to TFB (4 eq.) in DCM (30mL), and the resulting solution was stirred at room temperature for 72 hours. The solvent was then removed under reduced pressure, and the crude product re-dissolved in DCM and filtered to remove any insoluble precipitate. The solvent was removed in vacuo, before the solid was subsequently washed with ethyl acetate and the purified product collected by filtration.

	Mass of TFB (mg)	Mass of Amine A (mg)	Mass of Amine E (mg)	Volume of DCM (mL)	Mass recovery (g)	Yield (%)
<b>Original concentration</b> <sup>13</sup>	166.0	88.0	67.7	60	0.25	24
<b>3 times as concentrated</b>	498.0	263.0	203.0	60	0.57	54

**Appendix Table 2:** Summary of stock solutions in chloroform prepared for the high-throughput synthetic screen

Stock solution number	Reactant	MW (g/mol)	Stock solution concentration (mg/mL)	Stock solution concentration (mmol/mL)	Total volume of stock solution required (mL)	Total volume of stock solution made (mL)	Mass of reactant required for stock solution (g)	NEt <sub>3</sub> required per reaction (mmol/mL, 3.3 eq)	Total volume of NEt <sub>3</sub> added to stock solution (mL)
1	TFB	162.14	20	0.12	1341.61	1650.00	33.00	-	-
2	Amine A	88.15	20	0.23	408.86	500.00	10.00	-	-
3	Amine B	60.1	20	0.33	48.65	50.00	1.00	-	-
4*	Amine C	147.04	20	0.14	119.03	130.00	2.60	0.45	8.13
5	Amine D	114.19	20	0.18	92.44	95.00	1.90	-	-
6	Amine E	114.19	20	0.18	92.44	95.00	1.90	-	-
7	Amine F	212.3	30	0.14	120.96	125.00	3.75	-	-
8*	Amine G	217.18	30	0.14	106.20	95.00	2.85	0.46	5.08
9	Amine H	144.26	30	0.21	28.41	30.00	0.90	-	-
10	Amine I	200.37	30	0.15	49.23	40.00	1.20	-	-
11*	Amine J	297.31	30	0.10	53.46	55.00	1.65	0.33	5.11
12	Amine K	74.13	20	0.27	60.01	65.00	1.30	-	-

\*Diamine hydrochloride salts used, therefore triethylamine was added to the stock solutions prior to use

Appendix Table 3: Summary of precursor stock solution volumes used for each reaction in the HT screen

Reaction number	Scrambled cage	TFB volume (mL)	Amount of TFB (mmol)	Amount of amine A (mmol)	Amine A volume (mL)	Amine ratio (A:X)	Scrambling amine (Amine X)	Amount of Amine X (mmol)	Amine X volume (mL)	Additional volume of chloroform added (mL) (Total volume = 60 mL)
1	A <sup>6</sup> :B <sup>0</sup>	25.00	3.08	4.62	20.39	6:0	B	0.00	0.00	14.61
2	A <sup>5</sup> :B <sup>1</sup>	25.00	3.08	3.85	16.99	5:1	B	0.77	2.32	15.69
3	A <sup>4</sup> :B <sup>2</sup>	25.00	3.08	3.08	13.59	4:2	B	1.54	4.63	16.78
4	A <sup>3</sup> :B <sup>3</sup>	25.00	3.08	2.31	10.19	3:3	B	2.31	6.95	17.86
5	A <sup>2</sup> :B <sup>4</sup>	25.00	3.08	1.54	6.80	2:4	B	3.08	9.27	18.94
6	A <sup>1</sup> :B <sup>5</sup>	25.00	3.08	0.77	3.40	1:5	B	3.85	11.58	20.02
7	A <sup>0</sup> :B <sup>6</sup>	25.00	3.08	0.00	0.00	0:6	B	4.63	13.90	21.10
8	A <sup>5</sup> :C <sup>1</sup>	25.00	3.08	3.85	16.99	5:1	C	0.77	5.67	12.34
9	A <sup>4</sup> :C <sup>2</sup>	25.00	3.08	3.08	13.59	4:2	C	1.54	11.34	10.07
10	A <sup>3</sup> :C <sup>3</sup>	25.00	3.08	2.31	10.19	3:3	C	2.31	17.00	7.80
11	A <sup>2</sup> :C <sup>4</sup>	25.00	3.08	1.54	6.80	2:4	C	3.08	22.67	5.53
12	A <sup>1</sup> :C <sup>5</sup>	25.00	3.08	0.77	3.40	1:5	C	3.85	28.34	3.26
13	A <sup>0</sup> :C <sup>6</sup>	25.00	3.08	0.00	0.00	0:6	C	4.63	34.01	0.99
14	A <sup>5</sup> :D <sup>1</sup>	25.00	3.08	3.85	16.99	5:1	D	0.77	4.40	13.61
15	A <sup>4</sup> :D <sup>2</sup>	25.00	3.08	3.08	13.59	4:2	D	1.54	8.80	12.61
16	A <sup>3</sup> :D <sup>3</sup>	25.00	3.08	2.31	10.19	3:3	D	2.31	13.21	11.60
17*	A <sup>3</sup> :E <sup>3</sup>	25.00	3.08	2.31	10.19	3:3	E	2.31	13.21	11.60
18	A <sup>4</sup> :G <sup>2</sup>	16.66	2.06	2.06	9.06	4:2	G	1.03	7.44	26.84
19	A <sup>3</sup> :G <sup>3</sup>	16.66	2.06	1.54	6.79	3:3	G	1.54	11.16	25.39
20	A <sup>2</sup> :G <sup>4</sup>	16.66	2.06	1.03	4.53	2:4	G	2.06	14.88	23.93
21	A <sup>1</sup> :G <sup>5</sup>	16.66	2.06	0.51	2.26	1:5	G	2.57	18.60	22.48
22	A <sup>0</sup> :G <sup>6</sup>	16.66	2.06	0.00	0.00	0:6	G	3.08	22.32	21.02
23	A <sup>5</sup> :H <sup>1</sup>	16.66	2.06	2.57	11.32	5:1	H	0.51	2.47	29.55
24	A <sup>4</sup> :H <sup>2</sup>	16.66	2.06	2.06	9.06	4:2	H	1.03	4.94	29.34
25	A <sup>3</sup> :H <sup>3</sup>	16.66	2.06	1.54	6.79	3:3	H	1.54	7.41	29.14
26	A <sup>2</sup> :H <sup>4</sup>	16.66	2.06	1.02	4.53	2:4	H	2.06	9.88	28.93
27	A <sup>1</sup> :H <sup>5</sup>	16.66	2.06	0.51	2.26	1:5	H	2.57	12.35	28.72
28	A <sup>0</sup> :H <sup>6</sup>	16.66	2.06	0.00	0.00	0:6	H	3.08	14.82	28.52
29	A <sup>5</sup> :I <sup>1</sup>	8.33	1.03	1.28	5.66	5:1	I	0.26	1.72	44.29
30	A <sup>4</sup> :I <sup>2</sup>	8.33	1.03	1.03	4.53	2:4	I	0.51	3.43	43.71
31	A <sup>3</sup> :I <sup>3</sup>	8.33	1.03	0.77	3.40	3:3	I	0.77	5.15	43.13
32	A <sup>2</sup> :I <sup>4</sup>	8.33	1.03	0.51	2.26	2:4	I	1.03	6.86	42.54
33	A <sup>1</sup> :I <sup>5</sup>	8.33	1.03	0.26	1.13	1:5	I	1.28	8.58	41.96
34	A <sup>0</sup> :I <sup>6</sup>	8.33	1.03	0.00	0.00	0:6	I	1.54	10.29	41.38
35	A <sup>5</sup> :J <sup>1</sup>	16.66	2.06	2.57	11.32	5:1	J	0.51	5.09	26.93
36	A <sup>4</sup> :J <sup>2</sup>	16.66	2.06	2.06	9.06	4:2	J	1.02	10.18	24.10
37	A <sup>3</sup> :J <sup>3</sup>	16.66	2.06	1.54	6.79	3:3	J	1.54	15.27	21.27
38	A <sup>2</sup> :J <sup>4</sup>	16.66	2.06	1.02	4.53	2:4	J	2.06	20.37	18.45
39	A <sup>1</sup> :J <sup>5</sup>	16.66	2.06	0.51	2.26	1:5	J	2.57	25.46	15.62
40	A <sup>0</sup> :J <sup>6</sup>	16.66	2.06	0.00	0.00	0:6	J	3.08	30.55	12.79
41	A <sup>5</sup> :K <sup>1</sup>	25.00	3.08	3.85	16.99	5:1	K	0.77	2.86	15.15
42	A <sup>4</sup> :K <sup>2</sup>	25.00	3.08	3.08	13.59	4:2	K	1.54	5.71	15.69
43	A <sup>3</sup> :K <sup>3</sup>	25.00	3.08	2.31	10.19	3:3	K	2.31	8.57	16.23
44	A <sup>2</sup> :K <sup>4</sup>	25.00	3.08	1.54	6.80	2:4	K	3.08	11.43	16.77
45	A <sup>1</sup> :K <sup>5</sup>	25.00	3.08	0.77	3.40	1:5	K	3.85	14.29	17.31
46	A <sup>0</sup> :K <sup>6</sup>	25.00	3.08	0.00	0.00	0:6	K	4.63	17.14	17.86
47*	A <sup>3</sup> :E <sup>3</sup>	25.00	3.08	2.31	10.19	3:3	E	2.31	13.21	11.60
48	A <sup>2</sup> :D <sup>4</sup>	25.00	3.08	1.54	6.80	2:4	D	3.08	17.61	10.60
49	A <sup>1</sup> :D <sup>5</sup>	25.00	3.08	0.77	3.40	1:5	D	3.85	22.01	9.59
50	A <sup>0</sup> :D <sup>6</sup>	25.00	3.08	0.00	0.00	0:6	D	4.63	26.41	8.59
51	A <sup>5</sup> :E <sup>1</sup>	25.00	3.08	3.85	16.99	5:1	E	0.77	4.40	13.61
52	A <sup>4</sup> :E <sup>2</sup>	25.00	3.08	3.08	13.59	4:2	E	1.54	8.80	12.61
53	A <sup>3</sup> :E <sup>3</sup>	25.00	3.08	2.31	10.19	3:3	E	2.31	13.21	11.60
54	A <sup>2</sup> :E <sup>4</sup>	25.00	3.08	1.54	6.80	2:4	E	3.08	17.61	10.60
55	A <sup>1</sup> :E <sup>5</sup>	25.00	3.08	0.77	3.40	1:5	E	3.85	22.01	9.59
56	A <sup>0</sup> :E <sup>6</sup>	25.00	3.08	0.00	0.00	0:6	E	4.63	26.41	8.59
57	A <sup>5</sup> :F <sup>1</sup>	25.00	3.08	1.28	5.66	5:1	F	0.26	1.82	44.19
58	A <sup>4</sup> :F <sup>2</sup>	8.33	1.03	1.02	4.53	4:2	F	0.51	3.64	43.51
59	A <sup>3</sup> :F <sup>3</sup>	8.33	1.03	0.77	3.40	3:3	F	0.77	5.45	42.82
60	A <sup>2</sup> :F <sup>4</sup>	8.33	1.03	0.51	2.26	2:4	F	1.03	7.27	42.13
61	A <sup>1</sup> :F <sup>5</sup>	8.33	1.03	0.26	1.13	1:5	F	1.28	9.09	41.45
62	A <sup>0</sup> :F <sup>6</sup>	8.33	1.03	0.00	0.00	0:6	F	1.54	10.91	40.76

\*denotes a control reaction

**Appendix Table 4:** Summary of the characterisation data for the attempted scrambled cage reactions carried out in the high-throughput synthetic screen

Scrambled cage	Mass recovered (g)	Expected mass (g)	Yield based on mass recovery (%) <sup>*</sup>	Solid appearance	HRMS		HPLC		<sup>1</sup> H NMR (CDCl <sub>3</sub> )			
					Mass ions	Species	Scrambling visible?	Comment	Scrambled cage present?	Residual TFB?	Residual <small>(min. 0.5)</small>	Other species visible?
A <sup>6</sup> :B <sup>0</sup>	0.66	0.74	89	Colourless powder	961.6134	[M+H] <sup>+</sup>	✓	-	✓	✓	✓	*
A <sup>5</sup> :B <sup>1</sup>	0.65	0.72	90	Colourless powder	961.6130 933.5817 905.5501 877.5175 849.4856	[M+H] <sup>+</sup>	✓	-	✓	*	*	✓
A <sup>4</sup> :B <sup>2</sup>	0.56	0.70	80	Colourless powder	961.6131 933.5816 905.5504 877.5188 849.4866 821.4546 793.4227	[M+H] <sup>+</sup>	✓	-	✓	✓	*	*
A <sup>3</sup> :B <sup>3</sup>	0.52	0.68	77	Colourless powder	961.6090 933.5808 905.5501 877.5188 849.4873 821.4551 793.4232	[M+H] <sup>+</sup>	✓	-	✓	*	*	*
A <sup>2</sup> :B <sup>4</sup>	0.31	0.65	47	Colourless powder	905.5467 877.5176 849.4871 821.4558 793.4238	[M+H] <sup>+</sup>	✓	-	✓	*	*	✓
A <sup>1</sup> :B <sup>5</sup>	0.23	0.63	36	Colourless powder	849.486 821.456 793.4243	[M+H] <sup>+</sup>	✓	-	✓	*	✓	*
A <sup>0</sup> :B <sup>6</sup>	0.26	0.61	43	Colourless powder	793.4242	[M+H] <sup>+</sup>	✓	-	✓	*	*	*
A <sup>5</sup> :C <sup>1</sup>	0.13	0.73	18	Colourless powder	961.6126 947.5965 933.5802 919.5636	[M+H] <sup>+</sup>	✓	impurities (aldehyde and small oligomers)	✓	✓	*	*
A <sup>4</sup> :C <sup>2</sup>	0.22	0.72	31	Colourless powder	961.6107 947.5955 933.5799	[M+H] <sup>+</sup>	✓	impurities (aldehyde and small oligomers)	✓	✓	*	*

					919.563 905.547 7				
A <sup>3</sup> :C <sup>3</sup>	0.24	0.71	34	Hard orange glass	961.610 0 947.595 5 933.580 5 919.564 8 905.548 9 891.532 6	[M+H] <sup>+</sup>	✓	impuritie s (aldehyd e and small oligomer s)	✓ ✓ * *
A <sup>2</sup> :C <sup>4</sup>	0.18	0.70	26	Colourles s powder	947.594 1 933.579 3 919.564 2 905.548 7 891.532 9 877.516 4	[M+H] <sup>+</sup>	✓	impuritie s (aldehyd e and small oligomer s)	✓ ✓ * *
A <sup>1</sup> :C <sup>5</sup>	0.44	0.69	64	Hard orange glass	919.563 5 905.548 6 891.533 4 8.77517 5	[M+H] <sup>+</sup>	✓	impuritie s (aldehyd e and small oligomer s)	✓ ✓ * *
A <sup>0</sup> :C <sup>6</sup>	0.36	0.68	53	Colourles s powder	877.515 9	[M+H] <sup>+</sup>	✓	impuritie s (aldehyd e and small oligomer s)	✓ ✓ * ✓
A <sup>5</sup> :D <sup>1</sup>	0.38	0.76	50	Glassy orange solid	961.614 5 987.630 9	[M+H] <sup>+</sup>	✓	Possible scrambli ng but lots of impuritie s	* ✓ ✓ ✓
A <sup>4</sup> :D <sup>2</sup>	0.28	0.78	36	Glassy orange solid	935.548 2 961.611 4 987.628 5 1013.64 36	[M+H] <sup>+</sup>	✓	Possible scrambli ng but lots of impuritie s	✓ ✓ * *
A <sup>3</sup> :D <sup>3</sup>	0.48	0.80	60	Glassy orange solid	935.546 3 961.591 3 987.624 0 1013.64 24 1040.66 07	[M+H] <sup>+</sup>	✓	Possible scrambli ng but lots of impuritie s	✓ ✓ * *
A <sup>2</sup> :D <sup>4</sup>	0.61	0.82	74	Colourles s powder	1013.63 51 1039.65 61 1065.66 85 1091.68 42	[M+H] <sup>+</sup>	*		* * ✓ *
A <sup>1</sup> :D <sup>5</sup>	0.16	0.84	19	Colourles s powder	*	-	*		* ✓ ✓ ✓
A <sup>0</sup> :D <sup>6</sup>	0.16	0.86	19	Colourles s powder	1117.69 98	[M+H] <sup>+</sup>	*		* ✓ ✓ ✓
A <sup>5</sup> :E <sup>1</sup>	0.19	0.76	25	Colourles s powder	506.530 2 523.327 1	[M+2H] ] <sup>2+</sup>	✓		✓ * ✓ *

					545.488 1				
A <sup>4</sup> :E <sup>2</sup>	0.80	0.78	102	Colourless powder	481.2957 513.2970 523.33254 535.2703	[M+2H] <sup>2+</sup>	✓	✓	* ✓ *
A <sup>3</sup> :E <sup>3</sup>	0.25	0.80	31	Colourless powder	481.2900 494.3168 507.3263 520.3342 533.3422 546.3492	[M+2H] <sup>2+</sup>	✓	✓	* ✓ *
A <sup>2</sup> :E <sup>4</sup>	0.21	0.82	26	Colourless powder	523.3354	[M+2H] <sup>2+</sup>	✓	✓	* * *
A <sup>1</sup> :E <sup>5</sup>	0.15	0.84	18	Colourless powder	481.2638 523.3246 559.3670	[M+2H] <sup>2+</sup>	✓	✓	* * *
A <sup>0</sup> :E <sup>6</sup>	0.20	0.86	23	Colourless powder	*	-	✓	✓	* * *
A <sup>5</sup> :F <sup>1</sup>	0.19	0.84	23	Colourless powder	*	-	✓	✓	* *
A <sup>4</sup> :F <sup>2</sup>	0.13	0.93	14	Colourless powder	*	-	*	*	
A <sup>3</sup> :F <sup>3</sup>	0.03	1.03	3	Colourless powder	*	-	*	*	✓ ✓ ✓
A <sup>2</sup> :F <sup>4</sup>	0.08	1.12	7	Colourless powder	*	-	*	*	✓ ✓ ✓
A <sup>1</sup> :F <sup>5</sup>	-	1.22	0	Colourless powder	*	-	*	*	
A <sup>0</sup> :F <sup>6</sup>	0.02	1.32	2	Colourless powder	*	-	*	*	✓ ✓ ✓
A <sup>5</sup> :G <sup>1</sup>	0.15	0.78	19	Colourless powder	-	-	✓	Possible scrambling but some impurities	✓ ✓ ✓ Solvent
A <sup>4</sup> :G <sup>2</sup>	0.25	0.83	30	Waxy orange solid	961.6140 1017.6764 1073.7346	[M+H] <sup>+</sup>	✓	Possible scrambling but lots of impurities	✓ ✓ * *
A <sup>3</sup> :G <sup>3</sup>	0.32	0.87	37	Waxy orange solid	961.6111 1017.6741 1073.7367 1129.7971 1185.8594	[M+H] <sup>+</sup>	✓	Possible scrambling but lots of impurities	✓ ✓ * Solvent
A <sup>2</sup> :G <sup>4</sup>	0.47	0.91	51	Waxy orange solid	961.6150 1017.6762 1073.7369 1129.7974	[M+H] <sup>+</sup>	✓	Possible scrambling but lots of impurities	✓ ✓ * Solvent



					1185.86 13 1242.92 51 1297.99 11				
A <sup>1</sup> :G <sup>5</sup>	0.49	0.96	51	Waxy orange solid	1073.35 0 1129.79 88 1186.86 43 1242.92 61 1297.98 53	[M+H] <sup>+</sup>	✓	Possible scrambling but lots of impurities	✓ ✓ ✗ ✓
A <sup>0</sup> :G <sup>6</sup>	0.55	1.00	55	Waxy orange solid	1297.98 85	[M+H] <sup>+</sup>	✗		✓ ✓ ✗ ✓
A <sup>5</sup> :H <sup>1</sup>	0.28	0.78	36	Waxy orange solid	961.614 0 1017.67 64 1073.73 46	[M+H] <sup>+</sup>	✓	Possible scrambling but lots of impurities	✓ ✓ ✗ ✗
A <sup>4</sup> :H <sup>2</sup>	0.50	0.83	60	Glassy orange solid	961.613 2 1017.67 60 1073.73 64	[M+H] <sup>+</sup>	✓	Possible scrambling but lots of impurities	✓ ✓ ✗ ✗
A <sup>3</sup> :H <sup>3</sup>	0.38	0.87	44	Glassy orange solid	961.608 1 1017.67 30 1073.73 06	[M+H] <sup>+</sup>	✓	Possible scrambling but lots of impurities	✓ ✓ ✗ ✗
A <sup>2</sup> :H <sup>4</sup>	0.26	0.91	28	Glassy orange solid	✗		✗		✓ ✓ ✗ ✗
A <sup>1</sup> :H <sup>5</sup>	0.27	0.96	28	Glassy orange solid	✗		✗		✓ ✓ ✗ ✗
A <sup>0</sup> :H <sup>6</sup>	0.33	1.00	33	Glassy orange solid	✗		✗		✓ ✓ ✗ ✓
A <sup>5</sup> :I <sup>1</sup>	0.18	0.28	65	Waxy orange solid	961.614 0 1073.73 78	[M+H] <sup>+</sup>	✓	Possible scrambling but lots of impurities	✓ ✓ ✗ ✗
A <sup>4</sup> :I <sup>2</sup>	0.23	0.30	76	Waxy orange solid	961.612 9 1073.73 78	[M+H] <sup>+</sup>	✓	Possible scrambling but lots of impurities	✓ ✓ ✗ ✗
A <sup>3</sup> :I <sup>3</sup>	0.14	0.33	42	Colourless Powder	961.610 7 1073.73 57 1185.85 80 1298.98 90	[M+H] <sup>+</sup>	✓	Possible scrambling but lots of impurities	✓ ✗ ✗ ✗
A <sup>2</sup> :I <sup>4</sup>	-	0.36	0	-	✗	-	✓	Possible scrambling but lots of impurities	v. weak ✗ ✓ ✓
A <sup>1</sup> :I <sup>5</sup>	0.27	0.39	69	Glassy orange solid	✗	-	✓	Possible scrambling but lots of impurities	✓ ✓ ✗ ✓
A <sup>0</sup> :I <sup>6</sup>	0.30	0.42	71	Glassy orange solid	✗	-	✗		✓ ✓ ✗ ✓
A <sup>5</sup> :J <sup>1</sup>	0.35	0.28	124**	Waxy orange solid	961.611 6 1097.73 64	[M+H] <sup>+</sup>	✓	Possible scrambling but lots of	✓ ✓ ✓ ✓

					1233.8606			impurities				
A <sup>4</sup> :J <sup>2</sup>	0.34	0.32	107**	Waxy orange solid	961.6118 1097.7372 1233.8612	[M+H] <sup>+</sup>	✓	Possible scrambling but lots of impurities	✓	✓	*	*
A <sup>3</sup> :J <sup>3</sup>	0.48	0.35	136**	Waxy orange solid	961.6106 1097.7355 1233.8608 1370.9898	[M+H] <sup>+</sup>	✓	Possible scrambling but lots of impurities	✓	✓	*	*
A <sup>2</sup> :J <sup>4</sup>	0.49	0.39	127**	Waxy orange solid	961.6138 1097.7369 1233.8618 1370.9908 1507.1141	[M+H] <sup>+</sup>	✓	Possible scrambling but lots of impurities	✓	✓	*	*
A <sup>1</sup> :J <sup>5</sup>	0.56	0.42	133**	Waxy orange solid	961.6170 1097.7408 1233.8582 1370.9882	[M+H] <sup>+</sup>	✓	Possible scrambling but lots of impurities	✓	✓	*	*
A <sup>0</sup> :J <sup>6</sup>	0.43	0.46	94	Waxy orange solid	*	-	*		✓	✓	*	*
A <sup>5</sup> :K <sup>1</sup>	0.50	0.84	59	Hard brown solid	961.6135 947.5977 933.5822 919.5652	[M+H] <sup>+</sup>	✓		✓	*	*	*
A <sup>4</sup> :K <sup>2</sup>	0.46	0.83	55	Hard brown solid	961.6120 947.5979 933.5821 919.5665 905.5502 891.5331	[M+H] <sup>+</sup>	✓		✓	*	*	*
A <sup>3</sup> :K <sup>3</sup>	0.52	0.82	63	Foamy orange solid	933.5759 919.5606 905.5447 891.5291 877.5135	[M+H] <sup>+</sup>	✓		✓	*	✓	*
A <sup>2</sup> :K <sup>4</sup>	0.29	0.81	36	Glassy orange solid	919.5606 905.5447 891.5291 877.5135	[M+H] <sup>+</sup>	✓		✓	*	✓	*
A <sup>1</sup> :K <sup>5</sup>	0.30	0.80	38	Colourless powder	905.5443 891.5296 877.5139	[M+H] <sup>+</sup>	✓		✓	*	✓	*
A <sup>0</sup> :K <sup>6</sup>	0.25	0.79	32	Colourless powder	877.5142	[M+H] <sup>+</sup>	✓		✓	*	*	*

\*Mass TFB + Mass amines - mass water produced = maximum theoretical amount of isolated product, and reported yield based on comparison of mass recovery with this value

\*\* Impurities present

**Appendix Table 5:** Summary of results for solubility testing of **3<sup>3</sup>:13<sup>3</sup>** in common laboratory solvents

Vial number	Mass of <b>3<sup>3</sup>:13<sup>3</sup></b> cage (mg)	Solvent	Total volume added (mL)						Solubility (mg/mL)
			0.1	0.2	0.3	0.4	0.5	0.6	
1	26.1	Chloroform	✓						261.0
2	26.6	DCM	*	*	✓				88.7
3	25.5	Chlorobenzene	✓						255.0
4	26.9	1,1,1,3,3,3-Hexafluoro-2-propanol	✓						269.0
5	26.4	Trifluoroethanol	✓						264.0
6	27.5	Hexane	*	*	*	*	*	*	<50
7	27.5	Toluene	*	*	*	✓			68.8
8	27.5	<i>p</i> -xylene	*	✓					137.5
9	28	Methanol	*	*	*	*	*	*	<50
10	27.4	Ethanol	*	*	*	*	*	*	<50
11	28.3	Isopropanol	*	*	*	*	*	*	<50
12	27.9	Butanol	*	*	*	*	*	*	<50
13	27.7	1,4-Dioxane	*	*	*	*	*	*	<50
14	27.7	Acetonitrile	*	*	*	*	*	*	<50
15	27.9	THF	*	*	*	*	*	*	<50
16	28	Ethyl acetate	*	*	*	*	*	*	<50
17	28.4	Diethyl ether	*	*	*	*	*	*	<50
18	26.8	DMF	*	*	*	*	*	*	<50
19	27.6	DMSO	*	*	*	*	*	*	<50
20	27.5	DMAC	*	*	*	*	*	*	<50
21	26.7	NMP	*	*	*	*	*	*	<50
22	26.9	Acetone	*	*	*	*	*	*	<50
23	27.2	4-Formyl morpholine	*	*	*	*	*	*	<50
24	32.1	2,2-Dimethoxypropane	*	*	*	*	*	*	<50
25	28.5	Cyclohexanone	*	*	*	*	*	*	<50
26	28.4	1-Butyl-3-methylimidazolium tetrafluoroborate	*	*	*	*	*	*	<50
27	26.4	1-Ethyl-3-methylimidazolium bis(trifluoromethylsulfonyl) imide	*	*	*	*	*	*	<50
28	27.1	Anisole (Methoxybenzene)	*	✓					135.5

**Appendix Table 6:** Summary of solubility testing of **3<sup>3</sup>:13<sup>3</sup>** in bulkier solvent analogues

Solvent number	Solvent name	Mass of cage (mg)	Total volume added (mL)				Solubility (mg/mL)
			0.1	0.2	0.3	0.4	
1	2,4-Dichlorobenzyl chloride	29.7	✓				297.0
2	2-Chloro-4-toluene	30.5	✓				305.0
3	Hexafluoro-2,3-bis (trifluoromethyl) butane-2,3-diol	31.7	*	*	*	✓	79.3
4	2,3,5,6-Tetrafluoro-4-(trifluoromethyl)phenol	29.6	*	*	✓		98.7
5	3,5-Bis(trifluoromethyl) phenol	31.3	*	*	✓		104.3
6	4-(Trifluoromethoxy)benzyl alcohol	30.8	✓				308.0
7	2-Fluoro-5-(trifluoromethyl) phenol	30.3	*	*	✓		101.0
8	Dimethyl phthalate	28.7	*	*	*	*	<50
9	2-Hydroxyacetophenone	30.9	✓				309.0
10	Methyl salicylate	31.0	✓				310.0
11	4-Chloro-3-(trifluoromethyl)phenol	29.4	*	*	✓		147.0
12	4-( <i>tert</i> Butyl)benzyl alcohol	31.8	*	*	✓		106.0
13	Triisobutylamine	30.6	*	*	*	*	<50
14	$\epsilon$ -Caprolactone	28.8	*	*	*	*	<50

**Appendix Table 7:** Summary of the gas evolution screen on addition of bulky additives, with the volumes of xenon evolved to determine size-exclusivity of new potential porous liquid solvents

Bulky Additive (Bulky solvent from Appendix Table 6)	Solvent number	Total volume of gas evolved from porous liquid (cm <sup>3</sup> )		Total volume of gas evolved from perchloropropene (cm <sup>3</sup> )	
		After addition of bulky additive	After addition of bulky additive and then CHCl <sub>3</sub>	After addition of bulky additive	After addition of bulky additive and then CHCl <sub>3</sub>
2,4-Dichlorobenzyl chloride	1	0.5	2.4	0.5	0.1
2-Chloro-4-toluene	2	0.6	1.6	0.1	0.0
Hexafluoro-2,3-bis(trifluoromethyl) butane-2,3-diol	3	0.1	2.3	0.3	0.1
2,3,5,6-Tetrafluoro-4-(trifluoromethyl)phenol	4	0.0	1.5	0.1	0.2
3,5-Bis(trifluoromethyl)phenol	5	0.1	2.3	0.3	0.1
4-(Trifluoromethoxy)benzyl alcohol	6	0.7	2.4	0.1	0.2
2-Fluoro-5-(trifluoromethyl)phenol	7	0.4	1.9	0.6	0.3
2-Hydroxyacetophenone	9	0.7	3.9	0.4	0.7
Methyl salicylate	10	0.5	1.2	0.1	0.2
4-Chloro-3-(trifluoromethyl)phenol	11	0.9	2.2	0.5	0.2
4-( <i>tert</i> Butyl)benzyl alcohol	12	0.3	2.2	1.0	0.4

**Appendix Table 8:** Summary of results from the high-throughput solubility screen

Reaction Code	Scrambled cage (Amine A: Amine X)	Chemical formula	Average MW	Mass (mg)	Solvent	Fully dissolved in:			Overall solubility (mg/mL)	Overall solubility (mmol/mL)
						0.1 mL?	0.2 mL?	0.3 mL?		
A6	A <sup>6</sup> :B <sup>0</sup>	C <sub>60</sub> H <sub>72</sub> N <sub>12</sub>	961.320	31.4	1	*	*	*	<50	-
A12	A <sup>6</sup> :B <sup>0</sup>	C <sub>60</sub> H <sub>72</sub> N <sub>12</sub>	961.320	29.3	2	*	✓		146.5	0.152
A18	A <sup>6</sup> :B <sup>0</sup>	C <sub>60</sub> H <sub>72</sub> N <sub>12</sub>	961.320	32.3	3	*	*	*	<50	-
A24	A <sup>6</sup> :B <sup>0</sup>	C <sub>60</sub> H <sub>72</sub> N <sub>12</sub>	961.320	31.2	4	*	*	*	<50	-
A30	A <sup>6</sup> :B <sup>0</sup>	C <sub>60</sub> H <sub>72</sub> N <sub>12</sub>	961.320	28.7	5	*	*	✓	95.7	0.100
A36	A <sup>6</sup> :B <sup>0</sup>	C <sub>60</sub> H <sub>72</sub> N <sub>12</sub>	961.320	31.1	6	*	*	*	<50	-
B1	A <sup>5</sup> :B <sup>1</sup>	C <sub>58</sub> H <sub>68</sub> N <sub>12</sub>	933.266	29.0	1	*	*	*	<50	-
B2	A <sup>4</sup> :B <sup>2</sup>	C <sub>56</sub> H <sub>64</sub> N <sub>12</sub>	905.212	29.4	1	*	*	*	<50	-
B3	A <sup>3</sup> :B <sup>3</sup>	C <sub>54</sub> H <sub>60</sub> N <sub>12</sub>	877.158	30.8	1	*	*	*	<50	-
B4	A <sup>2</sup> :B <sup>4</sup>	C <sub>52</sub> H <sub>56</sub> N <sub>12</sub>	849.104	29.3	1	*	*	*	<50	-
B5	A <sup>1</sup> :B <sup>5</sup>	C <sub>50</sub> H <sub>52</sub> N <sub>12</sub>	821.05	28.6	1	*	*	*	<50	-
B6	A <sup>0</sup> :B <sup>6</sup>	C <sub>48</sub> H <sub>48</sub> N <sub>12</sub>	792.996	30.8	1	*	*	*	<50	-
B7	A <sup>5</sup> :B <sup>1</sup>	C <sub>58</sub> H <sub>68</sub> N <sub>12</sub>	933.266	29.5	2	*	*	✓	98.3	0.152
B8	A <sup>4</sup> :B <sup>2</sup>	C <sub>56</sub> H <sub>64</sub> N <sub>12</sub>	905.212	31.2	2	*	*	✓	104.0	0.115
B9	A <sup>3</sup> :B <sup>3</sup>	C <sub>54</sub> H <sub>60</sub> N <sub>12</sub>	877.158	30.5	2	*	*	✓	101.7	0.116
B10	A <sup>2</sup> :B <sup>4</sup>	C <sub>52</sub> H <sub>56</sub> N <sub>12</sub>	849.104	28.6	2	*	*	✓	95.3	0.112
B11	A <sup>1</sup> :B <sup>5</sup>	C <sub>50</sub> H <sub>52</sub> N <sub>12</sub>	821.05	29.5	2	*	*	✓	98.3	0.120
B12	A <sup>0</sup> :B <sup>6</sup>	C <sub>48</sub> H <sub>48</sub> N <sub>12</sub>	792.996	30.9	2	*	*	✓	103.0	0.130
B13	A <sup>5</sup> :B <sup>1</sup>	C <sub>58</sub> H <sub>68</sub> N <sub>12</sub>	933.266	31.8	3	*	*	*	<50	-
B14	A <sup>4</sup> :B <sup>2</sup>	C <sub>56</sub> H <sub>64</sub> N <sub>12</sub>	905.212	30.8	3	*	*	*	<50	-
B15	A <sup>3</sup> :B <sup>3</sup>	C <sub>54</sub> H <sub>60</sub> N <sub>12</sub>	877.158	30.7	3	*	*	*	<50	-
B16	A <sup>2</sup> :B <sup>4</sup>	C <sub>52</sub> H <sub>56</sub> N <sub>12</sub>	849.104	28.3	3	*	*	*	<50	-
B17	A <sup>1</sup> :B <sup>5</sup>	C <sub>50</sub> H <sub>52</sub> N <sub>12</sub>	821.05	29.3	3	*	*	*	<50	-
B18	A <sup>0</sup> :B <sup>6</sup>	C <sub>48</sub> H <sub>48</sub> N <sub>12</sub>	792.996	31.2	3	*	*	*	<50	-
B19	A <sup>5</sup> :B <sup>1</sup>	C <sub>58</sub> H <sub>68</sub> N <sub>12</sub>	933.266	30.2	4	*	*	*	<50	-
B20	A <sup>4</sup> :B <sup>2</sup>	C <sub>56</sub> H <sub>64</sub> N <sub>12</sub>	905.212	29.4	4	*	*	*	<50	-
B21	A <sup>3</sup> :B <sup>3</sup>	C <sub>54</sub> H <sub>60</sub> N <sub>12</sub>	877.158	30.2	4	*	*	*	<50	-
B22	A <sup>2</sup> :B <sup>4</sup>	C <sub>52</sub> H <sub>56</sub> N <sub>12</sub>	849.104	31.2	4	*	*	*	<50	-
B23	A <sup>1</sup> :B <sup>5</sup>	C <sub>50</sub> H <sub>52</sub> N <sub>12</sub>	821.05	27.9	4	*	*	*	<50	-

B24	A <sup>0</sup> :B <sup>6</sup>	C <sub>48</sub> H <sub>48</sub> N <sub>12</sub>	792.996	29.2	4	*	*	*	<50	-
B25	A <sup>5</sup> :B <sup>1</sup>	C <sub>58</sub> H <sub>68</sub> N <sub>12</sub>	933.266	29.3	5	*	*	*	<50	-
B26	A <sup>4</sup> :B <sup>2</sup>	C <sub>56</sub> H <sub>64</sub> N <sub>12</sub>	905.212	30.1	5	*	*	*	<50	-
B27	A <sup>3</sup> :B <sup>3</sup>	C <sub>54</sub> H <sub>60</sub> N <sub>12</sub>	877.158	31.0	5	*	*	*	<50	-
B28	A <sup>2</sup> :B <sup>4</sup>	C <sub>52</sub> H <sub>56</sub> N <sub>12</sub>	849.104	25.0	5	*	*	✓	83.3	0.100
B29	A <sup>1</sup> :B <sup>5</sup>	C <sub>50</sub> H <sub>52</sub> N <sub>12</sub>	821.05	29.6	5	*	*	*	<50	-
B30	A <sup>0</sup> :B <sup>6</sup>	C <sub>48</sub> H <sub>48</sub> N <sub>12</sub>	792.996	30.6	5	*	*	*	<50	-
B31	A <sup>5</sup> :B <sup>1</sup>	C <sub>58</sub> H <sub>68</sub> N <sub>12</sub>	933.266	31.2	6	*	*	*	<50	-
B32	A <sup>4</sup> :B <sup>2</sup>	C <sub>56</sub> H <sub>64</sub> N <sub>12</sub>	905.212	30.6	6	*	*	*	<50	-
B33	A <sup>3</sup> :B <sup>3</sup>	C <sub>54</sub> H <sub>60</sub> N <sub>12</sub>	877.158	31.6	6	*	*	*	<50	-
B34	A <sup>2</sup> :B <sup>4</sup>	C <sub>52</sub> H <sub>56</sub> N <sub>12</sub>	849.104	20.1	6	*	*	*	<50	-
B35	A <sup>1</sup> :B <sup>5</sup>	C <sub>50</sub> H <sub>52</sub> N <sub>12</sub>	821.05	29.5	6	*	*	*	<50	-
B36	A <sup>0</sup> :B <sup>6</sup>	C <sub>48</sub> H <sub>48</sub> N <sub>12</sub>	792.996	31.1	6	*	*	*	<50	-
C1	A <sup>5</sup> :C <sup>1</sup>	C <sub>59</sub> H <sub>70</sub> N <sub>12</sub>	947.293	27.4	1	*	*	*	<50	-
C2	A <sup>4</sup> :C <sup>2</sup>	C <sub>58</sub> H <sub>68</sub> N <sub>12</sub>	933.266	27.6	1	*	*	*	<50	-
C3	A <sup>3</sup> :C <sup>3</sup>	C <sub>57</sub> H <sub>66</sub> N <sub>12</sub>	919.239	31.1	1	*	*	*	<50	-
C4	A <sup>2</sup> :C <sup>4</sup>	C <sub>56</sub> H <sub>64</sub> N <sub>12</sub>	905.212	29.2	1	*	*	✓	97.3	0.108
C5	A <sup>1</sup> :C <sup>5</sup>	C <sub>55</sub> H <sub>62</sub> N <sub>12</sub>	891.185	30.4	1	*	✓		152.0	0.171
C6	A <sup>0</sup> :C <sup>6</sup>	C <sub>54</sub> H <sub>60</sub> N <sub>12</sub>	877.158	30.3	1	*	*	*	<50	-
C7	A <sup>5</sup> :C <sup>1</sup>	C <sub>59</sub> H <sub>70</sub> N <sub>12</sub>	947.293	27.9	2	*	*	✓	93.0	0.0982
C8	A <sup>4</sup> :C <sup>2</sup>	C <sub>58</sub> H <sub>68</sub> N <sub>12</sub>	933.266	29.8	2	*	*	✓	99.3	0.106
C9	A <sup>3</sup> :C <sup>3</sup>	C <sub>57</sub> H <sub>66</sub> N <sub>12</sub>	919.239	29.8	2	*	✓		149.0	0.162
C10	A <sup>2</sup> :C <sup>4</sup>	C <sub>56</sub> H <sub>64</sub> N <sub>12</sub>	905.212	27.2	2	*	✓		136.0	0.150
C11	A <sup>1</sup> :C <sup>5</sup>	C <sub>55</sub> H <sub>62</sub> N <sub>12</sub>	891.185	30.8	2	*	*	✓	102.7	0.115
C12	A <sup>0</sup> :C <sup>6</sup>	C <sub>54</sub> H <sub>60</sub> N <sub>12</sub>	877.158	28.9	2	*	✓		144.5	0.165
C13	A <sup>5</sup> :C <sup>1</sup>	C <sub>59</sub> H <sub>70</sub> N <sub>12</sub>	947.293	22.2	3	*	*	*	<50	-
C14	A <sup>4</sup> :C <sup>2</sup>	C <sub>58</sub> H <sub>68</sub> N <sub>12</sub>	933.266	28.7	3	*	*	*	<50	-
C15	A <sup>3</sup> :C <sup>3</sup>	C <sub>57</sub> H <sub>66</sub> N <sub>12</sub>	919.239	30.2	3	*	✓		151.0	0.164
C16	A <sup>2</sup> :C <sup>4</sup>	C <sub>56</sub> H <sub>64</sub> N <sub>12</sub>	905.212	29.7	3	*	✓		148.5	0.164
C17	A <sup>1</sup> :C <sup>5</sup>	C <sub>55</sub> H <sub>62</sub> N <sub>12</sub>	891.185	29.4	3	*	*	✓	98.0	0.110
C18	A <sup>0</sup> :C <sup>6</sup>	C <sub>54</sub> H <sub>60</sub> N <sub>12</sub>	877.158	30.9	3	*	*	✓	103.0	0.117
C19	A <sup>5</sup> :C <sup>1</sup>	C <sub>59</sub> H <sub>70</sub> N <sub>12</sub>	947.293	15.5	4	*	*	*	<50	-
C20	A <sup>4</sup> :C <sup>2</sup>	C <sub>58</sub> H <sub>68</sub> N <sub>12</sub>	933.266	29.3	4	*	*	*	<50	-
C21	A <sup>3</sup> :C <sup>3</sup>	C <sub>57</sub> H <sub>66</sub> N <sub>12</sub>	919.239	30.2	4	*	*	*	<50	-
C22	A <sup>2</sup> :C <sup>4</sup>	C <sub>56</sub> H <sub>64</sub> N <sub>12</sub>	905.212	30.4	4	*	*	✓	101.3	0.112
C23	A <sup>1</sup> :C <sup>5</sup>	C <sub>55</sub> H <sub>62</sub> N <sub>12</sub>	891.185	31.5	4	*	*	*	<50	-
C24	A <sup>0</sup> :C <sup>6</sup>	C <sub>54</sub> H <sub>60</sub> N <sub>12</sub>	877.158	30.3	4	*	*	*	<50	-
C25	A <sup>5</sup> :C <sup>1</sup>	C <sub>59</sub> H <sub>70</sub> N <sub>12</sub>	947.293	10.4	5	*	✓		52.0	0.0555
C26	A <sup>4</sup> :C <sup>2</sup>	C <sub>58</sub> H <sub>68</sub> N <sub>12</sub>	933.266	9.3	5	*	*	✓	31.0	0.0332
C27	A <sup>3</sup> :C <sup>3</sup>	C <sub>57</sub> H <sub>66</sub> N <sub>12</sub>	919.239	9.3	5	*	*	✓	30.7	0.0334
C28	A <sup>2</sup> :C <sup>4</sup>	C <sub>56</sub> H <sub>64</sub> N <sub>12</sub>	905.212	12.5	5	*	*	✓	41.7	0.0460
C29	A <sup>1</sup> :C <sup>5</sup>	C <sub>55</sub> H <sub>62</sub> N <sub>12</sub>	891.185	-	5	*	*	*	<50	-
C30	A <sup>0</sup> :C <sup>6</sup>	C <sub>54</sub> H <sub>60</sub> N <sub>12</sub>	877.158	17.0	5	*	✓		85.0	0.0969
C31	A <sup>5</sup> :C <sup>1</sup>	C <sub>59</sub> H <sub>70</sub> N <sub>12</sub>	947.293	10.3	6	*	*	✓	34.3	0.0362
C32	A <sup>4</sup> :C <sup>2</sup>	C <sub>58</sub> H <sub>68</sub> N <sub>12</sub>	933.266	29.5	6	*	*	*	<50	-
C33	A <sup>3</sup> :C <sup>3</sup>	C <sub>57</sub> H <sub>66</sub> N <sub>12</sub>	919.239	30.2	6	*	*	*	<50	-
C34	A <sup>2</sup> :C <sup>4</sup>	C <sub>56</sub> H <sub>64</sub> N <sub>12</sub>	905.212	30.3	6	*	*	*	<50	-
C35	A <sup>1</sup> :C <sup>5</sup>	C <sub>55</sub> H <sub>62</sub> N <sub>12</sub>	891.185	33	6	*	*	*	<50	-
C36	A <sup>0</sup> :C <sup>6</sup>	C <sub>54</sub> H <sub>60</sub> N <sub>12</sub>	877.158	30.7	6	*	*	*	<50	-
E1	A <sup>5</sup> :E <sup>1</sup>	C <sub>62</sub> H <sub>74</sub> N <sub>12</sub>	987.358	29.3	1	*	*	*	<50	-
E2	A <sup>4</sup> :E <sup>2</sup>	C <sub>64</sub> H <sub>76</sub> N <sub>12</sub>	1013.396	31.1	1	*	✓		155.5	0.153
E3	A <sup>3</sup> :E <sup>3</sup>	C <sub>66</sub> H <sub>78</sub> N <sub>12</sub>	1039.434	30.4	1	✓			304.0	0.292
E4	A <sup>2</sup> :E <sup>4</sup>	C <sub>68</sub> H <sub>80</sub> N <sub>12</sub>	1065.472	30.6	1	*	*	*	<50	-
E5	A <sup>1</sup> :E <sup>5</sup>	C <sub>70</sub> H <sub>82</sub> N <sub>12</sub>	1091.510	28.4	1	*	*	*	<50	-
E6	A <sup>0</sup> :E <sup>6</sup>	C <sub>72</sub> H <sub>84</sub> N <sub>12</sub>	1117.548	30.4	1	*	*	*	<50	-
E7	A <sup>5</sup> :E <sup>1</sup>	C <sub>62</sub> H <sub>74</sub> N <sub>12</sub>	987.358	29.7	2	*	✓		148.5	0.150
E8	A <sup>4</sup> :E <sup>2</sup>	C <sub>64</sub> H <sub>76</sub> N <sub>12</sub>	1013.396	31.4	2	*	✓		157.0	0.155
E9	A <sup>3</sup> :E <sup>3</sup>	C <sub>66</sub> H <sub>78</sub> N <sub>12</sub>	1039.434	29.1	2	✓			291.0	0.280
E10	A <sup>2</sup> :E <sup>4</sup>	C <sub>68</sub> H <sub>80</sub> N <sub>12</sub>	1065.472	30.4	2	*	*	✓	101.3	0.0951
E11	A <sup>1</sup> :E <sup>5</sup>	C <sub>70</sub> H <sub>82</sub> N <sub>12</sub>	1091.510	31.7	2	*	*	✓	105.7	0.0968
E12	A <sup>0</sup> :E <sup>6</sup>	C <sub>72</sub> H <sub>84</sub> N <sub>12</sub>	1117.548	30.3	2	*	*	*	<50	-
E13	A <sup>5</sup> :E <sup>1</sup>	C <sub>62</sub> H <sub>74</sub> N <sub>12</sub>	987.358	30.5	3	*	*	*	<50	-
E14	A <sup>4</sup> :E <sup>2</sup>	C <sub>64</sub> H <sub>76</sub> N <sub>12</sub>	1013.396	29.6	3	*	*	*	<50	-
E15	A <sup>3</sup> :E <sup>3</sup>	C <sub>66</sub> H <sub>78</sub> N <sub>12</sub>	1039.434	30.8	3	✓			308.0	0.296
E16	A <sup>2</sup> :E <sup>4</sup>	C <sub>68</sub> H <sub>80</sub> N <sub>12</sub>	1065.472	29.7	3	*	*	✓	99.0	0.0929
E17	A <sup>1</sup> :E <sup>5</sup>	C <sub>70</sub> H <sub>82</sub> N <sub>12</sub>	1091.510	31	3	*	*	*	<50	-
E18	A <sup>0</sup> :E <sup>6</sup>	C <sub>72</sub> H <sub>84</sub> N <sub>12</sub>	1117.548	32	3	*	*	*	<50	-

E19	A <sup>5</sup> :E <sup>1</sup>	C <sub>62</sub> H <sub>74</sub> N <sub>12</sub>	987.358	29.8	4	*	*	*	<50	-
E20	A <sup>4</sup> :E <sup>2</sup>	C <sub>64</sub> H <sub>76</sub> N <sub>12</sub>	1013.396	29.7	4	*	*	*	<50	-
E21	A <sup>3</sup> :E <sup>3</sup>	C <sub>66</sub> H <sub>78</sub> N <sub>12</sub>	1039.434	29.7	4	✓			297.0	0.286
E22	A <sup>2</sup> :E <sup>4</sup>	C <sub>68</sub> H <sub>80</sub> N <sub>12</sub>	1065.472	29.9	4	*	*	*	<50	-
E23	A <sup>1</sup> :E <sup>5</sup>	C <sub>70</sub> H <sub>82</sub> N <sub>12</sub>	1091.510	29.9	4	*	*	*	<50	-
E24	A <sup>0</sup> :E <sup>6</sup>	C <sub>72</sub> H <sub>84</sub> N <sub>12</sub>	1117.548	28.5	4	*	*	*	<50	-
E25	A <sup>5</sup> :E <sup>1</sup>	C <sub>62</sub> H <sub>74</sub> N <sub>12</sub>	987.358	24.0	5	*	✓		120.0	0.122
E26	A <sup>4</sup> :E <sup>2</sup>	C <sub>64</sub> H <sub>76</sub> N <sub>12</sub>	1013.396	28.3	5	*	*	*	<50	-
E27	A <sup>3</sup> :E <sup>3</sup>	C <sub>66</sub> H <sub>78</sub> N <sub>12</sub>	1039.434	28.6	5	✓			286.0	0.275
E28	A <sup>2</sup> :E <sup>4</sup>	C <sub>68</sub> H <sub>80</sub> N <sub>12</sub>	1065.472	29.1	5	*	✓		145.5	0.137
E29	A <sup>1</sup> :E <sup>5</sup>	C <sub>70</sub> H <sub>82</sub> N <sub>12</sub>	1091.510	29.4	5	*	*	✓	98.0	0.0900
E30	A <sup>0</sup> :E <sup>6</sup>	C <sub>72</sub> H <sub>84</sub> N <sub>12</sub>	1117.548	30.9	5	*	*	✓	103.0	0.0921
E31	A <sup>5</sup> :E <sup>1</sup>	C <sub>62</sub> H <sub>74</sub> N <sub>12</sub>	987.358	30.5	6	*	*	*	<50	-
E32	A <sup>4</sup> :E <sup>2</sup>	C <sub>64</sub> H <sub>76</sub> N <sub>12</sub>	1013.396	29.1	6	*	*	*	<50	-
E33	A <sup>3</sup> :E <sup>3</sup>	C <sub>66</sub> H <sub>78</sub> N <sub>12</sub>	1039.434	129	6	*	✓		109.5	0.105
E34	A <sup>2</sup> :E <sup>4</sup>	C <sub>68</sub> H <sub>80</sub> N <sub>12</sub>	1065.472	29.6	6	*	*	*	<50	-
E35	A <sup>1</sup> :E <sup>5</sup>	C <sub>70</sub> H <sub>82</sub> N <sub>12</sub>	1091.510	28.1	6	*	*	*	<50	-
E36	A <sup>0</sup> :E <sup>6</sup>	C <sub>72</sub> H <sub>84</sub> N <sub>12</sub>	1117.548	31.7	6	*	*	*	<50	-
F1	A <sup>5</sup> :F <sup>1</sup>	C <sub>70</sub> H <sub>76</sub> N <sub>12</sub>	1085.462	28.9	1	*	*	*	<50	-
F7	A <sup>5</sup> :F <sup>1</sup>	C <sub>70</sub> H <sub>76</sub> N <sub>12</sub>	1085.462	28.8	2	*	*	*	<50	-
F13	A <sup>5</sup> :F <sup>1</sup>	C <sub>70</sub> H <sub>76</sub> N <sub>12</sub>	1085.462	28.7	3	*	*	*	<50	-
F19	A <sup>5</sup> :F <sup>1</sup>	C <sub>70</sub> H <sub>76</sub> N <sub>12</sub>	1085.462	22.4	4	*	*	*	<50	-
F25	A <sup>5</sup> :F <sup>1</sup>	C <sub>70</sub> H <sub>76</sub> N <sub>12</sub>	1085.462	-	5	*	*	*	<50	-
F31	A <sup>5</sup> :F <sup>1</sup>	C <sub>70</sub> H <sub>76</sub> N <sub>12</sub>	1085.462	29.4	6	*	*	*	<50	-
G1	A <sup>5</sup> :G <sup>1</sup>	C <sub>64</sub> H <sub>80</sub> N <sub>12</sub>	1017.428	31.3	1	*	*	*	<50	-
G2	A <sup>4</sup> :G <sup>2</sup>	C <sub>68</sub> H <sub>88</sub> N <sub>12</sub>	1073.536	28.2	1	*	✓		141.0	0.131
G3	A <sup>3</sup> :G <sup>3</sup>	C <sub>72</sub> H <sub>96</sub> N <sub>12</sub>	1129.644	30.6	1	✓			306.0	0.271
G4	A <sup>2</sup> :G <sup>4</sup>	C <sub>76</sub> H <sub>104</sub> N <sub>12</sub>	1185.752	29.9	1	✓			299.0	0.252
G5	A <sup>1</sup> :G <sup>5</sup>	C <sub>80</sub> H <sub>112</sub> N <sub>12</sub>	1241.86	29.1	1	✓			291.0	0.234
G6	A <sup>0</sup> :G <sup>6</sup>	C <sub>84</sub> H <sub>120</sub> N <sub>12</sub>	1297.968	30.6	1	✓			306.0	0.236
G7	A <sup>5</sup> :G <sup>1</sup>	C <sub>64</sub> H <sub>80</sub> N <sub>12</sub>	1017.428	30.3	2	*	✓		151.5	0.149
G8	A <sup>4</sup> :G <sup>2</sup>	C <sub>68</sub> H <sub>88</sub> N <sub>12</sub>	1073.536	26.4	2	✓			264.0	0.246
G9	A <sup>3</sup> :G <sup>3</sup>	C <sub>72</sub> H <sub>96</sub> N <sub>12</sub>	1129.644	29.2	2	✓			292.0	0.259
G10	A <sup>2</sup> :G <sup>4</sup>	C <sub>76</sub> H <sub>104</sub> N <sub>12</sub>	1185.752	29.0	2	✓			290.0	0.245
G11	A <sup>1</sup> :G <sup>5</sup>	C <sub>80</sub> H <sub>112</sub> N <sub>12</sub>	1241.86	28.8	2	✓			288.0	0.232
G12	A <sup>0</sup> :G <sup>6</sup>	C <sub>84</sub> H <sub>120</sub> N <sub>12</sub>	1297.968	30.9	2	*	*	*	<50	-
G13	A <sup>5</sup> :G <sup>1</sup>	C <sub>64</sub> H <sub>80</sub> N <sub>12</sub>	1017.428	30.6	3	*	*	*	<50	-
G14	A <sup>4</sup> :G <sup>2</sup>	C <sub>68</sub> H <sub>88</sub> N <sub>12</sub>	1073.536	19.0	3	✓			190.0	0.177
G15	A <sup>3</sup> :G <sup>3</sup>	C <sub>72</sub> H <sub>96</sub> N <sub>12</sub>	1129.644	29.2	3	✓			292.0	0.258
G16	A <sup>2</sup> :G <sup>4</sup>	C <sub>76</sub> H <sub>104</sub> N <sub>12</sub>	1185.752	30.8	3	✓			308.0	0.260
G17	A <sup>1</sup> :G <sup>5</sup>	C <sub>80</sub> H <sub>112</sub> N <sub>12</sub>	1241.86	30.2	3	✓			302.0	0.243
G18	A <sup>0</sup> :G <sup>6</sup>	C <sub>84</sub> H <sub>120</sub> N <sub>12</sub>	1297.968	29	3	✓			290.0	0.223
G19	A <sup>5</sup> :G <sup>1</sup>	C <sub>64</sub> H <sub>80</sub> N <sub>12</sub>	1017.428	30.2	4	*	*	*	<50	-
G20	A <sup>4</sup> :G <sup>2</sup>	C <sub>68</sub> H <sub>88</sub> N <sub>12</sub>	1073.536	17.5	4	*	✓		87.5	0.0815
G21	A <sup>3</sup> :G <sup>3</sup>	C <sub>72</sub> H <sub>96</sub> N <sub>12</sub>	1129.644	27.2	4	✓			272.0	0.241
G22	A <sup>2</sup> :G <sup>4</sup>	C <sub>76</sub> H <sub>104</sub> N <sub>12</sub>	1185.752	29.9	4	✓			299.0	0.252
G23	A <sup>1</sup> :G <sup>5</sup>	C <sub>80</sub> H <sub>112</sub> N <sub>12</sub>	1241.86	29.3	4	✓			293.0	0.236
G24	A <sup>0</sup> :G <sup>6</sup>	C <sub>84</sub> H <sub>120</sub> N <sub>12</sub>	1297.968	31.5	4	✓			315.0	0.243
G25	A <sup>5</sup> :G <sup>1</sup>	C <sub>64</sub> H <sub>80</sub> N <sub>12</sub>	1017.428	17.2	5	*	*	✓	57.3	0.0563
G26	A <sup>4</sup> :G <sup>2</sup>	C <sub>68</sub> H <sub>88</sub> N <sub>12</sub>	1073.536	29.2	5	*	✓		145.5	0.136
G27	A <sup>3</sup> :G <sup>3</sup>	C <sub>72</sub> H <sub>96</sub> N <sub>12</sub>	1129.644	30.6	5	✓			306.0	0.271
G28	A <sup>2</sup> :G <sup>4</sup>	C <sub>76</sub> H <sub>104</sub> N <sub>12</sub>	1185.752	29.9	5	✓			299.0	0.252
G29	A <sup>1</sup> :G <sup>5</sup>	C <sub>80</sub> H <sub>112</sub> N <sub>12</sub>	1241.86	32.1	5	✓			321.0	0.258
G30	A <sup>0</sup> :G <sup>6</sup>	C <sub>84</sub> H <sub>120</sub> N <sub>12</sub>	1297.968	30.9	5	✓			309.0	0.238
G31	A <sup>5</sup> :G <sup>1</sup>	C <sub>64</sub> H <sub>80</sub> N <sub>12</sub>	1017.428	30.4	6	*	*	*	<50	-
G32	A <sup>4</sup> :G <sup>2</sup>	C <sub>68</sub> H <sub>88</sub> N <sub>12</sub>	1073.536	18.2	6	*	*	✓	60.7	0.0565
G33	A <sup>3</sup> :G <sup>3</sup>	C <sub>72</sub> H <sub>96</sub> N <sub>12</sub>	1129.644	20.3	6	✓			203.0	0.180
G34	A <sup>2</sup> :G <sup>4</sup>	C <sub>76</sub> H <sub>104</sub> N <sub>12</sub>	1185.752	30.8	6	✓			308.0	0.260
G35	A <sup>1</sup> :G <sup>5</sup>	C <sub>80</sub> H <sub>112</sub> N <sub>12</sub>	1241.86	29.2	6	✓			292.0	0.235
G36	A <sup>0</sup> :G <sup>6</sup>	C <sub>84</sub> H <sub>120</sub> N <sub>12</sub>	1297.968	29.4	6	*	*	*	<50	-
H1	A <sup>5</sup> :H <sup>1</sup>	C <sub>64</sub> H <sub>80</sub> N <sub>12</sub>	1017.428	29.4	1	*	*	*	<50	-
H2	A <sup>4</sup> :H <sup>2</sup>	C <sub>68</sub> H <sub>88</sub> N <sub>12</sub>	1073.536	27.5	1	*	*	*	<50	-
H3	A <sup>3</sup> :H <sup>3</sup>	C <sub>72</sub> H <sub>96</sub> N <sub>12</sub>	1129.644	31.1	1	*	*	*	<50	-
H7	A <sup>5</sup> :H <sup>1</sup>	C <sub>64</sub> H <sub>80</sub> N <sub>12</sub>	1017.428	29.8	2	*	*	✓	99.3	0.0976
H8	A <sup>4</sup> :H <sup>2</sup>	C <sub>68</sub> H <sub>88</sub> N <sub>12</sub>	1073.536	29.8	2	*	*	✓	99.3	0.0925
H9	A <sup>3</sup> :H <sup>3</sup>	C <sub>72</sub> H <sub>96</sub> N <sub>12</sub>	1129.644	30.9	2	*	*	*	<50	-
H13	A <sup>5</sup> :H <sup>1</sup>	C <sub>64</sub> H <sub>80</sub> N <sub>12</sub>	1017.428	25.4	3	*	*	*	<50	-

H14	A <sup>4</sup> :H <sup>2</sup>	C <sub>68</sub> H <sub>88</sub> N <sub>12</sub>	1073.536	29.3	3	*	*	*	<50	-
H15	A <sup>3</sup> :H <sup>3</sup>	C <sub>72</sub> H <sub>96</sub> N <sub>12</sub>	1129.644	31.6	3	*	*	*	<50	-
H19	A <sup>5</sup> :H <sup>1</sup>	C <sub>64</sub> H <sub>80</sub> N <sub>12</sub>	1017.428	23.8	4	*	*	✓	79.3	0.0780
H20	A <sup>4</sup> :H <sup>2</sup>	C <sub>68</sub> H <sub>88</sub> N <sub>12</sub>	1073.536	28.6	4	*	*	*	<50	-
H21	A <sup>3</sup> :H <sup>3</sup>	C <sub>72</sub> H <sub>96</sub> N <sub>12</sub>	1129.644	32.4	4	*	*	*	<50	-
H25	A <sup>5</sup> :H <sup>1</sup>	C <sub>64</sub> H <sub>80</sub> N <sub>12</sub>	1017.428	28.8	5	✓			288.0	0.283
H26	A <sup>4</sup> :H <sup>2</sup>	C <sub>68</sub> H <sub>88</sub> N <sub>12</sub>	1073.536	15.5	5	*	*	*	<50	-
H27	A <sup>3</sup> :H <sup>3</sup>	C <sub>72</sub> H <sub>96</sub> N <sub>12</sub>	1129.644	28.8	5	*	✓		96.0	0.0850
H31	A <sup>5</sup> :H <sup>1</sup>	C <sub>64</sub> H <sub>80</sub> N <sub>12</sub>	1017.428	23.9	6	*	*	*	<50	-
H32	A <sup>4</sup> :H <sup>2</sup>	C <sub>68</sub> H <sub>88</sub> N <sub>12</sub>	1073.536	29.9	6	*	*	*	<50	-
H33	A <sup>3</sup> :H <sup>3</sup>	C <sub>72</sub> H <sub>96</sub> N <sub>12</sub>	1129.644	31.3	6	*	*	*	<50	-
I1	A <sup>5</sup> :I <sup>1</sup>	C <sub>68</sub> H <sub>88</sub> N <sub>12</sub>	1073.536	28.1	1	*	*	*	<50	-
I2	A <sup>4</sup> :I <sup>2</sup>	C <sub>76</sub> H <sub>104</sub> N <sub>12</sub>	1185.752	28.9	1	*	*	*	<50	-
I3	A <sup>3</sup> :I <sup>3</sup>	C <sub>84</sub> H <sub>120</sub> N <sub>12</sub>	1297.968	29.6	1	*	✓		148.0	0.114
I4	A <sup>2</sup> :I <sup>4</sup>	C <sub>92</sub> H <sub>136</sub> N <sub>12</sub>	1410.184	30.0	1	✓			300.0	0.106
I7	A <sup>5</sup> :I <sup>1</sup>	C <sub>68</sub> H <sub>88</sub> N <sub>12</sub>	1073.536	29.8	2	*	*	*	<50	-
I8	A <sup>4</sup> :I <sup>2</sup>	C <sub>76</sub> H <sub>104</sub> N <sub>12</sub>	1185.752	29.8	2	*	✓		149.0	0.0838
I9	A <sup>3</sup> :I <sup>3</sup>	C <sub>84</sub> H <sub>120</sub> N <sub>12</sub>	1297.968	31.2	2	*	✓		156.0	0.0801
I10	A <sup>2</sup> :I <sup>4</sup>	C <sub>92</sub> H <sub>136</sub> N <sub>12</sub>	1410.184	31.1	2	✓			311.0	0.0735
I12	A <sup>5</sup> :I <sup>1</sup>	C <sub>68</sub> H <sub>88</sub> N <sub>12</sub>	1073.536	22.6	3	*	*	*	<50	-
I14	A <sup>4</sup> :I <sup>2</sup>	C <sub>76</sub> H <sub>104</sub> N <sub>12</sub>	1185.752	31.8	3	*	*	*	<50	-
I15	A <sup>3</sup> :I <sup>3</sup>	C <sub>84</sub> H <sub>120</sub> N <sub>12</sub>	1297.968	29.9	3	*	*	*	<50	-
I16	A <sup>2</sup> :I <sup>4</sup>	C <sub>92</sub> H <sub>136</sub> N <sub>12</sub>	1410.184	21.5	3	✓			215.0	0.152
I19	A <sup>5</sup> :I <sup>1</sup>	C <sub>68</sub> H <sub>88</sub> N <sub>12</sub>	1073.536	22.6	4	*	*	*	<50	-
I20	A <sup>4</sup> :I <sup>2</sup>	C <sub>76</sub> H <sub>104</sub> N <sub>12</sub>	1185.752	31.8	4	*	*	*	<50	-
I21	A <sup>3</sup> :I <sup>3</sup>	C <sub>84</sub> H <sub>120</sub> N <sub>12</sub>	1297.968	29.9	4	*	*	*	<50	-
I22	A <sup>2</sup> :I <sup>4</sup>	C <sub>92</sub> H <sub>136</sub> N <sub>12</sub>	1410.184	28.7	4	✓			290.0	0.206
I25	A <sup>5</sup> :I <sup>1</sup>	C <sub>68</sub> H <sub>88</sub> N <sub>12</sub>	1073.536	16.0	5	?	✓		80.0	0.0745
I26	A <sup>4</sup> :I <sup>2</sup>	C <sub>76</sub> H <sub>104</sub> N <sub>12</sub>	1185.752	30.2	5	✓			302.0	0.254
I27	A <sup>3</sup> :I <sup>3</sup>	C <sub>84</sub> H <sub>120</sub> N <sub>12</sub>	1297.968	22.1	5	✓			220.0	0.169
I28	A <sup>2</sup> :I <sup>4</sup>	C <sub>92</sub> H <sub>136</sub> N <sub>12</sub>	1410.184	28.7	5	✓			287.0	0.203
I31	A <sup>5</sup> :I <sup>1</sup>	C <sub>68</sub> H <sub>88</sub> N <sub>12</sub>	1073.536	n	6	*	*	*	<50	-
I32	A <sup>4</sup> :I <sup>2</sup>	C <sub>76</sub> H <sub>104</sub> N <sub>12</sub>	1185.752	30.9	6	*	*	*	<50	-
I33	A <sup>3</sup> :I <sup>3</sup>	C <sub>84</sub> H <sub>120</sub> N <sub>12</sub>	1297.968	31.2	6	*	*	*	<50	-
I34	A <sup>2</sup> :I <sup>4</sup>	C <sub>92</sub> H <sub>136</sub> N <sub>12</sub>	1410.184	29.8	6	*	*	*	<50	-
J1	A <sup>5</sup> :J <sup>1</sup>	C <sub>70</sub> H <sub>88</sub> N <sub>12</sub>	1097.558	30.8	1	*	✓		154.0	0.140
J2	A <sup>4</sup> :J <sup>2</sup>	C <sub>80</sub> H <sub>104</sub> N <sub>12</sub>	1233.796	31.0	1	*	✓		155.0	0.126
J3	A <sup>3</sup> :J <sup>3</sup>	C <sub>90</sub> H <sub>120</sub> N <sub>12</sub>	1370.034	31.1	1	*	✓		155.5	0.113
J7	A <sup>5</sup> :J <sup>1</sup>	C <sub>70</sub> H <sub>88</sub> N <sub>12</sub>	1097.558	28.9	2	*	✓		144.5	0.132
J8	A <sup>4</sup> :J <sup>2</sup>	C <sub>80</sub> H <sub>104</sub> N <sub>12</sub>	1233.796	30.9	2	*	✓		154.5	0.125
J9	A <sup>3</sup> :J <sup>3</sup>	C <sub>90</sub> H <sub>120</sub> N <sub>12</sub>	1370.034	29.8	2	*	*	✓	100.7	0.073
J13	A <sup>5</sup> :J <sup>1</sup>	C <sub>70</sub> H <sub>88</sub> N <sub>12</sub>	1097.558	29.3	3	*	*	*	<50	-
J14	A <sup>4</sup> :J <sup>2</sup>	C <sub>80</sub> H <sub>104</sub> N <sub>12</sub>	1233.796	31.9	3	*	*	*	<50	-
J15	A <sup>3</sup> :J <sup>3</sup>	C <sub>90</sub> H <sub>120</sub> N <sub>12</sub>	1370.034	30	3	✓			300.0	0.219
J19	A <sup>5</sup> :J <sup>1</sup>	C <sub>70</sub> H <sub>88</sub> N <sub>12</sub>	1097.558	30	4	*	✓		150.0	0.137
J20	A <sup>4</sup> :J <sup>2</sup>	C <sub>80</sub> H <sub>104</sub> N <sub>12</sub>	1233.796	28.8	4	✓			288.0	0.233
J21	A <sup>3</sup> :J <sup>3</sup>	C <sub>90</sub> H <sub>120</sub> N <sub>12</sub>	1370.034	31.3	4	*	*	*	<50	-
J25	A <sup>5</sup> :J <sup>1</sup>	C <sub>70</sub> H <sub>88</sub> N <sub>12</sub>	1097.558	28.6	5	*	*	✓	95.3	0.0868
J26	A <sup>4</sup> :J <sup>2</sup>	C <sub>80</sub> H <sub>104</sub> N <sub>12</sub>	1233.796	30.2	5	*	*	*	<50	-
J27	A <sup>3</sup> :J <sup>3</sup>	C <sub>90</sub> H <sub>120</sub> N <sub>12</sub>	1370.034	32.9	5	*	*	*	<50	-
J31	A <sup>5</sup> :J <sup>1</sup>	C <sub>70</sub> H <sub>88</sub> N <sub>12</sub>	1097.558	28.8	6	*	*	*	<50	-
J32	A <sup>4</sup> :J <sup>2</sup>	C <sub>80</sub> H <sub>104</sub> N <sub>12</sub>	1233.796	31.3	6	*	*	*	<50	-
J33	A <sup>3</sup> :J <sup>3</sup>	C <sub>90</sub> H <sub>120</sub> N <sub>12</sub>	1370.034	30.6	6	*	*	*	<50	-
K1	A <sup>5</sup> :K <sup>1</sup>	C <sub>59</sub> H <sub>70</sub> N <sub>12</sub>	947.293	30.3	1	*	*	*	<50	-
K2	A <sup>4</sup> :K <sup>2</sup>	C <sub>58</sub> H <sub>68</sub> N <sub>12</sub>	933.266	29.9	1	*	*	*	<50	-
K3	A <sup>3</sup> :K <sup>3</sup>	C <sub>57</sub> H <sub>66</sub> N <sub>12</sub>	919.239	31.1	1	*	✓		155.5	0.169
K4	A <sup>2</sup> :K <sup>4</sup>	C <sub>56</sub> H <sub>64</sub> N <sub>12</sub>	905.212	28.1	1	*	*	*	<50	-
K5	A <sup>1</sup> :K <sup>5</sup>	C <sub>55</sub> H <sub>62</sub> N <sub>12</sub>	891.185	29.9	1	*	*	*	<50	-
K6	A <sup>0</sup> :K <sup>6</sup>	C <sub>54</sub> H <sub>60</sub> N <sub>12</sub>	877.158	29.8	1	*	*	*	<50	-
K7	A <sup>5</sup> :K <sup>1</sup>	C <sub>59</sub> H <sub>70</sub> N <sub>12</sub>	947.293	28.9	2	*	*	✓	96.3	0.102
K8	A <sup>4</sup> :K <sup>2</sup>	C <sub>58</sub> H <sub>68</sub> N <sub>12</sub>	933.266	29.8	2	*	*	✓	99.3	0.104
K9	A <sup>3</sup> :K <sup>3</sup>	C <sub>57</sub> H <sub>66</sub> N <sub>12</sub>	919.239	30.8	2	✓			308.0	0.335
K10	A <sup>2</sup> :K <sup>4</sup>	C <sub>56</sub> H <sub>64</sub> N <sub>12</sub>	905.212	30.0	2	*	*	✓	142.5	0.160
K11	A <sup>1</sup> :K <sup>5</sup>	C <sub>55</sub> H <sub>62</sub> N <sub>12</sub>	891.185	28.5	2	*	*	*	<50	-
K12	A <sup>0</sup> :K <sup>6</sup>	C <sub>54</sub> H <sub>60</sub> N <sub>12</sub>	877.158	29.5	2	*	*	*	<50	-
K13	A <sup>5</sup> :K <sup>1</sup>	C <sub>59</sub> H <sub>70</sub> N <sub>12</sub>	947.293	28.4	3	*	*	*	<50	-
K14	A <sup>4</sup> :K <sup>2</sup>	C <sub>58</sub> H <sub>68</sub> N <sub>12</sub>	933.266	29.8	3	*	*	*	<50	-

<b>K15</b>	A <sup>3</sup> :K <sup>3</sup>	C <sub>57</sub> H <sub>66</sub> N <sub>12</sub>	919.239	31	3	*	*	*	<50	-
<b>K16</b>	A <sup>2</sup> :K <sup>4</sup>	C <sub>56</sub> H <sub>64</sub> N <sub>12</sub>	905.212	29	3	*	*	*	<50	-
<b>K17</b>	A <sup>1</sup> :K <sup>5</sup>	C <sub>55</sub> H <sub>62</sub> N <sub>12</sub>	891.185	31	3	*	*	*	<50	-
<b>K18</b>	A <sup>0</sup> :K <sup>6</sup>	C <sub>54</sub> H <sub>60</sub> N <sub>12</sub>	877.158	30.1	3	*	*	*	<50	-
<b>K19</b>	A <sup>5</sup> :K <sup>1</sup>	C <sub>59</sub> H <sub>70</sub> N <sub>12</sub>	947.293	31.1	4	*	*	*	<50	-
<b>K20</b>	A <sup>4</sup> :K <sup>2</sup>	C <sub>58</sub> H <sub>68</sub> N <sub>12</sub>	933.266	29.7	4	*	*	*	<50	-
<b>K21</b>	A <sup>3</sup> :K <sup>3</sup>	C <sub>57</sub> H <sub>66</sub> N <sub>12</sub>	919.239	28.8	4	*	*	*	<50	-
<b>K22</b>	A <sup>2</sup> :K <sup>4</sup>	C <sub>56</sub> H <sub>64</sub> N <sub>12</sub>	905.212	29.6	4	*	*	*	<50	-
<b>K23</b>	A <sup>1</sup> :K <sup>5</sup>	C <sub>55</sub> H <sub>62</sub> N <sub>12</sub>	891.185	31.4	4	*	*	*	<50	-
<b>K24</b>	A <sup>0</sup> :K <sup>6</sup>	C <sub>54</sub> H <sub>60</sub> N <sub>12</sub>	877.158	28.7	4	*	*	*	<50	-
<b>K25</b>	A <sup>5</sup> :K <sup>1</sup>	C <sub>59</sub> H <sub>70</sub> N <sub>12</sub>	947.293	29.4	5	*	*	*	<50	-
<b>K26</b>	A <sup>4</sup> :K <sup>2</sup>	C <sub>58</sub> H <sub>68</sub> N <sub>12</sub>	933.266	29.7	5	*	*	*	<50	-
<b>K27</b>	A <sup>3</sup> :K <sup>3</sup>	C <sub>57</sub> H <sub>66</sub> N <sub>12</sub>	919.239	29.1	5	*	*	*	<50	-
<b>K28</b>	A <sup>2</sup> :K <sup>4</sup>	C <sub>56</sub> H <sub>64</sub> N <sub>12</sub>	905.212	28.1	5	*	*	*	<50	-
<b>K29</b>	A <sup>1</sup> :K <sup>5</sup>	C <sub>55</sub> H <sub>62</sub> N <sub>12</sub>	891.185	30.5	5	*	*	*	<50	-
<b>K30</b>	A <sup>0</sup> :K <sup>6</sup>	C <sub>54</sub> H <sub>60</sub> N <sub>12</sub>	877.158	27.5	5	*	*	*	<50	-
<b>K31</b>	A <sup>5</sup> :K <sup>1</sup>	C <sub>59</sub> H <sub>70</sub> N <sub>12</sub>	947.293	29.8	6	*	*	*	<50	-
<b>K32</b>	A <sup>4</sup> :K <sup>2</sup>	C <sub>58</sub> H <sub>68</sub> N <sub>12</sub>	933.266	30.1	6	*	*	*	<50	-
<b>K33</b>	A <sup>3</sup> :K <sup>3</sup>	C <sub>57</sub> H <sub>66</sub> N <sub>12</sub>	919.239	32.3	6	*	*	*	<50	-
<b>K34</b>	A <sup>2</sup> :K <sup>4</sup>	C <sub>56</sub> H <sub>64</sub> N <sub>12</sub>	905.212	30.1	6	*	*	*	<50	-
<b>K35</b>	A <sup>1</sup> :K <sup>5</sup>	C <sub>55</sub> H <sub>62</sub> N <sub>12</sub>	891.185	31.3	6	*	*	*	<50	-
<b>K36</b>	A <sup>0</sup> :K <sup>6</sup>	C <sub>54</sub> H <sub>60</sub> N <sub>12</sub>	877.158	32.2	6	*	*	*	<50	-

**Appendix Table 9:** Volume of xenon evolved from porous liquids made from scrambled A<sup>3</sup>:E<sup>3</sup> cage in the different size-excluded solvents (200 mg mL<sup>-1</sup>) before and after purification

Solvent	Code	Purity (%)	Purification method	Xenon evolved (mL)	
				Measurement 1	Measurement 2
1	DCBC	97	As bought	0.6	0.8
		≥99	Distilled	1.7	1.0
2	TBA	97	As bought	1.5	1.8
		99	Distilled	2.2	1.9
		≥99	Distilled and alumina	2.8	2.8
3	MS	99	As bought	1.6	1.8
		≥99	Distilled	2.3	2.3
4	DCT	99	As bought	2.1	-
		≥99	Distilled	2.0	1.8
5	HAP	99	As bought	2.0	1.9
		≥99	Distilled	3.2	2.9
6	PCP	≥99	Alumina	4.3	4.5



## Chapter 3

Appendix Table 10: Possible intermediates during the formation of CC21.

Entry	No. of TFB	No. of DMHDA	No. of Imine Bonds	MW (calc.)	m/z (calc.)	calc. [M+H] <sup>+</sup>	calc. [M+2H] <sup>2+</sup>	calc. [M+Na] <sup>+</sup>	calc. [M+2Na] <sup>2+</sup>	calc. [M+H+Na] <sup>2+</sup>
1	1	1	1	288.3910	288.1837	289.1915	145.09965	311.1735	167.08165	156.0907
2	1	2	2	414.6380	414.3357	415.3435	208.17565	437.3255	207.16785	218.6628
3	1	3	3	540.8850	540.4877	541.4955	271.25165	563.4775	270.24385	270.2439
4	2	1	2	432.5200	432.2048	433.2126	217.1102	455.1946	216.1024	216.1024
5	2	2	3	558.7670	558.3568	559.3646	280.1862	581.3466	279.1784	279.1784
6	2	2	4	540.7520	540.3462	541.3540	271.1809	563.3360	270.1731	270.1731
7	2	3	4	685.0140	684.5088	685.5166	343.2622	707.4986	342.2544	342.2544
8	2	3	5	666.9990	666.4982	667.5060	334.2569	689.4880	333.2491	333.2491
9	2	3	6	648.9840	648.4876	649.4954	325.2516	671.4774	324.2438	324.2438
10	2	4	5	811.2610	810.6608	811.6686	406.3382	833.6506	405.3304	405.3304
11	2	4	6	793.2460	792.6502	793.6580	397.3329	815.6400	396.3251	396.3251
12	2	5	6	937.5080	936.8128	937.8206	469.4142	959.8026	468.4064	468.4064
13	3	2	4	702.8960	702.3779	703.3857	352.19675	725.3677	351.18895	351.189
14	3	3	5	829.1430	828.5299	829.5377	415.27275	851.5197	414.26495	414.265
15	3	3	6	811.1280	810.5193	811.5271	406.26745	833.5091	405.25965	405.2597
16	3	4	6	955.3900	954.6819	955.6897	478.34875	977.6717	477.34095	477.341
17	3	4	7	937.3750	936.6713	937.6791	469.34345	959.6611	468.33565	468.3357
18	3	4	8	919.3600	918.6607	919.6685	460.33815	941.6505	459.33035	459.3304
19	3	5	7	1081.6370	1080.8339	1081.8417	541.42475	1103.8237	540.41695	540.417
20	3	5	8	1063.6220	1062.8233	1063.8311	532.41945	1085.8131	531.41165	531.4117
21	3	5	9	1045.6070	1044.8127	1045.8205	523.41415	1067.8025	522.40635	522.4064
22	3	6	8	1207.8840	1206.9859	1207.9937	604.50075	1229.9757	603.49295	603.493
23	3	6	9	1189.8690	1188.9753	1189.9831	595.49545	1211.9651	594.48765	594.4877
24	3	7	9	1334.1310	1333.1379	1334.1457	667.57675	1356.1277	666.56895	666.569
25	4	3	6	973.2720	972.5510	973.5588	487.2833	995.5408	486.2755	486.2755
26	4	4	7	1099.5190	1098.7030	1099.7108	550.3593	1121.6928	549.3515	549.3515
27	4	4	8	1081.5040	1080.6924	1081.7002	541.354	1103.6822	540.3462	540.3462
28	4	5	8	1225.7660	1224.8550	1225.8628	613.4353	1247.8448	612.4275	612.4275
29	4	5	9	1207.7510	1206.8444	1207.8522	604.43	1229.8342	603.4222	603.4222
30	4	5	10	1189.7360	1188.8338	1189.8416	595.4247	1211.8236	594.4169	594.4169
31	4	6	9	1352.0130	1351.0070	1352.0148	676.5113	1373.9968	675.5035	675.5035
32	4	6	10	1333.9980	1332.9964	1334.0042	667.506	1355.9862	666.4982	666.4982
33	4	6	11	1315.9830	1314.9858	1315.9936	658.5007	1337.9756	657.4929	657.4929
34	4	6	12	1297.9680	1296.9752	1297.9830	649.4954	1319.9650	648.4876	648.4876
35	4	7	10	1478.2600	1477.1590	1478.1668	739.5873	1500.1488	738.5795	738.5795
36	4	7	11	1460.2450	1459.1484	1460.1562	730.582	1482.1382	729.5742	729.5742
37	4	7	12	1442.2300	1441.1378	1442.1456	721.5767	1464.1276	720.5689	720.5689
38	4	8	11	1604.5070	1603.3110	1604.3188	802.6633	1626.3008	801.6555	801.6555
39	4	8	12	1586.4920	1585.3004	1586.3082	793.658	1608.2902	792.6502	792.6502
40	4	9	12	1730.7540	1729.4630	1730.4708	865.7393	1752.4528	864.7315	864.7315

**Appendix Table 11:** Single crystal X-ray refinement details for; **CC21**·9(CHCl<sub>3</sub>)·10.5(CH<sub>4</sub>O)·(H<sub>2</sub>O) and **CC21-α**.

	<b>CC21</b> ·9(CHCl <sub>3</sub> )·10.5(CH <sub>4</sub> O)·(H <sub>2</sub> O)	<b>CC21-α</b> <sup>[a]</sup>
Crystallisation Solvent	CHCl <sub>3</sub> /MeOH	
Space Group	<i>P2</i> <sub>1</sub>	<i>P2</i> <sub>1</sub>
Wavelength [Å]	Mo-Kα	Mo-Kα
Collection Temperature	100 K	100 K
Formula	2(C <sub>84</sub> H <sub>120</sub> N <sub>12</sub> )·9(CHCl <sub>3</sub> )·10.5(CH <sub>4</sub> O)·(H <sub>2</sub> O)	2(C <sub>84</sub> H <sub>120</sub> N <sub>12</sub> )
<i>Mr</i>	4024.59	
Crystal Size (mm)	0.31 x 0.27 x 0.07	0.20 x 0.16 x 0.04
Crystal System	Monoclinic	Monoclinic
<i>a</i> [Å]	16.0941(13)	14.7314(3)
<i>b</i> [Å]	45.047(4)	41.6927(8)
<i>c</i> [Å]	16.4682(15)	15.9578(3)
$\alpha$ [°]		
$\beta$ [°]	105.336(2)	94.0143(19)
$\gamma$ [°]		
<i>V</i> [Å <sup>3</sup> ]	11514.2(17)	9777.1(3)
<i>Z</i>	2	2
<i>D</i> <sub>calcd</sub> [g cm <sup>-3</sup> ]	1.161	0.882
$\mu$ [mm <sup>-1</sup> ]	0.373	0.052
<i>F</i> (000)	4274	2832
2 $\theta$ range [°]	2.72 – 46.51	3.39 – 46.58
Reflections collected	84088	86289
Independent reflections, <i>R</i> <sub>int</sub>	27498, 0.0589	27809, 0.1257
Obs. Data [ <i>I</i> > 2 $\sigma$ ]	18041	17782
Data / restraints / parameters	27498 / 154 / 2135	27809 / 1 / 1777
Final <i>R</i> 1 values ( <i>I</i> > 2 $\sigma$ ( <i>I</i> ))	0.0999	0.0660
Final <i>R</i> 1 values (all data)	0.1259	0.1257
Final w <i>R</i> ( <i>F</i> <sup>2</sup> ) values (all data)	0.2647	0.1399
Goodness-of-fit on <i>F</i> <sup>2</sup>	1.500	1.005
Largest difference peak and hole [e·Å <sup>-3</sup> ]	0.421/-0.353	0.354 / -0.166
CCDC		

[a] After desolvating crystal of **CC21**—isolated by filtration from CH<sub>2</sub>Cl<sub>2</sub>—at 353 K and then running gas sorption analysis at 77.3 K, crystals of **CC21-α** were weakly diffracting at high angle. Consequently, a resolution limit of 0.9 Å was applied during structure refinement.

## Chapter 4

Appendix Table 12: Weight lost by parent solvents after being left under vacuum for 24 hrs

Solvent	Mass before (g)	Mass after 24 hrs (g)	Mass lost (g)
1	43.3360	43.2983	0.0353
2	43.6501	43.5273	0.1228
3	41.5774	41.3162	0.2612
4	44.3503	43.7963	0.554

Appendix Table 13: Summary of porosity testing carried out using chemical displacement of xenon to determine which of the new cage/solvent combinations were porous.

Porous liquid code	Scrambled cage	Solvent	Dissolved at 200 mg mL <sup>-1</sup>	Xenon evolved at 200 mg mL <sup>-1</sup>
E3	A <sup>3</sup> :E <sup>3</sup>	1	✓	1.4
E9	A <sup>3</sup> :E <sup>3</sup>	2	✓	2.8
E15	A <sup>3</sup> :E <sup>3</sup>	3	✓	2.3
E21	A <sup>3</sup> :E <sup>3</sup>	4	✓	1.9
E27	A <sup>3</sup> :E <sup>3</sup>	5	✓	3.1
G3	A <sup>3</sup> :G <sup>3</sup>	1	✓	1.4
G4	A <sup>2</sup> :G <sup>4</sup>	1	✓	0.8
G5	A <sup>1</sup> :G <sup>5</sup>	1	✓	1.0
G8	A <sup>4</sup> :G <sup>2</sup>	2	✓	0.5
G9	A <sup>3</sup> :G <sup>3</sup>	2	✓	0.8
G10	A <sup>2</sup> :G <sup>4</sup>	2	✓	1.2
G11	A <sup>1</sup> :G <sup>5</sup>	2	✓	1.0
G15	A <sup>3</sup> :G <sup>3</sup>	3	✓	1.2
G16	A <sup>2</sup> :G <sup>4</sup>	3	✓	2.8*
G17	A <sup>1</sup> :G <sup>5</sup>	3	✓	1.9
G21	A <sup>3</sup> :G <sup>3</sup>	4	✓	1.1
G22	A <sup>2</sup> :G <sup>4</sup>	4	✓	0.9
G23	A <sup>1</sup> :G <sup>5</sup>	4	✓	1.6
G27	A <sup>3</sup> :G <sup>3</sup>	5	✓	0.4
G28	A <sup>2</sup> :G <sup>4</sup>	5	✓	0.6
G29	A <sup>1</sup> :G <sup>5</sup>	5	✓	1.2
H25	A <sup>5</sup> :H <sup>1</sup>	5	✓	2.1
I4	A <sup>2</sup> :I <sup>4</sup>	1	✓	1.1
I10	A <sup>2</sup> :I <sup>4</sup>	2	✓	1.0
I16	A <sup>2</sup> :I <sup>4</sup>	3	✓	0.4
I22	A <sup>2</sup> :I <sup>4</sup>	4	✓	2.0
I26	A <sup>4</sup> :I <sup>2</sup>	5	✓	2.2
I27	A <sup>3</sup> :I <sup>3</sup>	5	✓	2.0*
I28	A <sup>2</sup> :I <sup>4</sup>	5	✓	1.7
K9	A <sup>3</sup> :K <sup>3</sup>	2	Gel formed	n/a

\*carried out at 100 mg in 0.5 mL due to low yield

NB. G16 appeared to have a reasonable xenon uptake when tested in the initial porosity screen (Table S12), but when gas evolution was attempted at a higher volume (>1 mL), the porous liquid suffered from gelation, so was not investigated further.

**Appendix Table 14:** Average viscosities calculated for the 3<sup>3</sup>:13<sup>3</sup> porous liquid family at 20% w/v

Porous liquid	Measurement 1 (cP)	Measurement 2 (cP)	Measurement 3 (cP)	Average $\pm$ SD (cP)	Average Temperature (°C)
3 <sup>3</sup> :13 <sup>3</sup> <sub>DCBC</sub>	14.91	14.90	14.97	14.93 $\pm$ 0.038	25.01
3 <sup>3</sup> :13 <sup>3</sup> <sub>TBA</sub>	31.93	32.48	32.98	32.46 $\pm$ 0.53	25.02
3 <sup>3</sup> :13 <sup>3</sup> <sub>MS</sub>	9.841	9.841	9.840	9.84 $\pm$ 5.7x10 <sup>-4</sup>	25.03
3 <sup>3</sup> :13 <sup>3</sup> <sub>DCT</sub>	3.694	3.698	3.700	3.70 $\pm$ 0.0031	25.03
3 <sup>3</sup> :13 <sup>3</sup> <sub>HAP</sub>	9.800	9.825	9.826	9.82 $\pm$ 0.015	24.97

**Appendix Table 15:** Average viscosities measured for the neat parent solvents after purification

Solvent	Measurement 1 (cP)	Measurement 2 (cP)	Measurement 3 (cP)	Average $\pm$ SD (cP)	Average Temperature (°C)
DCBC	3.291	3.281	3.291	3.29 $\pm$ 0.0058	24.99
TBA	7.924	7.920	7.930	7.92 $\pm$ 0.0050	25.01
MS	2.961	2.964	2.964	2.96 $\pm$ 0.0017	24.99
DCT	1.330	1.331	1.334	1.33 $\pm$ 0.0021	25.01
HAP	2.919	2.926	2.917	2.92 $\pm$ 0.0047	25.03

**Appendix Table 16:** Average densities calculated for the 3<sup>3</sup>:13<sup>3</sup> porous liquid family at 20% w/v

Porous liquid	Sample 1	Sample 2	Sample 3	Average density (g mL <sup>-1</sup> )	Standard deviation ( $\pm$ g mL <sup>-1</sup> )
	Mass (g)	Mass (g)	Mass (g)		
3 <sup>3</sup> :13 <sup>3</sup> <sub>DCBC</sub>	1.3073	1.3088	1.3135	1.3099	0.0032
3 <sup>3</sup> :13 <sup>3</sup> <sub>TBA</sub>	1.2656	1.2675	1.2612	1.2648	0.0032
3 <sup>3</sup> :13 <sup>3</sup> <sub>MS</sub>	1.1244	1.1236	1.1233	1.1238	0.0006
3 <sup>3</sup> :13 <sup>3</sup> <sub>DCT</sub>	1.1883	1.1931	1.1803	1.1872	0.0065
3 <sup>3</sup> :13 <sup>3</sup> <sub>HAP</sub>	1.0294	1.0226	1.0201	1.0240	0.0048

**Appendix Table 17:** Average densities measured for the neat parent solvents after purification

Solvent	Reported density (g mL <sup>-1</sup> )*	Sample 1	Sample 2	Sample 3	Average density (g mL <sup>-1</sup> )	Standard deviation ( $\pm$ g mL <sup>-1</sup> )
		Mass (g)	Mass (g)	Mass (g)		
DCBC	1.407	1.3218	1.3693	1.3403	1.3438	0.0239
TBA	1.326	1.2417	1.2362	1.2592	1.2457	0.0120
MS	1.174	1.1606	1.1441	1.1609	1.1552	0.0096
DCT	1.246	1.1524	1.1639	1.1913	1.1692	0.0200
HAP	1.131	1.0868	1.0844	1.0857	1.0856	0.0012

\*Reported from Sigma Aldrich

**Appendix Table 18:** Calculation of the scrambled cage to solvent ratio in each of the porous liquids at 20% w/v

Porous liquid	Mmol cage in sample	Mmol solvent in sample	Cage: Solvent
$3^3:13^3_{DCBC}$	0.192	7.20	1:37
$3^3:13^3_{TBA}$	0.192	6.90	1:36
$3^3:13^3_{MS}$	0.192	7.72	1:40
$3^3:13^3_{DCT}$	0.192	7.74	1:40
$3^3:13^3_{HAP}$	0.192	8.31	1:40
$3^3:13^3_{PCP}$	0.192	6.89	1:37

**Appendix Table 19:** Properties of the  $3^3:13^3$  scrambled cage used to calculate total pore volumes in the porous liquid family.

Scrambled Cage	Mass(g)	MW (g mol <sup>-1</sup> )	Moles of cage (mol)	Molecules of cage using Avogadro's constant	Pore volume of single cage (mL)
$3^3:13^3$	0.2	1039.43	$1.92 \times 10^{-4}$	$1.159 \times 10^{20}$	$6.545 \times 10^{-23}$

**Appendix Table 20:** Total pore volumes calculated for the scrambled  $3^3:13^3$  cage porous liquid family at 20% w/v (200 mg in 1 mL).

Porous liquid	Measured density of solvent (g mL <sup>-1</sup> )	Mass of PL sample (g)	Measured density of PL (g mL <sup>-1</sup> )	Overall PL volume (mL)	Pore volume (%)
$3^3:13^3_{DCBC}$	1.3438	1.5438	1.3099	1.18	<b>0.64</b>
$3^3:13^3_{TBA}$	1.2457	1.4457	1.2648	1.14	<b>0.66</b>
$3^3:13^3_{MS}$	1.1552	1.3552	1.1238	1.21	<b>0.63</b>
$3^3:13^3_{DCT}$	1.1692	1.3692	1.1872	1.15	<b>0.66</b>
$3^3:13^3_{HAP}$	1.0856	1.2856	1.0240	1.17	<b>0.65</b>

**Appendix Table 21:** Volume of xenon evolved from the different scrambled  $3^3:13^3$  porous liquids at 20% w/v by chemical displacement with chloroform.

Porous liquid	Volume of xenon evolved (mL)		Average $\pm$ SD (mL)	% occupancy
	Measurement 1	Measurement 2		
$3^3:13^3_{DCBC}$	1.7	1.0	$1.4 \pm 0.5$	30.4
$3^3:13^3_{TBA}$	2.8	3.0	$3.0 \pm 0.3$	65.2
$3^3:13^3_{MS}$	2.2	2.3	$2.3 \pm 0.1$	50.0
$3^3:13^3_{DCT}$	1.8	2.1	$1.9 \pm 0.1$	41.3
$3^3:13^3_{HAP}$	3.2	2.9	$3.1 \pm 0.2$	67.4
$3^3:13^3_{PCP}$	4.3	4.5	$4.4 \pm 0.1$	95.7

**Appendix Table 22:** Volume of xenon evolved from  $3^3:13^3$  porous liquids at 20% w/v in  $\mu$ mol

Porous liquid	Volume of xenon evolved ( $\mu$ mol)		Average $\pm$ SD ( $\mu$ mol)
	Measurement 1	Measurement 2	
$3^3:13^3_{DCBC}$	70.7	41.6	$56.2 \pm 20.6$
$3^3:13^3_{TBA}$	116.5	124.8	$120.6 \pm 5.9$
$3^3:13^3_{MS}$	91.5	95.7	$93.6 \pm 2.9$
$3^3:13^3_{DCT}$	74.9	87.3	$81.1 \pm 8.8$
$3^3:13^3_{HAP}$	133.1	120.6	$126.9 \pm 8.8$
$3^3:13^3_{PCP}$	178.9	187.2	$183.0 \pm 5.9$

**Appendix Table 23:** Volume of xenon evolved from the different scrambled porous liquids containing different cage components at 20% w/v by chemical displacement with chloroform.

Porous liquid	Xenon evolution (mL)	Xenon evolution ( $\mu\text{mol}$ )
$3^3:13^3_{\text{MS}}$	2.3	95.7
$3^3:13^3_{\text{HAP}}$	3.1	129.0
$3^3:13^3_{\text{PCP}}$	4.4	183.0
$A^3:G^3_{\text{MS}}$	1.2	50.0
$A^2:G^4_{\text{MS}}$	2.8	116.5
$A^1:G^5_{\text{MS}}$	1.9	79.0
$A^5:H^1_{\text{HAP}}$	2.1	87.3
$A^4:I^2_{\text{HAP}}$	2.2	91.5

**Appendix Table 24:** Calculated xenon uptake ( $\mu\text{mol g}_{\text{PL}}^{-1}$ ) from gas evolution measurements for scrambled  $3^3:13^3$  porous liquid family at 20% w/v

Porous liquid	Volume of xenon evolved ( $\mu\text{mol g}_{\text{PL}}^{-1}$ )		Average $\pm$ SD ( $\mu\text{mol g}_{\text{PL}}^{-1}$ )
	Measurement 1	Measurement 2	
$3^3:13^3_{\text{DCBC}}$	45.8	26.9	$36.4 \pm 13.4$
$3^3:13^3_{\text{TBA}}$	80.6	86.3	$83.5 \pm 4.0$
$3^3:13^3_{\text{MS}}$	67.5	70.6	$69.1 \pm 2.2$
$3^3:13^3_{\text{DCT}}$	54.7	63.8	$59.3 \pm 6.4$
$3^3:13^3_{\text{HAP}}$	103.5	93.8	$98.7 \pm 6.9$
$3^3:13^3_{\text{PCP}}$	93.6	97.9	$95.6 \pm 3.0$

**Appendix Table 25:** Calculated xenon uptake ( $\mu\text{mol mL}_{\text{PL}}^{-1}$ ) from gas evolution measurements for scrambled  $3^3:13^3$  porous liquid family at 20% w/v

Porous liquid	Measured Density of PL	Volume of xenon evolved ( $\mu\text{mol mL}_{\text{PL}}^{-1}$ )		Average $\pm$ SD ( $\mu\text{mol mL}_{\text{PL}}^{-1}$ )
		Measurement 1	Measurement 2	
$3^3:13^3_{\text{DCBC}}$	1.3099	60.0	35.3	$47.6 \pm 17.5$
$3^3:13^3_{\text{TBA}}$	1.2648	101.9	109.2	$105.5 \pm 5.1$
$3^3:13^3_{\text{MS}}$	1.1238	75.9	79.3	$77.6 \pm 2.4$
$3^3:13^3_{\text{DCT}}$	1.1883	65.0	75.8	$70.4 \pm 7.7$
$3^3:13^3_{\text{HAP}}$	1.024	106.0	96.1	$101.0 \pm 7.0$
$3^3:13^3_{\text{PCP}}$	1.6193	151.5	158.6	$155.1 \pm 5.0$

**Appendix Table 26:** Calculated xenon uptakes from gas evolution measurements for parent solvents

Solvent	Volume of xenon evolved (mL)	Mass of solvent used (g)	Density of solvent ( $\text{g mL}^{-1}$ )	Xenon uptake ( $\mu\text{mol}$ )	Xenon uptake ( $\mu\text{mol g}_{\text{sol}}^{-1}$ )	Xenon uptake ( $\mu\text{mol mL}_{\text{sol}}^{-1}$ )
DCBC	0.4	1.3438	1.3438	16.6	12.4	16.7
TBA	0.3	1.2457	1.2457	12.5	10.0	12.5
MS	0.3	1.1552	1.1552	12.5	10.8	12.5
DCT	0.6	1.1692	1.1692	25.0	21.3	24.9
HAP	0.2	1.0856	1.0856	8.3	7.7	8.4
PCP	0.2	1.7112	1.7650	8.3	4.9	8.4

**Appendix Table 27:** Methane uptake in scrambled 3<sup>3</sup>:13<sup>3</sup> porous liquids at 20% w/v

Porous Liquid	NCH integration relative to TMS = 1	NCH integration range (ppm)	Calculated [PL] concentration from calibration curve (mg <sub>cage</sub> mL <sup>-1</sup> )	Calculated [PL] concentration (mmol <sub>cage</sub> mL <sup>-1</sup> ) using average MW = 1039.43	Value cage NCH integration set to:	CH <sub>4</sub> integration relative to cage (4H)	CH <sub>4</sub> shift (ppm)	CH <sub>4</sub> integration range (ppm)	Cage: CH <sub>4</sub> Ratio (based on integrations)	Calculated CH <sub>4</sub> uptake (μmol mL <sup>-1</sup> )
3 <sup>3</sup> :13 <sup>3</sup> <sub>D</sub> CBC	11.90	3.50 to 2.60	197.4	0.190	12	0.30	-	-0.90 to -0.96	1:0.075	14.2
3 <sup>3</sup> :13 <sup>3</sup> <sub>T</sub> BA	8.59	3.61 to 2.80	142.5	0.137	12	0.55	-	-1.27 to -1.31	1:0.138	18.9
3 <sup>3</sup> :13 <sup>3</sup> <sub>MS</sub> <sup>a</sup>	9.87 <sup>a</sup>	8.16 to 7.74	163.8	0.158	24 <sup>a</sup>	0.52	-	-1.46 to -1.50	1:0.130	20.5
3 <sup>3</sup> :13 <sup>3</sup> <sub>D</sub> CT	10.73	3.64 to 2.94	178.0	0.171	12	0.41	-	-1.02 to -1.07	1:0.103	17.6
3 <sup>3</sup> :13 <sup>3</sup> <sub>HAP</sub>	9.13	3.92 to 3.28	151.5	0.146	12	0.70	-	-1.86 to -1.91	1:0.175	25.5
3 <sup>3</sup> :13 <sup>3</sup> <sub>P</sub> CP	10.45	3.67 to 2.70	173.4	0.167	12	1.96	-	-2.83 to -2.96	1:0.490	81.7

<sup>a</sup>Typically, the cage concentration in the porous liquid is calculated using the calibration curve by comparing the NCH integration, equating to 12H, to TMS = 1. However, the solvent peaks overlapped with the NCH peaks in the 3<sup>3</sup>:13<sup>3</sup><sub>MS</sub> porous liquid, which meant they could not be used to calculate the relative uptake in this system. In this case, the aromatic and imine protons in the cage were used which have an integration of 24. Therefore, the integration (ArH + N=CH = 19.74, relative to TMS = 1) was halved to account for this before the concentration of the porous liquid was calculated. TMS was integrated between 0.01 to -0.01 for all spectra.

**Appendix Table 28:** Methane uptake (μmol mL<sup>-1</sup>) for scrambled porous liquids containing different scrambled cages at 20% w/v

Porous Liquid	NCH integration relative to TMS = 1	NCH integration range (ppm)	Calculated [PL] concentration from calibration curve (mg <sub>cage</sub> mL <sup>-1</sup> )	Calculated [PL] concentration (mmol <sub>cage</sub> mL <sup>-1</sup> ) using average MW = 1039.43	Value cage NCH integration set to	CH <sub>4</sub> integration relative to cage (4H)	CH <sub>4</sub> shift (ppm)	CH <sub>4</sub> integration range (ppm)	Cage: CH <sub>4</sub> Ratio (based on integrations)	Calculated CH <sub>4</sub> uptake (μmol mL <sup>-1</sup> )
A <sup>3</sup> :G <sup>3</sup> <sub>MS</sub> <sup>a</sup>	8.46	8.33 to 7.59	140.4	0.249	24 <sup>a</sup>	0.60	-	-0.90 to -0.95	1:0.15	20.6
A <sup>2</sup> :G <sup>4</sup> <sub>MS</sub> <sup>a</sup>	7.77	8.22 to 7.58	128.8	0.217	24 <sup>a</sup>	0.76	-	-0.80 to -0.90	1:0.19	18.6
A <sup>1</sup> :G <sup>5</sup> <sub>MS</sub> <sup>a</sup>	6.74	8.19 to 7.58	111.7	0.179	24 <sup>a</sup>	0.84	-	-1.51 to -1.58	1:0.21	18.9
A <sup>5</sup> :H <sup>1</sup> <sub>HAP</sub>	10.01	4.10 to 3.28	166.1	0.163	12	0.57	-	-1.06 to -1.14	1:0.14	23.3
A <sup>4</sup> :I <sup>2</sup> <sub>HAP</sub>	6.09	4.10 to 3.20	101.0	0.085	12	0.89	-	-1.107 to -1.123	1:0.22	19.0

<sup>a</sup>Typically, the cage concentration in the porous liquid is calculated using the calibration curve by comparing the NCH integration, equating to 12H, to TMS = 1. However, the solvent peaks overlapped with the NCH peaks in the MS based porous liquids, which meant they could not be used to calculate the relative uptake in this system. In this case, the aromatic and imine protons in the cage were used which have an integration of 24. Therefore, the integration (ArH + N=CH = 19.74, relative to TMS = 1) was halved to account for this before the concentration of the porous liquid was calculated. TMS was integrated between 0.01 to -0.01 for all spectra.

**Appendix Table 29:** Calculation of the CH<sub>4</sub> uptake in each parent solvent

	Cage: CH <sub>4</sub> ratio based on integrations		Conversion to mmol mL <sup>-1</sup>		CH <sub>4</sub> integration range	Average CH <sub>4</sub> uptake from <sup>1</sup> H NMR (mmol mL <sup>-1</sup> )	Average CH <sub>4</sub> integration (4H) relative to TMS =1	Average calculated CH <sub>4</sub> uptake using integration ratios (mmol mL <sup>-1</sup> )	CH <sub>4</sub> uptake (μmol mL <sup>-1</sup> )
	Cage	CH <sub>4</sub>	Cage	CH <sub>4</sub>					
<b>3<sup>3</sup>:13<sup>3</sup><sub>DCBC</sub></b>	1	0.075	0.190	0.0142	-0.90 to -0.96	0.0142	0.30	0.0142	14.2
<b>DCBC</b>	-	-	-	-	-0.34 to -0.35	-	0.06	0.00284	2.8
<b>3<sup>3</sup>:13<sup>3</sup><sub>TBA</sub></b>	1	0.138	0.137	0.0189	-1.27 to -1.31	0.0189	0.55	0.0189	18.9
<b>TBA</b>	-	-	-	-	-0.12 to -0.13	-	0.12	0.00582	4.1
<b>3<sup>3</sup>:13<sup>3</sup><sub>MS</sub></b>	1	0.130	0.158	0.0205	-1.46 to -1.50	0.0205	0.52	0.0205	20.5
<b>MS</b>	-	-	-	-	-0.02 to -0.02	-	0.19	0.00927	7.5
<b>3<sup>3</sup>:13<sup>3</sup><sub>DCT</sub></b>	1	0.103	0.171	0.0176	-1.02 to -1.07	0.0176	0.41	0.0176	17.6
<b>DCT</b>	-	-	-	-	-1.02 to -1.07	-	0.13	0.00618	5.6
<b>3<sup>3</sup>:13<sup>3</sup><sub>HAP</sub></b>	1	0.175	0.146	0.0255	-1.86 to -1.91	0.0255	0.70	0.0255	25.5
<b>HAP</b>	-	-	-	-	0.13 to 0.11	-	0.15	0.00736	5.5
<b>3<sup>3</sup>:13<sup>3</sup><sub>PCP</sub></b>	1	0.490	0.167	0.0817	-2.83 to -2.96	0.0817	1.96	0.0817	81.7
<b>PCP</b>	-	-	-	-	-0.23 to -0.26	-	0.17	0.00817	7.1

**Appendix Table 30:** Comparison of the data for CH<sub>4</sub> uptake in the scrambled 3<sup>3</sup>:13<sup>3</sup> family of porous liquids at 20% w/v

	<b>3<sup>3</sup>:13<sup>3</sup><sub>DCBC</sub></b>	<b>3<sup>3</sup>:13<sup>3</sup><sub>TBA</sub></b>	<b>3<sup>3</sup>:13<sup>3</sup><sub>MS</sub></b>	<b>3<sup>3</sup>:13<sup>3</sup><sub>DCT</sub></b>	<b>3<sup>3</sup>:13<sup>3</sup><sub>HAP</sub></b>	<b>3<sup>3</sup>:13<sup>3</sup><sub>PCP</sub></b>
<b>CH<sub>4</sub> uptake in solvent (μmol mL<sup>-1</sup>)</b>	2.8	4.1	7.5	5.6	5.5	7.1
<b>CH<sub>4</sub> uptake in 20% w/v PL (μmol mL<sup>-1</sup>)</b>	14.2	18.9	20.5	17.6	25.5	81.7
<b>CH<sub>4</sub> peak in neat solvent (ppm)</b>	-0.34	-0.12	-0.02	-0.15	0.12	-0.24
<b>CH<sub>4</sub> peak in PL at 20% w/v (ppm)</b>	-0.93	-1.29	-1.48	-1.05	-1.88	-2.87
<b>Change in peak shift (ppm)</b>	0.59	1.17	1.46	0.90	2.00	2.63



**Appendix Table 31:** Comparison of the data for methane uptake in the scrambled porous liquids containing different scrambled cages at 20% w/v

	A <sup>3</sup> :G <sup>3</sup> <sub>MS</sub>	A <sup>2</sup> :G <sup>4</sup> <sub>MS</sub>	A <sup>1</sup> :G <sup>5</sup> <sub>MS</sub>	A <sup>5</sup> :H <sup>1</sup> <sub>HAP</sub>	A <sup>4</sup> :I <sup>2</sup> <sub>HAP</sub>
CH <sub>4</sub> uptake in solvent (μmol mL <sup>-1</sup> )	7.5	7.5	7.5	5.1	5.1
CH <sub>4</sub> uptake in 20% w/v PL (μmol mL <sup>-1</sup> )	20.6	18.6	18.9	23.3	19.0
CH <sub>4</sub> peak in neat solvent (ppm)	-0.02	-0.02	-0.02	0.12	0.12
CH <sub>4</sub> peak in PL at 20% w/v (ppm)	-0.91	-0.84	-1.54	-1.10	-1.17
Change in peak shift (ppm)	0.89	0.82	1.52	1.22	1.29

**Appendix Table 32:** Summary of the methane uptakes in the neat parent solvents (μmol mL<sub>sol</sub><sup>-1</sup> and μmol g<sub>sol</sub><sup>-1</sup>)

Solvent	Density (g mL <sup>-1</sup> )	CH <sub>4</sub> uptake (μmol <sub>sol</sub> mL <sup>-1</sup> )	CH <sub>4</sub> uptake (μmol g <sub>sol</sub> <sup>-1</sup> )
DCBC	1.3438	2.8	2.1
TBA	1.2457	5.1	4.1
MS	1.1552	7.5	6.5
DCT	1.1692	5.6	4.8
HAP	1.0856	5.5	5.0
PCP	1.7650	7.1	4.0

**Appendix Table 33:** Summary of the methane uptakes for the scrambled 3<sup>3</sup>:13<sup>3</sup> porous liquids at 20% w/v (μmol mL<sub>PL</sub><sup>-1</sup> and μmol g<sub>PL</sub><sup>-1</sup>)

Porous liquid	Density (g mL <sup>-1</sup> )	CH <sub>4</sub> uptake (μmol mL <sub>PL</sub> <sup>-1</sup> )	CH <sub>4</sub> uptake (μmol g <sub>PL</sub> <sup>-1</sup> )
3 <sup>3</sup> :13 <sup>3</sup> <sub>DCBC</sub>	1.3099	14.2	10.9
3 <sup>3</sup> :13 <sup>3</sup> <sub>TBA</sub>	1.2648	18.9	14.9
3 <sup>3</sup> :13 <sup>3</sup> <sub>MS</sub>	1.1238	20.5	18.2
3 <sup>3</sup> :13 <sup>3</sup> <sub>DCT</sub>	1.1872	17.6	14.8
3 <sup>3</sup> :13 <sup>3</sup> <sub>HAP</sub>	1.0240	25.5	24.9
3 <sup>3</sup> :13 <sup>3</sup> <sub>PCP</sub>	1.6073 <sup>13</sup>	81.7	50.9

**Appendix Table 34:** Average densities calculated for the 3<sup>3</sup>:13<sup>3</sup><sub>HAP</sub> porous liquid family at different concentrations

Concentration (% w/v)	Sample 1	Sample 2	Sample 3	Average density (g mL <sup>-1</sup> )	Standard deviation (± g mL <sup>-1</sup> )
	Mass (g)	Mass (g)	Mass (g)		
20	1.0294	1.0226	1.0201	1.0240	0.0048
30	1.0826	1.0851	1.0846	1.0841	0.0013
40	1.0915	1.0986	1.0954	1.0952	0.0036
60	1.1007	1.1052	1.1036	1.1032	0.0023

**Appendix Table 35:** Average densities calculated for the  $3^3:13^3_{TBA}$  porous liquid family at different concentrations

Concentration (% w/v)	Sample 1	Sample 2	Sample 3	Average density (g mL <sup>-1</sup> )	Standard deviation (± g mL <sup>-1</sup> )
	Mass (g)	Mass (g)	Mass (g)		
20	1.2656	1.2675	1.2612	1.2648	0.00323
40	1.2585	-	-	1.2585	-

**Appendix Table 36:** The range of concentrations of scrambled  $3^3:13^3_{HAP}$  porous liquids studied

Concentration (% w/v)	Mass of cage (g)	Mass of solvent (g)	wt%
20	0.2	1.0240	16
30	0.3	1.0841	22
40	0.4	1.0952	27
60	0.6	1.1032	35

**Appendix Table 37:** Summary of component amounts in  $3^3:13^3_{HAP}$  at various concentrations and the calculated cage to solvent ratio

Concentration (wt %)	Mmol solvent	Mmol cage	Cage: Solvent
8	0.0962	8.307	1:86
16	0.192	8.307	1:43
22	0.289	8.307	1:29
27	0.385	8.307	1:22

**Appendix Table 38:** The range of concentrations of scrambled  $3^3:13^3_{TBA}$  porous liquids studied

Concentration (% w/v)	Mass of cage (g)	Mass of solvent (g)	wt%
20	0.2	1.2648	14
40	0.4	1.2585	24

**Appendix Table 39:** Average viscosity for scrambled  $3^3:13^3$  porous liquids in HAP and TBA at various concentrations

Sample	Measurement 1 (cP)	Measurement 2 (cP)	Measurement 3 (cP)	Average (cP)	Average temperature (°C)
$3^3:13^3_{HAP}$ @8 wt %	4.772	4.771	4.761	4.77 ± 0.0061	25.01
$3^3:13^3_{HAP}$ @16 wt %	9.800	9.825	9.826	9.82 ± 0.015	25.03
$3^3:13^3_{HAP}$ @22 wt %	26.88	26.81	26.88	26.86 ± 0.040	25.01
$3^3:13^3_{HAP}$ @27 wt %	62.54	62.73	62.65	62.64 ± 0.095	24.97
$3^3:13^3_{TBA}$ @14 wt %	31.93	32.48	32.98	32.46 ± 0.53	25.02
$3^3:13^3_{TBA}$ @24 wt %	296.2	298.2	299.8	298.07 ± 1.8	25.07

**Appendix Table 40:** Volume of chloroform required to displace xenon from  $3^3:13^3_{\text{HAP}}$  at different concentrations (1.0 equiv. relative to cage)

Cage Present (mg)	Volume of chloroform ( $\mu\text{g}$ )
200	16
300	23
400	32
600	46

**Appendix Table 41:** Xenon uptake (mL and  $\mu\text{mol}$ ) for scrambled  $3^3:13^3_{\text{HAP}}$  and  $3^3:13^3_{\text{TBA}}$  porous liquids at various concentrations

Porous Liquid	Conc. (wt%)	Expected volume (mL)	Volume of Xenon (mL)		Average $\pm$ SD (mL)	Volume of Xenon ( $\mu\text{mol}$ )		Average $\pm$ SD ( $\mu\text{mol}$ )
			Sample 1	Sample 2		Sample 1	Sample 2	
$3^3:13^3_{\text{HAP}}$	16	4.6	3.2	2.9	$3.1 \pm 0.2$	133.1	120.6	$126.9 \pm 8.8$
$3^3:13^3_{\text{HAP}}$	22	6.9	4.9	4.7	$4.8 \pm 0.1$	203.8	195.5	$199.7 \pm 5.9$
$3^3:13^3_{\text{HAP}}$	27	9.2	6.6	6.1	$6.4 \pm 0.4$	274.5	253.7	$264.1 \pm 14.7$
$3^3:13^3_{\text{HAP}}$	35	13.9	4.0	4.0	4.0	166.4	166.4	166.4
$3^3:13^3_{\text{TBA}}$	14	4.6	2.8	3.0	$2.9 \pm 0.1$	116.5	124.8	$120.6 \pm 5.9$
$3^3:13^3_{\text{TBA}}$	24	9.2	2.9	2.9	2.9	120.6	120.6	120.6

**Appendix Table 42:** Xenon uptake ( $\mu\text{mol g}_{\text{PL}}^{-1}$ ) for scrambled  $3^3:13^3_{\text{HAP}}$  and  $3^3:13^3_{\text{TBA}}$  porous liquid at various concentrations

Porous Liquid	Concentration (wt%)	Mass of cage (g)	Mass of solvent (g)	Mass of PL (g)	Volume of Xenon ( $\mu\text{mol g}_{\text{PL}}^{-1}$ )		Average $\pm$ SD ( $\mu\text{mol g}_{\text{PL}}^{-1}$ )
					Sample 1	Sample 2	
$3^3:13^3_{\text{HAP}}$	16	0.2	1.0856	1.2856	103.5	93.8	$98.7 \pm 6.9$
$3^3:13^3_{\text{HAP}}$	22	0.3	1.0856	1.3856	147.1	141.1	$144.1 \pm 4.2$
$3^3:13^3_{\text{HAP}}$	27	0.4	1.0856	1.4856	184.8	170.8	$177.8 \pm 9.9$
$3^3:13^3_{\text{HAP}}$	35	0.6	1.0856	1.6856	98.7	98.7	98.7
$3^3:13^3_{\text{TBA}}$	14	0.2	1.2457	1.4457	80.6	86.3	$83.4 \pm 4.1$
$3^3:13^3_{\text{TBA}}$	24	0.4	1.2457	1.6457	73.3	73.3	73.3

**Appendix Table 43:** Xenon uptake ( $\mu\text{mol mL}_{\text{PL}}^{-1}$ ) for scrambled  $3^3:13^3_{\text{HAP}}$  and  $3^3:13^3_{\text{TBA}}$  porous liquid at various concentrations

Porous Liquid	Concentration (wt%)	Mass of cage (g)	Density of PL ( $\text{g mL}^{-1}$ )	Volume of Xenon ( $\mu\text{mol mL}_{\text{PL}}^{-1}$ )		Average $\pm$ SD ( $\mu\text{mol mL}_{\text{PL}}^{-1}$ )
				Sample 1	Sample 2	
$3^3:13^3_{\text{HAP}}$	16	0.2	1.0240	106.0	96.1	$101.0 \pm 7.0$
$3^3:13^3_{\text{HAP}}$	22	0.3	1.0841	159.5	153.0	$156.2 \pm 4.6$
$3^3:13^3_{\text{HAP}}$	27	0.4	1.0952	202.4	187.1	$194.7 \pm 10.8$
$3^3:13^3_{\text{HAP}}$	35	0.6	1.1032	108.9	108.9	108.9
$3^3:13^3_{\text{TBA}}$	14	0.2	1.2648	101.9	109.2	$105.5 \pm 5.1$
$3^3:13^3_{\text{TBA}}$	24	0.4	1.2585	92.2	92.2	92.2

**Appendix Table 44:** Methane uptake ( $\mu\text{mol mL}^{-1}$ ) for scrambled  $3^3:13^3\text{HAP}$  porous liquid at **8 wt%**

TMS integration: 0.10 to -0.10 ppm

NCH integration: 3.90 to 3.30 ppm

Total Methane Addition Time (min)	NCH integration relative to TMS = 1	Calculated [PL] concentration from calibration curve ( $\text{mg}_{\text{cage}} \text{mL}^{-1}$ )	Calculated [PL] concentration ( $\text{mmol}_{\text{cage}} \text{mL}^{-1}$ ) using average MW = 1039.43	Value cage NCH integration set to	$\text{CH}_4$ integration relative to cage (4H)	$\text{CH}_4$ shift (ppm)	$\text{CH}_4$ integration range (ppm)	Cage: $\text{CH}_4$ Ratio (based on integrations)	Calculated $\text{CH}_4$ uptake ( $\mu\text{mol mL}^{-1}$ )
5	4.23	70.18	0.0675	12	0.91	-1.05	-1.04 to -1.07	1:0.228	15.4
10	4.90	81.30	0.0782	12	0.88	-1.09	-1.07 to -1.11	1:0.220	17.2
20	4.87	80.80	0.0777	12	0.86	-1.14	-1.12 to -1.16	1:0.215	16.7
30	4.25	70.52	0.0678	12	0.91	-1.18	-1.17 to -1.20	1:0.228	15.4

**Appendix Table 45:** Methane uptake ( $\mu\text{mol mL}^{-1}$ ) for scrambled  $3^3:13^3\text{HAP}$  porous liquid at **16 wt%**

TMS integration: 0.10 to -0.10 ppm

NCH integration: 3.90 to 3.25 ppm

Total Methane Addition Time (min)	NCH integration relative to TMS = 1	Calculated [PL] concentration from calibration curve ( $\text{mg}_{\text{cage}} \text{mL}^{-1}$ )	Calculated [PL] concentration ( $\text{mmol}_{\text{cage}} \text{mL}^{-1}$ ) using average MW = 1039.43	Value cage NCH integration set to	$\text{CH}_4$ integration relative to cage (4H)	$\text{CH}_4$ shift (ppm)	$\text{CH}_4$ integration range (ppm)	Cage: $\text{CH}_4$ Ratio (based on integrations)	Calculated $\text{CH}_4$ uptake ( $\mu\text{mol mL}^{-1}$ )
5	8.36	138.71	0.133	12	0.61	-1.34	-1.32 to -1.37	1:0.153	20.4
10	8.53	141.53	0.136	12	0.54	-1.39	-1.38 to -1.42	1:0.135	18.4
20	8.54	141.70	0.136	12	0.61	-1.45	-1.43 to 1.48	1:0.153	20.8
30	8.33	138.21	0.133	12	0.63	-1.49	-1.47 to -1.52	0.158	21.0

**Appendix Table 46:** Methane uptake ( $\mu\text{mol mL}^{-1}$ ) for scrambled  $3^3:13^3\text{HAP}$  porous liquid at **22 wt%**

TMS integration: 0.10 to -0.10 ppm

NCH integration: 4.10 to 3.10 ppm

Total Methane Addition Time (min)	NCH integration relative to TMS = 1	Calculated [PL] concentration from calibration curve ( $\text{mg}_{\text{cage}} \text{mL}^{-1}$ )	Calculated [PL] concentration ( $\text{mmol}_{\text{cage}} \text{mL}^{-1}$ ) using average MW = 1039.43	Value cage NCH integration set to	$\text{CH}_4$ integration relative to cage (4H)	$\text{CH}_4$ shift (ppm)	$\text{CH}_4$ integration range (ppm)	Cage: $\text{CH}_4$ Ratio (based on integrations)	Calculated $\text{CH}_4$ uptake ( $\mu\text{mol mL}^{-1}$ )
5	11.27	187.00	0.180	12	0.49	-1.62	-1.58 to -1.66	1:0.123	22.0
10	11.61	192.63	0.185	12	0.53	-1.66	-1.62 to -1.71	1:0.185	24.6
20	12.11	201.00	0.193	12	0.54	-1.71	-1.64 to -1.76	1:0.193	26.1
30	11.04	183.18	0.176	12	0.58	-1.74	-1.70 to -1.78	1:0.176	25.6

**Appendix Table 47:** Methane uptake ( $\mu\text{mol mL}^{-1}$ ) for scrambled  $3^3:13^3_{\text{HAP}}$  porous liquid at 27 wt%

TMS integration: 0.10 to -0.10 ppm

NCH integration: 4.12 to 3.10 ppm

Total Methane Addition Time (min)	NCH integration relative to TMS = 1	Calculated [PL] concentration from calibration	Calculated [PL] concentration (mmol <sub>cage</sub> mL <sup>-1</sup> ) using average MW	Value cage NCH integration set	CH <sub>4</sub> integration relative to cage (4H)	CH <sub>4</sub> shift (ppm)	CH <sub>4</sub> integration range (ppm)	Cage: CH <sub>4</sub> Ratio (based on integrations)	Calculated CH <sub>4</sub> uptake ( $\mu\text{mol mL}^{-1}$ )
5	13.02	216.03	0.208	12	0.52	-1.76	-1.70 to -1.83	1:0.130	27.0
10	13.56	225.0	0.216	12	0.55	-1.80	-1.75 to -1.87	1:0.138	30.0
20	11.97	198.61	0.191	12	0.51	-1.85	-1.76 to -1.95-	1:0.128	24.4
30	13.29	220.51	0.212	12	0.57	-1.88	-1.82 to -1.96	1:0.143	30.2

**Appendix Table 48:** Methane uptake ( $\mu\text{mol mL}^{-1}$ ) for scrambled  $3^3:13^3_{\text{HAP}}$  porous liquid samples at increasing concentrations

TMS integration range: 0.10 to -0.10 ppm

(wt%)	NCH integration relative to TMS = 1	Calculated [PL] concentration from calibration curve (mg <sub>cage</sub> mL <sup>-1</sup> )	Calculated [PL] concentration (mmol <sub>cage</sub> mL <sup>-1</sup> ) using average MW = 1039.43	Value cage NCH integration set to	CH <sub>4</sub> integration relative to cage (4H)	CH <sub>4</sub> shift (ppm)	CH <sub>4</sub> integration range (ppm)	Cage: CH <sub>4</sub> Ratio (based on integrations)	Calculated CH <sub>4</sub> uptake ( $\mu\text{mol mL}^{-1}$ )	CH <sub>4</sub> uptake ( $\mu\text{mol mL}^{-1}$ )
8	4.96	3.90 to 3.30	82.30	0.0792	0.82	-1.46	-1.44 to -1.48	1:0.205	0.0162	16.2
16	9.12	3.90 to 3.25	151.32	0.1456	0.70	-1.88	-1.86 to -1.91	1:0.175	0.0255	25.5
22	12.33	4.10 to 3.10	204.58	0.1968	0.70	-2.10	-2.06 to -2.16	1:0.175	0.0344	34.4
27	18.15	4.12 to 3.10	301.14	0.290	0.57	-2.21	-2.18 to -2.24	1:0.143	0.0413	41.3

**Appendix Table 49:** Summary of properties for  $3^3:13^3_{\text{HAP}}$  at different concentrations

Concentration (wt %)	Methane uptake ( $\mu\text{mol mL}_{\text{PL}}^{-1}$ )	Chemical shift (ppm)	Viscosity (cP)
8	16.2	-1.46	4.77
16	25.5	-1.88	9.82
22	34.4	-2.10	26.86
27	41.3	-2.21	62.64

**Appendix Table 50:** Summary of the volume of chloroform or temperature needed to displace xenon in  $3^3:13^3_{\text{HAP}}$  porous liquid at various concentrations

Concentration (wt %)	Mass of cage (mg)	Maximum volume of Xe that can be evolved* (mL)	Volume of CHCl <sub>3</sub> needed to displace Xe* ( $\mu\text{L}$ )	Temperature required to release Xe (°C)
16	200	4.6	16	60-70
22	300	6.9	23	60-80
27	400	9.2	32	60-80
35	600	13.9	46	80-120

\*Based on a maximum 1:1 Xe: cage ratio

**Appendix Table 51:** Summary of the xenon evolution experiments for temperature release from  $3^3:13^3_{\text{HAP}}$  in mL

Concentration (wt%)	Mass of cage (mg)	Expected volume (mL)	Volume of xenon released (mL)			Average $\pm$ SD (mL)
			Sample 1	Sample 2	Sample 3	
16	200	4.6	2.9	3.0	-	3.0 $\pm$ 0.07
22	300	6.9	3.5	3.9	-	3.7 $\pm$ 0.28
27	400	9.2	6.0	6.0	6.4	6.1 $\pm$ 0.23
35	600	13.9	8.2	7.5	7.8	7.8 $\pm$ 0.35

**Appendix Table 52:** Summary of the xenon evolution experiments for temperature release from  $3^3:13^3_{\text{HAP}}$  in  $\mu\text{mol}$ 

Concentration (wt%)	Mass of cage (mg)	Expected volume (mL)	Volume of xenon released ( $\mu\text{mol}$ )			Average $\pm$ SD ( $\mu\text{mol}$ )
			Sample 1	Sample 2	Sample 3	
16	200	4.6	120.6	124.8	-	122.7 $\pm$ 3.00
22	300	6.9	145.6	162.2	-	153.9 $\pm$ 11.7
27	400	9.2	250.0	250.0	266.2	225.4 $\pm$ 9.35
35	600	13.9	341.1	312.0	324.4	325.8 $\pm$ 14.6

**Appendix Table 53:** Summary of the xenon evolution experiments for temperature release from  $3^3:13^3_{\text{HAP}}$  in  $\mu\text{mol g}_{\text{PL}}^{-1}$ 

Concentration (wt%)	Mass of cage (mg)	Expected volume (mL)	Volume of xenon released ( $\mu\text{mol g}_{\text{PL}}^{-1}$ )			Average $\pm$ SD ( $\mu\text{mol g}_{\text{PL}}^{-1}$ )
			Sample 1	Sample 2	Sample 3	
16	200	4.6	93.8	97.1	-	95.5 $\pm$ 2.33
22	300	6.9	105.1	117.1	-	111.1 $\pm$ 8.49
27	400	9.2	168.0	168.0	179.2	171.7 $\pm$ 6.45
35	600	13.9	202.3	185.1	192.5	193.3 $\pm$ 8.63

**Appendix Table 54:** Summary of the xenon evolution experiments for temperature release from  $3^3:13^3_{\text{HAP}}$  in  $\mu\text{mol mL}_{\text{PL}}^{-1}$ 

Concentration (wt%)	Mass of cage (mg)	Expected volume (mL)	Volume of xenon released ( $\mu\text{mol mL}_{\text{PL}}^{-1}$ )			Average $\pm$ SD ( $\mu\text{mol mL}_{\text{PL}}^{-1}$ )
			Sample 1	Sample 2	Sample 3	
16	200	4.6	96.1	99.4	-	97.8 $\pm$ 2.33
22	300	6.9	113.9	126.9	-	120.4 $\pm$ 9.19
27	400	9.2	184.0	184.0	196.3	188.1 $\pm$ 7.10
35	600	13.9	223.3	204.2	212.3	213.3 $\pm$ 9.59

**Appendix Table 55:** Volume of xenon released from the scrambled  $3^3:13^3_{\text{HAP}}$  porous liquid at a 16 wt% concentration after heating at 60-70 °C

Sample	Xenon evolved							
	(mL)		( $\mu\text{mol}$ )		( $\mu\text{mol g}^{-1}$ )		( $\mu\text{mol mL}^{-1}$ )	
	Cycle 1	Cycle 2	Cycle 1	Cycle 2	Cycle 1	Cycle 2	Cycle 1	Cycle 2
<b>1</b>	3.0	2.6	124.8	108.1	97.1	84.1	99.4	86.1
<b>2</b>	2.9	2.1	120.6	87.3	93.8	67.9	96.1	70.0

**Appendix Table 56:** The volume of xenon released from  $3^3:13^3_{\text{HAP}}$  at 26 and 35 wt% after setting as a gel

Concentration (wt %)	Sample 1	Sample 2	Sample 3	Sample 4	Average volume (mL)	Average volume ( $\mu\text{mol}$ )	Average volume ( $\mu\text{mol g}^{-1}$ )	Average volume ( $\mu\text{mol mL}^{-1}$ )
<b>27</b>	5.4	5.5	6.4	6.4	$5.9 \pm 0.55$	245.4	165.2	180.9
<b>35</b>	9.2	8.8	8.7	8.3	$8.8 \pm 0.45$	366.0	217.2	239.6

**Appendix Table 57:** The volume of xenon evolved from  $3^3:13^3_{\text{HAP}}$  at 27 wt% when heated at 60-85 °C (cycle 1) followed by chemical displacement carried out on the same sample

Porous liquid	Cycle 1		Cycle 2
	Temperature release		Chemical release
<b><math>3^3:13^3_{\text{HAP}}</math> at 27 wt%</b>	6.2 mL		0.2 mL

**Appendix Table 58:** Volume of xenon released, and percentage retained by  $3^3:13^3_{\text{HAP}}$  liquid after immediate release and after 48 hrs.

Time (hrs)	Volume of xenon released (mL)	Volume of xenon released ( $\mu\text{mol mL}^{-1}$ )	% Xe retained over time (%)
<b>0</b>	6.4	196.3	-
<b>48</b>	4.4	126.2	64

**Appendix Table 59:** Volume of xenon released from  $3^3:13^3_{\text{HAP}}$  gel after being left to stand for set amounts of time

Time after preparation (days)	Volume of xenon released (mL)	Volume of xenon released ( $\mu\text{mol mL}^{-1}$ )	% Xe retained over time (%)
<b>1</b>	8.8	222.4	-
<b>7</b>	6.0	151.6	68
<b>28</b>	4.4	111.2	50

**Appendix Table 60:** Volume of xenon released from 20% w/v porous liquids formed using recycled scrambled cage

Porous liquid	Mass of cage (mg)	Volume of xenon evolved (mL)	Volume of xenon evolved ( $\mu\text{mol mL}_{\text{PL}}^{-1}$ )
$3^3:13^3_{\text{TBA}}$	200	2.3	83.3
$3^3:13^3_{\text{HAP}}$	200	2.8	92.8

## Chapter 5

**Appendix Table 61:** Solubility of various ionic salts in methanol

Salt	Mass (mg)	Volume of MeOH (mL)	Solubility (mg/mL)
Na BARF	160	1	160
Li TFSA	100	1	100
Na TSA	10	5	2
Na XSA	100	5	20
Na NSA	x	x	Not soluble

**Appendix Table 62:** Summary of the stock solutions prepared for high-throughput cage salt screen

Stock solution number	Reactant	MW (g/mol)	Stock solution concentration (mg/mL)	Mmol per mL (stock sol)	Total volume of stock solution (mL)	Total volume of stock solution made (mL)	Mass of reactant required for stock solution (g)
1	RCC1.12HCl	1242.996	2.4	0.0019	40.0	50.0	0.12
2	RCC3.12HCl	1555.55	5	0.0032	40.0	50.0	0.25
3	RCC13.12HCl	1410.32	5	0.0035	40.0	50.0	0.25
4	$R3^3:R13^3.12HCl$	1489.34	5	0.0034	40.0	50.0	0.25
5	$R1^3:R3^3.12HCl$	1424.99	5	0.0035	40.0	50.0	0.25
6	Na BARF	886.20	150	0.169	12.52	20.0	3.00
7	Li TFSA	287.09	100	0.348	6.08	15.0	1.50
8	Na TSA*	194.18	6	0.031	68.57	80.0	0.48
9	Na XSA	226.225	20	0.088	23.96	30.0	0.60

\*Dispensed as a dispersion due to poor solubility

**Appendix Table 63:** Summary of the each reaction vessels content used in the high-throughput cage salt screen

Reaction Number	Cage	Volume of cage needed (mL)	Mmol of Cage	Salt	Eq. of salt needed	Mmol of salt	Volume of salt needed (mL)	Total volume (mL)	Additional volume of methanol added (mL) (Total volume = 15 mL)	
1	21	RCC1.12HCl	5	0.0097	NaBARF	12	0.1158	0.68	5.63	1.52
2	22	RCC1.12HCl	5	0.0097	Li TFSA	12	0.1158	0.33	5.33	1.87
3	23	RCC1.12HCl	5	0.0097	Na TSA	12	0.1158	3.75	8.75	0.00
4	24	RCC1.12HCl	5	0.0097	Na XSA	12	0.1158	1.31	6.31	0.89
5	25	RCC3.12HCl	5	0.0161	NaBARF	12	0.1929	1.14	6.14	8.86
6	26	RCC3.12HCl	5	0.0161	Li TFSA	12	0.1929	0.55	5.55	9.45
7	27	RCC3.12HCl	5	0.0161	Na TSA	12	0.1929	6.24	11.24	3.76
8	28	RCC3.12HCl	5	0.0161	Na XSA	12	0.1929	2.18	7.18	7.82
9	29	RCC13.12HCl	5	0.0177	NaBARF	12	0.2127	1.26	6.26	8.74



10	30	RCC13.12HCl	5	0.0177	Li TFSA	12	0.2127	0.61	5.61	9.39
11	31	RCC13.12HCl	5	0.0177	Na TSA	12	0.2127	6.88	11.88	3.12
12	32	RCC13.12HCl	5	0.0177	Na XSA	12	0.2127	2.41	7.41	7.59
13	33	R3 <sup>3</sup> :R13 <sup>3</sup> .12HCl	5	0.0168	NaBARF	12	0.2014	1.19	6.19	8.81
14	34	R3 <sup>3</sup> :R13 <sup>3</sup> .12HCl	5	0.0168	Li TFSA	12	0.2014	0.58	5.58	9.42
15	35	R3 <sup>3</sup> :R13 <sup>3</sup> .12HCl	5	0.0168	Na TSA	12	0.2014	6.52	11.52	3.48
16	36	R3 <sup>3</sup> :R13 <sup>3</sup> .12HCl	5	0.0168	Na XSA	12	0.2014	2.28	7.28	7.72
17	37	R1 <sup>3</sup> :R3 <sup>3</sup> .12HCl	5	0.0176	NaBARF	12	0.2110	1.25	6.25	8.75
18	38	R1 <sup>3</sup> :R3 <sup>3</sup> .12HCl	5	0.0176	Li TFSA	12	0.2110	0.61	5.61	9.39
19	39	R1 <sup>3</sup> :R3 <sup>3</sup> .12HCl	5	0.0176	Na TSA	12	0.2110	6.83	11.83	3.17
20	40	R1 <sup>3</sup> :R3 <sup>3</sup> .12HCl	5	0.0176	Na XSA	12	0.2110	2.39	7.39	7.61

**Appendix Table 64:** The physical appearance for the cage salts synthesised in the high-throughput screen

Reaction number	Cage salt	Chemical formula	MW	Physical appearance
1	RCC1.12BARF	C <sub>432</sub> H <sub>228</sub> N <sub>12</sub> B <sub>12</sub> F <sub>288</sub>	11187.926	White powder
2	RCC1.12TFSA	C <sub>72</sub> H <sub>84</sub> N <sub>24</sub> F <sub>72</sub> S <sub>24</sub> O <sub>48</sub>	4190.916	Brown oil
3	RCC1.12TSA	C <sub>132</sub> H <sub>168</sub> N <sub>12</sub> S <sub>12</sub> O <sub>36</sub>	2883.570	White powder
4	RCC1.12XSA	C <sub>144</sub> H <sub>192</sub> N <sub>12</sub> S <sub>12</sub> O <sub>36</sub>	3051.894	White powder
5	RCC3.12BARF	C <sub>456</sub> H <sub>264</sub> N <sub>12</sub> B <sub>12</sub> F <sub>288</sub>	11512.478	White powder
6	RCC3.12TFSA	C <sub>96</sub> H <sub>120</sub> N <sub>24</sub> F <sub>72</sub> S <sub>24</sub> O <sub>48</sub>	4515.468	Brown oil
7	RCC3.12TSA	C <sub>156</sub> H <sub>204</sub> N <sub>12</sub> S <sub>12</sub> O <sub>36</sub>	3208.122	White powder
8	RCC3.12XSA	C <sub>168</sub> H <sub>228</sub> N <sub>12</sub> S <sub>12</sub> O <sub>36</sub>	3376.446	White powder
9	RCC13.12BARF	C <sub>444</sub> H <sub>252</sub> N <sub>12</sub> B <sub>12</sub> F <sub>288</sub>	12185.534	White powder
10	RCC13.12TFSA	C <sub>84</sub> H <sub>108</sub> N <sub>24</sub> F <sub>72</sub> S <sub>24</sub> O <sub>48</sub>	5188.524	Brown oil
11	RCC13.12TSA	C <sub>144</sub> H <sub>192</sub> N <sub>12</sub> S <sub>12</sub> O <sub>36</sub>	3881.178	White powder
12	RCC13.12XSA	C <sub>156</sub> H <sub>216</sub> N <sub>12</sub> S <sub>12</sub> O <sub>36</sub>	4049.502	White powder
13	R3 <sup>3</sup> :R13 <sup>3</sup> .12BARF	C <sub>450</sub> H <sub>258</sub> N <sub>12</sub> B <sub>12</sub> F <sub>288</sub>	10424.642	White powder
14	R3 <sup>3</sup> :R13 <sup>3</sup> .12TFSA	C <sub>90</sub> H <sub>114</sub> N <sub>24</sub> F <sub>72</sub> S <sub>24</sub> O <sub>48</sub>	3427.632	Brown oil
15	R3 <sup>3</sup> :R13 <sup>3</sup> .12TSA	C <sub>150</sub> H <sub>198</sub> N <sub>12</sub> S <sub>12</sub> O <sub>36</sub>	2120.286	White powder
16	R3 <sup>3</sup> :R13 <sup>3</sup> .12XSA	C <sub>162</sub> H <sub>222</sub> N <sub>12</sub> S <sub>12</sub> O <sub>36</sub>	2288.610	White powder
17	R1 <sup>3</sup> :R3 <sup>3</sup> .12BARF	C <sub>444</sub> H <sub>264</sub> N <sub>12</sub> B <sub>12</sub> F <sub>288</sub>	12179.49	Brown powder
18	R1 <sup>3</sup> :R3 <sup>3</sup> .12TFSA	C <sub>84</sub> H <sub>186</sub> N <sub>24</sub> F <sub>72</sub> S <sub>24</sub> O <sub>48</sub>	5182.476	Brown oil
19	R1 <sup>3</sup> :R3 <sup>3</sup> .12TSA	C <sub>156</sub> H <sub>210</sub> N <sub>12</sub> S <sub>12</sub> O <sub>36</sub>	3875.13	Brown powder
20	R1 <sup>3</sup> :R3 <sup>3</sup> .12XSA	C <sub>60</sub> H <sub>102</sub> N <sub>12</sub> S <sub>12</sub> O <sub>36</sub>	4043.454	Brown powder

**Appendix Table 65:** Characterisation of the cage salts synthesised during the high-throughput screen

Reaction number	Cage salt	Mass (g)	Theoretical yield	% yield	HRMS		IR
					Expected	Found	
1	RCC1.12BARF	0.173	0.217	80	C <sub>48</sub> H <sub>84</sub> N <sub>12</sub> <sup>12+</sup> :	[M] <sup>+</sup> =	3660.2
					[M] <sup>+</sup> = 828.6942	817.5854	1609.4
					C <sub>48</sub> H <sub>84</sub> N <sub>12</sub> :	829.6807	1351.9
					[M] <sup>+</sup> = 816.6003		1351.9
							1273.6
							1106.7
2	RCC1.12TFSA	0.106	0.081	130	C <sub>48</sub> H <sub>84</sub> N <sub>12</sub> <sup>12+</sup> :	[M] <sup>+</sup> =	3565.3
					[M] <sup>+</sup> = 828.6942	817.5854	1634.3
					C <sub>48</sub> H <sub>84</sub> N <sub>12</sub> :	829.6807	1347.8
					[M] <sup>+</sup> = 816.6003		1197.4
							1129.4
							1044.9
							797.6
							603.8
							500.8
3	RCC1.12TSA	0.083	0.056	148	C <sub>48</sub> H <sub>84</sub> N <sub>12</sub> <sup>12+</sup> :	[M] <sup>+</sup> =	3649.8
					[M] <sup>+</sup> = 828.6942	817.5960	3439.6

						$C_{48}H_{84}N_{12}$ : [M] <sup>+</sup> = 816.6003	829.5946	2914.1 1626.0 1446.7 1199.4 1092.3 1016.0 809.9 676.0 568.8
4	RCC1.12XSA	0.093	0.059	157		$C_{48}H_{84}N_{12}^{12+}$ : [M] <sup>+</sup> = 828.6942 $C_{48}H_{84}N_{12}$ : [M] <sup>+</sup> = 816.6003	[M] <sup>+</sup> = 817.5923	3417.0 2932.7 1611.6 1446.7 1154.1 1088.2 1011.9 818.2 678.0 562.6
5	RCC3.12BARF	0.401	0.371	108		$C_{72}H_{120}N_{12}^{12+}$ : [M] <sup>+</sup> = 1152.9759 $C_{72}H_{108}N_{12}$ : [M] <sup>+</sup> = 1140.8820	[M+H] <sup>2+</sup> = 571.4409, 577.4398 [M+Li] <sup>2+</sup> = 582.1969	3388.1 1605.4 1351.9 1273.6 1106.7
6	RCC3.12TFSA	0.132	0.145	91		$C_{72}H_{120}N_{12}^{12+}$ : [M] <sup>+</sup> = 1152.9759 $C_{72}H_{108}N_{12}$ : [M] <sup>+</sup> = 1140.8820	[M+H] <sup>2+</sup> = 570.4932 578.5712 [H+Na] <sup>2+</sup> = 598.5095	3561.2 1636.4 1333.4 1187.1 1131.4 1053.1 795.5 599.7 496.7
7	RCC3.12TSA	0.085	0.103	82		$C_{72}H_{120}N_{12}^{12+}$ : [M] <sup>+</sup> = 1152.9759 $C_{72}H_{108}N_{12}$ : [M] <sup>+</sup> = 1140.8820	[M+H] <sup>2+</sup> = 571.4433 577.4362	3402.5 2924.4 1617.8 1455.0 1166.5 1007.8 816.1 680.1 560.6
8	RCC3.12XSA	0.094	0.109	86		$C_{72}H_{120}N_{12}^{12+}$ : [M] <sup>+</sup> = 1152.9759 $C_{72}H_{108}N_{12}$ : [M] <sup>+</sup> = 1140.8820	[M+H] <sup>2+</sup> = 571.4353 577.9389 [M+Li] <sup>2+</sup> = 583.4382	3427.3 2916.2 1603.4 1446.7 1160.3 1086.1 1009.8 820.2 680.1 568.8
9	RCC13.12BARF	0.241	0.431	56		$C_{60}H_{108}N_{12}^{12+}$ : [M] <sup>+</sup> = 996.882 $C_{60}H_{108}N_{12}$ : [M] <sup>+</sup> = 984.7881	[M+H] <sup>+</sup> = 985.7818	3388.1 2951.2 1613.7 1354.0 1273.6 1090.2
10	RCC13.12TFSA	0.147	0.184	80		$C_{60}H_{108}N_{12}^{12+}$ : [M] <sup>+</sup> = 996.882 $C_{60}H_{108}N_{12}$ : [M] <sup>+</sup> = 984.7881	-	3563.3 1634.3 1347.8 1185.0 1129.4 1044.9 797.6 568.8 500.8
11	RCC13.12TSA	0.077	0.137	56		$C_{60}H_{108}N_{12}^{12+}$ : [M] <sup>+</sup> = 996.882 $C_{60}H_{108}N_{12}$ : 984.7881	[M+H] <sup>+</sup> = 985.7755 997.7775	-
12	RCC13.12XSA	0.09	0.143	63		$C_{60}H_{108}N_{12}^{12+}$ : [M] <sup>+</sup> = 996.882 $C_{60}H_{108}N_{12}$ : [M] <sup>+</sup> = 984.7881	[M+H] <sup>+</sup> = 985.7757 997.7763	-

13	R3 <sup>3</sup> :R13 <sup>3</sup> .12BARF	0.179	0.350	51	[M] <sup>+</sup> =	[M+H] <sup>2+</sup> =	1140.882	2967.7
					1114.8663		1615.7	
					1088.8507		1356.1	
					1062.835		1275.7	
					1036.8194		1114.9	
					1010.8037			
					984.7881			
14	R3 <sup>3</sup> :R13 <sup>3</sup> .12TFSA	0.165	0.115	143	[M] <sup>+</sup> =	[M+H] <sup>2+</sup> =	1140.882	3480.9
					1114.8663		1634.3	
					1088.8507		1347.8	
					1062.835		1195.3	
					1036.8194		1127.3	
					1010.8037		1049.0	
					984.7881		791.4	
15	R3 <sup>3</sup> :R13 <sup>3</sup> .12TSA	0.079	0.071	111	[M] <sup>+</sup> =	[M+H] <sup>2+</sup> =	1140.882	3410.8
					1114.8663		2922.3	
					1088.8507		1626.0	
					1062.835		1455.0	
					1036.8194		1160.3	
					1010.8037		1007.8	
					0.109984.7881		822.3	
16	R3 <sup>3</sup> :R13 <sup>3</sup> .12XSA	0.078	0.077	101	[M] <sup>+</sup> =	[M+H] <sup>2+</sup> =	1140.882	3441.7
					1114.8663		2943.0	
					1088.8507		1613.7	
					1062.835		1450.9	
					1036.8194		1162.3	
					1010.8037		1090.2	
					984.7881		1007.8	
17	R1 <sup>3</sup> :R3 <sup>3</sup> .12BARF	0.26	0.429	61	[M] <sup>+</sup> =	[M+H] <sup>2+</sup> =	828.6942	3435.5
					882.7411		2918.2	
					936.7881		1601.3	
					990.835		1450.9	
					1044.882		1164.4	
					1098.9289			
					1152.9759			
18	R1 <sup>3</sup> :R3 <sup>3</sup> .12TFSA	0.183	0.182	100	[M] <sup>+</sup> =	[M+H] <sup>2+</sup> =	828.6942	3579.8
					882.7411		3404.6	
					936.7881		1642.5	
					990.835		1349.9	
					1044.882		1191.2	
					1098.9289		1133.5	
					1152.9759		1046.9	
19	R1 <sup>3</sup> :R3 <sup>3</sup> .12TSA	0.083	0.136	61	[M] <sup>+</sup> =	[M+H] <sup>2+</sup> =	828.6942	3425.2
					882.7411		2928.5	
					936.7881		1603.4	
					990.835		1455.0	
					1044.882		1170.6	
					1098.9289		1005.7	
					1152.9759		814.1	
20	R1 <sup>3</sup> :R3 <sup>3</sup> .12XSA	0.123	0.142	86	[M] <sup>+</sup> =	[M+H] <sup>2+</sup> =	828.6942	3431.4
					882.7411		2955.3	
					936.7881		1607.5	
					990.835		1452.9	
					1044.882		1154.1	
					1098.9289		1088.2	
					1152.9759		1009.8	
	824.4							
	678.0							
	566.7							

**Appendix Table 66:** Summary of the stock solution content for the cage salt scale out

Stock solution number	Precursor	Molar Mass (g mol <sup>-1</sup> )	Stock solution concentration (mg mL <sup>-1</sup> )	Mmol per mL (stock solution)	Total volume of stock solution
1	RCC1.12HCl	1242.996	15	0.0121	60
2	RCC3.12HCl	1555.550	19.6	0.0126	120
3	Sodium trifluoromethane sulfonimide	303.140	43.4	0.1432	240

**Appendix Table 67:** Summary of the stock solution content for the cage salt scale out

Vessel	Cage	Volume of cage stock solution (mL)	Mmol of cage	Salt	Salt equivalent	Mmol of salt	Volume of salt stock solution (mL)	Total Volume (mL)
1	RCC1.12HCl	2.5	0.0302	NaTFSA	12	0.362	2.53	5.03
2	RCC3.12HCl	5	0.0630	NaTFSA	12	0.756	5.28	10.28

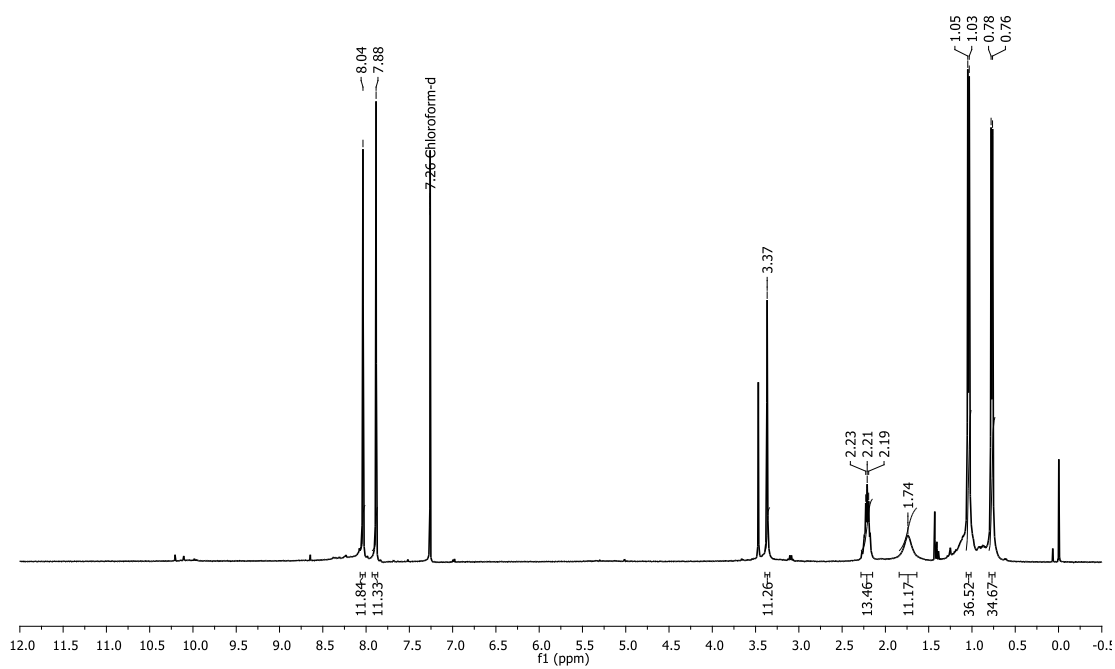
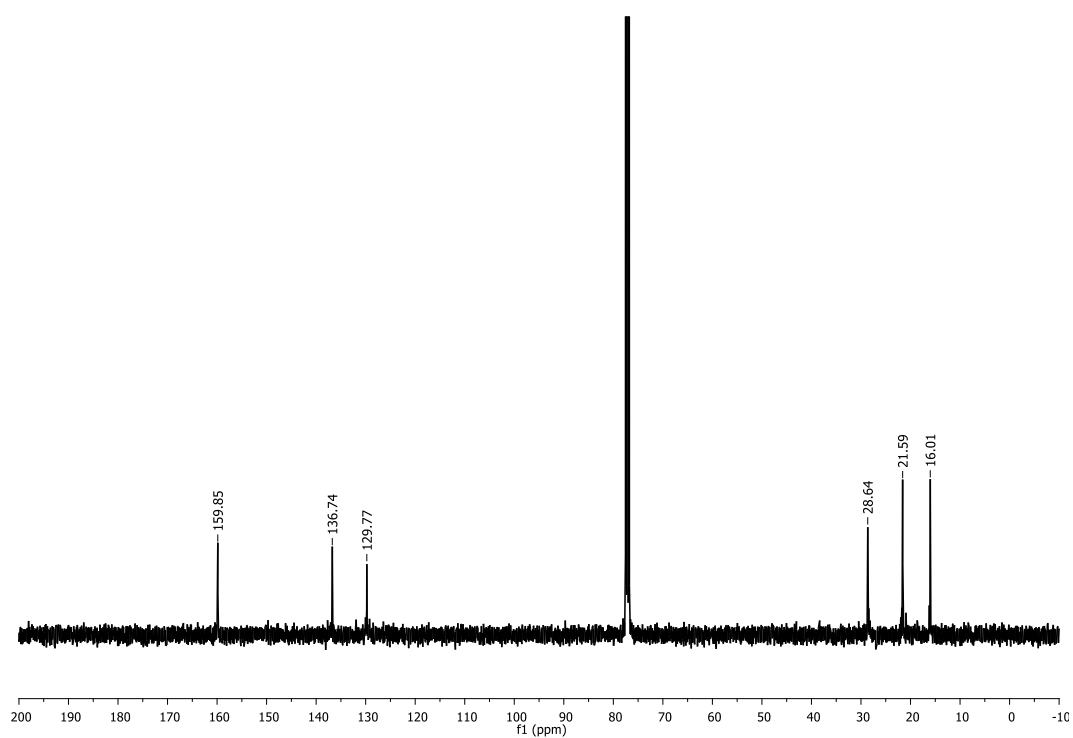
**Appendix Table 68:** Gas sorption results for porous liquids based on RCC3.12TFSA in a range of ionic liquids

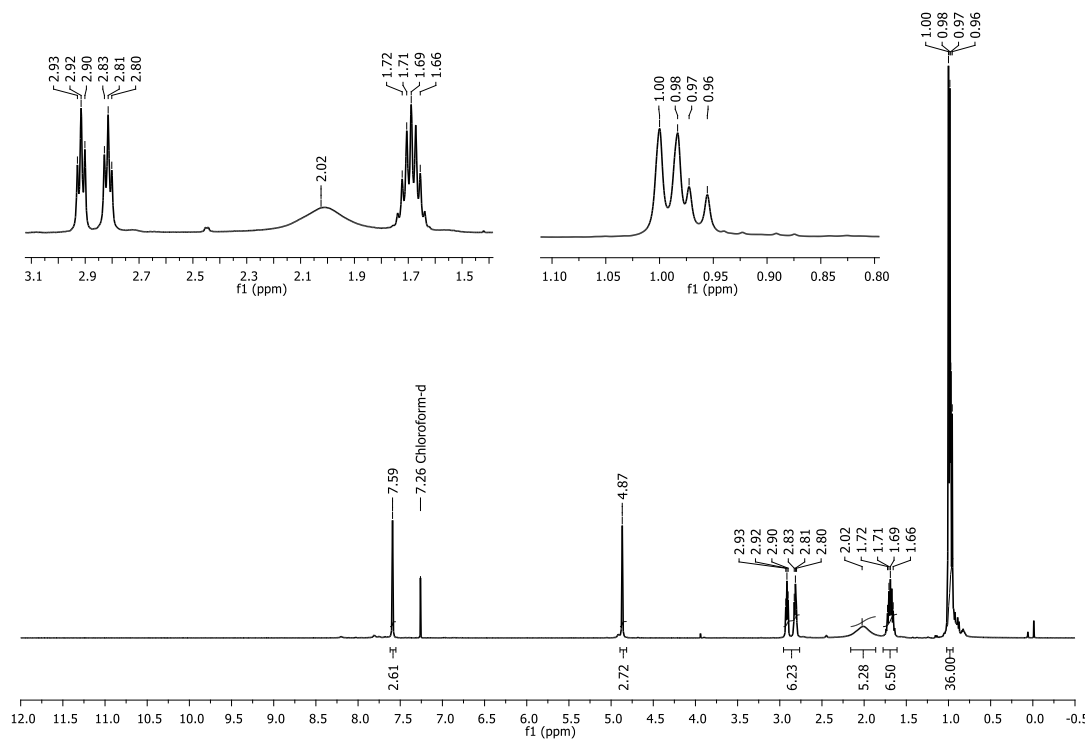
Sample	Gas uptake at 1 bar (μmol g <sup>-1</sup> )	
	CO <sub>2</sub>	CH <sub>4</sub>
PL-1	86.6	8.8
IL-1	72.4	6.2
PL-2	78.8	5.8
IL-6	63.4	3.8
PL-3	69.0	3.9
IL-7	76.7	4.2
RCC3.12TFSA solid	144.4	-6.8

## NMRs of new materials

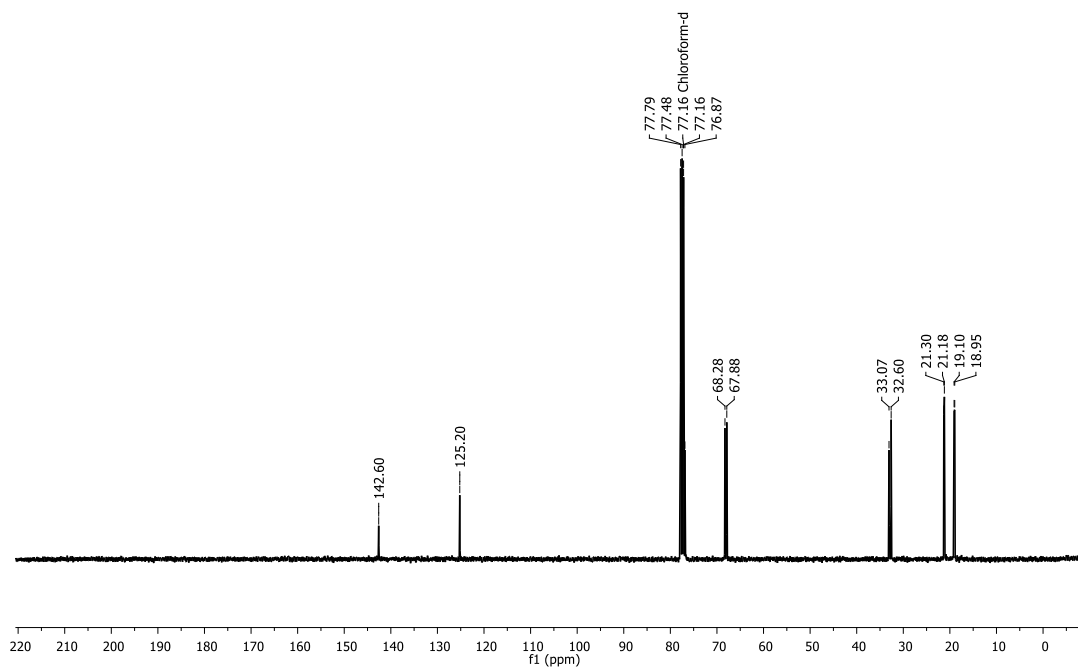
The materials presented in **Chapter 2** and **Chapter 4** are fully characterised in *Chem. Sci.*, 2019,10, 9454-9465.

## Chapter 3

Appendix Figure 1: <sup>1</sup>H NMR spectrum (CDCl<sub>3</sub>) of CC21 $\alpha$ Appendix Figure 2: <sup>13</sup>C NMR spectrum (CDCl<sub>3</sub>) of CC21 $\alpha$



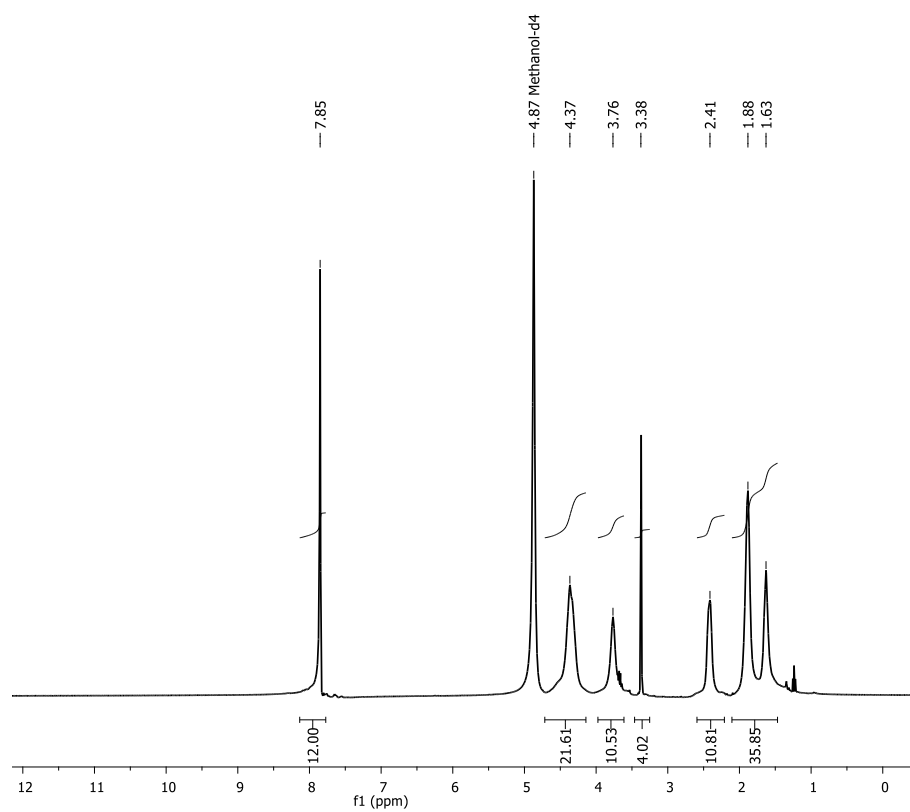
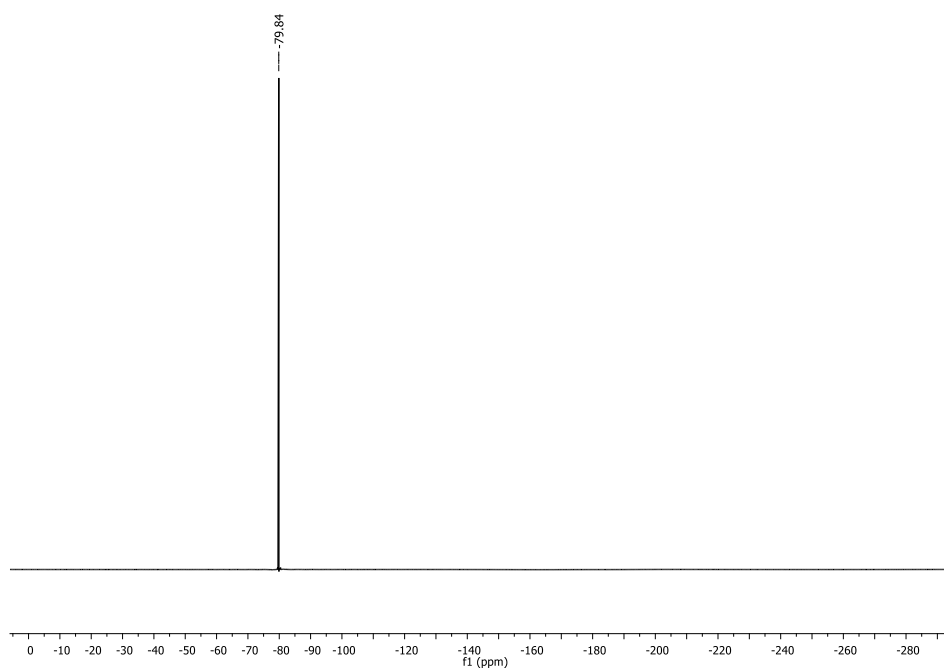
**Appendix Figure 3:** <sup>1</sup>H NMR spectrum (CDCl<sub>3</sub>) of 1,3,5-tris(4,5-diisopropylimidazolidin-2-yl)benzene



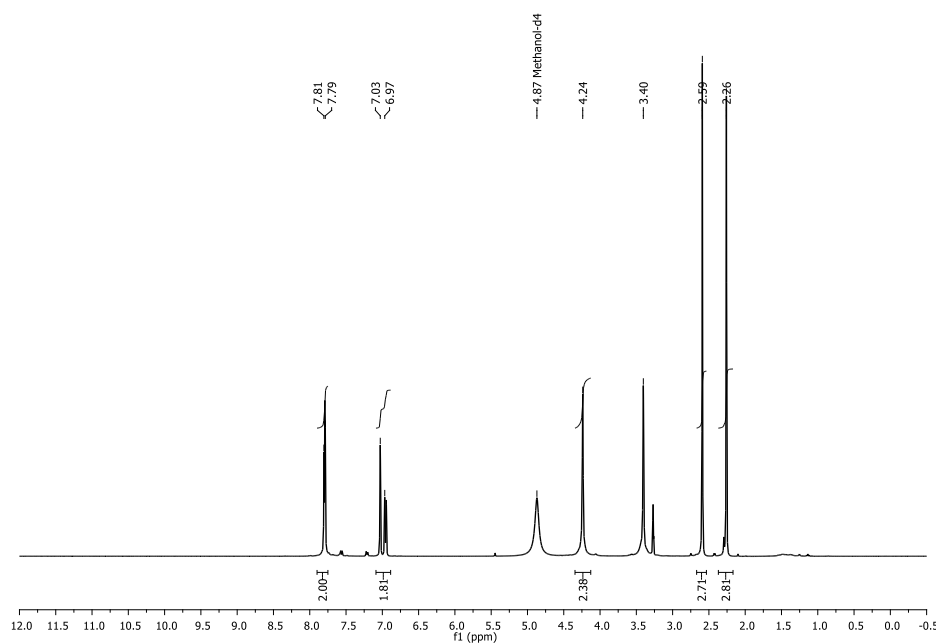
**Appendix Figure 4:** <sup>13</sup>C NMR spectrum (CDCl<sub>3</sub>) of 1,3,5-tris(4,5-diisopropylimidazolidin-2-yl)benzene

## Chapter 5

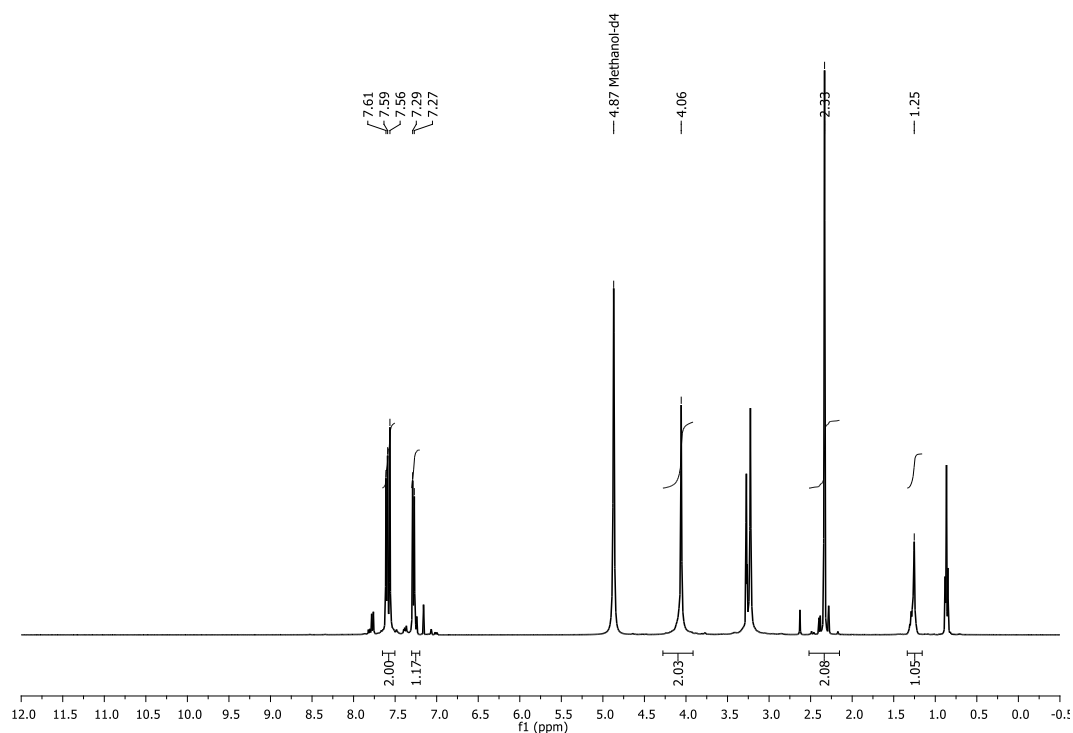
## RCC3.12TFSA

Appendix Figure 5:  $^1\text{H}$  NMR spectrum (MeOD) of RCC3.12TFSAAppendix Figure 6:  $^{19}\text{F}$  NMR spectrum (MeOD) of RCC3.12TFSA

## RCC1.12TSA

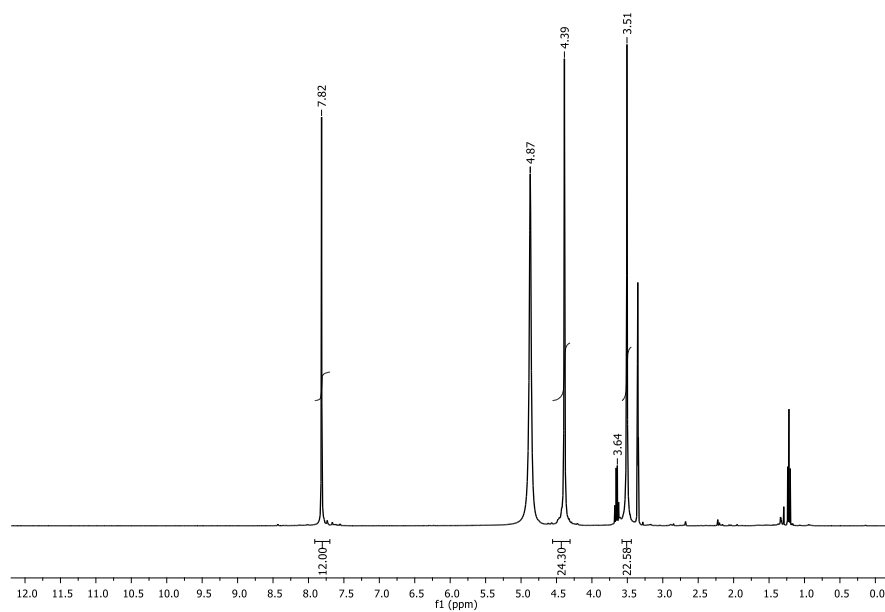
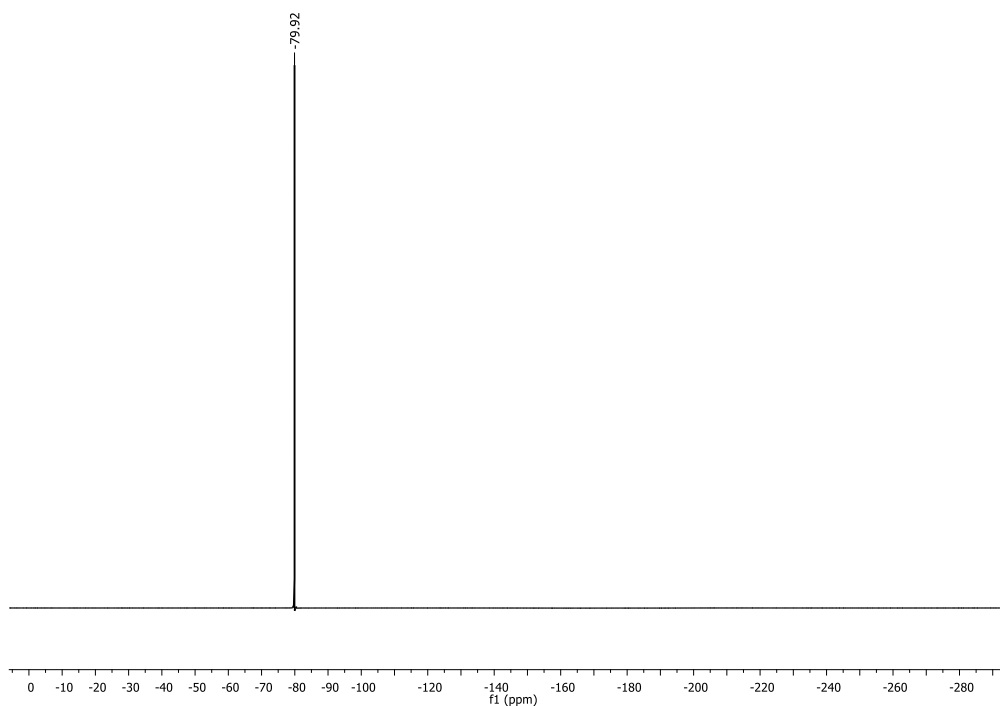
Appendix Figure 7: <sup>1</sup>H NMR spectrum (MeOD) of RCC1.12TSA

## RCC1.12XSA

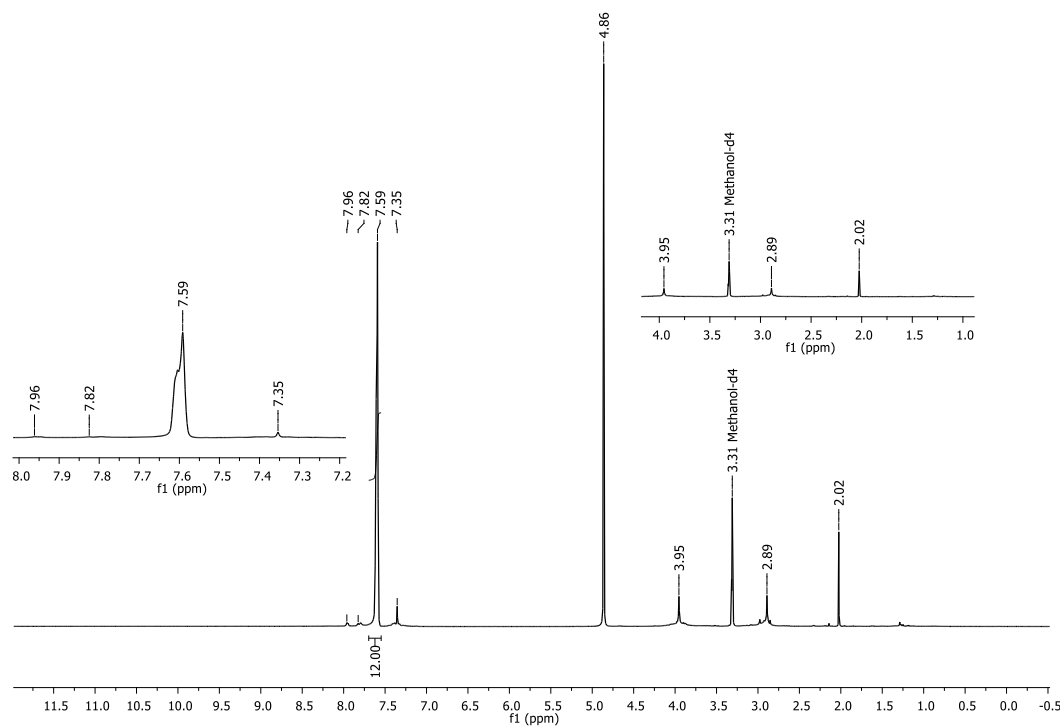
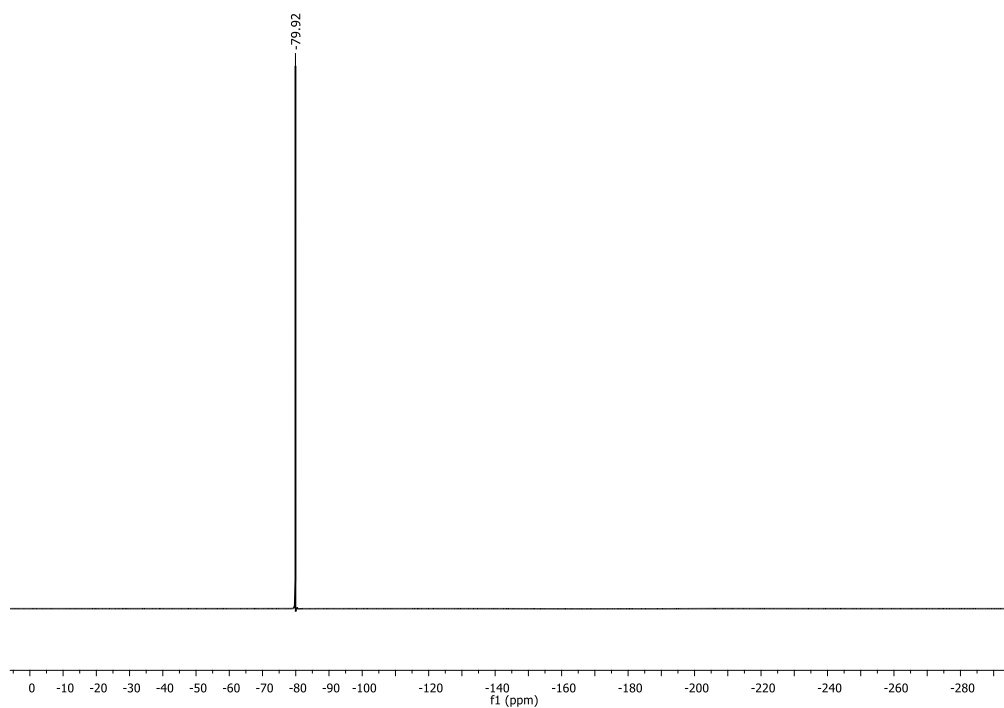
Appendix Figure 8: <sup>1</sup>H NMR spectrum (MeOD) of RCC1.12XSA



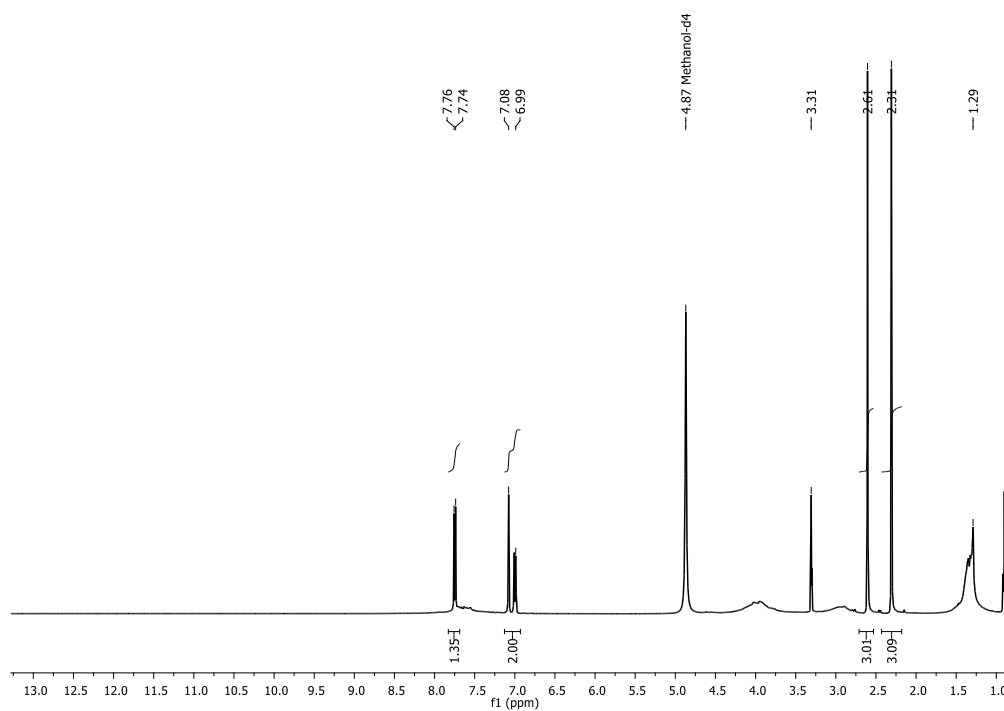
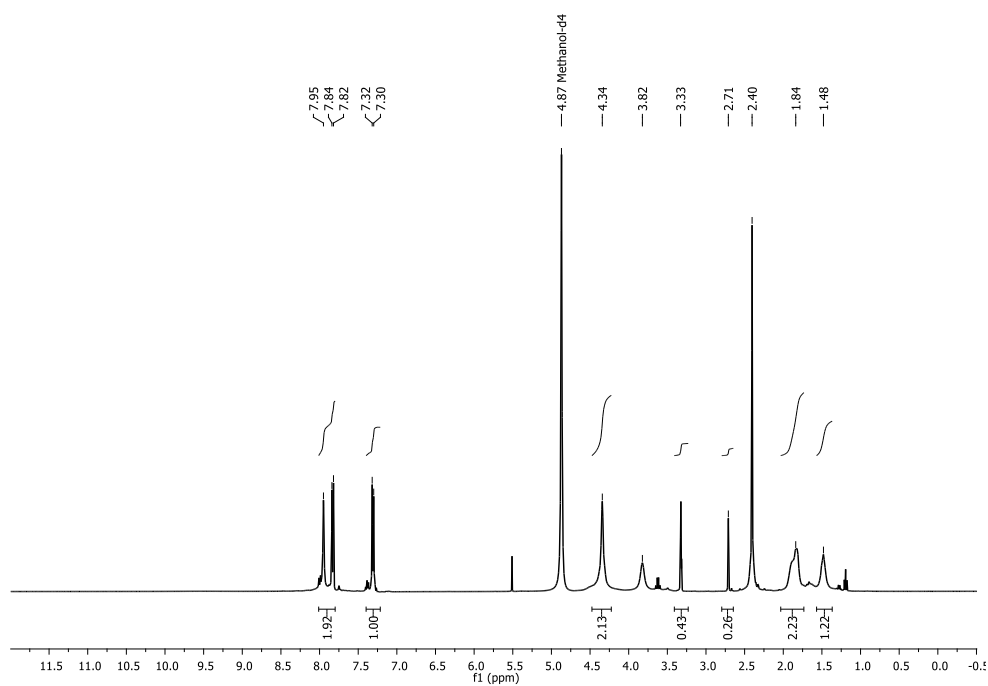
## RCC1.12TFSA

Appendix Figure 9:  $^1\text{H}$  NMR spectrum (MeOD) of RCC1.12TFSAAppendix Figure 10:  $^{19}\text{F}$  NMR spectrum (MeOD) of RCC1.12TFSA

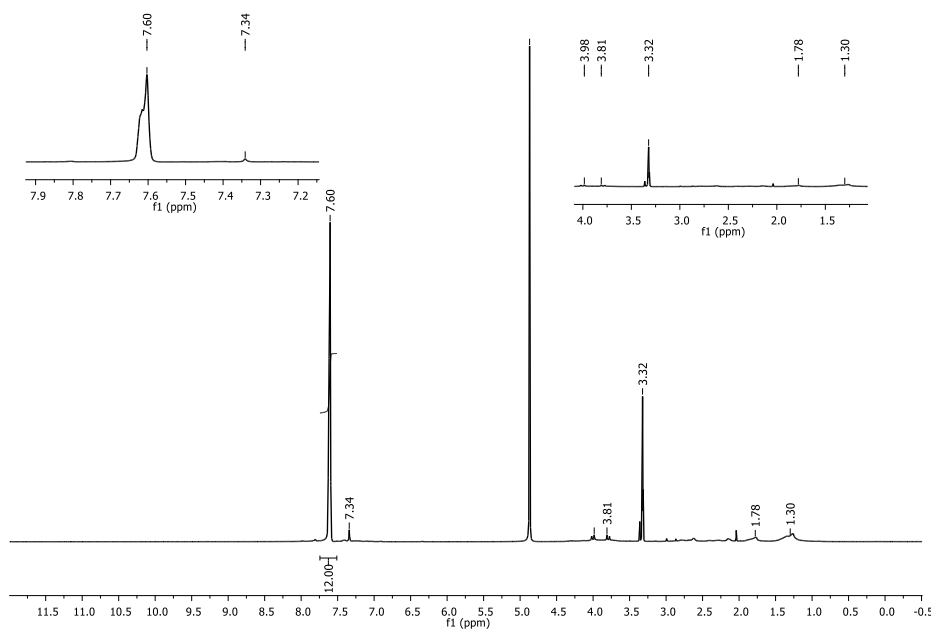
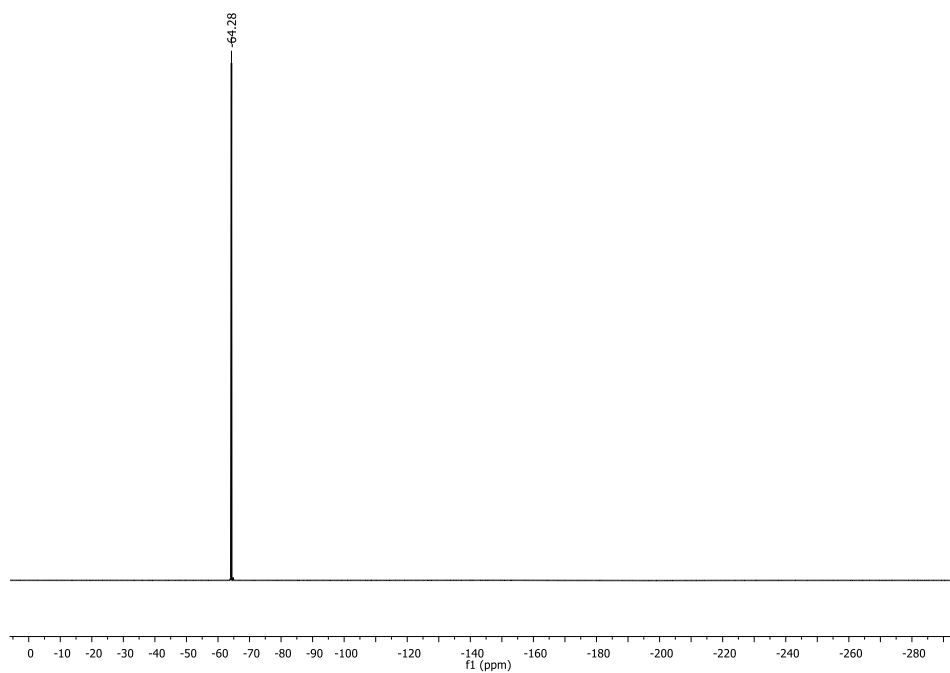
## RCC1.12BARF

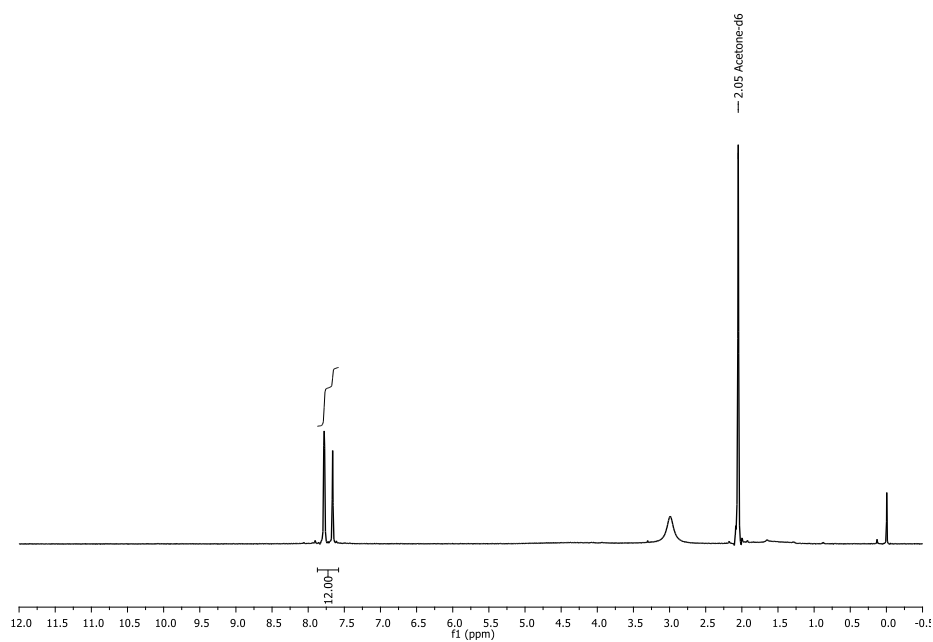
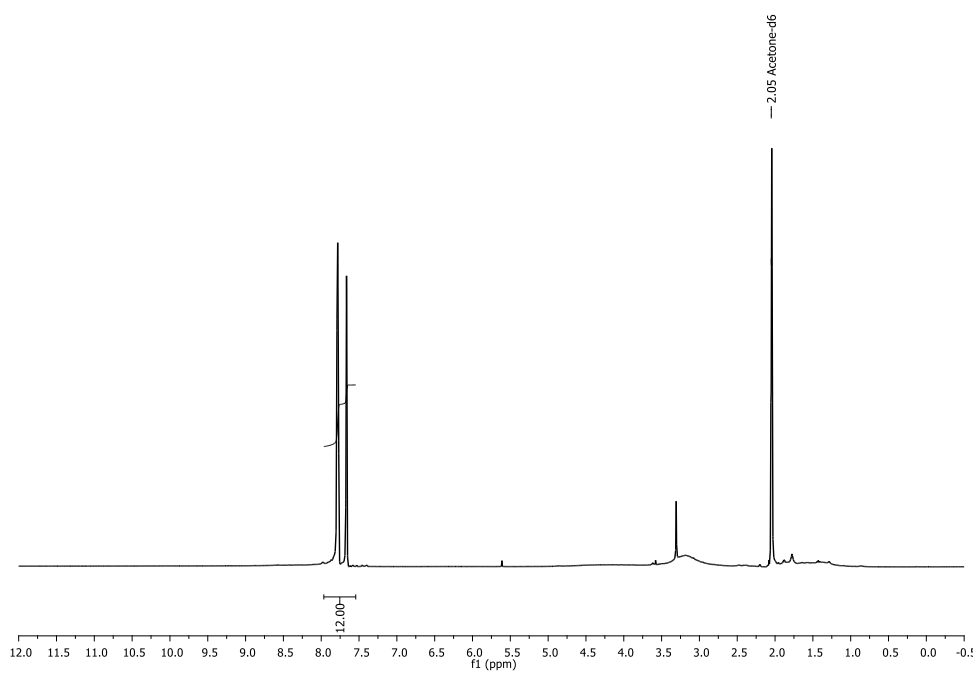
Appendix Figure 11:  $^1\text{H}$  NMR spectrum (MeOD) for RCC1.12BARFAppendix Figure 12:  $^{19}\text{F}$  NMR spectrum (MeOD) of RCC1.12BARF

## RCC3.12TSA

Appendix Figure 13: <sup>1</sup>H NMR spectrum (MeOD) for RCC3.12TSAAppendix Figure 14: <sup>1</sup>H NMR spectrum (MeOD) for RCC3.12XSA

## RCC3.12BARF

Appendix Figure 15:  $^1\text{H}$  NMR spectrum (MeOD) for RCC3.12BARFAppendix Figure 16:  $^{19}\text{F}$  NMR spectrum (MeOD) for RCC3.12BARF

**RCC13.12BARF****Appendix Figure 17:**  $^1\text{H}$  NMR spectrum (Acetone- $\text{d}_6$ ) for **RCC13.12BARF****R3<sup>3</sup>:R13<sup>3</sup>.12BARF****Appendix Figure 18:**  $^1\text{H}$  NMR spectrum (Acetone- $\text{d}_6$ ) for **R3<sup>3</sup>:R13<sup>3</sup>.12BARF**